TMX-18912382

Stock cy.
INTERNATIONAL WORKSHOP ON

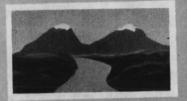
# EARTH RESOURCES SURVEY SYSTEMS

MAY 3-14, 1971

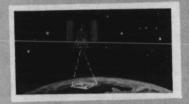
CASE FILE COPY













# UNITED STATES GOVERNMENT SPONSORS:















VOLUME II

# PROCEEDINGS OF THE INTERNATIONAL WORKSHOP

ON

# EARTH RESOURCES SURVEY SYSTEMS

Volume II

MAY 3-14, 1971

Sponsored by

NATIONAL AERONAUTICS AND SPACE ADMINISTRATION
DEPARTMENT OF AGRICULTURE
DEPARTMENT OF THE INTERIOR
NATIONAL OCEANIC AND ATMOSPHERIC ADMINISTRATION
of the
DEPARTMENT OF COMMERCE
NAVAL OCEANOGRAPHIC OFFICE
AGENCY FOR INTERNATIONAL DEVELOPMENT
DEPARTMENT OF STATE

#### PREFACE

In a statement before the United Nations General Assembly on September 18, 1969, President Nixon said, "Of all of man's great enterprises, none lends itself more logically or more compellingly to international cooperation than the venture into space. ...we are just beginning to comprehend the benefits that space technology can yield here on earth. And the potential is enormous. ... I feel it is only right that we should share both the adventures and the benefits of space. As an example of our plans, we have determined to take actions with regard to earth resource satellites as this program proceeds and fulfills its promise. The purpose of those actions is that this program will be dedicated to produce information not only for the United States but also for the world community."

As one of the actions foreseen in the President's message, the U.S. representative at the September 1, 1970, meeting of the United Nations Committee on the Peaceful Uses of Outer Space, announced that the U.S. would hold an International Workshop on Earth Resources Survey Systems. This Workshop has been organized to describe the Earth Resources Survey Program of the U.S., its content, techniques and results to date, and its future plans. The potential contribution of remote sensing data to the solution of resource problems and the experimental material which is expected to become available to other countries are also discussed. The Workshop also provided a forum in which other countries described their own related programs.

This volume of Proceedings contains the papers presented during the tutorial sessions of the second week of the Workshop (May 10-14, 1971). It has been prepared as a reference document for use during and after the Workshop sessions.

# CONTENTS

		Page
TIT	LE PAGE	i
PRE	FACE	ii
CON	TENTS	iii
	AGRICULTURE	
1.	Draeger, William C.	
	The Use of Small Scale Aerial Photography in a Regional Agricultural Survey	3
2.	Gausman, Harold W.	
	Photographic Remote Sensing of "Sick" Citrus Trees .	15
3.	Lauer, D. T.	
	Testing Multiband and Multidate Photography for Crop	
	Identification	33
4.	Pettinger, Lawrence R.	
	Field Data Collection An Essential Element in	
	Remote Sensing Applications	49
5.	Weigand, Craig L.	
	Agricultural Applications and Requirements for	
	Thermal Infrared Scanners	67
	FORESTRY	
6.	Aldrich, Robert C.	
	Forest and Range Inventory and Mapping	83
7.	Heller, Robert C.	
	Detection and Characterization of Stress Symptoms in	
	Forest Vegetation	109
8.	Hirsch, Stanley N.	
	Application of Infrared Scanners to Forest Fire	
	Detection	153

# CARTOGRAPHY

9.	McLaurin, John D.  Application of Remote Sensing to Planimetric, Thematic, and Topographic Mapping	171
	GEOGRAPHY	
10.	Anderson, James R. and Place, John L.  Regional Land Use Mapping: The Phoenix Pilot  Project	197
11.	Horton, Frank E.	
	The Application of Remote Sensing Techniques to Urban Data Acquisition	213
12.	Pease, Robert W.	
	Climatology of Urban-Regional Systems	225
13.	Wray, James R.  The Census Cities Project, and Atlas of Urban and Regional Change	243
	ENVIRONMENTAL QUALITY	
14.	Nelson, Harvey K.; Klett, A. T.; and Johnston, John E. Application of Remote Sensing Techniques for Appraising Changes in Wildlife Habitat	263
15.	North, Gary Remote Sensing of Environmental Pollution	291
16.	White, Peter G.	
	Remote Sensing of Water Pollution	303
	GEOLOGY	
17.	Jackson, Wayne H. and Eaton, Jerry P.	
	Satellite Relay Telemetry of Seismic Data in Earthquake Prediction and Control	323
18.	Smedes, Harry W.	
	Automatic Computer Mapping of Terrain	345

19.	Geophysical Aspects of Remote Sensing	409
	Geophysical Aspects of Remote Bensing	103
	HYDROLOGY	
20 a	. Baker, Donald	
	Remote Sensing of Snow Fields from Earth Satellites.	431
20 b	. Salomonson, Vincent V.	
	Nimbus 3 and 4 Observations of Snow Cover and Other Hydrological Features in the Western Himalayas	443
21.	Paulson, Richard W.	
	The Role of Remotely Sensed and Relayed Data in the Delaware River Basin	449
22.	Rabchevsky, George A.	
	Hydrologic Conditions Viewed by the Nimbus Meteorological Satellites	469
23.	Turner, Raymond M.	
	Measurement of Spatial and Temporal Changes in Vegetation from Color Infrared Film	513
	OCEANOGRAPHY	
24.	Duntley, Seibert Q.; Stevenson, R. E.; and Boileau, A. Exploration of Marine Resources by Photographic Remote Sensing	531
25.	Mairs, Robert L. Oceanographic Interpretation of Apollo Photographs .	553
26.	McClain, E. Paul	
	Remote Sensing of Sea Ice from Earth Satellites	581
27.	Rao, P. Krishna	
	Remote Sensing of Sea Surface Temperatures from Earth Satellites	595

# BIOGRAPHICAL SKETCH

William C. Draeger
Forestry Remote Sensing Laboratory
University of California
Berkeley, California 94720

Born in San Francisco, California in April, 1942. B.S. (Forestry), University of California, January, 1964; M.S. (Forestry-Photogrammetry), Univ. of Calif., June, 1965; Ph.D. (Wildland Resource Science), Univ. of Calif., March, 1970.

Presently is Leader of the Operational Feasibility Unit of the Forestry Remote Sensing Laboratory, University of Calif., Berkeley. Responsibilities include compilation of requirements for remote sensing data by resource management personnel, evaluation of remote sensing techniques in light of those requirements, and determination of the operational feasibility of large scale remote sensing applications. A member of the American Society of Photogrammetry and the Society of American Foresters.

#### THE USE OF SMALL SCALE AERIAL PHOTOGRAPHY

#### IN A REGIONAL AGRICULTURAL SURVEY

William C. Draeger

Forestry Remote Sensing Laboratory School of Forestry and Conservation University of California, Berkeley

#### INTRODUCTION

During the past year and a half, Maricopa County, Arizona has been the site of extensive NASA-sponsored research designed to investigate the potential usefulness of small-scale aerial and space photography in the inventory and evaluation of agricultural crops. Early in these investigations it became apparent that in order to fully assess the <u>operational</u> value of such photography, a regional approach to the research would be necessary.

One of the primary advantages of using small scale aerial or space photography is that it affords a synoptic view of the earth's surface (i.e., large areas of land can be seen in their entirety on one or a very few images), suggesting a particular potential usefulness for conducting broad regional resource analyses. Futhermore, few actual resource inventories as presently undertaken limit themselves to a small area, but rather are usually geared to larger managerial or policy-formulation units such as entire watersheds, counties or states. Thus, most remote sensing surveys, when performed operationally, would probable also be geared to fairly large areas so as to provide maximum utility to the ultimate user. Finally, while the development of remote sensing techniques on small test sites is often quite useful, especially in the early experimental stage, findings of limited tests often cannot be directly applied to the larger operational case. In addition to the obvious problems stemming from increased interpreter fatigue and data handling requirements when large areas are the subject of surveys, the phenomenon of environmental varibility often becomes a major factor to be dealt with in the design of information extraction techniques.

For these reasons, it seemed that one of the most meaningful experiments which could be performed with the imagery described above would be to attempt to make an agricultural survey, for Maricopa County as a whole. By so doing, an attempt could be made to answer questions which would arise only in such a semi-operational survey and which must be solved before the full benefits which might accrue from the use of high altitude or space photography can be realized. In addition, it was hoped that such a study might provide some clues as to the procedures to be followed in evaluating synoptic imagery which will become available from the Earth Resources Technology Satellites, ERTS-A and ERTS-B, due to be launched in early 1972 and 1973, respectively, and the manned Sky Laboratory, scheduled for launch in 1973.

could be the subject of such a survey, none are more important or more amenable to the application of remote sensing techniques than agricultural crops. According to recent records, over 10 percent of the land in Maricopa County is under cultivation. The county provides roughly half of Arizona's agricultural crop production, and ranks third among all U.S. counties in gross value of such products. In addition, many of the crops grown contribute directly to the livestock and cattle feeding industry, in which Arizona ranks eighth nationally. The nature of agricultural cropland makes it expecially well suited to such a study. By and large such land consists of discrete fields, each of which contains a fairly uniform stand of a particular type of vegetation that may vary quite rapidly in its phenological characteristics through a seasonal cycle. This characteristic presents an excellent opportunity for the development of techniques which could be quite valuable in their own right, and which hopefully could contribute to methods applicable to more varible wildland vegetation types. Finally, a very real need exists at the present time for inexpensive, accurate and up-to-date inventories of agricultural crops, as is evidenced by the extensive program carried out by the Statistical Reporting Serivce of the U.S. Department of Agricultire in cooperation with various state and county organizations.

#### PRELIMINARY TESTS

As has been described earlier (Lauer: Testing Multiband and Multidate Photography for Crop Identification), numerous photo interpretation tests were conducted on a 16-square-mile area within Maricopa County. These tests were intended to determine the relative value of small scale aerial photography and Apollo 9 space photography for the inventory of crops, and to evaluate the usefulness of multidate and multiband photography for these surveys.

These tests suggested that, at least for agricultural surveys in the area under study, no significant differences in identification accuracy resulted from the use of Apollo 9 and high altitude aerial photography. In addition, they emphasized the importance of the selection of specific dates for the inventory of particular crops, and the necessity for an understanding of the seasonal development of crops in a region prior to specification of optimum dates for obtaining photography.

operational survey for barley and wheat. This decision was based on the following factors: (1) small grains (of which barley and wheat are the only major varieties in Maricopa County) account for approximately 20% of the crop acreage in Maricopa County and thus are inportant crops for which agricultural statistics are currently prepared using conventional techniques, (2) these crops mature and are harvested within the first half of the calendar year, coincident with the time period for which monthly NASA aircraft missions were scheduled during 1970 and, (3) our previous results indicated that the highest percentage correct identification of any crop was achieved for barley (90% using Infrared Ektachrome photos and 91% using Pan-25 photos) by selecting the appropriate month (May) for conducting the test. For these reasons, it was felt that a survey for barley and wheat would provide the greatest opportunity for initial success using a previously untried technique.

Final preliminary tests were then conducted to determine the specific date or dates of photography and film/filter combinations which were optimum for the identification of barley and wheat. The results of these tests indicated that Ektachrome MS (2448) photography taken in the months of May and June should be used for the semi-operational survey.

#### DEVELOPMENT OF THE SEMI-OPERATIONAL SURVEY

Attempting to administer a photo interpretation survey involving an entire county, containing nearly 800-square-miles of agricultural land, immediately presented a number of problems not faced on the 16-square-mile study area. The principal questions raised were: (1) Will a sample provide a satisfactory estimate of crop acreage, or is 100% interpretation required? (2) Will stratification lead to a more accurate estimate? (3) How much ground information will be required for interpreter training and for evaluation of the interpretation? In an attempt to answer several of these questions simultaneously, the agricultural area within the county was delineated into six strata based wholly on their appearance on the Infrared Ektachrome Apollo 9 photo. Thirtytwo plots, each consisting of a square, two miles on a side, were allocated to the strata on the basis of proportional area, and plot centers were located randomly (Figure 2). Maps of each plot showing field boundaries were drawn based on their appearance on earlier high-flight photography, and each plot was visited by a field crew at the time of overflights for the months of April, May and June 1970. Information gathered in this manner included the category of crop growing in each field, the condition of the crop, the percent of the ground covered by vegetation, crop height, and the direction of rows, if any.

In order to facilitate access to this information pertaining to each of the more than 2500 fields present in the thirty-two four-square-mile sample plots (comprising a total of more than 80,000 acres), field data were punched on computer cards. Programs were then written which made possible the compilation of data by stratum, cell, crop type, and date, and which provided for subdivisions or consolidations of fields over time. Thus data are available not only for each date of photography, but for the sequential changes in crop type and condition through the growing season as well.

Based on a knowledge of the distribution and variability of crop acreage thus obtained, tests were conducted regarding the value of stratification based on gross appearance on space photography, and the possibility of sampling within the agricultural areas to obtain overall crop acreages for the county. Analyses of variance indicated that no significant differences existed between strata in terms of acreages of major field crops, thus indicating that stratification would not improve acreage estimates. In addition, calculations indicated that the acreage distribution of major crops was so variable that for any plot size, extremely large samples would be necessary in order to assure acreage estimates that would satisfy accuracy requirements. For example, in order to estimate the acreage of wheat with a standard error of  $\pm$  10% of the total acreage using a plot size of four-square-miles, a 75% sample would be necessary.

Thus, it was decided that the most efficient and realistic method of estimating crop acreage would entail a 100% photo interpretation of the agricultural areas, with ground data being gathered for thirty-two four-square-mile

plots only. In this way photo interpretation results could be compared with the ground conditions on the field plots, and the overall photo interpretation results adjusted as appropriate using standard ratio sampling procedures.

Some problems were also encountered in the development of the method of compilation of photo interpretation data. First of all, in order to make a measure of interpretation accuracy, interpretation findings must be tied to some actual unit of land area. However, the preparation of detailed field boundary maps from small-scale photos by the interpreter, while possible, would constitute an extremely time consuming task. Also, the tabulation of interpretation data on the basis of numbers of fields is not necessarily indicative of accuracy of acreage estimates which in most cases in the item of interest to the ultimate user. Furthermore, to evaluate "number of fields" data, the researcher must assign arbitrary weight to "correct", "omission error" and "commission error" values, a task which in many cases might best be left to the discretion of the ultimate user of the information.

In order to avoid these problems while still collecting data which would be as meaningful as possible, it was decided to require the interpreter merely to grid agricultural areas into regular square-mile cells (thus making possible direct comparisons with ground data on the thirty-two sample plots) and to tabulate extimates of the <u>acreage</u> of barley and wheat in each cell without regard to the specific location of individual fields.

The agricultural areas within Maricopa County were divided into three nearly equal portions, with one interpreter assigned to each area. The interpreters, chosen on the basis of high scores on preliminary tests, were first trained using photos and ground data maps of areas which they would not interpret later. Training included both indentification of wheat and barley, and estimation of field acreage. The interpreters were then supplied with Ektachrome photos for May 21 and June 16 (scale 1/120,000) of their test areas, as well as maps indicating township boundaries. Each township (norminally a six-mile square, but not invariably so because of ground survey errors made many years ago) was located on the test photography and interpreted as a unit, section by section. For each section the interpreter recorded total acreage of wheat, barley, and all cropland. (Deductions from cropland included farmhouse-barn complexes. freeways, major canals, and general urban and developed areas, but did not include secondary service roads or local irrigation ditches.) In addition, each interpreter was asked to interpret one township in another interpreter's area, as well as to repeat the interpretation of one township in his own area without reference to his earlier results.

#### RESULTS

The results of the semi-operational survey were obtained in the following manner:

- Each interpreter's estimates of acreage of barley, wheat, wheat and barley combined, and total cropland for the sample plots within his area were compared with the actual acreages for each of the plots as determined by on-the-ground surveys.
- 2. Ratios of actual acreages to interpretation acreages for each category were calculated for each interpreter, and this ratio was used to adjust

the results for the entire area as estimated by each interpreter by the formula

$$\hat{Y}_{T} = Y_{PT} X'R$$

where  $\gamma_{I}$  = estimate of total acreage of category within an interpreter's area

YPI = initial photo interpretation of acreage within an interpreter's area R = the correction ratio as derived from the sample plots.

- 3. The category estimates for the three interpreters were summed to form a total county estimate.
- 4. Sampling errors were calculated for the various category estimates by each interpreter as well as for the overall county estimates in order to give an indication of the accuracy of the crop estimates. In calculating the overall county statistics, each of the three interpreters' areas was handled as an individual stratum.

A summary of the survey results is presented as a precentage figure calculated by:

where

SY = standard error of the estimated acreage Y = estimated acreage.

A correction ratio greater than I indicates that the interpreter underestimated the acreage of that category, while a ratio less than 1 indicates that he overestimated the acreage.

# ACREAGE ESTIMATES AND SAMPLING ERROR (Table 1)

CATEGORY	TOTAL ESTIMATE (ACRES)	SAMPLING ERROR
Barley	50,044	11%
Wheat	41,714	13%
Barley and Wheat	92,207	8%
All Cropland	452 ,000	3%

# RATIO CORRECTION FACTORS (Table 2)

INTERPRETER	BARLEY	WHEAT	BARLEY AND WHEAT	ALL CROPLAND
1	1.1225	.9846	1.0481	.9913
2	1.1131	.9012	1.0352	.9809
3	1.1234	.9388	1.0309	1.0094

SAMPLING ERRO	R OF	INTERPRETERS	(Table 3)
---------------	------	--------------	-----------

INTERPRETER	BARLEY	WHEAT	BARLEY AND WHEAT	ALL CROPLAND
1	18%	17%	14%	5%
2	30%	32%	16%	3%
3	14%	21%	11%	6%
TOTAL AREA	11%	13%	8%	3%

# INTERPRETATION TIME (Table 4)

INTERPRETER	TRAINING TIME	INTERPRETATION TIME	AVERAGE TIME/TOWNSHIP
1	8 hr. 55 min.	26 hr. 20 min.	1 hr. 20 min.
2	7 hr. 30 min.	13 hr. 40 min.	1 hr. 03 min.
3	6 hr. 30 min.	28 hr. 05 min.	1 hr. 02 min.
TOTAL	22 hr. 55 min.	68 hr. 05 min.	1 hr. 08 min.

The results of greatest interest are, of course, the estimated acreages of each category for the entire county, and their accuracies. In this case, however, there are no reliable statistics gathered in the conventional manner with which to compare these results. While the Statistical Reporting Service does publish monthly estimates of crop acreages for the U.S. as a whole and for individual states, their methods are such that no accurate estimates are available for specific counties until months after the time of harvest, and even then they are mush less accurate than the state and national estimates. This, of course, only serves to emphasize the potential value of estimates obtained by means of the methods described here. It is possible, however, to discuss the accuracy of the estimates by reference to calculated measures of statistical reliability derived from the sample data.

The sampling error (standard error of the estimate expressed as a percent of the estimate) for barley was 11% and for wheat was 13%, while the figure for both barley and wheat combined was 8%, indicating that a good deal of error resulted from a confusion of the two small grain crops. This same phenomenon is evident in the correction ratio figures. In general, the interpreters underestimated barley and overestimated wheat, whild they were only slightly low in their estimates of the two grains combined. These results indicate that considerable improvement in the measurements could be realized if a more definite differentiation between the two small grains could be made. Nevertheless, the accuracies as shown are quite encouraging, especially considering the rapidity with which they could be compared.

In the table listing the individual interpreter's accuracy levels (Table 3) it can be seen that one of the interpreters. had a significantly higher error for both barley and wheat than the other two interpreters, but all three were nearly equal for barley and wheat combined. This indicates that while this one interpreter had more trouble differentiating between the two crops, he did nearly as

well as the others in distinguishing the two small grains from all other field conditions. Furthermore, the large differences in performance point up the importance of screening and training interpreters before undertaking operational surveys. The sampling error could have been significantly reduced if the performance of the one "inaccurate" interpreter had been equal to the other two. Also, all three interpreters indicated that their confidence in their interpretations increased as they progressed through the survey. Certainly any fully operational survey would include considerably more interpreter training than has been undertaken in this study.

#### CONCLUSION

The stated purpose of the experiment was to investigate the feasibility of performing inventories of agricultural resources using very small scale aerial or space photography. Further, it was hoped that by remaining cognizant at all times of the constraints that would be faced when carrying out an operational survey, findings would be more valuable than those resulting from the more usual limited-area tests.

Certainly the results to date are encouraging on two counts: (1) the questions posed initially are being answered, i.e., the very practical problems of an operational survey are being faced and solutions are being found, and (2) it would seem that a fully operational agricultural inventory using very small-scale photography is not beyond the scope of present technology.

Probably the biggest problems that will be faced in establishing a functional inventory system are those concerning logistics and data handling. For example, it will be necessary to ensure that ground crews are at the proper place at the proper time over widely scattered areas in order to provide calibration data. Imagery must be obtained at specific times to permit differentiation among various crop types, interpretation of large areas must be performed rapidly to ensure that the information is not outdated before it is available; and interpretation results must be compared with calibration data and the necessary adjustments made before distribution.

Finally, data must be provided, not at those times for those geographic units which lend themselves well to the data gathering techniques, but rather at times and for area units which are geared to user requirements as nearly as possible.

However, most of the data handling problems are not much more complex than those faced by government agencies gathering agricultural data by more conventional means at the present time. Furthermore, a number of systems are presently being developed which, it is hoped, will possess a capability to automatically extract image data from aerial or space photographs, perform crop identification functions, combine this information with other parameters keyed to the same geographic coordinate system, and produce graphical or tabular output in a wide variety of desired formats. It appears that such systems would lend themselves particularly well to agricultural surveys wherein nearly all the image interpretation is based on tone or color discrimination (a function much more accurately performed by a machine than a human interpreter) rather than complex deductive decisions. In fact, it is planned that further studies of agricultural inventory method by the Forestry Remote Sensing Laboratory will involve an

investigation of the extent to which automatic image interpretation and data handling methods can contribute to operational surveys of the type described in this paper.

#### LITERATURE CITED

Carneggie, D.M., et al. 1969. Analysis of earth resources in the Phoenix, Arizona area. In an Evaluation of Earth Resources Using Apollo 9 Photography. R.N. Colwell, et al. Final Report. NASA Contract No. NAS-9-9348. University of California, Berkeley, California.

Johnson, C.W., et al. 1969 A system of regional agricultural land use mapping tested against small scale Apollo 9 color infrared photography of the Imperial Valley. University of California, Riverside. USDI Status Report III, Tech, Report V, Contract 14-08-0001-10674.

Pettinger, L.R., et al. 1969 Analysis of earth resources on sequential high altitude multiband photography. Special Report Forestry Remote Sensing Laboratory, University of California, Berkeley. 31 December 1969.

U.S. Dept. of Commerce, Urban Renewal Administration. 1965. Standard Land Use Coding Manual. January 1965



Figure 1: This enlargement of Apollo 9 Infrared Ektachrome frame AS9-26-3801 shows the Maricopa County test site where the agricultural inventory was performed. The city of Phoenix appears in the right center, surrounded by extensive agricultural lands and wild areas valuable as rangeland and watershed.



Figure 2: This black-and-white enlargement of an Apollo 9 space photo shows the portion of Maricopa County containing agricultural lands, and for which the semi-operational survey was performed. The location of each of the 32 4-square-mile plots selected for ground survey at the time of each NASA overflight is as indicated.

Page Intentionally Left Blank

# BIOGRAPHICAL SKETCH Harold W. Gausman

Dr. Harold W. Gausman is a Plant Physiologist in the USDA's remote sensing program at the Rio Grande Valley Soil and Water Research Center, Weslaco, Texas. He obtained a B.S. degree at the University of Maine in 1949, and M.S. and Ph.D. degrees at the University of Illinois in 1950 and 1952, respectively. He has been employed in research and teaching by the Universities of Illinois, Texas A&M, Rutgers (New Jersey), and Maine. He was a Full Professor at the University of Maine from 1959 to 1967, and the University Radiation Protection Officer from 1956 to 1960. At the University of Maine, he taught Experimental Design, Soil and Plant Relationships, and Radiobiology. He has done Post-Doctoral studies in nuclear physics and radiochemistry, statistics, and plant physiology (NSF Fellowship) at the Universities of Rutgers, Florida, and Texas A&M respectively. He was on the visiting scientist panel of the American Society of Agronomy, 1964-1967.

Page Intentionally Left Blank

#### PHOTOGRAPHIC REMOTE SENSING OF "SICK" CITRUS TREES

Harold W. Gausman

Southern Plains Branch
Soil and Water Conservation Research Division
Agricultural Research Service
U. S. Department of Agriculture
Weslaco, Texas

#### INTRODUCTION

This paper considers remote sensing with infrared color aerial photography (Kodak Ektachrome Infrared Aero 8443 film) for detecting citrus tree anomalies ("sick" citrus trees). Illustrations and discussions are given to detecting nutrient toxicity symptoms, to detecting foot rot and sooty mold fungal diseases, and to distinguishing among citrus species. Also, the influence of internal leaf structure on light reflectance, transmittance, and absorptance will be considered; and physiological and environmental factors that affect citrus leaf light reflectance will be reviewed briefly and illustrated.

#### REVIEW OF LEAF STRUCTURE AND SPECTRA

# Internal Leaf Structure

Figure 1 is shown to review leaf structure. The leaf structure in Fig. 1 is similar to the structure of a citrus leaf that will be considered later.

The top layer of cells is the upper epidermis. The epidermal cells have a cuticular layer on their upper surfaces that diffuses but reflects very little light. The long narrow cells below the upper epidermis are palisade cells. They house many chloroplasts with chlorophyll pigments that absorb visible light. The cells below the palisade cells are spongy mesophyll cells. They have many air spaces among them (intercellular air spaces). It is here that oxygen and carbon dioxide exchange takes place for photosynthesis and respiration. The lower epidermis is like the upper epidermis, except a stoma or port is present where gases enter and leave a leaf.

The spongy mesophyll is important in remote sensing because it scatters near-infrared light. For a mature citrus leaf, approximately 55% of the incoming near-infrared light is reflected from the leaf, 40% is transmitted through the leaf, and 5% is absorbed within the leaf.

# Leaf Spectra

The 500- to 2500-nanometer (nm) spectral range will be considered. This spectral region can be divided into: the visible region of 500 to 750 nm, dominated by pigment absorption (chlorophylls and carotenoids); the 750- to 1350-nm near-infrared wavelength interval, a region of high reflectance and low absorptance that is affected primarily by internal leaf structure; and the 1350- to 2500-nm wavelength interval, a region of high absorption by water--the strongest water absorption bands occurring at 1450 and 1950 nm.

Figure 2 shows the diffuse reflectance, transmittance, and absorptance of mature citrus leaves (orange, <u>Citrus sinensis</u> (L.) Osbeck). The reflectance and transmittance spectra are each averages of measurements made on upper (adaxial) surfaces of 10 leaves. Measurements were made with a Beckman Model DK-2A spectrophotometer and its reflectance attachment<sup>1</sup>. Data were corrected for the reflectance of the MgO standard to obtain absolute radiometric values. Absorptance was then calculated as: [100 - (percent reflectance + percent transmittance)].

Figure 2 shows that reflectance, transmittance, and absorptance were 10, 2, and 90%, respectively, at the 550-nm green peak within the 500- to 750-nm visible wavelength range. Absorption in this region was primarily caused by pigments. Within the 750- to 1350-nm near-infrared range, there was approximately 55% reflectance, 40% transmittance, and 5% absorptance. Above 1350 nm, absorptance greatly increased because of water absorption of light energy.

FACTORS AFFECTING LEAF LIGHT REFLECTANCE AND THEIR DETECTION

#### Introduction

Citrus leaf light reflectance is affected by diseases, hormones, insects, leaf age, leaf drying, nutrient levels, and spray residues. For example, drying of a leaf increases its light reflectance, particularly over the 750- to 2500-nm wavelength interval. Because of limited time, we cannot discuss all of the factors listed. Thus we will consider only diseases, insects, leaf age, and nutrient levels.

# Leaf Age

A young citrus leaf is compact with few air spaces in its mesophyll, while an old or mature leaf is "spongy" or has many air spaces. The "spongy" effect in the mature leaf increases reflectance, because there are more intercellular air spaces. Scattering of light within leaves occurs at cell walls (hydrated

Use of a company or product name by the Department does not imply approval or recommendation of the product to the exclusion of others that may also be suitable.

cellulose)-air cavity interfaces that have refractive indices of 1.4 and 1.0, respectively. Healthy citrus leaves also had more spongy mesophylls (Fig. 4) than leaves from trees grown with too much salt. Their differences in light reflectance will be shown in Fig. 5.

Figure 3 shows that the mature leaf represented by the solid black line, compared with the young leaf represented by the dotted line, had about 5 and 15 percentage points more reflectance in the visible (550 to 750 nm) and near-infrared wavelength (750 to 1350 nm) ranges, respectively. This increase in reflectance was caused primarily by air voids (air spaces) in the "spongy meso-phyll" of the mature leaf.

# Nutrient Levels (Toxic Levels of Boron (B) and Chloride (CI)

Healthy citrus leaves also had more spongy mesophylls (Fig. 4) than leaves from trees grown with too much boron (B) and chloride (Cl<sup>-</sup>). Figure 5 shows that healthy compared with salt-affected leaves had approximately 12 percentage points less reflectance at the visible green peak of 550 nm within the 500- to 750-nm wavelength interval caused by light absorption by more chlorophyll; and about 4 percentage points more reflectance in the 750- to 1350-nm near-infrared range, caused by a more "spongy" mesophyll.

The use of infrared color photography to discriminate between healthy citrus trees and trees whose foliage exhibit boron (B) and chloride (Cl<sup>-</sup>) toxicity symptoms is being tested. Too much salt in the soil or irrigation water affects physiological functions of plants and subsequently plants become stunted and toxicity symptoms become apparent in their foliage. Too much boron (B) produces citrus leaves with yellowish areas on their leaf surfaces, and too much chloride (Cl<sup>-</sup>) gives a brownish tip burn.

An experiment with toxic levels of boron (B) and chloride (Cl<sup>-</sup>) is being conducted on citrus trees by A. Peynado, Research Chemist, Plant Science Research Division, Weslaco, Texas (Cardenas et al., 1971). There are 16 Red Blush grape-fruit (Citrus paradisi, Macf.) and 16 Valencia orange (Citrus sinensis (L.) Osbeck) trees within each of four blocks. The grapefruit and orange trees are each on 16 different rootstocks. The trees have grown together and individual trees can not be distinguished. Two treatments, that began in 1963, have been applied to the grapefruit and the orange trees within each block. Eight orange and eight grapefruit trees in each block have been irrigated with canal water (control treatment); and eight orange and eight grapefruit trees in each block have been irrigated with irrigation water with 4,000 ppm (parts per million) sodium chloride (NaCl) and calcium chloride (CaCl<sub>2</sub>) and 6 ppm of boron (B) added (salt treatment).

When aerial photographs were taken with infrared color film, 16 orange trees that showed no signs of being affected with salt and 12 grapefruit trees with salt-insensitive rootstocks photographed as dark-red trees. The photographs were taken at an altitude of 914 m with a 50-mm lens. Grapefruit trees with the salt-sensitive Troyer citrange rootstock gave whitish-tree images. Thus it seems feasible that remote sensing with aerial photography can be used to detect the presence of salinity-stressed citrus trees.

# Citrus Species Differences

Aerial infrared color photographs were taken of an orchard of Red Blush grapefruit, Valencia and Navel oranges, and Cleopatra tangerine trees. Photographs were taken at an altitude of 610 m with a 50-mm lens. All trees had new growth except for the tangerine trees. The tangerine trees gave dark red images on the infrared color transparencies in contrast to lighter red colored images for the grapefruit and orange trees; because new foliage on citrus trees is lighter green in color (less chlorophyll) than older foliage. One of the main problems in the photographic remote sensing of citrus maladies is to distinguish them from new foliage growth.

# Citrus Foot Rot (Fungus)

Citrus foot rot is a fungal disease caused by Phytophthora citrophthora (Sm. & Sm.) Leonian and Phytophthora parasitica Dast. These fungi produce a gummy exudate at or near the graft union on citrus trees; wood rots underneath, leaves lose color, and decline sets in (Gausman et al., 1970). The foliage of foot rotaffected citrus trees lose their chlorophyll and become chlorotic (yellowish-white) in contrast to the dark-green foliage of healthy trees.

Figure 6 is a negative print of Ektachrome color (film type B) and shows the photographic comparison of a white grapefruit leaf on the left (yellowish-white on color film) from a foot rot-affected tree with a dark leaf on the right (dark-green on color film) from a healthy tree.

An overflight of a grapefruit citrus orchard, Citrus paradisi Macf., Nucellar - CES-3 selection of Red Blush on Citrus aurantium Linn. Sour Orange rootstock, near Monte Alto, Texas was made at an altitude of 610 m (under cloudless skies with moderate haze), at 11:29 a.m., central standard time, December 5, 1968, in an easterly direction. Photographs were taken with a Zeiss, 150-mm focal length camera, using 229 mm Kodak Ektachrome Infrared Aero 8443 film (infrared color) and a Zeiss D light-orange filter, approximate 100% absorption edge at 500 nm.

On infrared color transparencies, healthy trees produced red images in contrast to white images for trees severely infected with foot rot.

Figure 7 is a negative print from an infrared color positive from an over-flight of a grapefruit orchard, showing images of dark-appearing (white on infrared color film) foot rot-infected trees, upper center; and white-appearing (red on infrared color film) healthy trees. Various degrees of white-appearing trees were detected among the red-appearing trees on the infrared color film. An outstanding example of a very white-appearing tree found on the color film is represented by the dark tree in the center of the upper row of the black and white negative print. Eventually, the foot rot fungus girdles the tree and kills it.

# Sooty Mold (Insect and Fungus)

Brown soft scale insects (Coccus hesperidum L.) start excreting large quantities of a sugary solution known as "honeydew" soon after establishment on the citrus leaf. The black sooty mold fungus, Capnodium citri, Berk. and Desm., develops rapidly on the leaf surface when the honeydew is abundant, and forms a dense black coating of interwoven filaments (hyphae). If the coating is heavy, it impairs plant growth and production. Light reflectance in the visible and near-infrared is considerably reduced (Hart and Myers, 1968).

Figure 8 shows that spectrophotometric measurements of diffuse reflectance of upper citrus leaf surfaces having varying amounts of sooty mold revealed that mature citrus leaves (spectrum 1) with no trace of sooty mold had reflectance values of 58 and 53% at 770 and 1300 nm, respectively. Leaves heavily coated with sooty mold (spectrum 4) had reflectance values of 9 and 23% at 770 and 1300 nm, respectively. A light sooty mold coating (spectrum 2) reduced reflectance 14 percentage points at 770 nm and 2 percentage points at 1300 nm.

When aerial photographs are taken with infrared color film, citrus trees with deposits of sooty mold give black images and noninfested trees give red images. It is, therefore, very easy to distinguish among infested and non-infested trees.

The detection of brown soft scale infestation of citrus trees with infrared color film has been demonstrated. A commercial service to the growers is feasible at the present time. It could function as entomological ground surveys now function; that is, a commercial service would photograph the trees, ground check suspicious areas in groves, and make recommendations for spraying of the orchards. It is estimated that the cost of surveys could be reduced up to 50% with this technique (Hart and Myers, 1968).

#### FUTURE PLANS

Further work is planned for comparing infrared color film transparencies of boron and chloride toxicities, iron deficiency, and foot rot of citrus trees. If visual interpretation among foot rot and the nutritional maladies is impractical, computer discrimination procedures (Richardson et al., 1970) will be applied to densitometer readings on infrared color film transparencies.

The detection of brown soft scale infestations of citrus trees with infrared color film is practical. A commercial service to the growers is a possibility in the near future.

Research is in progress to detect insect damage on citrus trees with infrared color films to assess the effectiveness of biological and chemical insect control applications.

#### ACKNOWLEDGEMENTS

The author is indebted to Marcia Schupp for preparing leaf transections, Ruben Cardenas for supplying an overflight transparency, Ron Bowen for photographic assistance, Guadalupe Cardona and Armando Berumen for illustrative assistance, and Jean Ryan for stenographic assistance.

#### LITERATURE CITED

- Cardenas, R., A. Peynado, H. W. Gausman, A. H. Gerbermann, and R. L. Bowen.

  Photographic sensing of boron and chloride toxicities of citrus trees. To
  be submitted to Jour. Rio Grande Valley Hort. Soc.
- Gausman, H. W., W. A. Allen, R. Cardenas, and R. L. Bowen. 1970. Detection of foot rot disease of grapefruit trees with infrared color film. 1970 Jour. Rio Grande Valley Hort. Soc., Vol. 24:36-42.
- Hart, W. G., and V. I. Myers. 1968. Infrared aerial color photography for detection of populations of brown soft scale in citrus groves. J. Econ. Entomol. 61:617-624.
- Richardson, A. J., R. J. Torline, D. A. Weber, R. W. Leamer, and C. L. Wiegand. Comparison of computer discrimination procedures using film optical densities. In House Technical Report, USDA, Weslaco, Texas.
- Van Nostrand's Scientific Encyclopedia. 1947. 2nd ed., D. Van Nostrand Co., Inc., New York. p 850.

#### GLOSSARY OF TERMS

Abaxial Leaf surface faces away from stem, or dorsal (lower)

side.

Adaxial Leaf surface faces toward stem, or ventral (upper)

side.

Air cavities Spaces among leaf mesophyll cells.

Carotenoids The yellow to orange pigments in plastids. Carotenes

and xanthophylls belong to the carotenoids.

Chlorophylls The green pigments present in chloroplastids.

Chloroplastid Specialized protoplasmic body containing chlorophylls

and other pigments.

Cuticle For this report it is considered as a waxy material

(cutin), on or within the outer epidermal cell wall.

Epidermis The outer layer of cells on both the dorsal and

ventral side of a leaf.

Intercellular spaces Spaces among cells within the leaf mesophyll.

Mesophyll Parenchyma tissue of a leaf between the epidermal

layers.

Mesophyll cell A cell located between the epidermal layers of a leaf.

If cell contains chloroplasts it is a chlorenchyma

cell.

Nanometer One billionth (10<sup>-9</sup>) of a meter.

Palisade layer A layer of elongated cells containing many chloro-

plasts.

Paradermal Refers to section made parallel with the surface of a

leaf.

Parenchyma Thin-walled cells capable of growth and division,

found in leaves between the lower and upper epidermis.

Refractive index The ratio of the velocity of light in a vacuum to the

velocity of light of a particular wavelength in any

substance.

Spongy parenchyma

Mesophyll parenchyma with noticeable air cavities.

Stoma

An opening in the epidermis with two guard cells surrounding it where gas exchange takes place between the plant and air.

Transection

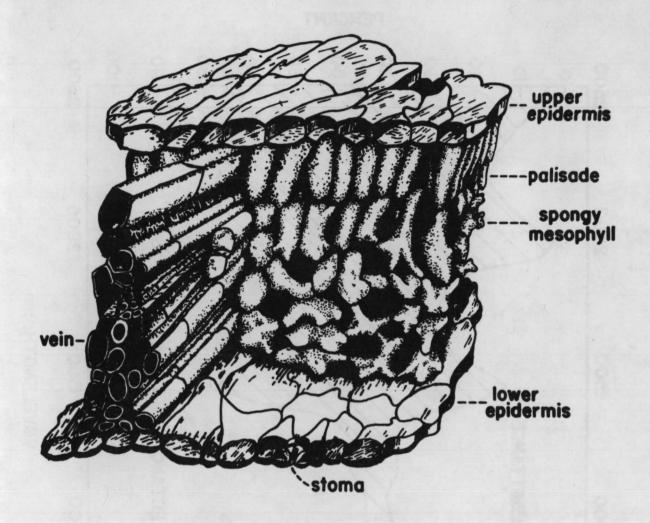
See transverse.

Transverse

A cross section. Section taken perpendicular to the longitudinal axis of the cell. Also called transection.

Vein

Strand of vascular material (in a leaf) containing xylem and phloem.



VAN NOSTRAND'S SCIENTIFIC ENCYCLOPEDIA COPYRIGHT, 1947

Figure 1. Three-dimensional drawing of a leaf structure that is similar to the structure of a citrus leaf (redrawn from <a href="Van Nostrand's Scientific Encyclopedia">Van Nostrand's Scientific Encyclopedia</a>, 1947).

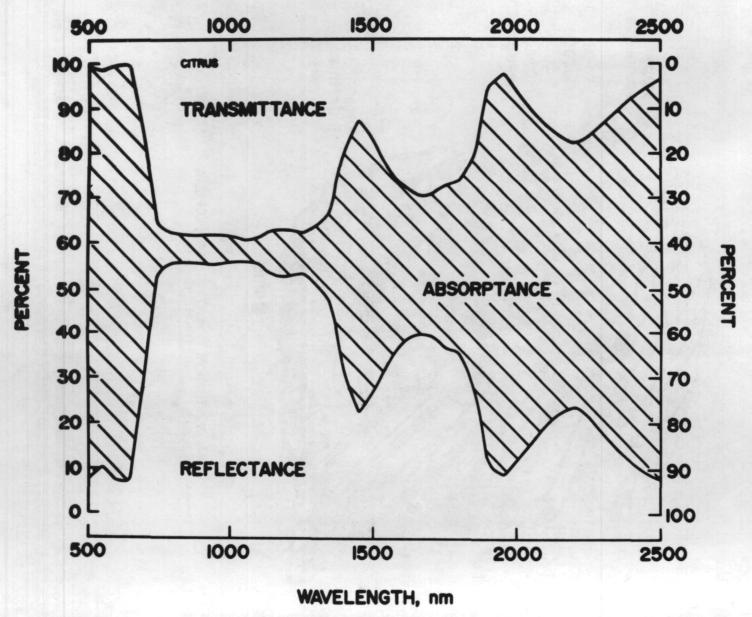


Figure 2. Diffuse reflectance, transmittance, and absorptance
[100 - (percent transmittance + percent reflectance)] of the upper (adaxial)

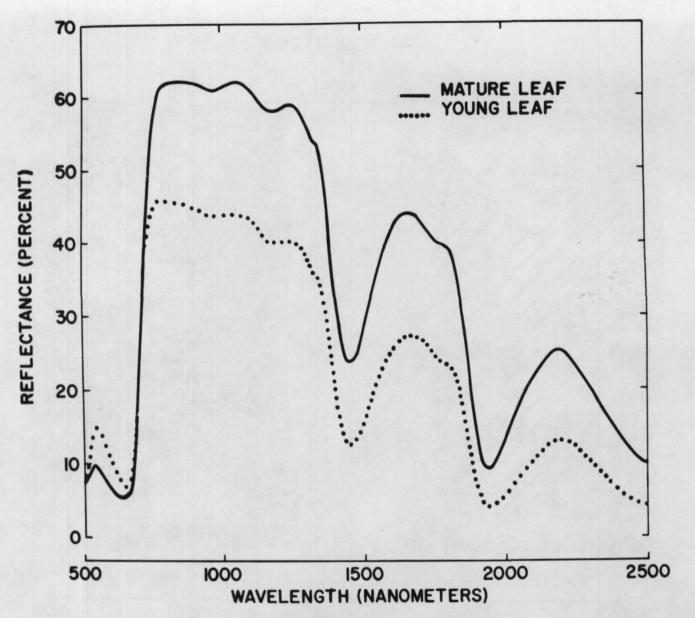
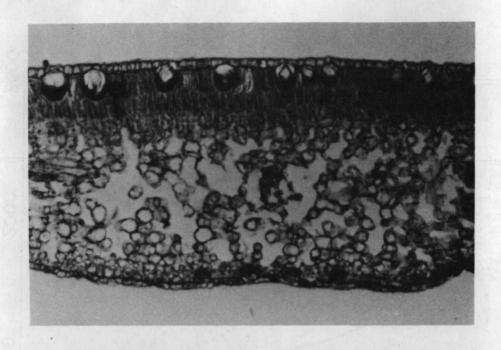


Figure 3. Diffuse reflectance of the upper (adaxial) surfaces of young (bottom dotted line spectrum) and mature (upper solid line spectrum) orange leaves (Citrus sinensis (L.) Osbeck).



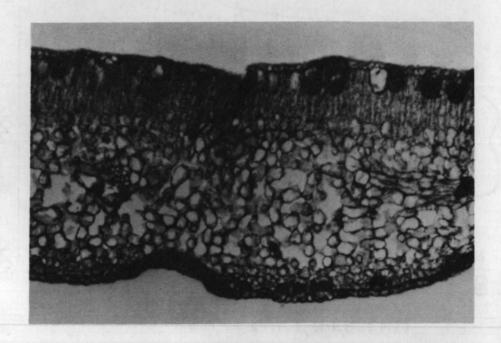


Figure 4. Photomicrographs of leaf transections of healthy (top, 200 X) and salt-affected (bottom, 200 X) citrus leaves.

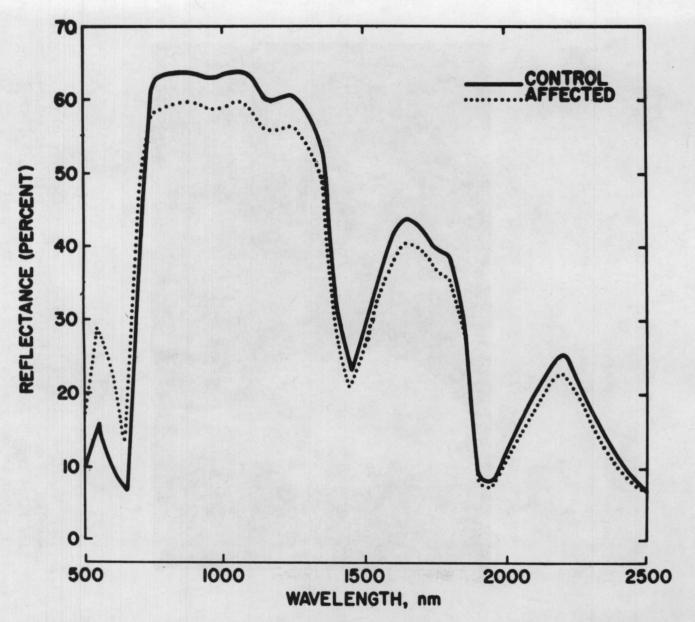


Figure 5. Diffuse reflectance of upper (adaxial) leaf surfaces of healthy (control, solid line) and salt-affected (dotted line) citrus leaves.



Figure 6. Negative print of Ektachrome color (film type B) photographic comparison of a white grapefruit leaf on the left (yellowish-white on color film) from a foot rot-infected tree with a dark leaf on the right (dark-green on color film) from a healthy tree.

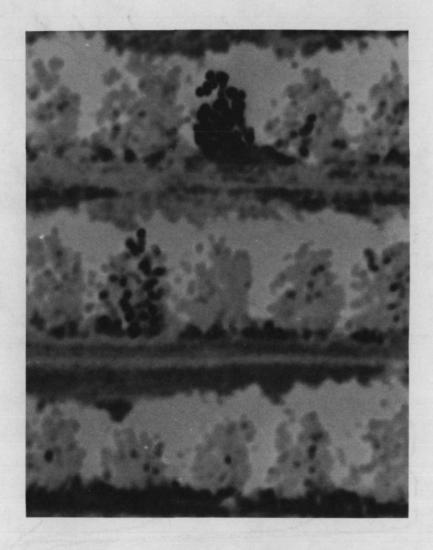


Figure 7. Kodak Ektaprint from a Kodak Ektachrome Infrared Aero 8443 (infrared color) positive from an overflight of a grapefruit orchard showing two images of dark-appearing (white on infrared color positive), foot rot-infected trees, and white-appearing (red on infrared color positive) healthy trees. The upper dark tree (top row) had a severe infection of foot rot, while the lower dark tree (middle row) was beginning to be affected by the foot rot fungus.

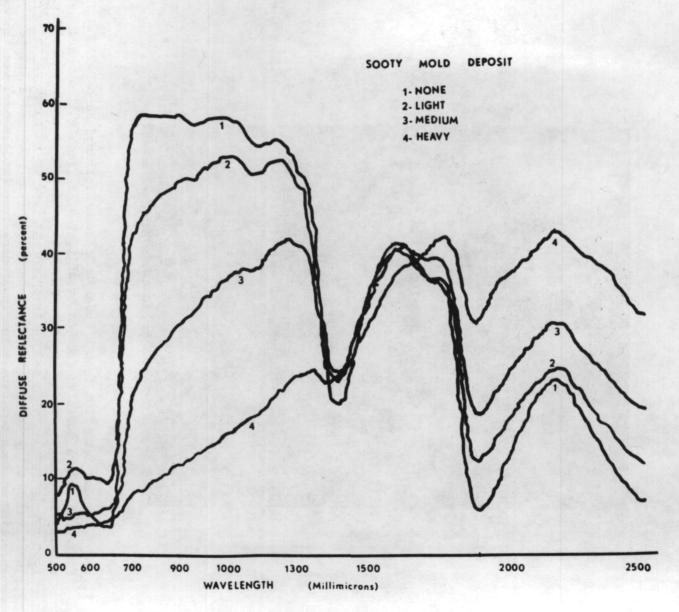


Figure 8. Effect of sooty mold on reflectance (percent) of leaves coated with varying amounts of the fungus (reproduced from Hart and Myers, 1968).

# Page Intentionally Left Blank

#### BIOGRAPHICAL SKETCH

Donald T. Lauer
Forestry Remote Sensing Laboratory
School of Forestry and Conservation
University of California
Berkeley, California

Page Intentionally Left Blank

Mr. Lauer was born on May 5, 1941 in Oakland, California. He is married and has two children. He received a B.S. degree in Forestry from the University of California, Berkeley in 1963 and a M.S. degree in Forestry and Remote Sensing in 1965. He is leader of the Image Interpretation and Enhancement Unit of the Forestry Remote Sensing Laboratory, University of California, Berkeley. His responsibilities include developing methodology for extracting useful resource information from remote sensing imagery -- using human photo interpreters. He is a member of the American Society of Photogrammetry and the Society of American Foresters.

## TESTING MULTIBAND AND MULTIDATE PHOTOGRAPHY

#### FOR CROP IDENTIFICATION

D.T. Lauer

Forestry Remote Sensing Laboratory School of Forestry and Conservation University of California, Berkeley

For several years, personnel at the Forestry Remote Sensing Laboratory have concentrated their efforts on developing techniques for extracting a maximum amount of information about vegetation resources in agricultural and wildland areas from aerial and space photos. Among the most significant research results obtained to date are our findings relating to agricultural crop surveys. Specifically, our recent investigations regarding the interpretability of photography taken in more than one spectral band and at more than one time of the year were so encouraging that we were able to attempt a semi-operational survey of the 1970 small grain crop growing in Maricopa County, Arizona. The purpose of this paper is to describe, with the aid of three case studies, the procedures used and results derived in a series of prerequisite interpretation tests that were performed on multiband and multidate photography. The results of these quantitative tests led to the selection of what was considered to be the best combination of multiband and multidate photographs for use in the Maricopa County survey.

The theoretical bases of the multiband and multidate concepts have been known for quite some time. For example, the tone or brightness with which an agricultural field or field condition is registered on a film emulsion is directly related to the amount of energy reflected from that field, through the camera lens system, to the film emulsion. Since most terrain features or conditions possess unique spectral reflectance characteristics -- depending on their atomic, molecular and physical structure -- they frequently possess unique tone signatures when viewed on photographs taken simultaneously in more than one spectral band. Consequently, multiband photography obtained in those spectral bands exhibiting the greatest differences in signatures between crops greatly facilitates the task of discriminating one crop from another. Furthermore, the reflectance characteristics of an agricultural field rapidly change throughout a growing season according to noticeable changes in plant phenology and to local or regional cropping practices. Generally, a field progresses in development as follows: unprepared bare soil, prepared bare soil (plowed, disced or diked), seedling plants, immature plants, mature plants, harvested field. Obviously, just about every agricultural crop has its own distinct life cycle, and these cycles are easily documented in a crop calendar. By studying a crop calendar for a particular region, one can predict when a crop might possess a unique tone signature when viewed on a series of photographs taken at more than one time of year. as is the case with multiband photography, multidate photography can aid the photo interpreter when trying to identify various agricultural crops. Logically, one could assume that both multiband and multidate photography, properly procured, would further enhance the interpreter's ability to perform an agricultural crop survey. The case studies presented below lend credence to this assumption -- in the form of interpretation test results.

#### CASE STUDIES

### A. Mesa, Arizona

Our Group first became involved in crop studies at the Phoenix-Mesa Test Site (NASA Test Site #29) while preparing for the Apollo 9 S065 multispectral photographic experiment. A 16-square-mile area, near Mesa, Arizona, was chosen for intense analysis; 125 fields within the study area included most of the economically important crop types found in irrigated regions of the southwest. In addition to the Apollo multiband photography, NASA made available high-altitude aircraft multiband-multidate photography for this area, and these aircraft over-flights occured sequentially at approximately one month intervals, beginning at the time of the Apollo flight. Given available multiband and multidate photography, a series of interpretation tests were devised to establish the best combination(s) of images for identifying all crop types and single crop types within the 16-square-mile area.

A large number of "test images" were presented to a group of skilled interpreters who were asked to classify each of the 125 fields within the study area into one of seven crop categories that included: barley (B), recently cut alfalfa (Ac), mature alfalfa (Am), wheat (W), sugar beets (SB), moist bare soil (BSm), and dry bare soil (BSd). Since the interpreters were not acquainted with the Mesa area, a photo interpretation key, in the form of training samples, was prepared. Individual fields from each crop category which represented a range in crop variability were selected, identified and presented to the interpreters (see figure 1). The interpreters were asked to study the appearance of each training sample, and once they became familiar with the identifying characteristics of each crop type, they attempted to correctly classify the remaining fields within the study area.

In order to minimize "familiarity" with the fields within the study area, an interpreter was asked to look at no more than five test images. Each image was examined by four different interpreters, and interpretation results were expressed as the cumulative number of fields seen by all four interpreters for each image. Table I shows actual interpretation results for eleven types of photography (i.e., various combinations of single band, multiband, single date, and multidate photography). The array of results shown in Table I were prepared in such a way as to aid the reader in comparing results derived from one image type with results from another. Note that each array includes ground truth, correct interpretations and incorrect interpretations (omission and commission errors). The correct interpretations, expressed in percent for all crops combined, have been summarized and are shown in Table II.

The interpretability of Apollo and high-flight photography (Pan-25, IR-89B, and Ekta Aero Infrared) were compared; and, in each case, the interpreters were able to identify the various crop categories field-by-field equally well on spaceborne and airborne photos.

In reference to multiband and multidate photography, note that single band photographs taken on single dates produce fairly low overall interpretation results, except for the Pan-25 image taken in May. Improved results were obtained with May photos since barley has sufficiently matured at that time allowing

it to be easily discriminated from all other crops. Overall interpretation accuracies for all crops improved impressively when single date photography. including the May photos, were viewed in a multiband form (i.e., Ekta Aero Infrared photo or optically combined color composite image) and when single band photos (Pan-25) taken on two different dates were viewed in a color composite form. Higher results were obtained on multiband images because bare soil is most easily separated from vegetated fields on film containing an infrared sensitive band, and mature barley is best discriminated from sugar beets and alfalfa on film containing a red sensitive band. However, the only sure means of identifying alfalfa is by searching for its characteristic harvest pattern on sequential images. Since alfalfa is periodically mowed, changing over time from mature to recently cut to mature, a distinct pattern for that crop is readily seen on multidate photography. Consequently, multiband-multidate photography (image #1) provides the maximum amount of discriminatory information for identifying barley, bare soil, sugar beets, and alfalfa and, therefore, image #11 (three separate Ekta Aero Infrared photos taken in March, April, and May and viewed together) gave better overall interpretation results than any other form of imagery tested.

# B. Imperial Valley, California

Concurrent with the Arizona study, an image interpretation experiment was being conducted in an adjacent and analogous agricultural area -- Imperial Valley, California. As in Maricopa County, agricultural cropping in the Imperial Valley is mainly on reclaimed desert land where the combination of deep rich soils, an abundance of solar energy, and available irrigation water has led to a level of agricultural productiveity equaled in only a few parts of the world.

Aircraft flights were arranged for this area during the summer of 1969 for the purpose of obtaining high quality single band, black-and-white multiband, and tri-emulsion color and false-color photographs. All photography was procured by the Science and Engineering Group at Long Island University; a boresighted multilens camera, equipped with infrared sensitive film, broad-band primary color absorption filters, and infrared cutoff filters, was used to obtain the multiband imagery. An experiment was designed, utilizing quantitative interpretation tests, to determine the usefulness of different kinds of multiband photography (flown in July) for identifying four Imperial Valley cropland categories: alfalfa, sorghum, cotton and bare soil.

Five sets of images were selected for testing -- one set of single band photos (IR-25) and four sets of multiband photos (Aerial Ektachrome, Ekta Aero Infrared, color enhancement 'A', and color enhancement 'B'). Color enhancement 'A', a close simulation of Ekta Aero Infrared film was made by optically combining an IR-58, IR-25 and IR-89B image projected through a blue, green and red filter, respectively; while color enhancement 'B' was made the same way but with the green and red filters reversed. Part of this experiment was to compare, through interpretation testing, the information content seen on enhanced black-and-white multiband photos with that seen on tri-emulsion subtractive reversal films.

Each set of imagery was examined by three interpreters, with no interpreter viewing more than one set. A set of images consisted of nine separate photos in print form, mosaiced together showing a total of 157 agricultural

fields. Several fields were randomly selected within each crop category and were used as training samples by the photo interpreter.

The results of the Imperial Valley Experiment are summarized in Table III in which test results are expressed as (1) mean percent correct identifications and (2) mean percent commission error -- for each of the four crop categories and all crop categories combined. (Percent commission error for a crop category is the percent of the total number of fields identified as that type which were actually same other crop type; therefore, a low percent commission error plus high percent correct identification indicates high interpretation accuracy.)

Probably what is most evident in these results is that accuracy of identification for all crop categories combined is relatively low (80%), no matter which type of test imagery was used. These poor results are probably a function of the improper timing of the photo mission rather than the lack of information content in multiband photography, per se. An analysis of a crop calendar for this region would indicate that both cotton and sorghum are in a mature, green state of development in July -- a condition rendering tone signatures for the two crops quite similar in appearance on single band and multiband photographs. The low percent correct identifications and high percent commission errors for cotton and sorghum indicate that the interpreter continually confused the two. Furthermore, the alfalfa fields were in any of several stages of development (ranging from recently cut to mature) at this single time of year which added to the difficulty of identifying one crop type from another. Nevertheless, some very prominent trends are evident in the data derived in this series of tests: (1) the single band black-and-white images when compared to the other four kinds of multiband photography, nearly always rendered the lowest percent correct identifications and the highest percent commission errors, (2) the color enhancement 'B" and Ekta Aero Infrared images tended to produce the most accurate results for each crop category and all crop categories combined, and (3) enough variability in interpretation results occurred within each group of interpreters working with a single type of imagery, that the significance of the results shown here could not be supported with statistical computations.

In summary, one might conclude from the data presented here that an accurate classification of Imperial Valley crops is not easily done on photography procured on a single day in July; however, if given the task of working with only July photos, multiband rather than single band (IR-25) photographs would be more useful for this purpose. In addition, black-and-white multiband photos properly procured and displayed as a color composite image can render as much information on crop types as conventional tri-emulsion layer color or false-color infrared films.

# C. Maricopa County, Arizona

Based on the above results, it was decided that a semi-operational regional agricultural crop survey would be a logical extension of the interpretation techniques initially developed. An inventory of the 1970 small grain crop (i.e., barley and wheat) growing in Maricopa County, Arizona became the survey objective since multiband-multidate photographs were available for the entire area and reliable ground truth data had been collected by FRSL personnel during these overflights. Prior to implementing the survey, it was necessary to apply the

crop calendar concept and an interpretation test to determine the best combination(s) of multiband-multidate photographs for discriminating wheat and barley from all other crops, and wheat from barley.

Studies of crop development patterns during early 1970 (data collected from FRSL field surveys and extracted from Arizona Crop and Livestock Reporting Service newsletters) indicated that the 1970 small grain crop was developing in a normal manner. Thus, general conclusions based on crop calendar information which indicated that small grains are mature and most easily distinguishable from other crops during the month of May, were assumed to be applicable for 1970. However, the studies conducted within the 16-square-mile area near Mesa, Arizona indicated that although barley could be consistently identified on May 21, 1970 photos, wheat and alfalfa were sometimes confused. It was noted that the identity of fields in question usually could be established by noting the appearance of these same fields on June 28, 1970 photos. For this reason, photos taken on May 21 and June 28 were ultimately provided for the survey.

In addition, the design of the previous tests, conducted in the Mesa area, regarding optimum film type, were not totally acceptable in terms of the survey for 1970. Since the 1970 photographs were taken at larger scales than the 1969 coverage (1/120,000 and 1/500,000 versus 1/950,000), giving better image resolution, and Aerial Ektachrome coverage was omitted in 1969, it was felt that a new test should be made, based primarily on May 21, 1970 photos, to determine the optimum film/filter combination for identifying barley and wheat. Consequently, five types of photography were tested for information content -- three kinds of single band imagery (Pan-58, Pan-25 and IR-89B) and two kinds of multiband imagery (Aerial Ektachrome and Ekta Aero Infrared).

Fifteen photo interpreters of equal ability were randomly placed in one of five three-man photo interpretation groups. Five four-square-mile test plots were chosen from thirty-two sample plots located throughout the county. The photo interpretation tests were administered so that (1) each interpreter group would interpret each of the five film/filter types, (2) each test plot would be interpreted using each of the five film/filter types, and (3) no interpreter group would interpret a test plot more than once. Thus each plot was interpreted fifteen times for a total of seventy-five interpretation tests:

Procedures used for training the interpreters were similar to those used in the Mesa and Imperial Valley studies. In this case, four additional four-square-mile plots were chosen and the fields within them were used as keys or reference materials. After each interpreter had trained himself to interpret a particular film/filter combination, he began the interpretation of the test plot assigned to him for that combination (each interpreter examined each of the five test plots on a different film/filter combination). In order to ascertain the optimum film/filter combination for inventorying wheat and barley, the results of the tests were analyzed in three ways: (1) mean-of-ratio variance analysis, (2) analysis of variance for % correct, and (3) analysis of variance for % commission error.

Mean-of-Ratio Test: In the actual crop survey, the acreage estimates by the photo interpreters were to be adjusted by using a mean-of-ratio estimator.

This estimator is defined as:

R= actual acreage of wheat (or barley)
interpretation acreage estimate for wheat (or barley)

This estimator is calculated for each of thirty-two sample plots, the mean of the ratios calculated, and the acreage estimation for the entire survey area adjusted by multiplying by this mean. The optimum film/filter type, therefore, is that in which the <u>variance</u> of ratios is lowest, (e.g., if the interpreter consistently interprets 60% correct, the adjusted total will be more accurate than if he fluctuates between 70% and 90%).

Variances of the ratios using each of the five film/filter types under consideration were tested at the 95% level of significance. No differences were found between the ratio variances for barley. For wheat, however, Aerial Ektachrome, Pan-25, and Pan-58 constituted a homogeneous sub-group of low variance, with Ekta Aero Infrared and Infrared-89B showing significantly higher variances. Thus, either Aerial Ektachrome, Pan-25 or Pan-58 would be optimum for the operational survey under this criterion.

% Correct and % Commission Error Analyses: Analyses of variance were run to ascertain whether there were differences (at the 95% level of significance) between the film/filter types in terms of % correct acreage and % commission error (Table IV). If significant differences were found, the types were to be ranked using the Duncan's new multiple range test.

The film/filter types proved to be different in terms of both % correct and % commission error for both barley and wheat, and hence were ranked. The results are illustrated in Table V. Percent correct is ranked with highest values at the top and % commission error with lowest values (and hence "best") at the top. However, types which are included within the same bracket are not significantly different according to Duncan's test at the 95% level of significance.

Based on the results of both the mean-of-ratio analysis and the analyses of % correct and % commission error, Aerial Ektachrome film was chosen as the film/filter type to be used for the operational survey. Although in some cases it was not significantly superior to other film types, it was the only type which was at least in the superior group in all tests. (For a discussion of the Maricopa County survey see Draeger, et al., 1970, or Draeger, 1971).

#### SUMMARY AND CONCLUSIONS

The research reported upon above was designed to answer two questions; (1) can a suitable methodology of interpretation testing be developed that would allow comparisons between the information content seen on various types of aerial and space photography? and (2) are multiband and/or multidate photographs useful to the photo interpreter as he attempts to identify various agricultural crops by means of remote sensing?

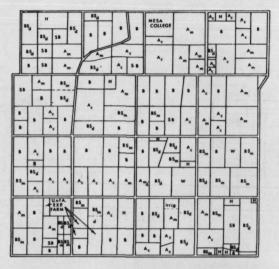
Drawing on the large pool of skilled photo interpreters at the Forestry Remote Sensing Laboratory, an efficient and reliable interpretation testing procedure has been developed that would be applicable to photography taken not only of agricultural resources but of nearly any resource environment. The technique consists mainly of presenting to a group of interpreters various types of photography on which resource patterns or conditions are to be identified. A large population of resource features is required so that an interpreter never looks at a particular terrain object more than once -- during training and testing. If several interpreters evaluate each type of photography, greater reliance can be placed on their cumulative results, which can be tabulated in various ways (e.g., total correct identifications, total omission errors, total commission errors, mean correct identifications, mean omission errors, mean commission errors) or analyzed statistically (e.g., one-way classification and Duncan's new multiple range test) in order to quantitatively determine the confidence which one should have in the results.

Such testing procedures were then applied to multiband and/or multidate photography taken over agricultural lands in southern California and southern Arizona. In each of these case studies involving the identification of several important crop types, the test results indicate that multiband photography consistently yields higher interpretation accuracies than any type of single band photography; but more importantly, proper timing of photography -- taken on more than one date -- will unquestionably insure a higher level of crop identification than that attainable with photos taken at any single point in time.

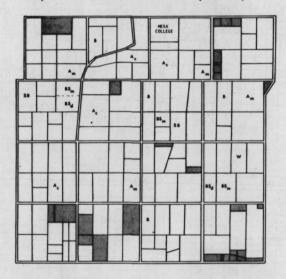
#### SELECTED REFERENCES

- Carneggie, D. M., L. R. Pettinger, C. M. Hay and S. J. Daus. 1969. An evaluation of earth resources using Apollo 9 photography -- Chapter 3. A report of research performed under Contract No. NAS9-9348 for the Office of Space Sciences and Applications, NASA, by personnel of the School of Forestry and Conservation, University of California, Berkeley.
- Draeger, W. C., L. R. Pettinger and A. S. Benson. 1970. Analysis of remote sensing data for evaluating vegetation resources -- Appendix I: A semi-operational agricultural inventory using small-scale aerial photography. Annual Progress Report, Contract No. R-09-038-003, for the Office of Space Sciences and Applications, NASA, by the personnel of the School of Forestry and Conservation, University of California, Berkeley.
- Draeger, W. C. 1971. The use of small-scale photography in a regional agricultural survey. Presented at the International Workshop on Earth Resources Survey Systems, Ann Arbor, Michigan, May 3-14, 1971.
- Lauer, D. T. and G. A. Thorley. 1971. Quantitative Analysis of Multiband Photography. Presented at the 37th Annual Convention of the American Society of Photogrammetry, Washington, D.C., March 7-12, 1971.
- Pettinger, L. R., et al. 1969. Analysis of earth resources on sequential high altitude multiband photography. A special report prepared for the Office of Space Sciences and Applications, NASA, by personnel of the School of Forestry and Conservation, University of California, Berkeley.

Pettinger, L.R. 1971. Field data collection - an essential element in remote sensing applications. Presented at the International Workshop on Earth Resources Survey Systems, Ann Arbor, Michigan, May 3-14, 1971.



Map With Ground Truth (March)



Map with Training Samples (March)

Figure 1: The type of reference material or "photo interpretation key" used to train the photo interpreters is shown here (bottom map). The interpreter was able to familiarize himself with the image characteristics of each crop category by studying each training sample seen on the test image. Once he was confident that he could correctly identify each field, he proceeded to annotate, on the map with training samples, the identity of the remaining fields. Accuracy of interpretation was then calculated by comparing the annotated map with the ground truth map. The symbols on the maps mean: "B" for barley, "Am" for mature alfalfa, "Ac" for cut alfalfa, "SB" for sugar beets, "W" for wheat, "BSm" for moist bare soil, and "BSd" for dry bare soil (from Carneggie, et al., 1969).

INTERPRETATION TEST RESULTS FOR MESA, ARIZONA STUDY AREA IMAGE #1 PAN-25A, APOLLO 9 IMAGE #2 PAN 25A. HIGH FLIGHT IMAGE #3 IR-898, APOLLO 9 IMAGE #4 IR-898, HIGH FLIGHT MARCH 12, 1969 MARCH 12, 1969 MARCH 12, 1969 by P. I. Ground Truth Ground Truth B Am Ac SB W BSm Am Ac SB W BSm BSd B Am Ac SB W BSm Ac SB W 8 35 13 Am 46 31 11 44 17 4 45 13 10 2 2 72 27 A 2 71 27 54 19 43 20 2 74 31 43 35 9 45 34 11 15 107 73 88 53 Am 38 34 16 89 58 7 97 63 Ac SB S Ac 25 S8 18 W 6 Ac Ac 25 14 54 13 37 3 1 12 10 1 37 7 Ac 13 3 113 59 1 38 4 69 31 SB 47 37 3 7 10 SB 17 20 11 6 10 30 3 17 6 56 50 1 ٧. 18 18 7 2 3 5 5 2 1 0 22 9 34 12 20 56 95 39 27 33 22 1 2 7 7 37 18 20 59 17 65 26 Total Fields 130 64 92 23 4 52 68 Total Fields 132 64 91 23 Total Fields 131 64 92 24 4 52 68 435 4 52 68 434 ields | 132 | 64 | 92 | 24 50 Incor- 86 30 55 20 4 19 31 89 30 54 18 86 29 55 13 4 30 9 Incor-rect 97 33 37 13 4 30 12 IMAGE #8 COLOR COMPOSITE-FRSL OPTICAL COMBINER IMAGE #5 PAN 25A, HIGH FLIGHT IMAGE #7 INFRARED EKTACHROME, HIGH FLIGHT IMAGE #6 INFRARED EKTACHROME, APOLLO 9 MARCH 12, 1969 HIGH FLIGHT, MARCH 12, 1969 MAY 21, 1969 MARCH 12, 1969 Pyd Pot. Ground Truth A SB BS W B Am Ac SB W BSm BSd B Am Ac SB W BSm B Am Ac SB W BSm В 8 43 17 1 2 Am 38 36 6 3 Ac 24 3 72 58 24 5 2 4 2 3 8 47 8 58 1 0 66 21 113 0 2 4 В A 1.130 15 48 4 82 46 57 51 15 198 68 2 8 2 133 82 31 33 SB 0 13 0 4 10 109 37 Ac 23 3 57 34 0 17 17 91 124 40 Ac 22 5 84 10 42 31 SB 12 3 59 5 BS 10 58 2 6 5 12 10 39 0 39 43 14 57 14 BSm BSd I BSm BSm 13 67 90 23 13 57 74 17 9 51 64 13 4 Total Fields 132 64 90 24 4 52 67 433 Total Fields | 132 | 64 | 92 | 23 | 4 ncor- 11 26 20 61 4 64 92 24 4 52 68 436 68 Total 132 Incor- 89 28 18 13 4 13 0 rect 85 13 35 18 4 13 11 122 66 31 8 18 2 9 17 Incor-Total Percentage Correct Identification: 64% Total Percentage Correct Identification: 7/9 THACE #10 MULTIDATE COLOR COMPOSITE IMAGE #11 MULTIBAND, MULTIDATE. EKTA AERO INFRARED (3 IMAGES) IMAGE #9 INFRARED EKTACHROME, HIGH FLIGHT FRSL OPTICAL COMBINER MAY 21, 1969 MARCH, APRIL AND MAY Ground Truth Ground Truth Am Ac SB W BS SB W B Am Ac SB W BS BA 108 107 1 1 2 102 1 2 Am 13 50 6 7 3 Am 21 80 30 8 7 113. 22 L Ac 3 4 70 Ac 6 71 25 0 17 8 4 9 8 8 SB 29 21 SB E SB 3 5 5 1 2 1. 0 4 4 v 1 0 1 g BS Poto I 5 34 1 112 2 8 126 10 Total 120 60 100 24 4 126 Total Fields 130 64 93 23 4 118 Total Fleids 118 152 24 Total Percent 23 14 23 15 3 2 Incor-rect 12 10 54 16 4 24 Incor-rect 16 39 24 4 15

The array of results for each image type illustrates the cumulative results of four interpreters (data along rows for each type) along with the actual ground truth (data down the columns). For example, consider the case of barley in the upper left array (Image #1). First, reading down the column marked 'B', out of a total of 131 fields known to be barley, 45 were correctly identified; however, 45 were called mature alfalfa, 13 cut alfalfa, 17 sugar beets, 5 wheat, 5 moist bare soil, and 1 dry bare soil, resulting in an omission error equal to 86. Reading across the row marked 'B', out of a total of 72 fields called barley by the interpreters, 45 were correctly identified; however, 13 mature alfalfa fields, 10 cut alfalfa fields, 2 sugar beet fields and 2 wheat fields were incorrectly identified as barley resulting in a commission error equal to 27. Hence, out of a total of 131 barley fields, 45 were correctly identified yielding a percent correct equal to 43% (from Carneggie, et al., 1969 and Pettinger, et al., 1969).

TABLE II: TEST RESULTS FOR MESA, ARIZONA STUDY AREA EXPRESSED AS PERCENT CORRECT IDENTIFICATIONS FOR ALL CROP CATEGORIES

TEST NUMBER	INTERPRETATION MODE	РНОТО (S)	DATE (S)	VEHICLE	%CORRECT
1	Single Band; Single Date	Pan-25	March	Apollo 9	43%
2		Pan-25	March	High-Flight	47%
3		IR-89B	March	Apollo 9	47%
4	1 m 10 i	IR-89B	March	High-Flight	45%
5		Pan <b>-2</b> 5	May	High-Flight	71%
6	Multiband; Single date	Ekta <b>Ae</b> ro Infrared	March	Apollo 9	65%
7		Ekta Aero Infrared	March	High-Flight	64%
8*		Color Composite	March	High-Flight	58%
9		Ekta Aero Infrared	May	High-Flight	72%
10**	Single band; Multidate	Color Composite Pan-25	March and May	High-Flight	76%
11	Multiband; Multidate	Ekta Aero Infra- red (3 images)	March, April	High-Flight	81%

<sup>\*</sup> A color composite image was made with the FRSL Optical Combiner Using Pan-58, Pan-25, and IR-89B images projected through a blue, green, and red filter, respectively.

(From Carneggie, et al., 1969 and Pettinger, et al., 1969).

<sup>\*\*</sup> A color composite image was made with the FRSL Optical Combiner using March Pan-25 and May Pan-25 images projected through a violet and green filter, respectively.

TABLE III: TEST RESULTS FOR IMPERIAL VALLEY, CALIFORNIA STUDY AREA EXPRESSED AS PERCENT CORRECT IDENTIFICATIONS AND PERCENT COMMISSION ERRORS

	ALL CROPLAND	ALFA	LFA	СОТ	TON	SOR	GHUM	BARE G	ROUND
IMAGE TYPE	% CORRECT	%COR %COM		%COR %COM		%COR %COM		%COR %COM	
Enhancement B	78	86	25	51	40	60	23	84	8
Ekta Aero IR	77	77	22	70	45	44	35	94	10
Aerial Ekta	72	74	25	48	45	60	43	82	11
Enhancement A	71	73	32	45	59	35	52	93	8
IR-25	67	60	30	54	73	48	38	87	14

TABLE IV: TEST RESULTS FOR MARICOPA COUNTY, ARIZONA STUDY EXPRESSED AS PERCENT CORRECT IDENTIFICATIONS AND PERCENT COMMISSION ERRORS

	BARL	WHEAT		
IMAGE TYPE (MAY)	%COR.	%сом.	%COR.	%сом.
Aerial Ekta.	71.19	5.73	49.25	49.67
Ekta Aero IR	65.06	24.89	59.05	44.73
Pan-58	32.35	44.69	38.11	85.19
Pan-25	46.65	41.43	20.15	77.77
IR-89B	44.55	45.40	30.87	77.49

Note: Accuracy of interpretation of wheat is significantly improved when the analysis is performed on May photography combined with June photography.

(From Draeger, et al., 1970)

TABLE V: TYPES OF PHOTOGRAPHY RANKED (BEST AT THE TOP) AND GROUPED (WHERE SUB-GROUPS ARE SIGNIFICANTLY DIFFERENT) IN TERMS OF PERCENT CORRECT AND PERCENT COMMISSION ERROR FOR BOTH BARLEY AND WHEAT

BARLEY INTERPRETATION					
% CORRECT	% COMMISSION ERROR				
Aerial Ektachrome	Aerial Ektachrome				
Ekta Aero Infrared	Ekta Aero Infrared				
Pan-25	Pan-25				
Infrared - 89B	Pan-58				
Pan-58	Infrared - 89B				

WHEAT INTERPRETATION					
% CORRECT	% COMMISSION ERROR				
Ekta Aero Infrared	Ekta Aero Infrared				
Aerial Ektachrome	Aerial Ektachrome				
Pan-58	Infrared - 89B				
Infrared - 89B	Pan-25				
Pan-25	Pan-58				

(From Draeger, et al., 1970)

# Page Intentionally Left Blank

# BIOGRAPHICAL SKETCHES

Lawrence R. Pettinger

Lawrence R. Pettinger was born in Altadena, California, in April, 1944. He received his B.S. degree in Forestry at the University of California, Berkeley, in 1967 and is completing requirements there for an M.S. degree in Forestry with an emphasis on remote sensing.

While fulfilling his educational objectives, he has been employed as a Project Leader for the Image Enhancement and Interpretation Unit of the Forestry Remote Sensing Laboratory where he has helped to develop interpretation techniques for performing resource inventories at the NASA test site at Phoenix, Arizona. He is a member of the American Society of Photogrammetry, Society of American Foresters and Xi Sigma Pi, and was a recipient of the ASP's Wild Heerbrugg Photogrammetric Fellowship Award in 1968.

\* Dr. Gene A. Thorley
Forestry Remote Sensing Laboratory
School of Forestry and Conservation
University of California
Berkeley, California

Dr. Thorley was born on May 28, 1940 in Mason City, Iowa. He is married and has one child. He received a B.S. degree in Forestry from the University of California, Berkeley in 1962 and a Ph.D. degree in Forestry and Remote Sensing in 1970. He is the Director of the Forestry Remote Sensing Laboratory, University of California, Berkeley. His experience includes work in private industry, government, and university research programs. He is a member of the American Society of Photogrammetry and the Society of American Foresters.

# FIELD DATA COLLECTION - AN ESSENTIAL ELEMENT

# IN REMOTE SENSING APPLICATIONS

Lawrence R. Pettinger

Forestry Remote Sensing Laboratory School of Forestry and Conservation University of California, Berkeley

#### INTRODUCTION

Field data collected in support of remote sensing projects are generally used for the following purposes: (1) calibration of remote sensing systems, (2) evaluation of experimental applications of remote sensing imagery on small test sites, and (3) designing and evaluating operational regional resource studies and inventories which are conducted using the remote sensing imagery obtained. In other words, field data may be used to help <u>develop</u> a technique for a particular application (uses 1 and 2 above), or to aid in the <u>application</u> of that technique to a resource evaluation or inventory problem for a large area (use 3 above). Scientists at the Forestry Remote Sensing Laboratory have utilized field data for both purposes. This paper will describe how meaningful field data has been collected in each case.

# FIELD DATA FOR TECHNIQUE DEVELOPMENT - THE SIMPLEST CASE

Studies of the first type (technique development) have been performed on several occasions using a stationary sensor platform 150 feet above the ground on the catwalk of a water tower at the Davis campus of the University of California (Figure 1). Over a period of several years, various kinds of target arrays have been positioned beneath this water tower such that they can be imaged using any of a variety of sensors.

For example, the usefulness of multiband photography has been investigated by photographing color panels, soil samples, and arrays of growing crops from the water tower (Figures 1 and 2). The same camera station is occupied for each camera exposure taken, thus eliminating one of the major problems, that of obtaining several matching multiband exposures of the same target array from an aircraft. All efforts to collect ground data are also simplified because there is only a single target array at one location. One field crew can record the condition of each target, obtain spectrometric data, and perform other operations as needed in an efficient manner (Figure 1).

Experiments using thermal infrared sensors have also been performed from the same platform. Thermal data can be obtained on an around-the-clock basis, and radiometric, surface temperature, and soil moisture measurements can be made at the time each thermal record is made from the tower (Figure 1). Continuous communication between the sensor operator and personnel on the ground below is made possible because the camera station and target array are both in a fixed position, separated by a short distance which can be bridged by voice or with portable battery-operated radios.

#### THE NEXT STEP: PROBLEMS ENCOUNTERED

A number of problems arise in attempting to apply remote sensing techniques to extended areas, and these must be acknowledged before the gap between technique development and application can be successfully bridged to extract meaningful resource information for potential users from remote sensing data.

First of all, studies of a large geographic area involve greater travel and the need for increased coordination between field teams. The need for communication among teams becomes more critical, especially in terms of coordinating field activities with the schedule of the remote sensing vehicle, be it aircraft or spacecraft. If there is a need for measurements to be made on the ground at the same time as the vehicle is overhead (e.g., spectrometric and radiometric readings, soil moisture determination, and enumeration of livestock), then frequent air to ground contact is essential.

Secondly, representative areas on the ground in which to gather information must be selected so that enough data will be collected within the economic constraints of the project. Preliminary sampling to determine the distribution and variability of each of the important resource features is helpful in this regard.

Thirdly, a rapid, efficient means must be developed for collecting large amounts of data in the field, storing it for later use, and extracting it in a meaningful fashion.

#### BRIDGING THE GAP: A CASE STUDY

Agricultural inventory techniques using small scale aerial and space photography of the Phoenix, Arizona area have been developed by personnel of the Forestry Remote Sensing Laboratory. This research which began in March, 1969, represents an interesting example of how remote sensing techniques were developed, and how the gap between technique development and application was bridged. The following discussion will concentrate upon the way in which field data collection methods were developed to provide information with which to evaluate the techniques developed, and to assess the application of these techniques on a regional basis.

Apollo 9 multiband photography was obtained in March, 1969, for use in developing improved capability for the inventory and analysis of earth resources. In addition to the Apollo 9 photography, the Phoenix test site has been the subject of regular high altitude (60,000 feet flight altitude) multispectral aerial photographic missions made possible through the NASA Earth Resources Survey Program. These missions, the first of which coincided with the Apollo 9 experiment, were flown at frequent intervals during the ensuing two years. Eighteen missions occurred between March, 1969, and March, 1971.

It became apparent at the outset of the experiment that the nature of the photography which was to be obtained -- i.e., broad areal coverage at regular intervals through a variety of seasonal conditions -- was such that it would lend itself well to performing regional resource surveys. The decision to orient the research towards performing surveys of agricultural crops in Maricopa County (which contains the city of Phoenix) was made for several reasons:

(1) there exists a need for accurate, timely, and inexpensive crop inventory information; (2) the seasonal variability which characterizes crop development patterns in the test site provided the basis for analysis on sequential aerial photography; and (3) the relatively uniform appearance of each crop type (as contrasted to the irregularity of wildland vegetation) simplifies the task of developing workable reference materials and photo interpretation keys for crop identification. The location of Maricopa County, where the survey was performed, and an indication of the distribution of agricultural land is presented in Figure 3. The first year's efforts were centered upon monitoring crop sequences and determining how high altitude aerial photography, obtained sequentially, could best be used to identify the major crops. Thus, procedures for crop identification constituted a major technique being developed, and agricultural inventory was the ultimate application under consideration. Data collected in the field consisted only of that information which affected crop identification directly (crop type, stage of maturity, percent cover, etc.). For this reason, no crop yield data or detailed vigor assessments were made.

Detailed field studies were begun in two areas south of Mesa, Arizona in March, 1969 at the time of the Apollo 9 overflight (Figure 4). A 16-square-mile area containing more than 125 individual fields was chosen as the primary study area. This site was chosen because (1) it was contiguous, (2) it was easy to reach for gathering crop data on a field-by-field basis, (3) it contained many of the important crop types found in the Phoenix area as well as a number of fields of each crop type, and (4) it was imaged clearly on the Apollo 9 photos as well as on most of the photography taken during subsequent aircraft missions. Additional ground data were also gathered during 1969 for another area of some 22 square miles (more than 250 fields) located in the same general region.

These two areas, totaling over 24,000 acres of agricultural land, were monitored at the time of each photo mission so that distribution and variability of crop type, crop development patterns, and crop signature could be adequately assessed. Coincident with each aircraft mission, each field was visited on the ground and notes were collected regarding crop type, condition, height of stand, and approximate ground cover percentage. Field maps of these test sites were prepared for field use and annotation. Boundary changes could easily be made while crop data was being recorded. Since the same field personnel were used to collect ground data at the time of each flight, they became familiar with the test site and crop patterns.

The most serious limitation to developing useful crop identification techniques lies in the variability of crop type and cropping practices. Any factor which affects the distribution, seasonal development and vigor of a crop will affect its photographic signature, and thus may influence the success with which that crop can be identified. The backlog of field data collected at the test sites near Mesa was used to develop some a priori knowledge regarding these factors which would be useful in developing practical interpretation techniques. Conclusions regarding these factors were as follows:

1. Crop type and distribution. It is generally true that agricultural practices in an area are relatively stable and that totally foreign crops are rarely introduced. For this reason, interpretation keys can be devised for

particular crops in a specific area with little fear that certain crops will totally disappear or that new crops will suddenly be introduced in large number. These generalizations were found to be valid for the main crops grown in central Arizona during a recent 4-year period.

- Seasonal development. Documentation of the seasonal development of crops is important for determination of optimum times of the year for crop type discrimination. Both within-season and between-season variability will affect the specification of optimum dates for obtaining photography. Knowledge of crop sequences and of the variations which affect these sequences must be understood. For agricultural areas, the cyclic changes and the approximate dates when they occur are best summarized in a table or chart known as a "crop calendar" (Figure 5). In addition to crop development information collected at the time of each flight, generalized crop conditions for the Salt River Valley (the major agricultural producing region of Maricopa County) were obtained from weekly crop condition reports released by the Arizona Crop and Livestock Reporting Service. Using this prepared information, tone values of individual fields (as seen on photography of a given date) can be related to the stage of maturity of the crops on that date, as summarized in the crop calendar. The calendar can then be used to determine either (1) at what single date a particular crop type has a unique signature that could be discriminated from signatures of all other crops, or (2) what combination of dates for sequential photography would best permit identification of that crop type.
- 3. Crop signature. Since little field detail is discernible at the scale and resolution of the high altitude Nikon photographs (scale 1/950,000) which were studies during 1969, photographic tone or color became the critical factor for identification. Either unique spectral signatures must exist at one date so that individual crop type can be identified, or else sequential patterns of tone or color must exist such that crop type can be distinguished on the basis of changing patterns (i.e., bare soil to continuous cover crop to bare soil) at particular dates through the year.

Interpretation tests were administered using photography of the test sites in which ground data were collected to determine which dates and film/filter combinations were best for identifying specific crop types. Some of the results of these tests are reported upon by Lauer in another workshop paper.

#### OPERATIONAL SURVEYS - THE FINAL STEP

During 1970, the area around Phoenix which was photographed by the NASA RB57F aircraft was increased to include most all the agricultural land in Maricopa County (Figure 3). At this point it was decided that the type of study initiated in the test sites near Mesa must be extended so that procedures developed might apply regionally instead of locally. The gap between technique development and application would hopefully be bridged at this point. Two aspects of the nature of this gap were assumed which would affect the direction of future work. First of all, it was recognized that crop distribution throughout the entire county would not be similar to the distribution found in the test sites near Mesa. Also, the photographic tone or color signature of given crop would vary throughout the test site as a result of variation in crop condition and development (stage of maturity at a single date, crop vigor, weediness, etc.).

This variation would mean that photo interpretation keys and reference materials prepared from images of the Mesa test sites could not be used with equal effectiveness as an aid to interpretation of an entire set of photography for the county. For these reasons it was decided to expand the scope of field data collection so that regional use of the data would be possible.

Examination of the Apollo 9 Infrared Ektachrome photography (AS9-26-3801) of Maricopa County suggested that there was enough variability in appearance of the cropland that some stratification might be desirable. Strata that appeared homogeneous were delineated on the space photo and 32 four-square-mile field plots were selected for detailed field-by-field study. These plots were allocated to the strata on a proportional area basis. Plot centers were chosen to coincide with the section corner nearest to the map point selected. In this way, the boundary of each square mile of a field plot would be identical to the boundary of a square mile as plotted on a topographic map. The objectives of collecting these data in conjunction with the April, 1970 NASA overflight and at the time of each successive flight were twofold: (1) to determine the distribution of the major crops in the county (determining whether the boundaries delineated on the space photo were meaningful in terms of accounting for crop variability); and (2) to evaluate the accuracy of crop type identification on photography obtained later in the year.

Thirty-two plots were chosen because this number could be completely field-checked within a two-day period by a team of three persons (economic constraint), and enough data would be provided for adequate statistical analyses (statistical restraint). A four-square-mile plot size (two miles by two miles) was chosen because it was large enough to contain a representation of the major crops growing in the particular area where the plot was located, yet small enough that several plots could be visited each day.

Maps of each plot showing field boundaries were drawn based on their appearance on earlier high altitude photography. Each plot was visited by a field crew at the time of each NASA overflight for the months of April, May, June, July, October, November, 1970, and March, 1971. Information gathered in this manner (Figures 6 and 7) included the category of crop growing in each field, its stage of maturity and condition, the percentage of ground covered by vegetation, crop height, and direction of rows (if any). The crop category code which was used is an adaptation of a coding system originally developed by the U.S. Government for categorizing land use (U.S. Department of Transportation, 1969) and subsequently refined for specific use in agricultural land use mapping by researchers at the University of California, Riverside (Johnson, et al., 1969).

Since more than 2500 fields were present in the 32 four-square-mile sample plots (comprising more than 80,000 acres), field data were punched on computer cards in order to facilitate access to this information in the future. Programs were then written which made possible the compilation of data by stratum, field plot, crop type, and date, and which provided for subdivisions or consolidations of fields over time. Thus, data are available not only for each date of photography, but for the sequential changes in crop type and conditions throught the growing season as well. An example of the computer printout for a few fields from one field plot appears in Figure 8.

Using the data which were derived from the first month's field inventory, the distribution and variability of crop acreage were evaluated to determine if the space photo strata delineations were useful in accounting for some of the variability in crop patterns. Analyses of variance indicated that there were no significant differences between strata in terms of acreages of major field crops. Therefore, it was assumed that acreage estimates from future surveys which used stratification as made on the Apollo 9 space photo of Maricopa County would not be improved. In addition, calculations indicated that the acreage distribution of major crops was so variable that for any plot size, extremely large samples for photo interpretation would be necessary in order to assure acreage estimates that would satisfy accuracy requirements. For example, in order to estimate the acreage of wheat with a standard error of  $\pm$  10% of the total acreage using a plot size of four square miles, a 75% photo interpretation sample would be necessary.

Once data for all 32 field plots were tabulated and prepared for computer analysis, they were used for two purposes: (1) providing training and reference material for photo interpretation testing for crop identification (as reported upon by Lauer in another International Workshop paper), and (2) adjusting photo interpretation estimates when regional surveys are performed (a workshop paper by Draeger summarizes this application). In addition, this data can be used to determine crop sequences that occur from season to season, and possibly may be employed to predict future crop patterns.

#### GROUND "TRUTH" - WHEN IT IS AND ISN'T

The term "field data" has been used in this discussion in preference to "ground truth", a term which is widely used among remote sensing scientists —but occasionally misunderstood by them. Such misunderstanding usually occurs when "ground truth" is accepted as an unbiased statement of the real conditions as they exist on the ground in the area being studied. This may well be a valid conclusion, yet the most rational approach should be to accept field data as an estimate of the ground condition. If measurements taken on the ground are carefully made and relevant kinds of measurement are selected for measurement, then it can be assumed that a near one-to-one correspondence exists between field measurements and the phenomena which they are supposed to characterize. If these precautions are ignored, however, then serious thought must be given to the usefulness of these data.

Since field data are collected by field personnel on the ground where the features and conditions can be seen "close-up", one's inclination is to accept them as "truth". However, two factors may affect the validity of this assumption and strengthen the admonition of the previous paragraph. First of all, ground measurements must be made which can be related to those parameters which are measured on remote sensing imagery. If the wrong field measurements are made, or if certain measurements are omitted which are critical for evaluation of the imagery, then conclusions regarding the worth of the imagery may mistepresent its true value. Secondly, once a set of ground measurements has been chosen, the care with which they are collected will determine the degree to which they can be relied upon for sound data analysis.

The effect of judgment errors which influence the first factor can be described by reference to the collection of field data in the Phoenix area. At present, information of the type summarized in the coded fraction in Figure 8 is collected. Personnel from our lab who have attempted automatic classification by means of scanning microdensitometer readings and computer analysis suggest that more detailed field measurements are needed for thorough analysis. Although no framework has been developed to determine how this added information may be of use in automatic image classification work, it has been suggested that the following items should also be recorded: soil moisture, presence and extent of invading species and weeds, percent bare areas in fields, vigor descriptions where applicable, and detailed mapping of the field environment (i.e., tractor access, storage pens, and drainage and irrigation lines). If this information is, in fact, required for automatic analysis, then current specifications fail to provide the needed information. Of course, requirements for field data collection may be constantly updated, and communication between co-workers (e.g., personnel working with automatic image interpretation and human image analysts) should be encouraged so that each field exercise might produce maximum return for the effort expended.

The importance of the second factor can also be stressed with reference to the Phoenix study, where errors by field personnel can easily lead to the collection of inaccurate 'ground truth'. If field teams must gather crop data on a field by field basis for several thousand acres (as has been done for the Phoenix study) in a short period of time, it is usually possible to visit only one portion of a given field as the crew moves by vehicle through the area. Identifications made at one side of a 40-acre field are extrapolated across that field. A careful look at that field will usually indicate whether the crop is continuous across the field, or if some other crop has been interplanted. However, an example of the possibility for errors to be made is given in Figure 9. This condition is usually corrected if the area is revisited at a later time. in conjunction with a future flight. Different routes through the test sites are generally followed on each date, and different sides of the same field can be visited. Any discrepancies between previous records (copies of which are carried by field teams) can be verified. Also, comparison of field data obtained on a particular date with the imagery obtained on that same date will expose boundaries and crop differences that were not evident to the field teams (Figure 9). Thus, the usefulness of field data for evaluating a set of imagery will depend upon the accuracy of the field estimates made on the ground. Some errors ascribed to photo interpreters should rightfully be ascribed to "ground truth". The possibility for encountering this type of error must be understood when a set of "ground truth" data is collected and used to evaluate remote sensing imagery.

#### CONCLUDING REMARKS

This paper has distinguished between field data collection for two differing uses: technique development and technique application. The scope of field data collection for each case was outlined and differences in terms of amount, timing, and format for collecting pertinent field data have been indicated. It is most important, for each application of remote sensing technology considered, that these distinctions be evaluated carefully in light of stated objectives so that reliable and timely data will be specified and collected. In addition,

care must be taken to ensure that any measurements are accurately recorded so that they do, in fact, provide an accurate estimate of "ground truth". Also the parameters which are chosen for field measurement should be those that relate most directly to image characteristics of the feature of interest.

The study of agricultural resources in Maricopa County, Arizona, has been described in depth to indicate how field data techniques were developed, first for a small "calibration" test site, then for a regional survey. As applications in other disciplines are pursued, the same kind of problems will no doubt be encountered. Not until regional studies are attempted will the considerations regarding field data collection have such far-reaching implications.

#### LITERATURE CITED

- Johnson, C.W., et al. 1969. A system of regional agricultural land use mapping tested against small scale Apollo 9 color infrared photography of the Imperial Valley. University of California, Riverside. USDI Status Report III, Tech. Report V, Contract 14-08-0001-10674.
- U.S. Department of Transportation. 1969. Standard Land Use Coding Manual. 111pp.



(a) Oblique aerial photo showing the water tower catwalk from which imagery was procured from a near-vertical angle of the target array below. Note that this target array contains crops, soil samples, soil moisture plots, water tanks, livestock, and color panels. Two Barnes Engineering thermal infrared sensors are mounted on the catwalk in this view.



(b) Surface temperature of objects in the array can be measured using a surface temperature probe.

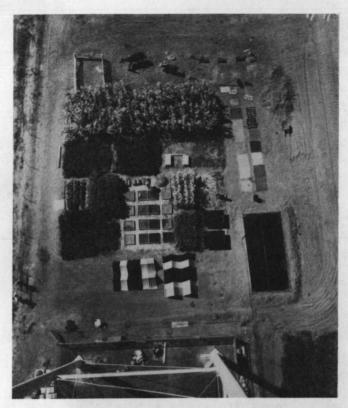


(c) Spectral reflectance data from each target in the array can be obtained at the time of image acquisition using an EG&G Spectroradiometer. Visible and near-infrared reflectance is measured in this manner.

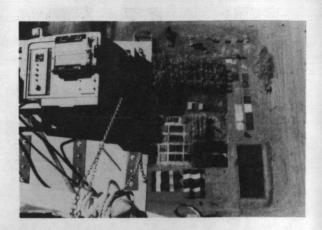


(d) The quantity and spectral distribution of incoming solar radiation can be measured with and ISCO Spectroradiometer.

Figure 1. An oblique aerial photo of the target array and water tower sensor platform at the University of California, Davis campus, appears at (a) above. Various instruments used to measure spectrometric and radiometric characteristics of objects in the array are shown at (b), (c), and (d).



(a) This photo is one of many multiband photos taken of the target array below by exposing panchromatic film with a Wratten 25 filter.



(b) Near-vertical view of target array in (a) as seen from water tower catwalk. One of two Barnes Engineering thermal infrared sensors is visible. An example of a thermal infrared image obtained with this sensor appears in (c).



(c) This photo-like image was made using the Barnes Engineering thermal infrared sensor seen in (b). Only the central part of the array was imaged because the field of view is somewhat limited. Light tones are indicative of relatively warm features while dark tones are cold features.

Figure 2. The images reproduced in (a) and (c) above were obtained on Sept., 14, 1967, from the sensor platform shown in Figure 1. Note that near-vertical imagery of the target array was procured in both cases from the catwalk of the water tower (c).

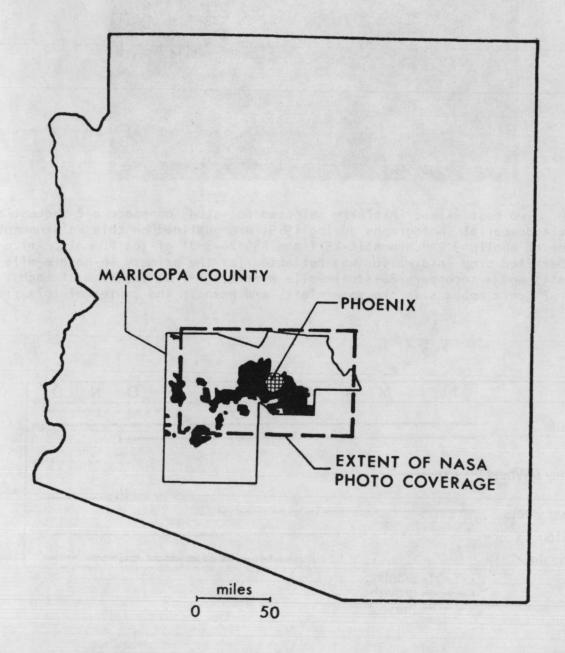


Figure 3. The location of the Maricopa County, Arizona test site is indicated on this map of the state of Arizona. The areal extent of NASA-obtained photographic coverage for each mission during 1970 is indicated. Note that essentially all agricultural cropland in the county is contained within the area photographed. As discussed in the text, 32 4-square-mile plots within the cropland area were selected for detailed field study.

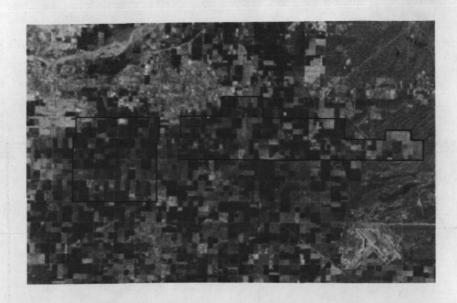


Figure 4. Two test sites, initially selected for study on space and sequential high altitude aerial photographs during 1969, are outlined on this enlargement of a portion of Apollo 9 Panchromatic-25 frame AS9-26-3801 of the Phoenix, Arizona area. Detailed crop information was collected for the primary 16-square-mile area (left) and a secondary 22-square-mile area (right) at the time of each flight. Phoenix appears in the upper left, and Mesa in the center of this frame.

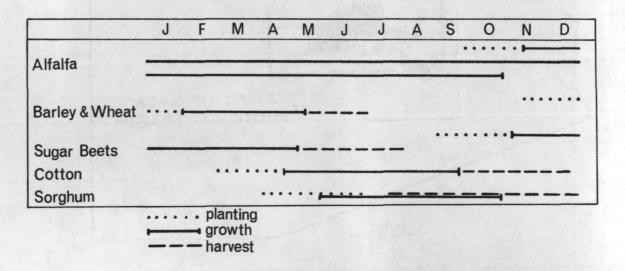
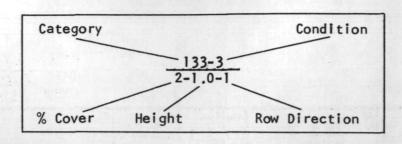


Figure 5. This crop calendar summarizes the development patterns of five major crop types in the Phoenix test site. The duration of each of the three main phases of development (planting, growth, and harvest) is indicated. It was prepared using field data and published crop status reports for Maricopa County. This kind of information is used to select optimum dates for discrimination of each crop type on aerial and space photography.

				DAT	L 2-1 E 7-20-70 W SLW
59 <sub>133-5</sub> 63 14-2 58 850 1-15-2	47 /-33-5 /4-2	133-3 14-1 1-1.0-1	45 133-5 14-1	41	40
57 61 <u>151-2</u> 800 <u>151-2</u> 51 1-25-2 1-25-1 850	850	14 133-3 1-1.5-1	43 /33-3 1:-1.0-1	850	850
850   133-3  -15-2	51a 52 850 930 51b 30 850 135-3 1-13-2	850/810	33 850	42 <u>/51-2</u> /-2.5-2 36 850	39  51-2  -25-  37  51-2  -25-
350 <u>  151-2</u>   1-2.5-	23a   23b   25   21   15   920	14 29 151-2 1-25-1	32 850 13 131-2 5-:3-1	35a  51-2  -1.5-2 35b  51-2  -20-2	850
8 850 850 7 850 810 920 2 810	3   <u>/51-2</u>  -2.5-1	//3-/ /-7.0-	/	10 151-2 1-2.5-1	9   <u>151-2</u>  -2.5-

Figure 6. This map contains field data collected for one of the 4-square-mile plots in Maricopa County at the time of a NASA high altitude overffight. The coded fraction in each field is explained in Figure 7. Computer storage of survey data, collected at the time of each flight on a field-by-field basis, facilitates sequential analysis of crop patterns as well as evaluation of photo interpretation test results.

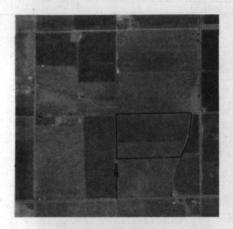


100	CATEGORY CODE (PARTIAL) Field and Seed Crops 111 Barley 114 Sorghum (grain) 118 Wheat 133 Alfalfa 142 Sugar Beets 151 Cotton	CONDITION CODE  1. seeded 2. Young 3. mature 4. dry (not harvested) 5. cut back (e.g., alfalfa)
200	Vegetable Crops	
300	Fruit and Nut Crops 331 Grapefruit 335 Orange	HEIGHT: Indicate average crop height in feet and tenths.
400	Livestock	
500	Animal Specialties	
600	Pasture and Rangelands 610 Pasture 620 Rangelands	% COVER CODE 1. 80-100% 2. 50-80%
700	Horticultural Specialties	2. 50-80% 3. 20-50% 4. 5-20%
800	Non-producing and Transition Cropland 810 Fallow 820 Plowed 850 Harvested 860 Prepared	5. 0-5%
900	Other Uses 910 Urban 920 Farmhouses and Farm-related Structures 930 Agricultural-related Activities 940 Native Vegetation	ROW DIRECTION CODE  1. N-S  2. E-W  3. NW-SE  4. NE-SW

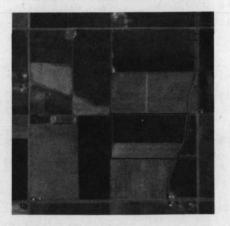
Figure 7. The fraction at the top of this page represents a typical field code as recorded by ground crews gathering information pertaining to the field plots. The example shown is a mature alfalfa field one foot in height, with 50-80% ground cover and rows running in a north-south direction. The complete category code is quite lengthy and therefore not reproduced here. Only the major headings (100, 200, etc.) and a few sub-headings (which are common to the Phoenix area) are presented.

	April 22	May 21	June 16	July 28
Test Site # Stratum # Plot # Field # Acreage	Category Condition Cover Height Row Direction Status	Category Condition Cover Height Row Direction Status	Category Condition Cover Height Row Direction Status	Category Condition Cover Height Row Direction Status
1111 1	1 11 1 11	1111111	111 1 11	1 11 1 11
1 1 3 1A 16.0	92000 0. 09	111 19	1[1 19	111 119
1 1 3 1B 24.0	11831 3.5 02	11841 3.0 02	85001 0.7 02 15123 0.7 22	850 9
1 1 3 2 37.0	86005 0 02	15103 0.2 22	15123 0.7 22	15121 2.5 22
1 1 3 3 9.0	92000 0. 29		9	15121 2.5 22 9 15121 2.5 12 850 850 13331 1.0 22
1 1 3 4 10.0	86005 0. 02	15105 0.3 12	15123 0.5 12	15121 2.5 12
1 1 3 5 42.0	11831 3.5 02	11841 3.0 02	85001 0.8 02 85001 0.3 12	850 2
1 1 3 6 25.0	11501 2.5 02	85001 0.5 02	85001 0.3 12	850 2
1 1 3 7 72.0 1 1 3 8 35.0	13351 0.3 02	13351 0.3 02	13331 1.0 02	13331 1.0 22
1 1 3 8 35.0 1 1 3 9 16.0	11821 1.5 Ø2 86005 Ø2	11831 2.0 Ø2 25623 Ø.3 22	25621 0.4 22	
1 1 3 10 24.0	86005 02	25623 0.3 22	25623 0.4 22	25622 ؕ5 22 25622 ؕ5 22
1 1 3 11 7.6	86005 02	25623 0.3 22	25621 0.4 22	810 1
1 1 3 12 56.4		13331 2.0 02	13331 0.7 22	13331 1.5 22
1 1 3 13 2.0	85005 02 92000 9	9	9	9
1 1 3 14 21.0	86005 02	25623 0.3 22	25621 0.4 22	25621 0.8 22
1 1 3 15 10.0	33502 9.0 21	1		
1 1 3 16 10.0	33504 2.0 21		1	
1 1 3 17 • 5	92000 29	9	9	9
1 1 3 18 3.0	92000 29	9	9	9
1 1 3 19 10.0	86005 23	19A, 19B	1	9 9 2
1 1 3 19A 5.Ø		13002 0. 22	13003 1.0 02	610
1 1 3 19B 5.0		23002 0. 12	800       1	

Figure 8. A portion of the computer printout for four consecutive months is reproduced here. This data for Phoenix test site (site #1), stratum #1, plot #3, fields 1A through 19B, was derived from field notes for each month. The key to each code appears in Figure 7. For example, field 7 is alfalfa which had been recently cut on the first two dates and was mature on the last two dates. Field 5 contained wheat during the first two months. It was harvested and contained stubble on the last two dates. Field 19 was divided into two 5-acre fields in May when pasture grasses were planted in 19A and a vegetable crop was planted in 19B. The system developed can easily handle divisions, consolidations and changes that occur from month to month.



MAY 21, 1970



JUNE 16, 1970

Figure 9. The possibility for errors in ground "truth" data is illustrated here. These two panchromatic photos were enlarged from RC-8 transparencies taken on May 21, 1970, and June 16, 1970. Seen in each photo is a one-square-mile area which is part of a four-square-mile plot where field data was recorded at the time of each aircraft overflight. All of the outlined field was recorded as barley on both dates by field personnel. However, by June 16 all fields containing cereal grain crops have matured and dried (note several light-toned fields on the June 16 photo); therefore, the upper portion of this field cannot contain barley because it still has a dark tone. Subsequent field checking during July has verified that the upper portion was, in fact, alfalfa, a crop which remains green during the entire growing season. This discrepancy occurred because the field crew reached the field along the route indicated by the arrow and, from where they viewed the field, it was identified as barley. Careful field checking and comparison of photography with ground data will help to minimize errors of this type.

Page Intentionally Left Blank

BIOGRAPHICAL SKETCH -- Craig L. Wiegand

Born: Santa Rosa, Texas; Jan. 11, 1933

Graduated: Texas A&M University, College Station, 1955, BS degree in Agronomy, and in 1956, MS degree in Soil Physics; Utah State University, Logan, 1960, PhD in Soil Physics (minors in Physical Chemistry and Mathematics).

Member of the American Society of Agronomy, Soil Science Society of America, Soil Conservation Society of America, International Soil Science Society, American Association Advancement of Science, and the Rio Grande Valley Horticultural Society.

Honor Society memberships include Sigma Xi, Phi Kappa Phi, and Alpha Zeta.

Dr. Wiegand first joined the U.S. Department of Agriculture in 1955 as a Soil Scientist working with Dr. E. R. Lemon at Texas A&M University. He worked with the late Dr. Sterling Taylor at Utah State University from 1956 to 1959. Dr. Wiegand rejoined the U.S. Department of Agriculture in 1959 as Research Soil Scientist at Weslaco, where he has served continuously since that time. In July 1966, he became Scientist in Charge of the Division's program at Weslaco, and in January 1969, Dr. Wiegand was named Director of the Rio Grande Soil and Water Research Center. This assignment involves both the direction of the Research Center and the conduct of creative research — one area being the adaptation and use of remote sensing techniques in agricultural research.

Dr. Wiegand has authored approximately 40 papers in his research field, many of these receiving special invitation for presentation before scientific societies and technical conferences.

# AGRICULTURAL APPLICATIONS AND REQUIREMENTS FOR THERMAL INFRARED SCANNERS

Craig L. Wiegand

Southern Plains Branch
Soil and Water Conservation Research Division
Agricultural Research Service
U. S. Department of Agriculture
Weslaco, Texas 78596

#### INTRODUCTION

The short wavelength energy of the sun strikes the earth where plants, soil, water, and other objects at the earth surface absorb, transmit or reflect it. The part of the sun's energy absorbed by the earth either heats the surface or evaporates water. In a desert practically all the absorbed energy heats the earth so there is a wide temperature difference between night and day. In humid climates most of the sun's energy evaporates water; consequently high daytime temperatures are not experienced. You can see that how the sun's energy is used at the earth surface is very important to mankind -- and to Agriculture.

The earth also gives off the heat it has absorbed by the process known as thermal emission. This energy given off is not absorbed by the atmosphere, but it is absorbed by clouds. Therefore, the temperature of the earth can be observed from spacecraft when clouds don't interfere. The temperatures observed tell us a great deal about earth conditions important to Agriculture.

In the short time I have today, I will list some of the applications of thermal scanner data in Agriculture; illustrate some factors affecting the temperature of plants, soil, and water; and, present a few examples of thermal imagery.

#### APPLICATIONS

Agricultural applications of thermal scanners include:

Detecting plant water stress due to --

Need for irrigation

Soil salinity

Shallow and droughty soil

Nematodes . . .

Indicating occurrence of rainfall

Measuring soil temperature for indicating when soil is warm enough to

Studying occurrence and pattern of freezes

Monitoring thermal pollution

Detecting springs and subsurface flow into lakes, rivers, and oceans Estimating evapotranspiration of farmland, forest, and rangelands Estimating water evaporation from lakes, ponds, and reservoirs

Most of the listed applications are obvious. A few may not be. For example, a question the farmer faces each spring is: "When is the ground warm enough to plant?" A seeding advisory based on earth surface temperature measured from space at night seems feasible. One needs to be able to locate the area he is interested in (ground resolution must be adequate) and the measuring instrument must be working properly (be calibrated).

## FACTORS AFFECTING EQUILIBRIUM TEMPERATURE

## Thermal Properties

The observed relation between incoming solar energy (insolation) and the temperature of cotton plant leaves, bare soil, and water in a reservoir are presented in the lower part of Figure 1 (Wiegand, Heilman and Gerbermann, 1968); air temperature measured at 5 ft above bare soil, with shielded thermocouples, is presented in the upper part of the figure. Incoming solar radiation is reported in langleys per minute which is numerically equal to calories per square centimeter per minute. The relations are linear in the bottom graph except for the leaves of the cotton plant. This is expected for cotton plants (Wiegand and Namken, 1966) because heat transfer between the cotton leaves and the air keep the leaf temperature near that of the air. Air temperature rises during the day. Cooling due to evaporation of water from the reservoir, the large amount of energy required to change its temperature (i.e., its high heat capacity), and thermal mixing keep the water temperature nearly constant. The dry soil, lower graph, for which the morning and afternoon curves follow separate paths, had large mass and poor thermal conductivity with a consequent strong thermal dependence on insolation. Wet soil behaves thermally like plant leaves, because the energy is used to evaporate water. As shown in Figure 1, the temperature of bare dry soil can be 30°C warmer than plant leaves.

A portable radiometer (Stoll, 1954) was used to make the measurements of Figure 1. It had been calibrated over a wide range in target temperature and internal reference temperature against a Leslie cube blackbody source. The temperatures for soil, plant, and other surfaces, then, are equivalent blackbody temperatures, i.e., the temperature these objects would have if they had unit emissivity. This reporting form is used because the measurements necessary for correcting for deviations from unit emissivity of targets and for radiation from the surroundings were not made (Fuchs and Tanner, 1966; Conaway and van Bavel, 1966).

#### Insolation

Figure 2 shows the influence of solar radiation on leaf temperature of cotton plants (Wiegand and Namken, 1966). The data in Figure 2 were obtained on different days when air temperature (TA) at plant height and relative turgidity (RT) were uniform among all experimental treatments. (Relative turgidity is the ratio of the water content of the leaf as sampled in the field to its water content after floating on water under illumination at room temperature overnight.) Air temperature at the time of measurement (2:30-3:00 p.m., central standard time (CST)) differed by 3.5°C, and relative turgidity of the cotton leaves differed by 10% on the two dates. The variable radiation was created by intermittent clouds.

In the study cited, it was found that individual cotton leaves equilibrated with a change in radiation intensity in about 45 seconds. Thus the leaf-temperature measurements were deferred until radiation remained steady for a minimum of 45 seconds.

The data show that the thermal response of leaves to changing radiation is linear, and they imply that if radiation conditions are variable it will be necessary to measure the incident radiation and leaf temperature simultaneously.

### Plant Water Stress

The effect of water deficiency (plant water stress) on cotton leaf temperature when air temperature ( $T_A$ ) and solar radiation ( $R_S$ ) were approximately constant is depicted in Figure 3. The variable plant moisture conditions M-1, M-2, and M-3 were achieved by timing of irrigation during a rainless period. In midafternoon, cotton plant leaves exhibited symptoms of wilt at 70 to 72% relative turgidity. Leaves at 60% relative turgidity were extremely flaccid. These data indicate that cotton leaf temperature can vary about 3.5°C with plant water stress.

The standard deviations of air temperature and solar radiation associated with these observations were 0.7°C and 0.04 ly min<sup>-1</sup>, respectively. The regression coefficient indicates that leaf temperature increased 0.15°C for each percent decrease in relative turgidity over the relative turgidity range 83 to 59%.

From the data for 37 individual days covering two crop seasons, it was determined that leaf temperature could be estimated with a standard error of 1°C from measurements of relative turgidity, solar radiation, and air temperature at plant height. For these measurements, solar radiation averaged 1.15 ly min-1, and leaf temperature minus air temperature averaged 4°C (Wiegand and Namken, 1966).

A panchromatic photograph of small, differentially irrigated cotton plots and the plant canopy temperature patterns obtained with an infrared camera are presented (Figure 4) (Myers, Wiegand, Heilman, Thomas, 1966a). The thermograms are a composite of 4 thermograms taken at the time of day (CST) indicated below each thermogram.

The cotton plot in the foreground and the one in the background of each thermogram were at about the same moisture condition, and have the same tone. The middle plot was drier than the others. The calculated temperature difference between dry and wet plots was 0.1, 0.3, 2.0, and 0.2°C at the hours 0540, 0935, 1520, and 2210, respectively.

The first thermogram of Figure 4 was obtained at 0540, well in advance of daybreak. The light areas from bottom to top on this thermogram -- ignoring the one at the very bottom of the thermogram -- are a man kneeling between the plot in the foreground and the center plot, an incandescent lamp in the far plot, and three side-by-side instrument shelters just beyond the plots. The other three thermograms depict the same target at later times during the day.

In all the thermograms presented, the lighter toned areas represent warmer plant temperatures. Interpretation of the thermograms is made by matching the tone of a target within the field of view with one of the 8 gray scale steps printed automatically at the top of each thermogram. From the electronic settings used to obtain the thermograms and a parameter corresponding to the gray scale step, the target radiance may be calculated and then converted to target temperature. It was necessary to vary the electronic settings as the crop surface warmed; therefore, temperature differences cannot be compared by visual inspection except relatively within individual thermograms.

# Soil Salinity

Soil salinity is a problem on irrigated, and on nonirrigated arid and semiarid land the world over. The presence of water soluble salts in the root zone causes an osmotic suction which reduces the availability of water to plants. This osmotic component plus the soil matric suction (Richards, 1949), which increases as plants extract water, constitute the total soil water suction. Plants growing in saline soil exhibit marked symptoms of moisture stress, and growth is retarded.

Figure 5 shows the relation between total soil water suction and leaf temperature of cotton growing in saline soil (Thomas and Wiegand, 1970). An increase in total soil water suction from 1 to 15 bars would raise the adjusted leaf temperature 1.82, 2.10, and 6.16°C, respectively, on May 27, June 4, and June 17. The osmotic suction accounted for nearly all the variation in leaf temperature attributed to total moisture suction.

A number of workers have applied remote sensing techniques to studying soil salinity (Myers, et al, 1963; Myers, Wiegand, Heilman, and Thomas, 1966a; Myers, Carter, and Rippert, 1966b; Myers and Allen, 1968; Myers, et al, 1970). Their findings demonstrate remote sensing's usefulness for this purpose.

## Ground Cover

If plants incompletely cover the soil, a scanning instrument will sense the mixture of plant and soil background emissions in the instrument's field of view. Figure 6, taken from Myers and Heilman (1969), relates equivalent blackbody temperature to percent plant cover. As percent plant cover increased, equivalent blackbody temperature decreased.

## Soil Survey

Another application of thermal data is in soil survey (Myers and Heilman, 1969). In this case, the soil profile characteristics influencing heat flow are related to surface temperatures. Timing of sensing, both diurnally and seasonally, must be carefully selected for this purpose. Park, Colwell, and Myers (1968) have suggested that soil moisture contrasts in bare soil can be detected using thermal infrared wavelengths.

For row crops, percent ground cover can be obtained by ground observers by measuring the distance between rows not occupied by leaves and dividing by the row spacing. Temperature of plant and soil mixtures have also been related to leaf area index and average plant spacing (Wiegand, Heilman, and Gerbermann, 1968). Ground cover can also be estimated from aerial photographs.

Gates (1970) presented energy balance equations which take the plant cover into account. However, the author is unaware that these equations have been applied in the field.

# Evapotranspiration

Another application of thermal scanner data is in evapotranspiration research. Surface temperature is required directly or indirectly to calculate the water vapor pressure at the plant (soil) surface for all equations in which the latent heat flux density (evaporation) is calculated (Wiegand and Bartholic, 1970).

#### Freezes

Freezes are another hazard in Agriculture. Figure 7 is a composite of a panchromatic photograph and three thermograms of a test citrus tree taken on a night when a radiational freeze was forecast and petroleum coke heater blocks were burned under the trees (Bartholic and Wiegand, 1969). The electronic settings of these thermograms were such that the lighter in tone the images are, the colder the temperature. At 0250, 0348, and 0603 the predominate external leaf temperatures were 3.3, 2.4, and 4°C, respectively.

Gray scales are immediately above each thermogram. The temperature range from gray scale step 1 (dark tone; warm) through step 8 (light tone; cold) is 4.2°C. For the 0603 thermogram, the temperature range is also 4.2°C but the signal was electronically offset so that each step is 1°C warmer than the corresponding step of the other thermograms.

The infrared camera senses longwave thermal radiation emitted by the exterior leaves only if the tree is heavily leafed. However, if there are holes in the tree canopy, interior leaves and limbs are sensed. In the 0348 hour thermogram (and to a lesser extent in the other thermograms) holes in the canopy resulted in interior warmer objects being sensed giving lateral and almost vertical, nearly continuous dark patches. Likewise, gradations in tone occur because some leaves were shielded from the sky by leaves above them while others were fully exposed to the sky. Temperatures of shielded leaves, as measured by attached thermocouples, were about 2°C warmer than exterior leaves.

#### INSTRUMENTATION

Lowe (1968) lists some of the features of scanners that make them attractive: (1) measurements are possible both within and outside the photographic range; (2) the electrical output signal can be readily transmitted, recorded, analyzed, and processed; (3) detectors generally have wide dynamic range; (4) the scanner is easy to calibrate to yield quantitative radiometric data; and (5) simultaneous data collection in many wavelength channels is possible.

In the thermal infrared, quantitative or semiquantitative thermal maps can be obtained if the signals which are ac coupled for ease of signal handling and recording have been dc restored -- a technique that introduces a repetitive signal of known constant level from a source whose position in the video is

known and which requires electronically sampling the output level of the known signal and adding or subtracting a dc voltage to make it constant. Then if the detector response is stable and reproducible and the amplifier gains are fixed, the instrument response can be calibrated from two or more internal or reference calibration sources (Lowe, 1968).

Myers and Allen (1968) have aptly stated: "The researcher must be warned, however, that use of relatively untried instruments with unknown characteristics with little or no attention to calibration may lead to wholly unsatisfactory research results. Radiometry is an exacting field and the use of poor experimental techniques will result in inadequate and misleading data, thus, the time of the experimenter and his readers will be wasted."

#### SUMMARY

There are many applications of thermal infrared scanners to problems faced by mankind in learning about the earth's resources and in managing and using them wisely. I hope that by talking about possible applications and factors affecting thermal measurements today you can better judge the usefulness of thermal scanners in your countries.

### REFERENCES

- Bartholic, J. F., and C. L. Wiegand. 1969. The environment in a citrus grove with and without heater blocks during cold conditions. Proc. First Int'l. Citrus Symp., Univ. of Calif., Riverside. 2:583-592.
- Conaway, J. and C. H. M. van Bavel. 1966. Remote measurement of surface temperature and its application to energy balance and evaporation studies of bare soil surfaces. Tech. Rpt. ECOM 2-67P-1, U.S. Army Electronics Command, Atmos. Sci. Lab., Fort Huachuca, Ariz. 136 p.
- Fuchs, M. and C. B. Tanner. 1966. Infrared thermometry of vegetation. Agron. J. 58:597-601.
- Gates, D. M. 1970. Physical and physiological properties of plants. Ch. 5, <u>In</u>
  Remote Sensing with Special Reference to Agriculture and Forestry. National
  Academy of Sciences, Washington, D.C. p. 224-252.
- Lowe, D. S., F. C. Polcyn and R. Shay. 1965. Multispectral data collection program. Proc. Third Int'l. Symp. Remote Sensing of Environ., Inst. Sci. & Tech., Univ. of Mich., Ann Arbor. Rpt. No. 4864-9-X. p. 667-680.
- Lowe, D. S. 1968. Line scan devices and why use them. Proc. Fifth Int'l. Symp. Remote Sensing of Environ., Inst. Sci. & Tech., Univ. of Mich, Ann Arbor. p. 77-101.
- Myers, V. I., L. R. Ussery and W. J. Rippert. 1963. Photogrammetry for detailed detection of drainage and salinity problems. Trans. Amer. Soc. Agr. Engin. 6:332-334.
- Myers, V. I., C. L. Wiegand, M. D. Heilman and J. R. Thomas. 1966a. Remote sensing in soil and water conservation research. Proc. Fourth Int'l. Symp. Remote Sensing of Environ., Inst. Sci. & Tech., Univ. of Mich., Ann Arbor. p. 801-813.
- Myers, V. I., D. L. Carter and W. J. Rippert. 1966b. Remote sensing for estimating soil salinity. J. Irrig. & Drain. Div., Proc. Amer. Soc. Civil Engin., Vol. 92, No. IR 4, Proc. Paper 5040, pp. 59-68.

- Myers, V. I. and W. A. Allen. 1968. Electrooptical remote sensing methods as nondestructive testing and measuring techniques in agriculture. Appl. Opt. 7:1819-1838.
- Myers, V. I. and M. D. Heilman. 1969. Thermal infrared for soil temperature studies. Photogramm. Engin. 35:1024-1032.
- Myers, V. I., M. D. Heilman, R. J. P. Lyon, L. N. Namken, D. Simonett, J. R. Thomas, C. L. Wiegand and J. T. Woolley. 1970. Soil, water and plant relations. Ch. 6, In Remote Sensing with Special Reference to Agriculture and Forestry. National Academy of Sciences, Washington, D.C. p. 253-297.
- Park, A. B., R. N. Colwell and V. I. Myers. 1969. Resource survey by satellite, Science fiction coming true. In 1968 Yearbook of Agriculture, U.S. Govt. Printing Office, Washington, D.C. pp. 13-19.
- Richards, L. A. 1949. Methods of measuring soil moisture tension. Soil Sci. 68:95-112.
- Stoll, Alice M. 1954. A wide-range thermistor radiometer for the measurement of skin temperature and environmental radiant temperature. Rev. Sci. Instru. 25:184-187.
- Thomas, J. R. and C. L. Wiegand. 1970. Osmotic and matric suction effects on relative turgidity, temperature and growth of cotton leaves. Soil Sci. 109:85-91.
- Wiegand, C. L. and L. N. Namken. 1966. Influences of plant moisture stress, solar radiation, and air temperature on cotton leaf temperature. Agron. J. 58:582-586.
- Wiegand, C. L., M. D. Heilman, and A. H. Gerbermann. 1968. Detailed plant and soil thermal regime in agronomy. Proc. Fifth Int'l. Symp. Remote Sensing of Environ., Inst. Sci. & Tech., Univ. of Mich., Ann Arbor. p. 325-341.
- Wiegand, C. L. and J. F. Bartholic. Remote sensing in evapotranspiration research on the Great Plains. Proc. Great Plains Agricultural Council Evapotranspiration Seminar, Publication No. 50, Kansas State Univ., Manhattan. p. 137-180.

# GLOSSARY OF TERMS

- Insolation (contracted from incoming solar radiation) -- In general, solar radiation received at the earth's surface. Langleys/cm<sup>2</sup>/min.
- Heat capacity (thermal capacity) -- The ratio of heat absorbed (or released) by a system to the corresponding temperature rise (or fall).
- Thermal conductivity (heat conductivity, coefficient of thermal conduction, coefficient of heat conduction) -- An intrinsic physical property of a substance, describing its ability to conduct heat as a consequence of molecular motion.
- Blackbody -- A hypothetical "body" that not only absorbs all wavelengths, but also emits at all wavelengths and does so with maximum possible intensity (has an emissivity of unity) for any given temperature.
- Equivalent blackbody temperature -- The temperature measured radiometrically corresponding to that which a "blackbody" would have. Most natural objects including soil, plant leaves, and water have emissivities >0.9 but <1.0.
- Relative turgidity (relative water content) -- The ratio of the water content of a leaf sampled in the field to its water content after floating on water under illumination at room temperature overnight.
- Leaf area index -- The cumulative one-sided leaf area per unit ground area projected from the canopy top to a plane at a given distance above ground level.
- Evapotranspiration -- The combined processes by which water is transferred from the earth's surface to the atmosphere; evaporation of liquid or solid water plus transpiration from plants.
- Internal reference temperature -- A standard surface or cavity of known temperature or radiometric intensity against which measurements of crops, soils, water, and other objects can be quantitized.

<sup>\*</sup> Definitions found in it are those given in <u>Glossary of Meteorology</u> edited by Ralph E. Huschke as published by American Meteorological Society, Boston, Mass. 1959.

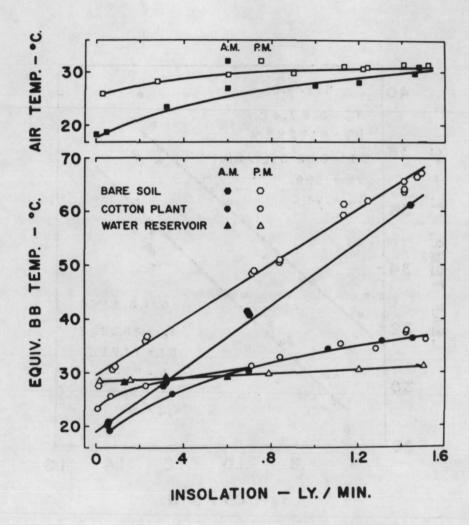


FIGURE 1. Equivalent blackbody temperature of dry soil, cotton plants, and a water reservoir and of air temperature versus incoming solar radiation on the day of a thermal scanner overflight, 6/1/66 (Wiegand, Heilman, and Gerbermann, 1968). Internal reference signal generation for the Univ. of Michigan scanner used (Lowe, Polcyn, and Shay, 1965) was not available until after these measurements were made. Therefore, the thermal imagery was calibrated against ground truth measurements such as the above taken simultaneously with the plane's overflight.

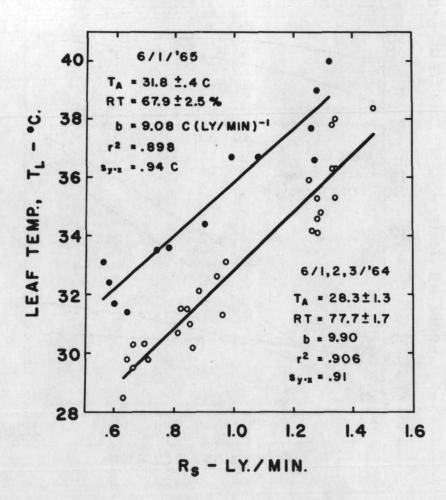


FIGURE 2. The influence of solar radiation ( $R_s$ ) on cotton leaf temperature when air temperature ( $T_A$ ) and relative turgidity (RT) were approximately constant. An increase in radiation from 0.6 to 1.6 ly min<sup>-1</sup> resulted in a 9° to 10°C increase in leaf temperature as indicated by the regression coefficient, b. The standard errors of estimate,  $S_{y.x}$ , indicate that leaf temperatures could be estimated  $\pm$  0.9°C two-thirds of the time (Wiegand and Namken, 1966).

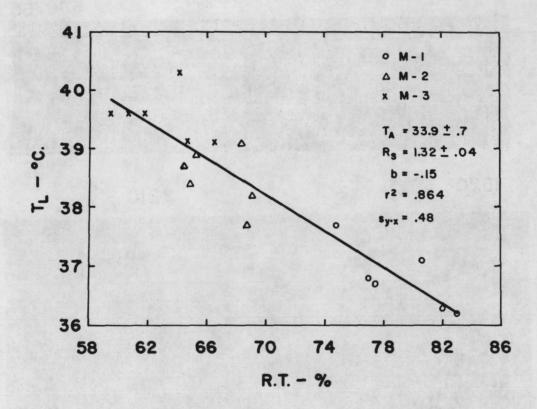


FIGURE 3. The effect of relative turgidity (RT) on leaf temperature when air temperature (T<sub>A</sub>) and solar radiation (R<sub>S</sub>) were approximately constant. The leaves on which relative turgidity measurements were made were sampled in midafternoon. Plant water condition ranged from freshly irrigated (83% RT) to extremely wilted (59% RT). Water stress is shown to cause a 3.5°C increase in plant leaf temperature. Therefore, plant temperatures should be useful for scheduling irrigations (Wiegand and Namken, 1966).

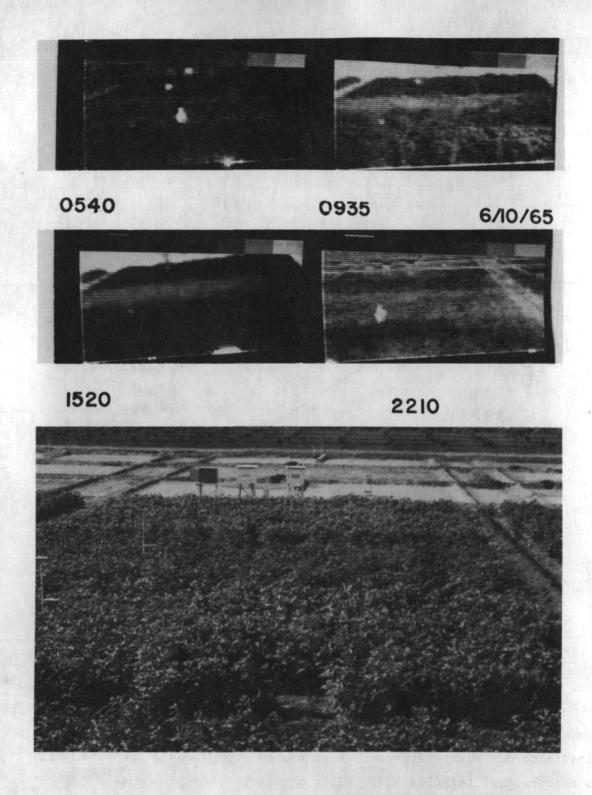


FIGURE 4. Panchromatic photograph and composite of 4 thermograms of small, differentially irrigated cotton plots. The center plot was drier than the others. The calculated temperature difference between the dry and wet plots was 0.1, 0.3, 2.0, and 0.2°C at the hours 0540, 0935, 1520, and 2210, respectively (Myers, et al., 1966a).

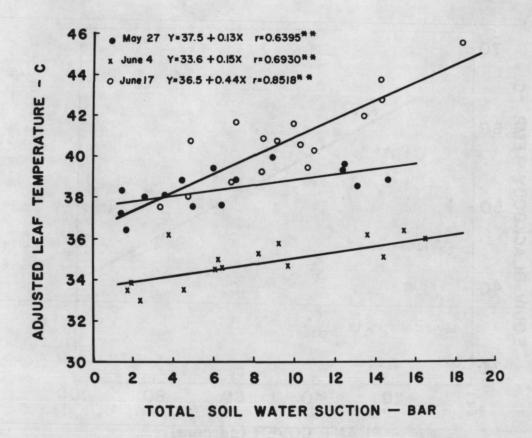


FIGURE 5. Leaf temperatures adjusted to mean solar radiation during the sampling period as related to total soil water suction (the sum of osmotic and matric suctions) on selected days in the growing season for cotton grown on saline soil. Nearly all the water suction was due to osmotic suction (Thomas and Wiegand, 1970).

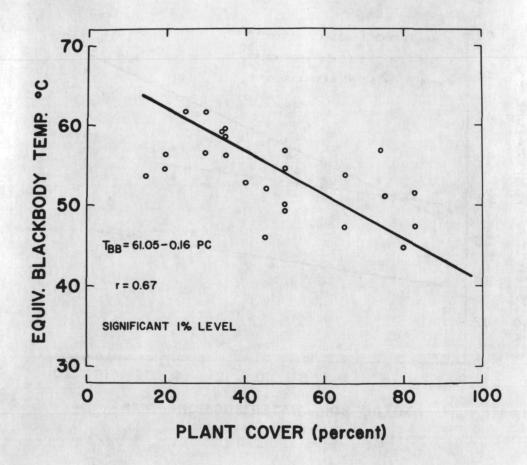


FIGURE 6. Relation between equivalent blackbody temperature of selected sites and percent plant cover for an overflight with the Univ. of Michigan scanner at 1400 hr on June 1, 1966 (Myers and Heilman, 1969). Incomplete plant cover results in the scanner recording a mixture of signals from the plant surfaces and the soil background.

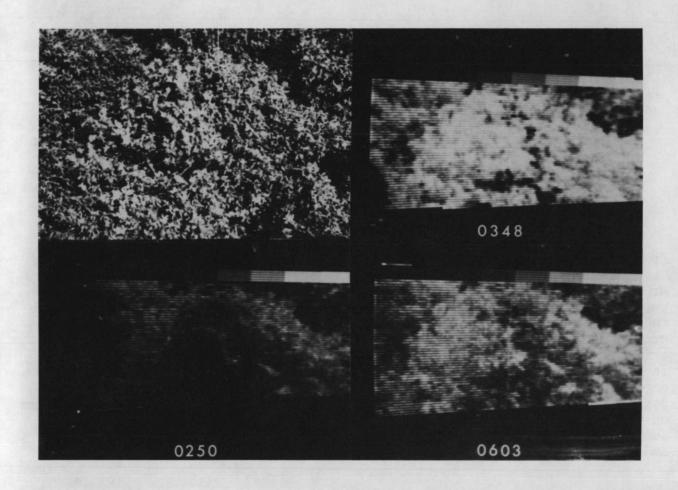


FIGURE 7. Panchromatic photograph (upper left) and thermograms taken in a citrus orchard at the hours indicated below each thermogram on a night of strong radiational cooling. For these thermograms, the temperature range depicted from gray scale step 1 (dark tone; warm) through step 8 (light tone; cold) is 4.2°C. Exterior leaves exposed to the sky were about 2°C colder than leaves shielded from the sky (Bartholic and Wiegand, 1969). The study of temperature distributions during a freeze is aided considerably by thermal scanners.

## FOREST AND RANGE INVENTORY AND MAPPING

by

Robert C. Aldrich

# BIOGRAPHICAL SKETCH

Robert C. Aldrich is Principal Research Forester with the Remote Sensing Project in Berkeley. He received his B. S. and M. F. degrees from the New York State College of Forestry at Syracuse University in 1944 and 1948, respectively. Mr. Aldrich has been employed by the Forest Service for 23 years and has devoted his career to the applications of remote sensing to forest surveys. Between 1948 and 1954 he was assigned to the Forest Survey unit at the Southeastern Forest Experiment Station at Asheville, North Carolina. In 1954, he transferred to the Forest Insect Laboratory at the Agricultural Research Center in Beltsville, Maryland, where he conducted research in survey techniques for detecting and evaluating forest insect outbreaks. He has been in his present position since 1965. Mr. Aldrich has authored or coauthored over 25 publications on the subjects of photo interpretation, aerial survey techniques, and remote sensing in forestry. He is a member of the American Society of Photogrammetry and the Society of American Foresters.

## FOREST AND RANGE INVENTORY AND MAPPING

by

# Robert C. Aldrich1

# INTRODUCTION

Gathering information about earth's forest and range resources will be a challenge for space-age remote sensing in the years ahead. Environmental experts are already saying that earth's rapidly expanding population will soon demand more food, forest products, and unpolluted water than present resource management practices can provide. To improve the situation, resource managers will require more information at much shorter intervals than is economical at the present time. Increasing the use of remote sensing may reduce costs and make surveys at more frequent intervals possible.

In the United States, demands for more highways, electric power, and consumer products are already creating rapid changes in the forest environment. We have a steadily increasing problem with air pollution and its effect upon vegetation (1), a shifting forest acreage caused by land-use changes, and a forecast for decreasing net forest growth and volume (2). To combat these effects, we must improve land management practices and policies to better utilize range and forest land and keep idle lands productive.

Remote sensing, including conventional aerial photography, is a tool for gathering information about the forest and range resources. And now since man has solved some of the mysteries of space, we have a new dimension in remote sensing--pictures taken from platforms 160-480 km (100-300 miles) above the earth with photographic or electronic sensors. Although these synoptic pictures have a ground resolution of only 46-122 meters (150-400 feet), they should be useful for generalized regional forest and range appraisals. Furthermore, prospects are bright for repeated earth coverage at intervals as short as every 18 days by polar orbiting spacecraft (ERTS); as this system develops, forest and range information systems and maps may be updated to show the situation as often as needed. In time, we feel that technological improvements in camera optics, films, and electronic scanner outputs will increase ground resolution and the kinds and quality of information taken from space imagery.

Regardless of ground resolution, imagery taken from space will never eliminate the need for larger scale aerial photographs and ground measurements. Foresters and range conservationists will always be a vital part of the information-gathering system. If we combine a limited amount of ground measurements with other levels of information in multistage sampling designs, the efficiency of extensive forest and range appraisals should be improved.

Research Forester, Pacific Southwest Forest and Range Experiment Station, Forest Service, U. S. Department of Agriculture, Berkeley, California, U. S. A.

# MULTISTAGE SAMPLING

The theory of sampling in more than one step is not new to forest or range inventories (3, 4, 5). Forest and range managers around the world have been using medium-scale aerial photographs, combined with ground data, for many years in two-step sample designs. Many of you are familiar with these. One classic example is the forest inventory using stratified sampling. First, the forest is stratified into relatively homogeneous vegetative types and volume classes on aerial photographs. This reduces variation between population units within classes. As a result, fewer ground plots are needed to attain the same sampling error that can be achieved by simple random sampling alone, and total survey costs are minimized. But multistage sampling, by including several stages, can make even greater improvements in efficiency. The gains are made because we use the additional information found at each stage to select the next stage. We can use existing medium-scale photographs, high-altitude small-scale photographs, space photographs, and even maps and combine them with large-scale photographs and ground samples in a survey design by using probability sampling theory (6). This theory is commonly referred to as p.p.s.--probability proportional to size.

# PROBABILITY SAMPLING THEORY

Langley (7) extended the theory of probability sampling to multistage sampling designs in conjunction with timber mortality surveys and National Forest management plan inventories. This technique was first used successfully on a forest insect damage survey to estimate the volume of dead timber (8). Since then, it has been extended to general forest surveys that use more than one photographic scale. These are multistage sampling surveys with arbitrary probabilities of sample selection at each stage (photographic scale). In this technique, the sampling probabilities are derived by using the information made available through the use of increasingly finer ground resolution of remote sensors at each stage. At the last stage, detailed measurements are made for the survey parameters on the ground. These measurements are then projected back through the sampling formula to obtain estimates for the entire survey area.

Basically, probability sampling allows us to select the sample in each stage based upon some prior information. In a forest survey, the prior information is most likely to be a prediction of something related to volume--perhaps stand density, type, or area. The better the correlation between the prediction and the estimate at each stage, the lower the variance will be. However, if there is a negative correlation, the sampling variance will be higher than if we had used simple random sampling at that stage.

Probability sampling designs have several advantages over other sampling designs. One is that the number of costly ground samples required to obtain estimates of volume within acceptable limits of error can be reduced significantly. In addition to being efficient, the design provides unbiased estimates and statistically valid sampling errors at all stages. Furthermore, it improves operational efficiency by concentrating our effort in those areas of the greatest interest at each stage.

Let's look at an example of multistage sampling using photographs taken from space as the first level of information.

# A MULTISTAGE FOREST INVENTORY

The vertical photographs of earth taken during NASA's Apollo 9 multiband photography experiment (SO-65) gave foresters their first good look at extensive forested areas from space. Of the four film and filter combinations tested in this experiment, infrared color film (Ektachrome Infrared, SO-180) with a Photar 15 filter (0.510 to 0.890 µm), showed the greatest promise for separating forest from nonforest areas. Extensive range lands also were photographed in this experiment, but we decided to test our sampling theories in two forested areas (9). One of these is in the Mississippi River valley and includes about 2 million hectares (5 million acres). The other area covers about 1.9 million hectares (4.7 million acres) in the states of Georgia and Alabama southwest of Atlanta, Georgia (Fig. 1).

Please keep in mind that we were concerned only with determining the potential usefulness of space photographs in an operational survey environment. We wanted to answer two basic questions: (1) can information obtainable from space photographs make a contribution toward reducing the sampling error of a timber inventory, and (2) how can support aerial photography be used in controlling the variation within relatively large primary sampling units delineated on space photographs?

Our first task was to examine the infrared color transparencies and relate color and film densities to land classes on the ground. We also needed to decide what parameter on the photo could be related to forest volume. A variable-intensity light table and a Bausch and Lomb Zoom 70 Stereoscope<sup>3</sup> were used for this examination (Fig. 2).

From this preliminary examination, we decided that the best relationship would be between forest area (proportion) and cubic-foot volume. As a population unit we selected a 6.4- x 6.4-kilometer (4- x 4-mile) block. Our reason for this was intuitive. We felt that units this large would (1) be readily identifiable from an aircraft for photographing at a larger scale, (2) be large enough that we could make a meaningful prediction of timber volume, and (3) be large enough that between-unit variation in timber volume per acre of forest land would be relatively low within identifiable strata.

Range scientists at the Rocky Mountain Forest and Range Experiment Station, Forest Service, U. S. Department of Agriculture, Fort Collins, Colorado, are studying correlations between vegetation types and photographic images in preparation for multistage sampling surveys in Southwestern United States.

Trade names and commercial enterprises or products are mentioned solely for necessary information. No endorsement by the U. S. Department of Agriculture is implied.

We found there are two fairly homogeneous strata within the Mississippi area (10). One stratum is predominantly upland pine and hardwood and the other stratum is predominantly bottomland or upland hardwoods without any significant pine (Fig. 3). Since the Apollo 9 mission was flown in early March when the hardwood (deciduous) forests were defoliated, these forests were represented by a bluish green color on the infrared film. Hardwoods that occurred along streams and rivers (bottomland hardwoods) registered as a medium to dark blue. The darker blue occurred in many places in the Mississippi valley where streams and rivers had overflowed their banks. Pine forest, primarily loblolly pine (Pinus taeda L.), and shortleaf pine (Pinus echinata Mill.) in pure stands were highly infrared reflectant and had a dark purplish red color on infrared color transparencies. We also found that pine is darker than pure hardwoods. Thus, stands appear to have a mottled texture where small clumps of pine and hardwoods grow together.

In the Georgia-Alabama area, homogeneous strata were more difficult to define on the space photograph. Here the entire area is more or less homogeneous with blocks of pure pine, hardwood, and mixed stands broken by agricultural fields (Fig. 4). However, we finally decided on two strata--one that is predominantly agricultural and one that is predominantly forest. Our reason for this was intuitive. We felt that forest land in a predominantly agricultural area would reflect differences in site and should represent a different population strata. I will discuss the results of this a little later. For now, I would like to limit myself to the Mississippi valley portion of the forest inventory test.

The first level of information for the forest inventory was derived by subdividing the space photograph into blocks approximately 6.4- x 6.4-kilometers (4- x 4-miles) in size or 4,144 hectares (10,240 acres) (Fig. 5). There were 480 of these population units. After the primary sample units had been delineated, each block was examined with the aid of a 7X power stereoscope (Fig. 2). From this examination the interpreter estimated the proportion of forest land. This estimate was used as a prediction of the relative timber volume in the block. After all squares had been examined and predictions made, a sample of five blocks were drawn at random with probability proportional to the predicted volume. One of these blocks is shown enlarged about 16 times in Figure 6.

Between April 15 and April 24, 1969, the Forest Service remote sensing research aircraft<sup>4</sup> and crew flew photographic missions in support of this inventory study. The five primary sample blocks selected were flown with a camera package that consisted of a Crown Graphic camera with a Polaroid back and two Maurer KB-8 70 mm. cameras mounted in a single frame (Fig. 7).

The first stage of the inventory was a 1:60,000 scale Polaroid mosaic for each primary sample block. We used Polaroid to obtain and rapidly interpret the imagery while still airborne. Why this was necessary will be explained later.

Stationed at the Pacific Southwest Forest and Range Experiment Station, Berkeley, California.

The 1:60,000 scale was chosen so that the entire sample block would fit within a 101.6- x 127.0-mm. (4- x 5-inch) film format in one photographic pass. When the Polaroid mosaic had been constructed, a transparent overlay was used in the aircraft to divide the primary samples into 12 equal strips (Fig. 8). These strips represented a path approximately 536 meters (1,760 feet) wide on the ground. Here is where Polaroid photos were necessary. We could examine the strips quickly while still in the aircraft and predict the timber volume based upon the proportion of forest in each strip. The forest information on these photographs was sufficient for predicting timber volumes as a basis for selecting strips for the next stage. Using this second level of information, we selected two random strip samples in each block with probability proportional to the predicted volume in each strip. A hand-operated adding machine and a book of random numbers were all that were required to do this.

The selected strips were marked on the Polaroid mosaic and the mosaic handed to the aircraft pilot. Using the mosaic as a flight map, the pilot flew over the two strips with two 70 mm. cameras operating simultaneously. One camera with a 38 mm. (1-1/2 inch) lens photographed the strip at a 1:12,000 scale in negative color (Fig. 9). Meanwhile, the second camera with a 228-mm. (9-inch) lens was triggered in bursts of 3 exposures at 8- to 10-second intervals to produce three 1:2,000 scale color transparencies with 60 percent overlap (Fig. 10). The 1:12,000 photography covered the entire strip, whereas the 1:2,000 scale photo triplets consisted of a systematic sample with a random start taken down the center of the strip (Fig. 11).

We returned to our headquarters in Berkeley where the 1:12,000 scale photographs were printed and assembled into strip mosaics. The exact boundaries of the strips were delineated on the mosaics. Then, the photo coordinates of these boundaries were digitized at 0.254 mm. (0.01 inch) intervals using a Bendix Datagrid digitizer (Fig. 12). The area within each strip was computed from these data. The proportion of the strip covered by the 1:2,000 scale photos was computed from the number of 1:2,000 scale photographs obtained in a strip and the area of the strip. The inverse of this proportion was used to expand the timber volume estimates from the cluster to the strip level.

The 1:2,000 scale clusters of color transparencies made up stage three of the survey design. They were made up of three pictures with 60 percent overlap to provide stereoscopic coverage of the center frame. There were from 13 to 20 triplets per strip, depending on airspeed and altitude; the total for all triplets was 175.

The center photograph of each triplet was divided into 4 square plots equal to approximately 0.25 hectare (0.6 acre) each (Fig. 9). This size plot is convenient for locating and measuring on the ground.

Each large-scale photo plot was examined stereoscopically and stand height, crown closure, and crown diameter measured. Stand height was measured with a parallax wedge, crown diameter with a crown diameter wedge, and crown closure with a dot grid. With these three measurements, a composite cubic-foot volume table was entered and the volume read for each plot (11). Separate estimates were made for pine and for hardwood. From the total photo plots in each strip, one plot was selected for measurement on the ground. Again, the selection

probabilities were proportional to the predicted timber volume at this level.

Each selected plot was located on a 23-  $\times$  23-cm. (9-  $\times$  9-inch) enlargement of the 1:12,000 scale and 1:2,000 scale photographs. A packet of these photos was given to a field crew to aid in locating the plots on the ground.

Each plot was precisely located on the ground and the perimeter marked with a string line. Each tree's diameter was measured and recorded by species. A separate tally was kept for hardwoods and softwoods. The tree diameters were used to predict each tree's volume from a volume table. The timber cruiser adjusted each tree volume for defects and deformities in the tree. Then using these predictions, four to six trees were selected (a minimum of two in hardwoods and two in softwoods) on which precise measurements were made of bole characteristics using an optical dendrometer (Fig. 13). The solid wood volumes of these sample trees were calculated by computer from the dendrometer measurements.

After the tree volumes were obtained at the last stage, they were expanded back through the sampling formula to obtain an estimate of the total volume of timber present in the survey area, i.e., the area covered by the Apollo 9 photography.

The estimated timber volume in each stratum is computed from this equation:

$$v = \frac{1}{m} \sum_{i=1}^{m} \frac{1}{p_{i}n_{i}} \sum_{i=1}^{n_{i}} \frac{1}{p_{i}} \frac{A_{j}}{a_{c}} \frac{1}{p_{p}t_{p}} \sum_{i=1}^{n_{p}} \frac{v_{k}}{p_{k}}$$

in which

v<sub>k</sub> is the measured volume of the k<sup>th</sup> sample tree on a selected ground plot,

p<sub>k</sub> is the probability of selecting the k<sup>th</sup> sample tree,

p is the probability of selecting the p<sup>th</sup> plot from the cluster of plots delineated on the 1:2,000 scale 70 mm. photos in a strip

p, is the probability of selecting the j<sup>th</sup> sample strip in a sample 4- by 4-mile square area,

p, is the probability of selecting the ith sample square

 $a_{\ \ c}$  is the area covered by the cluster of 1:2,000 scale 70 mm. photographs within a strip,

A is the total area of the j<sup>th</sup> sample strip,

t is the number of sample trees measured on the pth plot,

n<sub>i</sub> is the number of sample strips in the i<sup>th</sup> 4- by 4-mile square, m is the number of 4- by 4-mile squares included in the primary sample.

Judging our results in relation to the original objectives, we would have to say that we met both success and setbacks. In the Mississippi area, we estimated the gross total volume at 63 million cubic meters (2.225 billion cubic feet) of timber with a sampling error of 13 percent using only 10 ground plots. This constitutes a sampling intensity of one to one million in terms of area. Half the error was attributed to the tree volume tables used on the ground to relate to dendrometer measurements. If we had used the sampling plan, but used random sampling with equal probabilities at the first stage and without stratification, the sampling error would have been 30.7 percent. By combining the benefits from stratifying on the space photographs with the benefits of variable probability, we reduced the error to 13 percent. This is a 58 percent reduction in sampling error (from 30.7 percent to 13 percent) directly attributable to information interpreted on the Apollo 9 photographs.

There is no standard sampling design for all forest inventories. This was exemplified in the Georgia area inventory where we were not very successful; in fact, the results were disappointing. Using exactly the same sampling plan as in Mississippi, we estimated a gross total volume of 75.6 million cubic meters (2.670 billion cubic feet) of timber. The sampling error was a high 30 percent. More important to our test, we were unable to show a gain in sampling efficiency as a result of using information on the space photographs. This failure was a result of poor correlation between our predicted volumes on the primary sample units--made on the space photographs--and estimated volumes on the corresponding sample blocks found by subsampling on the ground.

We are continuing to study the Georgia area to isolate the sources of variation at each stage in the sample. By this means we hope to be able to learn ways of reducing the sampling error and improve the multistage sampling design to suit this area.

# DISCUSSION

I have devoted most of my lecture to one forest inventory application of remote sensing. This was necessary because of time limitations. However, it would be unfair not to mention a few other challenging applications of remote sensing that are related to surveys of our forest and range resources. One of these--remote sensing to detect stress symptoms in forest and range vegetation-is being discussed at another session. Another potential application of remote sensing that is being studied is the relationship between vegetation, soil, and water. Here, hydrologists hope to find relationships that will be useful in managing surface and subsurface water supplies (12).

One of our Forest Service range research projects at Fort Collins, Colorado, is studying remote sensing in connection with rangeland inventories (13). They have found that infrared color photographs taken from space provide a synoptic base for classifying and prestratifying groups of associated plant communities. These photographs provide information on the location and areal extent of

generalized vegetation types and are useful for broad land-use planning and management decisions. However, for quantitative information about the plant communities in these generalized strata, multiscaled sample photography is necessary. For instance, range scientists have found 1:80,000 color and infrared color films good for mapping ecosystem boundaries. But, 1:20,000 scales are required to map units where only subtle image differences exist between units. To measure range plant density and dispersion by species, range scientists have found that scales larger than 1:2,400 are most helpful.

I hope that I have, in this very short period, brought to you a reasonable picture of the state of the art in remote sensing for forest and range inventories and mapping. We still have a long way to go before some of these techniques can be used on an operational basis. However, by the time the Earth Resources Technology Satellites (ERTS) and Skylab space missions are flown in 1972, we should be able to tell what kind and what quality of information can be extracted from remote sensors and how it can be used for surveys of forest and range resources.

## REFERENCES

- 1. Larsh, R. N., P. R. Miller and S. L. Wert. 1970. Aerial photography to detect and evaluate air pollution damaged ponderosa pine. Jour. of the Air Pollution Control Assoc. 20(5):289-292.
- Forest Service, U. S. Dept. of Agr. 1965. Timber trends in the United States. Forest Resource Report No. 17, p. 113-136.
- 3. Wilson, R. C. 1950. Controlled forest inventory by aerial photography. The Timberman, 51(4). 4 pp.
- 4. Harris, R. W. 1951. Use of aerial photographs and subsampling in range inventories. Jour. of Range Mangt. 4(4):270-278.
- 5. Seely, H. E. 1964. Canadian forest inventory methods. Dept. of Forestry Pub. No. 1068. Forestry Research Branch, Ottawa, Canada. 11 pp.
- 6. Cochran, W. G. 1959. Sampling techniques. Ed. 2, 330 p. New York: John Wiley & Sons, Inc.
- 7. Langley, P. G. 1969. New multi-stage sampling techniques using space and aircraft imagery for forest inventory. Sixth Internat1. Symposium on Remote Sensing of Environment Proc. 1969:1179-1192.
- 8. Wert, S. L., and B. Roettgering. 1968. Douglas-fir beetle survey with color photos. Photogramm. Engng. 34(12):1243-1248.
- 9. Langley, P. G., R. C. Aldrich and R. C. Heller. 1969. Multi-stage sampling of forest resources by using space photography--an Apollo 9 case study. Second Annual Earth Resources Aircraft Program Status Review. Vol. I, Geology and Geography. Manned Spacecraft Center, NASA, Houston, Texas. Section 19:1-21.

- 10. Aldrich, R. C. 1970. Space photographs separate land use and aid in forest inventories. Paper presented at the March 1970 joint annual meeting of the ACSM and ASP, Washington, D. C. (In Press.)
- 11. Avery, G. 1958. Composite aerial volume table for southern pine and hardwoods. Jour. For. 56:741-745.
- 12. Stewart, Joseph W. 1969. Synoptic remote sensing survey of lakes in west-central Florida. Second Annual Earth Resources Aircraft Program Status Review. Volume III, Hydrology and Oceanography. Manned Spacecraft Center, NASA, Houston, Texas. Section 38:1-31.
- 13. Driscoll, R. S. 1969. The identification and quantification of herbland and shrubland vegetation resources from aerial and space photography. Annual Progress Report for the National Aeronautics and Space Administration. Rocky Mountain Forest and Range Exp. Sta., Fort Collins, Colorado.

# GLOSSARY OF TERMS

Cluster: All photo triplets within a sample strip.

Crown closure: Proportion of total ground covered when tree crowns are projected vertically to the ground (measured with a dot grid template).

Crown diameter wedge: A simple device printed on transparent film to measure tree crowns in units of 0.0254 mm. (0.001 inch) between two diverging calibrated lines.

DBH (d.b.h.): Diameter at breast height.

Dendrometer (optical): An optical device somewhat similar to a range finder used to measure precise tree bole diameters and vertical heights.

Dot grid: A systematic pattern of dots printed on transparent film. The number of dots per unit of area is varied depending on the intensity of sampling required.

Hardwoods: Angiosperms. Usually deciduous but sometimes persistent leaves.

Hardwoods, upland: Occurring on upland, dry or well-drained sites.

Hardwoods, bottomland: Occurring on low, wet, poorly drained sites.

Large-scale: Aerial photographs with a representative fraction of 1:500 to 1:10,000.

Medium-scale: Aerial photographs with a representative fraction of 1:12,000 to 1:30,000.

Multistage: More than two sampling levels in the sampling design.

Multiscaled: More than one aerial photographic scale used in the sampling design

Parallax wedge: A simple device printed on transparent film used to measure parallax difference between the bottom and tops of trees on overlapping photographs. Differences in parallax are usually measured in units of 0.001 mm. and converted to tree height using conversion tables.

Photo coordinates: The x and y position of data points referenced to a common origin.

Plot: A unit of area selected for measurement of forest variables; type, volume site, growth, etc.

Population unit: A single member of a defined population.

Primary sample: Population units selected for the first stage in multistage sampling surveys.

- Probability: The mathematical basis for prediction. For an exhaustive set of outcomes, probability is the ratio of the outcomes that would produce a given event to the total number of possible outcomes.
- Probability, arbitrary: Samples selected at random without judgment.
- Probability, variable: Samples selected at random from a variable set of values. The probability of selecting any member of the set is dependent on its value; size, area, volume, diameter, height or others.
- Probability proportional to size: The probability of a sample being selected is dependent on the size of the units to be sampled; area, volume, diameter, height, or others.
- Sampling error: The standard error of the estimate. A measure of the variation that might be expected between sample estimates if repeated estimates were made. Variation depends on the sampling method, the sample size, and the variability among the individual units in the population sampled.
- Small-scale: Aerial photographs with a representative fraction smaller than 1:40,000.
- Strata: Areas of the same or similar forest type, volume, site, or other interpretable quality.
- Stratification: Dividing an area into strata.
- Timber cruiser: Term used to describe a forester or forestry technician who estimates, measures, marks, and records a tally of forest trees according to some prescribed sampling design.
- Triplet: Three overlapping (60 percent) aerial photographs used as a photo sample.
- Volume table: Tree volumes by d.b.h. and merchantable height by tree species.
- Volume table, composite: A volume table for both softwoods and hardwoods.

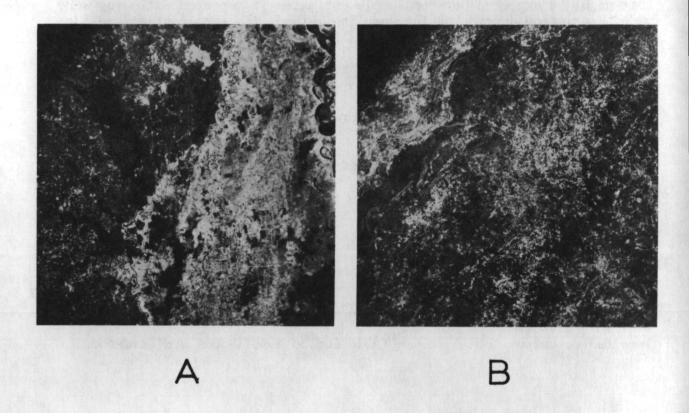


Figure 1. Apollo 9 photographs of the Mississippi area (A) and the Georgia-Alabama area (B). These illustrations were made from infrared color transparencies.

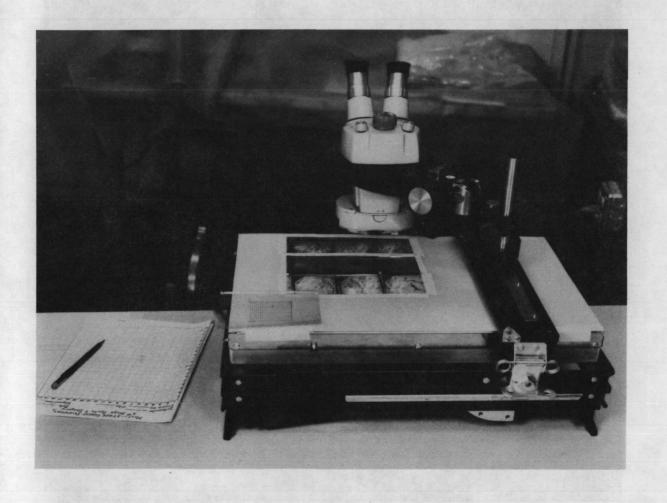


Figure 2. A Bausch and Lomb Zoom 70 Stereoscope on a Richards variable-intensity light table was used to interpret the small-scale imagery.



Figure 3. Apollo 9 frame 3740 enlarged 2.5X to illustrate two strata; predominantly pine with upland and bottomland hardwoods (A), and predominantly upland and bottomland hardwoods with little or no pine and associated with cultivated fields (B).



Figure 4. Apollo 9 frame 3792 enlarged 2.5X to illustrate two strata; predominantly agricultural  $(\underline{A})$  and predominantly mixed pine and hardwoods  $(\underline{B})$ .

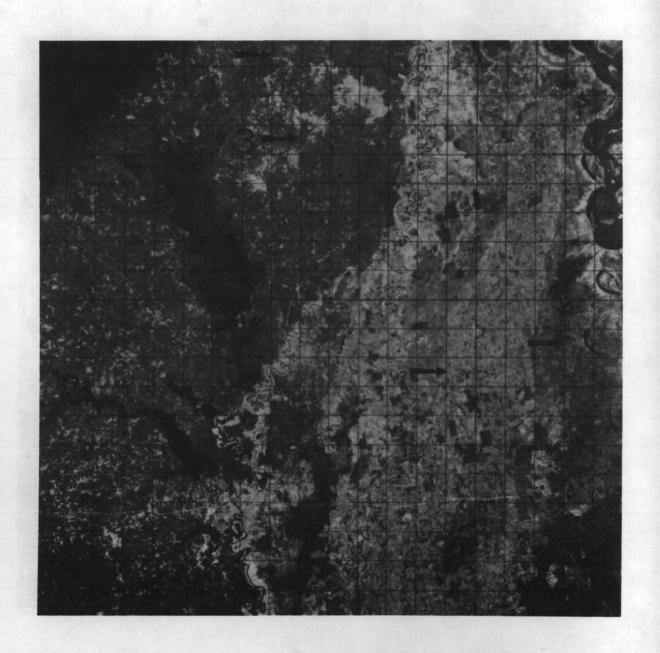


Figure 5. The interpreted portion of Apollo 9 infrared color frame 3740 for the Mississippi area shown with 6.4- x 6.4-km. (4- x 4-mile) grid template attached. Black arrows point to first-stage sample blocks--the sample block at (3) in the upper left-hand corner appears in Figure 6.

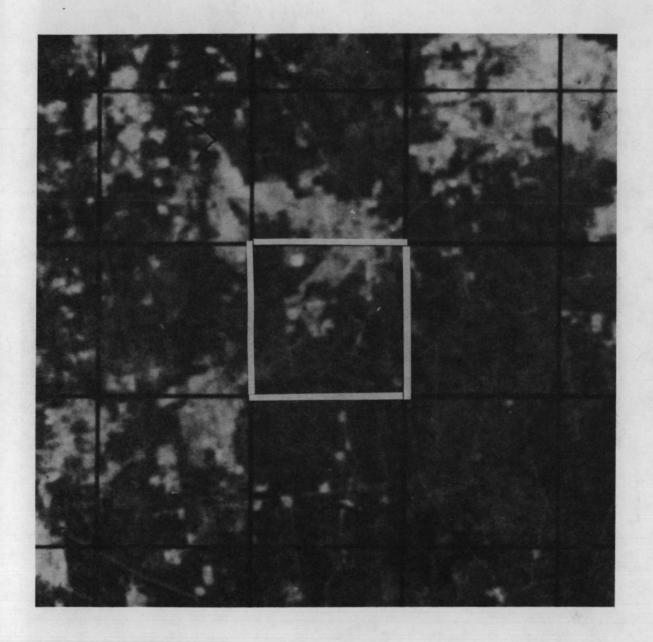


Figure 6. This 16X enlargement of a portion of the space photo shows one of the first-stage samples in the Mississippi area. The block outlined in white appears at (3) in Figure 5 and is also shown in Figure 8.

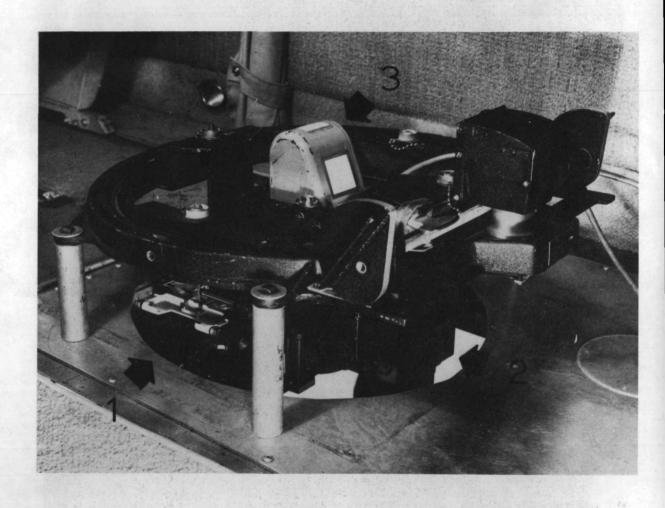


Figure 7. This aerial camera setup was used to obtain support photography for primary sampling units selected from the space photographs: (1) Crown Graphic with Polaroid back and 75 mm. lens; (2) J. A. Maurer KB-8 70 mm. camera with 38 mm. lens; and (3) J. A. Maurer KB-8 with a 228 mm. lens.

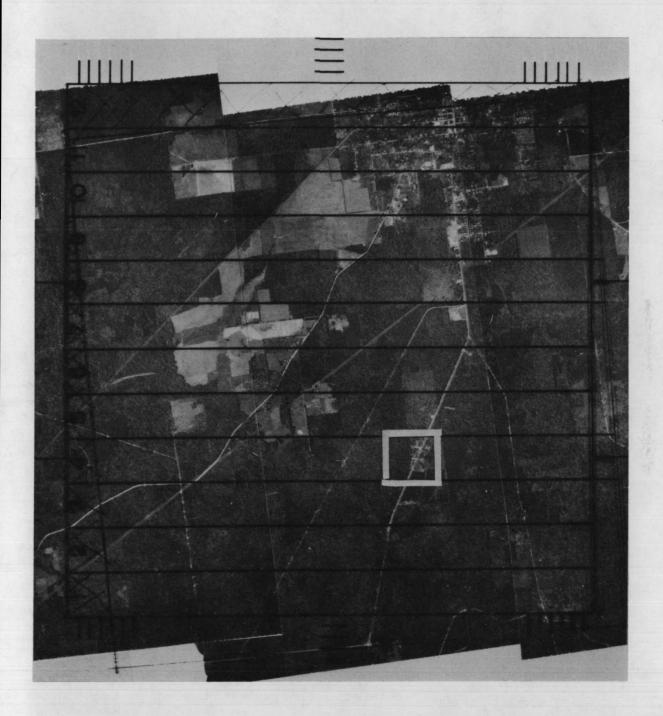


Figure 8. The first stage of the forest inventory is a 1:60,000 scale Polaroid photo mosaic for each sample block selected from the Apollo frames. Block (3) is shown with a grid overlay used to select two strips for the next sampling stage. This block appears at (3) in Figure 5 and also in Figure 6. The area outlined in white corresponds to the 1:12,000 photo coverage in Figure 9.

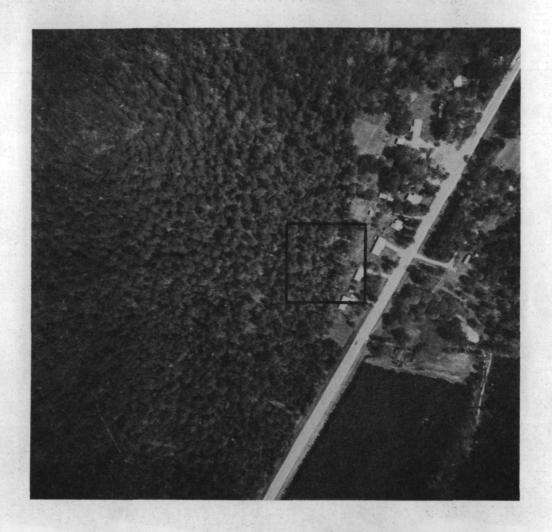


Figure 9. This 1:12,000 scale photograph covers the area outlined in white in Figure 8. The area outlined in black corresponds to the coverage of the 1:2,000 scale photograph shown in Figure 10. Each sample strip was completely covered by 1:12,000 scale photography. The photo shown is a 2.2X enlargement made from negative color film.



Figure 10. This 1:2,000 scale photograph corresponds to the area outlined in black on the 1:12,000 scale photograph in Figure 9. The grid divides the center photograph (shown) of each sample triplet into four plots approximately 0.25 hectares (0.6 acres) in size. Photo is a 2.2X enlargement made from the original 70 mm. color transparency.

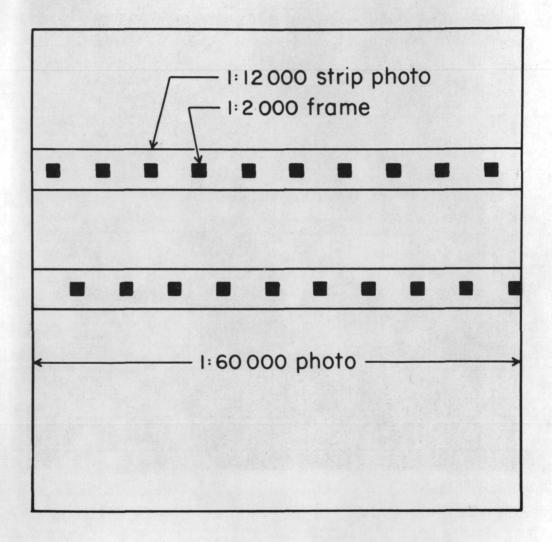


Figure 11. The scaled diagram shows how the two 1:12,000 scale 70 mm. photo sample strips and 1:2,000 scale 70 mm. color samples are related to each other and to the 1:60,000 scale Polaroid photograph.



Figure 12. Photo coordinates of sample strip boundaries outlined on 1:12,000 scale photo mosaics were digitized at 0.254 mm. (0.01 inch) intervals by using this Bendix Datagrid digitizer.



Figure 13. Ground crews used Barr and Stroud optical dendrometers to measure the boles on 4 to 6 trees on each ground plot.

Page Intentionally Left Blank

# DETECTION AND CHARACTERIZATION OF STRESS SYMPTOMS IN FOREST VEGETATION

by

Robert C. Heller

## BIOGRAPHICAL SKETCH

Robert C. Heller is a research forester and project leader of a Forest Service, U. S. Department of Agriculture nationwide project called "Remote Sensing Related to the Forest Environment." The project is located at the Pacific Southwest Forest and Range Experiment Station in Berkeley, California. Studies are being conducted in forest and range inventory, insect and disease detection, spectral reflectance and emittance responses from forest vegetation, and automated interpretation systems.

He attended Duke University, Durham, North Carolina, for both his undergraduate and graduate studies in botany and forest management. Supplementary graduate work was taken at the University of Maryland in entomology. Aerial color, infrared color, and 70 mm. sampling photography have been adapted to many forestry applications as a result of Mr. Heller's efforts. He has been a member of the Committee on Remote Sensing for Agricultural Purposes formed by the National Academy of Sciences - National Research Council. This committee recently published (1970) a comprehensive book called Remote Sensing, with special reference to agriculture and forestry which is relevant to the presentation at this meeting.

#### DETECTION AND CHARACTERIZATION

#### OF STRESS SYMPTOMS IN FOREST VEGETATION

by

## Robert C. Heller<sup>1</sup>

#### INTRODUCTION

Forest managers in the United States must keep 212 million hectares (509 million acres) of commercial forest land under their surveillance. Much of this area is roadless. The condition of the forest varies seasonally and annually, depending upon weather and destructive agents at work. About 40 percent of the ownerships are large and employ some level of forest management; the remaining ownerships are small, privately owned, and mostly are not under management. Inaccessibility, rapid changes, and differences in practice have made it increasingly clear that better remote sensing methods are needed to develop new techniques to aid decision making in resource management.

I know that remote sensing requirements will vary widely in your own countries, according to size and availability of timber stands and the level of forest management practiced. Let me describe our work, at the Pacific Southwest Forest and Range Experiment Station, to detect advanced and previsual symptoms of vegetative stress. Perhaps you can benefit from our good and bad experiences.

I will talk primarily about stresses caused by bark beetles in coniferous stands of timber, because beetles induce stress more rapidly than most other destructive agents. Bark beetles are also the most damaging forest insects in the United States. Our studies have been carried out jointly by the Forest Service, U. S. Department of Agriculture, and the Earth Resources Survey Program, National Aeronautics and Space Administration. In the work on stress symptoms, we have two primary objectives: (1) to learn the best combination of films, scales, and filters to detect and locate injured trees from aircraft and space-craft and (2) to learn if we can detect stressed trees before visual symptoms of decline occur.

# VIGOR LOSS IN PLANTS

What do we mean by stress symptoms in vegetation? Stress is caused by loss of vigor which indicates an abnormal growing condition. Causes for loss of vigor are disease, insects, moisture deficiency, soil salinity, absence of trace elements or soil fertility, etc. Because stress symptoms to vegetation are similar regardless of agent, the particular cause must be verified on the ground. Unique patterns or differential rates of spread often reveal the cause. Such a situation

Research Forester, Pacific Southwest Forest and Range Experiment Station, Forest Service, U. S. Department of Agriculture, Berkeley, California, U. S. A.

occurred in Honduras, Central America, in 1963 and 1964, when a tiny bark beetle (Dendroctonus frontalis, Zimm.) multiplied to epidemic proportions and killed about 60 percent of the merchantable sawtimber in an 18-month period. Successive rings of dying trees could be marked by the differential coloring of the pine foliage. The first-killed timber appeared red, the next ring yellow-red, then yellow to yellow-green, and around that green timber, perhaps dying from the insect attack but not yet showing discoloration.

When the foliage discolors over wide areas, aerial color photography (natural color or false-color transparencies) is an efficient sensor at medium scales (1:5,000 to 1:8,000). For example, photo interpreters with training can locate, separate, and plot dying trees accurately enough on transparencies to plan control and salvage operations (1, 3). They can also estimate losses from epidemics over wide areas (11) in a short period of time. One must recognize, however, that such techniques provide the forest manager with de facto evidence. That is, the vegetation has long passed the stress point and is, in fact, dead.

The forest manager could be many times more effective if he could detect the trees in early stages of stress. He could apply insecticides or remove the beetle populations from the woods by salvage operations before new and perhaps larger beetle populations emerged and began a new round of tree killing. Forest entomologists hope to locate, by remote sensing methods, trees which are under stress to give advance notice of an abnormal condition and to permit early evaluation of insect population trends.

This is just one example of the importance of detecting tree stress before visible symptoms occur. Recently, sensors that detect conditions beyond the visible spectrum have been developed. Consequently, we designed a study aimed not only at detecting discolored vegetation from aircraft, but also at the previsual detection of ponderosa pine trees (Pinus ponderosa, Laws.) being attacked by the Black Hills beetle (Dendroctonus ponderosae, Hopk.).

# LOCATION OF STUDY AREA

The Black Hills, in western South Dakota and eastern Wyoming, rise to 2,200 meters (7,250 feet) from the surrounding flat to rolling plains, at about 1,100 meters (3,500 feet). Ponderosa pine is the principal commercial tree. It occurs primarily above 1,200 meters (4,000 feet). The total sawtimber volume in the Black Hills is estimated to be 2.3 billion board feet.

A serious epidemic of the Black Hills bark beetle has been under way since 1960 (Fig. 1). A study area about 1.6 by 5 kilometers (1 by 3 miles) was selected northwest of Rapid City, South Dakota (Fig. 2). In areas where no control efforts were exerted, beetle populations from the outbreak were continuing to kill trees in large numbers. Groups of several hundred trees were infested annually, whole hillsides of timber were destroyed, and the total infestation ran to many thousands of trees killed each year.

## COLLECTION OF GROUND AND AIRBORNE DATA

Whenever a remote sensing study is undertaken, we need to make a great many ground observations to correlate with data from the airborne platform. Usually as we learn more about the characteristics of our target areas, less ground work is needed, and we can extrapolate our airborne data over wider areas. Both ground and airborne data were measured on and over the Black Hills study site, from August 1965 through August 1969. Most ground data were monitored continuously during the tree growing season, while the aerial imagery was collected intermittently.

#### GROUND DATA COLLECTION

Biological observations which involve ecological, physiological, and meteorological interactions must be made over a time continuum. Since one of our objectives is to detect loss of tree vigor before visual symptoms occur, we are interested in the rate at which stress changes take place. To capture these changes, we measured beetle populations, numbers of infested trees, foliage color, foliage internal temperatures, needle moisture tensions, transpiration, solar radiation, soil moisture, air temperature, humidity, and wind velocity.

Most of these data are needed to compute the total energy budget which affects tree growth. For example, the data permit one to explain why trees under moisture stress may produce higher temperatures at one time of the day but not at another--even under similar sunlight conditions. One can then deduce how thermal imagery may differentiate less vigorous trees from healthy ones in one time period and not in another.

Another objective is to learn which sensors provide us with reliable evidence of past stress in the event previsual detection fails. For aerial photography, what scales, films, and filters are optimum? We know that during a bark beetle epidemic, trees likely to be attacked in the future are more likely to be related to past stressed trees. There is ample evidence that beetles tend to attack trees in clusters and usually near the site of older attacked trees. Aerial photography is particularly helpful in locating the older stressed trees, and thus we can direct our attention to these areas.

Finally, we want to learn what sizes of infestations can be detected from high-flying aircraft or even satellites. Thus, we may be able to relate known infestation sizes (groups of discolored, killed trees) to the expected and actual resolution of the Earth Resources Technology Satellite (ERTS).

## Visual Determination of Tree Decline

Once a tree is attacked by beetles, the success or failure of the attack may be in doubt to the observer--even when close ground examination is continued. One manifestation of heavy attack is the presence of pitch tubes on the outer bark. Another is boring dust--like fine sawdust--caused by the attacking beetles when boring in the cambial zone. This dust lodges in bark crevices near the ground and must be searched for very carefully. The surest method of determining whether the attack is successful and the tree will succumb is to look for blue

stain fungus (Ceratostomella spp.) in the xylem. This fungus is carried into the cambial galleries on the legs and body of the beetle and is an accelerating agent in the death of the tree. Blue stain is discovered by making small hacks into the wood with an axe. The time required to kill a tree and the likelihood that an attacked tree will succumb are both uncertain; therefore, intensive ground examinations are required for accurate appraisal. The detection of small changes in tree vigor, even on the ground, is most difficult.

The rate of foliage discoloration was followed in two ways: (1) by taking 35 mm. color photographs on the ground of 10 selected dying trees at weekly intervals from May 1 to August 30, 1967, and (2) by having one person with full color perception check all infested and healthy trees on four occasions: May, June, July, and August in both 1967 and 1968. Tree colors were identified by the Munsell color notation system described by Nickerson (7). One experienced observer compared the color of foliage of the upper tree crown in full sunlight with a series of Munsell color cards also held in sunlight.

The color chips are mounted on hue cards with holes punched between the chips to aid comparison. The foliage is viewed through the punched holes; thus, the foliage and color chip are adjacent and the eye can readily compare them. Similar vegetation studies using Munsell notations have been conducted by Nickerson (8) to discriminate between grades of cotton and by Heller et al. (4) to identify northern tree species.

By relying on one observer we reduced subjective bias and permitted quantification of the color attributes. Furthermore, we hoped to compare the ground observer's Munsell notations with ground and aerial photographs of the trees.

To assess the accuracy of photo interpretation, one must know the locations and sizes of the dying groups of pine trees, how many trees in each group, and their foliage color. Over our selected study area (1.6 by 5 kilometers) we made ground visits to over 260 known and suspected infestation centers (Fig. 3).

## Biophysical Measurements taken on Healthy and Infested Trees

A great many techniques were developed and improved over the course of this study. Most methods for previsual detection are discussed in detail by Weber  $(\underline{10})$  and Heller  $(\underline{5})$ , but a brief description follows:

Spectral reflectance of healthy, newly infested, and discolored foliage was measured by the Bureau of Standards, U. S. Department of Commerce, using General Electric, Cary Model 14, and Cary White Model 90 recording spectrophotometers. A Beckman DK-2 recording spectrophotometer was also used in later studies. Reflectance was recorded from 0.35 to 22.22 micrometers.

Internal needle temperatures of the healthy and dying pine trees were recorded continuously by means of copper-constantan thermocouples inserted into the

Mention of commercial products does not imply endorsement by the U. S. Department of Agriculture.

pine needles. Thus, we could follow the heat patterns between healthy and infested trees as they differed by time of day and by solar conditions.

Apparent (emitted) temperatures were monitored by aiming a Barnes PRT-5 (precision radiation thermometer) at healthy and insect-attacked trees from a high tower (Fig. 4). Net and total radiation thermometers are now being used in a related study (9) from tower-supported moving tramways suspended above the trees (Fig. 5). Thus, solar radiation and emitted foliage temperatures can be monitored continuously.

Relative transpiration was determined by measuring the differential sap flow between healthy and affected trees (Fig. 6).

Needle moisture tension, a measure of the tightly bound water within needles, was determined by a hydrostatic pressure bomb. Stressed foliage has less water than healthy, and by inserting the coniferous needles into a pressure bomb the amount of gas pressure required to force out the water can be related to the vigor of the tree (Fig. 7). Stressed trees require more gas pressure than healthy trees and this difference is an early indicator of stress.

Soil moisture data were collected at first with a Colman soil moisture meter, but later by a neutron probe (Fig. 8). This device measures the differential bombardment of neutrons from a nuclear source through moist and dry soils to a detector. It is important that we know soil moisture levels so that we may relate changes in transpiration rates to sap flow, solar radiation, or to soil moisture.

Wind velocity and direction are also recorded so that we may know whether excessive heat loss of foliage may be ascribed to high wind speed.

In the early stages of the study, most of the data were collected independently on separate recording instruments and analyzed separately--a slow, tedious process. In 1970, we used a data logger and the moving tramway described by Wear and Weber (9) to collect up to 38 channels of data, digitize it, and store it on magnetic tape (Fig. 9). This system permits rapid access to the data and is in computer-compatible form. It saves up to one year in the analysis of the energy budget data. I would recommend continuous ground data recording of this kind if your funding will permit it.

#### AIRBORNE DATA COLLECTION

# Aerial Photography

Color films (both natural and false color) have generally been more useful than panchromatic or black-and-white infrared emulsions for locating and accurately mapping discolored coniferous trees. In using color films, we wanted to determine (1) whether infrared color film could serve as a previsual sensor and (2) the smallest scale and best film for detecting discolored groups of beetle-infested pine trees.

To answer the first objective, we obtained very large-scale (1:1,584) photographs over known green infested trees for a two-year period. We used two KB-8 70 mm. aerial cameras equipped with 150 mm. Schneider Xenotar lenses (Fig. 10) and extremely high-speed shutters (up to 1/4,000 second). These cameras were triggered simultaneously at 0.5-second intervals for stereo overlap. Anscochrome D/200 normal color film (with a Wratten 1A filter) was used in one camera and Kodak Ektachrome Infrared film (with a Wratten 12 filter) in the other. The photographs were taken at five time periods: in October just after the trees were attacked by the beetle, the following May after snow had left the ground and the trees began growing, and in June, July, and August almost one year after attack and when foliage color progressed from green to green-yellow, yellow, and finally yellow-red.

To determine the smallest infestation size in meters (or feet) that we could resolve, we used high-altitude photography by our own Forest Service aircraft and NASA's RB-57. Tables 1 and 2 summarize the photographic combinations, taken in July and August 1969, of the large study area (1.6 by 5 kilometers). August is usually the month in the Black Hills when maximum color contrast occurs between old-killed trees, newly dying trees, and healthy green trees. Consequently, this is the one seasonal period when likelihood of detection would be greatest and resolution could be measured most accurately on film.

## Optical-Mechanical Scanning Imagery

You have already been introduced into the operation and capabilities of optical scanning instruments in your earlier session on Sensors. In 1966 and 1967, we tested infrared line scanners adapted by Stanley Hirsch for fire detection and fire mapping purposes. The instruments were designated as HRB Singer Reconofax 11 and Texas Instrument RS-7; they were primarily designed to pick up high-energy returns from forest fires. We learned a great deal about interpreting single channels of line scan imagery from these tests but could not detect dying trees. The infrared fire scanner was not designed to detect the subtle temperature differences (2° to 6° C.) occurring between healthy and infested trees.

In 1968 and 1969, the University of Michigan multispectral line scanner was flown over our instrumented test sites. It used the discrete channels shown in Table 3. Data were collected at four time periods (early morning, midmorning, early afternoon, and late afternoon) in May 1968 and July 1969. These periods coincided with maximum changes in tree metabolic activity as determined from our field measurements. We used handy-talky radios for ground-to-air communications, primarily to inform the operator of the thermal scanner about the range of apparent temperatures in ground targets. This information permits him to adjust his temperature-controlled reference plates on the thermal line scanner.

# Interpretation of Aerial Photos

The 70 mm. color and color infrared transparencies were viewed over a balanced white light source by several unbiased interpreters with 2.25X magnification lens stereoscopes. On photographic scales smaller than 1:63,360, a Bausch

and Lomb stereomicroscope was used to discriminate the healthy green from the discolored infested trees (Fig. 11). To test the previsual capabilities of color and false-color film, we built a special Munsell color comparator (4) (Fig. 12) to assign colors to the dying trees in connection with the film tests taken at very large scale (1:1,584). The Munsell film colors in the comparator permitted an interpreter to compare foliage colors on the aerial photos with Munsell colors. In turn, these Munsell notations were compared with those taken of the identical trees on the ground.

The 210 mm. format color and false-color transparencies resulting from the RB-57 flight were examined over our viewing tables with Old Delft stereoscopes (Fig. 13). The interpretations of suspected infestations were plotted on templates and the trees counted within each discolored group. In turn, these interpretations were compared with the known ground conditions on the study area. Thus we could draw conclusions on the limits of resolution at various scales.

## Multispectral Processing

#### 0.4 to 1.0 micrometer

The processing equipment at the University of Michigan's Infrared and Optics Laboratory (IROL) reflects an advanced technology in the field of multispectral image processing. The details of the multispectral discrimination technique, which employs a tape-loop training device, are described by Hasell et al. 1968 (2). In effect, we are trying to exploit the energy return from our targets in very narrow segments of the electromagnetic spectrum; some segments, or wavebands, contribute more than others. The analog and digital computers connected with the electrical signal outputs are programmed to select those wavebands which, when combined, best identify the targets we are interested in. The targets for which we furnished ground information and wished positive separation were: healthy pines, nonfaded-infested pines, faded (discolored) infested pines, and old-killed pines with few or no needles.

To locate training examples on the scanning imagery, the operator needs a good aerial photograph (color or black-and-white) showing the images in their proper spatial orientation. Next, analog printouts of each waveband are made on 70 mm. film strips which preserve the shape and pattern relationship of the original scanner imagery. These printouts (analogs) are useful to a new investigator who may be unfamiliar with each waveband response. Of more interest are the combined wavelength printouts which are made on individual transparent film strips only of the targets of interest. Through the use of special color diapositive material, these combined waveband printouts can be coded in color. Then, each color-coded strip and its respective recognition spots are placed over the analog of the original imagery to re-establish spatial orientation with respect to the "ground truth." Color prints can be made of this packet of templates. The prints show the tree condition classes of interest, and each class is recognized as a different color spot (Fig. 14).

## Reflective IR and Thermal Processing

#### 1.0 to 13.5 micrometers

On the Infrared and Optics Laboratory (IROL) scanner, because there is not perfect registration of all five channels of reflective and thermal infrared imagery to satisfy requirements for multiple-channel processing, some infrared channels are processed individually. There are several techniques for displaying the thermal responses of the target temperatures on the infrared imagery. Two of the most effective are: (1) combining two channels of reflective infrared with the 4.5 to 5.5 micrometer thermal channel and then varying voltage levels to produce reliable signatures of the targets and (2) using the 8.5 to 13.5 micrometer channel and producing a series of color printouts which represent targets of equal temperature (Fig. 15). This latter technique, known as thermal contouring, capitalizes on the fact that the calibration plates in the scanner are set to include the range of temperatures of the ground targets. Targets of higher or lower temperatures can be overlooked.

## ANALYSIS AND RESULTS

Let us first consider the application of aerial color photography to stress detection--including previsual possibilities, comparison of color and false-color film, and the effect of smaller scales on detection accuracies. Next, the results on previsual detection with multispectral scanners and processors.

#### AERIAL PHOTOGRAPHY

In general, we have learned a great deal about the biological and physical changes in pine trees as they begin to die and how these changes are reflected in the photographic image. The visual and photographic color changes which show up on the ground and on large-scale aerial transparencies (1:1,600) vary with the length of time since the stress (beetle attack) was imposed.

## Visual Determination of Tree Decline

The visual comparisons of foliage color made by one ground observer with the prepunched Munsell hue charts are shown in Figure 16. At a glance one can see the shift in hue of the dying trees (sample size 209) as the season progressed from May through August. For example, in May about 75 percent of the infested trees were green-yellow, whereas in August the same percentage of trees were yellow-red. The greatest shift from the normally healthy green-yellow (5 GY and 2.5 GY) foliage to off-green foliage (2.5 GY and 10 Y) seems to take place during the fall following attack until the next May.

About 10 to 15 percent of the healthy trees in May, June, and August have a slightly yellow hue (2.5 GY) which is similar to early fading of infested trees. In July, the healthy trees appeared greener; this is probably a result of new needle growth and dropping of old (dead) needles.

When foliage is healthy, it is fairly dark--the average Munsell value (lightness or darkness) being 5 and the chroma (color strength) 4 to 6. When the tree loses vigor it becomes lighter (the Munsell value goes up to 6 and 7). The ground observer also noted during May and June that infested trees appeared lighter and more silvery than healthy trees while both still had the same hue. As infested foliage changes to yellow, the trees become still lighter and the Munsell value becomes 7 to 8 with little change in chroma. The chromas increase appreciably as the foliage becomes drier later in the summer and tends toward the orange or yellow-reds (7.5 YR and 5 YR). It is at this stage in late July, August, and September that the infested trees have their highest reflectivity in the visible spectrum. Note that even in August about 12 percent of the infested trees have the same hues as healthy trees. These trees may either not die, and consequently not change color, or may succumb, and discolor in September and October. The ground inspection in October revealed that 17 percent of the infested trees did not die or change color.

Munsell readings made from the ground of 10 sample infested trees are compared with Munsell readings made from ground color photos and with aerial color photos in the discussion of photo interpretation results.

Ground readings of infested trees were made one year later (1968) of an entirely different population of trees, but it was interesting to note that the August foliage colors were nearly identical to the 1967 August readings. The use of Munsell cards in the field is a reliable indicator of early and late stress symptoms and can be used in similar studies of vegetative stress.

Munsell notations vary by the three methods in which they were used, namely: (1) by ground comparison of the Munsell charts with the 10 sample trees in the field, (2) by comparison of the aerial photo images with Munsell transparencies, <sup>3</sup> and (3) by comparison of the 35 mm. color photos taken of the same 10 trees on the ground with Munsell transparencies. The hue comparisons made from the 10 representative trees are shown graphically in Figure 17. There is good agreement between the ground observations and those made of the identical aerial photo images; they are not over one hue apart at any time period. Note that the aerial photos detected an earlier changeover from the GY (green-yellow) hues to the Y (yellow) hues as compared with the ground observations. The ground photography did not correlate at all well with either the aerial transparencies or the visual ground Munsell comparisons of foliage. We advise against using ground color photography if very accurate comparisons are to be relied upon.

# Infrared Color versus Normal Color Film for Stress Detection

In coniferous timber, our studies over a three-year period have shown that photo interpreters can distinguish discolored pines as well on normal color film

A special viewer, developed and described in a previous study (4), permits an interpreter to select Munsell color chips by transmitted light while viewing 70 mm. transparencies stereoscopically, also by transmitted light.

as on false-color film (Fig. 18) in the Black Hills (5). Even at very small scales (1:174,000) no differences in interpretation accuracies could be ascribed to films (Fig. 19). At no time did either normal color film nor false-color film detect stressed pine trees before the foliage discolored. In other words, infrared color film cannot be used as a previsual sensor of stress for ponderosa pine. Probable reasons are described in detail by Knipling (6) and Heller (5).

Infrared color film does show advantages for other forest applications, particularly when coniferous and hardwood species are difficult to distinguish, or when atmospheric haze is unfavorable. The Wratten 12 or 15 yellow filter, always used with infrared color film, absorbs blue light and permits better atmospheric penetration. Under severe haze, infrared color film should always be used.

## Detection Success of Finding Various

## Sizes of Discolored Infestations on Aerial Photographs

How small a discolored spot (infestation) can we detect on small\_scale aerial photography? You will recall that we hope to relate known infestation sizes with resolution capabilities of sensors used on very high-flying aircraft (above 15,000 meters) or satellites (ERTS, Skylab, etc.).

The large study area (1.6 by 5 kilometers) was found to have a distribution of infestations and trees grouped into the following size classes:

Size Class (number of discolored trees per infestation)	Average Largest Dimension (meters)		Number of Infestations	Percent of Total	
	<u>m.</u>	(ft.)			
1 - 3	5	(16)	109	52	
4 - 10	13	(43)	49	23	
11 - 20	24	(80)	27	13	
21 - 50	45	(149)	16	8	
51 - 100	53	(175)	3	1	
100+	122	(403)	7	3	
			211	100	

Our results are shown in Figures 19, 20, and 21. Figure 19 compares interpretation success on two films (color and color infrared) by seven scales, and with two seasonal differences. Again, we see very little difference between the two films; a "t" test showed no significant differences. As might be expected, detection success fell off as the scales and images became smaller. July photography, taken before all stressed trees became discolored, was significantly poorer than August photography.

Figure 20 indicates that small infestations, 1-3 trees (5 m.), are not likely to be detected at acceptable accuracies when scales are smaller than 1:31,680. However, infestations of 4 to 10 trees (13 m.) can be detected at scales around 1:100,000 with an accuracy of about 20 percent. Not good but still detectable.

Figure 21 again compares the two color films (color and false color) but by infestation size in meters. Again, as infestation size (or resolution size) becomes large, detection success improves; however, detection success is acceptable only on the larger infestations (over 30 m. in size and more than 20 trees) when scales are as small as 1:174,000. For determining stress in the early stages of an epidemic, it is apparent that we will need good resolution capabilities—probably 5 meters (16 feet). For discovery of stress in very remote areas or in developing countries, we may be able to detect discolored timber with resolution capabilities of 30-50 meters (100-200 feet). Based on the expected resolution (100 meters) of the two ERTS sensors—the return-beam vidicon and the 4-channel line scanner—it seems unlikely that we will be able to detect any but the largest discolored areas. Resolution and sensor capabilities of Skylab I and II sound more promising. For stress detection, perhaps ERTS data will prove most helpful in learning how to use the mass of data most effectively.

#### PREVISUAL DETECTION WITH MULTISPECTRAL SCANNERS

I should emphasize that our studies with multispectral scanners are still experimental and not ready for application. The results are encouraging, and we should expect more improvements with better sensors and automatic processors. Line scanning is readily adaptable to automatic combining and processing of waveband data. Automatic data processing is a necessity for handling the great mass of data which will pour out from ERTS.

The "ground truth" data collected continuously through the growing season permitted us to learn the optimum conditions for sensing with the Infrared and Optics Laboratory (IROL) multispectral scanner. We learned, for example, that needle temperatures of both healthy and stressed ponderosa pine trees reached ambient air temperatures after sundown; therefore, thermal sensing for stress would be useless at night.

Figure 22 represents the ground conditions that existed at the instrumented test site in May 1968. Note particularly the first three graphs which reflect the respiratory conditions of the stressed and healthy trees. Inhibition of transpiration in stressed trees is probably the main factor which permits us to sense temperature differences. The dying tree still transpires, but at a reduced rate, because of stomata and needle desiccation (Fig. 23) and because of reduced sap flow. Needle and foliage temperatures—measured with thermocouples and radiation thermometers—at the time of the flight (1530 hours) showed a 5° C. emission temperature difference. This difference is detectable on the IROL thermal scanner. Such basic physiological information is needed to predict when thermal or spectral differences should occur. It also permits the investigator to specify what kind of sensor is required to detect targets on the ground.

## Multispectral Processing

The spectral processing and recognition computer (SPARC) at the IROL could discriminate the four target signatures for which training samples were established, namely healthy pines, nonfaded infested pines, faded infested pines, and old-killed pines. The combination of wavebands which best identified these targets are shown in Table 4.

Four analog printouts are shown in Figure 14; the target identifications show as dark spots on the darker analog print of the area. A color slide of this scene has been prepared which shows these black spots in color; the color code is: green for healthy trees, amber for nonfaded infested trees, red for faded infested trees, and blue for old-killed trees. The level of accuracy of correctly identifying the nonfaded trees is low, and the rate of making commission errors in this class quite high.

A digital processing program has been developed by the Laboratory for Agricultural Remote Sensing (LARS) at Purdue University, Lafayette, Indiana, which uses the Michigan IROL multispectral scanner data. This program was tried from the same analog tapes taken over our test site to test Purdue's digital method of computer processing and readout. Figure 24 is a representation of their output. For this trial, we were unable to identify green infested trees. The faded infested trees showed up very well, but the training sample for old dead trees must have been incorrect because it grossly overstated this target by about 5 times.

## Thermal Processing

Improvements in thermal processing methods in 1969 and 1970 provided us with more evidence that previsual detection is possible. Figure 15 is a thermal contour map; targets of equal temperature can be depicted in separate colors, but the gray tones represented in this illustration are not as easily deciphered as the color print. Nevertheless, this technique was successful in identifying the discolored trees over a wide area (2 by 5 kilometers). The dying green trees are distinguishable from the healthy green trees in many cases; however, there are still too many other objects that have the same temperature range as the stressed trees and hence appear as the targets we wish to recognize.

## CONCLUSIONS

Stress induced on forest vegetation is best detected when symptoms exhibit foliage discoloration. At our present state of the art, color or false-color photography is still our most efficient sensor. There are many examples of successful programs using one or more scales of aerial color photography to detect and locate efficiently areas of affected timber. Some of these examples of multistage aerial photography include air pollution injury to ponderosa pine near Los Angeles, bark beetle epidemics in California, South Dakota, Washington, and Southeast United States, hardwood diebacks in Northeast United States, and spruce-fir defoliators in Northern United States. We must remember that one of the stages of any stress-detection program includes limited ground sampling to identify causal agents and to make the correlation between the photographic images.

Because aerial color photography has high resolution, is inexpensive, and is readily available to most user agencies, I predict it will continue to be one of our most useful sensors for stress detection for some time to come.

Multispectral scanners are still research tools for stress detection. Because the causal agent, such as air pollution or Dutch elm disease (Ceratocystis ulmi [Buism.] C. Moreau), often affects single trees and produces subtle foliar symptoms, we require sensing systems with high resolution capabilities. Most available scanners do not have good enough resolution to separate individual tree crowns when flown from aircraft at altitudes above 1,500 meters. Our ground studies indicate that when a multispectral scanner and ground processor, with perfect spatial registration in wavebands from 0.38 to 13.5 micrometers, is available, we will be more successful in previsual detection.

The ERTS program will be a useful exercise in learning how to handle large masses of data. Because of the low resolution capability of the 4-waveband scanner and the 3-band return-beam vidicon (RBV), probably only the largest areas of discolored timber will be detected.

#### LITERATURE CITED

- (1) Ciesla, W. M., C. J. Bell, Jr., and J. W. Curlin. 1967. Color photos and the southern pine beetle. Photogramm. Engng. 33(8):883-889.
- (2) Hasell, P. G., N. Spansail, and F. Thomson. 1968. Investigations of spectrum-matching techniques for remote sensing in agriculture. In Report to U. S. Dept. of Agr. by Univ. of Michigan, Infrared and Optics Laboratory, Ann Arbor, Mich.
- (3) Heller, R. C., R. C. Aldrich, and W. F. Bailey. 1959. An evaluation of aerial photography for detecting southern pine beetle damage. Photogramm. Engng. 25(4):595-606.
- (4) Heller, R. C., G. E. Doverspike, and R. C. Aldrich. 1964. Identification of tree species on large-scale panchromatic and color aerial photographs. U. S. Dept. of Agr. Handbook 261, Washington, D. C. 17 p., illus.
- (5) Heller, R. C. 1968. Previsual detection of ponderosa pine trees dying from bark beetle attack. Fifth Symposium on Remote Sensing of Environment Proc. 1968: 387-434.
- (6) Knipling, E. B. 1967. Physical and physiological bases for differences in reflectance of healthy and diseased plants. Proceedings of Workshop on Infrared Color Photography in Plant Sciences. Florida Dept. of Agr., Div. of Plant Indus., Winterhaven, Fla. 24 pp.
- (7) Nickerson, D. 1940. History of the Munsell color system and its scientific application. Opt. Soc. Amer. J. 30:575-586.
- (8) Nickerson, D. 1958. Color measurement and its application to the grading of agricultural products. U. S. Dept. of Agr. Misc. Pub. 580, 62 p.

- (9) Wear, J. F., and F. P. Weber. 1969. The development of spectro-signature indicators of root disease impacts on forest stands. Fourth Annual Progress Report. Available in microfiche from NASA, Washington, D. C. Scientific and Technical Aerospace Reports.
- (10) Weber, F. P. 1969. Remote sensing implications of water deficit and energy relationships for ponderosa pine attacked by bark beetles and associated disease organisms. Ph. D. Thesis. University of Michigan, Ann Arbor, Mich. 143 pp. Available in microfiche from University of Michigan.
- (11) Wert, S. L., and B. Roettgering. 1968. Douglas-fir beetle survey with color photos. Photogramm. Engng. 34(12):1243-1248, illus.

#### GLOSSARY OF TERMS

- Bark beetle infestation (or spot): A single pine tree or group of pine trees which have been successfully attacked by pine bark beetles (Scolytidae, Dendroctonus ponderosae, Hopk.), and this stress causes the foliage to discolor and the tree to die.
- Faded pine trees: The result of discoloration of pine foliage caused by bark beetle attack which in turn causes pine needles to change color progressively, from green to yellow to yellow-red.
- Pitch tube: An exudation of pitch or resin from the inner bark of the tree.
- Previsual detection: Detection of vegetation under stress before visible symptoms (foliage discoloration) occur.
- "t" test of significance: A statistical test designed to compare two (or more) groups of experimental data to determine whether they came from the same populations.

Table 1. Film-filter-scale combinations exposed during RB-57 Flight Mission #101 - August 3 and 8, 1969

Film	Filter	Camera	Focal Length	Scale	Format
Color IR (SO 117)	Zeiss ''B'' (15)	Zeiss	304 mm.	1:55,000	210 mm.
Color (2448)	HF-3	RC-8	152 mm.	1:110,000	210 mm.
Color IR (SO 117)	15	RC-8	152 mm.	1:110,000	210 mm.
Color (SO 368)	2A	Hasselblad	76 mm.	1:220,000	70 mm.
Color (SO 368)	12	Hasselblad	76 mm.	1:220,000	70 mm.
Color IR (SO 180)	15g	Hasselblad	76 mm.	1:220,000	70 mm.
Panchromatic (3400)	58	Hasselblad	76 mm.	1:220,000	70 mm.
Panchromatic (3400)	25A	Hasselblad	76 mm.	1:220,000	70 mm.
Panchromatic IR (SO 246)	89B	Hasselblad	76 mm.	1:220,000	70 mm.

Table 2. Film-filter-scale combination exposed during Aero Commander flight on July 21, 1969, with KB-8 70 mm. camera

Film	Filter	Focal Length	Scale	
Color D/200	HF-3	150 mm.	1:7,920	•
EIR (8443)	12	150 mm.	1:7,920	
Color D/200	HF-3	150 mm.	1:15,840	
EIR (8443)	12	150 mm.	1:15,840	
Color D/200	HF-3	150 mm.	1:31,680	
EIR (8443)	12	150 mm.	1:31,680	
Color D/200	HF-3	38 mm.	1:63,360	
EIR (8443)	12	38 mm.	1:63,360	
Color D/200	HF-3	38 mm.	1:120,000	
Color D/200	12	38 mm.	1:120,000	
EIR (8443)	12	38 mm.	1:120,000	
Color D/200	HF-3	38 mm.	1:170,000	
EIR (8443)	12	38 mm.	1:170,000	

Table 3. Spectrometer channels used for target recognition by University of Michigan aircraft and processing unit and their respective spectral colors

Spectral Color	Wavelength (Microme	eters) Channel Number
Violet	.4044	1
	.4446	2*
Blue	.4648	3
Blue-Green	.4850	4*
Green	.5052	5
Yellow-Green	.5255	6
Yellow	.5558	7
Yellow-Red	.5862	8
Light Red		
	.6266	9
Deep Red	.6672	10
	.7280	11
Reflective Infrared	.80 - 1.0	12
	1.0 - 1.4	13
	1.5 - 1.8	14
	2.0 - 2.6	15
Thermal Infrared	4.5 - 5.5	16
	8.2 - 13.5	17

<sup>\*</sup> Not used in the course of this study.

Table 4. Optimum target recognition channels for detecting stressed pine trees on the Michigan multispectral processor

Target		Wavelength Channels <sup>1</sup>	Threshold Voltage		
	Healthy trees	1, 6, 7, 8, 9, 10, 11, 12	2.00		
	Nonfaded infested trees	1, 3, 5, 6, 7, 8, 9, 10, 11, 12	1.75		
	Faded infested trees	6, 9, 10	2.87		
	Old-killed trees	1, 3, 9, 10, 11, 12	1.00		

Channel numbers refer to specific wavelengths listed in Table 3.



Figure 1. Flag shows location of the Black Hills National Forest near Rapid City, South Dakota. Ponderosa pine (Pinus ponderosa, Laws.) is the principal tree species and is under stress from attack by the Black Hills bark beetle (Dendroctonus ponderosae, Hopk.).



Figure 2. An oblique view of a portion of the study area looking down the drainage where over 3,000 ponderosa pine trees have been killed since 1967. Made from an Ektacolor negative. Whitish trees are most recently killed; light gray trees were killed one year earlier; dark gray images are mostly uninfested healthy trees.

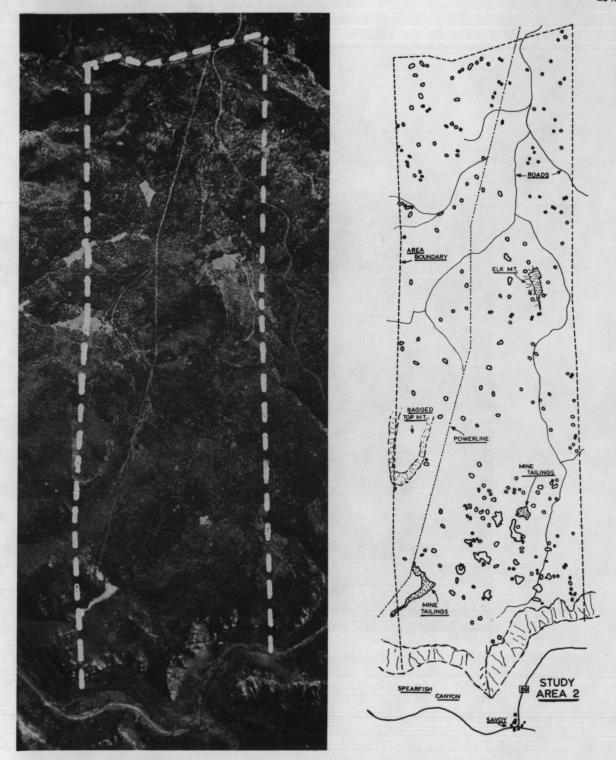


Figure 3. Aerial mosaic, left, of 1.6 by 5 kilometer study area near Savoy, N. D. Right, the 211 infestations are plotted at the same scale.



Figure 4. Measurements of apparent emittance (°C) are taken of healthy and infested trees from a tower overlooking infested and healthy ponderosa pine trees.



Figure 5. Net and total radiation thermometers are supported on moving tramway system above 30-meter-tall Douglas-fir (Pseudotsuga menziesii [Mirb.] Franco) trees. These trees are being monitored for stress induced by Poria weirii root rot.

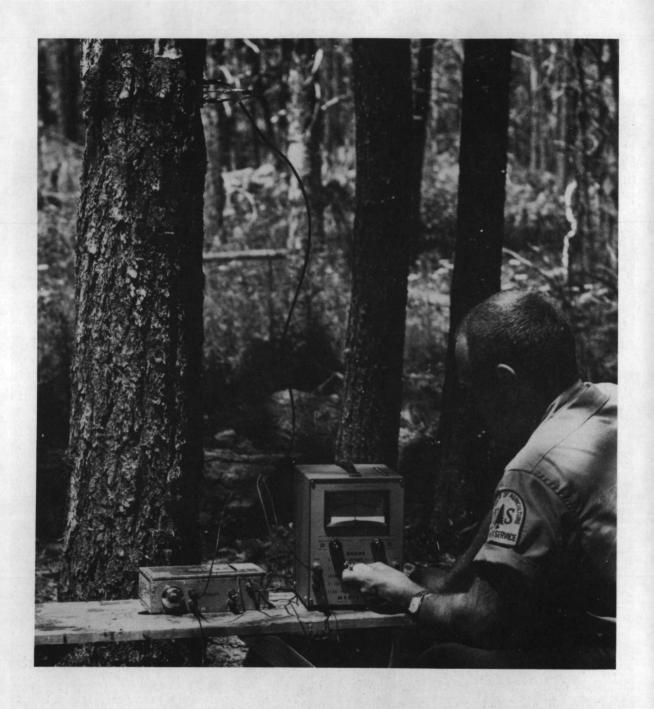


Figure 6. Rate of sap flow is measured by measuring the rate of heat loss from a small, high-energy heat source by means of thermocouples. Sap flow is related to transpiration; normal transpiration of foliage tends to keep foliage cooler than when transpiration is reduced by a stress of some kind.

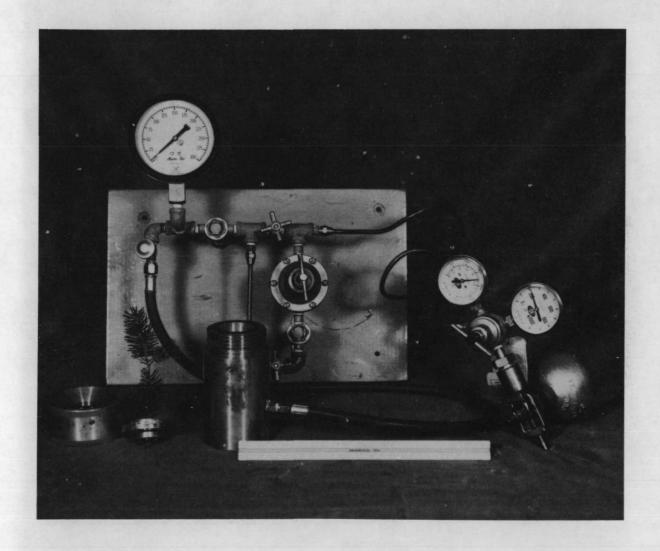


Figure 7. Hydrostatic pressure cell with pressure manifold is taken into field to measure leaf moisture tension. Induced pressures are closely related to moisture stress conditions and general tree vigor. Relatively low pressures are indicative of healthy trees; high pressures are needed to force moisture from stressed twigs.



Figure 8. Neutron probe device is used to measure soil moisture at known depths of the soil.

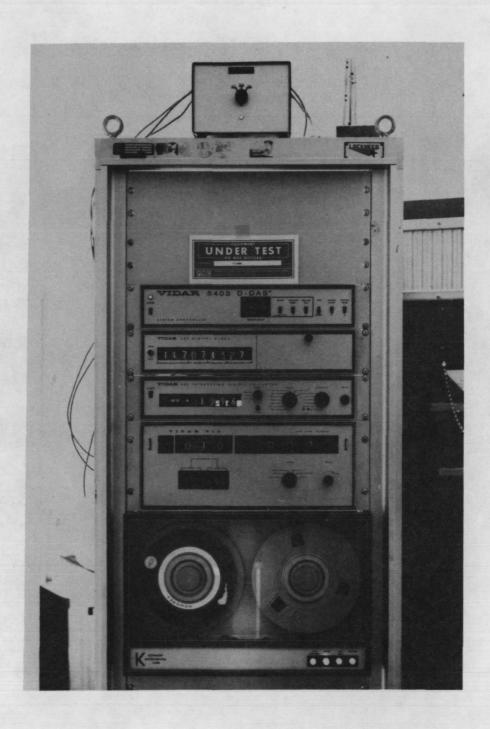


Figure 9. Field data logger can collect, digitize, and store on magnetic tape up to 38 channels of field data.



Figure 10. Two 70 mm. Maurer KB-8 cameras were triggered simultaneously from one intervalometer to get identical coverage with color and false-color film. 150 mm. Schneider Xenotar lenses were used from medium altitudes (to 6,000 meters); 38 mm. Zeiss Biogon lenses were used at higher altitudes.

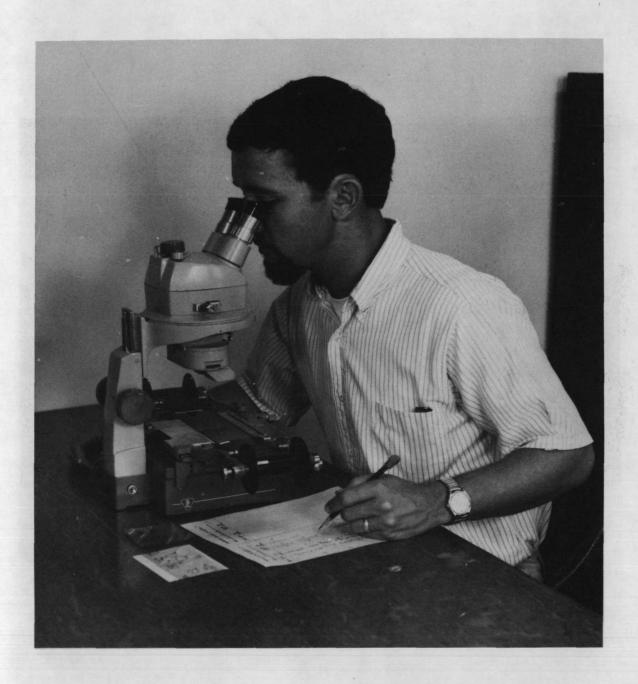


Figure 11. Bausch and Lomb Zoom stereoscope was used to interpret small-scale color and infrared color transparencies (1:116,000 to 1:174,000). Magnifications used by the three photo interpreters varied from 12X to 28X.

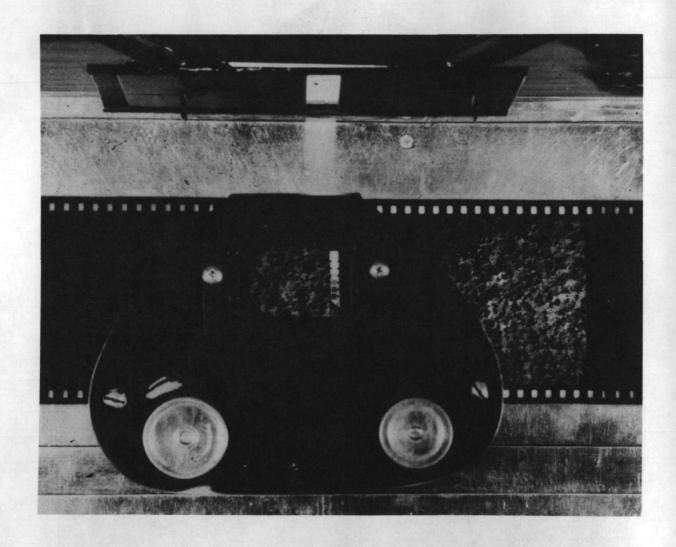


Figure 12. Munsell comparator permits a photo interpreter to compare film transparencies of Munsell charts with images of interest on aerial color photographs. The same light source is used in making this comparison.

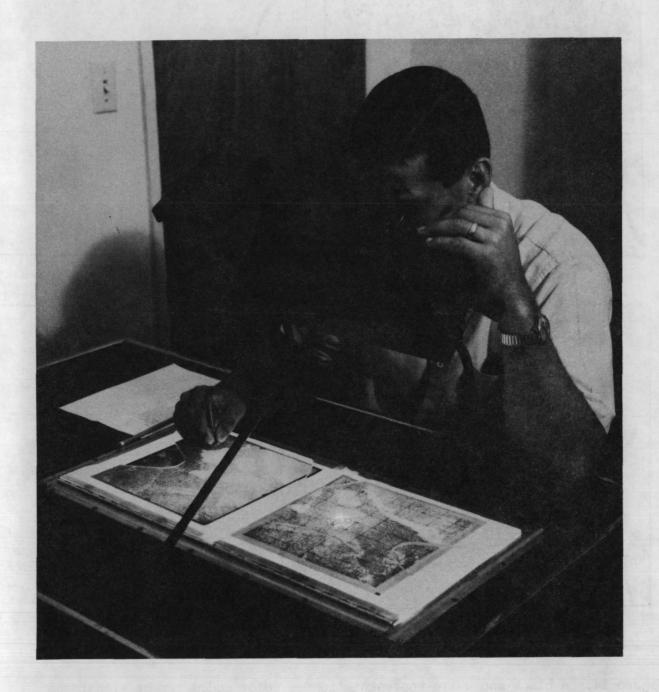


Figure 13. Aerial color and false-color transparencies taken from the RB-57 air-craft (high altitude) were examined with Old Delft scanning stereoscopes at 4.5 magnifications.

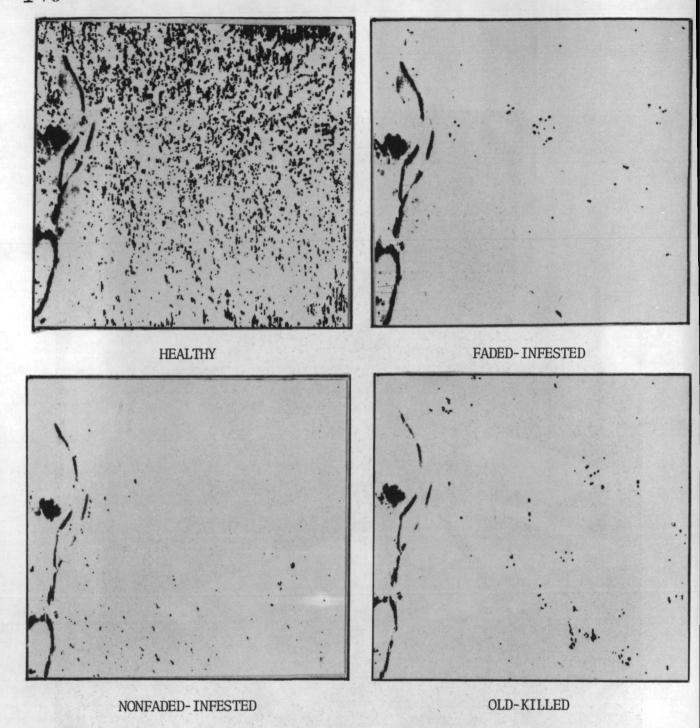


Figure 14. A black-and-white representation of color-coded target signatures identifying four tree condition classes made from successive combined waveband overlays. Each overlay is derived mathematically as the best combination of wavebands which identify a particular target. The multispectral scanner and processor operated in 10 wavebands from 0.40 to 1.0 micrometer.

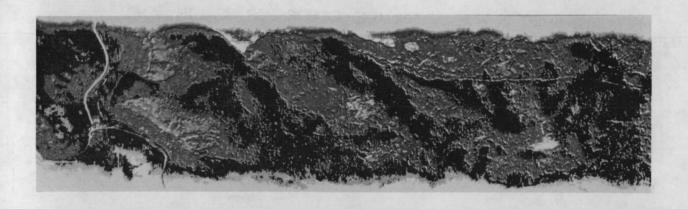




Figure 15. Upper: A black-and-white representation of a color print made from "temperature contouring" techniques developed at IROL, University of Michigan. Each gray level depicts a particular ground emission target temperature. Objects of equal temperature are more easily distinguished on color prints or transparencies. Lower: Infrared line scan imagery in analog form of upper picture. This imagery covers the study area shown in Figure 3.

# PERCENT SHIFT IN HUE OF FOLIAGE COLOR FOR HEALTHY AND INSECT INFESTED TREES

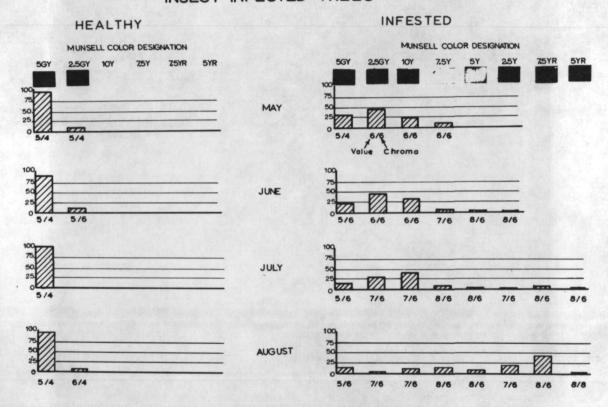


Figure 16. The shift in foliage color of healthy and stressed ponderosa pine trees over a four-month period. Munsell estimates of foliage color were made on the ground for 209 infested and 47 healthy trees in May, June, July, and August 1967. Almost identical readings were obtained in 1968.

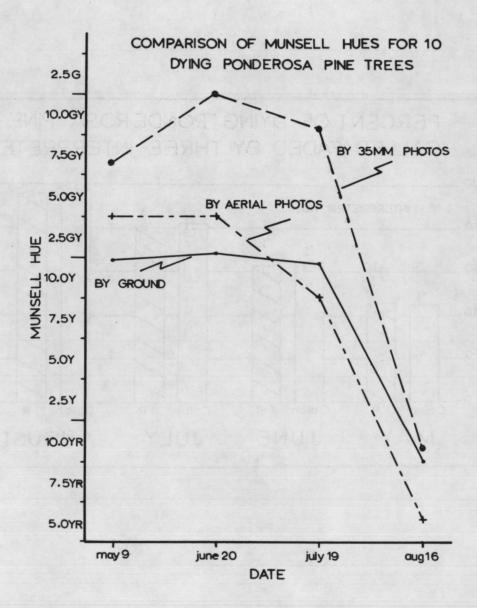


Figure 17. Comparison of Munsell hues of 10 sample trees taken by three methods at four time periods.

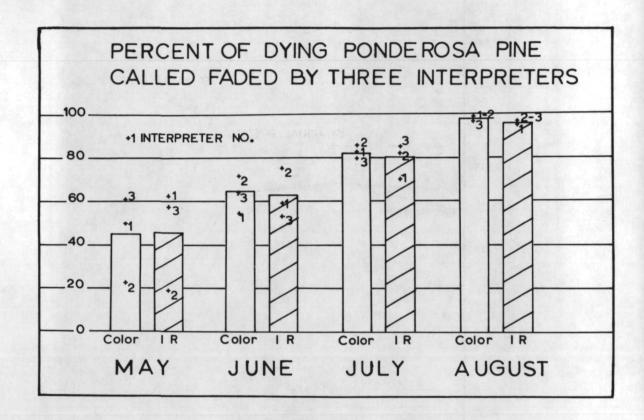


Figure 18. Photo interpretation results from three experienced photo interpreters, using Anscochrome D/200 and Ektachrome Infrared Aero films at 1:1,584 scale. Note the increased ability to detect infested trees as the season progresses, and the greater consistency among interpreters in July and August.

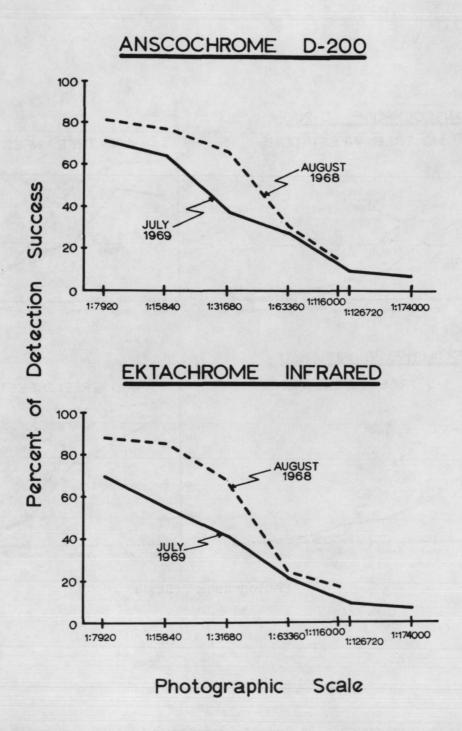


Figure 19. Detection of beetle-attacked trees in 1968 and 1969. The 1968 data represent the mean for three interpreters—the 1969 data for two. Accuracy of photo interpretations is expressed as a percent of the total number of discolored infestations present. Note the significant drop in 1969 detection because maximum discoloration of foliage had not occurred by July 1969.

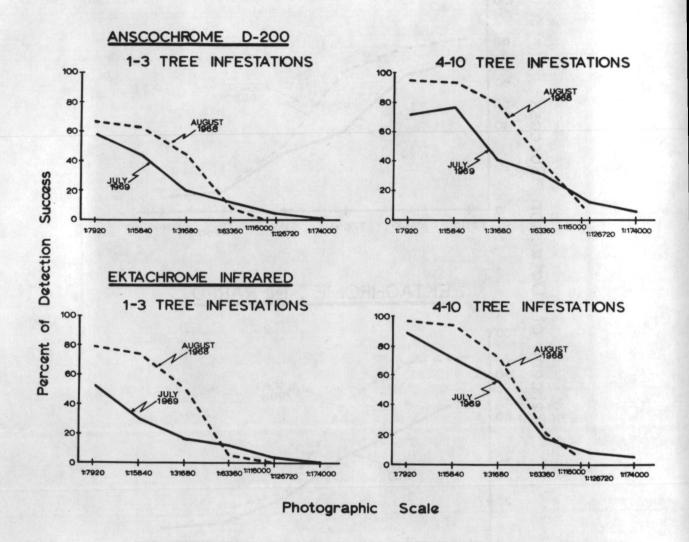


Figure 20. Detection success in August 1968 and July 1969 for small bark beetle infestations. Small infestations are representative of stress conditions showing up early in the cycle of a bark beetle epidemic. Note the similarity in detection success of the two films (color and false color) and also the drop in detection accuracies when photos were taken in July 1969 before maximum foliage discoloration occurred.

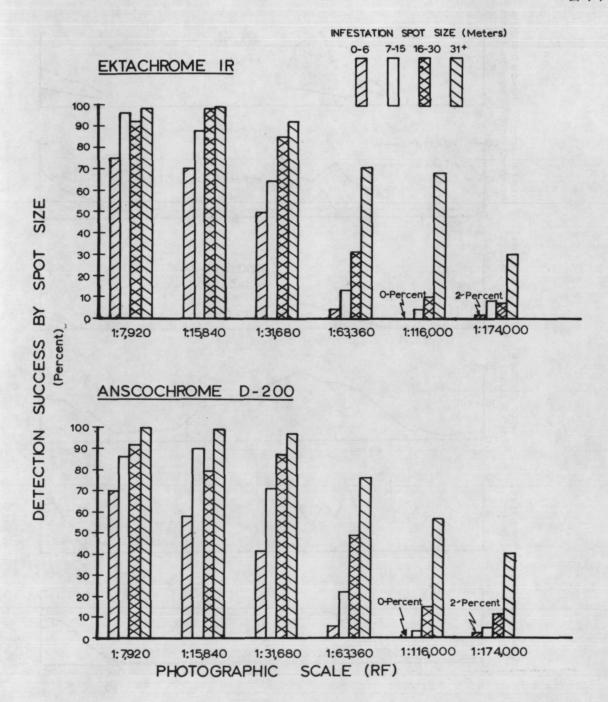


Figure 21. Detection successes (mean of three interpreters) expressed as a percent of 4 infestation size classes, 6 photographic scales, and 2 films. The upper chart is for infrared color film; the bottom chart for color film. Note the high level of detection success on 1:31,680 transparencies even for infestations 7 to 16 meters in diameter (average of 4 to 10 trees). The big drop in detection success occurs at scales smaller than 1:31,680.

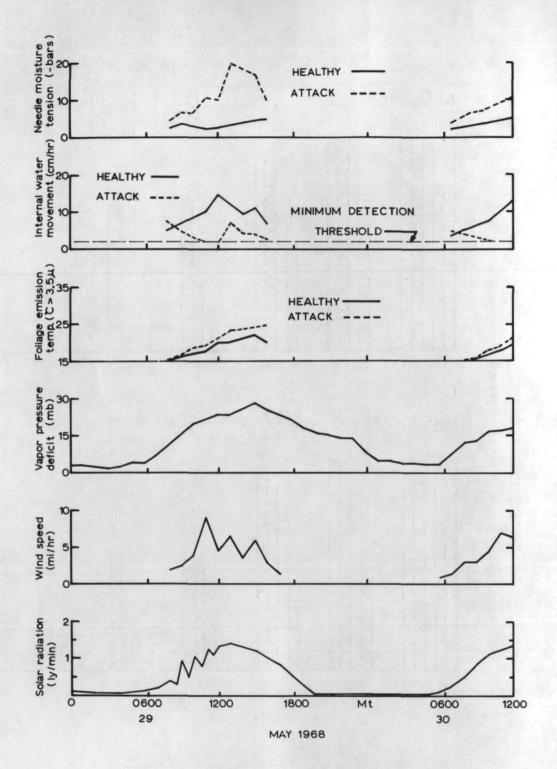


Figure 22. Meteorological and tree physiological data collected at instrumented test site, May 29 and 30, 1968. Sampling intervals cover the period during which overflights were made with the University of Michigan C-47 aircraft equipped with the 17-channel scanner system.



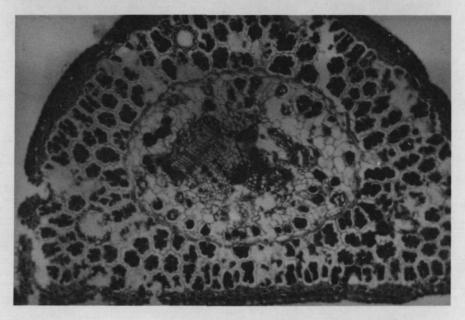


Figure 23. Cross section of needle tissue from ponderosa pine. Upper: from healthy needle; most cell walls are intact and are filled with cytoplasm. Lower: from needle taken from infested tree; many cell walls are broken, vascular bundles, resin canals, and stomata are collapsed, and cytoplasm is absent or shrunken.

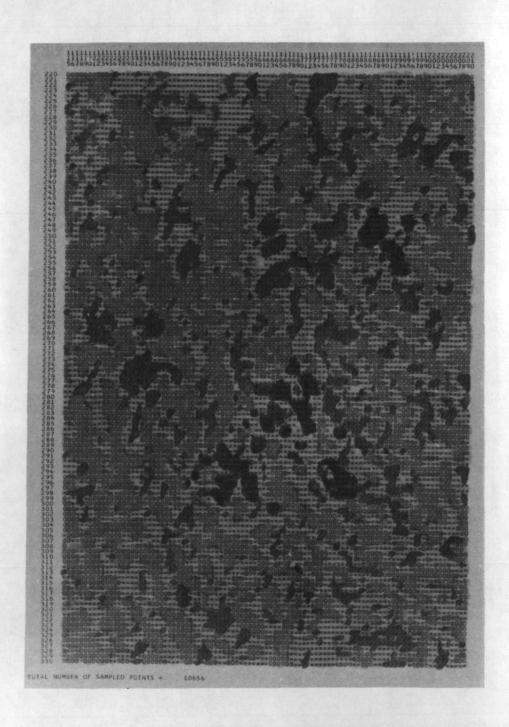


Figure 24. This display printout of the Black Hills test site was made from the Purdue LARSYAA target-recognition program. The various shades of gray and black represent six different condition classes. The discolored pine trees were accurately identified; other targets were not accurately identified.

Page Intentionally Left Blank

#### APPLICATION OF INFRARED SCANNERS TO

#### FOREST FIRE DETECTION

Stanley N. Hirsch, Project Leader

U.S. Department of Agriculture, Forest Service Intermountain Forest and Range Experiment Station Northern Forest Fire Laboratory Missoula, Montana

Stanley N. Hirsch received his B.S. degree in electronic engineering at the University of New Mexico and has done graduate work at the University of Idaho. Prior to joining the Forest Service in 1961, Mr. Hirsch served as Senior Instrumentation Engineer for Sandia Corporation and General Electric Company.

As Project Leader for Project Fire Scan, Mr. Hirsch has received international recognition for his work in remote detection of heat sources obscured by smoke and timber cover. His involvement in the development of airborne electronic fire surveillance systems led to a fire mapping system which became operational in the USDA Forest Service's Division of Fire Control in 1966. The unique bispectral IR fire detection system, developed under his leadership, was successfully tested in 1970 and will become operational within the Forest Service in 1971. Mr. Hirsch has served as a member of the forestry committee of NASA's remote sensing group and also in an advisory capacity to the remote sensing project at Pacific Southwest Forest and Range Experiment Station, Berkeley, California.

## APPLICATION OF INFRARED SCANNERS TO FOREST FIRE DETECTION

### Stanley N. Hirsch1/

Forest fires frequently spread slowly immediately after ignition. During this period they are easily suppressed. The function of a detection system is to find fires before they grow large enough to cause serious suppression difficulty. Outputs of smoke and radiant energy, which are the key characteristics in forest fire detection, are extremely variable. During the time from ignition until a fire has grown to a size where it is difficult to control, the radiant energy and the smoke outputs may increase continuously with time. More commonly, however, there is a high initial output of either smoke or flame or both smoke and flame, followed by long dormant periods interrupted occasionally by bursts of flame and/or puffs of smoke. Outputs of both smoke and heat usually decrease significantly at night. We have not been able to find any direct correlation between outputs of smoke and radiant energy (Fig. 1).

All forest fire detection systems now being used rely upon visual observation of smoke from lookout towers or aircraft. Such systems are only efficient during daylight hours when a column of smoke is well developed and rises above the trees and when the atmosphere is clear, not contaminated.

Because of these limitations, our project began to investigate the potential of infrared (IR) detection systems. We recognized that an IR device could not be operated from lookout towers because rough topography and heavy timber severely limit the probability of obtaining an unobscured line of sight to ground fires burning under a timber canopy. A direct "look" is needed because reliable detection cannot be achieved from the small amount of radiant energy produced by smoke columns rising above a fire. Therefore, we proceeded with a study of the IR detection probability from aircraft.

At the outset of our studies, we did not know the probability of having an unobscured line of sight between an aircraft and a fire burning under a timber canopy (Fig. 2). We suspected it was strongly dependent on timber characteristics (stand height, bole diameter, number of stems per acre, live crown ratio, and crown characteristics) as well as angle of view and fire size. Therefore, we conducted rather extensive tests in 1963-65 in timber

Author is Project Leader for Project Fire Scan, USDA Forest Service, Intermountain Forest and Range Experiment Station, Ogden, Utah; stationed at the Northern Forest Fire Laboratory, Missoula, Montana.

types representative of stands found on the North American Continent [1],[2],[3],[4]. Initially, we conducted flight tests; later we added a mountaintop test because the cost of obtaining sufficient data using aircraft would have been prohibitive. We found that reliable detection for simulated fires of 5 square feet2/could be achieved at angles up to 60° from the nadir (as shown in Fig. 3).

An IR system scanning 120° at 15,000 feet at ground speeds in excess of 200 knots could economically compete with an airborne visual detection system which costs approximately 6¢ per square mile. From 15,000 feet, a 2-milliradian (mrd) resolution system has a ground resolution of 30X30 feet directly under the aircraft and 60X120 feet at 60° from the nadir. This provides enough terrain detail to determine target location. Fire targets of the size we must detect (1 to 10 square feet) will occupy between 1.4X10-4 to 1.1X10-2 of the instantaneous field of view, depending on the angle of observation and size of the fire. The effective target size may be further reduced because of obscuration by timber. Many of the targets detected in the mountaintop tests were up to 95 percent obscured.

The radiant energy from a forest fire (600°C) peaks in the 3- to  $6-\mu$  (micron) region. We obtained a 2-mrd IR line scanner with about 1/2° temperature sensitivity (InSb) and began to evaluate its performance. After 2 years of flight testing we found that many of the fires we detected produced very marginal targets. If an interpreter knew the target locations he was usually able to detect them, but the signatures produced on the imagery were so marginal that randomly located targets in a large search area were not detectable.

If a 600°C target fills less than  $2\times10^{-2}$  field of view of the scanner, the target's signal-to-background ratio in the 3- to 6- $\mu$  region is insufficient to distinguish fire targets from background

 $P_n = 1 - (1 - P_5)n/5$ 

where:

n = area of fire in ft.2.

<sup>2/</sup> The probability of detecting a fire of any size may be inferred by assuming that the probability of detecting a fire with 5-ft.<sup>2</sup> of burning material is equal to the probability of seeing at least one of five 1-ft.<sup>2</sup> fires. To extrapolate the data in figure 3 to fires of smaller or larger areas, the following may be used:

 $<sup>3/\</sup>mu = 1 \times 10^{-6}$  meters.

thermal anomalies. In the 8- to 14- $\mu$  region, the target's signal-to-background ratio is less than it is in the 3- to 6- $\mu$  region. We began to wonder if we could use the 3- to 6- $\mu$  and 8- to 14- $\mu$  regions in combination to enhance the target.

Figure 4 shows the 3- to 4- $\mu$  (A) and 8.5- to 11- $\mu$  (B) signals from both terrain background and fire targets as seen by a 2-mrd system from 15,000 feet plotted in two-dimensional vector space [5]. The lower curve contains all background temperatures from 0° to 60°C. The set of points above (shaded area) contains target signatures from fires ranging in temperatures from 600° to 800°C, areas ranging from 1 to 10 square feet, angles of view from 0° to 60°, and obscuration ranging from 0 to 95 percent. Amplitude discrimination in the A channel (horizontal line) would not provide effective separation of targets from background, nor would amplitude discrimination in the B channel (vertical line).

A sloping, straight line drawn between the lower curve and the target points does provide discrimination for most targets. The equation of that line is:

A = KB + C

where:

$$A = {}_{3}\int^{4} W_{\lambda} T_{A} T_{F_{A}} R_{D_{A}} d_{\lambda}$$

$$B = {}_{45}\int^{11} W_{\lambda} T_{A} T_{F_{B}} R_{D_{B}} d_{\lambda}$$

K = slope of discrimination line

C = displacement from origin

W, = Planck function

 $T_A$  = transmission of atmosphere

 $T_{F_A}$  = transmission of A channel filter

 $T_{F_D}$  = transmission of B channel filter

 $R_{D_A}$  = responsivity of A channel detector

R<sub>DR</sub> = responsivity of B channel detector

<sup>4/</sup> Variations in spectral emissivity will spread the back-ground points forming a band rather than the discrete curve shown in figure 4.

or, rewriting and redefining K:

#### K'A - B - C = 0

If the background temperature range can be predicted for a given flight, an optimum K can be selected. An effective decision rule and one that is easy to implement in an analog system is: A target exists if the signal is greater than KA - B. A nonlinear function that more closely matched the lower curve would be an even more efficient rule, but it would be more difficult to implement. We employed the KA - B function and found it quite effective.

To minimize the effects of changes in atmospheric moisture, we selected the 3- to 4- $\mu$  and 8.5- to 11- $\mu$  bands rather than the total 3- to 6- $\mu$  and 8- to 14- $\mu$  windows. We empirically selected spectral regions centered around 3 $\mu$  and 8 $\mu$ , where the ratio of the power is relatively insensitive to changes in atmospheric moisture.

The way we implemented the bispectral system is shown in figure 5. The 8.5- to  $11-\mu$  channel produces high quality infrared imagery from which the position of targets can be accurately determined with respect to terrain features.

The KA - B signal is pulse-height/pulse-width discriminated. A pulse above a preset threshold and within the pulse-width2/limits produces a logic pulse that is stored in a digital memory for one scan line. If a logic pulse is produced at the same point in two successive scan lines, an output pulse is generated. To eliminate false alarms caused by electrical noise, sufficient overscan is available to permit scan-to-scan comparison. The output pulse produces a mark on the edge of the film and rein-serts a pulse in the video, which cues the operator (Figs. 6 and 7).

The curvature of the function shown in figure 8 permits selection of two temperatures where the signal amplitude is equal. To calibrate the system we select a pair of temperatures that will produce equal signals in the difference channel for the desired K value. We set the internal calibration sources at these temperatures, of and then adjust the gain of the 8.5- to 11-µ

<sup>5/</sup> Pulse-width limit is set to equal the dwell time for one resolution element.

<sup>6/</sup> Atmospheric transmission is not included in the integration for A and B in figure 8 since the path between the detector and calibration sources is short.

channel until the signal from the two sources is equal. This simple procedure assures that the ratio of total gain (amplifier, detector, and optics) in both channels is optimum for differentiating between targets and any preselected background range.

We calculated the performance of both the single and bispectral systems and predicted that the bispectral system could produce a 12:1 improvement in detecting 1-ft.<sup>2</sup>, 600°C targets against backgrounds ranging from 0° to 50°C. To check our calculations we performed flight tests using thermal anomalies in Yellowstone National Park to provide a high contrast background. The results of these tests showed a 10:1 improvement.

The test was performed in April 1970 when nighttime surface temperatures were -10°C in areas unaffected by geothermal activity. As shown in figure 9, the temperature at Fire Hole River was 10°C, and that for Hot Lake, which is located adjacent to a geyser, was 50°C. Buckets of glowing charcoal were used as targets with surface areas of 1/2, 1, and 2 ft.<sup>2</sup>.

We overflew the area at 15,000 feet above terrain. In addition to the normal film recording and TDM marks, we recorded the 3- to 4- $\mu$ , 8.5- to 11- $\mu$ , and KA - B signals on magnetic tape. After the flight we photographed the video signals from the tape recordings.

The signals from the 1/2- and  $1-ft.^2$  targets were easily differentiated from signals for Hot Lake in the KA - B channel. The signal from the  $1-ft.^2$  target was slightly larger than the signal from Hot Lake in the 3- to  $4-\mu$  channel. None of the targets produced measurable signals in the 8.5- to  $11-\mu$  channel.

During July and August of 1970, the equipment was operationally tested in an 8,000-square-mile area adjacent to Missoula, Montana. On 42 patrol flights, of 5-1/2 hours' duration each, over 800 hot targets were detected and plotted. More than 200 of the targets were wildfires. Forty-five of these were detected by the IR system before they were detected by the presently used visual system of 59 lookout towers and seven patrol aircraft (Fig. 10).

Many fires were detected visually but missed by the IR system, and many fires were detected by the IR system but missed visually. Until we learn more about the relationship between heat output and smoke output from latent fires we cannot determine the relative effectiveness of visual and IR systems. The results of the 1970 tests convinced us that IR used in combination with

visual detection will result in a more efficient system than visual alone. Even with our limited knowledge of the relative effectiveness of the two systems we can begin operational use of a combined system and substantially reduce total firefighting costs (detection plus suppression) [6]. The ultimate potential will not be realized until we are able to arrive at optimal combinations.

#### REFERENCES

- [1] S. N. Hirsch, "Applications of remote sensing to forest fire detection and suppression," 1962 Proc. Second Symp. Remote Sensing Environ., pp. 295-308, illus., 1963.
- [2] , "Preliminary experimental results with infrared line scanners for forest fire surveillance," 1964 Proc. Third Symp. Remote Sensing Environ., pp. 623-648, illus., 1965.
- [3] , "Project Fire Scan-summary of 5 years' progress in airborne infrared fire detection," 1968 Proc. Fifth Symp. Remote Sensing Environ., pp. 447-457, illus., 1968.
- [4] R. A. Wilson, "Fire detection feasibility tests and system development," 1968 Proc. Fifth Symp. Remote Sensing Environ., pp. 465-477, illus., 1968.
- [5] Committee on Remote Sensing for Agricultural Purposes, "Remote sensing (with special reference to agriculture and forestry)," Wash., D.C.: Nat. Acad. Sci., pp. 360-410, 1970.
- [6] P. H. Kourtz, "A cost-effectiveness analysis of a simulated airborne infrared forest fire detection system," Ph.D. dissertation, Univ. of California, Berkeley, 1970.



Fig. 1. These two photographs point up the role that smoke and radiant energy play in the development of forest fire detection systems. A, Flames indicate a high output of radiant energy. In such instances this fire could be readily detected by an IR system, but not by a visual system. B, The output of radiant energy from the fire is too small to enable detection by an IR system, but the well-developed smoke column would be readily detected by a visual system.



Fig. 2. This photograph of the western white pine stand used in the tests shows the "obscuring" effect of a typical forested area.

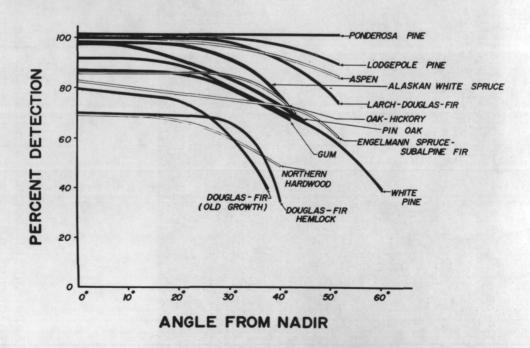


Fig. 3. Shown here are detection probability curves for the 13 timber types tested. Target arrays were five 1-ft.<sup>2</sup> buckets of glowing charcoal placed on the circumference of a 9-ft. circle. Flight passes were flown at 10° angular increments from 0° to 60° from the nadir.

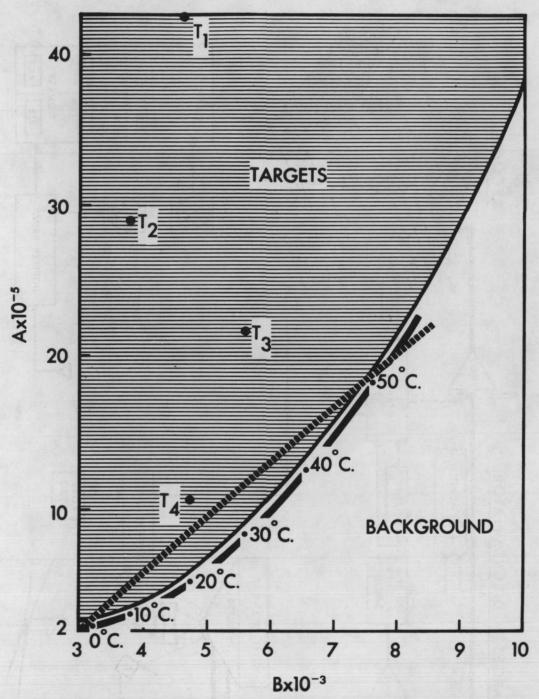


Fig. 4. The signals for both targets and background, as seen by the 2-mrd IR detection system from 15,000 feet, are plotted in two-dimensional vector space, where A is the 3- to 4- $\mu$  and B is the 8.5- to 11- $\mu$  vector. Annotation of the target and background temperatures, areas, and angles of view for detected targets is as follows:  $T_1$ =1 ft², 600°C, 20° background, 0° angle;  $T_2$ =1 ft², 600°C, 10° background, 30° angle;  $T_3$ =1 ft², 800°C, 30° background, 60° angle; and  $T_4$ =1 ft², 600°C, 20° background, 60° angle.

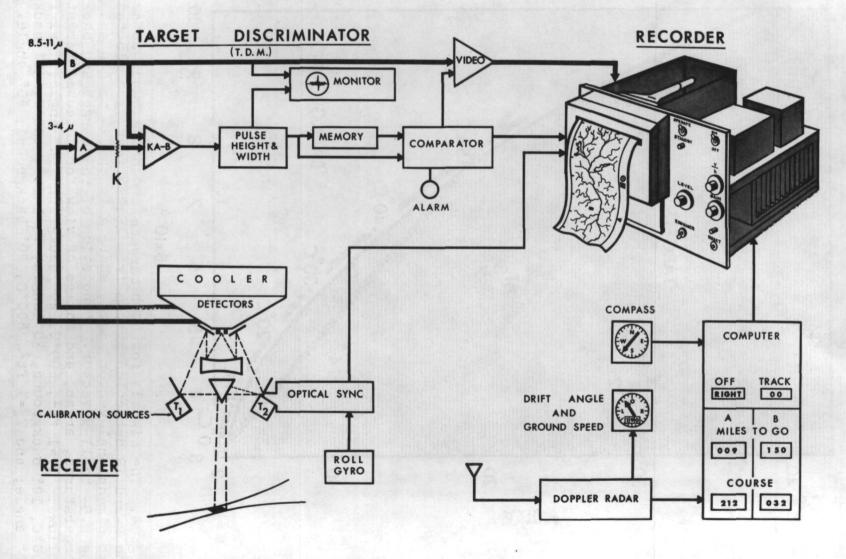


Fig. 5. Shown is a block diagram of the bispectral IR fire detection system.



Fig. 6. The IR fire detection system is designed for operation in a twin turbo-prop, light executive, pressurized aircraft.

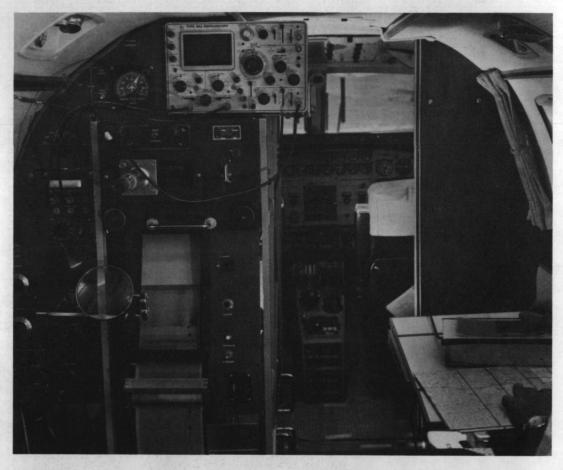


Fig. 7.  $\underline{A}$ , Looking forward, the scanner control console, which uses 5-inch film (left foreground) that is processed in near real time.



Fig. 7. B, The special equipment for the IR fire detection system required a modification of the fuselage by the factory. Looking aft, scanner mounted in specially constructed hatch. When closed, the cover for the hatch forms a pressure seal. Helium refrigerator shown provides detector cooling.

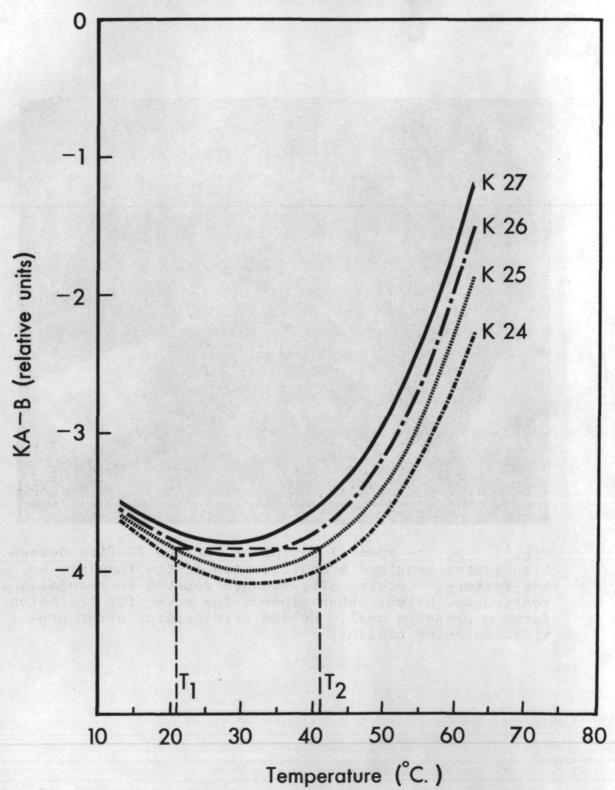


Fig. 8. Shown here is the KA - B signal plotted against temperatures for several values of K. To calibrate the system,  $T_1$  and  $T_2$  are selected to produce equal signals in the difference channel for the desired K value.

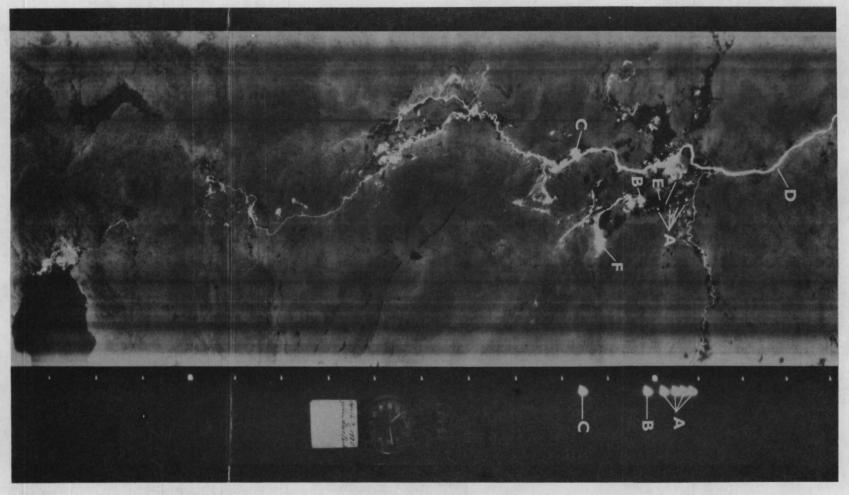
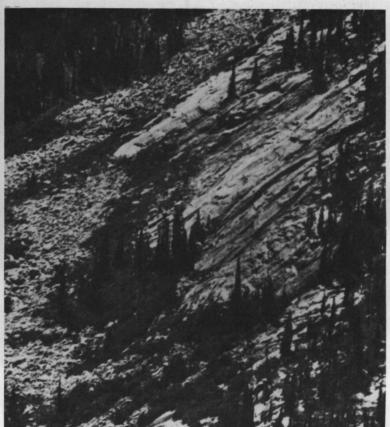


Fig. 9. Shown here is imagery from the test flight over Yellowstone National Park on April 7, 1970, at 2115 hours, and is annotated as follows:  $\underline{A}$ , Trips on test targets (600°C);  $\underline{B}$ , Kaleidoscope Geyser;  $\underline{C}$ , Excelsior Geyser;  $\underline{D}$ , Fire Hole River (10°C);  $\underline{E}$ , snowfield (-13.6°C);  $\underline{F}$ , Hot Lake (52°C); and  $\underline{G}$ , asphalt road (-9°C).





A



Fig. 10. This lightning-caused, latent or incipient-type fire (A) occurring in one tree in this area (B) was first spotted in this imagery (C) which was recorded at 0005 hours on July  $\overline{16}$ , 1970, in an aircraft flying at 21,000 feet. The fire was still burning when photo B was taken. The imagery is annotated as follows: (1) Target is a campfire at Twin Lakes; (2) TDM marks (double marks at the latent fire are due to aircraft pitching during the run); (3) actual fire; and (4) navigation marks at 1-mile intervals.

#### Personal Resume - John D. McLaurin

Mr. McLaurin is a Research Civil Engineer in the Branch of Photogrammetry of the Topographic Division, U.S. Geological Survey. He received BSE and MSE degrees in Civil Engineering at the University of Michigan in 1961 and 1965 respectively. He was admitted to candidacy toward a Ph.D in Forestry and Remote Sensing in 1970, also at the University of Michigan. He has spent several years working in the field surveys and photogrammetric phases of topographic mapping with the Geological Survey. In recent years Mr. McLaurin has been conducting research in computational photogrammetry and the applications of remote sensor data to mapping. He is presently working with the cartography discipline of the EROS Program in studying the metric properties of line scanning and television systems and the correlation of multispectral imagery.

#### APPLICATION OF REMOTE SENSING TO PLANIMETRIC, THEMATIC, AND TOPOGRAPHIC MAPPING

By

John D. McLaurin
Topographic Division
U.S. Geological Survey
1340 Old Chain Bridge Road
McLean, Virginia 22101

#### INTRODUCTION

For centuries men have been mapping the earth's surface. The first maps were probably made from estimated distances and directions and from reports of travelers; later, astronomic and field measurements were used. Until about the 1920's, almost all original maps were made with ground surveying techniques. The advent of aerial cameras and photogrammetric plotting instruments produced a significant increase in production, geometric accuracy, and content of topographic maps. However, despite over 50 years of continuous effort, the availability of map data for the world is woefully inadequate. A recent study by the United Nations 1 has shown the magnitude of the mapping problem with an estimate of the availability of map data. Table 1 is extracted from this study.

Table 1. -- Current Status of Topographic Maps

Scale	World	U.S.
1:1,250 - 1:31,680	6.0%	40.5%
1:40,000 - 1:75,000	24.5%	44.7%
1:100,000 - 1:126,720	30.2%	20.8%
1:140,000 - 1:253,440	72.0%	100.0%

Of even more concern is the rate of obsolescence of maps, particularly in urban areas. The rate of obsolescence is increasing and may soon equal the production rate, and therefore with present techniques and capacities the world mapping task will never be completed. In addition, for some maps the production cycle from photography to distribution is from 3 to 4 years, so a map may be as much as 4 years out of date on the day it is published.

Doyle  $\frac{2}{}$  has summarized the world's mapping needs as follows:

 Complete and revise where necessary the International Map of the World (IMW) at 1:1,000,000 scale.

<sup>1/</sup> United Nations, The Status of World Topographic Mapping, World Cartography, Vol. X, 1970.

<sup>2/</sup> Doyle, F. J., Mapping Techniques and the World Mapping Problems, paper presented at the Canadian Institute of Surveying Meeting, Halifax, N.S., April 16, 1970.

- Complete and revise where necessary synoptic maps at 1:250,000 scale for the entire world.
- Provide up-to-date medium-scale (1:100,000 or 1:62,500) maps for all settled areas.
- Provide current large-scale (1:25,000 or 1:24,000) maps for all urban, suburban, and cultivated areas.

The capability of revising maps at intervals inversely proportional to their scale is also needed.

Another need is for thematic maps at various scales. These maps depict water areas, wooded areas, cultivated areas, and the massed works of man. Their main use is in locating and measuring natural and man-related features and in monitoring their changes.

To help fill current mapping needs, considerable effort is being devoted to developing new methods for producing and updating maps. For instance, the U.S. Geological Survey is now producing orthophotomaps as a standard product in selected areas. Orthophotomaps contain photoimagery, processed so that the scale is true and uniform, and selected cartographic symbols and labels to enchance important map detail. One of the main advantages of this type of map is that the map production cycle is shortened. In addition, the orthophotomap includes terrain detail that cannot be shown on a standard line map.

Another relatively new technique used by the Geological Survey is interim revision. In this procedure, recent aerial photographs are used to plot cultural and drainage changes which have occurred since the previous survey. The changes are printed on the revised map in purple. Significant cost and time savings result because no fieldwork is required. This technique permits the timely updating of maps.

These new procedures alone will not completely accomplish the world mapping task, however, and cartographers and photogrammetrists are naturally looking for new methods to solve the problem. One of the most promising methods is the use of data from earth-orbiting satellites. Satellites are a logical progression from high-altitude aircraft, and they provide platforms which are inherently global in operation. Analyses and experiments have indicated that space imagery can be used for compiling and revising maps of medium and small scale. Because of its synoptic coverage, space imagery also provides valuable data for thematic mapping because it has no local anomalies in tone as in mosaics of aircraft photographs.

#### Selection of the Sensor

One of the basic requirements for any sensor to be used for mapping is geometric accuracy. A second requirement is resolution sufficient to identify features to be shown on the map. These requirements follow from the basic purpose of maps, that is, to show the location and extent of features of general interest. In addition to these requirements, thematic mapping requires imagery in selected spectral bands so that signature analysis techniques may be used to separate the features to be shown on the map.

The geometric accuracy requirements are a function of the scale of the map. In the United States these requirements are set by the National Map Accuracy Standards, which for maps of publication scales of 1:20,000 or smaller may be paraphrased as follows:

Horizontal

90% of all well-defined points tested shall be within 0.02 inch (.50mm) of their correct position.

Vertical

90% of all elevations tested shall be within one-half contour interval (with allowance for the permissable horizontal error).

Thus, maps at a scale of 1:250,000 require 90% of the well-defined points to be located within 127 meters of their true position; this corresponds to a standard error of position of 77 m. For a contour interval of 100 meters, 90% of the interpolated elevations should be within 50 m, or a standard error of 32 m.

The National Map Accuracy Standards apply only to the position and elevation of features on the final product—the map. The sensor requirements must be stringent to allow for the inevitable loss of positional accuracy and resolution in producing the map from the sensor image. If the image is used directly to produce a photomap, the loss in horizontal accuracy can be minimized but not completely eliminated.

The sensor resolution requirements are set by factors other than those that affect map accuracy. The main factor is the map content, which is primarily a function of map scale. For instance, 1:24,000-scale maps usually include detail, such as houses, trails, and mines, not normally shown on 1:250,000-scale maps. Consequently, the resolution requirements for a sensor to be used in producing 1:250,000-scale maps are not as stringent as they would be for a sensor to be used in producing 1:24,000-scale maps.

One criterion which can be used to estimate the sensor resolution requirements for producing photomaps is that the resolution of the image at map scale should be just discernible by the eye. A resolution of approximately 10 line pairs per millimeter can be used for the average eye at the usual viewing distance.

Table 2 summarizes the ground resolution and accuracy requirements for various planimetric and topographic map publication scales. These are the basic requirements for any sensors to be used for mapping.

Table 2.--Map Accuracy and Resolution Requirements

Map scale	Std. error of position	Ground resolution	Contour*	Std. error of elevation
	meters	meters	meters	meters
1:1,000,000	300	100	500	150
1:250,000	75	25	100	30
1:100,000	30	10	50	15
1:50,000	15	5	25	8
1:25,000	7.5	2.5	10	3

\*The contour interval actually used depends on the topography. Average values are used in this table.

For the production of thematic maps, the spectral band of the sensor becomes important. For instance, water bodies are best identified in the near infrared band (0.8 to 1.0  $\mu m$ ) since water reflects very little energy at these wavelengths. Most healthy vegetation, on the other hand, is highly reflective in the near infrared, so this band can also be used for identification of vegetated areas. For the identification of the massed works of man, such as urban areas and transportantion routes, the red band (0.6 to 0.7  $\mu m$ ) is the most useful. In some cases, combinations of bands are required to identify the features to be shown on the thematic map. Thus, the spectral response of the sensors used for thematic mapping should be selected on the basis of features to be mapped. The main requirement is that the spectral bands chosen yield the maximum enhancement of the items of interest.

Thus, sensors to be used for planimetric, topographic, and thematic mapping require good geometry, relatively high resolution, and spectral response which will enhance the features to be mapped. To meet the first requirement, which is important primarily for planimetric and topographic mapping, photogrammetric frame cameras with film to record the image are usually required. However, for small-scale mapping (1:1,000,000) it is possible that high-resolution television systems will be adequate. It is necessary to calibrate TV systems, however, so that the geometric distortions may be removed. Some panoramic cameras and line-scanning systems can meet the resolution or spectral response requirements, but they generally do not have sufficient geometric accuracy for use in mapping. However, increased attention to geometric fidelity could permit these sensors to be used, at least for small-scale mapping.

#### Collection of the Data

There are at least three basic modes which can be used to acquire imagery for mapping. These are:

- 1. Aircraft
- 2. Data transmission from spacecraft
- 3. Film return from spacecraft

The aircraft mode is the one most widely used at the present time, and it will very likely continue to play a major role in the acquisition of mapping imagery, particularly for large-scale maps. Aircraft are the least expensive

platforms when small areas are to be mapped, and they are the best platform to use when the recovery of photographic film is required. However, aircraft platforms have several disadvantages. For example, many photographs are required to cover a large area, and it is very difficult to match tones in mosaicking a large number of photographs. The time and cost of map production vary directly with the number of photographs involved. In figure 1 the number of photographs and control points required to cover an area of 8,700 square km with spacecraft and with aircraft are compared. Another disadvantage of aircraft platforms is that the varying sun angle causes similar features to be enhanced or obscured on different photographs. The wide angle cameras normally used to cover large areas from aircraft can also introduce tonal problems when constructing mosaics.

The second mode is that which is planned for the Earth Resources Technology Satellites (ERTS A and B). This mode relies on a television system or scanner as the sensor, with transmission of the data to the ground by a wide-bandwidth telemetry link. The primary advantage is that the satellite can remain in orbit for a long period of time and provide the potential for repetitive coverage on a global basis. The large amount of data transmitted from the satellite can create a data-handling problem on the ground, however, so the rate of data acquisition must be controlled. The television and scanner sensors do not provide the geometric accuracy and resolution required for large-scale mapping. Small-scale (1:1,000,000) mapping will be possible, however, if sufficient care is taken in calibrating the sensors.

Perhaps the best mode for acquiring imagery for mapping large areas is film return from spacecraft. This mode could use a spacecraft in a relatively low-altitude orbit. After all of the film has been exposed, the film package would be returned to earth for processing. Photographs obtained in this manner could have very high geometric fidelity and resolution, thus being ideally suited for mapping. A study by the U.S. National Academy of Sciences 2 recommends such a system for mapping.

The sensors proposed by NAS for this system include the following:

- vertical frame camera; 300 mm focal length, 225 × 370 mm format
- vertical frame camera; 150 mm focal length, 225 x 225 mm format
- narrow-angle convergent camera; 600 mm focal length, 225 × 450 mm format
- stellar attitude camera
- laser altimeter

All cameras in this system would provide the necessary ground resolution for mapping at 1:100,000 and 1:50,000 scales, and the 600-mm focal length camera would have sufficient resolution for 1:25,000-scale mapping. This system has been designated by NASA for ERTS C and D, but no approval has yet been given to build these satellites.

<sup>3/</sup> National Academy of Sciences, Useful Applications of Earth Oriented Satellites, Geodesy-Cartography, Panel 13, Washington, D.C. 1969.

Of course, the use of film-return satellites assumes the need to map large areas. Because of the high fixed cost of the satellite system, which has been estimated as \$15 to \$20 million, the cost is the same to acquire photographs of  $1000 \, \mathrm{sq} \, \mathrm{km}$  as it is to acquire photographs of  $10 \, \mathrm{x} \, 10^6 \, \mathrm{sq} \, \mathrm{km}$ . The use of a satellite system for mapping can be justified, therefore, only if large areas are to be mapped or repetitive coverage, such as that provided by a data-transmission satellite, is essential.

Regardless of which mode of data acquisition is used, there are two basic sensor calibration requirements which must be considered—geometric and photometric. Geometric calibration is the determination of the changes in image position which result from various imperfections in the <a href="sensor">sensor</a>. The calibration data are obtained by measuring lens distortion, lens alinement, electronic distortions, and so on, and are used to correct the locations of points on the image so that accurate positions may be determined. In addition, movements of the sensor platform can introduce geometric distortions in the images, particularly for scanning systems, and these must be removed during the image processing.

Photometric calibration is the determination of the response of the imaging element to different levels of illumination. Thus, for a television system, it is necessary to determine how the output signal varies with illumination on different areas of the photosensitive surface, illumination levels, spectral regions, temperature, and so on. Similar considerations apply to photographic systems, although the calibration is more difficult because of inherent nonlinearities in photographic systems. Photometric calibration is important primarily for thematic mapping. It is necessary to know whether a tonal variation on the image is due to changes in sensor response or changes in the ground target so that a correct interpretation can be made.

Most of the available earth-oriented images are photographs taken with handheld Hasselblad cameras on the Gemini and Apollo missions. Nevertheless, these photographs have been useful for indicating the potential applications of space photographs for mapping. Some results of mapping from these photographs will be presented in the last section of this paper.

#### Processing of the Image Data

After imagery is acquired for mapping, several procedures must be used to process it into a map. First, the geometric and photometric distortions caused by the sensor must be removed. The techniques for removing distortions vary from relatively simple optical methods to quite sophisticated digital computer processing. A detailed discussion of these techniques is beyond the scope of this workshop, but there is sufficient evidence to indicate that most of these distortions can be minimized.

After distortions are removed, the images must be rectified and scaled to fit a map projection. This usually requires the use of ground control points that are visible on the image and have known coordinates in the map reference system. The most common map reference system is the geographic coordinate system. It is based on an assumed ellipsoidal shape for the earth and datum which defines the location

of some initial point on this spheroid. For North America, the figure and datum used are Clarke Spheroid of 1866 and the North American Datum of 1927. Most other areas of the world use the International Ellipsoid.

Because no spherical or ellipsoidal surface can be transformed into a plane without some kind of distortions, several different map projections are used to minimize distortions, depending on the size and shape of the area to be mapped. In the United States, the systems of State plane coordinates based on the transverse Mercator and Lambert conformal conic projections have been widely used in mapping and surveying. These projections, however, vary from State to State and even within States, so problems are encountered when mapping across State or zone boundaries. One system which overcomes most of these problems and can be used worldwide is the Universal Transverse Mercator (UTM) projection and associated grid. This system covers the earth with 60 zones, each of which is 6° in longitude and extends north to 84° latitude and south to 80°. In the polar regions another system can be used—the Universal Polar Stereographic (UPS) projection and grid system. The main advantage of these projections is their worldwide applicability and the availability of tables for their construction.

Regardless of which projection and map reference system is used, the sensor image must be transformed into the selected system. This is normally done by rectifying and scaling the image and superimposing grid intersections. Factors such as earth curvature and terrain elevation must also be considered. Several image correction techniques can be employed, ranging from simple graphical methods to computer-controlled differential rectification.

In the production of photomaps, scaling and rectification are followed by mosaicking and cartographic enhancement. Cartographic enhancement requires the use of auxiliary data to add names, road designations, boundaries, and other information to the map.

For producing thematic maps with imagery of more than one spectral band, registration of the bands becomes important. Each band must be superimposed on the others to within about one resolution element so that the spectral signature of various image points can be determined. Very accurate calibration of the sensors is a prerequisite for good registration. In particular, if separate cameras are used to acquire the imagery, the precision of boresighting, or relative alinement of the optical axes, must be known. The camera lenses should also be matched with respect to focal length and lens distortion. With multispectral scanners, many of these problems are avoided since the same optical system is used for each spectral band.

One technique for automatic thematic mapping now being studied by the U.S. Geological Survey is density slicing. This is a photographic process which isolates very small density ranges on the photographs. Each density range or slice is then printed in a distinctive color, and several slices can be overlaid to produce a composite. One goal is to isolate specific features, such as water, in a unique density range on the photograph so that one density slice can be used as a map of these features. Electronic and optical techniques for automatic thematic mapping are also being studied in an effort to determine which is the most accurate and efficient.

In summary, then, several steps are required to produce a map from sensor images. Figure 2 is a flow diagram of the data-handling concept for earth resource imagery which is being investigated by the U.S. Geological Survey. An image correlator is used to obtain the registration data for several sensor images. A spatial and/or spectral transformation is then done to remove sensor distortions and fit the images to map projection. Fitting the images to a map projection requires the use of ground control and/or orbital data. At this point, planimetric photomaps may be produced. To produce thematic maps, additional processing, either analog or digital, is required. In the analog mode, density slicing or similar techniques are used to identify the signatures of the desired features. In the digital mode, the same process can be performed, but it requires the conversion of the image data into a digital format.

#### Results and Conclusions

Several studies have been done with the available Gemini and Apollo photographs which indicate some of the potential usefulness of space data. Figure 3 is a color photograph of the Dallas-Ft. Worth, Texas, area taken on the unmanned Apollo 6 mission in 1968. The extent of urbanized area is readily apparent. This photograph was compared with a 1:250,000-scale map prepared in 1954 and updated in 1963 to determine what changes had occurred. Figure 4 shows these changes.

This space photo provided a means of updating the map. If periodic coverage was available, space photos could be used to monitor changes in urban areas.

An example of map revision with space photographs is shown in figure 5. Two photographs taken on the Apollo 9 mission in March 1969 were rectified and overlaid on a 1:250,000-scale map of the Phoenix, Arizona, area. The map was considered current in March 1969, but from figure 5 it can be seen that at least two changes had occurred since the map was made. Figures 6 and 7 show comparisons between the standard line map and the map with a space imagery base. Considerably more detail is visible on the space imagery. The map accuracy was also improved using the space photograph. Figure 8 shows portions of the original map and the corrected map. The map planimetry was moved about 1 mm to conform with the detail on the space photo. This map is for sale by the U.S. Geological Survey.

A second photomap, this one at a scale of 1:500,000, has been prepared from space photographs. Photos from several Gemini and Apollo missions were used in its production. Copies of this map are available from the U.S. Geological Survey for those who would like to make comments on it. The addition of space imagery on the map base holds promise for improving the content, currency, and even the accuracy of conventional line maps or charts.

Several experiments have been done to develop automatic techniques for thematic mapping. Figure 9 shows the results of an experimental effort to extract the surface water distribution from Apollo 9 color infrared photographs. This work was done by RCA, under contract to the U.S. Geological Survey, using an electronic scanning technique.

Figure 10 shows the automatic separation of thick and thin snow areas from an Apollo 9 color infrared photograph. This work was done by Philco-Ford Corporation with photographic techniques. This type of information would be useful to water-supply managers if it were available on a periodic basis.

Other work has been done using photoenhancement techniques to increase the interpretability of the space photographs. For instance, figure 11 shows enchancement on an infrared photograph of the Ouachita River in Arkansas at flood stage. This image provides an excellent view of the extent of flooding. Figure 12 is an enhancement of a selected portion of the photograph used in figure 11. The tone differences in the flooded area are believed to be the result of vegetation on or above water level. Figure 13 shows a photoenhancement of the mouth of the Colorado River. The sedimentation patterns in the water are clearly visible on the enhanced image.

The results of the studies shown in this presentation indicate some of the potential applications of space photography to mapping. The imagery used was certainly not optimum for mapping purposes, and there is considerable room for improvement. The planned ERTS A and B satellites are expected to provide imagery that will be useful for small-scale mapping, both planimetric and thematic. The repetitive coverage capability will certainly be useful for monitoring changing phenomena.

However, to really solve the world mapping problems, other imaging systems will have to be flown. Film-return satellites, as proposed by the National Academy of Sciences, and geosynchronous satellites may have to be used together with aircraft to provide imagery for rapid and efficient mapping operations. Until such systems are in use on a worldwide basis, there is little likelihood that the planimetric and topographic map needs, particularly of the developing countries, will be met.

#### Glossary

- Cartographic Enhancement The addition of names, boundaries, road and railroad designations and other information to the map base or photoimagery to produce a useable map.
- Cartographic Referencing The scaling, positioning, and gridding of the map information or photoimagery to place it in a map reference system.
- Differential Rectification The process of removing the effects of tilt, relief, and other distortions from imagery by correcting small portions of the imagery independently.
- Image Correlator An electro-mechanical device for locating the corresponding point on two or more images.
- Image Enhancement The manipulation of image density to more easily see certain features of the image.
- Map Projection A systematic drawing of lines on a plane surface using a mathematical transformation to represent the parallels of latitude and the meridians of longitude of the earth or a section of the earth.
- Map Revision Updating, improving and/or correcting map content to reflect the current status of an area.
- Mosaicking The assembling of photographs or other images whose edges are cut and matched to form a continuous photographic representation of a portion of the earth's surface.
- Orthophotomap Maps consisting of photoimagery, which has been processed so that the scale is true and uniform, and certain cartographic symbols and labels which enhance certain map detail.
- Planimetric Map A map which presents only the horizontal positions for features represented.
- Rectification The process of projecting a tilted or oblique photograph onto a horizontal reference plane.
- Register The correct position of one band of a multiband composite image in relation to the other bands or to images collected at a different time.
- Resolution The number of black and white line pairs which can be separately recorded in a dimension of 1 mm. on the image.
- Signature Analysis Techniques Techniques which use the variation in the spectral reflectance or emittance of objects as a method of identifying the objects.
- Spectral Band Portions of the electromagnetic spectrum where the information on a particular image was collected.

# Glossary (cont'd)

- Synoptic Coverage Imagery which covers a large area in one frame.
- Telemetry Link The system for transmitting data over long distances using radio techniques.
- Thematic Map A map showing the location and distribution of a certain feature such as water or vegetation.
- Topographic Map A map which represents the horizontal and vertical positions of the features represented.

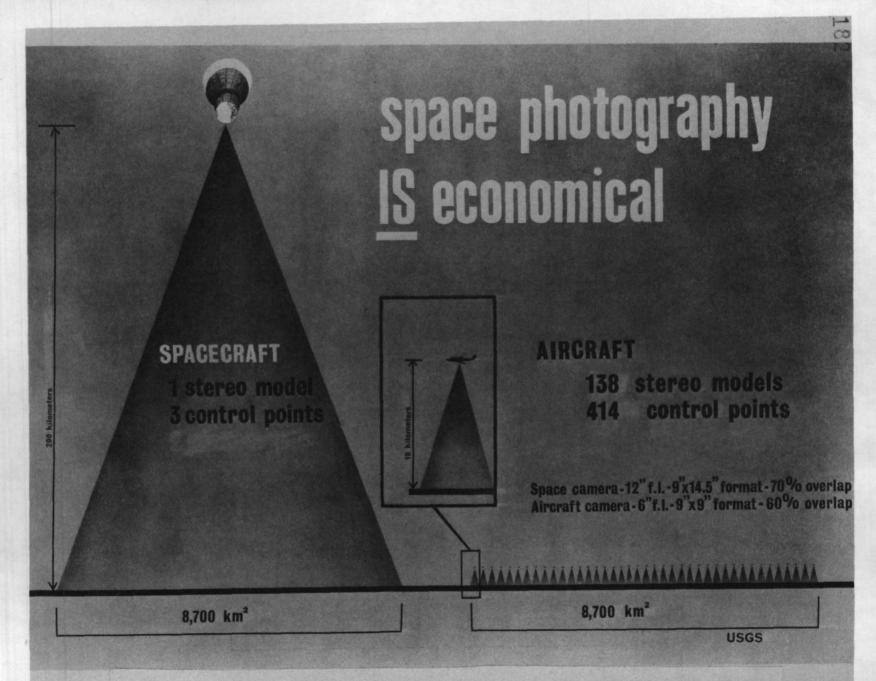


Figure 1. -- Comparison of ground coverage of spacecraft and aircraft photographs.

# DATA HANDLING CONCEPT FOR EARTH RESOURCE IMAGERY

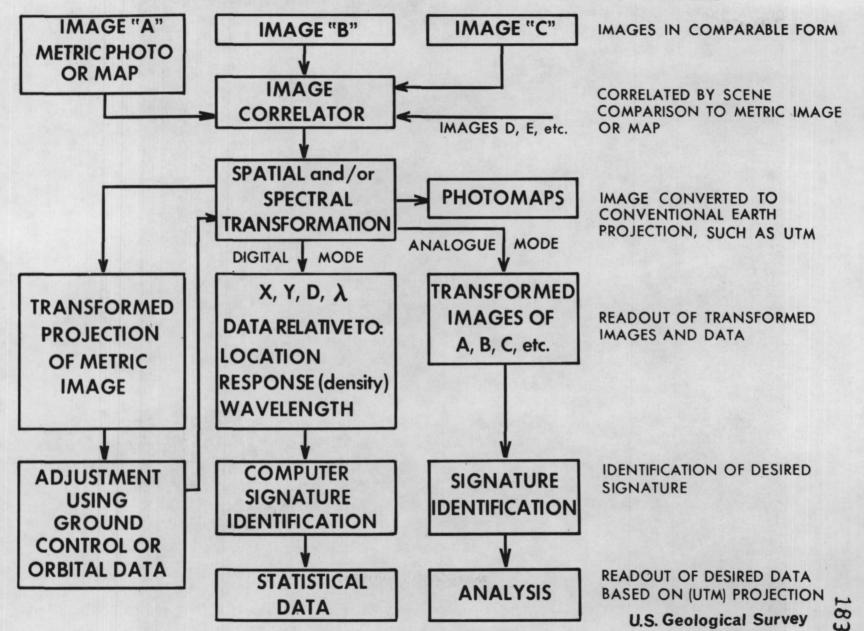


Figure 2.



Figure 3.--Apollo 6 photograph of the Dallas-Fort Worth, Texas, area.

# FORT WORTH, TEXAS AND VICINITY

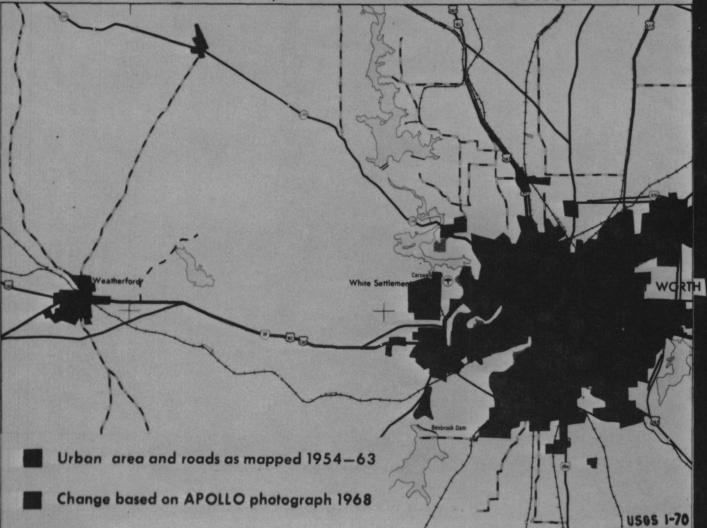


Figure 4.—Revision of the urban area shown on existing map using Apollo 6 photograph.

# 1969 MANUSCRIPT REVISED BY 1969 SPACE (APOLLO) PHOTOGRAPHY



(1) EXTENSION TO INTERSTATE

Figure 5.-- the manuscript (1:250,000 scale, Phoenix sheet) was developed by the USGS from all available sources and was considered current as of March, 1969, which is the same date as the Apollo 9 space photograph. On this particular section of the map the space photo indicated both additions and positional corrections to be made to the road net.

# 1:250,000-SCALE MAP - PHOENIX





···with space imagery base

standard line map

USGS 1-70

Figure 6.--Comparison of standard line map and map with space imagery base.

# 1:250,000-SCALE MAP - PHOENIX



standard line map

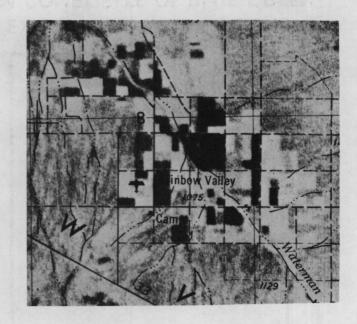


...with space imagery base

US68 1-70

# Map Accuracy Improved By Space Photo





Original Map

Corrected Map

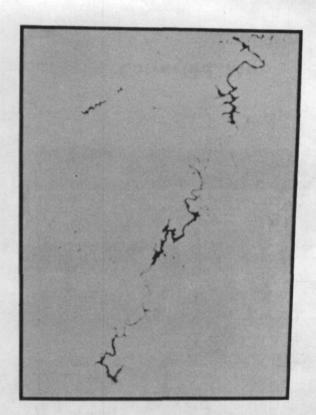
Figure 8.

Map detail (planimetry) was moved about 1 mm (0.04") on this 1:250,000-scale map (Phoenix) to conform with the detail on the space photo (Apollo 9). The photo was found to be correct.

# AUTOMATIC MAPPING OF SURFACE WATER DISTRIBUTION FROM INFRARED SPACE PHOTOGRAPH, ALABAMA

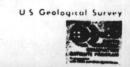


APOLLO SO65 FRAME No. 3790 COLOR IR GADSDEN, ALA. AREA

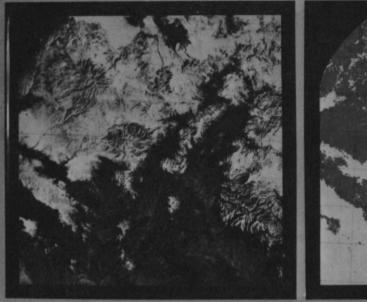


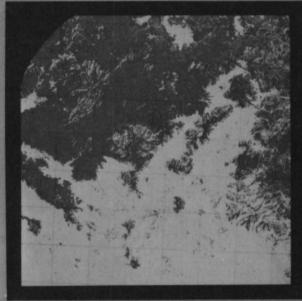
FROM COMPOSITE OF BLUE-GREEN
AND PHOTO IR BANDS

Image enhancement by RCA, Advanced Video Technology Group



### **AUTOMATED SNOW MAPPING**





COLOR IR PHOTO

**THIN SNOW** 

**THICK SNOW** 

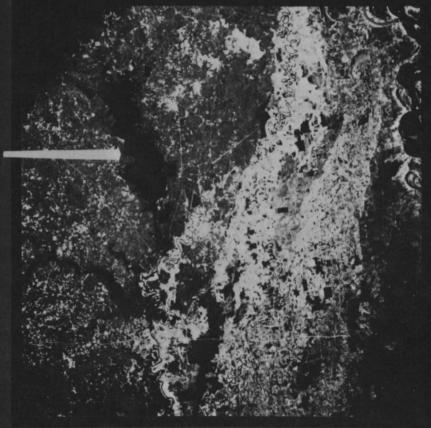
ARIZONA SNOW SCENE

BASED ON "DENSITY SLICING" BY PHILCO FORD IN COOPERATION WITH THE USGS

Figure 10.--Extraction of snow information from Apollo 9 space photograph.

# SPACE PHOTO MAPS FLOOD LOUISIANA - ARKANSAS

OUACHITA RIVER IN FLOOD MARCH 9, 1969

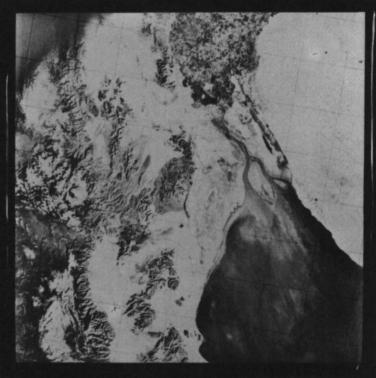


AS 9-26A-3740



# MOUTH OF THE COLORADO RIVER





COLOR IR PHOTO

ENHANCED B&W PRINT OF COLOR IR PHOTO

Enhancement of water detail using conventional photolab procedures

Page Intentionally Left Blank

#### BIOGRAPHICAL SKETCHES

Dr. James R. Anderson Dr. John L. Place

- Dr. James R. Anderson was born in the state of Indiana.

  He received a doctorate in Geography from the University of Maryland in 1950, and presently is a Professor of Geography at the University of Florida. Formerly he had been employed by the U.S. Department of Agriculture where he conducted a number of land use studies. More recently, he served as Chairman of the Commission on Geographic Applications of Remote Sensors of the Association of American Geographers from 1967 to 1969. He has prepared and revised maps of land use for the National Atlas of the United States of America which was released in January 1971.
- Dr. John L. Place was born in California. He received a doctorate in Geography from the University of California in Los Angeles in 1970. He has been working on research related to the NASA Earth Resources Program since 1964 and presently is in charge of regional studies in the Geographic Applications Program of the U.S. Geological Survey.

#### REGIONAL LAND USE MAPPING: THE PHOENIX PILOT PROJECT

James R. Anderson

University of Florida

and

John L. Place

U.S. Geological Survey

#### INTRODUCTION

Regional land use mapping and inventory should be a major component of effective regional analysis. Land use maps, topographic maps, soil maps, as well as other kinds of maps can be effective tools in the planning and management of land resources. However, if land use maps are to be used effectively in making planning and management decisions at local, state, and national levels, such maps and inventories should be accurate and up-to-date, and should provide the appropriate information in a format most useable for planning and management purposes.

Numerous examples of national, regional and local programs which have utilized aerial photographs effectively in land use inventory and mapping can be cited. A few are briefly mentioned here to illustrate how widely the aerial photograph has been accepted as a tool in carrying out inventory and mapping programs at different scales of refinement and detail.

Currently Canada is conducting a land inventory for all of Canada that has been settled, which is approximately 800,000 square miles. In this inventory an effort is being made to assess and map land "according to its capabilities for various uses" and then relate these uses to various social and economic conditions. To do this in an intelligent manner there is "a need to collect a mass of information on the land's characteristics, and to organize this knowledge so that it can be put to good use." The inventory is a cooperative project between the several provinces and the federal government, which is being conducted under the Agricultural and Rural Development Act.

The Canada Land Inventory, Department of Forestry and Development - Canada, Ottawa, 1966, p.1.

Recognizing that conventional maps have data limitations which need to be complemented by other analytical techniques, a geo-information system has been developed in order to cope effectively with the storage, analysis, and presentation of many different kinds of data about the many characteristics of land and the numerous physical, social, economic, and other conditions affecting the use of land resources. Aerial photography is being used extensively in collecting the great variety of information inputs for the Canadian land inventory and airphoto interpretation is being used as an analytical tool. However, the use of the computer is the major new dimension in land inventory presently being carried out in Canada.

Another example of an integrated survey which made extensive use of aerial photographs and of the techniques of airphoto interpretation in a semi-detailed land use mapping program was the Proyecto Aerofotogrametrico OEA-Chile. This survey covered nearly all of the agricultural land of Chile. Land use information was needed more or less simultaneously for a number of different purposes including (1) the design of a new taxation program for rural areas; (2) research and planning for land reform; and (3) for agricultural development and conservation of soil resources. By sharing the costs of the survey among several related programs it was possible to make the land use survey economical.<sup>2</sup>

In the late 1940's Francis J. Marschner, working in the former Bureau of Agricultural Economics of the U.S. Department of Agriculture, undertook the compilation of land use information at a scale of 1:1,000,000 by using aerial mosaics, which had been prepared as index sheets for the aerial photography then available for the United States. These unpublished maps, now preserved in the National Archives, constituted the most comprehensive single attempt to make a thematic map of land use for the United States. The map, which was a generalization of the unpublished maps compiled by states, was published in 1950 under the title,

Physical Resource Investigations for Economic Development: A Casebook of OAS Field Experience in Latin America. General Secretariat, Organization of American States, Washington, D.C. 1969, pp. 288-293.

Major Land Uses in the United States at a scale of 1:5,000,000. Thus the use of airphoto interpretation in making a definitive study of the major uses of land on a national scale was firmly established by the publication of this map.

Another current example of land use and natural resource inventory is being carried out with major reliance upon the technique of airphoto interpretation and computer compilation, storage, retrieval, and mapping and tabular analysis by the Office of Planning Coordination of the State of New York. This inventory was designed specifically to "identify and record how the State's land resources are being utilized" in order to provide the necessary information for the "long range planning of the State's physical resources."

Several aspects of the methodology of the New York land use and natural resource inventory are worth noting. In the first place, the scale of the aerial photography has been specifically keyed to the 1:24,000 scale of existing topographic maps for the State, thus making effective use of earlier large-scale maps. Secondly, the land use classification represents a compromise between the anticipated data requirements of various potential users and the main source of information which was aerial photographs. Thirdly, both land use areas and point data have been identified and mapped. For example, an agricultural area being identified is orchard land. "Active farmsteads" is an example of point data being obtained through airphoto interpretation. In order to make a meaningful generalization of the massive amount of information contained in the 989 maps at a scale of 1:24,000 necessary for total State coverage, a summarization of data by grid cells is being employed. By using appropriate referencing units, such as political subdivisions, several different statistical analyses can be made by use of the computer. Thus there is a clear recognition of the importance of the prompt analysis of inventory data if such information is to be used effectively for a wide variety of existing needs.

<sup>3</sup>Marschner, Francis J., Major Land Uses in the United States, U.S. Department of Agriculture, Washington, D.C., 1950.

<sup>4</sup>Land Use and Natural Resource Inventory of New York State, Office of Planning Coordination, State of New York, 1969, p. 1.

The Phoenix Pilot Project, which is being carried out under the Geographic Applications Program in the U.S. Geological Survey, has been designed to make effective use of past experience in making land use maps and collecting land use information. The first specific objective of the Phoenix Pilot Project is to make a land use map at a scale of 1:250,000 by using Apollo 9 and aircraft imagery as well as some other supplemental information. In making a land use map at this scale from the sources indicated, it was hoped that at least eight major categories and several subcategories could be identified and mapped. A second major objective in the pilot project is to create a geographically oriented data bank of land use information. It is hoped that a workable scheme can be developed for digitizing land use data on the basis of a one-kilometer grid on the Universal Transverse Mercator Projection and for programming of the electronic computer to print out on call, land use maps, land use information in tabular format, and to make several different kinds of analyses of land use.

Land use information and maps are widely used for a number of purposes, a few of which are cited here as examples.

- (1) In regional and local planning an inventory and mapping of the present uses of land furnishes the most effective base from which to plan needed changes in land uses.
- (2) Officials charged with making assessments for the collection of taxes on land and improvements are very interested in locating uses of land by ownership units. Changes in the use of land and improvements made to land must be carefully assessed if taxes are to be fairly levied.
- (3) State and Federal agencies charged with land management and environmental planning functions must have information about the present use of land resources.
- (4) Utility companies, banks, and other private industries and businesses are interested in land use changes.
- (5) Effective prediction of sediment loads and flood hazards on streams is dependent upon having current information about the distribution of the several different uses of land and the changes in land use that occur. Clearing of forests,

increasing the area of cultivated land, and the expansion of urban areas are examples of changes that greatly affect stream flow.

Among the reasons for selecting the Phoenix quadrangle of the 1:250,000 series of topographic maps of the U.S. Geological Survey were the following:

- (1) Rectified photographs from the Apollo 9 mission of March 1969 have been converted by the U.S. Geological Survey into a photo map which could be effectively used as a base map for land use plotting and analysis.
- (2) Considerable analytical work has already been done in the Phoenix area by the U.S. Geological Survey during the past five years. This meant also that a large collection of recent imagery was available.
- (3) Clear skies and low latitude make it more certain that additional imagery from future manned and other satellite missions will be available for comparative purposes.

#### SELECTION OF SENSORS

The types of sensors used on NASA aircraft to obtain the images in the Phoenix area were mostly conventional aerial cameras utilizing a variety of film-filter combinations, but some experimental testing was also done with side-looking radar. A very large number of pictures were taken from airplanes flying at altitudes as low as several hundred meters to as high as 18,000 meters above the Earth's surface. Of additional interest were the many color photographs taken from orbital altitudes by astronauts using hand-held Hasselblad cameras. After experimentation, it was determined that the most useful sensor image for geographic research was the color infrared photograph. This was found to be true for studies for both rural and urban areas.

One of the cameras used to photograph the Earth from the Apollo 9 spacecraft contained color infrared film. Another finding from the NASA aircraft program was that multiband photography could be of assistance in the study of man-made features, especially surfaces of concrete, asphalt, and roof materials. In order to verify the interpretations obtained from the color and multiband photographs, ground information was collected by field teams and from low-flying aircraft. In some cases the airplanes were equipped with metric cameras with long focal lengths which were intended to collect spot type of information as samples of prevailing conditions on the ground. This served as an additional check in the interpretation of the lower-resolution, satellite-type photographs.

#### DATA COLLECTION

Data being used in the Phoenix Pilot Project include Apollo 9 imagery, photographs taken from both high-flying (17,000 to 19,000 meters) and low-flying aircraft (1,500 to 4,500 meters), and results of ground observation and enumeration. Much pertinent information was also collected from government and commercial offices. The Apollo 9 mission took place in March 1969. The high altitude and low altitude photography, although not taken simultaneously with the Apollo 9 mission was taken sufficiently close in time to be used effectively for preparing a land use map at a scale of 1:250,000 for 1969. Comp. Complete photographic coverage from high-altitude flights was not available for the Phoenix Pilot Area, but such photography was available for Phoenix and vicinity where it was most needed. Mosaics of aerial photographs (1:62,500) taken on lower altitude flights were used for selected areas where more detailed information was necessary for effective delineation of land use categories. Ground observations were made in June 1970 to check the actual land use situation against the available imagery. Some use was also made of the Phoenix urban area.

#### DATA ANALYSIS

# A Land Use Classification Scheme for

## Use with Orbital Imagery

Although it is very unlikely that the one ideal classification of land use will ever be developed or universally accepted, there is a growing appreciation for the advantages of more standardized approaches to land use classification for urban and regional planning and other purposes. In developing a land use classification scheme for application in the Phoenix Pilot

Project, several working criteria were established for the purpose of giving guidance in adopting a workable scheme of classification for mapping land use in the Phoenix area.

Among the criteria used were the following:

- 1. A minimum level of accuracy of about 85 to 90 percent or better should be approached in the interpretation of the imagery being used.
- 2. A well-balanced reliability of interpretation for the several categories included in the classification scheme should be attained.
- Repeatable or repetitive results should be obtainable from one interpreter to another and from one time of sensing to another.
- 4. The classification scheme should be useable or adaptable for use over an extensive area.
- 5. The categorization used in the classification scheme should permit vegetative and other cover types to be related to be activity-oriented categories whenever possible.
- 6. The classification scheme should be suitable for use with imagery taken at different times during the year.
- 7. The classification scheme should permit effective use of sub-categories that can be obtained from ground surveys or from the use of imagery available at a larger scale or with the use of color photography.
- 8. A need to collapse the categories of the classification scheme into a smaller number of categories must be recognized.
- 9. Comparison with land use information compiled at earlier points in time and with data that will be collected in the future should definitely be possible.
- 10. The classification scheme should recognize the multiple-use aspects of land use whenever possible.

The following classification scheme was adopted for use in the Phoenix Pilot Project.

# Land Use Classification Scheme for Mapping Land Use from High-Altitude Imagery in the Phoenix Area

## I. Agricultural

- A. Cropland (All cropland except orchards, groves, and vineyards. All cropland will be irrigated in the Phoenix area.)
- B. Orchards, Groves, Vineyards (A more permanently established cover type than generally exists for other cropland.) All of this use will be irrigated in the Phoenix area.

### II. Grazing

- A. Rangeland
- B. <u>Pasture</u> (irrigated) may need to be included as part of cropland (IA)

#### III. Forestry

- A. Arid woodland (Generally of little commercial value for timber or wood products but may be of value for watershed protection, grazing, wild-life habitat, and recreation.)
- B. Forest Land (Very little such land will be found on the Phoenix Quadrangle.)
- IV. Mining and Quarrying (There is no oil or gas production on the Phoenix Quadrangle.)
- V. Transportation, Communications, and Utilities
  - A. Highways
  - B. Railroads
  - C. Airports

## VI. Urban Activities

- A. <u>Urbanized Areas</u> (1970 definition not yet determined by the Bureau of the Census)
  - 1. Industrial

- 2. Commercial
- 3. Residential
- 4. Other
- B. Other Urban (Populated places of more than 2,500 but not including urbanized areas)
- VII. Towns and Other Built-Up Areas (With a lower areal limit which is identifiable through interpretation)

#### VIII. Recreational Activities

- A. Mountain Oriented
- B. Desert Oriented
- C. Water Oriented

When this adopted land use classification scheme was evaluated against the established criteria, it was obvious that all of the criteria could not be satisfied immediately by the classification scheme. Some of the criteria are not always satisfactorily met in classification schemes used in conjunction with field or enumerative surveys. It has been possible to meet some of the criteria more easily than others. Generally, however, the adopted land use classification scheme has worked staisfactorily when used with Apollo 9 as well as aircraft imagery available for the Phoenix Pilot Area.

In developing the land use classification scheme for the Phoenix area, it seemed highly desirable to maintain effective rapport with existing schemes of land use classification that are currently in widespread use. The more basic the categorization used in a classification scheme, the more variable the uses that can be made of the classification. Categories containing a combination of two or more discrete land uses have been avoided, since a grouping of uses during the interpretation stage would prevent alternative groupings from being made later.

## Interpretation of Imagery

The preparation of the land use map of the Phoenix quadrangle in Arizona was done in the following steps.

First, two of the Apollo 9 photographs were put together to fit the existing map of the Phoenix area. These photographs served as the base for the land use map. Study of the Apollo photographs permitted the selection of areas with more intensive land use, such as settled areas and irrigated cropland. For these areas, aerial photographs were procurred. For most of the area, the Apollo photographs are the best quality recent photographs available. To supplement the Apollo photographs, mosaics of aerial photographs taken by the U.S. Department of Agriculture during February 1970 were used. The aerial photographs and orbital photographs were found to be mutually supporting, especially for delimiting cropland boundaries and the urban fringe of Phoenix. clutter in the aerial mosaic is clarified by the Apollo photograph and aided in the delimiting of the urban fringe. Rangeland, a category of grazing, could not be uniformly isolated at a desirable level of reliability. This problem was particularly noticeable when arid woodland types were being used for grazing, as they frequently are in southwestern United States.

It was found that, where choices of film types were available, color infrared photographs proved to be the most useful for the interpretation of land use. For the Phoenix metropolitan area, NASA had provided multispectral photography, including color infrared, conventional color, and multiband photography. Of the multiband photographs, the red band of the spectrum produced the clearest pictures of urban areas. The photographs that were taken from satellites or from very-high aircraft were so small in scale that it was difficult to separate the residential from the commercial districts. Some differences in texture were detectable between urban and commercial districts; however, lower altitude photographs, or other supplemental data, were needed for accurate identification of commercial districts of Phoenix.

Since it is improbable that a complete well-balanced land use map can be compiled solely from orbital and aerial imagery, it seems desirable to supplement these useful sources of information with other land use data when available. Use of inference by knowledgeable persons, which is based on such supplemental information, will probably continue to be much needed at least until further technological improvements have been made in remote sensors and until a more standardized approach to interpretation has been developed.

The actual drawing of the land use map was done on a

sheet of transparent plastic which was overlain first upon the Apollo photographs and verified by overlaying upon the published topographic map of the Phoenix area at this same scale. In this way, the boundaries of the land use patterns could be aligned more accurately with the roads, streams, canals, and other topographic features, and with governmental boundaries. The land use patterns were then represented in color on the finished map. It should be noted that this map was not intended for publication; it was intended as a working tool in reading off the land use data into a computer.

After the land use map was completed, a grid overlay of lines spaced one kilometer apart was placed upon the map. The land use at each grid intersection was identified and recorded on computer tape for future analysis, automatic updating, and print out in map form.

### Auto-Processing of Interpreted Imagery

In addition to making a land use map of the Phoenix area at a scale of 1:250,000 by combining the use imagery from high altitude aircraft and satellites, the Phoenix Pilot Project was designed to devise a system for land use data collection, storage, retrieval, and up-dating. Such a digitized data bank is almost absolutely necessary if large masses of data are to be handled efficiently and economically. Since the analysis of land use changes is considered to be a prime objective of any future national program of land use mapping and inventory, it will be important to employ prompt and accurate data processing techniques.

One of the important components of electronic computer handling of data will be a means of geographically isolating cells of information about land use. In the pilot project it was decided to use a l km² cell keyed to the Universal Transverse Mercator grid. Since each UTM grid unit is a square of constant size, the use of this grid makes computer handling of data easier. In order to compare data obtained mainly from the use of remote sensing techniques with information available from other sources, several different identification codes are being keyed to the l km² cells. Thus it will be possible to group these cells by counties, census tracts, watersheds, land management agency areas, and in other ways that may be needed.

Highways will be read from photographs and recorded as changing line patterns in the computer data bank. Other line patterns such as railroads, which rarely change significantly at this scale and within a short time frame, will be shown as a fixed overlay on the printed map output. Each of the land use categories and line patterns will be shown in a different color. In order to increase the value of the data bank for purposes of planning and management, a soils map is also being placed on computer tape. These soils data will be allocated to the same one-kilometer grid points.

At each kilometer grid point the date of the photograph from which the land use was interpreted is also recorded. Presumably, the land use information in the data bank will be updated at intervals of one to five years, depending on how rapidly changes in land use are occurring. If good geometric control is maintained, the computer can report changes occurring at each grid point at each updating. Thus, a map of land use change could be printed out automatically on the computer.

This spatial identification of interpreted uses of land will form an important basis for further study of land changes that are occurring. Prompt, efficient, and flexible analysis of the changes is necessary if a data bank of land use information is to be an effective toll in regional land use mapping and inventory. It will also be essential to have the capability to relate the present land use situations and the changes that occur from time to time to other characteristics of land. Some examples of influences on land use are natural soil, slope, and climatic conditions; assessed and sale values; size and type of ownership units; distance from centers of population of various size; and access to different types of transportation.

#### CONCLUSIONS

Some conclusions reached from the Phoenix Pilot Project are:

- (1) Land use maps and accompanying statistical information of reasonable accuracy and quality can be compiled at a scale of 1:250,000 from orbital imagery.
- (2) Orbital imagery used in conjunction with other

sources of information when available can significantly enhance the collection and analysis of land use information.

- (3) Orbital imagery combined with modern computer technology will help resolve the problem of obtaining land use data quickly and on a regular basis, which will greatly enhance the usefulness of such data in regional planning, land management, and other applied programs.
- (4) Agreement on a framework or scheme of land use classification for use with orbital imagery will be necessary for effective use of land use data.

#### GLOSSARY

Data bank is a term used to indicate the information stored in the electronic computer.

Mosaic is a composite of aerial photographs.

Print out in map form refers to the capability of the electronic computer to make a map by printing symbols of various kinds on a sheet of paper.

Page Intentionally Left Blank

#### BIOGRAPHICAL SKETCH

#### Frank E. Horton

Dr. Horton is Director of the Institute of Urban and Regional Research and Professor of Geography, at the University of Iowa. He is principal investigator of a contract with the Geographic Applications Program, U.S.G.S.: The Application of Remote Sensing to Intra and Inter-Urban Systems. In addition he is on the research and training staff of the Center for Urban Transportation Research and Training, a member of the research team dealing with Quantitative Spatial Methodology, a member of the research staff on an Urban Policy Study for the State of Iowa. Amoug his many committee memberships, Dr. Horton is currently serving as Chairman of the Remote Sensing Commission, of the Association of American Geographers, is a member of the International Committee on Remote Sensing and Data Processing, International Geographical Union, is a member of the National Highway Research Board's Travel Forecasting Committee, and is a member of the Urban Symposium Subcommittee, Committee on Geography, National Academy of Sciences; and in the past year served as a member of the Urban Information Systems and Measurement Committee of the National Highway Research Board. Also during the past year Dr. Horton served as Associate Director for the Institute for Comparative Urban Analysis, sponsored by the National Science Foundation; a member of the Earth Observations Committee, Study on Space Science and Earth Observation Priorities, Space Science Board, National Academy of Sciences. In April 1970 Dr. Horton's book entitled: Geographic Perspectives on Urban Systems: With Integrated Readings, (with Brian J.L. Berry), was published by Prentice Hall. He has written numerous articles dealing with remote sensing of urban environments, urban planning and geography, and urban transportation analysis.

# THE APPLICATION OF REMOTE SENSING TECHNIQUES TO URBAN DATA ACQUISITION

Prepared by

Dr. Frank E. Horton
Director, Institute of
Urban and Regional Research
and Professor of Geography
University of Iowa

# Introduction

Current research related to the application of remote sensing techniques to problems concerning the acquisition of data useful in urban and regional planning, management, and research clearly indicates a potentially powerful data acquisition system is feasible. One of the most perplexing problems facing urban planners, managers, and analysts is the dearth of pertinent, timely, and reliable information. In an earlier paper it was stated "...data performs a vital, two-fold task: (1) it provides a basis for testing research hypotheses..." about processes "...and (2) it provides a basis for current decision-making as well as a means of monitoring the outcome of past decision." The collection of data concerning a variety of urban phenomenon is a continuing and costly problem.

Recently there has been in this country an increasing concern with the development of information systems, data handling procedures, and data processing technology. In my opinion, and in the opinion of others, it can truthfully be stated that our ability to handle data is much greater than our ability to collect reasonably accurate data for input to operating urban information systems. It is in this context that remote sensing offers a significant opportunity to help improve the effectiveness of urban management, to help guide urban growth and development, and to help maintain and improve the quality of metropolitan environments.<sup>2</sup>

Frank E. Horton and Duane F. Marble, "Regional Information Systems: Remote Sensing Inputs," <u>Technical Papers</u>, Proceedings of the 35th Annual Meeting of the American Society of Photogrammetry, March, 1969, p. 262.

<sup>&</sup>lt;sup>2</sup>Duane F. Marble and F. E. Horton, "Remote Sensing: A New Tool for Urban Data Acquisition," <u>Urban and Regional Information Systems: Federal Activities and Specialized Programs</u>, J. Rickert (ed.), Kent State University, 1969, pp. 252 - 257.

It should be pointed out that of all the remote sensing technology available to us, remote sensing applications in urban environments has been primarily restricted to photographic sensors. This is not to say that others may not be more useful, nor that new remote sensing technologies not yet applied may not provide greater utility to urban analysts, rather this statement rests upon the fact that we have been unable, at least to date, to mount a major research program in evaluating alternative remote sensing technology applications in an urban context. In addition, and just as important, is the fact that no large scale operational demonstration programs of the utility of remote sensing in urban data acquisition have been completed to date.

While the above comments may seem somewhat negative, they should not deter us from research goals and the development of a continuing research program, nor should they be construed to mean that positive developments in this area have not occurred. Utilizing primarily photographic sensors, and for the most part fairly primitive straight forward photo interpretation techniques, we have learned a great deal about the amount of data which can be extracted and converted into useful information for decision-makers and analysts in metropolitan areas.

In studies supported by the Geographic Applications Program, United States Geological Survey, and NASA, photographic sensors, and to a limited extent radar, have been evaluated in terms of their ability to provide information about cities. These include the application of remote sensors to the acquisition of data concerning housing and population characteristics, urban travel, identification of urban land use and activities, general evaluation of urban change detection systems, utility of space photography in urban data acquisition, the identification of intra-urban commercial centers and their functions, identification of the economic position of single cities with respect to all other cities within a region or nation, and with respect to the latter, the use of that knowledge in monitoring regional economic growth. In addition, research activities are being carried out which relate to urban geographic information systems and the interface between imagery and operational urban information files.

In the time available to me here today it is impossible for me to detail all of the projects completed and underway. Therefore, I will discuss the application of remote sensing techniques useful in acquiring data concerning housing quality.

<sup>&</sup>lt;sup>3</sup>Many of these topics are discussed in detail in Duane F. Marble and Frank E. Horton, <u>Remote Sensors as Data Sources for Urban Research and Planning</u>, Remote Sensing Laboratory, Northwestern University, Evanston, Ill. (forthcoming).

# Remote Sensing Applications to Housing Quality Definition 4

Federal and local agencies have shown an increasing interest in methods for the rapid survey of housing conditions over large urban areas in order to:
(1) evaluate the magnitude of such problems within the city, (2) identify those neighborhoods most in need of immediate remedial action and (3) to qualify for Federal funds for neighborhood improvement. At present expensive ground surveys covering a large number of parcels, and involving many variables, are required. Recent research at Northwestern University attempted to evaluate the following hypotheses with respect to housing quality and surveys and potential remote sensing inputs: (1) due to high redundancy levels, an excessive number of variables are currently collected by public agencies in their attempt to identify housing quality areas; (2) a reduced set of these variables exists which are potentially observable via remote sensing techniques; (3) a viable classification algorithm can be developed utilizing the reduced variable set which would quantitatively assign a particular areal unit of observation to a unique quality class; (4) measures of the reduced variable set can be extracted from remote sensor imagery.

# Analysis of Ground Data

Ground data was obtained from a survey conducted by the Los Angeles County Health Department in the spring of 1968 covering some 1,300 city blocks in three districts in the Los Angeles area containing some of the country's worst housing. This data set constituted the basic ground truth information for the Northwestern University participation in NASA's Earth Resources Aircraft Mission 73 and were used to explore the hypotheses noted above.

A 1% sample of parcels (478 parcels) was drawn from the Los Angeles housing data set (A parcel is a piece of land under single ownership). The 37 structural and environmental variables utilized are given in Table 1. It is unfortunate that many of these variables are subjectively defined and hence suffer from severe scaling problems. However, they are representative of the current state of the art of housing studies. A statistical technique called principle axes factor analysis was applied to the sample set. This analysis produced a factor structure which indicated that the basic factors produced were consistent with those found in existing public agency statements. However, this analysis also demonstrated that for each basic housing element, the variables acting as indicators of that element tended to be highly correlated with other variables within the element. This strongly suggests that a more critical evaluation is needed of the cost effectiveness of collecting data on large numbers of variables as practiced in existing housing quality studies.

<sup>&</sup>lt;sup>4</sup>The major portion of this section has been taken from Duane F. Marble and F. E. Horton, "Extraction of Urban Data from High and Low Resolution Images," Proceedings of the Sixth International Symposium on Remote Sensing of Environment, Vol. II, October, 1969, pp. 807 - 814.

Of particular interest was that, for the observations which made up the parcel sample, the structural variables emerged as a single set of variables which were uncorrelated with environmental variables. This led to the rejection, for this study area, of the notion of estimating overall housing quality (as currently defined by public agencies) at the parcel level based only upon remote sensor observation of environmental variables. It is felt, however, that such a finding may be unique to Los Angeles (or at least to cities of the Southwest) which are dominated by single-family structures with a high degree of variation in the level of maintenance of individual parcels. In other U.S. cities, particularly those of the East and Midwest, the set of relationships between structures and environment may be substantially modified in those poorer areas possessing a predominance of apartment buildings, town houses, and other kinds of multi-unit structures.

Using the city block as the unit of study, a similar analysis was undertaken for observations on a 20% sample of blocks (268 units). The resulting factor structure was markedly different from that generated at the parcel level. Other research has indicated that simple correlations between variables tend to increase as the units of observation encompass larger and larger areas; in the several variable case this also results in a larger proportion of the differences being accounted for by a small number of factors and also increasing correlation levels between previously uncorrelated variable sets. In particular, in the present case, the factor comprised of structural variables no longer represented an isolated variable set, but was associated with a number of environmental variables, primarily those which identified the level of upkeep of lots and the existence of land uses which are generally thought to be inappropriate for location near residential developments. This finding is extremely important since it implies that overall housing quality may be estimated at the block level utilizing observations on environmental condition variables alone.

The results of the two analyses indicated not only that the clear factors defined at the individual parcel level had been lost at the block level, but also that the factors used to judge housing quality must be examined anew each time the observational units are made larger, such as the traffic zone or census tract. The results of this study lead to a research concentration upon the assignment of blocks to housing quality classes through remote sensor generation of environmental variables appeared most feasible.

An objective grouping of the sample blocks into five quality classes ranging from high quality to extremely poor housing was made based on similar profiles of factor scores derived from an analysis of observations on all 37 variables. Comparing this grouping with the subjective evaluations made by individuals working on the ground, it was found that the general trends of the two classification structures were similar, with the most deficient blocks being well identified on both; however, considerable differences existed in the drawing of boundaries between the higher rated blocks. The objective grouping is more compact than that of the

enumerators, suggesting that the latter did not utilize the full range of data recorded in making their subjective assignments. Further, it suggests that the ground enumerators tend to be somewhat conservative in assigning blocks to the highest or lowest categories.

The blocks were classified on the basis of scores generated by a factor analysis of the environmental variables. The results showed a strong agreement with those of the previous state with 75.4% of the block assignments being the same in both groupings. The errors occurred in the assignment of a number of marginal blocks and do not constitute a major problem.

The final stage of the ground data analysis examined the feasibility of further reducing the set of 21 environmental variables in effecting the classification. Using a statistical method called stepwise multiple discriminant analysis it was found that a high level of performance (82.2% correct assignment) could be attained using only seven environmental variables, namely measures relating to:

- 1. On-street parking
- 2. Loading and parking hazards
- 3. Street width
- 4. Hazards from traffic
- 5. Refuse
- 6. Street grade
- 7. Access to buildings

Table 2 displays the linear discriminant coefficient, pertaining to each of the five quality classes.

Although it is not claimed that these results possess complete generality in the sense that an analysis of all urban areas would result in the same variables being selected for use in classification, it is highly encouraging that the seven variables listed above, all presumably measurable using remote sensing techniques, can effect a classification of city blocks which is very similar to that obtained by using all 37 environmental and structural variables in combination. This, in itself, is an extremely important finding of the research which could lead to large financial savings in urban data acquisition.

# Imagery Analysis

The imagery analysis consisted of an evaluation of black and white, color, and color infrared photography obtained as part of NASA Aircraft Mission 73 with respect to the identification of the reduced variable set listed above. Color infrared photography was found to be the most useful in estimating the seven variables important in housing quality identification. (Photography was from an RC-8 camera flown at 3,000 feet).

After some interpreter training, sub-sample of 53 contiguous blocks in the Firestone area was chosen for an evaluation experiment. Definition of the variables and subsequent assignment using the multiple discriminant functions made up of the coefficients shown in Table 1 satisfactorily classified 50% of the blocks, when compared to the 37 variable classification, into the five housing groups. Because of the subjective nature of some of the variables, it was necessary to use three relatively inexperienced imagery interpreters and assign blocks on the basis of two out of three interpreters giving the same value. Further investigation indicated that within the area chosen, the differences between Groups 2 and 3 were not critical and upon aggregating Groups 2 and 3, thus reducing the number of housing quality classes to four, the level of accuracy was increased to 69%. Thus, when remote sensor imagery was utilized to estimate the values of the seven variables, it was possible to correctly classify 69% of the blocks into four classes when compared to the four-way classification based upon use of all 37 variables. Once again this percentage is based on a two out of three interpreter agreement, with individual interpreters scoring higher and higher.

Further evaluation of the seven variables utilized suggested that a further reduction in their number would remove some which suffered from severe interpretation difficulties. The original 37 variable set was then reduced to four: (1) street width; (2) on-street parking; (3) street grade; and (4) hazards from traffic, by methods identical to those used in the original analysis. Comparison of the capability of the four variable discriminant functions to classify blocks correctly with respect to the 37 variable classification showed that use of the reduced variable set led to a correct assignment in 78% of the cases.

When estimates of these four variables were derived from the Firestone imagery and inserted into the new linear discriminant functions, 53% of the 53 block test area was correctly classified.

# Conclusions with Respect to Housing Quality Studies

The use of individuals with a higher degree of training in photo interpretation should significantly increase the percentage of successful classifications. Other problems which remain but which seem to fall outside the purview of the Earth Resources Program are:

- (1) Redefinition of variables into a more objective form.
- (2) Development discriminant coefficients for major U.S. cities.
- (3) More critical evaluation of the statistical methods used in the present study.
- (4) Determine how sensitive the classification methods are when giving variables different weights.

Based upon the pilot study outlined here, it seems reasonable to conclude that small area classification of urban housing quality can definitely be accomplished via high resolution aerial photography. Such surveys, at the levels of accuracy

demonstrated here, can be of major utility in quick look surveys. They will not replace ground surveys, but they can permit the ground surveys to function more efficiently by enabling them to focus on true problem areas within the city.

Total costs of the Los Angeles ground survey were over \$50/block. Given the method outlined here, survey costs should be very significantly reduced even when the costs of image acquisition are included. The significant time savings are of at least equal importance since survey delays result in critical delays in implementing urgently needed social action programs. A significant amount of development and calibration work remains to be done before this approach can be considered operational in the context of the typical urban planning office, but there is little doubt of its ultimate validity.

A similar study is currently underway to delineate methodologies for identifying population density surfaces of cities. That is, how population density varies within metropolitan areas. This study is similar to the housing quality study in the sense that population density per se cannot be extracted directly from imagery but only through statistical analysis of other variables which can be acquired from imagery. In addition, variables are also used which are acquired from the 1970 census, such as number of persons per family. In other words, we cannot in all instances rely solely on data items generated by remote sensing techniques but from time to time we will have to fall back on secondary sources of information to help in the accurate definition of particular urban data sets. In the case of evaluating the level of transportation demand in different parts of the city, population density and land use are incorporated into data sets used to define travel demand. Thus, data derived from imagery in previous studies is then incorporated into studies to define other urban data sets. In this way, we can maximize the amount of information gained and minimize the costs of acquiring such information.

# Final Comments

In addition to the problem of information about internal variation in cities, we are also interested in evaluating and defining relationships between sets of cities. <sup>5</sup> Changes in individual cities and their environs often are indicative of changing social and economic conditions within regions of a nation or the nation itself. Many of us are interested in the derivation and implementation of policies

<sup>&</sup>lt;sup>5</sup>An application of side looking airborne radar to this problem is discussed in the Marble and Horton paper cited in Footnote 4 and the utilization satellite imagery is discussed in Gerard Rushton and Nancy Hultquist, "Remote Sensing Techniques for Evaluating Systems of Cities: A Progress Report," Technical Report No. 2, Remote Sensing Project, Institute of Urban and Regional Research, University of Iowa, November, 1970.

related to economic development or regional growth. For example, in our own country we would like to evaluate the effect of certain policies on regional economic growth in Appalachia. Similarly, in other countries where a particular development policy is being pursued, it is appropriate and important to be able to evaluate the impact of alternative policy considerations. Does the policy we have implemented in fact generate the type of development we wanted or expected? In some parts of the world, it is difficult to collect information concerning the impact of specific policies. Either it is too costly or suitable mechanisms have not been developed to acquire such information. It is in this context that we are interested in defining changes in the economic and social characteristics of cities vis-a-vis one another within a region. In this case, geographers at the University of Iowa are evaluating various kinds of indices which can be measured from satellite imagery either manually or automatically which then can be evaluated statistically to define significant regional changes. We feel that this type of research will be particularly useful and feasible using the ERTS-A satellite returns.

The latter problem denotes a new element important in all phases of current urban related remote sensing research endeavors. That is, an ability to detect change over time. Thus, the fact that specific data sets can be defined for one point in time would indicate that changes occurring between two points in time should be definable. While in their simplest form change detection systems would evaluate data acquired in the first time period and data acquired in the second time period in order to discern changes, but more sophisticated methods could be applied Generally, this area of research might fall under the general rubric of information systems. Issues to be resolved in the general area of geographic information systems based on remote sensing inputs are: (1) compatibility with the operational needs of a host of interested public agencies at the local, regional, federal, and international level, (2) the integration of urban and regional information systems requirements, (3) the setting of urban and regional information systems into a national or international program of land use or environmental monitoring, and (4) specific recommendations for hardware and software systems. 6 In addition to these considerations, there is a general problem of the development of imagery analysis procedures designed to automatically define changes which are occurring in metropolitan regions. In other words, if one bit of information did not change between the two observation points, it is unnecessary to recollect that information. Automated change detection systems would clearly be a step forward.

<sup>&</sup>lt;sup>6</sup>Kenneth J. Dueker and Frank E. Horton, "Remote Sensing and Geographic Urban Information Systems," Technical Report No. 3, Remote Sensing Project, Institute of Urban and Regional Research, University of Iowa, January 1971.

While I am not aware of the state of cities in all of your countries, it is clear that in my country, cities are moving toward unprecedented stagnation and even lower levels of efficiency. If we are to achieve solutions to our problems, we must acquire knowledge about the processes which lead to those problems. If theory is developed concerning urban processes and empirically verified and translated into operational programs for the alleviation of those problems, we will be in an excellent position to stem the blight and decay attacking our cities. While this latter discussion may seem somewhat esoteric, it is a plea for us, as well as for you, to continually be alert for new methods of acquiring information which can increase our knowledge of diverse processes and apply that knowledge in order to alleviate critical problems facing the world society.

# TABLE 1

# ENVIRONMENTAL AND STRUCTURAL VARIABLES

#### UTILIZED IN THE LOS ANGELES STUDY

1. ]	Land	Use -	Suitability	for	Residential	Development
------	------	-------	-------------	-----	-------------	-------------

- 2. Condition of Street Lighting
- 3. Presence of On-Street Parking
- 4. Street Width
- 5. Street Maintenance
- 6. Street Grade
- 7. Condition of Parkways
- 8. Hazards from Traffic
- 9. Adequacy of Public Transportation
- 10. Number of Buildings/Lot
- 11. Number of Units/Lot
- 12. Condition of Fences
- 13. Adequacy of Lot Size
- 14. Access to Buildings
- 15. Condition of Sidewalks
- 16. Condition of Landscaping
- 17. Refuse
- 18. Parcel Use
- 19. Adverse Effects of Residences
- 20. Nuisances from Loading/Parking
- 21. Unclassified Nuisances from Industry, etc.
- 22. Overall Block Rating
- 23. Noise/Glare (Block)
- 24. Smoke
- 25. Condition of Accessory Buildings
- 26. Premise Rating
- 27. Noise, Fumes and Odors (Parcel)
- 28. Construction Type
- 29. Age of Dwelling
- 30. Condition of Structure
- 31. Condition of Walls
- or. Condition of Walls
- 32. Condition of Roofs
- 33. Condition of Foundation
- 34. Condition of Electrical Installations
- 35. Condition of Paint
- 36. Other Exterior Factors
- 37. Overall Parcel Rating

Environmental

Variables

Potentially

Measurable Using Remote

Sensors

(1-21)

Structural

Variables Not

Observable

Using

Remote Sensors

(22 - 37)

TABLE 2
ESTIMATED VALUES OF SEVEN VARIABLE DISCRIMINANT
FUNCTION COEFFICIENTS FOR FIVE HOUSING
QUALITY CLASSES

Variables	Highest Quality				Lowest Quality
Entered	Group 1	Group 2	Group 3	Group 4	Group 5
Street Parking	11.98	11.71	14.30	26.83	33.83
Street Width	9.58	12.75	12.84	23.94	29.37
Street Grade	-0.10	2.27	-2.14	-8.22	-15.35
Traffic	6.30	6.97	10.26	14.83	19.92
Access to Buildings	.74	7.53	.92	4.82	-23.01
Refuse (B)	. 89	.32	1.45	2.78	8.69
Loading/Parking	-0.13	.15	.06	.19	13.68
Constant Term	-14.39	-23.73	-24.20	-66.00	-179.58

#### RESUME

Robert W. Pease, Ph.D. Age 53. Doctorate in Geography, University of California, Los Angeles with specializations in climatology, geomorphology, and historical geography. Sixteen years experience prior to doctorate teaching secondary and junior college physics and astronomy. Since 1967 have specialized in the use of remote sensing systems for geographic purposes, including urban and agricultural climatology. Publications include: "The Photosynthesis Potential of the Energy Components of Climate, "Yearbook of the Association of Pacific Coast Geographers, Vol. 16, 1954; "Mapping Terrestrial Radiation Emission with the RS-14 Scanner," Technical Report, USGS; "Making Color Infrared Film a More Effective High Altitude Remote Sensor," Remote Sensing of the Environment, Vol. 1, No. 1, 1969; "More Information Relating to the High Altitude Use of Color Infrared Film," RSE Vol. 1, No. 2, 1970; "Color Infrared Film as a Negative Material," RSE Vol. 1, No. 3, 1970; Modoc County: A Time Continuum on the California Volcanic Tableland, Univ. of Calif. Pubs. in Geography, Vol. 17, 1965. Now on staff as Associate Professor and Associate Research Professor in the Department of Geography, University of California, Riverside.

# CLIMATOLOGY OF URBAN-REGIONAL SYSTEMS

Robert W. Pease

Department of Geography University of California Riverside, CA 92502

Urbanized areas have come to be significant if not dominant components of many regional land surfaces. They represent perhaps the most dramatic recent change man has made in his environment—a change that may well burgeon in the foreseeable future as greater percentages of world populations crowd into metropolitan areas. The climate of urban—regional systems is involved because temperature, air, and pollutants added to the air are significant aspects of this change. During the past two years, substantial progress has been made in the application of remote sensing techniques to the study of urban climatology by programs jointly sponsored by NASA and the United States Geological Survey. The initial effort has endeavored with considerable success to map terrestrial radiation emission or the general thermal state of the land surface with the aid of imaging radiometers (mechanical—optical scanners).

As its name implies, urban-regional climatology is dual in nature. One line of inquiry delves into the climate of the city itself. How do the various objects man has made create for him a different and perhaps detrimental environment? How do his activities create climates distinctly urban? The other line of inquiry is concerned with the way cities modify the climates of larger regions of which they are parts. Are temperatures developed over urban areas carried by winds out over adjacent rural lands? And what is the effect of a blanket of polluted air on the larger area?

It is useful to analyze urban climates in terms of energy systems. This helps in understanding the role of the large quantities of heat man adds to the city which must be dissapated in addition to the energy received from the sun. It gives quantitative insight into the disposal of solar energy by distinctive urban surfaces. Through the use of energy, the way pollutants hold back solar energy can also be studied

quantitatively. Absorption of solar energy and the radiation of energy from the terrestrial surfaces are parts of energy budgets which can be measured by the energy exchanges that are taking place. Most commonly measured are radiant fluxes, the shortwave energy from the sun and the interchange of longwave radiant energy between the surface and overlying air. A measurement from which useful inferences can be made is the balance of incoming to outgoing radiant energy flows, or "net radiation." A long-term net radiation deficit, for example, indicates that energy is being transferred from surface to air by non-radiant means such as transpiring plants. A long-term surplus might well indicate the transport of non-radiant energy into an area of concern such as a city. A change in this balance toward a consistent surplus is fundamental to the existence of cities as "heat islands" in their respective regions. Oppressive heat may be worsened when the energy absorption by living plants is diminished and a great deal of non-solar heat is liberated which sooner or later must be emitted from the urban surface.

The mating of remote sensing techniques to urban-regional energy climatology is desirable because of certain characteristics of the urban surface.

- (1) It is highly three dimensional. Streets between rows of buildings become "thermal canyons" with many of the characteristics of the blackbody cavity of Kirchhoff. Radiant energy, absorbed and re-emitted repeatedly between building walls, results in almost total absorption of solar and atmospheric inputs despite albedos and emissivities of surface. An observer at street level, using traditional radiation measuring instruments, is within the cavity structure and, although he may be able to sense well the environment around him, he cannot assess the energy contribution to the open air over the city as well as can measurements made from above.
- (2) The urban surface is a mosaic of smaller surfaces, each with its own radiant and thermal properties. A ground observer must attempt to extrapolate his point observations into a spatially complex system by assigning proportionality to the many types of surfaces he measures. This is an almost impossible endeavor without an airborne perspective (Figure 1). The new generation of mechanical-optical imaging radiometers capable of self-calibration automatically demarcates and measures characteristics of the many small surfaces that make up the urban mosaic. In Figure 1 both the urban mosaic and the urban-rural interface of Houston show well, imaged solely by the energy they are emitting in the thermal spectral band.

(3) Urban patterns of radiant exchange are constantly changing during diurnal and annual cycles. Relative radiant states may reverse between day and night. Blacktop is a good reservoir for solar energy, for example, and may not become as hot during the day as poorly conducting dry soil. This is apparent when one compares the cleared areas in the non-urban lands with the apparent radiation temperatures of the freeway and city streets in Figure 1. Had we a view of the same area made late at night, the pavement would be the warmer of the two. Thus there is reason to believe that synoptic maps of radiant exchange and thermal states may be of greater value in the analysis and monitoring of urban energy phenomena than maps laboriously compiled from statistical averages of difficult-to-obtain data collected at street level.

The application of remote sensing techniques to radiation climatology here described was carried out in conjunction with the Barbados Oceanographic and Meteorological Experiment (BOMEX) on the island of Barbados in the summer of 1969. The test site was a portion of the city of Bridgetown and adjacent agricultural lands. The imaging radiometer used was the RS-14 manufactured by the Texas Instruments Company. This instrument was one of the first of a new generation of "scanners" capable of quantitative calibration. A type of direct current electronic circuitry permitted operation along flightline without a change in the gain of the amplifier. In older types, frequent automatic change in gain prevented consistent calibration because a relation between surface radiation and instrument output established for one part of the image would not apply to other parts. Calibration is aided by initial recording of the full range of detected energy modulations onto magnetic tape. When these energy signals are converted to a photographic image in the laboratory, further adjustments can be made to maintain the full range of energy modulations as density differences on the film. A further aid that should become increasingly useful in the future are internal reference energy sources within the instruments which record with the image and aid in quantitative calibration. Although the initial experimental work relied primarily upon ground calibration targets, internal energy sources in the RS-14 although still without final calibration, permitted tentative equations to be formulated which in the future may reduce the dependence upon ground cross-calibration.

It should be understood that an imaging radiometer does not make a photograph of the surface it images. Rather, it records the energy being emitted by the surface, not reflected sun energy. Thus if it can be calibrated it becomes a true radiometer with the

added capability that energy it records can be converted to an aerial-type image from which a map of energy emission can be made. Further, since the energy emission is related to the temperature of the land surface, a fairly good picture of surface temperatures is obtained. Since the earth is much cooler than the sun, it emits energy in wavelengths much longer than light. In reality, the earth surface is imaging itself with its own energy emission. Quantitative calibration of the image is useful in the study of the climatic relationships of the surface being imaged.

The flightline chosen for the mapping experiment extended inland from the west coast of the island of Barbados across the northern suburbs of Bridgetown to sugar cane fields inland and presented a good contrast of rural and urban lands. Cloud shadows from a daily cumulus buildup presented a problem, since these comprised short-lived areas of cool surface that persisted for some moments after the shadow had moved on.

Initial cross-calibration between the surface and the airborne sensor was empirical. Ground calibration surfaces or "targets" had been selected, the radiation temperatures of which were measured during the overflight. The adjacent sea surface, of known temperature, was also used for calibration. Surfaces chosen as targets were large enough that the optical transmittance of them on image transparencies could be subsequently measured during data reduction. Target radiances were measured with an absolute calibration instrument, the Barnes Engineering Company PRT-5 Precision Radiation Thermometer.

The initial data reduction problem was to relate transmittances of the radiometric image to surface radiances at the time of overflight. This was accomplished with the aid of a transmission densitometer by measuring the transmittances of the images of ground targets. Since the image was positive, transmittance was used rather than density to avoid an inverse relationship. Sea-surface radiance was used to anchor one end of an appropriate conversion curve and land calibration targets the other in order to make the graphical plot shown as curve A of Figure 2.

To make isoline maps that would show meaningful patterns of terrestrial radiation, it was necessary to generalize the minute patterns of the radiometric image, particularly over the urban area. To accomplish this, the image was divided into a matrix of choropleth cells one centimeter square or close to one-half kilometer square on the ground. A silicon cell device with an area equal to a matrix cell was first calibrated to the densitometer (curve B, Figure 2) and was then used to integrate each cell

transmittance. The matrix, superimposed upon the scan image, is shown in Figure 3a, and derived averaged transmittances in Figure 3b. With the aid of a computer, slope equations for curve B then converted the averaged cell transmittances to the radiances shown in Figure 3c. Mapping (Figure 3d) involved the use of the centers of the averaged cells as control points from which to plot the desired isolines. Maps in other radiation terms were made in the same manner and appropriately all showed the same radiation patterns.

As previously noted, the RS-14 has built-in calibration sources which give the instrument a self-calibration potential. The radiances received aloft by the instrument, however, are not the same as the radiances emitted by the surface being imaged. Intervening air, even in the 8-14 micron wavelength water vapor window, both attenuates the surface signal and adds an energy component of its own. Realization of the full potential of an imaging radiometer, then, necessitates that the error induced by the atmosphere be systematized in order that a correction without elaborate ground controls be carried out. For the Barbados data, this has been accomplished by using a gray-window model for the intervening air expressed by the equation:

$$I_z = \epsilon \left[ E_{bb} \left( \overline{T} \right) \right] + (1 - \epsilon) I_o$$

where  $(I_Z)$  is the radiance at the sensor,  $(I_O)$  the radiance of the surface target,  $[E_{bb}(\bar{T})]$  the blackbody equivalent of the mean temperature of the intervening air column, and epsilon the effective emissivity of the air column in the spectral band being sensed. When values for sensor and surface radiance  $(I_Z$  and  $I_O)$  are known from instrument readout and ground calibration and a mean air temperature has been established, the effective emissivity of the air, or epsilon (6) in the equation, can be determined. This value permits the mathematical computation of surface radiances  $(I_O)$  for all values of sensor radiance  $(I_Z)$  which in turn permits plotting a correction curve (Figure 4) that will fit all parts of the scan image if the intervening air is considered to be relatively homogeneous.

Although at the time of the Barbados flight, the internal calibration sources of the RS-14 were not deemed to be working properly, Victor Whitehead of the NASA Earth Observation Program systematized the error well enough to obtain image vs radiation temperature values which, when corrected for the effects of the atmosphere by the foregoing equation, corresponded closely to values derived from ground calibration targets.

Certain characteristics of the relationships just described may in the future significantly reduce the amount of ground calibration necessary. The slope of the correction curve is equal to the reciprocal of the air transmissivity (1/1-6) and can thus be set by a single ground calibration which permits determination of the effective air emissivity in the spectral band being utilized. The position of the curve with respect to the Iz axis of the graph is established by the fact that the curve must interesect a line of equal value at a radiance equal to the blackbody equivalent of the mean temperature (T) of the intervening air column. Further, according to Beer's Law, the transmissivity of the air is also equal to the natural log base (e) to the minus (ku) power where (k) is the absorption coefficient of the spectral band of concern and (u) the optical depth of the intervening air in gram-centimeters squared of precipitable water. Thus the slope of the correction curve is also equal to

# 1/e-ku

a relationship which should permit setting the slope without the aid of ground controls, solely from atmospheric data, when more knowledge has been collected regarding absorption within the water vapor window. Elimination of ground controls may be particularly important when the system is applied to earth-viewing satellites with a thermal sensing capability, such as ERTS-B.

The foregoing radiation mapping project must be considered a pioneer effort. The optical integration method has certain inherent potential errors relating to the linearity of translating energy received by the airborne sensor to film densities. Computer programs are now being adapted to yield the matrix cell generalization directly from the magnetic tapes to reduce this possible source of error. It is recognized that sides of a scan are not viewed vertically which may produce errors since three-dimensional surfaces in all probability do not emit equally in all directions. Planimetry of the maps must be adjusted for changes in airplane course and attitude. The maps are successful enough, however, to indicate that rapid production of synoptic radiant emission maps with imaging radiometer data is sufficiently feasible to warrant further study toward refinement and adaptation as an operational system.

Future progress in achieving an ability to remotely monitor urban-regional energy budgets must follow two paths. First, the sensing capability must be extended to include fluxes other than terrestrial longwave emission. Investigation this past summer

indicates that surface albedos can be determined photographically or perhaps better by the use of other channels of the imaging radiometer that will sense solar radiation. With ground pyranometers to check solar input, the addition of albedo measurements may make possible the construction of synoptic maps of net radiation, adding this valuable analytical tool to radiation analysis.

The second path toward improvement involves the application of the methods developed from data acquired in the single flight over tropical Barbados to a sequence of flights over a midlatitude city in the United States. Derived maps can show patterns of both diurnal and annual change for a variety of phenomena related to radiant exchange. First will be an initial sequence of four flights with appropriate sensors to sample a diurnal period. This sequence logically should be followed by similar diurnal sequences at other seasons to demonstrate annual change in patterns.

The continuing effort is a logical preliminary toward giving the earth resource satellites the capability to monitor urbanregional climatic elements. A "pre-calibrated" city will help in calibrating ERTS instruments. Previously acquired knowledge pertaining to the target city will be augmented by aircraft and ground data observed at the time or times of satellite passage. Present planning calls for establishment of several automatic platforms around the city which will transmit at least daily records of selected surface radiation information to ERTS for subsequent retrieval.

If we are successful in quantifying ERTS outputs for the target city, attempts will then be made to apply the methods to other urban-regional complexes without resorting to ground truth.

The question naturally arises as to the practical use of the methods of study described. Rapidly made radiation maps should help in understanding the causes of problems in urban environments that relate to climate. With a better understanding of the problems either remedial action can be taken to alleviate them or they can be lessened by wise future urban planning. The three-dimensional nature of a city, for example, creates what Lettau and others have termed a "roughness factor." This roughness can interfere with ventilating winds creating problems of excess temperature and stagnation of air. Proper spacing of high-rise buildings can reduce interference with city ventilation, improve the temperature environment, and reduce the collection of atmospheric pollutants. Measurement of conditions of net radiation may indicate the desirability of providing "greenbelts" and

open spaces within an urban area and give suggestions as to the most effective locations for them in a particular city situation. Study of the thermal cavity structure of a city may suggest that a variety of building heights along a given street is preferable to the common thermal canyon structure. On the other hand, winter maps may show that changes beneficial to summer climates make winter cold more severe. Only with a considerable body of knowledge derived from the operation of such a mapping program can problems of these types be best solved.

Since cities are dynamic and growing, change is an important factor to study. In a sense we have simply drifted into our present urban-regional climates. Rapidly made synoptic radiation maps, perhaps derived from satellite observations, will enable governments to monitor the changes that are taking place and replace aimless drift with wisely planned change.

As Outcalt has broadly stated, "... a reasonable programme goal is the prediction of the effects of land-use manipulation on the climates of urban areas." To this we add, "... and on the regional climates which urban areas help to create." At this point, a path toward an operational capability beings to take shape. By the endeavors of this program of investigation it is hoped we can gain the ability to monitor rapidly urban-induced changes in the climatic aspects of man's environment.

#### REFERENCES

- Holter, M. R., S. Niedelman, G. Suite, W. L. Wolfe, and G. Zissis, <u>Fundamentals of Infrared Technology</u>, 1962. Macmillan, New York.
- 2. Lettau, Heinz, "The Physical and Meteorological Basis for Mathematical Models of Urban Diffusion Processes," <u>Proceed-ings of the Symposium on Multiple Source Urban Diffusion Models</u>, Dept. Health, Education, Welfare, 1970, Washington, D.C.
- 3. Lowe, D. S., "Line Scan Devices and Why Use Them," Proceedings of the Fifth Annual Symposium on Remote Sensing, Infrared Physics Laboratory, University of Michigan, Ann Arbor, Mich., September, 1968.
- 4. Mohr, Don M., "Unique Design of the RS-14 Multi-Spectral Scanning System," Proceedings of the 1970 Electro-Optical Systems Design Conference, Electro-Optical Systems Design, 222 W. Adams St., Chicago, Illinois.

- Myerup, L. O., "A Numerical Model of the Urban Heat Island," <u>Journ</u>. <u>App</u>. <u>Met</u>., Vol. 8, No. 6, pp. 908-918.
- 6. Outcalt, Samuel I., "A Plan for Urban Climatology within the Geographic Applications Branch, USGS, Interior," Geographic Applications Program Discussion Paper, June, 1970.
- 7. Pease, Robert W., "Mapping Terrestrial Radiation Emission with the RS-14 Scanner," Technical Report 4, U. S. Department of Interior Contract 14-08-0001-11914, July, 1970.
- 8. Remote Sensing, National Academy of Sciences, 1970, Washington, D.C.

# DEFINITION OF TERMS (In order of appearance in text)

Energy exchange system: Local climates as well as world wide are to a great extent conditioned by the exchange of energy between the surface and overlying air. The overall system includes the transfer of energy by radiant exchange, by conduction, and in a non-sensible form through evaporation and the transpiration of plants.

Longwave radiation: The peak wavelength of a radiant energy package depends upon the temperature of the source. Since the sun is very hot, the energy it emits is shortwave. Energy emitted by the much cooler earth is considered longwave.

Radiant flux: The flow of radiant energy in a given direction. Most commonly we speak of downwelling and upwelling fluxes.

Energy sink: Objects or processes by which energy is aborbed or removed from a radiant exchange system.

# Blackbody cavity: See emissivity.

Albedo: The fraction of solar or shortwave radiation reflected by a surface. The fraction reflected is usually expressed as a percent.

Emissivity: The effectiveness of a surface in emitting radiant energy for a given temperature as compared to the radiation of a perfect blackbody. It is equal to the effectiveness of absorption of the surface or absorptance. A perfect blackbody, according to the concepts of Kirchhoff, absorb all radiant energy striking it. A blackbody cavity increases the efficiency of

absorption by emitting and reabsorbing energy within it until virtually all energy entering the cavity has been absorbed, regardless of actual emissivities of the cavity surfaces.

Imaging radiometer: A device, capable of calibration, for imaging radiant energy too long in wavelength to affect photographic film. It consists of mirror systems and a detector capable of reacting to the desired wavelengths. Although the imaging is done electronically, a final display may be made on photographic film. Also termed mechanical-optical scanner and electro-optical scanner, although the term "radiometer" should not be applied to older type instruments.

Thermal spectral band: Radiant energy varies according to wavelength. Visible light has wavelengths that range from .4 to .7 microns. One micron is 1/1000 of a millimeter. The near infrared extends from .7 microns to 3 microns. Thermal infrared or the thermal spectral band extends from 3 to 100 microns. It gains its name from the fact that the general range of temperatures found at the surface of the earth emit radiant energy mostly with these wavelengths. See also longwave radiation.

Blacktop: The common name given to asphaltic concrete used for pavement. Also known as "tarmac" and "Macadam."

Synoptic maps: Maps made to portray conditions as of a given instant.

Radiance: A quantitative measurement of the intensity of radiation emitted by a surface. It is defined as watts per square centimeter per solid angle or steradian.

Optical transmittance: The fraction of the light falling upon a substance that passes through it, in this case an area of a photographic transparency.

<u>Density</u>: The measure of the opaqueness of a photographic transparency. It is the logarithm of the reciprocal of the optical transmittance.

<u>Densitometer</u>: An instrument for measuring the transmittance and ensity of a transparency.

<u>Isoline</u>: A line connecting points of equal value. Examples are isotherms and isobars on a weather map. Lines mentioned here connect points of equal radiance.

<u>Chloropleth</u>: A statistical area treated as a whole. For purposes of convenience, all parts of the area are considered to have the same value or an average value.

<u>Air transmissivity</u>: The measure of the fraction of radiant energy that will pass through a given mass of air. That not transmitted is either absorbed or scattered.

Water vapor window: In the thermal infrared spectral band, water vapor is an efficient absorber of radiant energy, effectively reducing the transmissivity of the air. Between 8 and 12 microns, on the other hand, water vapor is a poor absorber and radiant energy with these wavelengths penetrates air best. This spectral band is commonly called the "water vapor window," although other smaller windows occur.



Figure 1 -- The interface between rural and urban surfaces at the edge of Houston, Texas as imaged by the RS-14 scanning thermal radiometer. Light tones represent relatively high emission of radiant energy or "radiance." Dark tones are lower levels of emission. From this image it can be clearly seen that an urban surface is a mosaic of sub-surfaces, each with its own thermal and radiant properties.

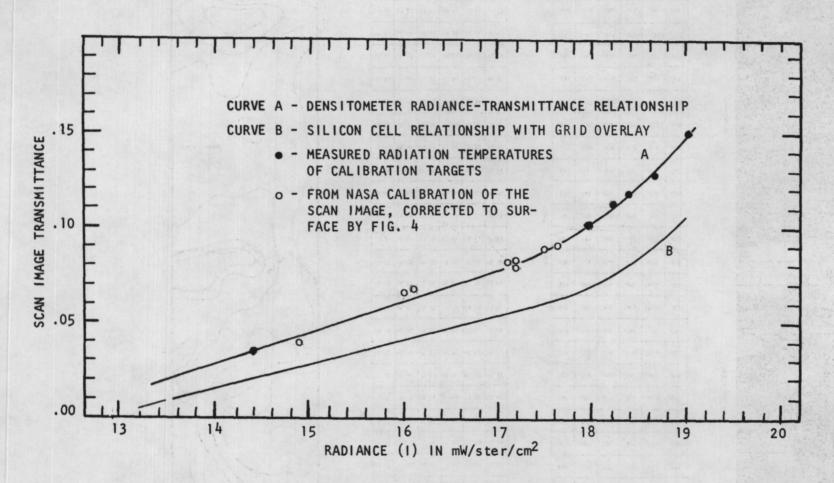


FIG. 2. RADIANCE - TRANSMITTANCE RELATIONSHIPS



SUGAR CANE FIELDS

BRIDGETOM

.034	.042	.025	610.	810.	610.	.023	780.	.023	.029	.028	.023	.023	.025	.024	.033	.028	.028	.026	.027	.037	.043	.026	.022
.020	.027	960.	710.	410.	120.	.023	940.	.032	0.030	.034	380.	.030	¥60.	.032	.032	.033	.032	160.	160.	.040	450.	660:	100
420.	.045	060.	.020	.022	160.	.038	540.	.043	960.	840.	180	.048	840.	.035	760.	.028	960.	.028	.035	.064	670.	.043	160
040	070.	950.	620.	.023	.029	450.	.032	960.	.042	940.	80.	.053	140.	.038	660.	.032	060.	050.	150.	170.	.082	.029	020
840.	.062	750.	.058	040.	.042	.038	A£0.	050	640.	070.	.083	.049	940.	.035	660.	.038	.038	040.	.042	.060	870.	032	910
050	450	043	450	190	950	980	150.	.042	.043	0,00	8/	.042	.034	.033	.029	.032	.032	.039	.047	.050	950.	9.	160

RURAL URBA

15.45	16.05	14.78	14.33	14.25	14.33	14.63	15.68	14.62	15.08	15.00	14.63	14.63	14.78	14.70	15.37	15.00	14.96	14.85	14.93	15.67	16.13	14.85	
14.40	14.93	15.60	14.17	13.95	14.48	14.63	16.50	15.30	15.15	15.45	15.5	15.15	15.45	15.30	15.30	15.38	15.30	15.23	15.23	15.90	16.95	15.83	1
14.70	16.28	15.15	14.40	14.55	15.23	15.75	16.28	16.13	15.60	16.50	17.25	16.50	16.50	15.53	15.68	14.96	15.60	15.00	15.53	17.70	18.17	16.13	1
15.90	18.15	17.10	15.07	14.63	15.08	16.95	15.30	15.60	16.05	16.35	18.34	16.88	16.20	15.75	15.83	15.30	15.15	16.65	16.73	18.03	18.41	15.08	
16.50	17.55	17.18	17.25	15.90	16.05	15.75	15.45	16.65	16.57	18.15	18.44	16.58	16.35	15.53	15.82	15.75	15.75	15.90	16.05	17.40	18.27	15.30	
16.65	16.95	16.13	16.95	17.70	17.03	15.75	17.18	90.91	16.13	8.15	7.93	16.05	15.45	15.38	15.08	15.30	15.30	15.83	16.42	16.65	17.10	16.58	1

c.

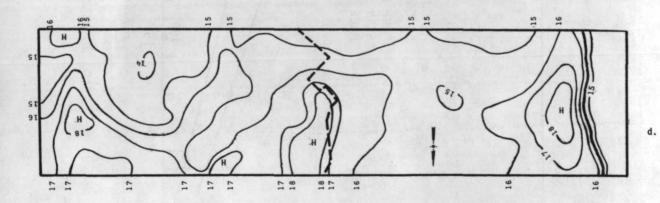


Fig. 3.

Figure 3 -- The sequence of operations to transform a thermal scan image into a generalized map of radiance, utilizing optical means. The maps are for Bridgetown, Barbados, made June 27, 1969 by NASA Mission 98, 10:30 AM local time.

- (a) The calibrated image from the RS-14 scanning radiometer. Included in the image are two control targets for which radiation temperatures at the time of overflight are known. Average transmittances for each cell of the choroplethic grid are optically determined with a silicon integrating device.
- (b) The matrix of chloropleth cells with average optical transmittance indicated for each.
- (c) The matrix of choropleth cells with transmittances converted to average radiances according to a transmittance-radiance relationship determined both by the ground control targets and by mathematical equations. Computerized methods were used to facilitate the many transformations required. Radiant emission could also have been expressed as radiation temperature or as radiant flux in either milliwatts per square centimeter or langleys per minute.
- (d) An isoline map of generalized radiance for Bridgetown and adjacent rural lands, drawn by using the centroids of the choropleth cells as control points. This map gives a picture of both the thermal state of the mapped area at the moments of overflight as well as the contribution of energy emitted by the surface to the overlying air.

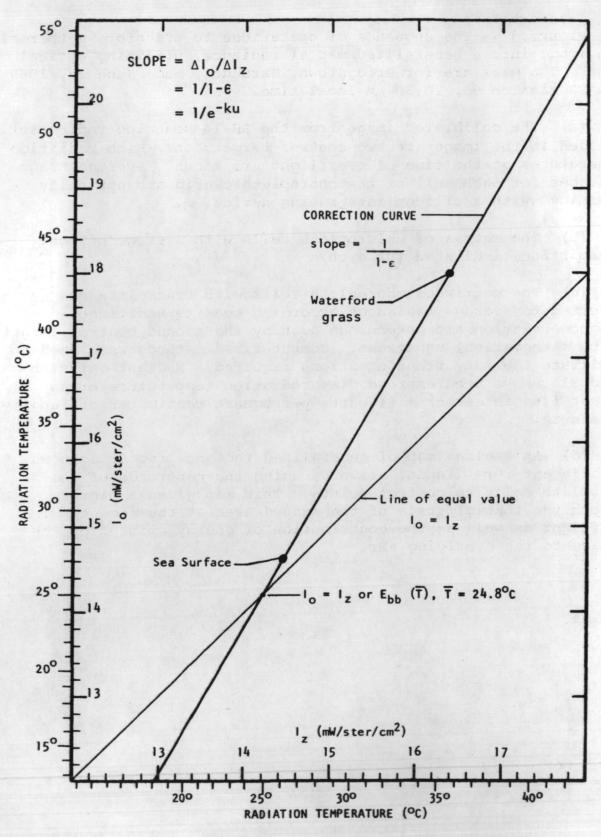


FIG. 4. SURFACE-TO-SENSOR RADIANCE ADJUSTMENT

raye Intericionary Lere Dialik

Page Intentionally Left Blank

#### **BIOGRAPHY**

# James R. Wray

James R. Wray is a senior geographer-cartographer in the U.S. Geological Survey's Geographic Applications Program. He is responsible for urban aspects of the Program, and for design of cartographic aspects of a geographic information system, including such user-oriented end products as the looseleaf Atlas of Urban and Regional Change. Mr. Wray earned degrees in Geography at the University of Chicago. He is author of "Photo Interpretation in Urban Area Analysis" in the Manual of Photographic Interpretation, published by the American Society of Photogrammetry. His earlier work, reported in this Manual, partly inspired the "Census Cities Project." Mr. Wray has taught geography, cartography, or remote sensing at his alma mater and at four other universities. As consulting geographer-cartographer he designed urban data systems which combine use of image interpretation and map tools to serve the specific needs of government, planners, and private industry. Among systems he has helped to develop are applications in public utilities, advertising and marketing, civil defense, and census planning.

Page Intentionally Left Blank

#### CENSUS CITIES PROJECT AND

#### ATLAS OF URBAN AND REGIONAL CHANGE

by

### James R. Wray

U.S. Geological Survey Geographic Applications Program Washington, D.C.

#### INTRODUCTION

A large segment of the USGS Geographic Applications
Program is concerned with the urban applications of remote
sensing. The Program's current urban research goals can be
demonstrated by an experiment on the combined use of sensors and
census data, and of aircraft and spacecraft sensor platforms.
Early phases of this experiment received some attention as the
"Census Cities Project," and one of the user oriented end-products
will be a looseleaf "Atlas of Urban and Regional Change," hence
the double theme in the title of the paper.

The Census Cities Project has several related purposes:

- to assess the role of remote sensors on high altitude platforms for the comparative study of urban areas;
- to detect changes in selected U.S. urban areas between the 1970 census and the time of launching of an Earthorbiting sensor platform prior to the next census;
- 3. to test the utility of the satellite sensor platform to monitor urban change (When the 1970 census returns become available for small areas, they will serve as a control for sensor image interpretation.);
- to design an information system for incorporating graphic sensor data with census-type data gathered by traditional techniques;
- to identify and design user-oriented end-products or information services; and
- to plan an effective organizational capability to provide such services on a continuing basis.

#### THE RESEARCH DESIGN

The design of the "Change Detection Experiment" is illustrated in Figure 1. In this figure each of the rectangles is a symbol representing a page in the Atlas of Urban and Regional Change, a user oriented end-product. The horizontal rows represent steps in the research design. The vertical columns represent imagery and imagery interpretation at different times and from different sensor platforms. The experiment begins with the procurement of high altitude aircraft photography near the dates of the 1970 census for a sample of U.S. cities. From that photography a rectified mosaic is made for each city and is fitted with a grid, or rectangular coordinate system. next step is to prepare an overlay showing the 1970 census statistical areas and their centroids. This overlay helps to relate the census data to the information generated from the aerial photography. The next step is to complete the land use analysis and measurement of land areas in each category and each census tract. An additional step, not illustrated in Figure 1, calls for listing the land use information for 1970 in computer-retrieval format.

When the Earth Resources Technology Satellite (ERTS) is launched in 1972, we will also receive high altitude aircraft photography over the same test sites, plus television imagery from the satellite itself. From the aircraft photography, we plan to make another land use analysis, but we will not need to repeat the making of a gridded photo mosaic or the overlay showing the census statistical areas. Another overlay will show changes detected between the 1970 land use and the 1972 land use. Besides the locational details recorded on the overlay, the new land use information will also be recorded in computer retrievable format. The 1972 land use analysis will serve as a basis for interpreting the imagery from the satellite. Thus, it will become possible to determine how well the imagery from the satellite can be used to detect the location, kind, and intensity of urban land use change between 1970 and 1972.

#### ACQUISITION OF REMOTELY SENSED IMAGERY

Twenty-six urban test sites selected for this experiment are shown in Figure 2. A twenty-seventh test site is the Pittsburgh metropolitan area in southwestern Pennsylvania. These sites represent a ten percent rank-size sample of U.S. urban areas. Inland and coastal cities are represented and so also are most regions of the country. There are more cities in the South because we already have Gemini and Apollo photography for the lower latitudes. For twenty of the urban test sites, photo missions were completed during the April-to-July period when the 1970 census was being taken.

One of the test sites for which photography was received is the Washington, D.C. Urbanized Area. Figure 3 shows the flight lines and areas covered by that mission. The Washington coverage was acquired on NASA Mission 128-d, June 28, 1970, with an RB-57B aircraft at 50,000 feet above terrain. There were three north-south flight strips spaced about 18.5 kilometers apart. The diagram in the lower right corner shows the area covered by each of the cameras aboard the aircraft. The legend shows there were nine cameras.

Figure 4 is a diagram of the nine photo-sensors for a central frame over the Washington test site. One the left are sample frames from three metric cameras, and on the right, sample frames from six Hasselblad cameras. The cameras for the planning of the mission are the two RC-8s, which use roll film 24 centimeters wide. Both cameras have a focal length of 152.6 millimeters, and produce an image scale of 1:100,000 at a flight altitude of 15.2 kilometers. One of these cameras has color infrared film with a minus-blue filter. The other camera has black-and-white panchromatic film used with the same filter. A portion of the RC-8 color infrared photo is shown in Figure 5. Each of the full RC-8 photos covers a square 22.8 kilometers on a side, or an area of 520 square kilometers. Photographs are taken with sixty percent overlap in line of flight and about thirty percent sidelap between flight lines. This provides stereoscopic coverage and permits three-dimensional viewing. A backup camera is also provided in the 24-centimeter film width format. This is a Zeiss camera with a 305 millimeter focal length lens. It procures pictures at 1:50,000 and covers a square 11.4 kilometers on a side, or an area of 129 square kilometers. This camera also is loaded with color infrared film but the lens is fitted with a "D" filter. With the Zeiss camera there is edge-to-edge coverage in the line of flight, but there is some gap in coverage between flight lines.

The Hasselblad cameras all use roll film, 70 millimeters wide. Three are loaded with black-and-white film, three with color film. Two of the cameras have a black-and-white panchromatic film, one filtered with a green filter and one with a red filter. The third contains black-and-white infrared These three cameras simulate the three television film. cameras which are expected to be aboard the ERTS-A platform. In the ERTS data handling systems these three different television images can be combined to form one false color image. The composite image is represented by the fourth camera, which contains color infrared film and the same minus-blue filter used on the RC-8 cameras with color infrared film. fifth camera contains panchromatic color film with a stronger blue filter for additional haze penetration. The sixth camera also has panchromatic film; it is filtered with a number three filter to render the scene about as you and I would see it looking through the camera sight at the time the picture was

taken. Each of the Hasselblad cameras has a 40 mm focal length lens which covers about 438 square kilometers (slightly less than the RC-8 camera), producing an image scale of 1:382,000 from a flight altitude of 15.2 kilometers above terrain.

This same multispectral, census-contemporaneous imagery has been received for most of the urban test sites. This data base represents a truly unique opportunity for comparative urban study!

#### UTILIZATION OF THE IMAGERY

As called for by the research design, the first step in the analysis is the preparation of a rectified photo mosaic, fitted with a rectangular coordinate grid. Figure 6 shows a portion of the mosaic for Washington, D.C. This portion is a simulated page in the Atlas of Urban and Regional Change. The grid interval is one kilometer. The publication format will have a mosaic square 20 kilometers by 20 kilometers at 1:100,000. This square is placed to the left of the center on a page measuring 28 centimeters from north to south and about 38 centimeters east to west. This is the same size as one standard page used for computer printout. The right hand panel provides legend space for overprints or overlays, or for extension of the map area. Pages may be bound at top or at left, or used singly, and folded into reports using the page size of conventional office stationery.

As in other experiments proposed for the Department of the Interior's Earth Resources Observation Systems (EROS) Program, the Universal Transverse Mercator projection and rectangular coordinate system is in use, and all distances and areas are expressed in metric units. Geographic coordinates and bar scales in non-metric units will also be shown, however, and the various State coordinate systems can be indexed for users who require them.

The next step in the urban analysis is the preparation of an overlay showing the census statistical areas. A simulation of the census overlay is shown in Figure 7. The fine solid lines in the figure represent the census tract boundaries at the same scale as in Figures 6 and 8. The numbers represent the census tract identification. Some of the tract lines are state boundaries, county boundaries, or boundaries of incorporated cities. These delimit political areas and other "user" areas for planning and decision-making. A supplementary overlay would show additional point and line features appearing on the mosaic, or essential to its interpretation.

The next step is the analysis of area features, especially land use. This is illustrated in Figure 8, a simulated overlay or overprint for the same area in Washington, D.C. The land use interpretation is done directly on an overlay to the color infrared photography at 1:100,000. The smallest mapping unit is a square 0.2 kilometer on each side, or four hectares, or about 11 acres. This is not much larger than the area covered by the blunt end of the color pencil used in the image interpretation. The minimum sized mapping unit is larger than the anticipated resolution cells. The legend shows the nested land use classification system presently being tested in the prototype analysis of the Washington test site. There are eight urban classes and five non-urban classes. Three of the classes are repeated, so there are really only ten different categories. The Urban and Non-Urban land use categories can be expanded or contracted according to the scale and minimum-size area for mapping purposes. Land ownership information garnered from "ground truth" may be shown on the supplementary overlay.

After mapping land use to the limits of the mosaic, a single boundary line is drawn around the central mass of "Urban" land uses. This is taken as the boundary of the urban area at the time of the photography. It becomes the "real estate" definition that will form the basis for comparison with other urban areas similarly delimited, or for analyzing changes in one urban area at different times.

The next step in the analysis is to measure the area of land in each land use category and to report the totals by census tract. The information for a particular time period is then stored in computer retrievable format. The land use overlays and area measurements for two different time periods will form the basis for change detection, and for the analysis of location, kind, and intensity of change.

#### STATUS OF THE WORK

The graph in Figure 9 provides a frame of reference for reporting what the Census Cities Project has accomplished so far and what remains to be done. This figure is a graph, on which are plotted 213 U.S. Urbanized Areas having more than 50,000 population in 1960. Population is scaledon the X-axis. The Y-axis shows land area in square kilometers. The "Urbanized Area" is an official census delimitation of the built-up area around central cities of 50,000 or more population. Adjoining cities, whether entirely built-up or not, are either wholly included, or wholly excluded. The minimum density is about four hundred persons per square kilometer. This definition is more inclusive than the corporate city; but it is less

inclusive than the Standard Metropolitan Statistical Area, since the latter is comprised of whole counties. The Urbanized Area, then, is more nearly comparable to the mass of urban land use that is likely to be detected and delimited by interpretation of air photos and other sensors. Even so, a delimitation based on actual urban land use, as derived by image interpretation, can effect more meaningful area comparison than a delimitation that may include large tracts of open unimproved land which happens to have corporate status. On the graph, the small dot in the upper left corner represents the New York Urbanized Area, with 14,000,000 persons on 4,650 square kilometers. The small dot in the lower right corner represents Mayaguez, Puerto Rico, with 53,000 persons on 10 square kilometers. Ranging between these extremes are all other urban areas. Some regional central tendencies can be discerned although they are not annotated on the graph as it is reproduced here. The Census Cities test sites are represented by triangles and are identified in the diagonal legend. This reads from left to right in population rank order and comprises roughly a ten percent sample. A similar model, refined by land use delimitation and regional interpretation, will be one result of our experiment. It can be used to estimate inter-censal population and to project the cost of analyzing land use in all U.S. urban areas.

Land use analysis is underway on the three largest urban test sites: San Francisco, Boston, and Washington. Work in seven smaller areas is also underway. In all on-going work, special attention is being given to the identification of urban environmental problems which can be studied by spatial analysis—including the use of remote sensors, and computer mapping techniques. We are also giving attention to the identification and direct involvement of prospective users in the applications of remote sensing techniques to the solution of environmental problems.

\* \* \*

#### GLOSSARY OF TERMS

- Census statistical area. A clearly defined area of any size used for reporting the results of a census. Boundaries are either those established by law or which are clearly visible roads or streams which are not likely to change. In this way, the census reports data for political areas, and changes from one census to the next. In urban areas, the census statistical area for which the greatest variety of socio-economic data are reported is the census tract. It varies in area size and population size, but on the average it will have between 4,000 and 5,000 persons.
- Centroid. An arbitrarily selected coordinate point within a small area delimited on a map or photograph. The point may be described in any coordinate system. It is used as an "address" to describe the <u>location</u> of all data counted within the area outlined.
- Gridded photo mosaic. A composite of several aerial photographs, corrected (or rectified) for distortions due to camera tilt (but not necessarily those due to relief), and fitted with a grid of squares. The grid is preferably a rectuangular coordinate system with a clearly defined relationship to the geographic coordinate system and to an appropriate map projection.
- Land use analysis. A systematic classification of areas with respect to their use by man. Point and line features in an aerial photograph are usually interpreted first. Land use analysis is essentially the interpretation of area features or areal associations of point and line features (depending on scale or resolution). Land use analysis is often the first step in the many specialized applications, any one of which imposes limits on the classes chosen. For urban mapping land use by image interpretation it is appropriate to use classes that are based on apparent use; details can be added by applying information not necessarily derived from the photos.
- Simulated overlay. Figures 6, 7, and 8 are "simulations" of pages in the Atlas of Urban and Regional Change. They are not actual pages or overlays, but are simplified for presentation as illustrations. The actual pages or overlays will be larger, more detailed, and executed with finer line work.

- Standard Metropolitan Statistical Area (SMSA). Another census statistical area. It is comprised of whole counties and some central cities which are not parts of counties. (The county is the principal political subdivision of a state.) The SMSA includes much more land than the "Urbanized Area."
- Urbanized Area. One kind of census statistical area. It most closely resembles the mass of built-up urban area one would recognize as "urban" and delimit on a small scale air photo. However, whole corporate cities are included, so extensive areas of non-urban land use may also be included.
- <u>Atlas of Urban and Regional Change</u>, a flexible photographic, cartographic, and statistical tool that will provide a basic synthesis of land use and related data. Yet, it also leaves to the user the opportunity to re-interpret the data, and to make additional thematic studies.

# Change Detection Experiment

Geographic Applications Program



1972 ERTS-A Satellite sensors

1972 (ERTS-A) Aircraft photog.



incl. gridded Mosaic, other remote sensors



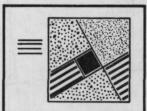
1970 (Census)

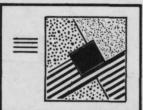


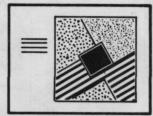


LAND USE ANALYSIS:

Use boundaries, and area measurement

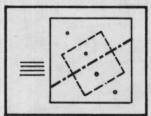


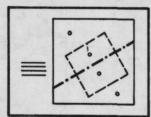


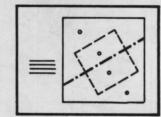


CENSUS STAT. AREAS:

Area measurement, other Ground Truth





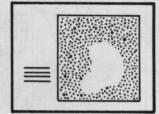


CHANGE DETECTION:

Analysis, and interpretation

End products shown are pages or overlays in Atlas of Urban and Regional Change. Others will include tabulated data, interpretation of changes and research design, and allied research on spatial models and theory.





U.S. Geological Survey April 1970

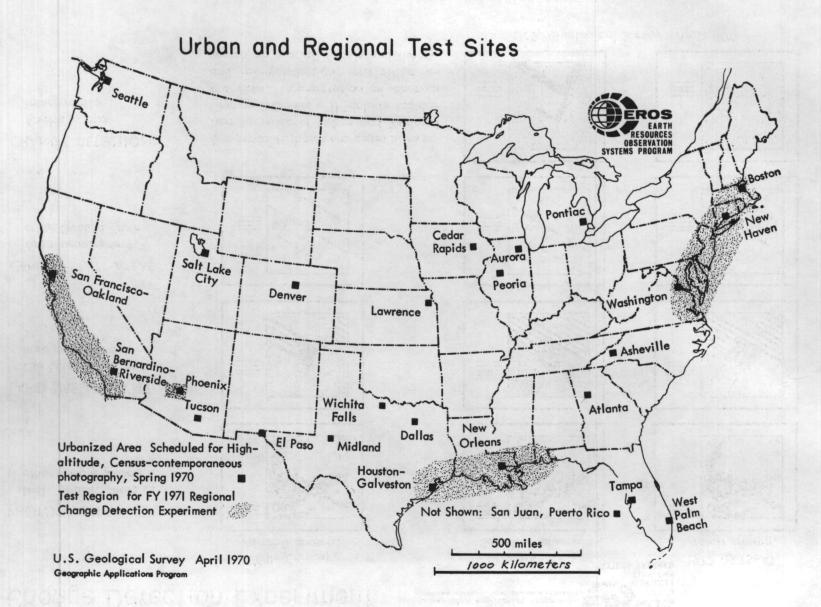


Figure 2.- Map showing urban and regional test sites.

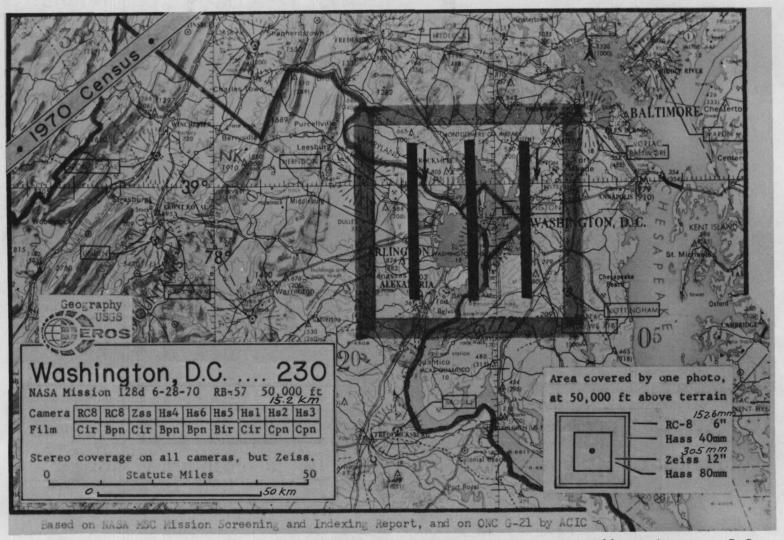


Figure 3.- Map showing flight lines and sensor coverage area, Mission 128, Washington, D.C.

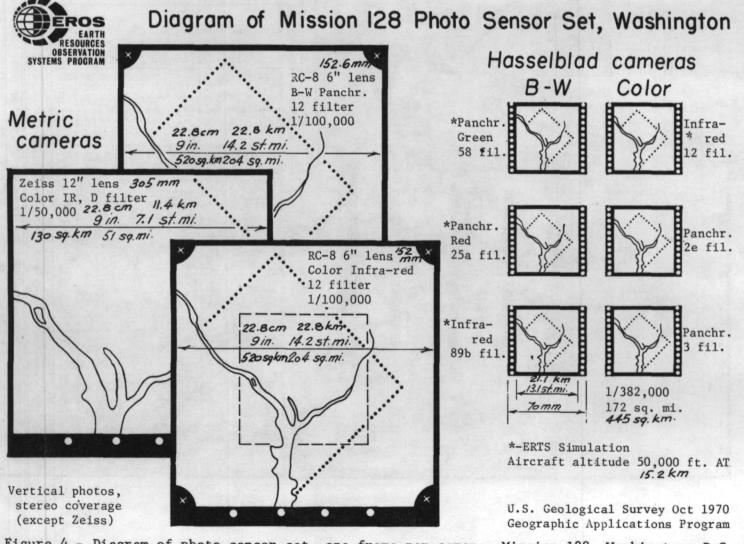


Figure 4 .- Diagram of photo sensor set, one frame per camera, Mission 128, Washington, D.C.



Figure 5.- Portion of RC-8 color infrared photo, Mission 128, Washington, D.C.

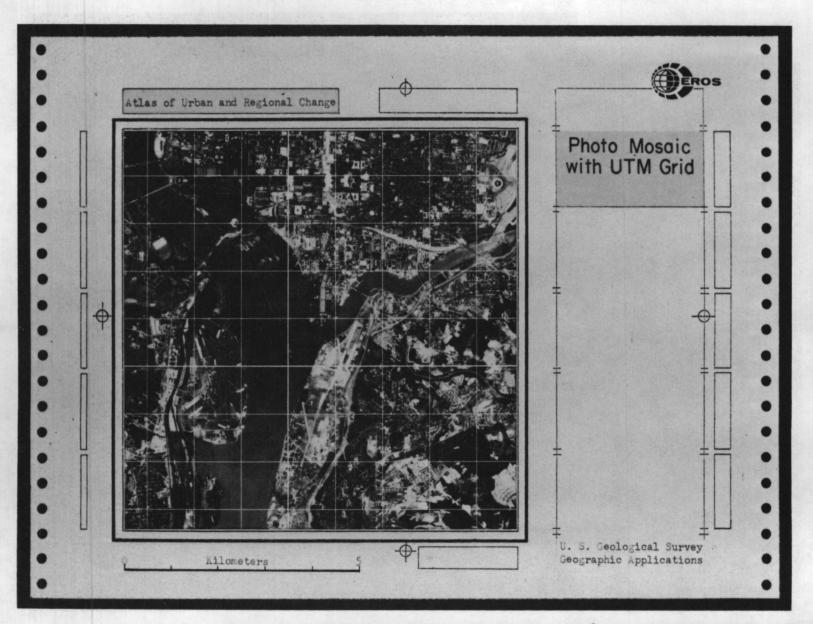


Figure 6.- Atlas of Urban and Regional Change, simulated page with gridded photo mosaic.

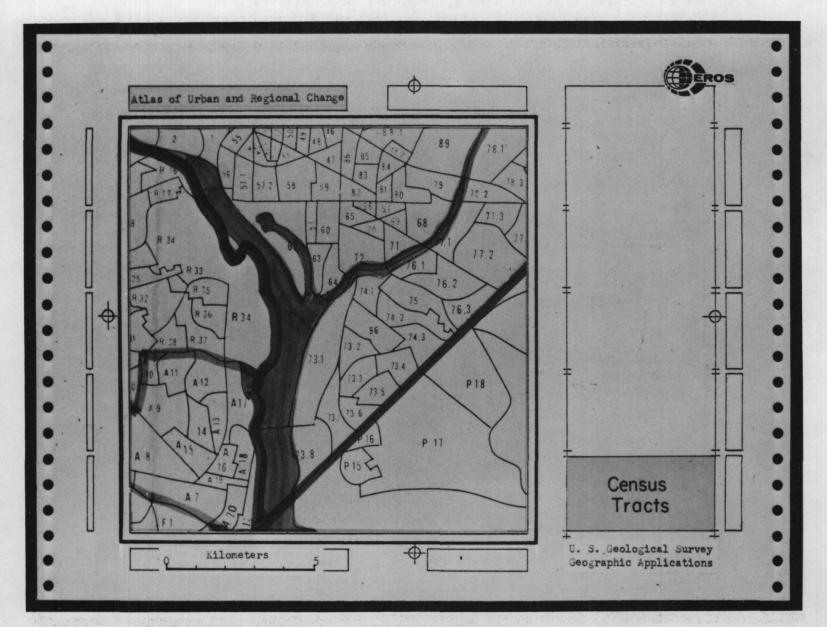


Figure 7.- Atlas of Urban and Regional Change, simulated page with Census Tract boundaries.



Figure 8.- Atlas of Urban and Regional Change, simulated page with land use interpretation compiled directly over the color infrared photo.

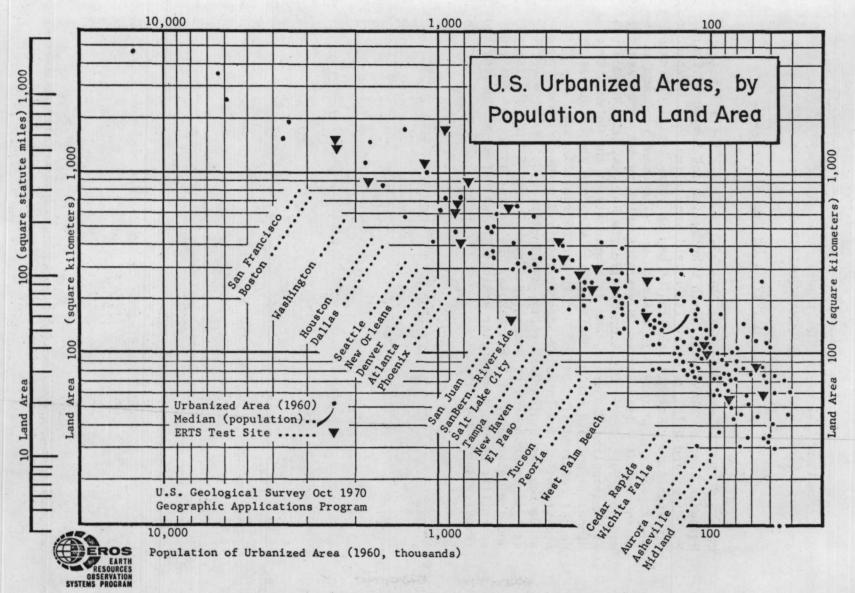


Figure 9.- U.S. Urbanized Areas, 1960, by Population and Land Area. Note ERTS test sites.

#### BIOGRAPHICAL SKETCH

#### Harvey K. Nelson

Karvey K. Nelson has served as Director, Northern Prairie Wildlife Research Center, Jamestown, North Dakota, for the Bureau of Sport Fisheries and Wildlife since its establishment in 1963. Preceeding his appointment to this position he had 13 years experience with the Bureau's migratory bird research and management programs in the north central United States, 8 years of which he served as Assistant Regional Supervisor, Division of Wildlife Refuges, with headquarters at Minneapolis, Minnesota. He is a graduate of the University of Minnesota and did his graduate work at Michigan State University. He has received a number of honors and awards from the U.S. Department of the Interior and has received graduate scholarships at George Washington University, Washington, D.C. He also serves as Adjunct Professor of Zoology at North Dakota State University and the University of North Dakota. He is the author of numerous scientific papers and popular articles on waterfowl management and research subjects.

#### BIOGRAPHICAL SKETCH

#### John E. Johnston

John E. Johnston is the Inter-Bureau Liaison and Coordinating Representative for the Department of the Interior/U.S. Geological Survey, Earth Resources Observation Systems (EROS) Program. Prior to this position, Mr. Johnston spent a year with NASA's earth resources programing office. He holds a B.S. degree in Geology from the University of North Carolina and did graduate work there and at the University of Kentucky, while with the U.S. Geological Survey. He is the author of numerous reports pertaining to surveying resources, and has a particular interest in the methodology of surveying and measuring earth resources.

#### BIOGRAPHICAL SKETCH

#### A. T. Klett

Albert T. Klett has been employed as a Wildlife Research Biologist with the Bureau of Sport Fisheries and Wildlife at the Northern Prairie Wildlife Research Center, Jamestown, North Dakota since 1965. Prior to that he worked with Bureau's wetland preservation program in the prairie region for 3 years, served as a Wildlife Biologist for the North Dakota Game & Fish Department during the period 1953 to 1962 and worked for the Utah Game & Fish Department for 3 years. He attended Utah State University and received his Master's Degree there in 1953. He is the author of more than 20 scientific papers and popular articles concerning research and management of upland game birds, waterfowl and furbearing animals.

### APPLICATION OF REMOTE SENSING TECHNIQUES FOR APPRAISING

#### CHANGES IN WILDLIFE HABITAT

Harvey K. Nelson
A. T. Klett
Northern Prairie Wildlife Research Center
Jamestown, North Dakota

John E. Johnston
Remote Sensing Evaluation & Coordination Staff
U. S. Geological Survey
Washington, D. C.

#### INTRODUCTION

Most Americans consider wildlife as an important national resource. Historically, the Indians, Eskimos, and pioneers depended on the native fish, mammals, and birds for survival. Wild animals are still a source of food and clothing in some areas. Today, since the agricultural and industrial development of the continent, wildlife is valued for its contribution to such recreational pursuits as nature study, bird watching, photography, and sport hunting. Many species are beneficial to mankind and there is a growing awareness of the ecological importance of wild animals. Many Americans feel that the presence of a variety of wildlife in the environment adds important dimensions to the quality of life.

In general, economic development has resulted in a decline in the number of many wild animals, and some species have become endangered or extinct. Laws of various types have been enacted to protect wildlife. Species that migrate across international boundaries have been given additional protection through treaties between Canada, the United States, and Mexico.

The Bureau of Sport Fisheries & Wildlife, in the U. S. Department of the Interior, is the agency responsible for the protection of migratory birds in the United States. Most migratory birds are given complete protection. One exception is the gamebird group that may be hunted under regulations set annually by the respective governments. These migratory gamebird groups include waterfowl, cranes, rails, shorebirds, and doves. Government administration of game management and public hunting at the Federal and State level is traditional in North America. Although we are largely dependent on operations of private land owners and management of public domain lands for preservation and maintenance of wildlife habitats, governmental agencies establish restrictions on areas open to hunting, bag limits, shooting hours, season length, and species that

can be taken. One significant aspect of game management in the United States and Canada is that the Federal government assume major responsibility for migratory species. State and provincial governments have primary jurisdiction over most resident species.

In 1965, 1,650,000 U. S. waterfowl hunters spent \$87,136,000.00 for 13,526,000 recreation-days (U.S.D.I., 1965) utilizing one aspect of the waterfowl resource (Figure 1). In addition, as shown in Figure 2, bird watchers and other groups obtained millions of days of satisfying recreation (Clement, 1964). Unlike most resident small game species, waterfowl populations may be influenced greatly by hunting regulations (Geis, 1963). Populations also fluctuate with changes in weather and water conditions on the breeding grounds (Crissey, 1969; Geis et al., 1969). Efficient management of this renewable resource depends upon annual adjustment of hunting regulations to insure that a sufficient number of birds remain after the hunting season to provide for production the following year.

An estimate of the size of the fall flight must be available at the time hunting regulations are set. This estimate must be reasonably accurate since, for a number of species, hunting is the largest cause of mortality once the young have attained flight age. Regulations based on faulty estimates of current waterfowl numbers could result in loss of hunting opportunity or reduction of the breeding population to undesirably low levels. A need exists, therefore, to accurately predict the magnitude of the annual fall flight from the breeding grounds (Figure 3).

To meet this need, the U. S. Bureau of Sport Fisheries & Wildlife, (BSF&W), the Canadian Wildlife Service (CWS), and the various provinces and states have developed systematic procedures for predicting fall waterfowl populations (Geis et al., 1969; Crissey 1957; U.S.D.I. 1969). Aerial surveys conducted in May and July are used to provide indices for habitat conditions and waterfowl breeding populations and production. The stratified sampling plan for the United States and Canada is shown in Figure 4. Sample ground surveys are also made to provide correction factors for the aerial data, and the corrected data are then used to make predictions. Hunting season recommendations, presented at the annual national waterfowl regulations meeting, must be prepared in early August, but the last aerial surveys often are not completed until the end of July. Administrators, therefore, are often pressed to evaluate the data and develop recommendations in time to meet this deadline.

Although these surveys have been generally successful for providing essential data for management, biologists have proposed that remote sensing techniques might be used to improve and extend current methods. William A. Fischer (1967) of the USGS has pointed out that information obtained by remote sensing techniques from aircraft or spacecraft are particularly valuable if: (1) The problem is on a

regional or global scale (2) Repeated observations on such a scale can provide a "motion picture" of time dependent changes (3) Data collection, reduction, and interpretation are more economical than those obtained by current, conventional methods (4) The problem can be solved without direct samples of the material sensed (5) A map or plan showing a pattern of distribution of the remote sensed element will aid in solution of the problem. Other capabilities of remote sensing and automatic data processing include rapid processing of large volumes of data and data collection over inaccessible regions and terrain.

Many of these characteristics of remote sensing technology have application to the waterfowl production and habitat surveys. The area surveyed is transcontinental in scope, extending from coast to coast and from the far north into the central United States. A large important portion of the North American waterfowl breeding range is located in the prairies of north central United States and south central Canada, an area subject to extreme variability in surface water Repeated observations are needed seasonally and annually conditions. to monitor changes in surface water and other environmental conditions. Some portions of the migratory bird breeding grounds, especially in Northern Canada and Alaska, are inaccessible to ground surveys and pose problems for surveys from small aircraft. Other indices of water conditions and waterfowl production would be helpful in meeting the inflexible time schedule required for the establishment of annual hunting regulations.

Remote sensing technology has not advanced to the point that small mammals and birds can be recognized and counted. However, because of the relationship between reproductive success and habitat quantity and quality, particularly surface water conditions in ponds and small lakes, biologists have speculated that a reliable production index for waterfowl could be derived from an inventory of such water areas during the nesting and rearing period. Remote sensing from aircraft or spacecraft might provide such an inventory or perhaps some other annual indices to wetness that could be used as a base for predictions.

For the project under consideration here, an attempt was made to investigate the potential of airborne, multispectral, line-scanner data-acquisition and computer-implemented automatic recognition techniques for providing useful information about waterfowl breeding habitat in North Dakota. Previous to this project, field-oriented investigations had been carried out by personnel of the Willow Run Laboratories, University of Michigan over agricultural areas (Hasell 1968; Nalepka, 1970), over portions of the International Biological Program (IBP) Grasslands Biome site (Wagner et al. in press), over selected areas of an urbanized landscape (Colwell 1970), and over

hydrobiological features in the Everglades National Park (Higer et al. 1970). These investigations demonstrated that techniques for airborne data acquisition using multispectral line scanners, and data processing techniques using analog and digital computers, provide useful information about landscape materials, features, and processes not obtainable from conventional aerial photographic techniques. The study was planned by the BSFW and the USGS and carried out with the support of NASA through contracts with the University of Michigan. The principal information presented in this paper is based on two reports resulting from the study (Burge et al. 1970; Nelson et al. 1970).

#### **OBJECTIVES**

Arrangements were made with the University of Michigan to fly a multispectral remote sensing mission over the Woodworth study area in May 1968 (Figure 5). The mission was part of an experiment to determine what characteristics of wetland habitats and adjacent uplands could be detected multispectrally and processed automatically with the special computer equipment at the University of Michigan's Willow Run Laboratories. The specific kinds of information sought were:

1. Number of ponds containing water.

2. Number of dry ponds.

3. Number of ponds by size class and wetland type.

4. Identification of major land use types.

- 5. Distribution of ponds within different land use types.
- 6. Identification of major associations of marsh plants.
- 7. Measurement of pond depth, area and shoreline perimeter.

8. Area and distribution of cultural features.

9. Effects of increased flight altitude on accuracy of measurements.

Fortunately these objectives are of mutual interest to hydrologists, geologists, geographers, agriculturalists and others. These overlapping interests justify work on projects of secondary economic importance such as waterfowl ecology. The results can be used to advantage in a number of disciplines.

#### THE STUDY AREA

The topography of the test site is typical of the stagnation moraine that lies along the eastern edge of the Missouri Coteau in North Dakota. The 15.5 km² area has been studied intensively by biologists from the Northern Prairie Wildlife Research Center, BSF&W, since 1964 (Kirsch, 1968). Pond basins of various sizes and types are numerous, averaging nearly 40 per km² (Figure 6). During the past 4 years, the breeding population of ducks has ranged from 27-43 pairs per km². Most of the land in private ownership is cultivated for small grains or is used for pasture. Some lands owned by the BSFW have been

maintained in a variety of idle cover types since 1963. A small percentage remains as native prairie. Ground conditions on the day of the flight presented a composite of fields in different stages of tillage, wet and dry ponds, and upland and aquatic vegetation in early stages of growth.

#### **PROCEDURES**

The mission was flown with the University of Michigan C-47 aircraft using a 17 channel multispectral scanner and four aerial cameras. The scanner channels included contiguous but discrete wavelength bands in the ultraviolet, visible, and infrared regions. Thirteen runs were completed at 610 m and 3,050 m above the terrain between 0830 and 1030 on May 31, 1968. Ground measurements of air, soil surface, and water surface temperature; soil moisture; relative humidity; water depth; and vegetative development were made at selected study sites on the morning of the flight. Data on land use, wetland types, and cultural features were collected at different times as part of the routine monitoring of the area. A further source of control data was the photographic information obtained during the flight with four film/filter combinations. These data provided the necessary background for interpreting the scanner imagery and assessing recognition success obtained with the automatic processing equipment. A number of welldocumented areas were chosen for test sites.

The Willow Run Laboratories' airborne scanning spectrometer is currently configured to sense radiation simultaneously in 12 spectral bands ranging from 0.4 um (blue) to 1.0 um (near infrared) (Figure 7). The scanning spectrometer, which is mounted in the belly of an airplane, accomplishes the scanning function by means of a mirror which rotates about an axis parellel to the aircraft heading. The forward motion of the aircraft causes succeeding scans to view different portions of the scene below. Thus, by appropriately setting the aircraft velocity and mirror rotation rate, each point in the ground scene that is within the total system field of view may be scanned.

The radiation from each point of the scan is collected and directed through a prism. Radiation in different portions of the spectrum is then picked off by 12 fiber optic bundles, each of which directs the radiation to a different photomultipler. The voltages produced in each of the photomultipliers are then amplified and recorded on magnetic tape. Thus, the data recorded on tape, which is used as an input to the recognition processor, consists of 12 scanner signals, each signal corresponding to information gathered over a different spectral band. Four additional detectors were used to provide data in the 1.0- to 1.4-, 2,0- to 2.6-, 4.5- to 5.5-, and 8.0- to 13.5-um regions.

Preliminary analyses of the scanner imagery and computer recognition maps were completed at the Willow Run Laboratories in late 1969. Five

of the runs were selected for processing: four from 610 m data and one from 3,050 m data. A segment of one 610 m run over a representative part of the study area was processed most intensively. The 3,050 m data used were selected because they covered most of the study area and contained the least amount of cloud shadow. Both analog and digital procedures were tested for the identification of materials; digital techniques were used to measure the perimeter and area of the ponds.

Several analog processing experiments were conducted with the 610 m imagery using six data channels in the visible and near infrared region. Materials tested for automatic recognition included open water, marsh vegetation, croplands, pastures, idle areas, hayland and cultural features. In some instances, attempts were made to identify components within these broad categories such as standing marsh vegetation, matted marsh vegetation, or a given species such as cattail. At other times materials were combined to identify a broader group, e.g. open water and marsh vegetation were combined to delineate entire pond basins (Figure 8). Spectral signatures were established by the analog computer for each test site and the signatures were then used to recognize similar materials within the recorded field of view.

The 3,050 m data were not completely analyzed. The objective was to determine in a general way some of the advantages and disadvantages of sensing from higher altitudes and to simulate results obtainable from similar sensors aborad space craft. Three channels in the 0.62 to 1.0 um region were selected because they were synchronous with one another and may have an advantage over shorter wavelength data at higher altitudes because longer wavelengths are less affected by atmospheric scattering.

One line of 610 m coverage was processed with a CDC-1604 digital computer. Outputs from this process are recognition maps that are similar to analog color coded recognition maps. In addition to maps, the digital computer was used to produce statistics on the perimeter and area of individual ponds by flight line segment and by size class distribution. Five channels in the reflective wavelength region (0.4 to 1.0 um) were selected for this digital processing. These computations were compared to measurements of shorelines and area made on aerial photographs with a wheel-type map measurer and a dot grid counter.

#### RESULTS

## Analog Processing of 610 m Data

An important objective of this project was to determine the use-fulness of multispectral techniques in identifying components of migratory bird habitat. In general, the analog processing experiments with the 610 m data were successful. The features of greatest interest were ponds, which were recognized with almost 100 percent accuracy on one line in the study area. Ponds less than 0.25 ha in size printed out clearly in

the analog recognition maps. In order to recognize all ponds, it was necessary to combine the signatures for open water and two types of aquatic vegetation (Figure 8).

Technical problems prevented analysis of the data for water depth during the period of the contract. This information, however, can now be obtained for those ponds having water clear enough to permit light to penetrate to and be reflected from the bottom using a recently developed digital program.

Dry pond basins were not recognized in the visible portions of the spectrum analyzed in this study. The types of vegetation in these temporary ponds was so similar to those in surrounding area that no differentiation could be made. Recently, however, examination of video prints in the near-infrared channels indicates that dry ponds can be recognized.

Recognition of principal aquatic vegetative associations was unsatisfactory because development of plant communities is incomplete in late May. Much of the new growth was still concealed by the remains of previous growth. Also, vegetation at or just above the water surface produced a hybrid signature that made differentiation between water and aquatic vegetation difficult. Collection of data later in the season, such as mid-July, when the vegetative communities are at peak growth should permit much more accurate differentiation. Additional data were collected in July 1970 when the vegetative growth was mature. These data are now being processed for recognition of aquatic plant communities.

The recognition of land use types and upland vegetation was successful. Bare soil, new growth, and dead vegetation could be separated in most cases (Figure 8). All the bare soil areas recognized were tilled fields. Some differentiation was obtained between fields that may have been due to soil moisture, stage of tillage, or soil type. New vegetative growth was evident in a variety of land use types where agricultural operations resulted in the removal of the dead vegetation from the previous year. Attempts to recognize wild hay, overgrazed pasture, and idle alfalfa-brome grass mixtures were only partially successful. Areas of brush were not recognized because of the dominance of grasses within the brush training sets, but the appropriate spectral signature for woody species can be developed. The result is a hybrid signature similar to the example of marsh vegetation growing in water. When consideration is given to the fact that the original land use training sets were chosen from mapped information and not from on-site observations, these results are reasonable. The selection of more representative test sites would have eliminated much of the misclassification. This aspect can be corrected in future remote sensing work by establishing a more coordinated ground data collection effort.

No signatures were established for cultural features. For most purposes roads, towns and farm buildings can be recognized satisfactorily from photographs or spectral imagery (Figure 9). Automatic recognition of these features from high altitude may be difficult because of the relatively small dimensions and the great diversity of materials that would have to be detected. This conclusion is supported by findings obtained on another project at the University of Michigan (Colwell, 1970). These findings do show, however, that buildings and road materials can be mapped using data in the reflective and infrared wavelengths together.

## Recognition Digital Processing of 610 m Data

The digital processor can provide mapped recognition outputs which are comparable with those obtained from the analog equipment (Figure 10). A portion of a digital recognition map is shown in Figure 12. There is, in general, a good correlation between the materials represented by the gray levels on the digital maps and the colors on the analog maps.

## 3,050 m Analog Imagery

As expected, recognition results from 3,050 m data were of lesser quality than those from 610 m data (Figure 11). Aerial coverage was about five times greater from 3,050 m than at the lower altitude. In general, the loss of spatial information did not exceed the lower size limit of features of interest, e.g. the smaller ponds. However, 3,050 m appears to be a practicable upper limit to the altitude at which such results can be obtained with the 3 milliradian resolution capability of the University of Michigan scanner. Recognition of ponds larger than 1 to 2 ha will probably be resolved with instruments being designed for use in space craft by 1972 or later.

Recognition results using the higher altitude data were complicated by partial cloud cover during the flight. Better results could be expected with more representative test sites and an optimum selection of synchronized channels. Fewer resolution elements cover a given area at a higher altitude and hence provide a less dense sample for a test site. Since all features are reduced in size, the probability of including extraneous or unwanted material in the test site is greatly increased. However, if large, homogeneous, and representative training sets are available, recognition of areas about four resolution elements in size (40 m x 10 m) can be achieved at the 3,050 altitude.

## Quantitative Digital Processing of 610 m Data

Quantitative results on the perimeter and size of ponds were obtained using low altitude data on the digital processor (Figure 12). Computations of pond perimeters averaged higher than control measurements obtained with aerial photographs and a wheel-type map measuring device.

The map measuring device tends to smooth out irregularities in the shoreline that are included in the digital processing. Acreages derived from aerial photographs were about the same as the computed estimates. Automatic processing of multispectral data may make it possible to derive these measurements faster than by conventional methods with equal or greater precision.

#### CONCLUSIONS

The spectral characteristics of the components of a landscape containing waterfowl habitat can be detected with airborne, multispectral scanners. By analyzing these spectral characteristics it is possible to identify and map the landscape components through analog and digital processing methods.

The recognition results obtained with the 610 m data are reasonably accurate. Pond identification was accomplished successfully by combining the spectral signatures of open water and marsh vegetation. In addition, by operating on the digital recognition data, statistical summaries and distributions were obtained that appear to be more accurate than those obtained by standard office measurements. Progress was made in the recognition of broad categories of land use and vegetation. Recognition of land use types and further development of automatic measurement techniques will make it possible to better interpret the relationship of such parameters as land: water ratios, changes in the relative amounts of cropland and grassland, and specific land-use practices. Greater differentiation will be possible by collecting data later in the growing season, selecting large homogeneous areas for test sites, obtaining better on-site ground data, and using optimum data channels as determined by digital techniques.

At the present stage of development multispectral remote sensing techniques are not ready for operational application to surveys of migratory bird habitat and other such resources. Further developments are needed to (1) increase accuracy, (2) decrease retrieval and processing time, and (3) reduce costs.

New studies are in progress using multispectral data collected by the University of Michigan in 1970. High altitude photography, collected by NASA, is also available for comparative evaluation. Hopefully, the results of these investigations and future studies with ERTS data will assist us in attaining our previously stated goals.

#### LITERATURE CITED

- Burge, W. G., and W. L. Brown. 1970. A study of waterfowl habitat in North Dakota using remote sensing techniques. Univ. Michigan, Inst. Sci. and Tech., Willow Run Laboratories.
- Clement, R. C. 1964. Viewpoint of a naturalist. Pp. 699-705. In Waterfowl tomorrow, J. P. Linduska (editor). U. S. Gov't. Printing Office. 770 pp.
- Colwell, J. E. 1970. Multispectral remote sensing of urban features. Univ. Michigan, Inst. Sci. and Tech., Willow Run Laboratories Report No. 2772-6-F.
- Crissey, W. F. 1957. Forecasting waterfowl harvests by flyways. Trans. N. Am. Wildl. Conf. 22:256-268.
- \_\_\_\_\_\_. 1969. Prairie potholes from a continental viewpoint.

  Saskatoon Wetlands Seminar, Canadian Wildl. Serv. Report Series 6:161-171.
- Fischer, W. A. 1967. Geological applications of remote sensors. A.I.A.A. Annual Meeting and Technical Display 4:13-19.
- Geis, A. D. 1963. Role of hunting regulations in migratory bird management. Trans. N. Am. Wildl. Conf. 28:164-172.
- , R. K. Martinson, and D. R. Anderson. 1969. Establishing hunting regulations and allowable harvest of mallards in the United States. J. Wildl. Mgmt. 33(4):848-859.
- Hasell, P. G. 1968. Investigations of spectrum matching techniques for remote sensing in agriculture. Univ. Michigan, Inst. Sci. and Tech., Willow Run Laboratories Report No. 8725-13-P, vol. 1.
- Higer, A. L., N. S. Thomson, F. J. Thomson, and M. C. Kolipinski. 1970. Applications of multispectral remote sensing techniques to hydrobiological investigations in Everglades National Park. Univ. Michigan, Inst. Sci. and Tech., Willow Run Laboratories Report No. 2528-5-T.
- Kirsch, L. M. 1968. Effect of land use on waterfowl and other wildlife on the Woodworth study area. Pp. 14. In Research Accomplishments. Northern Prairie Wildlife Research Center, Bur. Sport Fish. and Wildl. 55 pp. multilithed.

- Nalepka, R. F. 1970. Investigation of multispectral discrimination techniques. Univ. Michigan, Inst. Sci. and Tech., Willow Run Laboratories Final Tech. Report No. 2264-12-F.
- Nelson, H. K., A. T. Klett, and W. G. Burge. 1970. Monitoring migratory bird habitat by remote sensing methods. Trans. N. Am. Wildl. and Nat. Resources Conf. 35:73-84.
- U. S. Department of the Interior. 1965. National survey of fishing and hunting. Bur. Sport Fish. and Wildl., Resource Publ. No. 27:13.
- . 1969. Standard procedures for waterfowl population and habitat surveys -- the prairies. Bur. Sport Fish. and Wildl., Div. Management and Enforcement. 68 pp.
- Wagner, T. W. et al. An investigation of grassland resources using multispectral processing and analysis techniques. Univ. Michigan, Inst. Sci. and Tech., Willow Run Laboratories Report No. 34795-1-F. (In press)

#### DEFINITIONS \*

- Aerial survey: An estimate of populations and/or species composition through the use of an airplane.
- Air-ground correlation: The use of data from intensive ground surveys to correct extensive observations from low flying aircraft.
- Aquatic: An animal or plant living in the water.
- Bird Treaty Act: A law making it illegal to hunt, kill, sell, purchase or possess migratory birds except as permitted by annual regulations adopted by the Secretary of the Interior.
- Breeding population: The number of breeding pairs of birds present on a given unit of habitat.
- Daily bag limit: The legal limit of game animals per day as defined by law.
- Fall migration: Movement of waterfowl from nesting range to wintering range.
- Forecast-fall flight: An estimate of the number of waterfowl that move from the northern nesting grounds to the southern wintering grounds.
- Ground survey: A study or inventory of wildlife activities or numbers from the ground as contrasted to study or inventory from an airplane.
- Habitat: A set of ecological conditions required by any one species.
- Hunting: The act of attempting to take game.
- Hunting season: The period during which game animals can be legally taken for sport.
- Inventory: An estimate of population levels.
- Migratory: To move periodically or seasonally from one region or climate to another.
- Production: The yield of a wildlife population through reproduction.
- Production index: Ratio of young of the year to adult segment of a population.
- Protection: Safeguard against natural enemies and/or hunters.

- Range: The extent of an area covered by the breeding population of a particular species.
- Surface water: Water that is stored above ground in natural or artificial basins.
- Training set: A test site; a representative feature, object or material that is used to establish a spectral signature.
- Waterfowl: A grouping of birds including brant, wild ducks, geese, and swans.
- Wetland classification: A system for categorizing and rating the value of wetlands based on permanency, emergent vegetation, size and use by migratory birds.
- \* Most definitions taken from Glossary of Waterfowl Management Terms, J. R. Singleton and Monte M. Dodson. The Central Flyway Council. Publ. by: Texas Game and Fish Commission. 1959.

# Waterfowl Hunting, 1965







# Birds and Other Wildlife Provide Outdoor Activities for

8,196,000 Birdwatchers



3,113,000
Bird and Wildlife Photographers

FIGURE 2



278



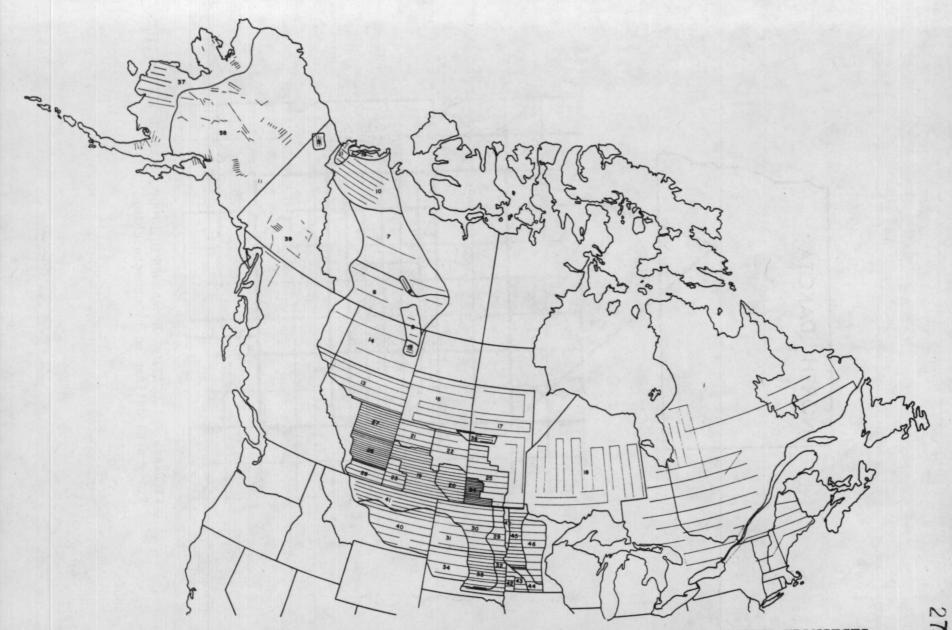


FIGURE 4. WATERFOWL BREEDING POPULATION AND PRODUCTION AERIAL SURVEY TRANSECTS AND STRATA

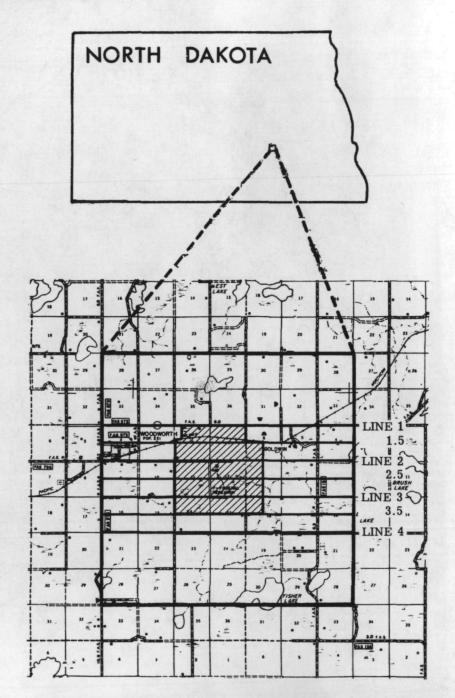


FIGURE 5. LOCATION OF WOODWORTH STUDY AREA AND FLIGHT LINES. Study area delineated by crosshatching.

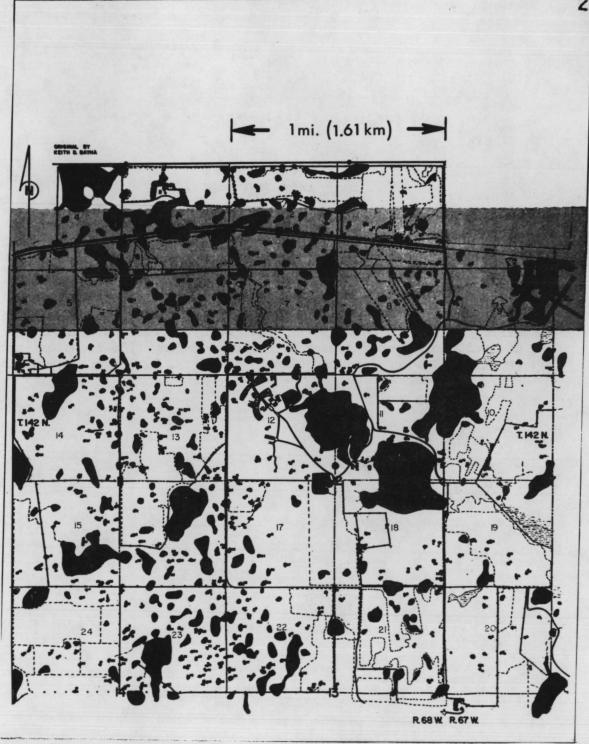
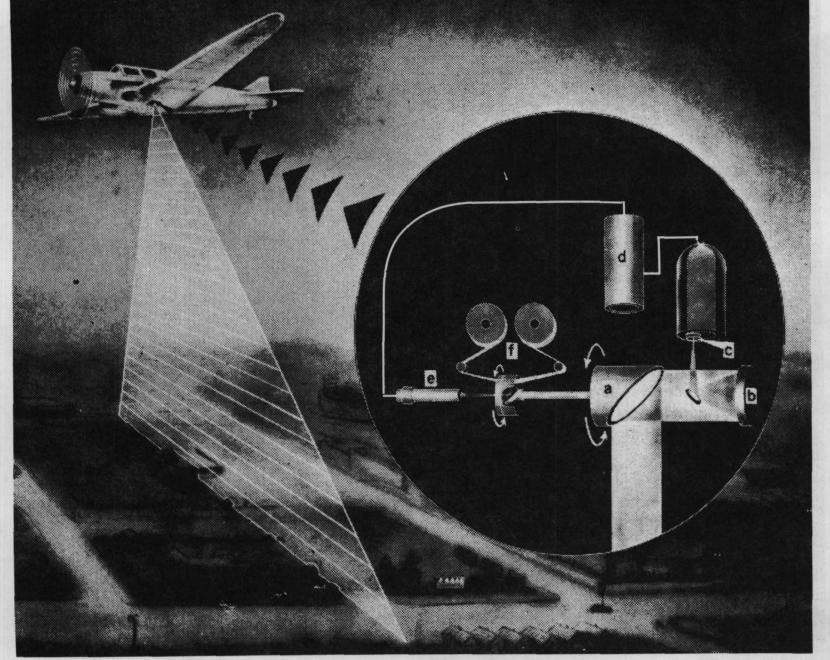


FIGURE 6. WOODWORTH STUDY AREA, NORTH DAKOTA. Wetlands shown in black; flight line 1.5, run 9 shown stippled.

Figure 7. (See next page.)

INFRARED SCANNING SYSTEM. Radiation from the earth is collected on the surface of a rotating miror a, reflected to the surface of a parabolic mirror b, and thence to the surface of a solid state detector c. The output of the detector is amplified d and modulates the output of a light source e. The modulated light is recorded on film f. Interal coverage is obtained by rotation of the collecting mirror a; forward coverage is provided by forward movement of the aircraft and is coordinated with the recording film-transport mechanism. (Modified from diagram supplied by the H. R. B. Singer Corporation.)



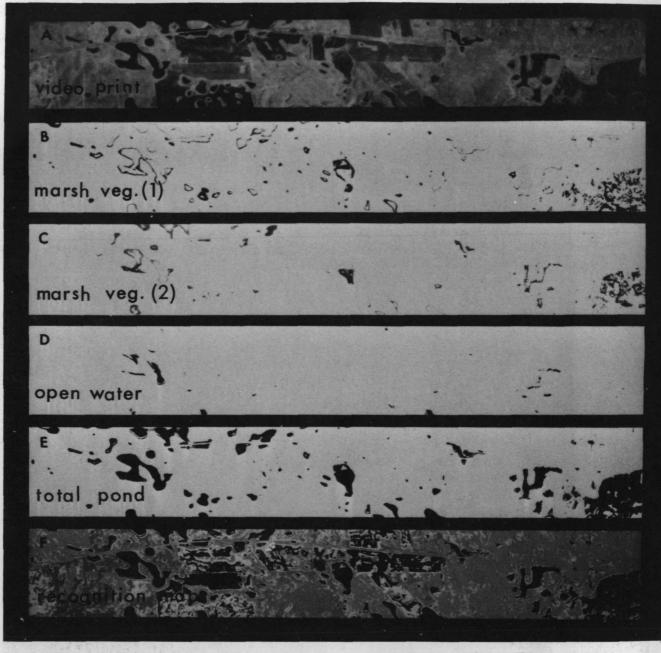


FIGURE 8. STEPS IN THE ANALOG PROCESSING OF MULTISPECTRAL SCANNER DATA, WOODWORTH STUDY AREA. Strip E is the recognition map of wet basins obtained by combining the information in strips B, C, and D. The recognition map F includes other materials in the scene.

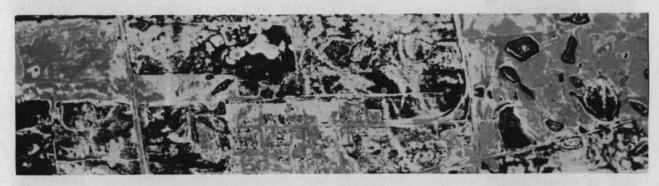


FIGURE 9. ANALOG RECOGNITION MAP OF CULTURAL FEATURES. Village of Woodworth, North Dakota

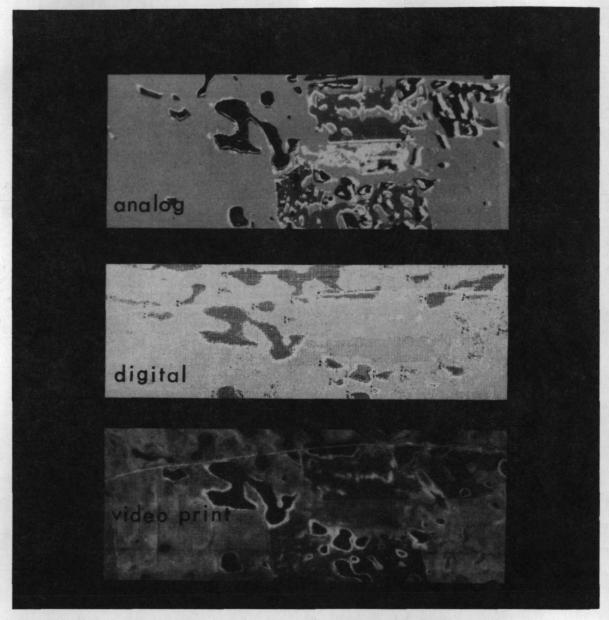


FIGURE 10. COMPUTER RECOGNITION MAPS FROM MULTISPECTRAL SCANNER DATA.



FIGURE 11. ANALOG RECOGNITION MAP FROM DATA COLLECTED AT 3,050 METER ALTITUDE

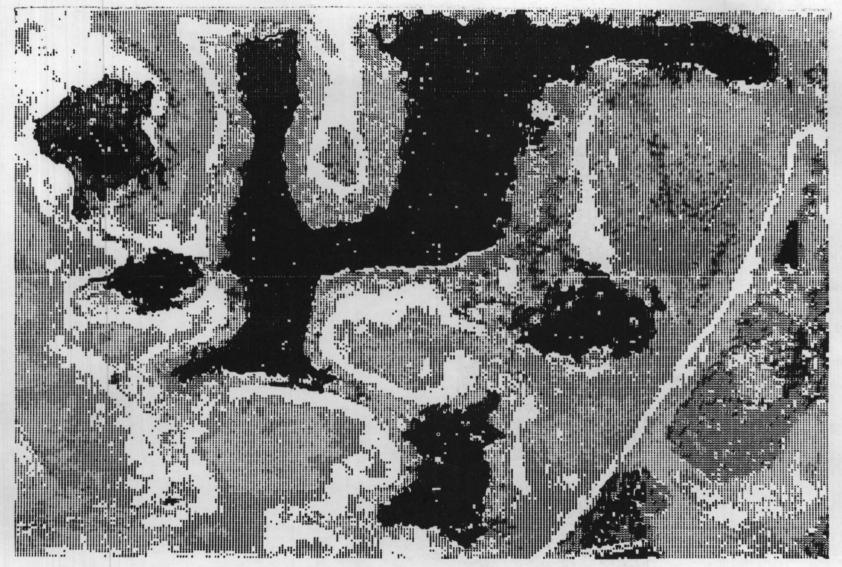
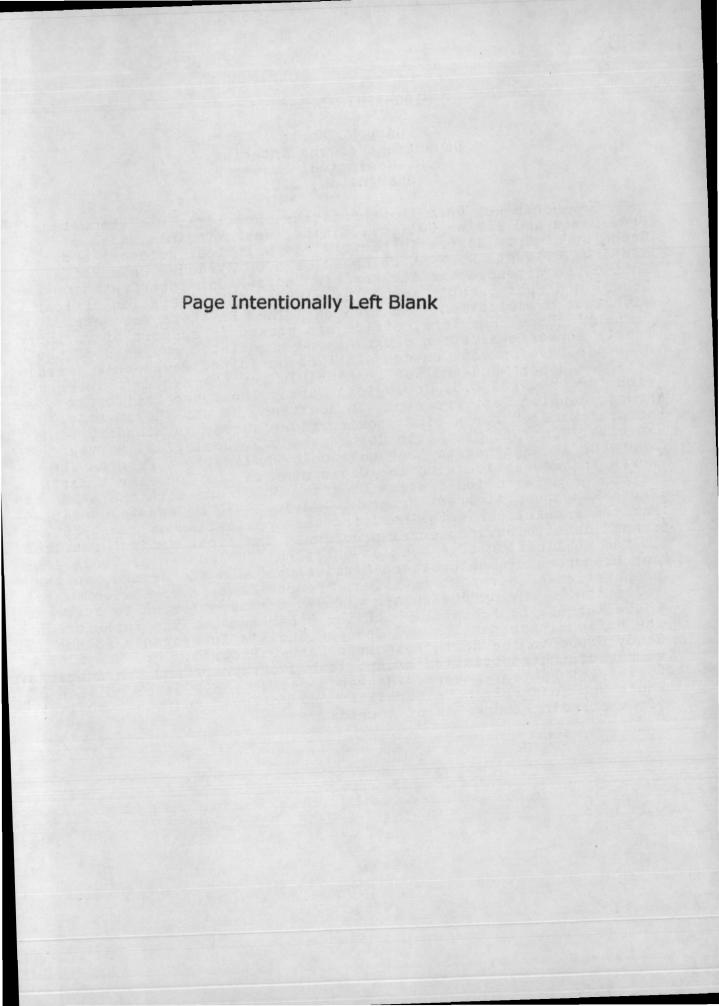


FIGURE 12. DIGITAL RECOGNITION MAP OF POND 9-1, WOODWORTH STUDY AREA, NORTH DAKOTA



#### BIOGRAPHICAL SKETCH

Gary W. North
Department of the Interior
U.S. Geological Survey
Washington, D.C.

Mr. North was born in Schenectady, New York; was graduated from Davis and Elkins College, Elkins, West Virginia, with a Bachelor of Arts degree in history and political science; and has done graduate work at Utica College of Syracuse University. In 1962 he attended the Air Force's Photo-Radar Interpretation School and subsequently served as a photo interpretation officer with that organization. In 1965 he joined Raytheon Autometric Company's Rome, New York, office and worked in support of various remote sensor evaluation programs and associated projects of the Rome Air Development Center. In 1968 he joined Raytheon's terrain sciences department and was responsible for the system's integration for the NASA/U.S. Geological Survey, Southern California Remote Sensing Test Program. In addition, he was the on-site program manager for a side looking radar survey in Ecuador, South America. In 1969 Mr. North joined the U.S. Geological Survey where he is assigned to the Geographic Applications Program and works in association with the Department of the Interior's Earth Resources Observation Systems Program (EROS) and with the NASA Earth Resources Aircraft Program. During 1970 he was responsible for two special projects involving the application of remotely sensed data to environmental problems. The first project resulted in the publication of a booklet entitled "Environmental Conditions and Resources of Southwestern Mississippi" and the second, in the preparation of a report entitled, "Remote Sensing of Environmental Pollution." During the summer of 1970 he was selected to serve as the alternate representative of the Department of the Interior on the National Aeronautics and Space Council's Interagency Ad Hoc Study Group on the Earth Resources Survey Program. Mr. North is a member of the Association of American Geographers and the American Society of Photogrammetry. He was named to the 1961-62 edition of Who's Who in American Universities and Colleges and the 1970 list of Outstanding Young Men of America.

REMOTE SENSING
OF
ENVIRONMENTAL POLLUTION

by

Gary W. North

Department of the Interior U.S. Geological Survey Washington, D.C. 20242

#### ABSTRACT

Environmental pollution is a problem of international scope and concern. It can be subdivided into problems relating to water, air, or land pollution. Many of the problems in these three categories lend themselves to study and possible sollution by remote sensing. Through the use of remote sensing systems and techniques, it is possible to detect and monitor; and in some cases, identify, measure, and study the effects of various environmental pollutants. As a guide for making decisions regarding the use of remote sensors for pollution studies, a special five-dimensional sensor/applications matrix has been designed. The matrix defines an environmental goal, ranks the various remote sensing objectives in terms of their ability to assist in solving environmental problems, lists the environmental problems, ranks the sensors that can be used for collecting data on each problem, and finally ranks the sensor platform options that are currently available.

Examples of remote sensor data relating to various environmental problems will be shown during the oral presentation of this
paper. These examples have been extracted from a special report
entitled "Remote Sensing of Environmental Pollution." This report
was prepared by the Geographic Applications Program of the U.S.
Geological Survey for the Department of the Interior's Earth
Resources Observations Systems Program, and for the Earth Observations Program of the National Aeronautics and Space Administration.

#### INTRODUCTION

Several days ago, during the first part of this International Workshop, many of you heard a paper outlining the various steps required to carry out a regional assessment of environmental quality through the use of remote sensing. The objective of this paper is to concentrate on one of those steps and look in detail at many of the detrimental factors that tend to lower the quality

of an environment. We are going to examine some of the problems of land, air, and water pollution and discuss many examples of how remote sensing devices can detect, identify, measure, monitor, or determine the effects of various environmental pollutants. Within each category an attempt will be made to show what can be observed, interpreted, and/or monitored from currently available experimental and operational spacecraft, high and low altitude aircraft, and ground based platforms. Examples of special processing, enhancement, and analysis techniques will not be discussed in detail, since they have already been, or will be, covered in several of the other papers during the workshop.

The illustrations shown during the oral presentation of this paper were taken from a special report entitled "Remote Sensing of Environmental Pollution" prepared by the U.S. Geological Survey, with substantive contributions from many different governmental agencies and commercial firms. This report covers more than 50 of the environmental problems faced by this nation. Many of these may be problems in your own country and if they are not, they represent potential problems that you may face in the near future.

#### REMOTE SENSING SYSTEMS

Various remote sensing devices can be used to collect the different kinds of data relating to pollution. In many cases a single sensor can provide the necessary data while for others, a specialty sensor or combination of sensors may be required.

# Cameras:

Perhaps the oldest, best known, and most widely used remote sensor is the camera. You will probably find this to be the easiest, cheapest, and most flexible sensor to use. With lens options and different film/filter combinations, much can be accomplished with a camera system.

# Infrared and Multispectral Line Scanners:

A second family of sensors includes the infrared and multispectral line scanners. Infrared scanners are built to detect the
thermal infrared, or heat energy emitted by objects. They are most
useful in detecting heated effluents from power plants, industrial
processes, or monitoring the surface temperatures of rivers, lakes,
and streams. They can be used during the day or night, since they
record energy emittance and not the sun's reflected energy. Various models of these scanners are available commercially and can be
carried about in suitcase size boxes and used in small aircraft.

Multispectral scanners operate on the same principle as the infrared scanners except that they record data in other portions of the spectrum, in addition to the infrared. Only a few of these sensors are being flown experimentally in this country. They are very expensive to operate and maintain, and often require a computer system to effectively analyze the raw data.

## Radiometers:

Radiometers are non-imaging sensors which measure emitted or reflected electromagnetic energy and graphically display this information on a strip chart recorder. They can be built to be sensitive to a range of energy from the ultraviolet portion of the spectrum to the infrared region, and are useful in recording spectral signatures for various objects. When flown in conjunction with a thermal scanner, they can provide temperature measurements of the ground or water which can then be correlated with the different grey tones of the thermal imagery. By using radiometers and scanners together, it is possible to eliminate the need for taking temperature samples on the ground. Another application of these sensors involves using them to determine the thickness of crude oil slicks lying on water surfaces.

## Side Looking Radar:

Side looking radar is an all weather, day/night sensor that is particularly effective in imaging large areas of terrain. A special advantage of this sensor is that it penetrates most clouds and thus, if you live in a perpetually cloud covered region of the world, it may be practical to acquire radar coverage instead of photography. This sensor, while not specifically designed for pollution detection, is effective in monitoring strip and open pit mining operations and other large scale changes to the landscape. It could also be used to monitor extent and level of content changes in large industrial waste ponds or tailings dumps and for monitoring oil spills.

# Correlation Spectrometer:

Another specialty sensor is the correlation spectrometer. This non-imaging sensor was built to detect quantities of gases in the atmosphere from either an aircraft, or hopefully, spacecraft platform. This device measures the concentrations of a single air pollutant in a column of air between the ground and the platform and then prints out the concentrations on a strip chart recorder. Even though it is undergoing development tests, it has demonstrated its usefulness in detecting, from aircraft, sulfur dioxide and nitrogen dioxide, two pollutants that are major

components of smog. These sensors can also be placed in mobile vans to be moved about on the ground to check on various smokestack emissions.

## Decibel Recorders:

A decibel recorder is a device to measure the relative intensity of sound. The sensor detects and records various noises on a strip chart recorder thus producing a graphic record of its intensity. Such devices could be used to determine whether or not housing should be allowed near such things as airports, expressways, heavy industry, etc.

## Fraunhofer Line Discriminator:

The Fraunhofer Line Discriminator was built specifically to detect and measure fluorescence. Currently undergoing flight development tests in a helicopter, the device has effectively detected concentrations of Rhodamine WT dye as small as five parts per billion. This alone is encouraging since this dye is often used to study current and mixing patterns in water bodies. By mixing portions of the dye with particular pollutants, it may be possible to determine to a greater extent what the fate of these substances may be once they enter a stream or lake. It is hoped that additional instruments will be built to detect small quantities of such things as crude oil, fish oil, pulp mill wastes, and other substances that fluoresce.

## Scintillation Detectors:

Scintillation detectors are often referred to as aeroradioactivity equipment and are placed in low flying aircraft to detect and monitor gamma radiation. The sensors record radioactivity in counts per second, and by plotting flight paths and sensor readings, individual ranges or radioactivity levels can be assigned to specific areas. These instruments are useful in monitoring radioactive waste material disposal areas and in checking radioactivity levels of nuclear power plant effluents.

# SENSOR/APPLICATIONS MATRIX

With the sensors that have just been described it is possible to detect and monitor; and in some cases, identify, measure, and study the effects of various environmental pollutants. There are, of course, many variables involved and once a basic photographic coverage has been fully interpreted for current and potential pollution sources, new decisions requiring supplementary data will be necessary. As a guide for making these decisions, a special fivedimensional matrix has been designed. The matrix defines an envi-

ronmental goal, lists the environmental problems, ranks the sensors that can be used for collecting data on each problem, and finally ranks the sensor platform options that are currently available.

Figure 1 shows the matrix for water, air, and land pollution problems. To use the matrix one simply reads the numbers and letters in each of the blocks, and checks them against the key to see what they mean. Each block represents a decision involving two factors. For example, if the environmental problem is oil spills, the matrix indicates that remote sensing is an excellent way to detect, identify, and monitor such spills and that it represents an excellent input for environmental planning and modeling. This is shown by the use of the number (1) in the appropriate blocks. Remote sensing is only a fair way, however, to determine the effects of oil spills on the environment, since this requires supplemental ground level sampling and analysis. This is shown by the use of the number (4). In the blocks involving the sensor/ problem interaction, the matrix indicates that a multispectral scanner is the best, or (A), sensor for providing data, but that either a camera with color infrared film, a side looking radar system, or a microwave radiometer would be good (B) choices to provide additional oil spill data. The last of the matrix blocks suggests that an aircraft flying at altitudes of 600 - 6,000 meters would be an excellent, or (1), platform for the chosen sensor or sensors.

To show the overall range of effectiveness of remote sensing to assist in solving environmental problems, the numbers in the Remote Sensing Objectives block have been totaled. By checking the total for each environmental problem, one is able to determine which problems are most amenable to solution by remote sensing.

### ENVIRONMENTAL PROBLEMS

## A. Water

Water pollution is a world-wide phenomena, and irresponsible human attitudes and activities will probably create an even more critical problem in the future. Water pollution is not a local problem for once a pollutant has been added to the water it is carried downstream into lakes, underground acquifer systems and eventually the oceans. Multiple demands for water will continue to increase, especially near the urban centers of the world. As this demand increases, we must remember that the discharge from one user becomes part of the water supply for the next. Thus, it is critical that each time water is used it must be released in a safe condition. Remote sensing can detect and monitor many of man's activities regarding the use and misuse of water.

The following list represents a few selected examples of various water pollution problems in the United States. By examining remote sensor data covering these subjects and then studying the matrix, one may gain a better understanding of how effective remote sensing is in trying to find a means to solve these problems.

- 1. Incompatible Urban Water Uses
- 2. Municipal Sewage Discharges
- 3. Algae
- 4. Contaminated Ground Water Systems
- 5. Acid Mine Drainage

## B. Air

The Earth's atmosphere is the most mobile of the three basic components of our environment. It is a dynamic system which has neither regional boundaries nor ownership attached to it. Nature contributes particulate matter to the atmosphere when a volcano errupts, when a forest burns, and when winds blow across a barren area. Man does a comparable thing when he burns fossil fuels, drives his automobiles, or runs his factories. In fact, where concentrations of people are the greatest, so are the concentrations of air pollutants. Because cities have become heat and particulate anomolies, they are beginning to affect the climate of areas around them. Polluted air masses also cost these same areas a significant number of days of sunshine per year. Add to this the fact that respiratory illnesses and even deaths increase with high levels of air pollution, and one can see the severity of the problem we face.

Remote sensing systems have a significant role to play in the collection of air pollution data. They will not replace the present ground monitoring systems and laboratory analyses which are performed, but they can add a new dimension to air pollution control by providing a regional perspective, by detecting sources and some specific types of pollutants, and by determining representative sample points. The combination of both the more common ground sampling networks and the synoptic view provided by remote sensors can provide an effective detection and monitoring system. Eventually we may even be able to plot and trace concentrations of various pollutants around the globe in much the same way that we presently monitor cloud and weather systems.

The following list represents examples of air pollution problems that are also included and ranked on the Sensor/Applications Matrix.

- 1. Smog
- 2. Dust Storms
- 3. Fire and Volcanoes
- 4. Contrails from Aircraft and Ships
- 5. Ore Smelter Smokestack Plumes

## C. Land

The land resources of the world are neither unlimited in areal extent nor equally capable of supporting human activity. Some of it has been abused and some of it has actually been destroyed for any future productive capability by exploitation and uncontrolled growth. In areas where the land is adaptable to a variety of productive purposes, the demand is greatest and the competition between various land uses is most intense. At present, land use policy is usually determined by who will pay the highest price for each parcel of land. In the years ahead it will become increasingly important for each nation to decide what value it places on each activity and each parcel of land. Each of you should make these decisions based on scientific data and human values in an attempt to establish an environmentally sound master plan for future development. In this way each activity will be allocated the proper amount and type of land, many land pollution problems will be eliminated, and the quality of the overall environment will be improved.

Land pollution problems are different from air and water problems because with land ownership is involved. Parcels of land belong to someone but no one owns the air or a river and besides, unless they are detected at their source, water and air pollutants drift or float away. Land problems, however, remain stationary and until the owner and probable cause are identified and forced to correct the situation, the problem will remain.

Remote sensing can locate and identify these problems and monitor any remedial actions that are taken. The following list of examples from the matrix will illustrate various land problems and how they can be observed by remote sensing.

- 1. Parking Lots
- 2. Garbage and Solid Waste Disposal
- 3. Hillside and Coastal Housing Developments

- 4. Open Pit Mining
- 5. Underground Fires
- 6. Underground Gasoline Leaks
- 7. Lumbering Activities
- 8. Disasters

#### CONCLUSION

On February 10, 1970, the President of the United States made an address to Congress on the environment. In this speech he said:

"... We came only late to a recognition of how precious and how vulnerable our resources of land, water, and air really are... The time has come when we can wait no longer to repair the damage already done, and to establish new criteria to guide us in the future... The tasks that need doing require money, resolve, and ingenuity -- and they are too big to be done by government alone. They call for fundamentally new philosophies of land, air, and water use, for stricter regulation, for expanded government actions, for greater citizen involvement, and for new programs to ensure that government, industry, and individuals all are called on to do their share of the job and to pay their share of the cost ... The fight against pollution, however, is not a search for villains. For the most part, the damage done to our environment has not been the work of evil men, nor has it been the inevitable by-product either of advancing technology or of growing population. It results not so much from choices made, as from choices neglected: not from malaign intention, but from failure to take into account the full consequences of our actions."

This message applies not just to Americans, but to the citizens of all the nations of the Earth. If you too can accept this as a challenge, and perhaps employ some of the remote sensing techniques you have learned about at this workshop, we can all work together to build a quality environment for the many generations who will follow us here on the Earth.

### GLOSSARY OF TERMS

Acid Mine Drainage - Phrase used to describe the acidic water which commonly drains from strip and underground coal mines. Its presence can usually be inferred whenever a stream has a bright yellow/orange color. This color is produced by a liquid called "yellow boy" which is the result of the chemical reaction of the acidic water with iron.

Aeroradioactivity Equipment - Sensor or instrument that is used in low flying aircraft to detect and monitor gamma radiation.

Anomolies - Quantities which increase uniformily with time.

Correlation Spectrometer - A sensor built to detect gasses in the atmosphere. This device analyzes the column of air between the sensor and the ground and then plots out the concentrations of each gas on a strip chart recorder. By plotting these readings along the line of flight, a verticle profile map of gas concentrations can be made. It is used primarily to detect sulfur dioxide.

Decibel Recorder - A sensor used to measure the relative intensity of sounds.

Effluent - Term used to describe any liquid discharge.

Enhancement - Process by which certain details or grey tones of a piece of remote sensor data are magnified and/or intensified.

Flourescence - Property possessed by certain substances of emitting light following exposure to external radiation.

Fraunhofer Line Discriminator - A remote sensing device built specifically to detect and measure flourescence.

Infrared Line Scanner - A remote sensing device built to detect the thermal infrared energy emitted by objects. The word scanner is used in connection with this sensor because the detection system involves the use of a rotating mirror which directs the incoming radiation through a detector and onto a piece of film at the rate of one scan line per rotation.

Matrix - A form which shows the linkages between two or more
interrelated subjects.

Multispectral Line Scanner - A remote sensing device which operates on the same principle as the infrared scanner except that it is capable of recording data in the ultraviolet and visible portions of the spectrum as well as the infrared.

Platform - Term used to describe the vehicle or equipment on which a remote sensing device can be mounted. An aircraft or spacecraft is often referred to as a sensor platform since it is capable of having sensors attached to it.

Radiometer - A non-imaging sensor which measures emitted or reflected electromagnetic energy.

Remote Sensing - Term used to describe the use of instruments that measure properties of objects without coming into direct contact with them. It is also used to describe a series of related problem solving activities involving data acquisition, collection, processing, distribution, and analysis.

Rhodamine WT Dye - A red dye used in hydrology studies. The WT indicates a specific type of rhodamine which has a peak fluorescence of between 5,800 and 5,820 angstroms.

Scintillation Detector - A remote sensing device built to detect gamma radiation with energy levels greater than 50 Kev (thousand electron volts).

Side Looking Radar - An all weather, day/night remote sensor which is particularly effective in imaging large areas of terrain. It is called an "active" sensor since it generates its own energy which is transmitted and received out the side of the aircraft to produce a photo-like picture of the ground.

Smog - Term used to describe a polluted air mass comprised of a mixture of smoke, fog, gasses, and other particulates.

Spectral Signature - Quantitative measurement of the properties of an object at several wavelength intervals.

Tailings - Term used to describe the material separated as residue in the preparation of various products, grains or treated ores.

D. Some Possibility

X. Not Acceptable

\*Partial Listing-Includes only

those problems covered by this report

### Figure 1 U.S. GEOLOGICAL SURVEY

234553 33332554545 5555444345

Spacecraft (this category applies only

to unmanned satellites.)

### Peter G. White

Mr. White is manager of the Electro-Optical Sensors Department of TRW Systems in Redondo Beach, California. He has directed a number of programs in the remote sensing of water bodies, in order to relate the remotely sensed data to the quality of the water. Most of these programs have involved the use of spectrometers, cameras, and thermal infrared imagers flown in aircraft in conjunction with suitable surface truth measurements obtained from boats.

Mr. White was registered as a Professional Engineer in 1954 by the Association of Professional Engineers of Ontario, Canada. He has published a number of papers on the subject of remote measurement of water quality, and holds patents on two instruments specifically designed to make such measurements.

## REMOTE SENSING OF WATER POLLUTION

By

Peter G. White

TRW Systems Group

Remote sensing, as a tool to aid in the control of water pollution, may prove to be exceptionally valuable in the next few years. It offers a means of making rapid, economical surveys of areas that are relatively inaccessible on the ground. At the same time, it offers the only practical means of mapping pollution patterns that cover large areas.

New sensors and techniques, under development for the past several years, will obtain information about the nature and extent of pollution that previously could only be obtained by water sampling. Some of these sensors operate in daylight only, while others will work either day or night.

Data are presently being obtained from aircraft in conjunction with analyses of water samples taken on the ground to correlate the airborne data with such parameters as sediment count, algae concentration and type, degree of thermal pollution, and oil slick extent and thickness.

Figure 1\* shows the regions of the electromagnetic spectrum of most interest in this type of remote sensing. The right-hand bar indicates the relationship of the ultraviolet, visible, and infrared portions of the spectrum. It should be noted that the radiation which is detected by a passive remote sensor has two different sources - reflected or scattered sunlight, and thermal emission of the water itself. As with the atmosphere, at short wavelengths, light is heavily scattered by the molecules of water, and above 0.7 microns water abosrbs most of the energy which reaches it.

Finally, the two left-hand bars show the regions in which we can perform our passive remote sensing after allowing for all the previous effects. The only radiation from beneath the surface which reaches the sensor is constrained to the visible and near ultraviolet. Material floating at the surface, such as oil slicks, can be detected at longer wavelengths, including the infrared region around 10 microns. As the source energy at 10 microns is emitted, rather than reflected, its absolute value is indicative of the temperature and emissivity of the surface, whether it contains floating matter or not.

Detection of oil slicks, thermal pollution, sewage and algae will be discussed in the following paragraphs.

<sup>\*</sup> Unless otherwise credited, all illustrations and data used in this report were obtained by TRW Systems Group, in large part under the sponsorship of the Spacecraft Oceanography Project.

### OIL SLICKS

As oil floats on the water surface, it offers the possibility of detection in any spectral region in which a suitable atmospheric windiw and adequate detectors exist. Optical contrast between oil and water is high in the ultraviolet and sometimes in the thermal infrared regions of the spectrum, as shown in Figure 2. In Figure 2, the upper two images were obtained by a multispectral linescan sensor which simultaneously images many different spectral regions. The lower image is a photograph of the same scene, in this case the large oil spill in the Santa Barbara Channel in early 1969. It can be seen from Figure 2 that the Panchromatic film/K-2 filter combination (sensitive from 0.48 to 0.65 microns) does a poor job of rendering contrast. On the other hand, the Kodachrome II film used in Figure 3 shows good contrast between the oil and water. This is because this film (used without a filter) has good sensitivity in the near ultraviolet region of the spectrum. Some purple tones are evident in Figure 3, indicating a contribution to the signal in the red as well as blue/ultraviolet. This is in agreement with some spectral reflectance measurements made of the oil slick with a spectrometer that indicate a relatively high oil-to-water contrast in the 0.60 to 0.67 micron region of the spectrum.

Although dramatic in appearance, the reverse Infrared Ektachrome print of Figure 4, shows less contrast between oil and water.

In summary, oil slick photography is best accomplished with ultraviolet sensitive film such as unfiltered Kodachrome II or 103-0. If the altitude is very high or haze conditions are such that atmospheric scattering is a problem, thermal infrared imagery obtained with an infrared linescanner should probably be substituted for photography.

## THERMAL POLLUTION

Thermal anomalies are characteristic of many types of pollution. Biochemical action at sewage outfalls is capable of raising the temperature of the surrounding water many degrees. Discharge of cooling water from electrical generating plants has a similar effect. Oil slicks are frequently at a different temperature than the surrounding water, resulting in the contrast shown in the infrared image of Figure 2.

As water, or any other substance with high emissivity and temperature within the range of 0 to 25 degrees Centigrade emits maximum radiation in the spectral region of 10 microns, a detector which is sensitive in the atmospheric window of 8 to 13.5 microns is well suited to this type of measurement.

A simple radiometer containing a temperature controlled reference black body is capable of remotely measuring temperature within an absolute accuracy of better than ± 0.5°C. Infrared linescanners can give good imagery of thermal gradients. Figure 5 is a picture showing the thermal diffusion from the cooling water discharge of a large electric generating station. This picture was obtain obtained with an infrared linescanner operating between 8 and 13.5 microns in an aircraft at 1000 ft. altitude. In the picture, higher temperatures are indicated by lighter tones. Temperature differences of about 0.2°C are probably evident.

One of the primary advantages of thermal imagery of the type shown, is that it may be obtained either day or night. As the long wavelength infrared radiation being sensed is emitted by the water itself, sunlight is not required. In fact, sunlight contains virtually no energy in this region of the spectrum. Figure 5 was obtained in the daytime, and as a result, the land areas appear lighter (warmer) than the water as they have been heated by the sun. A similar picture taken on a cool night would show the land areas as darker (cooler) than the water. The thermal patterns in the water itself, however, would remain unchanged.

## SEWAGE AND ALGAE

Particulate and dissolved matter released from sewage outfalls is characterized by various changes in the visible region of the spectrum. Some of the more dramatic visual effects are shown in Figure 6, which was taken with Kodachrome II film. Usually, however, the visual appearance is much less pronounced. Work is currently unquerway to attempt to quantitatively relate these color changes to the condition of the water, with the intention that type, concentration, and distribution of the pollutants may be determined remotely. As water transmits light in the visible spectrum, the signal received by the sensor gives information about the condition of subsurface water instead of only the surface condition.

Probably the most useful instrument for this type of measurement is the rapid scanning airborne spectrometer. When pointed at an area on the surface of the water, it gives a continuous scan through the visible spectrum in about one second, measuring spectral radiance with good spectral resolution. When the resulting signal is divided by a similar scan of a known surface of constant reflectance, the spectral reflectance of the water body is obtained.

Current tests are underway to relate these remotely obtained spectral signatures to measurements made at the water surface. Figure 7 is a map of Los Angeles Harbor showing areas in which spectrometer scans were made from 1000 feet altitude (shown as rectangles on the map) and points at which turbidity measurements were made from a boat (shown as dots on the map). Figure 8 is a photographic montage of the area taken from 8000 ft. altitude within 30 minutes of the spectrometer measurements. The positions of the spectrometer scans are marked on the picture. Two distinct types of matter can be seen in the water. Particulate matter from three sewage outfalls is evident near the top of the picture. Algae of a type known as gonyaulax or "red tide" may be seen in the lower half of the harbor and also outside of the breakwall.

Spectral signatures from scans 2, 5, and 11 (positions indicated on Figure 8) are shown in Figure 9. Scans 2 and 5 are from regions of high particulate matter from the sewage outfalls, while scan 11 is from an area with a high algae concentration. Absorptions in the algae signature indicate the presence of pycobilin pigment and chlorophyll- $\alpha$ , both present in the algae gonyaulax. Characteristic features of the other signatures are still under investigation.

In order to utilize the airborne spectrometer measurements to obtain quantitative data about the type and concentration of the water pollution, correlation must be obtained between certain characteristics of the spectral signatures and the data obtained at the water surface itself. In the tests currently underway,

water samples are taken from one foot beneath the surface and at the surface. Portions of the samples are fixed with formaldehyde and counts made under a microscope of different organisms and particles. As another measure of water turbidity, a Secchi disk is lowered into the water until the depth is reached at which it is no longer visible to observers in the boat.

Certain parameters have been selected to characterize the spectrometer curves. Figures 10, 11, and 12 show these parameters plotted against the Secchi depth, which is a measure of water turbidity. The parameters have been defined as follows:

$$K_{1} = \frac{R_{4000\text{Å}} - R_{5250\text{Å}}}{R_{5700\text{Å}}}$$

$$K_{2} = 1 - \frac{R_{5250\text{Å}}}{R_{5700\text{Å}}}$$

$$K_{3} = \frac{R_{7000\text{Å}} - R_{6700\text{Å}}}{R_{5700\text{Å}}}$$

In all cases  $R_{\lambda}$  is the reflectance of the water at wavelength  $\lambda$ .

K<sub>1</sub> (Figure 10) was selected to indicate the amount and direction of the slope of the reflectance curves in the blue-green region of the spectrum. High concentrations of sewage result in a rising reflectance with increasing wavelength in this spectral region whereas high concentrations of algae produce a decreasing reflectance. The parameter can be seen to relate to concentrations of sewage, but not to concentrations of algae, at least in high concentrations.

K<sub>2</sub> (Figure 11) is a measure of the drop in reflectance due to absorptions around 5250Å. It is in this region that pycobilin pigment of the type from the algae gonyaulax is found. In this case a correlation is apparent with high concentrations of algae as well as a different correlation with sewage.

 $K_3$  measures the chlorophyll- $\alpha$  absorption at 6700Å and again shows different correlations with sewage and algae.

It is expected that as better, faster, methods of analyzing many water samples become available, better correlations with spectrometer data will be obtained. However, the present data is most promising in that it indicates a capability to differentiate between types of pollution and at the same time give a measure of the concentration of each type.

A factor which can contribute to the inaccuracy of this type of measurement is the speed of the spectrometer in taking each spectral scan. As the aircraft is moving at a velocity of some 150 ft/sec., within a one-second scan time, the area on the surface being viewed by the spectrometer has moved 150 ft. To illustrate this effect, Figure 13 is a photographic montage of the northern portion of the test area in Los Angeles Harbor described earlier. The distance

that the aircraft has moved during each scan is marked on the picture. In some areas, these lines cross boundaries in the water. This will result in a spectrum composed at short wavelengths from one type of water and longer wavelengths from another. To overcome this difficulty, faster scanning spectrometers are under development.

## **NEW DEVELOPMENTS**

Certain other instruments and techniques are in various stages of development. One of the most promising new instruments is the imaging spectrophotometer. This device is capable of sensing radiation from many small areas on the surface simultaneously and obtaining a spectral signature from each. After properly processing the data, maps of pollution concentration may be prepared. The imaging spectrophotometer and associated data processing techniques are currently being developed.

Certain other techniques are in early stages of investigation. Image intensifiers and low light level television cameras which are sensitive to extremely low levels of illumination may be used to detect phosphorescence of decaying material at night. Some investigations currently underway are attempting to utilize the very narrow regions of the solar spectrum in which no light reaches us from the sun (Fraunhofer lines) to measure fluorescence during daylight. These techniques offer interesting possibilities for the future.

In summary, remote sensing of water pollution is rapidly progressing to the point where quantitative measurements may be obtained from aircraft. The benefits which will be derived from the ability to rapidly monitor and evaluate the condition of our environment will be of major value.

### GLOSSARY

Algae - Microscopic living organisms found in oceans and lakes

Atmospheric Window - Portion of the electromagnetic spectrum in which the atmosphere does not attenuate radiation.

Emissivity - The fraction of radiation emitted by a body, compared to a perfect radiator of the same temperature.

Oil Slick - The film formed on a water surface by oil.

Reference Black Body - A perfect thermal radiator.

<u>Sediment Count</u> - The number of particles per unit volume of water sample.

<u>Thermal Anomaly</u> - A localized region of different temperature from the surrounding water.

Thermal Emission - Radiation given off by a body due to its temperature.

Thermal Pollution - Water of a higher temperature which is adde to a body of natural water, usually as a by-product of an industrial process.

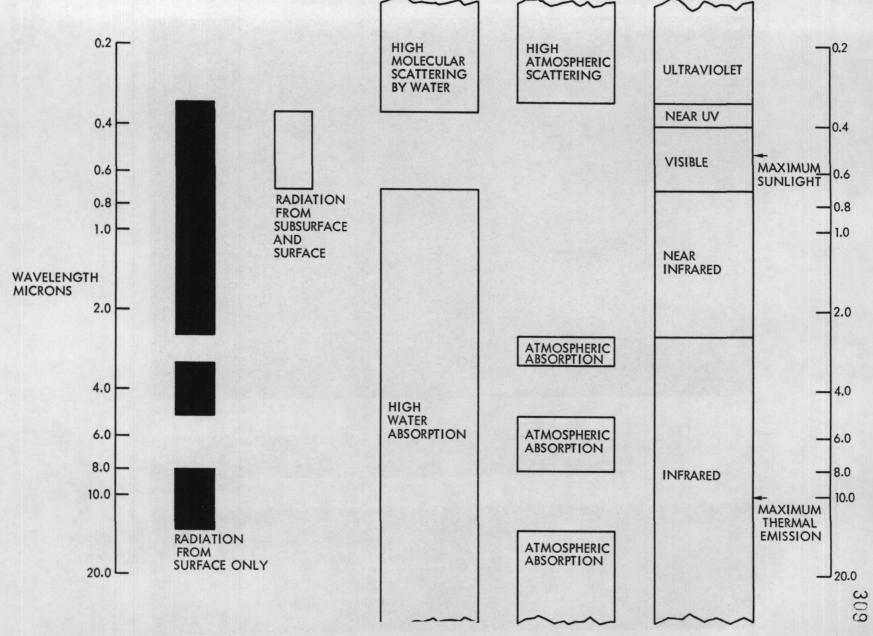
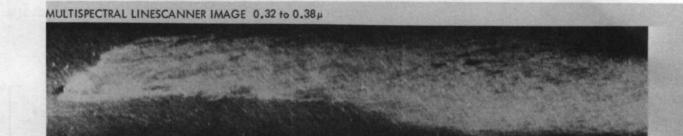


Figure 1 Electromagnetic Spectrum Relative to Water Pollution.



MULTISPECTRAL LINESCANNER IMAGE 8.0 to 13.5 µ

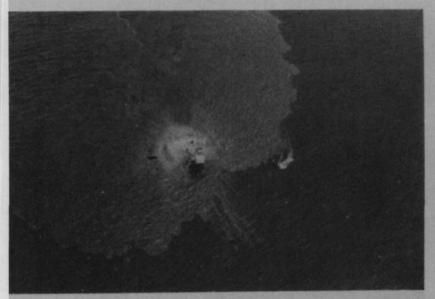


PANCHROMATIC PHOTOGRAPH K-2



Figure 2 Santa Barbara Oil Slick.

PHOTOS COURTESY WILLOW RUN LABORATORIES, U of M



HEAVY OIL SLICK

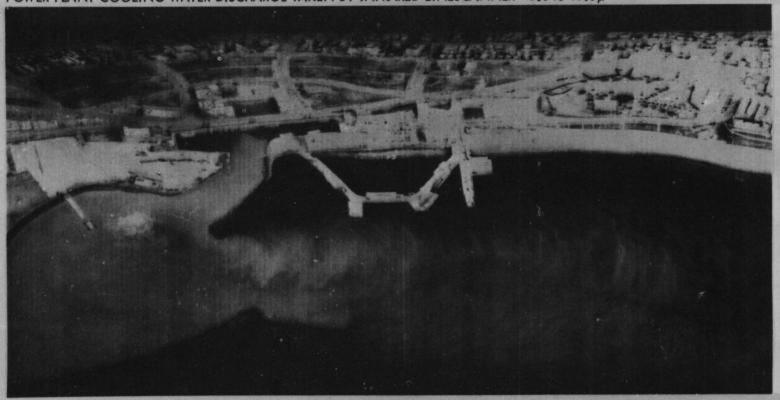


LIGHT OIL SLICK



Figure 4 Reverse Infrared Ektachrome Print of Oil Spill. PHOTO COURTESY U.S.G.S.

POWER PLANT COOLING WATER DISCHARGE TAKEN BY INFRARED LINESCANNER 8.0 to 13.5  $\mu$ 



TRW PHOTO

Figure 5 Example of Thermal Infrared Imagery.

## CONVENTIONAL COLOR PHOTOGRAPHY

INNER CHANNEL - LOS ANGELES HARBOR 8000 FT



SEWAGE OUTFALLS - LOS ANGELES HARBOR 3000 FT



Figure 6 Conventional Color Photography.

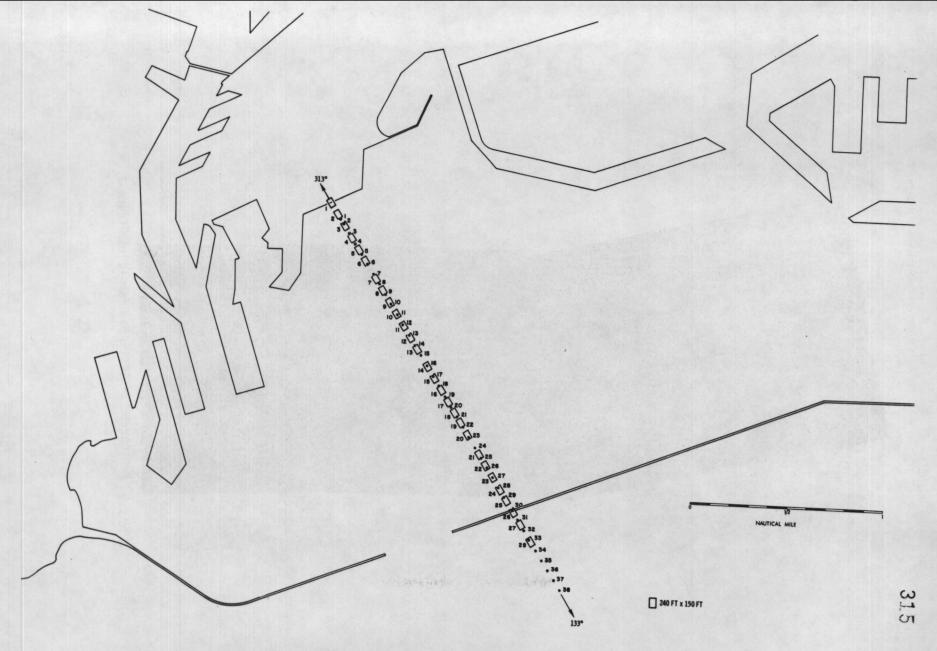


Figure 7 Map Showing Locations of Spectrometer Scans and Surface Test Stations.

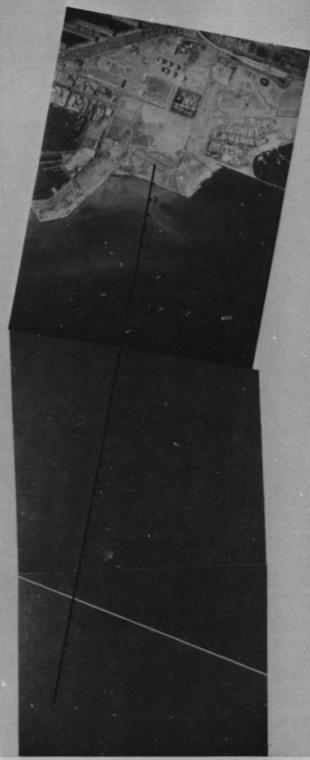


Figure 8 Photograph of Test Area Mapped in Figure 7.

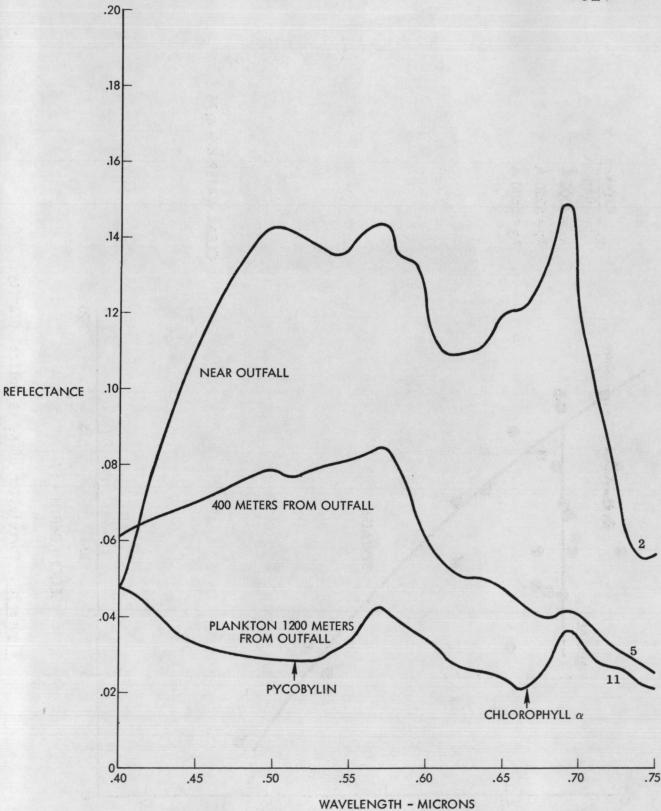


Figure 9 Reflectance Curves From Three Locations.

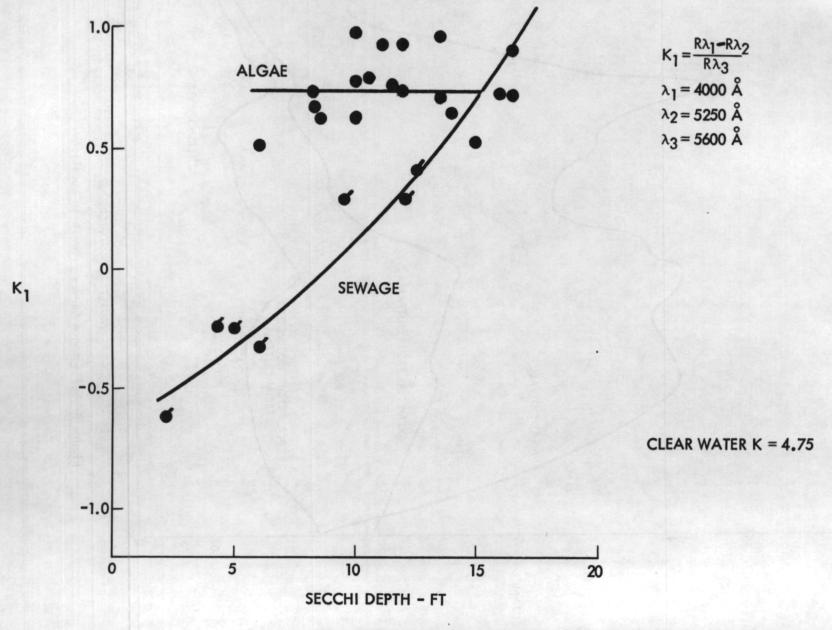


Figure 10 Correlation of K<sub>1</sub> vs Optical Clarity.

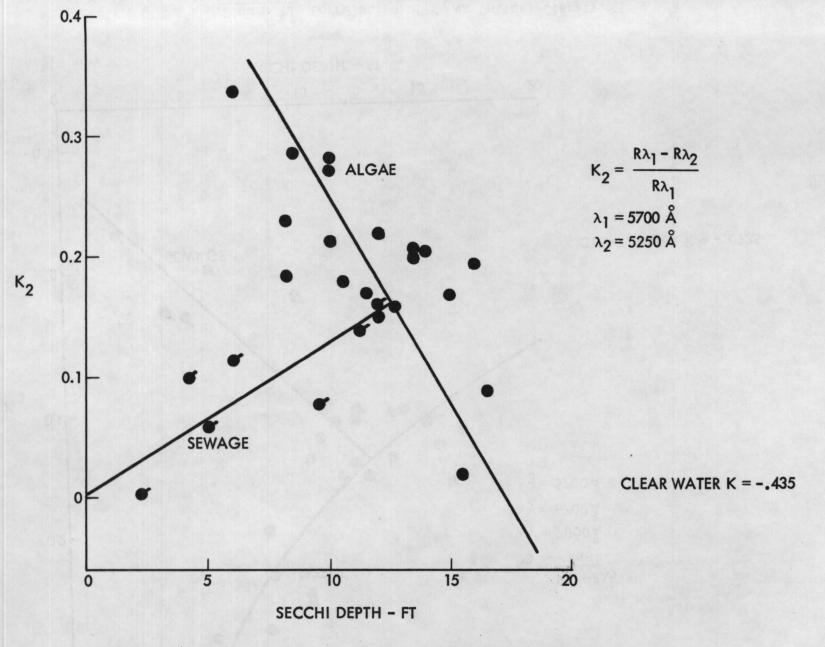


Figure 11 Correlation of K2 vs Optical Clarity.

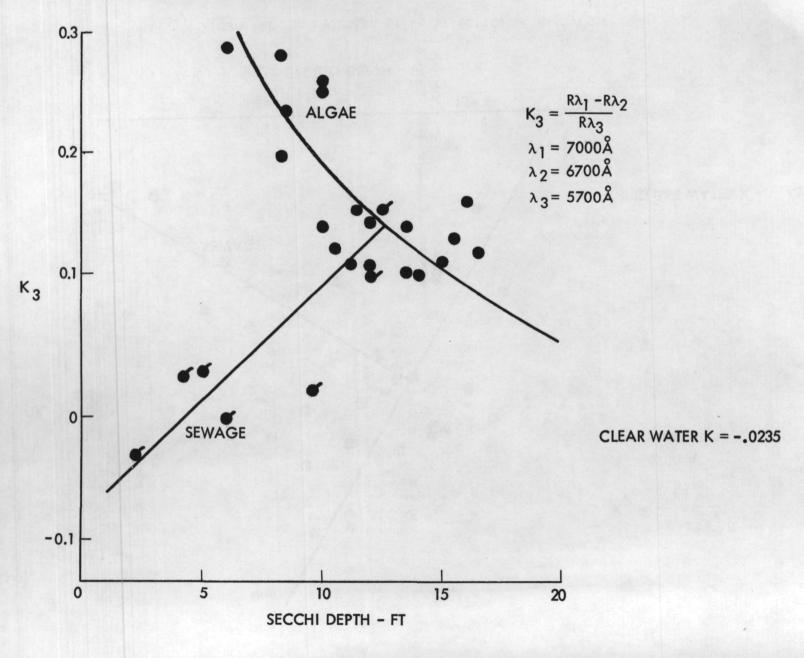
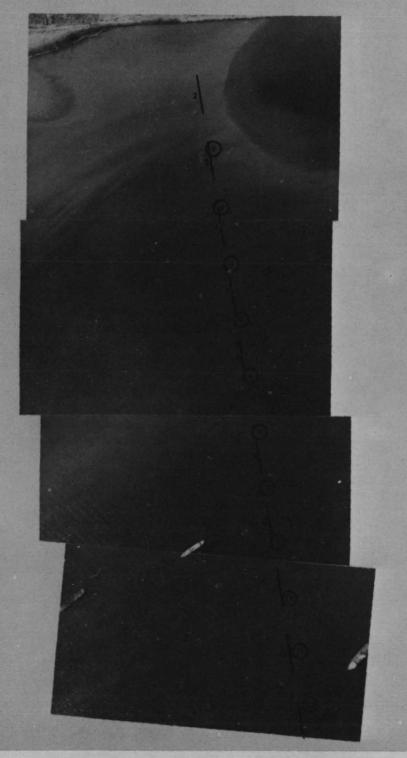


Figure 12 Correlation of  $K_3$  vs Optical Clarity.



ure 13 Location of Spectral Scans on Photograph of Northern Portion of Los Angeles Harbor.

#### **BIOGRAPHY**

Jerry P. Eaton has done geophysical research with the U.S. Geological Survey since being awarded the Ph.D. in Geophysics from the University of California, Berkeley, in 1953. Until 1961, he was associated with the Geological Survey's Hawaiian Volcano Observatory, first as Geophysicist and later as Scientist-in-Charge. At the Observatory, he organized and conducted research in seismology and general geophysics on Hawaiian volcanoes and correlated the results of those studies with geophysical and geochemical investigations of the volcanoes. In 1961, he joined the Geological Survey Crustal Studies Branch, where he developed an earthquake seismology program in the Rocky Mountain-Great Plains region, and participated in the analysis of data from explosion-seismology crustal-refraction studies of crustal and uppermantle structure in the western United States. He joined the staff of the National Center for Earthquake Research (NCER) at its formation in 1965, and has played a major role in shaping of facets of the NCER Program. Dr. Eaton is Past President (1966-67) and Member of the Board of Directors (1961-1970) of the Seismological Society of America, and is currently Acting Chief of the Office of Earthquake Research and Crustal Studies, U.S. Geological Survey.

Wayne H. Jackson received a degree in Geophysical Engineering from the Colorado School of Mines in 1951. Following a year of work as Physicist with the U.S. Navy Electronic Laboratory, he joined the U.S. Geological Survey, where he served as Geophysicist, first on gravity, seismic, and magnetic projects in the Colorado Plateau area, and later in Cuba. From 1956 to 1965, Mr. Jackson worked on laboratory and field studies using seismic and gravity methods in the western United States. He has been in charge of all seismic operations of the National Center for Earthquake Research Program (NCER) since it was established in 1965. Mr. Jackson is author or co-author of more than 40 papers and reports on geophysical subject.

### PREDICTION AND CONTROL

Wayne H. Jackson and Jerry P. Eaton

#### INTRODUCTION

The Satellite Telemetry Earthquake Monitoring Program was started in FY 1968 to evaluate the applicability of satellite relay telemetry in the collection of seismic data from a large number of dense seismograph clusters laid out along the major fault systems of western North America. Prototype clusters utilizing phone-line telemetry were then being installed by the National Center for Earthquake Research (NCER) in 3 regions along the San Andreas fault in central California; and the experience of installing and operating the clusters and in reducing and analyzing the seismic data from them was to provide the raw materials for evaluation in the satellite relay telemetry project.

Initially, it was assumed that the satellite relay would provide a large number of continuous voice-grade communications channels that would link clusters to a central data recording and processing facility. The principal advantages of the satellite relay system over commercial telephone or microwave systems were: (1) it could be made less prone to massive failure during a major earthquake; (2) it could be extended readily into undeveloped regions; and (3) it could provide flexible, uniform communications over large sections of major global tectonic zones.

Fundamental characteristics of a communications system to cope with the large volume of raw data collected by a short-period seismograph network are discussed.

Aside from the relay system itself, which was outside the scope of this study, the most urgent need was for the development of a flexible, reliable, inexpensive means of gathering data from individual sensors in a cluster into a central point from which the satellite relay would be reached. Accordingly, during FY 1968, emphasis was placed on the investigation of available or promising systems for collecting seismic-cluster data at a central point in a format which would be convenient for long-range telemetry via relay satellite or phone line. To stimulate development of a low-power radio data link, a development contract was issued (to DEVELCO, Mountain View) for the construction of a 0.1-watt FM VHF transmitter.

Near the end of FY 1968, we learned that the first satellites (ERTS) that might become available for testing a seismic-data-relay system would provide only for periodic relay of a very small amount of data. These restrictions forced a fundamental reevaluation of the experiment that was being formulated. Our best information on the cost and complexity of the electronic equipment required to transmit data to the satellite indicated that a number of such platforms should be kept to a minimum. Thus, a high priority was maintained on the development of a reliable inexpensive communications link to transmit data from a number of sensors to a central platform.

The project was extended into FY 1969, with some additional support, to study possible applications of the ERTS system to earthquake prediction and related geophysical problems. Work was continued on several topics:

- 1. 7 VHF radio data-transmission links were purchased. They were tested and evaluated under a variety of field conditions in California, Nevada, Colorado, and Hawaii and were found to operate reliably over line-of-sight paths more than 50 km long with only 0.1-watt of radiated power. A summary of the work on the development and testing of the low-power radio links is presented.
- 2. Various sources of power for the low-power seismic units and radio data links were investigated. The simplest inexpensive, large capacity power source discovered is the air cell, a primary cell utilizing oxygen from the air as a depolarizing agent. These cells were tested extensively under field conditions of extreme heat and cold. The principal results of investigations of power supplies are summarized.
- 3. A number of slowly varying non-seismic geophysical parameters that might contribute to a better understanding of earthquakes were studied from the viewpoint of the instrumentation required to measure them and the volume of data required to specify them. Tilt, strain, and fault-creep measurements, which are important because they characterize kinematic changes in the earthquake-producing system, were the subjects of chief concern.

As a result of the studies carried out in FY 1968 and FY 1969, a shift in emphasis in the satellite-relay telemetry of seismic data experiment was proposed. Pending the perfection of methods and equipment for the in-the-field automatic processing of seismic network data, nothing short of a continuously-available synchronous satellite will suffice for telemetry of raw data from even a moderate size microearthquake network. On the other hand, the polar-orbit ERTS system will fulfill the data collection requirements of global volcano surveillance networks based on condensed-data seismic and tiltmeter systems in-stalled on the individual volcanoes under study.

The problems and requirements of a worldwide volcano surveillance system are briefly discussed, along with descriptions of the new instrumentation that will be needed for such a network and of preliminary field studies that will be required to test these instruments. Sixteen preliminary platform locations in Hawaii, Continental United States, and Central America are suggested for initial tests.

#### SEISMOGRAPH DATA TRANSMISSION

# A. Basic Methods

Real-time transmission of seismic data from a number of remote stations to a data-collection center is generally accomplished by radio, commercial telephone line, or a combination of these two. The usable band of frequencies available with the transmission link is in the range of 300 to 3000 Hz, a bandwidth of about 2700 Hz. The desired range of short-period seismic signals is generally from 0.1 to 25 or 30 Hz, which lies below the band of frequencies that can be handled directly by the communciations link. Remote seismograph stations are generally arranged in "clusters" so even if direct transmission of seismic data were possible over radio and telephone links, a separate link for each station would be impracticable.

There are two basic methods of transmitting more than one data signal over a communications link: frequency-division multiplexing and time-division multiplexing. With frequency-division multiplexing, all channels occupy the entire frequency band, but each channel is connected to the transmission medium for a short time. Each has advantages and disadvantages.

# B. Frequency-Division Multiplexing

Frequency-division multiplexing (FDM) is the oldest and most widely used method. FDM equipment has been made extremely reliable throughout its many years of use. The telephone company's carrier equipment, a type of FDM, has been in use for many tens of years. In using FDM for transmitting seismograph data, the signal from a seismometer (figure 1) is amplified and used to frequency-modulate a subcarrier frequency which is compatible with the transmission link. The frequency is generated by an oscillator, commonly called a voltage controlled oscillator (VCO) because the output frequency is controlled by the amplitude of the input signal. The electronic circuit of the VCO is arranged so that an upward ground motion (positive output voltage from a vertical seismometer) results in an increased VCO frequency, or a positive deviation from center frequency; while a downward ground motion results in a decreased VCO frequency or a negative deviation. With a zero input signal, the VCO oscillates at its center frequency.

An important consideration in the design of a seismograph data transmission system is in the bandwidth of the data channel. Since all data channels are expected to carry similar signals (0.1 to 25 Hz), a constant-bandwidth system is indicated, or each channel will occupy the same bandwidth. It is common practice to design a VCO so that the peak deviation from center frequency is 5 times the data frequency, or its deviation ratio is 5. Lower deviation radios are used to reduce data channel bandwidth but at the expense of data accuracy, harmonic distortion and signal-to-noise improvement. Another important consideration is in channel spacing. Guardbands, or the unused spacing between channels should be as wide as possible to prevent "crosstalk" between adjacent channels.

The seismic data transmission system now in use at NCER utilizes a total of 7 data charmels of 250 Hz each, separated by guardbands of 90 Hz. An 8th channel, of center frequency 3060 Hz, has been added when the telephone lines pass frequencies as high as 3185 Hz.

# C. Time-Division Multiplexing

Time-division multiplexing (TDM) is becoming more prevalent as the costs of digital equipment is being reduced, as computer data processing and analysis is required, and as high speed and greater precision is needed. Various types of pulse modulation are in use, but pulse-code modulation (PCM) appears to be the most useful in the transmission of large amounts of earthquake data. With PCM, each data channel is sampled in a regular sequence, and the signals are converted into a series of digits or characters. The samples from the various channels are interleaved in time to form a single-pulse train.

The primary advantage of PCM is its ability to be adapted for direct use with digital data-processing equipment and computers. It has an unlimited dynamic range and exceptionally good data accuracy. The Large Aperture Seismic Array (LASA) in Montana uses digital transmission even over the relatively short distances involved. The analog signal from each station of a subcluster is transmitted by buried cable to the Data Center at Billings. The LASA raw data has a dynamic range of over 72 db. Good FDM, or analog, data transmission may expect no greater than 60 db dynamic range.

An important disadvantage of PCM transmission is its bandwidth extravagance. If frequencies below 3000 cycles per second are to be transmitted by PCM, a theoretical minimum of 6000 samples per second are needed. Assuming a 7-bit sample (42 db dynamic range) is required, a total of 42,000 bits per second will be transmitted. To transmit this bit rate, a bandwidth of 21 kilohertz is necessary.

# D. Comparing FDM and TDM

There is no simple way to compare analog, or FM transmission, with digital, or PCM transmission, because of the large variation in data to be transmitted. These methods, however, can be contrasted in general terms.

Costs of terminal equipment are important. Little, if any of the circuitry is common to the separate FM channels. Frequency-division multiplexing costs are essentially proportional to the number of channels transmitted over one transmission link. With time-division multiplexing, much of the circuitry is common so this type of transmission is more economical for large numbers of channels. A few channels of high frequency data could absorb the entire capacity of a PCM system. PCM transmission is very well suited for handling large numbers of low-speed data channels.

One of the most important points of comparison is the dynamic range of the system. Over an optimum transmission path a maximum of 60 db may be expected from FM equipment. If a better dynamic range is required, a PCM system will be necessary. PCM transmissions are superior to FM transmissions over noisy communications links.

An extremely important advantage of the FM over the PCM system is the manner of combining, or multiplexing, data channels for transmission over a communications link. The multiplexing of FM channels is simply a summation, or mixing process, that can be accomplished at any point along the transmission path. This is very useful in transmitting earthquake data by radio to a collecting point. Each radio relay station can also be a seismograph station and/or a subcollecting point. Additional data channels can be inserted into the transmitted "stream" of data with little or no additional equipment. The addition of channels in a TDM system cannot be done as easily because of the difficulties in synchronizing the additional channel data bits with the available time gaps in the data "stream." There are many ways of solving this problem, but usually at the expense of flexibility, additional equipment, and channel capacity. Multiplexing in a TDM system is best accomplished at a central point, such as is done at the LASA subarray vaults.

The proper system to be used in the collection of earthquake data will depend upon the cost, noise characteristics, available bandwidth, etc., of the transmission path. It is most likely that, for remote sensing, the data will be collected locally for processing using a frequency division system, then the processed data would be retransmitted via satellite by a time-division system. This would maintain flexibility and yet require a relatively uncomplicated electronic system.

#### RADIO TRANSMISSION LINKS

## A. Practical Considerations

For the radio transmission link to be useful in collecting and transmitting earthquake data, it is essential that the remote equipment, including power supplies, be portable; reliable; require as little power as possible; be able to run for 12 to 18 months before changing batteries; and provide continuous 24-hr per day duty over wide ranges of temperature and humidity. Under most circumstances, it should be possible to arrange instrument locations so that line-of-sight transmission will be possible. Although eventually the collected data will be processed at one point for retransmission to an orbiting or stationary satellite, for purposes of evaluating data, it would be useful if each radio link have similar bandpass characteristics as telephone voice-grade lines. This would make it possible to have data collected either by a radio link, a telephone line, or both, for transmission to a data collection center. Voice-grade telephone lines pass, in general, frequencies in the range 300 to 3000 Hz.

# B. Transmitter Modulation and Frequency

For continuous line-of-sight transmission, frequency modulation in the range above 100 MHz is less affected by atmospheric noise than amplitude-modulated radio at lower frequencies. Therefore, FM is preferable to AM. Of the frequencies in the VHF (30 to 300 MHz), UHF (300 to 3000 MHz), and the microwave frequencies (above 3000 MHz), the VHF frequencies were preferred because of the availability of suitable equipment. UHF and microwave radio equipment were available but at considerably higher cost per radio link. Although radio frequency assignments in this band are becoming extremely scarce, 9 splinter channel frequencies (167 to 170 MHz) became available on a non-interference basis. Even though the radio propagation path is not precisely an optical straight-line path at these frequencies, the same frequencies can be used over and over again in many sites provided they are not in optical sight of one another

## C. Transmitter Power

An extremely important consideration in the design of the telemetry system is the power required by the radio transmitter to provide reliable transmission over the maximum distance to be expected. Power requirements for the entire remote system must be kept to a minimum; over half of the weight is expected to be that of the batteries; and a large part of the maintenance costs are expected to be in replacing batteries over regular periods.

There is, however, a practical limitation on the minimum radio-frequency power supplied to the antenna. In the RF power range (5 watts and less) required for this work, the efficiency of power output to power input increases with increased RF output power. This is due in part to the constant power drain of the early stages of the transmitter that do not contribute to the output power.

Assuming a transmitter output power of 100 milliwatts is the minimum practical power, its performance may be calculated using the range equation:

Let Prad = radiated power, watts

Prec = received power, watts

r = distance, transmitter to receiver, meters

 $G_T$  = transmitter antenna gain

A<sub>R</sub> = receiver antenna capture area

G<sub>R</sub> = receiver antenna gain

The power at the receiver is given by

$$P_{rec} = \frac{P_{rad}G_{T}A_{R}}{4\pi r^{2}}$$

The signal-to-noise ratio at the receiver is given by

 $S/N = \frac{P_{rec}}{P_{SEN}}$  where  $P_{SEN}$  is receiver threshold sensitivity

For example:

$$P_{rad} = {}^{100} \text{ mw}$$

$$r = 10 \text{ km}$$

$$G_{T} = 6 (7.8 \text{ db})$$

$$A_{r} = {}^{2G_{r}} = {}^{(c/f)^{2}G_{r}} = {}^{(\frac{3 \times 10^{8}}{4\pi})} \times 6$$

$$P_{SEN} = 0.5 \times 10^{-16}$$

$$= 1.49 \text{ m}^{2}$$

Then

$$\frac{P_{\text{rec}}}{(4\pi)(10^4)^2} = 0.71 \times 10^{-9} \text{ w}$$

$$S/N = \frac{0.71 \times 10^{-9}}{0.5 \times 10^{-16}} = 1.42 \times 10^7 = +71.1 \text{ db}$$

For 100 km, S/N = 71.1-20 = 51.1 db

For 10 km, S/N = 71.1 db

The calculations suggest that for line-of-sight transmission, under ideal circumstances, a 100-milliwatt transmitter could be used to send data over distances as great as 100 km.

A DEVELCO, Model 3401, VHF 100-milliwatt transmitter was delivered in June 1968. Preliminary tests indicated that the performance of the radio link did not deviate greatly from the calculated performance for line-of-sight travel paths, but the signal-to-noise ratios of 6 db and less were measured for grazing paths through industrial areas, high-power lines, etc.

In July 1968, a seismograph station was installed on Poverty Ridge in the Diablo Range about 45 km southeast of Menlo Park using the prototype radio transmission link. Through the 1-yr. period, July 1968 to July 1969, seismograph data of excellent quality was recorded.

Since this time radio links have been utilized by a number of projects throughout the country to transmit seismic data from remote locations to telephone terminals. Presently a total of 24 VHF radio links are in use at locations in California, Nevada, Colorado, and Hawaii.

The advancement in the state-of-the-art has made a second generation of radios possible. Motorola Communications has delivered radio transmitters and receivers requiring considerably lower input power than the first generation.

### POWER SUPPLIES

The utilization of an efficient system to power the remote sensors and associated equipment is extremely critical. A large part of the weight of the remote station, and a large part of the attention necessary for operation of the station, can be attributed to the power supply. The seismograph station, because it is continuously operated, requires the highest power drain of all the fault-zone instruments. Studies of available power supplies have therefore been based upon the requirements of a remote station consisting of a seismic pre-amplifier-subcarrier oscillator and a 100-milliwatt VHF transmitter.

When properly installed, a seismograph station has a yearly survival probability of about 95%. Proper installation includes avoiding areas susceptible to flooding, care taken to minimize pilferage, etc. Failure has been due, in large part, to lightning strikes in the vicinity of a station or telephone line. Lightning arrestors utilized in interfacing the equipment to telephone lines and to radio transmitters may have reduced the failure rate, but we have not been able to devise a reliable method to measure potentially damaging voltage transients in a given area. When possible, radio transmitters are not placed on peaks, ridges, or other locations which may receive lightning strikes.

Assuming a power supply will be required for a minimum of one year, various types of sources were investigated. Power drain for the remote seismograph station (table 1) indicates that about 7000 watt-hours will be required to operate the VCO preamplifier and the VHF transmitter for one year, and 12,600 watt-hours per year for a relay station.

Various types of power sources were studied (table 2) to determine the cost, weight, life, and other factors having a bearing on suitability to power remote stations. Lead-acid batteries are immediately rejected because of their short shelf-life. The most promising battery tested to date for powering remote stations is made up of Union Carbide "air cells," primary, or non-rechargeable, cells. Each cell is made up of zinc-carbon electrodes with potassium hydroxide electrolite. These batteries have been in use for many years in powering railway signals and in maritime lighting. Carnegie Institute, Washington, D. C., used "air cells" to power seismograph stations in South America several years The high-power density, low-cost per watt-hour, and long shelf-life features are particularly important in considering power supplies for remote locations. The batteries are rated at operating temperatures down to 0° F. One possible disadvantage offered by these batteries is in the necessity of supplying air as required in the depolarizing process. In cold regions (temperature below 0° F), all equipment will have to be buried beneath the ground surface; a "snorkel" will be required to supply air.

Isotope generators may be useful in remote areas to power a permanent station, but the extremely high purchase cost (about \$9000 at this time) must be weighed against transportation and maintenance costs of less expensive power supplies.

Although solar cell charging systems are relatively expensive, the power yield per pound is extremely high. Use of this type of power supply is especially advantageous for stations located in areas serviced by small aircraft or in locations where equipment and batteries have to be packed in, or for other reasons where weight may be a problem. The primary disadvantage of this power supply is the cost, which for an average station may be on the order of \$1000.

In areas where propane or butane gas is available, thermoelectric generators are probably the most economical type of power supply for unattended stations requiring from 10 to 20 watts. On the other hand, the power yield per pound is the lowest of all the supplies described, suggesting that if fuel is to be transported by air or some other high-cost route, perhaps another type of power would be preferable. Thermoelectric generators have been used in extremely cold climates by utilizing the generated heat to keep the fuel from freezing and in maintaining the electronic components within the operating range.

# A. Background

It is becoming increasingly apparent that a comprehensive attempt to understand the mechanics of earthquake generation and to predict the time and place they will occur must be based on massive collection of pertinent data over large areas and the real-time analysis of that data at a central facility. Our current studies of the San Andreas fault system in central California (truly a small part of the region of concern) have already turned up some formidable telemetry problems: lack of adequate commercial facilities in large areas that require dense instrumental coverage, long waits for installation and/or improvement of phone systems, expectation that commercial communications links will fail during large earthquakes when continuity of data gathering is essential, etc. When one considers extension of such networks outside well-developed populated areas, it appears that a flexible, easily accessible, large capacity, long-range data transmission system is required (perhaps one based on a synchronous satellite). At NCER we have pondered these questions at length, and it seems clear that networks like the one we are operating in California generate such a large flow of data that a continuous multi-channel data transmission system is needed.

We are now beginning to experiment with automatic processing of seismic data from the California net. It may be possible to reduce the data flow from such a regional network by four or five orders of magnitude by "local" automatic event detection and timing and, thus, correspondingly to reduce the load on a data link to the central collection and analysis facility. In terms of present networks and processing capabilities, however, it is difficult to see how the proposed ERTS data collection system can be used. If the experiment in automatic processing leads to a workable system, the picture would change of course. There are also slowly changing geophysical parameters—earth strains (including tilting of the surface magnetic field, etc.—that could be sampled at intervals and relayed to a central processing facility via an ERTS-type system. Our understanding of the relationship of such parameters to earthquakes is still too poor to justify a large "prediction" system based on them alone, however.

In short, we cannot yet identify a simple set of parameters that can be sampled once a day, for example, that will permit us to judge whether a damaging earthquake is about to occur in the vicinity of the data collection point. The heart of the data collection and analysis problem lies in the earthquake-generating process itself. The region from which energy is drained to produce a large earthquake measures tens or hundreds of kilometers in length. Within this region, smaller earthquakes are frequent; and whether a given earthquakeproducing "tear" will be arrested (and produce a small earthquake) or extend to dimensions that will result in a truly catastrophic one depends on the physical properties and initial state of the "system" that comprises a very large region. It appears that a more detailed understanding of the structure, history, and ambient state of such a region is needed than we believe can be acquired by periodic sampling of a few poorly understood geophysical parameters. At this time, it appears that the time of occurence, magnitude, and precise location of all significant earthquakes in such a region is the indispensable core of the data that are required. And as indicated above, until massive automatic digestion of seismic data from regional networks, yielding extremely condensed results such as arrival times and amplitudes (or even times, hypocenters, and magnitudes), is possible, the volume of seismic data that must be transmitted is enormous.

The hazard to man posed by volcanic eruptions around the world, however, is comparable to that posed by earthquakes, and the scientific tools used to study volcanoes include all of these pertinent to the study of earthquakes. Indeed, large numbers of small earthquakes occurring in or beneath a volcanic structure, together with measurable tilting of the ground around the volcano have turned out to be among the most easily detected and most readily interpretable manifestations of volcanic activity, except for the eruptive outbreaks themselves.

The habit of most volcanoes, especially the most dangerous ones, to lie dormant for decades or even hundreds of years between eruptions makes them extremely difficult to study individually. It is virtually impossible to maintain an effective up-to-date surveillance system on such a volcano during the long period of its quiescence. And by the time it reawakens, such systems as may have been established after a previous eruption almost invariably have degenerated till they are useless, if not abandoned altogether. It appears that a program of modest observations at a very large number of active volcanoes, organized and conducted by a single dedicated organization, would have an excellent chance of developing effective methods for predicting dangerous eruptions. Volcanoes also seem to be more amenable to simple schemes for condensing pertinent observations into concise numerical form than major earthquake-producing faults. The volcano itself is the focal point of activity: one knows in advance where to look for the symptoms related to changes in the internal condition of the volcano. Thus, a few multi-level earthquake-event counters placed thoughtfully around the volcano and queried daily may be expected to provide a useful and interpretable summary of earthquake activity in or near the volcano. Several tiltmeters strategically located around the eruptive center, also queried once or several times a day, should provide the most important strain data relative to the final buildup to an eruption.

For such a program of volcano observation to succeed, it will be necessary to collect data automatically recorded at many volcanoes and to transmit it to the center carrying out the volcano studies program. The volume and sampling interval of the required data seem to be compatible with the ERTS system; and the worldwide scope of the ERTS data collection system suggests that the most dangerous and interesting volcanoes of the entire world could be brought under continuous surveillance by its use.

# B. Equipment

A total of about 50 platforms should be established initially in seven regions. It may be advantageous to collect data for each region at a central collection point; however, this would not appreciably affect the total data collected. Each platform will consist of 4 tiltmeters and 2 seismic-event counters.

Tiltmeters-Tiltmeters will detect changes of tilt in the earth with a resolution of 0.1 microradian. The sensors will be emplanted downhole to minimize surface and temperature effects and to insure a stable installation. At the present time tiltmeter electronics are being supplied by Develco, Inc., Mountain View, California, and the sensors are being constructed at the NCER machine shop. The present meter is not believed to be suited for the ERTS-proposed system, and although several different types are now under development, a suitable meter is not to be expected earlier than in one to two years. The present system will operate for a period of one year without a change of batteries; this will be a minimum requirement for all the components of the proposed system.

Seismic-Event Counters--This equipment is available commercially (Geotech Division, Teledyne Industries, Garland, Texas), but its high power consumption makes it unsuitable for the ERTS system. It is relatively simple to develop a low-power unit with the required specifications. Each event counter will have 3 outputs corresponding to input level separations of from 30 to 40 db, providing means of determining numbers of large intermediate, and small earthquakes.

Interfacing Equipment--Equipment will have to be developed to collect and store data from each sensor of a platform awaiting the satellite command for transmission.

# C. Data Rates

Twelve-bit words are preferred for both seismic and tilt data although 8-bit words could be tolerated. One reading per day is required for each seismic-event counter, and three readings per day are preferred for each tilt-meter. It is assumed the data could be collected and stored by the interfacing equipment for transmission to the satellite upon interrogation. Assuming one interrogation per day, the following bit rates would be required per day:

a. Seismic-event counters:

72 bits

b. Tiltmeters:

144 bits

216 bits/day/platform

# D. Platform locations

Although we see an eventual need for at least 50 platforms throughout the circum-Pacific belt to monitor volcanic activity, we feel that the start of the program should be limited to a few test areas. This would allow us to evaluate the entire data collecting system, to study data obtained under an operational mode, and to gain experience in all phases of a volcano-surveillance network from site location and installation through data analysis.

We recommend that the program be started with a total of 16 platforms in the following test areas: Hawaii, the Cascade Range of Oregon and Washington, and in Central America.

Hawaii--Data recorded continuously at the Hawaii Volcano Observatory will provide a check on accuracy and completeness of platform data. Personnel at HVO will evaluate field installation and make recommendations for modifications. HVO will be the central data collection point. Volcanoes to be instrumented are: Kilauea, Manuna Loa, Hualalai, Two additional platforms will be moved from place to place in the Hawaiian Islands.

### 1. Kilauea

a. Location: Southwest part of Island of Hawaii

Lat. N19° 25.5'

Long. W. 155° 17.5

b. Height: 1222 meters above sea level

c. Type: Shield volcano

d. History: The historic activity of Kilauea has been largely concentrated within its caldera. Explosive activity has played only a very minor part in the building of Kilauea. Approximately 3.4 billion cubic meters of lava has been extruded by this volcano during historic time.

## 2. Mauna Loa

a. Location: Southwestern part of the island of Hawaii

Lat. N19° 28.5'

Long. W155° 36.5'

b. Height: 4170 meters above sea level

c. Type: Shield volcano

d. History: Eruptions of Mauna Loa consist almost exclusively of the relatively quiet extrusion of fluid basaltic magma. From its first historic eruption, in 1832, to the present, Mauna Loa has averaged one eruption every 3.6 years and has been active approximately 6 percent of the time.

#### 3. Hualalai

a. Location: Western part of island of Hawaii

Lat. N19° 41.5' Long. W155° 52'

b. Height: 2515 meters above sea level

c. Type: Shield volcano

d. History: The only eruption of Hualaiai during historic times took place around 1800, when several flows were extruded. Several villages were buried, but there is no record of any casualties.

Continental United States--The volcanoes in the Cascade Range have been inactive for 80 to 100 years, but are important because of their proximity to populated areas. The volcanoes are in a seismically active region. Data from five platforms will be telemetered to one central collection point. The volcanoes to be instrumented are: Mount Baker, Mt. St. Helens, Mt. Adams, Mt. Hood, and Mt. Rainier.

#### 1. Mount Rainier

a. Location: Approximately 100 km southeast of Seattle, Washington, in Mount Rainier National Park.

Lat. N46° 52' Long. W121° 45.5'

b. Height: 4395 meters above sea level

c. Type: Strato-volcano

d. History: Records exist of six eruptions between 1843 and 1882. Steam is still issuing from the rocks along the smallest, and best defined, crater rim at the summit in sufficient volume to keep the rim free of snow and ice.

## 2. Mt. St. Helens

a. Location: On the western slope of the Cascade Range in Washington, 65 km north of the Columbia River. About 85 km NNE of Portland, Oregon.

Lat. N46° 12' Long. W122° 11'

b. Height: 2975 meters above sea level

c. Type: Strato-volcano with small domes

d. History: The younger lave flows from Mt. St. Helens is estimated to be around 100 years old. Between 1842 and 1854 five eruptions have been recorded. Steam jets were reported in 1941.

## 3. Mt. Adams

a. Location: In the Cascade Range of Washington. About 115 km NE of Portland, Oregon.

Lat. N46° 12.30' Long. W121° 29.50'

b. Height: 3751 meters above sea level

c. Type: Strato-volcano

d. History: Inactive during recent times

### 4. Mt. Hood

a. Location: In the Cascade Range of Oregon. About 75 km east of Portland, Oregon.

Lat. N46° 22.40' Long. W121° 41.70'

b. Height: 3427 meters above sea level

c. Type: Strato-volcano

d. History: Inactive during recent times

#### 5. Mt. Baker

a. Location: 25 km south of the Canadian border, Washington.

Lat. N48° 47.1' Long. W121° 49.0'

b. Height: 3316 meters above sea level

c. Type: Strato-volcano

d. History: Five eruptions occurred between 1843 and 1870. Inactive at present.

Central America--Four volcanoes in Guatemala and two in El Salvador have been chosen to test an active area outside the United States where volcanoes are extremely hazardous to life and property. A detailed study will determine the number of data collection points, but two or three may be required. The volcanoes to be instrumented are: Santa Maria, Acatenango, Fuego, and Pacaya.

### 1. Santa Maria Volcano

a. Location: Southwest Guatemala, Departmento Quezaltenango.

Lat. N14° 45.5' Long. W91° 32.9'

b. Height: 3768 meters above sea level

c. Type: Strato-volcano with explosion crater on SW slope and lava dome

d. History: Activity first noted in 1902 when a vast explosion removed 5.5 cubic kilometers of rock. Occasional eruptions have continued on through recent times. Greatest activity occurred between 1928 and 1932 causing loss of life and property. In November 1929 at least 23 people were killed.

# 2. Acatenango Volcano

a. Location: 40 km WSW of Guatemala City.

Lat. N14° 30.2' Long. W90° 52.4'

b. Height: 3960 meters above sea level

c. Type: Strato twin volcano

d. History: Recent activity (after 1924) has been limited to eruptions of ash and bombs. This volcano is included because of its proximity (1 km) to Fuego.

# 3. Fuego Volcano

a. Location: About 45 km WSW of Guatemala City.

Lat. N14° 28.9' Long. W90° 52.9'

b. Height: 3835 meters above sea level

c. Type: Compound strato volcano

d. History: Fuego is the most active volcano in Guatemala.

Eruptions, landslides, and earthquakes attributed to activity in Fuego have resulted in property losses since 1582. In 1932 ashes fell as far as Salvador and Honduras and 140 kg meter of ash fell in one hour in Guatemala City.

# 4. Pacaya Volcano

a. Location: About 30 km SSW of Guatemala City

Lat. N14° 23.0' Long. W90° 36.2'

b. Height: 2544 meters above sea level

c. Type: Complex, strongly faulted volcanic mountain with two young cones at its SW peak, and a cluster of domes at its NW foot.

d. History: Eruptions, often accompanied by earthquakes and subterranean rumblings, have been recorded. In October 1965, covered near by towns with rocks and ashes. Flaming lava was visible in Guatemala City. In 1961 Pacaya erupted for three days forcing the evacuation of 1,000 residents from the area.

#### 5. Santa Ana Volcano

a. Location: Western Salvador

Lat. N13° 51.2' Long. W89° 37.8'

b. Height: 2181 meters above sea level

c. Type: Strato volcano

d. History: Weakly active through 1955. Primary interest in this volcano is its proximity to Izalco.

## 6. Izalco Volcano

a. Location: Western Salvador, on the southern slope of Santa Ana Volcano.

Lat. N13° 48.9' Long. W89° 38.1'

b. Height: 1965 meters above sea level (January 1956)

c. Type: Strato volcano

d. History: This volcano has been active continually since the late 1700's with outflow of lavas interrupted by strong explosions, which were generally accompanied by subterranean rumbling. Life and property have been lost during an eruption of this volcano.

The above platform locations are tentative, and after coordinating the work with other local university and government organizations, we may wish to make minor modifications. It is understandable that there are other equally important areas such as the Aleutians, Philippines, etc., but these regions have special environmental, logistics maintenance, and other problems that can be solved after the volcano-surveillance network is operating satisfactorily.

Each platform will consist of 4 tiltmeters and 2 seismic-event counters. A total of 216 bits/day/platform will be required.

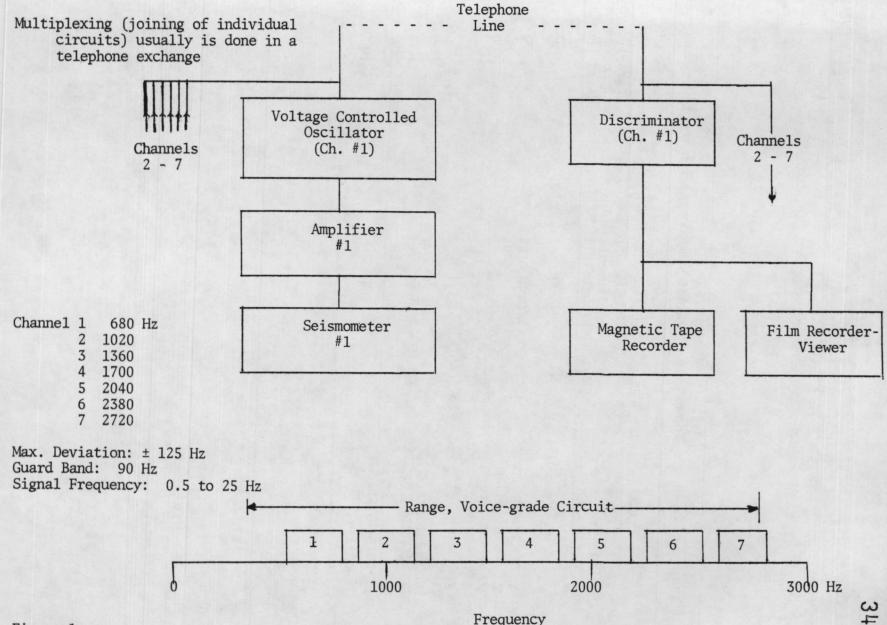


Figure 1.

Frequency

Table 1. Power requirements for various components of a remote seismograph station.

Unit	Power Requirement (watts)	Yearly Power Requirement (watt-hours)	
1. VCO-Preamplifier	0.30	2,600	
2. Transmitter	0.48	4,200	
3. Receiver	0.66	5,800	
Remote Station (1 and 2)	0.78	6,800	
Relay Station (1, 2 and 3)	1.44	12,600	

Table 2. Power Sources.

Type of Power Source	Power Rating	Voltage	Life	Weight (Pounds)	Watt-Hours per pound	Watt-Hours per dollar
Lead-acid battery (Sears)	80 AH	12	6 mos	48	20	64
Air Cell (Union Carbide Model 2S10)	1000 AH	2.5	3 yrs	32	78	122
Solar Cell (Central Lab Model CSP14D) charging a Nickel Cadmium battery	6 watt-hrs per day (av)	12	?	12	?	<u>/</u> 1
Thermoelectric Generator (3M, Model 515)	20 watts	12	?		15 /2	260 /2
Isotope Generator (U.S. Underseas Cable Corp., Model ITG-101/5)	1 watt	12	5 yrs	350	125	5

<sup>/1</sup> Assuming life of 3 years.

<sup>/2</sup> Rating based on cost and weight of propane fuel only.

#### BIOGRAPHICAL SKETCH

Dr. Smedes has been a research geologist for the United States Geological Survey since 1953. Prior to that he served in the U.S. Navy during World War II and taught in the Geology Department at Kansas State University.

His career has included geologic and mineral deposits studies in Oregon, Montana, and Wyoming where he specialized in the study of volcanic and plutonic igneous rocks. He coordinated and engaged in studies of remote sensing as part of his volcanologic studies in Yellowstone National Park, and is now responsible for research in geologic mapping techniques.

He received a B.S. degree with honors and a Ph.D degree in Geology at the University of Washington, with minors in Physics and Chemistry. He is a Fellow of the Geological Society of America and the Mineralogical Society of America; a Corporate Member of the American Society of Photogrammetry; and a Member of the Colorado Scientific Society and the Society of Sigma Xi.

Dr. Smedes' biography is listed in American Men of Science, Who's Who (South and Southwest), and the Dictionary of International Biography. He has published numerous maps and technical reports in his fields of specialization and has been selected as author-editor of the section on image enhancement of the new Manual of Remote Sensing (in preparation).

### AUTOMATIC COMPUTER MAPPING OF TERRAIN\*

by

Harry W. Smedes U.S. Geological Survey Denver, Colorado

## ABSTRACT

Computer processing of 17 wavelength bands of visible, reflective infrared, and thermal infrared scanner spectrometer data, and of three wavelength bands derived from color aerial film has resulted in successful automatic computer mapping of eight or more terrain classes in a Yellowstone National Park test site.

The tests involved: 1) supervised and 2) non-supervised computer programs; 3) special preprocessing of the scanner data to reduce computer processing time and cost, and improve the accuracy; and 4) studies of the effectiveness of the proposed Earth Resources Technology Satellite (ERTS) data channels in the automatic mapping of the same terrain, based on simulations, using the same set of scanner data.

The following terrain classes have been mapped with greater than 80 percent accuracy in a 12-square-mile area with 1,800 feet of relief: 1) bedrock exposures, 2) vegetated rock rubble, 3) talus, 4) glacial kame meadow, 5) glacial till meadow, 6) forest, 7) bog, and 8) water. In addition shadows of clouds and cliffs are depicted, but were greatly reduced by using preprocessing techniques.

<sup>\*</sup>Publication authorized by the Director, U.S. Geological Survey Work done in cooperation with the National Aeronautics and Space Administration

Harry W. Smedes

## PURPOSE AND SCOPE

For several years now there have been discussions and expressions of concern about the need to examine vast areas of the earth's surface, the advantages of high-altitude aircraft and satellite-borne remote sensors to gather the needed data, and at the same time concern about the immense quantity of data that is needed and would become available. Handling these data will require automatic processing by computer--not to make the <u>final and only</u> decisions of classification, but to perform one or more of the following three basically different tasks:

- 1) to perform the first-approximation rough interpreting, calling attention to special places that warrant examination by a human interpreter;
- 2) to enable us to extend our interpretation far beyond the range of human vision into the reflective infrared and thermal infrared, at the same time combining and integrating the data from many different parts of this expanded spectrum--something which cannot be done from the study of any single image; and
- 3) to enable us to extract additional information by either amplifying very small differences in radiance which are on or even below the limit of visual recognition, or by portraying broad ranges in radiance uniformily as a single value in order to determine or clarify relations previously obscured by mottled radiance.

For some of these operations a human can do a better job of interpreting, but the computer can do it faster. In this case, computer processing is largely a matter of data compression. However, some others of these operations cannot be done directly by a human interpreting some image or images. In these cases the computer processing enables man to extend his capability and perform tasks not otherwise possible.

It is for these reasons that the U.S. Geological Survey engaged in this study of automatic data processing by computer, that includes:

- A. Testing the suitability of existing sensors and computer software;
- B. Determining how many and what kinds of natural and manmade terrain classes can be satisfactorily classified in this particular climatic region;
- C. Simulating the spectral response of the proposed Earth Resources Technology Satellite (ERTS) sensors.

This report summarizes the current status of studies of computer processing of airborne multispectral data and color photographs, the success of automatic recognition and mapping of the distribution of eight or more different terrain classes, and the effectiveness of the proposed ERTS data channels in the automatic recognition and mapping of the same terrain classes based on simulations, using the same set of scanner data.

<sup>\*</sup>Publication authorized by Director, U.S. Geological Survey Work done in cooperation with the National Aeronautics and Space Administration

This study involves the data from one flight over a test area of about 12 square miles in a region of moderate relief (1,800 feet) comprising a wide variety of terrain types (Figures 1 and 2).

The data were acquired and processed in analog and digital form by the Institute of Science and Technology of the University of Michigan; and were processed in digital form by the Laboratory for Applications in Remote Sensing (LARS) at Purdue University; the Center for Research (CRES) at the University of Kansas; and EG&G, Inc. of Bedford, Massachusetts. The project also involved limited studies of spatial pattern recognition using optical lasers, and image enhancement by electronic and optical methods, but these studies are not described in this report.

## COLLECTION OF THE DATA

A multispectral survey was made of selected test areas in Yellowstone National Park during flights by the University of Michigan in September 1967, on a NASA-sponsored contract to the U.S. Geological Survey.

The University of Michigan 12-channel scanner-spectrometer in the 0.4 to 1.0 $\mu$ m range (Table I) provided the principal data for the computer processing described in this report. In addition, two scanner systems recorded a total of five channels of reflective and thermal infrared data in the region from 1.0 to 14 $\mu$ m.

Photographs taken at the same time the scanner data were acquired provide important supplements to the control data. These photographs consist of color, color infrared, black and white panchromatic, and black and white infrared film on board the aircraft, and color film from stations on the ground. Special computer processing was performed on some of the color aerial film for comparison with scanner data.

A simplified diagram of the Michigan scanner-spectrometer is shown in Figure 3. As the aircraft flies over the test area, the ground surface is scanned in overlapping strips by successive sweeps as a mirror is rotated at about 3,600 rpm. The radiant energy from the earth's surface is reflected off the rotating mirror and focused, by other mirrors (M, Figure 3) onto the slit of a prism spectrometer, thus refracting the rays into a wavelength spectrum.

Fiber optics placed at appropriate places lead to photomultiplier tubes which measure the amount of radiant energy received in each of 12 overlapping bands or channels of this spectrum from 0.4 to 1.0  $\mu$  m (visible violet to reflective infrared). This energy, which is now a voltage, is fed to a multitrack tape recorder where each of the 12 channels is recorded as a separate synchronized signal on magnetic tape. Similar, separate scanners recorded the infrared part of the spectrum from 1 to 14  $\mu$  m (see Table I).

Table I. Wavelength bands of University of Michigan multispectral system.

Channel number	Wavelength band µm	Channel number	Wavelength band ~~ m
	SCANN	ER NO. 1	
1	0.40-0.44	7	0.55-0.58
2 3 4 5 6	.4446	7 8 9	.5862
3	.4648		.6266
4	.4850	10	.6672
5	.5052	11	.7280
6	.5255	12	.80-1.00
	SCANN	ER NO. 2	
1	1.0 -1.4	3 4	3.0 - 4.1
2	2.0 -2.6	4	*4.5 - 5.5
	SCANN	ER NO. 3	
	*8.0-14.0		

\*Denotes thermal infrared channels; others are reflective

## TERRAIN CLASSES MAPPED

The eight terrain classes discussed on the following pages were selected arbitrarily during field study and the early part of computer processing. They were selected not on the basis of composition or genesis, as we traditionally do in the course of geologic mapping, but on the basis of their overall surface color and radiance (brightness) inasmuch as that is what the sensor was recording.

For example, geologists are more interested in the areal distribution of a sand and gravel unit, such as glacial till, than in the distribution of forest. Conventional maps would show the extent of till regardless of whether it was the site of a meadow or was covered with dense forest. The terrain classes of this study necessarily show the unforested till as one class (till) and the forested till as a different class (forest). In fact, all forested terrain, regardless of underlying rock or soil unit, is shown as a single class (forest).

Initial processing disclosed that at least 13 classes could be separated. Several of these were subunits which have been combined to make the display shown in Figure 25. The following is a brief description of the nine classes (including shadows) mapped.

1. BEDROCK EXPOSURES

This class (Figure 4) consists of bare bedrock exposed by glacial and stream erosion and mantled by minor amounts of loose rubble. These are unvegetated except for lichens and sparse tufts of dry grass, and have high reflectance in nearly all channels.

2. TALUS

This class includes blockfields, talus, and talus flows of basalt lava flows, volcanic tuff, and gneiss, formed by frost-riving and solifluction from outcrops. These are blocky and well-drained deposits; trees are widely spaced or absent (Figure 5). Blocks generally are covered with dark-gray lichens (Figure 6). The blocks range from a few centimeters to about 1 meter in diameter; most are larger than 10 centimeters. The slopes range widely, from 35°-45° at the head, to 5° or less at the toe. In places, a basin or trough lies just inside the distal margin of talus flows.

VEGETATED ROCK RUBBLE

This class consists of locally derived angular rubble, frost-riven from basalt lavas, volcanic tuff and breccia, and gneiss. Grasses, lichens, evergreen seedlings, and mosses now cover more than three-fourths of the surface underlain by this debris (Figures 7 and 8). Blocks range in diameter from less than 1 centimeter to about 1 meter, and occur on slopes of from 0° to about 25°.

4. GLACIAL KAME MEADOW

These are meadows underlain by sand and gravel, and mantled by sandy silt (Figures 9 and 10). The deposits are well-drained and are vegetated by grass and sagebrush. About one-fourth of the area of this class is exposed mineral soil. Deer and elk manure locally covers as much as one-fourth the surface area.

5. GLACIAL TILL MEADOW

This class consists of meadow areas underlain by glacial till. These are grassland and sagebrush areas (largely dormant at time of flight) with mineral soil exposed over about one-fifth of the area (Figures 11, 12, and 13). Mineral soil consists of mixtures of silty to bouldery debris. Deer and elk manure locally is abundant in these meadows.

6. FOREST

Depicted here are Douglas Fir and lodgepole forest (see Figure 5). Local clusters of deciduous trees were recognized separately, but combined with evergreens in the displays.

7. BOG

These are moist areas supporting tall lush growth of sedges and grasses. Bogs are rather abundant because of glacial scour and derangement of drainages.

- 8. WATER
  The Yellowstone River and Floating Island Lake are present in the test area. Phantom Lake was dry at the time of flight, and was considered therefore as bog rather than water.
- 9. SHADOWS
  Cloud shadows are near west and south-central margins of the test area,
  and deep shade occurs at base of north-facing cliffs and along north edge
  of forest areas.

## DATA PROCESSING BY ANALOG COMPUTER

This section of the report, dealing with analog processing, was conducted at the University of Michigan.

Any given channel of magnetic tape data can be reproduced by photographing a cathode-ray tube video (C-scope) presentation of the tape data (Figure 14). By changing the gain and amplitude, and thresholding out certain upper and (or) lower limits, different levels of radiance can be enhanced. Quantizing and contouring of thermal infrared data are examples of this technique.

For example, the continuous curve of image density versus log of exposure (Figure 15) can be broken electronically into discrete steps of variable width-all densities within each step being displayed in analog as a single density. Examples of density slicing of this sort are shown for thermal infrared data in Figure 16. The continuous-tone image is on the top, the n-level density-sliced equivalent in the middle. Electronic triggering at changes of density steps can produce a "spike" which can be displayed as a thermal contour, shown on the bottom on Figure 16. Ground temperature measurements or other control data can be used to convert this into a quantitative thermal contour map (the Michigan thermal scanner has internal calibrations, so that no ground control is required).

If each density slice is reproduced separately, copied on a colored transparent film and then the films stacked together, the result is a color-coded quantized thermal map (Figure 17).

Each of the 12 reflective and 5 thermal channels can be printed as video images comparable to that of Figure 14. These prints would constitute 17-channel multiband imagery. These images contain differences in tone (density)--hence, information--that is on or even below the limit of visual recognition, but that can be amplified or enhanced and made visible by electronic means. However, now that the data are recorded as signals on magnetic tape, they can easily be processed electronically in several ways to enhance selected features and to determine the statistical parameters of the spectral radiance (reflectance or emittance of each class of material in the scene. This was done in analog form for data from the 12-channel scanner, that is, from the visible violet to the near infrared, or about 0.4 to 1.0 µm.

Specific targets in the scene can be selected. By electronically measuring the mean and standard deviation of the signals in each of the 12 channels, spectral signatures and covariance functions can be obtained for each target class, and the optimum channels for separating each object class from all other classes can be determined in the computer by spectral-matching or by maximum-likelihood statistical decision rules.

For example (Figure 18), radiance (a voltage now) is measured for each of the channels for water (W) and forest (F). A vertical line two standard deviations long, centered about the mean radiance, is shown for each of the 12 channels.

Note that these two classes overlap only in the reflective IR part of the spectrum (right side). Other materials overlap these two and each other in various places; some have dissimilar and others have closely similar spectral reflectance.

The radiance in channel 1 can be compared to that in channel 2 for each class of material. The distribution of this spectral covariance data might have the form shown diagrammatically in Figure 19, where each cluster represents a different material. R1 and R2 represent radiance in channels 1 and 2, respectively. A-D represent classes of material.

On a frequency diagram the covariance radiance data may appear like that shown in Figure 20, where the seemingly topographic surface is the surface that bounds the distribution of data points. RI and R2 are radiance in channels 1 and 2, as before; f is the frequency of distribution of data.

This surface is topologically similar to, and can be considered as, a probability diagram. Each class (A-D) has its own peak value and falls off in all directions, generally in Gaussian fashion.

Statistically, if radiance values in channels 1 and 2 are r<sub>1</sub> and r<sub>2</sub>, they fall under the peak of class A and should be classified as belonging to class A. They have high probability of belonging to that class. But values that fall in the regions of low relief are highly questionable in terms of which class they belong to. They have low probability values.

Part of the computer processing involves maximum-likelihood theory to establish what plane or contour level should be applied as a threshold limit--for instance outside the area of intersection of the "topographic" surface and the vertical cylinder (shaded) of Figure 20. Any value falling outside that area would be rejected for that class by the computer. For simplicity, the threshold limit (cylinder) is shown only for class A in Figure 20. The "contour" at which the thresholds are set for other classes may be different for each class, depending on the distribution of data (shape of the probability surface) and overlap of different classes.

The peak positions and the entire "topography" of this surface would be different in a plot of channel 1 vs 3, 1 vs 4 . . . 7 vs 9, 7 vs 10 . . . etc. The computer compares the radiance in channel 1 with that in 2, 1 vs 3, 1 vs 4 . . . 7 vs 9, 7 vs 10 . . . etc.—until all 144 combinations of the 12 channels have been computed. From this data, the complex 12 X 12 covariance matrix function is computed and stored for making decisions of classification. These data represent the multispectral characteristics or "signatures" of each designated terrain class. A diagram cannot be drawn to illustrate this 12-dimensional space—it exists only in a mathematical sense. That is why the computer is needed.

After the spectral distribution and the covariance functions are determined for all classes sought, the entire tape of the traverse can be run through and the computer instructed to recognize and show only areas whose spectral reflectance matches that of one class, for example FOREST. A photograph of the cathode-ray tube shows the distribution of all areas recognized as FOREST by this spectral matching technique (Figure 21).

Separate runs for recognition of other terrain classes can be printed in different colors and overlayed, resulting in a sandwich which is a colored map presentation of the data.

Although there are the advantages of real-time mapping of terrain units by having the analog computer in the aircraft during acquisition of data, for most scientific applications it has proven more feasible and more accurate to use digital programs to determine optimum channels and threshold levels and to feed this data back to the analog computer for the actual display and mapping in analog form.

# DATA PROCESSING BY DIGITAL COMPUTER

Three basically different digital computer processing studies or tests were conducted. These involved:

- 1. Supervised programs using the scanner data
  - a. without preprocessing
  - b. with preprocessing of two different types
- 2. Non-supervised programs using the scanner data and clustering techniques
- Non-supervised programs using the aerial color film and clustering techniques

#### SUPERVISED PROGRAMS

Although the digital and computer programs used at Purdue and at Michigan differ in detail, they are closely similar. The Purdue program was used without preprocessing of data; the Michigan programs were used to test different preprocessing techniques and to closely simulate the spectral response of the ERTS data channels.

#### TESTS WITHOUT PREPROCESSING

In contrast to processing the data in analog form such as that in Figure 14, they can be processed in digital form by making a digitized copy of the original magnetic tape. This is the procedure used by the Laboratory for Applications in Remote Sensing (LARS), Purdue University. This section of the report will discuss the Purdue method of handling multispectral scanner data, and preliminary results obtained on a section of one flight-line of the Yellowstone Park data.

This particular run was digitized in such a manner that, on the average, there was neither overlap nor underlap of adjacent scan lines (Figure 3). The scanner resolution is three milliradians, and the aircraft altitude was about 6,000 feet above terrain. This required that every 10th scan line be digitized. Also, each scan line contains 220 ground resolution cells. The scanner mirror rotates at constant angular rate whereas the digitizing was done at constant linear rate. This, plus the effect of topographic relief, changes the size and shape of the ground resolution cell from the midpoint to both ends of the scan line. Even so, the average dimensions of the ground resolution cell are approximately 20 by 20 feet. There is a gap of about 20 feet between cells along each scan line, making each cell effectively 20 by 40 feet.

The analog data were quantized to 8-bit accuracy. Therefore, each resolution element of each spectral band has one of 256 possible values.

A computer printout of the data from any given channel is made to simulate the analog video display by breaking the continuous tones of the gray scale into a finite number of discrete gray levels by assigning a letter or symbol to each level in accordance with the relative amount of ink each symbol imprints onto the paper. An example is given in Figure 22. Each of the 15 reflective and 2 thermal channels could be printed as video and (or) digital printout images. constituting 17-channel multiband imagery (for example, see Lowe, 1968, figs. 12a and 12b, p. 94 and 95). The area coordinates are fed to a computer system\*, which then computes the statistical parameters of each class of material. These statistics are calculated from the relative response in each channel (Figures 23 and 24). Relative response can be considered as an uncalibrated reflectance measurement, where the lack of calibration between channels allows only relative comparisons of the various classes of materials within each channel. The statistical parameters calculated are based on an assumed Gaussian distribution of the data, and include the mean, standard deviation, covariance, and divergence (i.e., the statistical measure of the separability of classes). These statistics are stored by the computer, and are used to represent the multispectral characteristics of each designated class of material. These statistics constitute the

<sup>\*</sup>An IBM 360 model 44 computer with 64K bytes (8 bits per byte) of core storage was used. The principal computer language used was FORTRAN, with ASSEMBLY used for some of the support programs.

multispectral pattern or "finger-print" of each terrain class, and are used in the computer program to 1) determine which channels are most useful for recognition of all object classes studied, and 2) actually classify the unknown data points into the known classes using a Gaussian maximum-likelihood decision scheme.

Four channels were used in the Purdue study. This decision was based on experience at LARS-Purdue which has shown that the use of only 4 of the 12 channels in the 0.4 to 1.0 m range results in approximately as good a classification as does the use of more channels. Computer time, which increases in a geometric fashion with the number of channels used in the classification, is costly; therefore, some optimum for the number of channels used, the quality of results, and funds expended must be achieved. The channels selected are shown in Table II.

The channel-selection part of the computer program provides the capability of measuring the degree of separability of Gaussianly-distributed classes and determining the optimum set of channels for doing so. This is done by calculating the statistical distance in N-dimensional space between the classes, N being 12 in this case.

The classification part of the computer program involves the actual classification (mapping) of an arbitrary number of classes using an arbitrary number of channels and a Gaussian maximum-likelihood scheme. The display part of the program displays the results in line-printer form, and analyzes the recognition performance in each training area.

A thresholding capability is provided in the display process. If the resolution element does not exceed a predetermined threshold—that is, if the element does not look sufficiently like a member of the class to which it has tentatively been assigned even though that is the most likely class—then final classification of that element is declined and that element is assigned to a null class (rejected) and displayed as a blank. Different thresholds may be assigned to each of the classes individually.

A segment of the digital computer terrain map is shown in Figure 25. The part shown is composed of about 57,860 data points--about 22 percent of the full map. The full map covers an area of about 2 by 6 miles and is composed of 269,060 data points.

Initial processing disclosed that at least 13 classes could be separated. Several of these were subunits which have been combined to make the displays shown in Figure 25.

Hand-colored maps give a more graphical portrayal of the distribution of classes, but could not be reproduced here.

Table II. Channels used in the terrain classification and mapping, and to simulate the ERTS data channels using Purdue University's computer programs.

	Wavelength band used Um	Color or Michigan scanner spectral region channel number
Post li	0.44-0.46	Blue 2
Best 4	.6266	Orange 9
channels	.80-1.0	Red 10 Infrared 12
	.6672	Red 10
	.80-1.0	Infrared 12
The state of the s	2.0 -2.6	Infrared
	8.0 -14	Thermal infrared
ERTS scanner channels:	re tradition and exercise	the grad on by her and the
0.5-0.6µm	.5255	Green 6
.674m	.6266	Orange 9
.784m	.728	Infrared 11
.8-1.2 и т	.8 -1.0	Infrared 12
ERTS RBV cameras:		
0.535 M m peak	.5255	Green 6
.680 ит "	.6672	Red 10
.760 um "	.728	Infrared 11

## Thermal overlay

Another aspect of the work underway is a terrain classification made by substituting one or more data channels from the infrared scanners  $(1.0-14 \mu m)$  for those of the 12-channel scanner  $(0.4-1.0 \mu m)$ .

For this test, channels 1, 3, 5, 7, 9, 10, 11, and 12 of the 12-channel scanner were combined with the 1.0-1.4 \( \mu\), 2.0-2.6 \( \mu\), 4.5-5.5 \( \mu\), and 8-14 \( \mu\) m channels. A computer program recently developed at LARS-Purdue made it possible to overlay the data from these two separate scanner systems. The computer selected the best set of four of these channels (Table II) for classification of the terrain in the same manner as before. The maximum mismatch of registry is no more than three ground resolution cells, and probably is mostly no more than one cell.

The "map" of Figure 26 is the result of overlaying one thermal and three reflective channels (0.66-0.72, 0.80-1.0, 2.0-2.6, and 8-14 $\mu$ m). Only one of these channels is in the visible range. Because the scan angle of the thermal scanner was much narrower than that of the reflective scanner, this display covers only the middle east-west strips of those shown in Figure 25. The close correspondence of this display with the others indicates the accuracy of classification.

These studies should enable us to further extend the range of potential diagnostic spectra for existing classes and may point out some additional terrain classes. In addition, they will be useful tests of how well computer programs can take data from different scanner systems and automatically overlay them to produce a single set of multispectral data.

## Simulation of ERTS data channels

Along with the studies of evaluating the accuracy of performance, we are studying how well data in wavelength bands tentatively designated for the proposed Earth Resources Technology Satellite (ERTS) might serve for automatic mapping of the same eight terrain classes in the same area.

The existing computer programs of Purdue did not allow a simulation of the wider wavelength band width of the ERTS sensors. Instead, the midpoints of the channels of the proposed ERTS 4-channel scanner, and the peak transmissions of the three Return Beam Vidicom (RBV) cameras were matched with the closest channels of the University of Michigan 12-channel scanner. These data are summarized in Table II.

The classification using the <u>simulated</u> ERTS 3-RBV cameras is shown in Figure 27. Note the close agreement with Figure 25--that based on the computer-selected best set of four channels. A segment of the display of the simulated ERTS 4-channel scanner data classification is shown in Figure 28, for comparison with the RBV camera simulation and the computer-selected 4-channel display (Figures 25 and 27).

# Accuracy

In general, the products are highly satisfactory terrain maps which portray PHYSIOGRAPHIC UNITS or units which are unique associations of ROCK-SOIL-VEGETATION

The following generalizations about accuracy of classification of the terrai classes is based on comparison of the computer-generated maps with the ground control data.

- 1. BEDROCK EXPOSURES
  - This class is present mainly in the western part of the test area, along the banks of the Yellowstone River, and in a quarry where it was moderately well classified. Where misidentified, it generally was classified as vegetated rock rubble--a closely similar unit into which it grades.
- 2. TALUS
  All of the known areas of this class and a few previously undetected are clearly delineated.
- 3. VEGETATED ROCK RUBBLE
  The general areas classified are realistic, but in detail this class is the least well classified. Because of the small size of the individual areas occupied by this unit, it is not possible to locate precisely a homogeneous training area.

4. GLACIAL KAME MEADOW

Areas of kame meadows are accurately depicted. Areas of forested kame sand and gravel between open meadows of kame were erratically classified by the computer, mostly as other units. Control data show that in some places this class occurs as small scattered patches surrounded by till; in those places it was misidentified by the computer.

5. GLACIAL TILL MEADOW

This class was first classified as four separate subunits on the basis of change in illumination across the flight path, but the four were later combined into one unit for the map printout. Classification is estimated as about 95 percent accurate over the entire flight strip. The other classification symbols scattered throughout areas of this class generally are correct, for there are small areas of vegetated rubble and of bogs in meadow areas underlain by till.

Although both the till and kame deposits are the sites of meadows, the differences in amount of soil exposed and the subtle differences in soil composition and texture apparently permit these two classes to be accurately distinguished by the computer.

6. FOREST

This class generally is well recognized in large, almost uniformly-symboled blocks. All forest areas seem to be consistently recognized. Local clusters of deciduous trees were recognized separately, but combined with evergreens in the displays.

7. BOG

This is one of the best recognized classes. All known bogs and many previously unknown small bogs were correctly mapped.

8. WATER

The Yellowstone River and Floating Island Lake (see Figure 5) were clearly recognized. Phantom Lake (not on this segment of map) was dry at the time of flight, and so was correctly classified as bog rather than water. Parts of the Yellowstone River were omitted or generalized, principally because the width of the river is near the threshold of resolution, and because some data points were integrated values of river plus some other class or classes. Stretches of white-water rapids were rejected. In places, the shaded north edges of patches of forest were printed as scattered points of water or talus.

9. SHADOWS

All shadows were recognized well.

10. OTHER

All data points whose reflectance did not closely fit the statistical data for any of the above nine classes were rejected, and shown as blank regions on the map. A few of these are very light and bright areas of shallow water where bottom deposits show through, or are white-water rapids and gravel bars.

A blacktop road can be detected in places as a line of anomalous symbols, but is not consistently recognized as any particular class. The road is about as wide as a single data point and hence is at the threshold of resolution.

Although all bedrock types were classified as a single unit, the spectral reflectance histograms, spectrograms, and the divergence data indicate good possibility of distinguishing among several of the rock types present. Further testing over areas of larger rock exposure seems justified.

Where terrain classes covered large areas, they were correctly identified by the computer. Most inaccuracies occurred where the units were small and where some were below the threshold of resolution; accordingly, the radiance for a given resolution cell was a complex combination of several classes. Presumably, the computer usually selected the dominant terrain class or, by thresholding, indicated that the spectral properties did not clearly fit any of the classes.

For comparison of the performance of classification using the ERTS simulations with the best sets of four channels, the computer rated itself in the training areas only. For example, of the total of 5,418 data points used in training the computer, less than 20 of those were subsequently classified (using the best set of four channels) as something other than what they were called during the training. The ratings are as follows:

Best set of four channels99.6	percent
Thermal overlay98.8	
ERTS 4-channel scanner97.7	
ERTS 3 RBV93.8	

The figures are a good measure of the <u>relative</u> accuracy of each test. They are misleading in part because the computer assumes that each training area is homogeneous, consisting 100 percent of what it was labeled. The 0.4 percent error probably is a close measure of the degree of inhomogeneity of the material in the training areas.

When coordinates of other known areas (test areas) are fed to the computer, the computer determines the classification of those areas and computes the accuracy of classification. Appraisal of numerous test areas gives a more complete and meaningful evaluation of the overall recognition performance of the computer program.

Preliminary results of computer studies which rate the accuracy of classification of test areas give the following overall performance (data from unpublished report by Marc G. Tanguay):

Best set of four channels86	percent
Simulated ERTS four channels83	
Simulated ERTS 3-RBV cameras82	
Thermal overlay81	

These figures should be taken as approximations only. They agree with a preliminary visual estimate that the overall accuracy of all displays is more than 80 percent, and indicate that the best set of four channels gives slightly better results than the other three displays, all of which are about equally good.

The drop in accuracy from 99 to 86 percent, etc., from the training to the test areas, is understandable, because we would expect the computer to perform well in the areas where it was trained unless the reflectances of two or more classes were closely similar in all channels used.

For the training areas, the classification made using the overlay of thermal and reflective channels was virtually as accurate as the best classification—that using the computer-selected best set of four reflective channels (98.8 vs 99.6 percent, respectively). However, for the test areas, the thermal overlay was least accurate (about 81 vs 86 percent). The slight mismatch of registry in parts of the thermal overlay test undoubtedly results in a less accurate classification than if all channels were in complete registry, as would occur if a single scanner system could cover the range of 0.4 to 14 µm or more.

Nevertheless, these studies indicate that the infrared region is promising in the classification of some terrain units. For example, in the test areas the thermal overlay classification was better than the computer-selected best four-channel classification for glacial till (95 vs 93 percent), glacial kame (82 vs 74 percent), and bog (81 vs 80 percent). The accuracy of classification of talus in the test areas was only about 49 percent; however, most of the error was due to talus being misclassified as vegetated rock rubble, a unit which actually is quite similar to talus. If talus and rock rubble are combined as a single unit, the accuracy jumps to about 83 percent, whereas the same combination was classified only about 76 percent when using the best set of four channels in the test areas.

In geologic applications it is more desirable to know what kind of material the forest is growing on than simply to know where the forest is. The thermal overlay classification has some potential in this regard; it has been shown (Waldrop, 1969) that thermal infrared in forested areas can in places indicate the sites of thick, unconsolidated, well-drained gravels vs bare or thinly mantled bedrock.

An obvious advantage of infrared data channels for space applications is the haze penetration ability. Further investigations are needed to adequately assess the potential of these channels, particularly over areas of extensive rock outcrops.

Studies underway also include careful evaluation of the overall accuracy by point-to-point comparison with ground-truth maps. It is important to recall the recognition of previously undetected areas of occurrence of some terrain units. This means that errors in the control maps are being detected at the same time errors in the computer printout are being sought.

In general, the ERTS simulations differed from the computer-selected best four channels as follows:

- 1. For areas correctly shown as FOREST on the classification using the best four channels, the ERTS 4-channel classification showed small to moderate amounts of TALUS and WATER, whereas the RBV 3-channel classification showed greater amounts.
- 2. In places, both ERTS classifications showed considerably more BOGS than are present in areas that were correctly classified by the best four channels.
- 3. Slightly poorer classification of water was performed in the ERTS classification. However, few of the bodies of areas of water in the test area are of sufficient size to serve as good training areas, so I do not view this part of the classification as a good test of the ability of the ERTS data channels to permit automatic identification of water.

I wish to point out that these are not complete simulations of the ERTS data channels, but are only first approximations, because no attempt was made to simulate 1) the poorer resolution of the satellite sensors due to vast differences in scale, 2) the effects of atmospheric attenuation, or 3) the broader wavelength bands of most of the ERTS sensors (see Table II). Studies at the University of Michigan aimed at more closely simulating the actual wavelength bands of the ERTS sensors, are described in a later section of this report.

All four of the experiments produced good results. They are good classifications. I do not wish to set any specific limits on how good "good" is. Obviously, some are better than others, and none is perfect—but neither is the manmade control map—and preprocessing of the data, as described below, further improves the accuracy of the computer—generated maps. I am convinced, however, that all can be considered as more than adequate for the reconnaissance first—approximation kind of interpreting and mapping which we expect to accomplish with the satellite data.

#### TESTS OF PREPROCESSING OF DATA

Programs for terrain classification using multispectral data, such as described above, are based on the assumption that the spectral radiance of all objects of a given class in the scene is substantially the same. During these studies we soon determined that this was not true because of various factors such as cloud shadows, haze, variations in topography, and changes in scanner "look" angle. As a result, the performance of classification schemes based on spectral signatures was degraded, both in analog and digital tests. This was partly overcome by selecting multiple training sets for each class, each set effective over a narrow range of data along the scan line. However, this lengthened the preparation and computer-processing time. This is described more fully in a paper by Smedes, Spencer, and Thomson (1971).

Preprocessing of the data to compensate for the angular variations was studied using digital computer programs developed by the University of Michigan. This allowed the use of a single training set for each class of objects anywhere in the field of view. It shortened the preparation and computer-processing time, gave more accurate results, and, in places, enabled areas under cloud shadow to be classified as to the correct terrain class.

In a way shadows and topography pose similar problems, in that they affect the total level of irradiance. North-facing slopes, and shadows, result in lowering the total level, whereas south-facing slopes reflect more light back to the sensor and result in a raising of the total level. However, in both cases, the ratio of observed (recorded) spectral radiance in two spectral channels will be independent of variations in the level of radiance.

The topographic and other scan-angle-dependent variations may be deduced and corrected for by dividing by a function of the scan angle.

Results of preprocessing of these two types--ratio transformation and scanangle function transformation--are described below.

# Ratio Transformations

Three ratio preprocessing techniques, previously reported by Kriegler and others (1969), make use of the fact that if the scene radiance varies, this variation is present in all spectral channels. Ratios of channel signals therefore will show less variation with scene changes than will the signals themselves.

These ratio transformations, which have been previously used as techniques for preprocessing the scanner-spectrometer data to reduce illumination variations, are:

- 1. Ratio of each channel to the sum of all channels, e.g., channel 1 Σchannels.
- 2. Ratio of adjacent channels, e.g., channel 2 channel 1
- 3. Ratio of the difference to the sum of adjacent channels, e.g., channel 2 - channel 1. channel 2 + channel 1

If the original scanner-spectrometer data consist of N channels, then after performing any of these three ratio transformations there would be (N-1) independent channels of data. Therefore, one channel must be eliminated. Arbitrarily, the twelfth channel was eliminated in these studies by Michigan. The data of Table III show that the first ratio transformation (ratio of each to the sum) gives lower probability of misclassification than do the other two ratio transformations.

Table III. Probabilities of misclassification of training area classes using different preprocessing of the original data and ERTS scanner simulations. The higher the value, the greater the probability of misclassification.

Preprocessing technique	Probability of misclassification			
	Best channel	2 Best channels	3 Best channels	
Ratio transformation 1	0.088	0.037	0.026	
$\frac{\text{channel } n}{\Sigma \text{ channels}}$	(n=1)	(n=1,5)	(n=1,5,10)	
Original data ERTS RBV simulation ERTS scanner simulation	0.101	0.039	0.035	
Ratio transformation 2 (channel $\frac{12}{11}$ etc.)	0.179 (12)	$(\frac{0.087}{11})$ , $(\frac{10}{9})$		
Ratio transformation 3	0.186	0.091		
$\left(\frac{\text{channel } 12 - 11}{\text{channel } 12 + 11} \text{ etc.}\right)$	$\left(\frac{12-11}{12+11}\right)$	$\left(\frac{12-11}{12+11}\right), \left(\frac{1}{12}\right)$	10 - 9 10 + 9	
Normalized scan-angle function transformation	<u>0.070</u> (5)	0.015 (5, 12)	0.009 (5,12,2)	

# Scan-angle Transformation

More knowledge of the scene is required for the use of this preprocessing technique than for the ratio preprocessing. It is assumed that the variations in scene radiance in each spectral channel can be described by a function of scan angle, which may be determined by analyzing spectral signatures from one or more classes of materials distributed along the scan line. Enough information must be available to locate samples of a given class of material at various scan angles.

If the ratio of spectral radiances of two classes as a function of scan angle is constant, then we can derive a single correcting function which we can assume will be valid for all data in each spectral channel for all classes. This assumption is equivalent to assuming that the bidirectional reflectance variations as a function of scan angle of different classes are the same.

A universal scan-angle correcting function for each channel is obtained by normalizing the function of signal vs scan angle for any one material at some particular scan angle.

For one spectral channel (channel 1, Table I), the variation in the means and standard deviations of the training areas of FOREST, BOG, and TILL as the scan angle is varied are shown in Figure 29. In this example, a radiance value of 0.8 could be interpreted as any one of the three classes depending on the scan angle.

Figure 30 shows the same data after the scan-angle transformation. Now the classes are clearly separated, and a radiance value of 0.8 could only be interpreted as TILL.

If the preprocessing technique is successful, the wide separation in mean values of spectral signatures of classes at different scan angles (Figure 29) has been eliminated for training sets of the same class of material. One could easily obtain combined signatures for each class using unpreprocessed data, as was done in the Purdue study. Because this results in signatures with large standard deviations, the signatures of different materials are far more likely to overlap, causing increased probabilities of misclassification. Because of this, the Purdue tests using non-preprocessed data required that most materials be treated as subunits, in terms of scan-angle position—the subunits later combined as complete units (classes) during the printout stage.

As with the non-preprocessed data studied by Purdue, the Michigan computer program\* utilizes a supervised training program which involves a maximum-likelihood decision scheme for selecting the best spectrometer channels, and closely similar techniques of digitizing the data of the analog magnetic tapes.

Studies of the training areas of all classes enabled the computer to calculate the probability of misclassification by using the different preprocessing techniques described above. The results, summarized in Table III, indicate that use of the normalized scan-angle function transformation would result in the lowest probability of misclassification. Hence, that transformation was used in making the recognition map of Figure 31. The symbols used to designate the different terrain classes are shown in Table IV.

# Simulation of ERTS Data Channels

The existing Michigan computer programs allowed a closer simulation of the full band width and spectral response of the ERTS sensors.

<sup>\*</sup> A CDC-1604 computer with 32K bytes (8 bits per byte) of core storage was used. The computer language used was FORTRAN IV. An IBM-1401 computer was used for peripheral work and for the actual printing of the recognition of maps in color.

Table IV. Symbols and colors used to represent the different terrain classes shown on the maps of Figures 28, 31, and 32.

Material	Color				
	Blue	Red	Green	Black	White
Bog			*		
Forest			車		
Glacial Till Meadow		車			
Glacial Kame Meadow		*			
Bedrock	車				territoria di
Vegetated Rock Rubble	*			12.25.27.3	
Water				*	
Talus				*	
Shadow					
Not classified					(No Symbol

The spectral responses\* of the ERTS 4-channel scanner and the three RBV cameras were used to construct nominal spectral sensitivity curves. The detailed spectral response of each scanner-spectrometer channel (Larsen and Hasell, 1968) were fitted graphically to the specified ERTS data using a technique described by Nalepka (1970). Further corrections to account for peak sensitivity variations in photomultipliers were determined from radiance standard lamp data. The result was a set of weighting coefficients to be assigned to each spectrometer channel to simulate the ERTS sensor data. These are summarized in Table V.

These data were used with the signatures previously obtained from the training areas, using preprocessing with the ratio transformation in which the spectral channel is divided by the sum of spectral channels, using channels 1, 5, and 10 (see Tables I and IV). The terrain map made using this data is shown in Figure 32.

<sup>\*</sup> Data obtained by F. Thomson and M. Spencer of the University of Michigan from L. Goldberg and O. Weinstein of NASA-Goddard.

Table V. Weighting factors for simulation of ERTS sensors with original scanner spectrometer data.

Michigan spectrometer channel number	ERTS 4-channel scanner and RBV camera	Weighting of Michigan channels
5 6 7 8	channel 1	0.68 .86 .98 .70
8 9 10	channel 2	.74 .96 .72
11	channel 3	1.00
12	channel 4	1.00
4 5 6 7	camera l	.72 .82 .95 .86
9	camera 2	• 94 • 59
11	camera 3	1.00

The probability of misclassification of training area classes using simulated ERTS scanner data is 0.035 (Table III) and the average percentage of correct recognition is 81 (Table VI). Although no recognition map was run for the simulated ERTS 3 RBV cameras, the data from the training areas indicate probability of misclassification as 0.039 using the same ratio transformation. If the simulations had been made with normalized scan-angle transformation, the probability of misclassification surely would have decreased, and the accuracy of recognition would probably have increased to about 90 percent (deduced from data of Table VI).

### Accuracy

The accuracy of classification using preprocessing techniques of the original spectrometer data and the simulated ERTS scanner data is indicated in part by the data of Table VI, which is based only on the training areas.

The ERTS simulations were made using the best of the three previously tested ratio processing techniques before Margaret Spencer had developed and tested her program for normalized scan-angle preprocessing. Had the scan-angle preprocessing

been used, it would have permitted use of all four ERTS channels rather than the three which resulted from the (N - 1) loss inherent in all ratio preprocessing techniques, as described above.

Table VI. Accuracy of recognition in training areas using different preprocessing of original spectrometer data and ERTS scanner simulations (maps of Figures 28, 31, and 32).

	Results of training area evaluation of the recognition map, in percent correct recognition			
Catagory	Normalized scan-angle transformation	Ratio transformation $\left(\frac{\text{channel } n}{\Sigma \text{ channels}}\right)$	ERTS scanner simulation using (channel n')*	
Bedrock Talus Vegetated Rock Rubble Glacial Kame Meadow Glacial Till Meadow Forest Bog Water Shadows	96.7 91.9 94.4 100 98.6 97.0 95.0 94.7 97.4	80.0 81.0 91.9 93.3 74.4 88.8 92.7 94.7 91.8	47.7 63.1 95.3 94.7 89.0 85.5 88.9 93.4 71.3	
Average percentage of correct recognition	96.2	87.7	81.0	
Average percentage of incorrect recognition	3.4	11.6	18.4	
Average percentage of no recognition	0.4	0.7	0.6	

<sup>\*</sup> n' indicates the simulated ERTS channel which is a non-linearly weighted summation of several original spectrometer channels (see Table V) and does not correspond to n which represents the non-weighted original spectrometer channel.

The simulated ERTS data gave poor results for three classes—bedrock, talus, and shadows. However, bedrock and talus basically are exposures of rock blocks, the blocks in talus simply having moved down slope a short distance, and the two units actually are gradational. If these two gradational classes are combined, the recognition performance would rise to values comparable to those of other classes, for nearly 18 percent of the bedrock was misidentified as talus and nearly 28 percent of the talus was misidentified as bedrock. The apparently poor performance of the ERTS data for shadows (71.3 percent) is misleading because

10.4 percent of the training area was identified as forest, which is the true terrain unit that was under the shadow. This suggests that, somehow, the simulated ERTS data can "see" through the shadow better than can the other recognition techniques.

As with the non-preprocessed data, the most meaningful test of accuracy is not in the areas for which the computer was trained, but throughout the entire map, through use of numerous test areas or a point by point comparison with the ground control data.

At the time of this writing, studies are underway to determine more closely the accuracy of these preprocessed classification maps. Preliminary results indicate that the most important improvement in accuracy has resulted from the fact that, because of preprocessing, the area of shadow was markedly reduced and the true terrain unit beneath the shadow accurately mapped. Because the terrain class generally under cloud shadow was forest, the classification of forest was greatly improved over that of the non-preprocessed maps.

In comparing the accuracy of these maps made using preprocessing techniques with those made without preprocessing, the following generalizations are valid: bog, glacial kame meadow, water, and vegetated rock rubble were as accurate or slightly more accurate; forest, glacial till meadow, bedrock, and talus were definitely more accurate.

Thus, in spite of far fewer training areas (24 vs 187) and fewer channels used (3 vs 4), these maps are more accurate and required less computer time than those made without preprocessing.

#### NON-SUPERVISED PROGRAMS

The various techniques described above required that we train the computer on known areas. This requires some prior knowledge of the region. The techniques described below are based on non-supervised processing that requires no prior knowledge of the area. These techniques utilize the fact that the radiance of different classes tends to cluster in different places in n-dimensional space. The programs allow the computer to determine these clusters and to plot each class based on clustering, whatever the class may be.

One such natural class might be printed in map form by the letter S, for example; and, although you would not know what that class really was, you would know everywhere it occurred. Limited field checking or photo interpretation would then give an identity to each of the classes mapped by this clustering technique.

In addition to the fact that no prior knowledge is required, there is the further advantage that no calibration is required.

Non-supervised digital computer processing of data using cluster techniques has been done using the multispectral scanner data and color aerial film.

### SCANNER DATA

In order to reduce computer time, the original twelve channels of data were preprocessed by a principal-components analysis to yield four different classes, but with almost all (more than 99 percent) of the statistical and spatial structure preserved. The cell size was reduced by taking every third row of resolution cells and every third resolution cell on each such row taken. This is the equivalent of a cell 60 by 60 feet. Each of the four classes consists of a binary vector of 25 components.

From this principal-components analysis, clustering and inverse clustering functions (described briefly below) were generated for a sample of 1,908 data elements out of 30,044.

Any clustering procedure assigns data elements to clusters such that the elements within a cluster are closely similar or related, and elements of any two clusters are dissimilar or unassociated.

The clustering technique used at the University of Kansas is an iterative clustering procedure (Haralick and Dinstein, 1970) programmed for the GE 635 computer.

Viewed as a geometric approach, the data elements are represented as vectors of N binary components, each of which has a value of +1 or -1. Hence, each data element can be considered as a vertex of an N-dimensional unit hypercube in an N-dimensional Euclidian space. The clustering function f projects those points into vertices of a K-dimensional unit hypercube. The points that are projected into a vertex of the K-dimensional hypercube form a cluster whose code is the coordinates of the vertex in the K-dimensional space. The inverse clustering function g projects these vertices of the K-dimensional hypercube back into some vertices of the N-dimensional hypercube.

The computer program enables the K-dimensional hypercube to be iteratively "rotated" until the sum of the distances between the original and respective projected-back data points is minimum.

The f and g functions are chosen from a class of parametric functions derived from linear threshold functions. "Rotation" of the K-dimensional hypercube is accomplished by iterative small changes in these parameters.

The cluster map derived from this iterative clustering technique by digital computer contained symbols delimiting four classes. These classes were outlined, traced onto a blank sheet and coded with drafting patterns. This final product is shown in Figure 33. The classes correspond generally with the following:

Medium gray = Till, kame, locally vegetated rock rubble White = Forest, water, and shadow

The topographic and scan-angle functions have obviously degraded the classification as indicated by the different patterns for materials along the north edge (south-facing slopes at low elevation). Preprocessing by ratio or scanangle function transformations undoubtedly would improve the accuracy.

#### COLOR AERIAL FILM

Traditionally, multispectral data from film have been from multilens cameras using black and white film, each lens filtered to pass only a limited wavelength band. In the present study, conducted with EG&G, Inc., the three emulsion layers of color infrared film were used as a three-band spectrometer. This film was acquired at the same time as was the scanner data. Because of the focal length of the cameras, the film covers only the central part of the full scan width.

This study is underway at the time of this writing, so only preliminary results can be presented in this report.

The three emulsions of color infrared film are most sensitive to the broad spectral bands (approximate) listed below, as normally exposed with appropriate filters:

Emulsion	Color recorded	Band width	Equivalent spectrometer channel numbers
blue	green	0.50-0.58 4m	5,6,7
green	red	.5868	8,9,(and half of 10)
red	infrared	.6890	10,11,(and half of 12)

Image density data from each of the three color emulsions were entered into a digital computer program that produces terrain maps by using clustering techniques.

The 70-mm color transparencies were scanned by a Mann Trichromatic Microdensitometer at a resolution of 4504, corresponding to a spot about 30 feet in diameter on the ground. All three color film layers were sampled simultaneously by means of beam-splitters and filters. Triads of density values were obtained from each area element on the transparency, as shown diagrammatically in Figure 34, and were recorded on magnetic tape. The data were digitized to nine-bit accuracy (though less accuracy would suffice). Characteristic spectral signatures inherent in the data -- presumably representing terrain classes -- were identified by the application of clustering techniques in three-color space. Each datum point was assigned on the basis of its spectral signature, to one of these classes, and each class was then assigned a letter character (for example, A and B. Figure 34). Computer-generated overlays were made to fit photographic enlargements of the transparency at a scale of approximately 1:4,000 (Figure 35). Existing control data enabled these classes to be labeled as to true terrain class. This technique is described more fully in a paper by Smedes. Linnerud, and Hawks (1971).

The following terrain classes were automatically mapped from color infrared film, with overall accuracy equal to or better than those of previous multispectral scanner classification (better than 85 percent): 1) deciduous trees, bushes, and bogs, 2) evergreen trees, 3) bedrock, largely granitic gneiss, and rhyolite tuff (in a quarry), 4) bedrock, largely basalt and amphibolite, 5) talus, 6) rock and talus in shade, and 7) shade of trees and cliffs.

The resolution cell size of the present study closely simulates the computergenerated maps previously made from multispectral scanner data. Studies underway include classification of the same areas using smaller ground area elements.

The present study indicates that color film can be used as an accurate means of multispectral terrain mapping by computer. An important additional advantage is that the results can be directly overlaid on the photograph. Geometric distortions can be rectified by using stereoscopic pairs of aerial photographs and simple standard photogrammetric techniques. Color aerial photographs are readily available at low cost, whereas scanner data are sparse and are expensive to obtain.

The widths of the bands used in this study are similar to those of the ERTS sensors. The accuracy of classification (better than 85 percent) indicates how well the ERTS sensors might be expected to perform in classifying similar terrain, and agrees closely with the results of ERTS simulations made using scanner data.

## CONCLUSIONS AND RECOMMENDATIONS

Direct comparisons cannot be made between any of the computer maps and the control data for several reasons. With the exception of the test with the color aerial photos, it is not possible to transfer the class boundaries accurately from the scanner format to the topographic base map or to annotated aerial photos on which the control data are plotted. Scanner distortions and size of the computer ground resolution cell place constraints on the accuracy of locating these boundaries. Continuing research and development at the Universities of Michigan, Kansas, and Purdue are minimizing these constraints.

The control data consist of a surficial geologic map, a bedrock geologic map (both of which ignore the vegetation), and a map in which percentage of classes within broader areas are indicated (Figure 36). Thus, because we cannot accurately locate and check accuracy of mapping of specific small clumps of trees or small and scattered outcrops, we can only compare percentages of these classes within the broader areas on the computer map with those on the generalized control map. But, for the purposes of these tests, we are really only interested in the larger features, anyway--those that constitute a large resolution cell comparable to that which can be resolved by the satellite sensors.

Furthermore, a direct comparison cannot be made of the results obtained using different computer techniques because of the differences in digitizing the data, number and size of training areas used, and resulting differences as summarized below. However, the objectives of the Michigan study were principally to test the effectiveness of preprocessing and of more closely simulating the ERTS data channels.

il same minden the back of the displayer than ever	Purdue	Michigan
Total number data points Number of training areas	269,060 187	187,131
Total number of data points in training area	5,418	3,521
Percent of total area used for training	2%	1.9%
Maximum number of channels used in classification	4	3

The University of Kansas cluster processing used only every third row of cells and every third cell of such a row, resulting in a ground resolution cell of about 60 X 60 feet in contrast to the cells of 20 X 20 feet and 30 X 30 feet used in the other tests. However, in this regard, it more closely simulates the resolution of the satellite sensors.

In spite of this inability to be able to make a point by point (cell by cell) comparison of the computer maps with the control data, the overall accuracies can be rather well determined, as indicated in previous chapters.

One of the overwhelming problems of automatic mapping of terrain classes is that the spectral signatures of a given class vary widely with such things as time of day, season of the year, latitude and flight direction (illumination-angle functions), and recency of rain in the region. I doubt that we can adequately sample the spectra of many classes of material under a wide enough range of conditions so that by the spectra alone we could identify materials.

Lacking complete samples of spectral signatures, we would have to rely on supervised computer techniques, thus requiring some prior knowledge of the terrain.

However, after studying the results of these tests, and on the basis of discussions with Dr. Robert Haralick of the University of Kansas, I am convinced that there is great potential in the cluster processing technique, and that automatic mapping will be most successful where the two kinds of processing--non-supervised and supervised--are performed in concert. Specifically, I suggest that the (non-supervised) cluster techniques be used to determine what the natural terrain classes are and where they are. Then, sample spectra of these classes can be compared to spectral signatures in a master computer data bank to determine which class or classes of material most closely correspond to the spectra from these natural terrain classes. Although several specific classes may be equally likely on the basis of the data bank, several may be eliminated by mutual exclusiveness with adjoining classes, by reference to model studies such as described by Watson at this Workshop, or by some very general knowledge of the region surveyed. It may thus be possible to identify specific natural classes of terrain without field check.

Preprocessing of the data is an important part of the concept because it normalizes the data and thus minimizes the effects of variations in illumination due to scanner "look" angle, topography, and shadows. Subsequent sets of data over the same area could be processed using conventional supervised techniques.

If we examine the spectral range spanned for each of the displays (Tables II, V, and Figure 37), we see that they vary by a factor of nearly 50, from 0.28 µm for the 3-camera ERTS system to 13.34 µm for the thermal overlay classification. This implies that, for a broad range of terrain categories, many combinations of three or four channels of data in the 0.4-14 m range would be satisfactory. More complete simulations, in which the effects of the atmosphere are considered, undoubtedly will require identification as to which channels would be suitable. For example, the haze penetration ability of some reflective infrared channels, mentioned earlier, is an obvious advantage for satellite applications; the blue part of the spectrum is apt to have low signal-to-noise ratio and therefore be of limited use except for oceanography. We need worry about careful selection of specific wavelength bands only if a specific category is being sought. Inasmuch as the ERTS program is aimed at covering many scientific disciplines and user groups -- hence involving many terrain categories -- the highly specific requirements are not now pertinent to tests of the suitability of the proposed satellite sensors.

I believe that the concept, rather than the specific immediate results of these studies, is the most important product. Admittedly, it is not really important to find that talus occurs on the shore of a lake here or that a narrow bog lies there—we already know most of that for this particular area. The important point is that eight or more widely different terrain units could be accurately mapped automatically. For the moment it does not really matter what the units are or where they occur—they could as easily have been orchards, barns, municipal parks surrounded by streets and buildings, beaches, polluted or clean water, marshlands, etc.

In fact, I believe that these particular maps are <u>over-classified</u> in comparison with what we will want to attempt from space--at least for our first attempts. It may well suffice to map out such features as WATER, VEGETATION, BARE SOIL, and ROCKS, and to interpret other things, such as geologic structure, from the resulting patterns and their relations to topography.

Especially significant applications in geology and other fields will be for those features that are time-dependent, changing with the seasons or with a few years' time. Once an area has been mapped by computer, the areas of change can be periodically mapped automatically in terms of material, location, and the amount of area changed

I suggest that economically feasible geologic applications will include those that contribute to regional mapping, engineering geology, hydrology, and volcanology. Other applications may be in the fields of agriculture, cartography, landuse and land-management studies, and in still other fields in which seasonal and other changes are more rapid than in most geologic applications. In many fields, these data will become more useful by combining them with other (nonspectral) data--for example, the engineering application to trafficability studies--by combining these terrain data with slope (from radar images or topographic maps).

The fact that we are sensing surface material emphasizes the need for multidisciplinary approach to terrain mapping, because the surface involves the complex interplay of at least bedrock and surficial geology, hydrology, soils, vegetation, and meteorology. Traditionally, in mapping many regions of the earth, we interpret the geology secondarily from the patterns of other materials and features.

I hope that, in this brief review of the steps involved in acquiring and processing the data, you can see in the results some applications to your own fields of interest.

### ACKNOWLEDGMENTS

The data which form the subject of this preliminary report were derived from work done by the U.S. Geological Survey and on NASA- and USGS-supported contracts by the following research groups: (1) Institute of Science and Technology, Willow Run Laboratories, University of Michigan: airborne multispectral survey, analog processing of data and digital computer test involving preprocessing of data and ERTS simulations; (2) Laboratory for Applications in Remote Sensing, Purdue University: digital computer processing including techniques of overlaying data from two scanner systems; (3) Center for Research, Inc., Engineering Science Division, University of Kansas: digital computer processing of scanner data using cluster techniques; and (4) EG&G, Inc., Bedford, Massachusetts: digital computer processing of aerial color film using cluster techniques.

The U.S. Geological Survey conducted field studies before, during, and after flight, and actively participated in the computer processing and evaluation of all data. This report has incorporated data from reports by Smedes and others (1970) cited below, and from unpublished reports by Dr. Robert Haralick, Stanley Hawks, Dr. Harold Linnerud, Margaret Spencer, Frederick Thomson, and Dr. Lawrence Woolaver.

## REFERENCES

More detailed information on optical-mechanical scanners and the various techniques and computer programs described in this report can be found in the following. Those cited in this report are preceded by an asterisk.

- Cardillo, G. P., and Landgrebe, D. A., 1966, On pattern recognition: Purdue Univ. Laboratory for Agricultural Remote Sensing Inf. Note 010866, 18 p. mimeographed.
- \*Haralick, R. M., and Dinstein, I., 1971 (in press), An iterative clustering procedure, in Institute of Electrical and Electronics Engineers Trans. Systems Science and Cybernetics.
- \*Kriegler, F. J., Malila, W. A., Nelapka, R. F., and Richardson, W., 1969, Preprocessing transformations and their effects on multispectral recognition,

- in Proceedings of the Sixth Int. Symposium on Remote Sensing of Environment: Ann Arbor, Michigan Univ. Inst. of Science and Technology, v. 1, p. 97-131.
- Landgrebe, D. A., and staff, 1968, LARSYAA, A processing system for airborne earth resources data: Purdue Univ. Laboratory for Agricultural Remote Sensing Inf. Note 091968, 34 p. memeographed.
- \*Lowe, D. S., 1968, Line scan devices and why use them, in Proceedings of the Fifth Symposium on Remote Sensing of Environment: Ann Arbor, Michigan Univ. Inst. of Science and Technology, p. 77-100.
- \*Smedes, H. W., Linnerud, H. J., and Hawks, S. G., 1971, Digital computer mapping of terrain by clustering techniques using color film as a three-band sensor, in summary of papers presented, Seventh Int. Symposium on Remote Sensing of Environment, May 17-21, 1971: Ann Arbor, Michigan, Univ. Mich.
- \*Smedes, H. W., Pierce, K. L., Tanguay, M. G., and Hoffer, R. M., 1970, Digital computer terrain mapping from multispectral data, and evaluation of proposed Earth Resources Technology Satellite (ERTS) data channels, Yellowstone National Park: Preliminary report: Am. Inst. of Aeronautics Earth Resources Observations and Information System Mtg., Annapolis, Md., March 1970; AIAA Paper No. 70-309, 18 p.
- \*Smedes, H. S., Pierce, K. L., Tanguay, M. G., and Hoffer, R. M., 1970, Digital computer terrain mapping from multispectral data: Journ. of Spacecraft and Rockets, v. 7, no. 9, p. 1025-1031. (This is a condensed version of the AIAA paper listed above.)
- \*Smedes, H. W., Spencer, M. M., and Thomson, F. J., 1971, Preprocessing of multispectral data and simulations of ERTS data channels to make computer terrain maps of a Yellowstone National Park test site, <u>in</u> summary of papers presented, Seventh Int. Symposium on Remote Sensing of Environment, May 17-21, 1971: Univ. of Michigan, Ann Arbor, Michigan.
- Swain, P. H., and Germann, D. A., 1968, On the application of man-machine computing systems to problems in remote-sensing: Purdue Univ. Laboratory for Agricultural Remote Sensing Inf. Note 051368, 10 p. mimeographed.
- \*Waldrop, H. S., 1969, Detection of thick surficial deposits on 8-14 infrared imagery of the Madison Plateau, Yellowstone National Park: U.S. Geol. Surv. open-file report, 7 p., 2 figs.
- Watson, Kenneth, 1971, Geophysical aspects of remote sensing, in Proceedings of the Int. Workshop on Earth Resources Survey Systems.
- Willow Run Laboratories Staff, 1968, Investigations of spectrum-matching techniques for remote sensing in agriculture; final report, January 1968 through

September 1968: Ann Arbor, Michigan Univ. Inst. of Science and Technology Infared and Optical Sensor Laboratory report no. 1674-10-F, 48 p. This report contains numerous pertinent references.

#### GLOSSARY OF SPECIAL TERMS USED

- Basalt lava. Fine-grained, dark colored lavas relatively rich in calcium, iron, and magnesium, and low in silica.
- Breccia (volcanic). A rock formed of compacted volcanic fragments embedded in a tuff matrix.
- Cathode ray tube. A vacuum tube that generates a focused beam of electrons which can be deflected by electric and/or magnetic fields. The terminus of the beam is visible as a spot or line of luminescence caused by its impinging on a sensitized screen at one end of the tube. These tubes are used to reproduce pictures in television receivers or to study the shapes of electric waves.
- Control data. This refers to all that is known about the site conditions, including types and distribution of materials (determined from conventional field mapping and examination supplemented by study of photographs taken from the air and ground), and measurements of such parameters as temperature, relative humidity, porosity, moisture content, and spectral reflectance of surface materials. Collectively, these constitute the control data with which the test data can be compared.
- Covariance. The manner in which one feature or parameter varies in relation to another.
- ERTS. Acronym for the Earth Resources Technology Satellite.
- Gneiss. A coarse-grained metamorphic rock in which bands rich in granular minerals alternate with bands in which platy minerals predominate. These are derived from pre-existing impure sandstone, shale, or granite during the dynamic and thermal processes involved in mountain-building.
- Kame. A mound composed chiefly of gravel and sand, whose form is the result of original deposition by settling during the melting of glacier ice against or upon which the sediment accumulated.
- <u>Maximum-likelihood</u>. The maximum probability or chance. The statistical parameters of radiance may somewhat resemble those of two (or more) different classes of material. The relative likelihood (probability or "odds") that the data in question belong to class A as opposed to class B or C is P(A)/P(B) or P(A)/P(C). When the statistical parameters are chosen so that these ratios are optimum, then the likelihood is maximum and the data are assigned to that class (A,B, or C) which has maximum probability.
- Mm. Micrometer; the millionth part of a meter. Formerly called micron.
- Rhyolite. Fine-grained, light colored lavas and other igneous rock bodies relatively rich in potassium, sodium, and silica, and low in calcium, magnesium, and iron.

- Solifluction. The process of slow downhill flowage of masses of soil and unconsolidated surface debris saturated with water.
- Till. Nonsorted, nonstratified sediment carried or deposited by a glacier.
- Tuff. A rock formed of compacted volcanic ash and other fragments generally smaller than 4 mm in diameter.

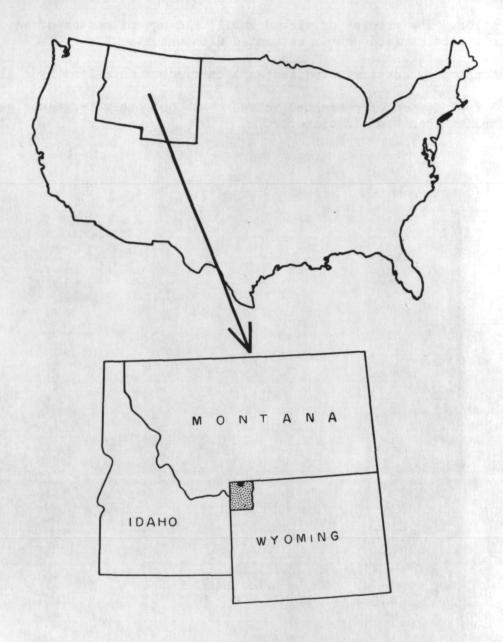


Figure 1. Index map of United States showing location of Yellowstone National Park (shaded) and the test site (black).

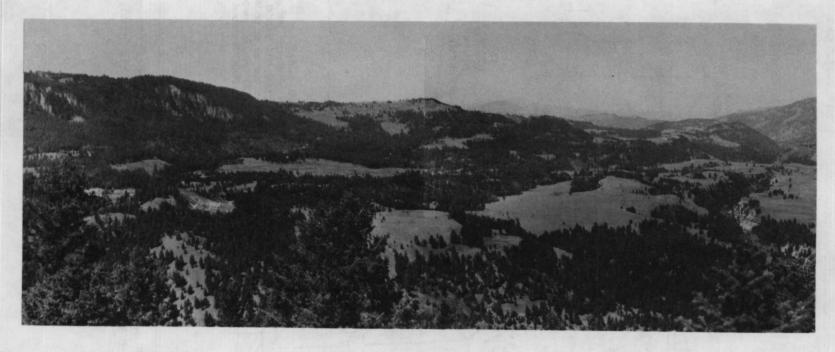


Figure 2. Panorama photo of test site looking west from near east edge. Crescent Hill is on the left edge.

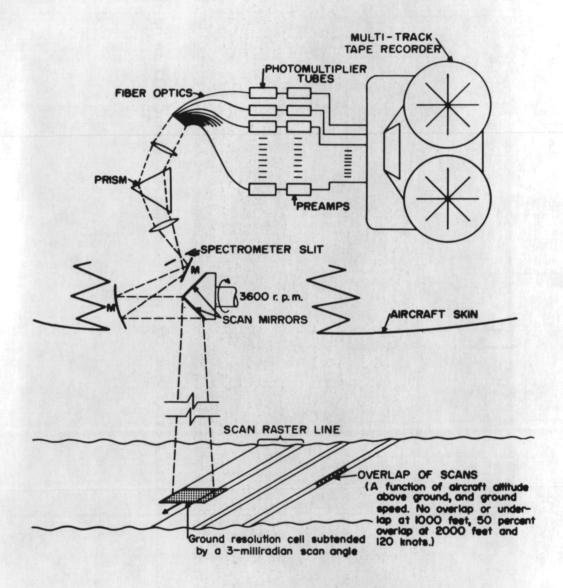


Figure 3. Diagram of optical-mechanical scanner and spectrometer used by the University of Michigan in gathering data for this study.

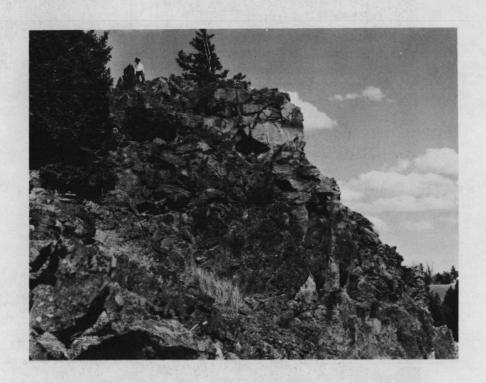


Figure 4. Bedrock exposure of basalt lava flows.



Figure 5. Talus of rhyolite tuff at Floating Island Lake. Crescent Hill is in the background.



Figure 6. Blocks of rhyolite tuff in talus showing contrast between fresh surfaces (below hammer head) and surfaces coated with dark lichens, which is what the scanner records.



Figures 7 and 8. Vegetated rock rubble. These are mixtures of angular blocks of basalt (fig. 7), bedrock slabs and blocks of gneiss (fig. 8), lichens, soil, dry grass, sagebrush, weeds, evergreen seedlings, and twigs.



Figure 9



Figure 10

Figures 9 and 10. Glacial kame meadow, showing grass, mineral soil, weeds, dead vegetation, elk manure (fig. 9) and sagebrush debris (fig. 10).







Figures 11, 12, and 13. Glacial till, showing sand, rock chips, and boulders in mineral soil, grass, sagebrush, weeds, and twigs. Wide range in texture is shown: fine-grained (fig. 11), mixed (fig. 12), and coarse-grained (fig. 13).

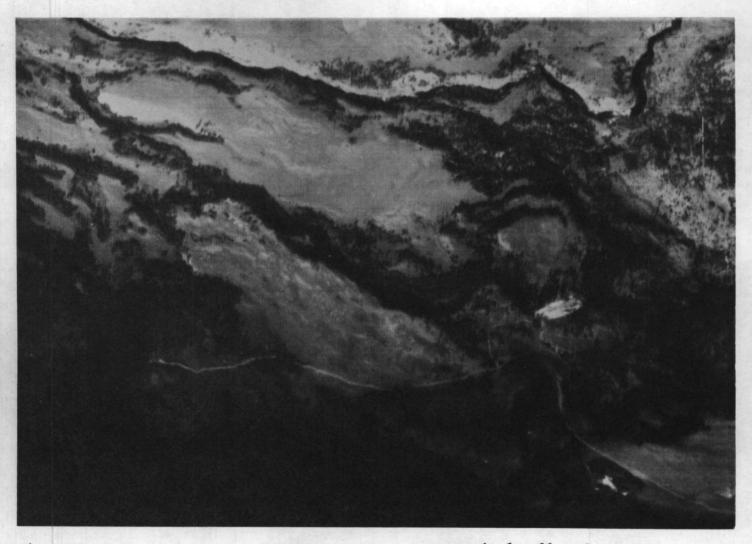


Figure 14. Gray-scale video display of radiance from channel 9 (0.62-.66  $\mu$  m). Area is same as shown in eastern parts of figures 26 thru 30.

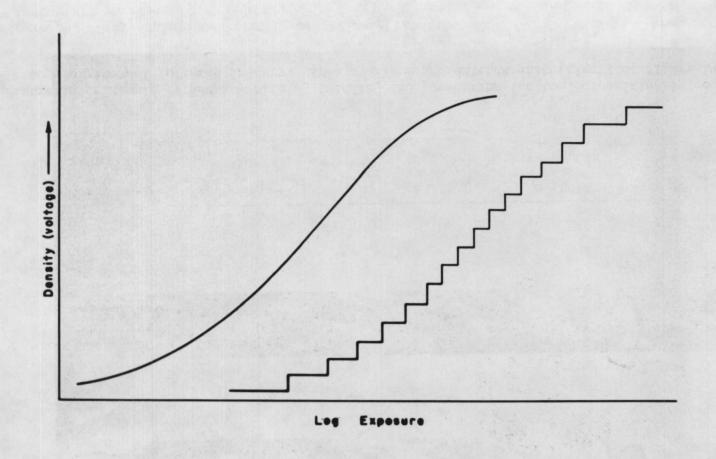


Figure 15. Example of electronic density slicing of continuous curve of film density (on the left) into discrete steps (on the right).

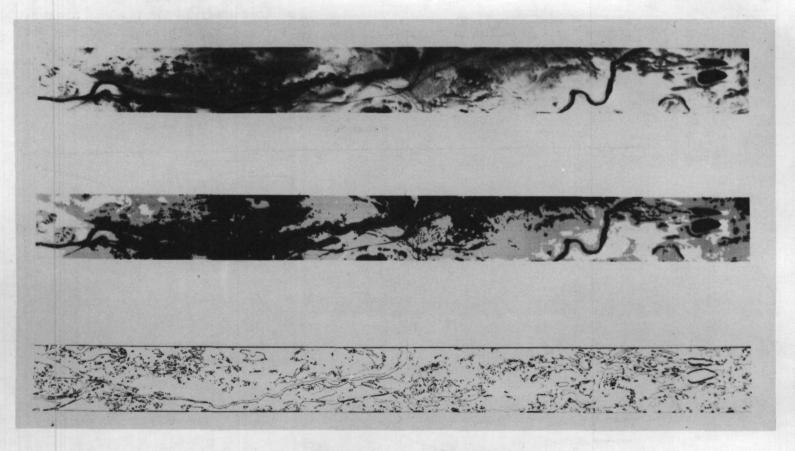


Figure 16. Example of density slicing (middle) and contouring (bottom) of originally continuous tones (top) of thermal infrared imagery. Area overlaps and extends east (right) of Figure 14.



Figure 17. Color coded quantized thermal infrared image. Temperatures, from coldest to warmest, are shown on original color print by white, blue, yellow, red, green, and black, but are portrayed by different shades of gray on this black and white copy.

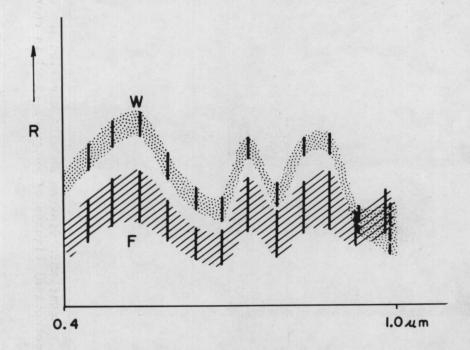


Figure 18. Radiance of water (W) and forest (F). Radiance (R) increases upward. A vertical line two standard deviations long, centered about the mean radiance, is shown for each of the 12 spectrometer channels.



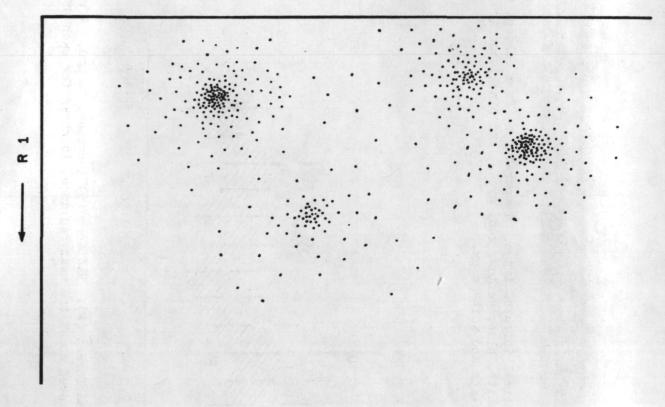


Figure 19. Covariance diagram showing distribution of radiance data for four hypothetical classes of material (A-D) in channels 1 and 2 (R1, R2).

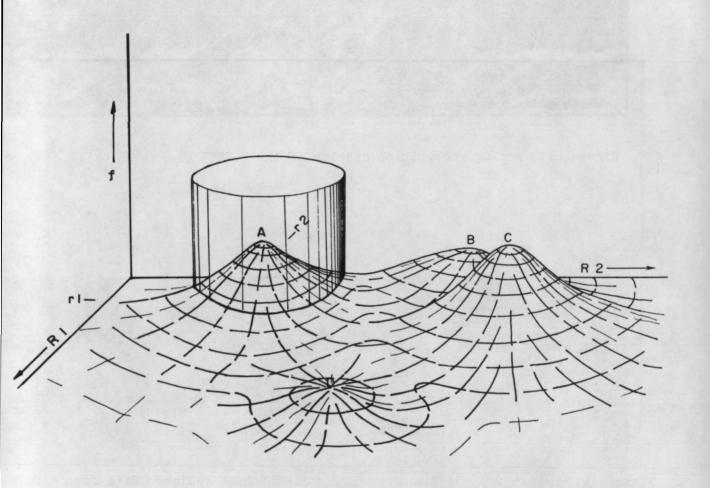


Figure 20. Frequency diagram of covariance data of same four classes (A-D) and channels (R1, R2) as in figure 19. The surface is that which bounds the distribution of data points, and is topologically equivalent to a probability surface. The cylinder indicates placement of threshold limits; for simplicity, it is shown for class A only.



Figure 21. Analog recognition display of the FOREST class (white).



Figure 22. Ten-level gray-scale digital computer display of radiance from channel 9 (0.62-.66  $\mu$  m), as obtained by University of Purdue. Area shown is the bottom (south) half of that shown in Figure 14.

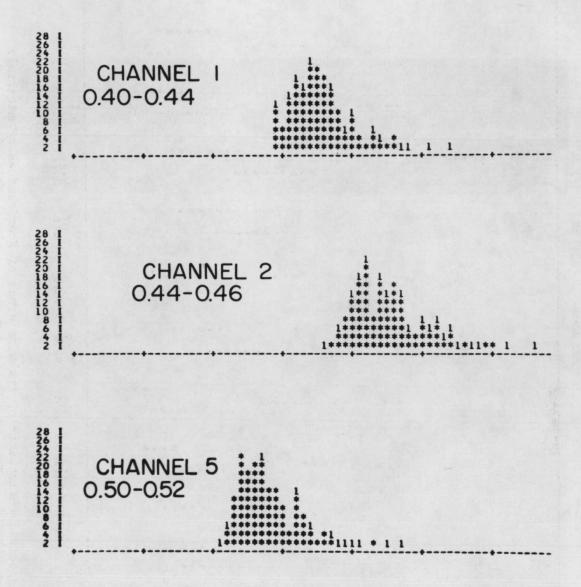


Figure 23. Histograms of reflectance of talus in channels 1, 2, and 5. The abscissa is relative radiance (brightness), increasing to the right. On this copy of the computer printout, the ordinate gives the number of resolution elements with a given relative radiance. Band width of each channel given in micrometers.

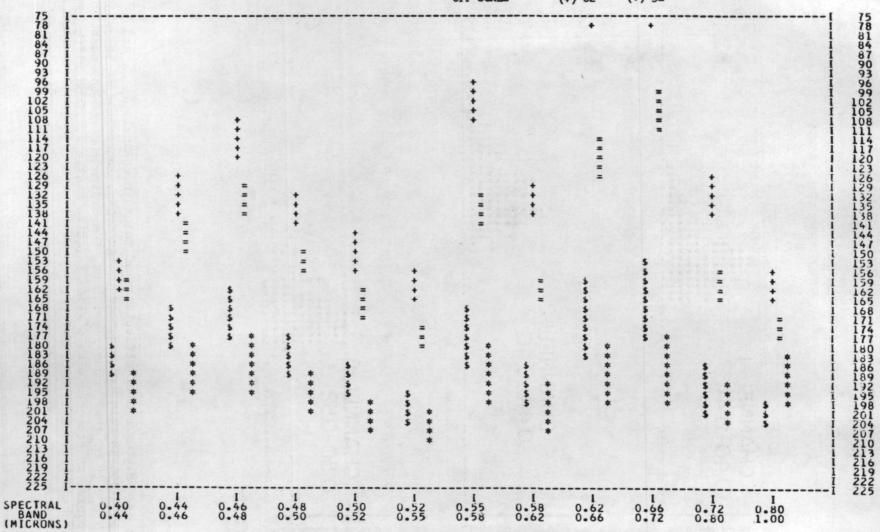


Figure 24. Comparisons of spectral reflectance of training areas of four classes of material: \$ Talus, + Vegetated rock rubble, = Kame, \* Forest. Reflectance or radiance, increasing upward, is shown for each of the 12 channels of the Michigan scanner data. A vertical line two standard deviations long, centered about the mean radiance, is drawn using alphanumeric symbols.

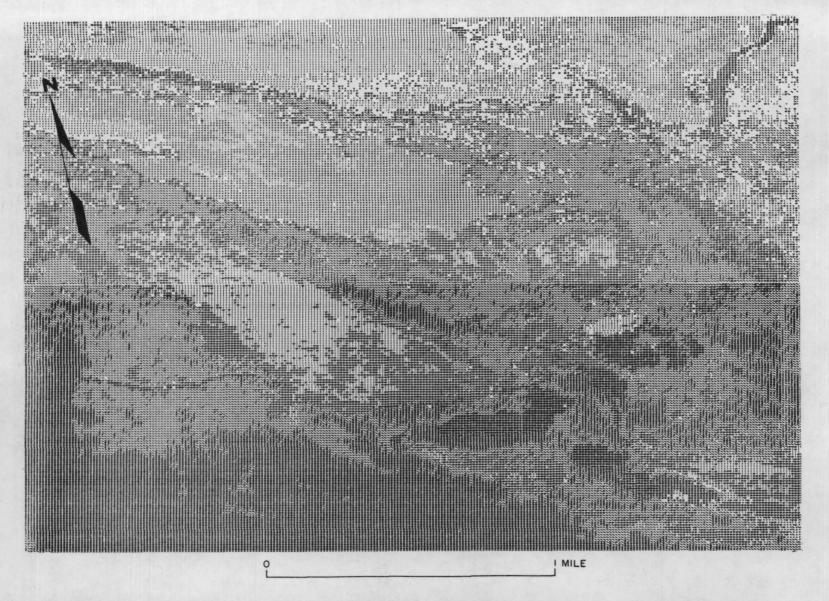


Figure 25. Segment of terrain map obtained by using Purdue University's digital computer-selected best set of four channels of radiance data. Symbols used to designate the terrain classes are:

. Bedrock Exposures, \$ Vegetated rock rubble, - Glacial till meadows, : Bog, H Shadows, 8 Talus,

= Glacial kame meadows, / Forest, W Surface water, (Blank) Rejected.



Figure 26. Segment of terrain map obtained by combining one thermal infrared and three reflective channels of data. Symbols used to designate the terrain classes are the same as in figure 25 (water and bedrock are not present in this display). Because the scan angle of the thermal scanner was much narrower than that of the reflective scanner; this display covers only the middle strip of those shown in figures 25, 27, and 28.

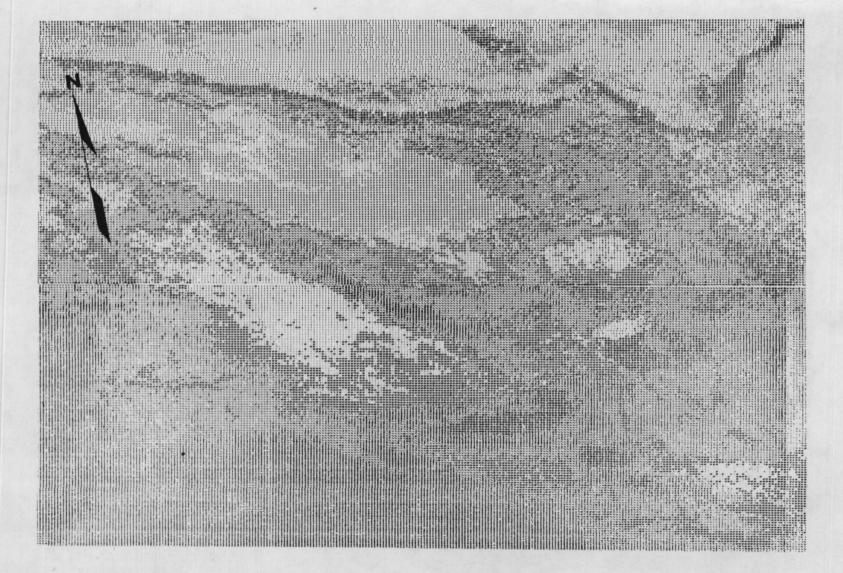


Figure 27. Segment of terrain map obtained by using simulations of ERTS 3-RBV camera data. Symbols used to designate the terrain classes are the same as in figure 25.

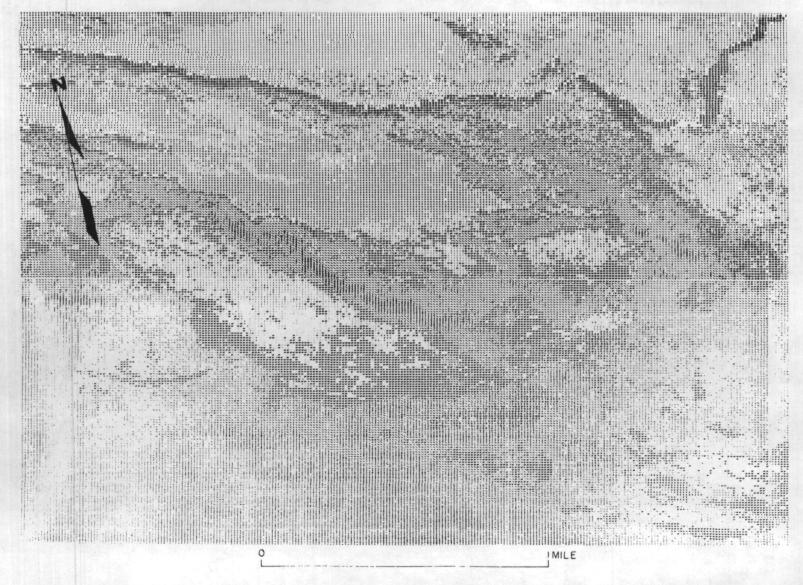


Figure 28. Segment of terrain map obtained by using simulation of ERTS 4-channel scanner data. Symbols used to designate the terrain classes are the same as in figure 25.

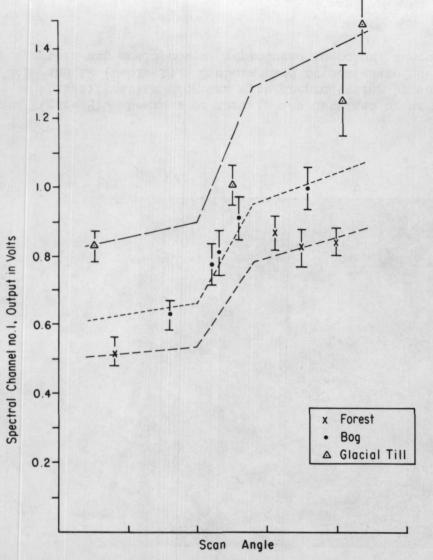


Figure 29. Spectral channel output versus scan angle for three classes, showing the scan angle functions. Each vertical bar is two standard deviations long, centered about the mean.

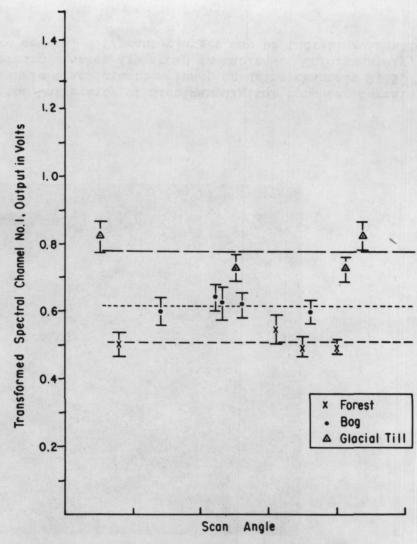


Figure 30. Transformed spectral channel output versus scan angle for three materials, showing mean values of combined (transformed) signatures. Each vertical bar is two standard deviations long, centered about the mean.



Figure 31. Segment of terrain map obtained by using the University of Michigan digital computer terrain classification programs with preprocessing by scan-angle transformation function using channels 2, 5, and 12 (table 1). Symbols used to designate the terrain classes are shown in table 4. Unfortunately, this map could not be reproduced in color; therefore several different classes may be indistinguishable.



Figure 32. Segment of terrain map obtained by using the University of Michigan digital computer terrain classification programs with preprocessing by ratio transformation using simulated data of the ERTS 4-channel scanner. Symbols used to designate the terrain classes are shown in table 4.



Figure 33. Computer-generated terrain map of entire test site, produced by University of Kansas using spatial clustering techniques.

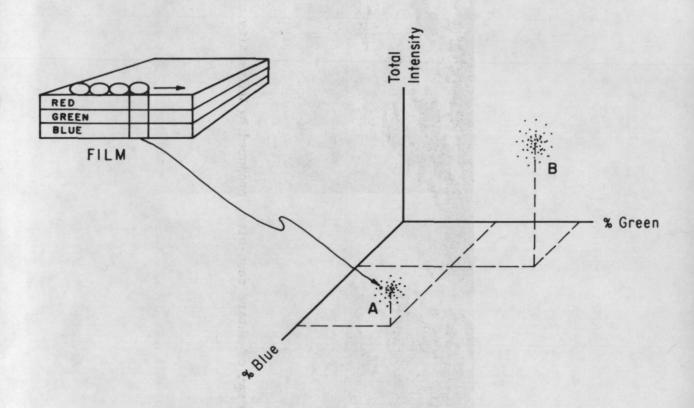


Figure 34. Schematic diagram showing scanning of color infrared aerial film and the distribution of the density data from the three film layers in three-color space. Four successive resolution cells along the microdensitometer scan direction are shown. Hypothetical clusters A and B represent two classes whose means have coordinates indicated by the dashed lines. The arrow indicates the plotted position of density data for one of the resolution cells, which falls within the cluster of class A.

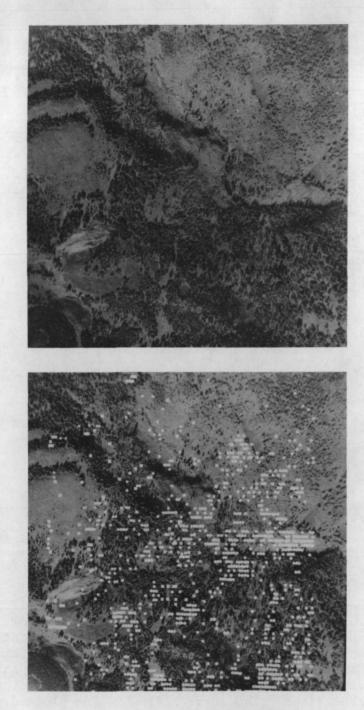


Figure 35. Black and white copy of color infrared aerial film used in the clustering study (top image) showing two of the terrain classed derived by computer processing as white circles (deciduous trees) and squares (bedrock of basalt and amphibolite).

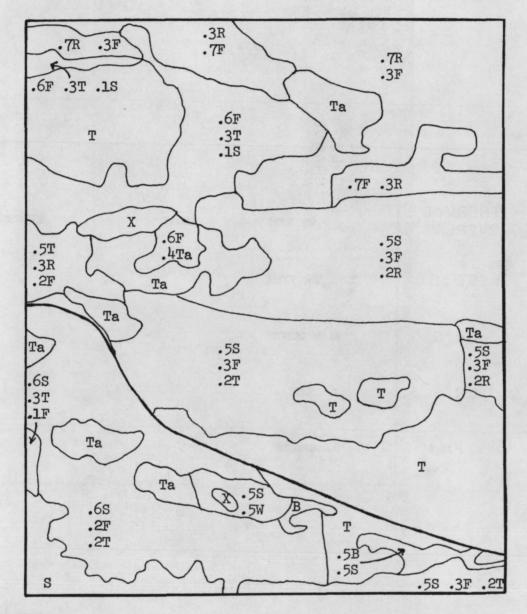


Figure 36. Segment of ground-control map, southeast corner of test site.

Numbers indicate decimal proportion of classes present in each outlined area. Classes are indicated by letters:

- T glacial till meadow
- Ta talus
- F forest
- R vegetated bedrock rubble
- X bedrock
- W water
- S shadow
- B Bog

The dark line is a road

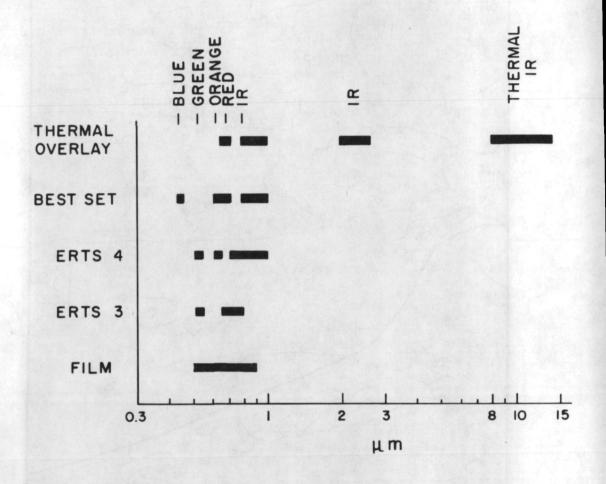


Figure 37. Comparison of wavelength bands used in the computer studies.

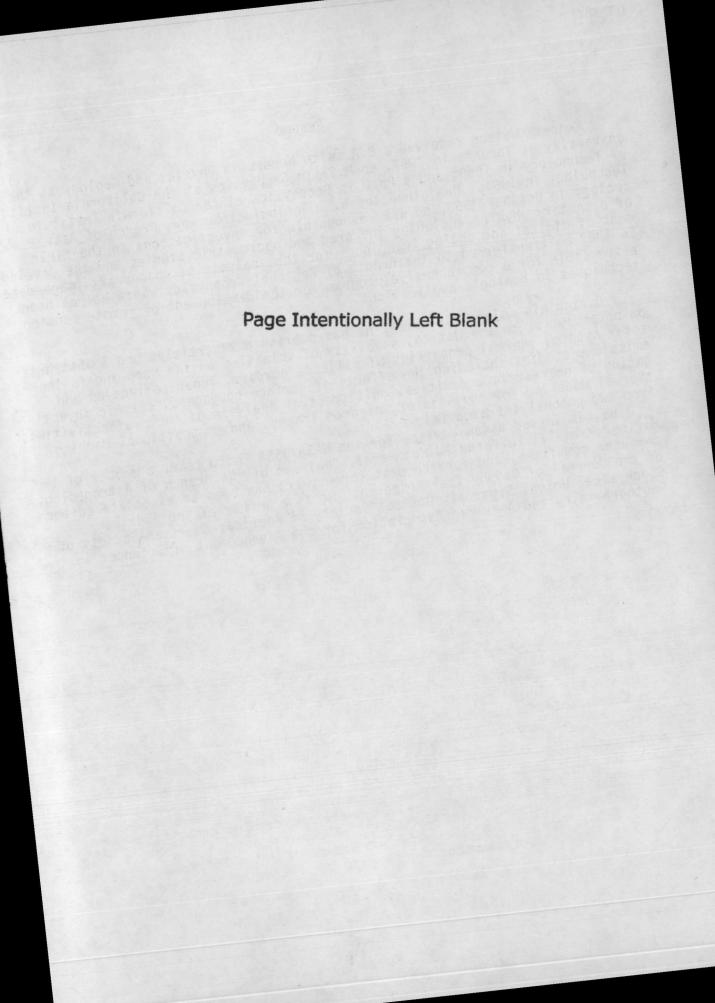
THERMAL OVERLAY: four channels were combined and overlaid by the computer to make a single set of data from three scanner systems, using one reflective and two thermal scanners.

BEST SET: computer-selected best set of four reflective channels of data from the 12-channel scanner.

ERTS 4: simulation of the ERTS 4-channel scanner data.

ERTS 3: simulation of the ERTS 3 RBV camera data.

FILM: use of the three emulsion layers of color infrared film as a 3-band spectrometer for mapping by clustering techniques.



# Resumé

Kenneth Watson received a B.A. with honors in Physics and Geology at the University of Toronto in 1957, an M.S. in Geophysics at the California Institute of Technology in 1959, and a Ph.D in Geophysics at the California Institute of Technology in 1964. He joined the U.S. Geological Survey, Branch of Astrogeology in October 1963 and was responsible for investigations in the field of planetary physics including infrared and photometric studies and the development of digital and analog techniques for the analysis of spacecraft image data. In 1967 he transferred to the Branch of Regional Geophysics where he has been responsible for a comprehensive program for the development of remote sensing techniques in geologic applications.

During his scientific career he has published 27 articles and 5 abstracts on potassium-argon age dating, stability of volatiles on the Moon and in the solar system, thermal properties of silicate powders, lunar reflection and emissions studies including the effects of surface roughness, seismic investigation of near-surface cavities, multispectral analysis of rock reflectivities, thermal modeling for analysis of infrared images, and compositional mapping from two-channel infrared imagery.

He has served as an advisor for the NASA/OSSA Photo team, a member of the Mariner Mars '71 Infrared Ad Hoc Panel, Chairman of the Branch of Astrogeology computer committee, and for the past three years has been an associate editor of the Journal of Geophysical Research. He is a member of the American Geophysical Union, Sigma Xi, Optical Society of America, American Society of Photogrammetry and American Association for the Advancement of Science.

Geophysical Aspects of Remote Sensing 1/

by Kenneth Watson U.S. Geological Survey Denver, Colorado

#### Introduction

Our ability to budget the natural resources of this planet will determine, in large measure, the course of future civilization. We must develop new resources for the needs of an expanding society and, at the same time, extract and use our current resources with greater concern for the damage that can be inflicted on our environment. Remote sensing techniques provide a means to explore for new resources and to identify the sources of environmental destruction.

The study of large regions of the Earth's surface is now feasible through the use of satellites. It is possible to observe how the surface reflects, stores, and reradiates solar energy. Techniques are also available to illuminate the ground, using controlled energy sources, and to record the reflected energy. Finally, we can remotely sense the interior of the Earth by measuring its gravitational and magnetic fields.

Remote sensing observations are made by using a variety of detectors ranging from simple photographic films to complex devices such as spectrometers, gravimeters, and multispectral scanners, all with the disarmingly simple goal of measuring electromagnetic energy or force fields. Techniques for data analysis are equally diverse, ranging from conventional photointerpretation to the use of a host of electro-optical devices and high-speed digital computers.

But the most important ingredient in the use of remote sensing to solve our resource problems must still remain our ability to interpret correctly new observations on the basis of previous experience. In mathematical theory this ability should be axiomatic, in the physicist's laboratory it may be a rational extension of physical laws, but in nature it is truly astonishing! When you consider the seemingly infinite variety of materials, natural settings, and climatic conditions it is difficult to believe that results obtained at one area under one set of conditions could have any application to a new area under a different set of conditions.

There are basically two different approaches to this problem. One can attempt to remotely sense many materials under many conditions and hence derive, by empirical relationships, a basis for interpreting remote sensing observations of a poorly known area. A number of statistical techniques can be applied to quantify the empirical relations and to automate some of the analysis procedure using computers to "recognize" similar relationships. In some cases, where well-defined problems and good observations occur, this approach has led to fundamental discoveries in physics. Examples include Newton's law of gravitational

attraction which was derived from the empirical laws of Kepler describing planetary-motion observations and Planck's empirical formula derived to explain blackbody radiation. This led to his discovery of quantum physics.

But, when observations are made not to establish new physical laws but, rather, to discriminate and identify different materials it is more appropriate to base the approach on contemporary scientific principles than on empirical relations. In order to apply these principles in a systematic manner we must start with well-defined problems and a small number of variables, progressing logically to more complex situations. In science one of the most useful techniques to apply, in this kind of approach, is a "mathematical model." Model, in this context, refers to a simplified abstraction of a physical object.

For some purposes we might wish to model the Earth as a flat multilayered object, for others as a rigid sphere or as a point mass. The fact that these entirely different models are used to describe the same physical object does not mean that one is more precise than the other but rather that different physical processes are being studied. Thus a flat layered Earth model may be perfectly appropriate to study explosion seismology but quite inappropriate for satellite orbital mechanics. A rigid sphere might be quite useful to model lunar eclipses but utterly irrelevant to discussions of elastic wave propagation. Models provide a means to consider a problem with only a small number of key variables so that their importance can be evaluated for predicting other phenomena. In essence the test of a model is how well it can explain the observations.

One further question concerning models that bears consideration is: How complicated should a model be? The question is important, because it affects the complexity required in analysis and the type and precision of measurements which will have to be made. The most effective way to handle this problem is to develop an iterative model that is initially chosen to be very simple; that is, with only a few variables. In gravity analysis the initial model might be a point mass; in heat-flow analysis, a flat homogeneous solid heated by a regularly varying energy source. By starting with an elementary model which only grossly matches the preliminary observations and continually increasing its sophistication as new observations are made we can use a systematic approach in developing our iterative model. This technique also suggests the desirability of selecting the field test areas in the same manner as the iterative approach: starting with areas which are relatively simple and progressing to more complex areas which present a great diversity of problems.

In summary then, an effective approach in applying remote sensing techniques to resource studies is to start with observations of simple areas, analyze the results in terms of simple mathematical models which are based on scientific principles, and iteratively increase the complexity of the models and sites in a systematic manner. This approach, which I will call the "geophysical method", has been successfully applied in traditional geophysical studies of seismology, gravity, magnetism and electromagnetic induction. It should be equally appropriate to the latest remote sensing techniques involving the measurement of the reflection and emission of electromagnetic energy from terrain.

#### Problem Area

The long-range goal of the U.S. Geological Survey in remote sensing is to develop techniques which augment traditional field observations in order to provide a more complete understanding of the geologic resources of the United States. A new unit was established within the Geological Survey in 1968 to investigate remote sensing as a geophysical technique applied to geologic mapping and interpretation (Watson, 1971). Our initial approach has been to select field areas for remote sensing observation which display common rock types with good exposure and little vegetation cover. Through the use of mathematical models we then planned to evaluate the discrimination of these rock types and their structural and stratigraphic setting based on physical-property differences and also to evaluate the influence of some important variables associated with the atmosphere and the surface state. We then planned to extend the models to other common rock types and, in a systematic manner, to more complex rock types and geologic settings.

For the purpose of this discussion the results from our most intensively studied site, at Mill Creek, Oklahoma, are described in detail. Common rock units exposed in this area are relatively pure dolomite, limestone, sandstone, and granite (figure 1). A detailed study of the stratigraphic relations of the area (Ham, 1955) provided us with geologic information necessary in the analysis of remote sensing observations. In addition to conventional information recorded for geologic analysis it was necessary to observe the surface state of the geologic materials to a degree commonly ignored in conventional studies. Electromagnetic reflection and emission depends not only on conventional rock properties such as color, topographic expression, and composition, but also on surface roughness, lichen, plant, and tree cover as well as chemical and vegetative staining.

We planned to use remote sensing observations of the Mill Creek area to test whether we could measure differences between three common rock types that could be used to develop models for discrimination of rock types in unknown areas. We also wished to examine the application of remote sensing to structural and stratigraphic analysis and its potential for identification of rock types.

Perhaps I should explain what I mean by identification versus discrimination of rock types and why this represents an important concept in remote sensing. Discrimination means recognizing the difference among rock types, i.e., one unit, A, is different from another unit, B. Identification means labeling the rock type, i.e., unit A is granite and unit B limestone. The actual process is really one of degree of confidence, with identification and discrimination representing the end members. The recognition of rock types from remote sensing observations is a complicated process which is performed at a number of different confidence levels. This approach is a familiar one in conventional geologic studies. Rock types can be identified directly from standard petrographic analysis; indirectly, from infrared spectroscopy by relating molecular resonance to crystal species; inferentially, from physical property measurements of, for example, density, thermal inertia, and dielectric constant; or presumptively, from topographic expression or vegetative cover. Thus as the level of confidence in the approach decreases, identification of rock types requires a greater

understanding of the limitations of the methods and more detailed knowledge of the geologic environment.

Because our initial interest at Mill Creek was to discriminate rock types, we chose as our prime experiment the observation of ground thermal emission by means of an infrared scanner. We hoped to be able to see temperature differences among the rock types that would be attributable to differences in their thermal properties. We also planned to observe the reflection of solar radiation in the visible and near infrared, the spectral emission in the infrared and microwave, and the reflection of radar energy. These observations, which are dependent on other physical properties, would then provide a consistent framework for development of additional models. It would then be possible to examine a variety of remote sensing techniques under controlled conditions and in a systematic way. Thus we would develop a group of models which can be used individually to discriminate rock types and define their stratigraphic and structural settings, collectively as a potential tool for rock-type identification, and which could be extended to other areas of geologic interest.

# Mission Objectives and Results

Because the initial remote sensing flights of the Mill Creek area (Mission 84) were to be flown as part of the larger overall objectives of the NASA Earth Resources Aircraft Program which include many disciplines, the mission flight parameters had to be planned several months in advance of the actual overflight. We decided to limit this initial flight to survey coverage with primary emphasis on photographic and thermal infrared scanner data. Several flight lines were selected over key areas so that images would have contiguous edges but virtually no overlap. A flight altitude of 1800 m above mean terrain was selected to insure reasonable useful resolution on the infrared data. Flight times were selected that seemed a reasonable compromise to obtain maximum utility from thermal and photographic data during the daytime and optimum thermal contrast at night: midmorning, midafternoon, and predawn.

In addition images, multiband photographs, and microwave line scan data were requested. This information was considered useful for examining the application of spectral reflectivity to characterize rock types and for determining albedo which would be necessary in the thermal analysis (albedo of a surface is a number equal to the fraction of incident sunlight which it reflects), and for comparing microwave and infrared temperatures over a diurnal cycle. Instrument operational problems during the flight and lack of data analyses facilities were later to restrict severly the use of these data.

In support of the overflight measurements we also planned a number of ground observations to calibrate the aircraft data and to measure additional parameters for thermal modeling. Later data analysis illustrated some of the limitations of this initial ground data recording, including the need to investigate more fully the density of "point" ground measurements, the difficulty of comparing measurements made at different scales, and the need to monitor continuously the relevant atmospheric parameters for several days before the actual overflights.

Despite the preliminary nature of the initial overflights, the results were extremely promising (Rowan and others, 1970). The infrared data in particular contained significant stratigraphic and structural information. relatively pure limestone and dolomite of the test area can be differentiated in the predawn infrared images, and facies changes between them can be detected along and across strike (see figure 2). The daytime images display much stratigraphic and structural detail (see figure 3). Small-scale bedding detail is enhanced in the morning images of areas of low elevation difference, and contrasts of alternating formations that form ridges and valleys are enhanced in the afternoon images of areas of high elevation differences. The difference in features displayed in morning and afternoon images appears to be a function of the insolation (solar flux at the ground) on sunward and shadowed slopes of differing scale. Fault or fracture zones are best displayed in the predawn image; they appear cooler than surrounding ground, because of greater water content and concomitant evaporation. The abundance and throughgoing nature of lineaments (which coincide for the most part with joint systems) are more obvious in the infrared images than in aerial photographs. Lineaments striking northwest are preferentially enhanced in the morning images and lineaments striking northeast are preferentially shown in the afternoon images.

# Data Analysis

The interpretation of remote sensing observations obtained to study Earth resources is complicated by both the number and the magnitude of factors which affect the signal received by the detectors. The use of simple mathematical models, which are based on scientific principles, is essential in the application of the "geophysical method" to these observations. Correlations between selected variables can be found, assumptions about suspected major factors can be tested, and unsuspected factors can be discovered and analyzed. To illustrate this point more fully a case history example is presented describing the modeling of thermal emission data obtained at the Mill Creek, Oklahoma, test site (Watson, 1971).

A simple initial model which describes the diurnal heating and cooling of the ground can be selected in the following manner. Let us consider the sinusoidal heating of a semi-infinite solid with homogeneous thermal properties. Then the flux into the ground F can be written as

where  $F_0$  is the flux at time t=0 for a periodic function with a time periodicity  $T=2\pi/w$ . The time t=0 will correspond to the time of maximum heating, local noon, and the period T is 1 day. The surface temperature V for this periodic flux (Carslaw and Jaeger, 1959, p. 68) can be derived from the equation of heat conduction and is

$$V = \frac{F_0}{K} \sqrt{\frac{k}{w}} \cos (wt - \pi/4)$$

where k is the thermal diffusivity and K the thermal conductivity of the homogeneous solid. For convenience we shall introduce a parameter, P, called the

thermal  $P = K / \sqrt{k}$ . Using a single quantity is clearly more convenient than the ratio of two quantities. Thus, we can write

$$V = \frac{F_0}{P\sqrt{W}} \quad \cos (Wt - \pi/4).$$

From this simple model we recognize an important parameter in characterizing terrain: the thermal inertia. The model also implies that materials with high thermal inertia have a smaller amplitude and hence they heat and cool less than materials with low thermal inertia. This behavior illustrates why P is called the thermal inertia.

But the model has some obvious limitations. It assumes that all materials are heated in the same manner, ignoring the fact that dark materials which have low albedos absorb more solar energy than light materials which have high albedos. In order to treat this phase of the problem more precisely we must first examine the insolation. If atmospheric transmission effects are ignored, the insolation, I, is proportional to the cosine of the sun's zenith angle, Z, which is the angle between the sun and the zenith.

$$I = I_0 \cos Z$$

where  $I_0 = Solar Constant$ 

A simple formula describes the change of sun's zenith angle with time for different latitudes and seasons (sun's declination).

 $\cos Z = \cos \lambda \cos \delta (\cos wt + \tan \lambda \tan \delta)$ 

where

 $\lambda$  = local latitude

 $\delta$  = sun's declination

Our new model for the flux absorbed by the ground during the daytime is expressed as

$$I = I_0 (1 - A) \cos Z$$

where A is the ground albedo and hence (1 - A) is the fraction of the insolation which is absorbed. During the day and night the ground loses heat primarily by radiation and this term can be approximated by the Stefan-Boltzmann law which states that the total radiative flux is proportional to the fourth power of the temperature.

Thus, our simple flux boundary condition  $F = F_0$  cos wt is now replaced by one of greater utility but more complexity:

$$F = I_0 (1 - A) \cos Z - \sigma V^4$$
 daytime  
 $F = -\sigma V^4$  nighttime

Where o is the Stefan-Boltzmann constant.

Two mathematical techniques exist to solve the equation of heat conduction, subject to the flux boundary conditions described above: the method of harmonic analysis (Carslaw and Jaeger, 1959, p. 64-68; Jaeger and Johnson, 1953) and the method of Laplace transforms (Carslaw and Jaeger, 1959, p. 399-402; Jaeger, 1953). Both methods require an iterative approach (i.e., repetitively improved solutions based on an initial guess) to handle the nonlinear term V4 in the flux equation. Suffice it to say that the problem can be solved numerically using digital computers, provided that sufficient care is taken in the analysis to avoid convergence problems.

This revised model can now be applied to interpret the Mill Creek thermal observations. Values for the thermal inertia of limestone, dolomite, and granite are obtained from published data (Clark, 1966; National Research Council, 1933). Albedo values are selected partly on the basis of field measurements and partly from qualitative examination of the photographic film data. The insolation is computed for the site latitude (34.5°) and the appropriate sun's declination (-23.3°) for the December flight. The computed surface temperature variation with time for a single diurnal hearing cycle is then determined for the three materials (see figure 4). The model is then evaluated by comparing its results with the thermal images obtained at three times during the diurnal cycle. During both daytime flights no obvious contrast is apparent among the three rock types; however, the predawn contrast is striking between the warmer dolomite and the cooler limestone and granite. These observations are consistent with results predicted by the thermal model.

Several additional improvements in the model have been made to include the effects of atmospheric transmission as a function of sun's altitude, cloud cover, atmospheric heating, and topographic slope.

Some generalized conclusions can be drawn from the model results. is the most appropriate time for flights in order to show maximum thermal inertia differences because then the thermal contrast is high (see figure 5) and the insolation effects are least (see figure 6). The pronounced influence of atmospheric heating effects on the diurnal temperature range is illustrated in figures 7 and 8. As expected, the greatest temperature contrast--and hence the greatest response to the rock parameters (albedo, thermal inertia), excluding vegetation and water content effects--occurs when the insolation is great (i.e., sun's declination is equal to the site latitude and clear-sky conditions) and the sky radiation is low (i.e., low day and night effective air temperatures). To examine this obvious consequence of the model a comprehensive overflight program was performed in June 1970 at Mill Creek, Oklahoma, through the auspices of the NASA Earth Resource Aircraft Office. Although some of the features of the limestone-dolomite contrast were observed, clearly (see figure 9) the most striking features of the predawn images are the relatively warm granite outcrops. This result is not consistent with the model results using the same thermal inertia and albedo values as in the initial study for the winter flight (see figure 10). It is tempting to speculate that the differences are due solely to the insolation changes. However our reliance on physical principles restricts us to the obvious conclusion that either the thermal inertia and albedos of the rock types have changed seasonally or some transient heating event occurred. Added credence is given to the latter explanation by the observation at the overflight time of a warm airmass moving into the area. A simple model of transient heating was constructed. If we assume, for discussion purposes, that the granite has a lower thermal inertia than the limestone, the model predicts that at predawn the granite would be warmer than both the dolomite and the limestone (see figure 11). The presence of a significant lichen cover over the granite outcrops is supporting evidence for a low thermal inertia for this granite.

### Summary

Remote sensing techniques provide a means to explore for new resources and to identify the sources of environmental destruction. An extensive variety of platforms, detectors, and data analysis techniques is available but the most important ingredient is the ability to apply previous experience in the correct interpretation of new observations. An effective approach to this problem is the geophysical method which relies on observation of simple areas, analyzed in terms of simple mathematical models based on scientific principles. Increasingly complex models and sites can thus be examined in a systematic manner.

Results obtained through the NASA Earth Resources Aircraft Program at Mill Creek, Oklahoma, provide a case history example of the application of remote sensing to the identification of geologic rock units. Thermal-infrared images are interpreted by means of a sequence of models of increasing complexity. The roles of various parameters are examined: rock properties (thermal inertia, albedo, emissivity), site location (latitude), season (sun's declination), atmospheric effects (cloud cover, transmission, air temperature), and topographic orientation (slope, azimuth).

The results obtained at this site also illustrate the development of an important application of remote sensing in geologic identification. Relatively pure limestones and dolomites of the Mill Creek test area can be differentiated in nighttime infrared images, and facies changes between them can be detected along and across strike. The predominance on the Earth's surface of sedimentary rocks, of which limestone and dolomite are major members, indicates the importance of this discrimination.

#### References

- Carslaw, H. S., and Jaeger, J. C., 1959, Conduction of heat in solids (2d ed.): Oxford Clarendon Press, 510 p.
- Clark, S. P., Jr., 1966, Handbook of physical constants (Rev. ed.): Geol. Soc. America Mem. 97, 587 p.
- Ham, W. E., 1955, Regional stratigraphy and structure of the Arbuckle Mountain region, in Field conference of geology of the Arbuckle Mountain region: Oklahoma Geol. Survey, Guide Book III, pt. 2, 61 p.

- Jaeger, J. C., 1953, Conduction of heat in a solid with periodic boundary conditions, with an application to the surface temperature of the Moon: Cambridge Philos. Soc. Proc., v. 49, pt. 2, p. 355-359.
- Jaeger, J. C., and Johnson, C. H., 1953, Note on diurnal temperature variation: Geofisica Pura e Applicata, v. 24, p. 104-106.
- National Research Council, 1933, International critical tables of numerical data, physics, chemistry and technology: New York, McGraw-Hill Book Co., Inc. v. 7, 507 p.
- Rowan, L. C., Offield, T. W., Watson, Kenneth, Cannon, P. J., and Watson, R. D., 1970, Thermal infrared investigations, Arbuckle Mountains, Oklahoma: Geol. Soc. America Bull., v. 81, no. 12, p. 3549-3561.
- Watson, Kenneth, 1971, Part A, Introduction and summary, and Part B, Data analysis techniques, in Remote sensor application studies progress report July 1, 1968 to June 30, 1969: U.S. Geol. Survey Rept. USGS-GD-71-004; available from Dept. Commerce, National Technical Information Service, Springfield, Va. 22151.



Figure 1. An aerial photograph of the Mill Creek test site showing the major rock units; L-limestone, D-dolomite, G-granite. The Regan fault and a minor fault to the south are indicated with an F. North is at the top of the photograph.



Figure 2. A predawn thermal infrared image of the Mill Creek test site (Dec. 1968). It can be directly compared with the aerial photograph of the same area shown in figure 1. Geometric distortions at the sides of the image are due to the perspective of a line scanner. Note that the dolomite is warmer than the limestone and that the granite is somewhat intermediate.

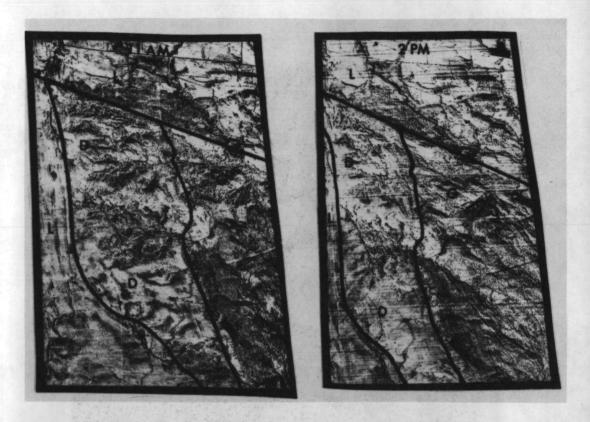


Figure 3. Two daytime thermal infrared images of the Mill Creek test site obtained at 11:00 A.M. (left) and 2:00 P.M. (right). Comparison with figure 2 illustrates that the limestone and dolomite are indistinguishable from each other. Lineaments (which coincide for the most part with joint systems) are more obvious in the infrared images than in aerial photographs. Lineaments striking northwest are preferentially enhanced in the 11:00 A.M. image (see region near left-hand L) and lineaments striking northeast are preferentially shown in 2:00 P.M. image (see region near bottom D).

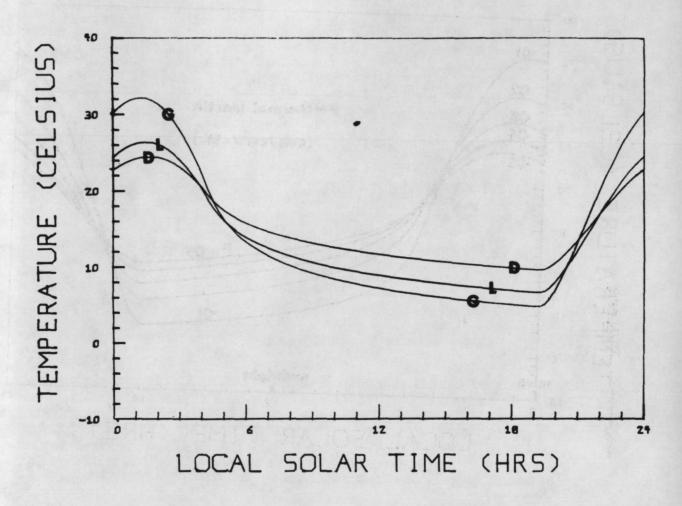


Figure 4. The computed surface temperature variation with time for a single diurnal heating cycle in December for three materials; L-limestone, D-dolomite, G-granite. Values for the thermal inertia and albedo were determined from published data, field measurements, and qualitative examination of the photographs. The model results are in qualitative agreement with the thermal images shown in figures 2 and 3. Noon is at 0 hours and midnight is at 12 hours local solar time.

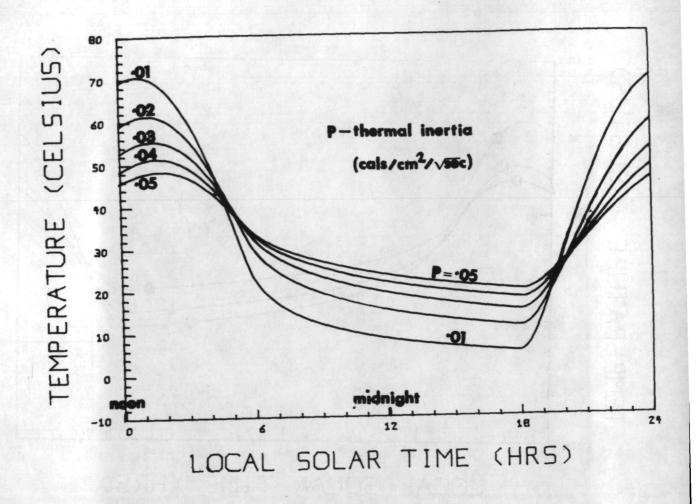


Figure 5. The computed surface temperature variation with time for materials with various thermal inertias. Note that materials with high thermal inertias go through a smaller temperature change from day to night than materials with low thermal inertias.

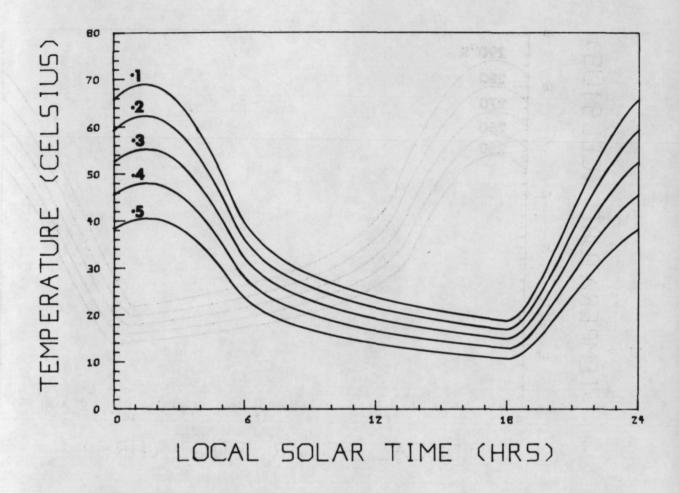


Figure 6. The computed surface temperature variation with time for materials with various albedos. Note that the temperature contrast between materials of different albedos is greatest during the daytime and least at dawn. Noon and midnight are as shown in figure 5.

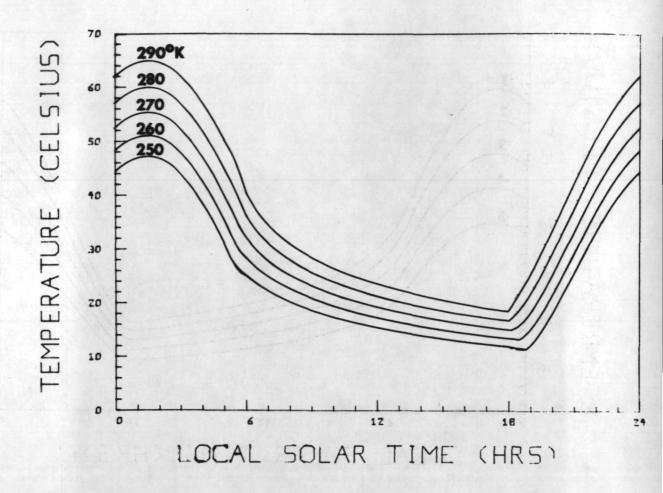


Figure 7. The computed surface temperature variation with time for daytime atmospheric heating of the ground.

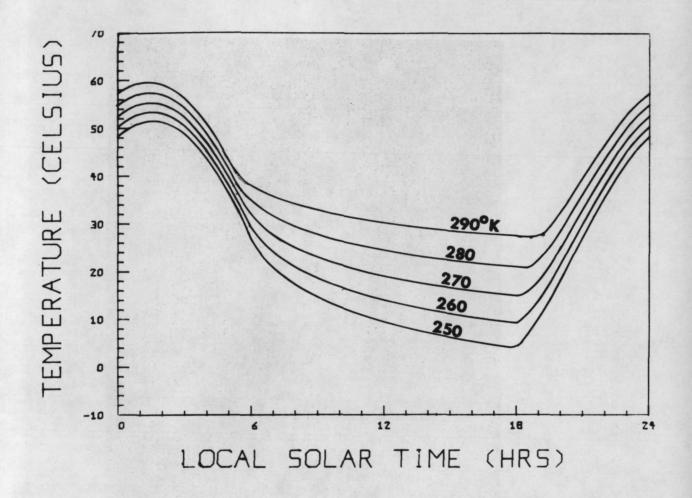


Figure 8. The computed surface temperature variation with time for nighttime atmospheric heating of the ground.



Figure 9. A predawn thermal infrared image of the Mill Creek test site (June, 1970). Contrast with the Dec. 8, 1968, results in figure 2. The most striking features are the relatively warm granite outcrops (G) in the June image. L, limestone; D, dolomite.

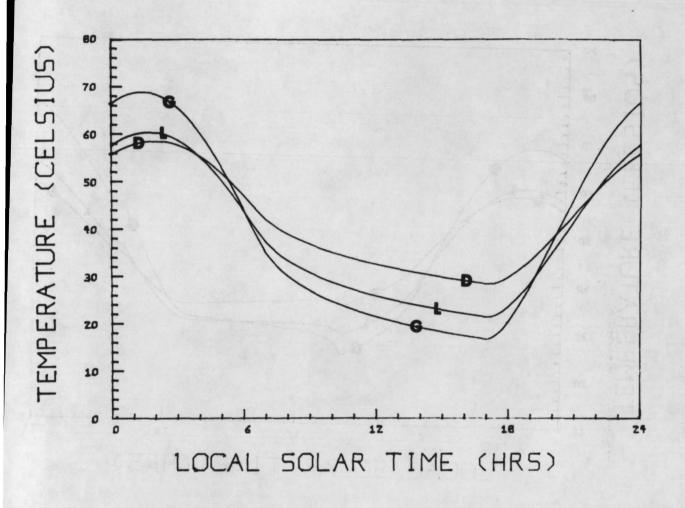


Figure 10. The computed surface temperature variation with time for a single diurnal heating cycle in June for the three materials: L, limestone; D, dolomite; G, granite. Compare with figure 4 to see the effects of the increased insolation during the summer flight.

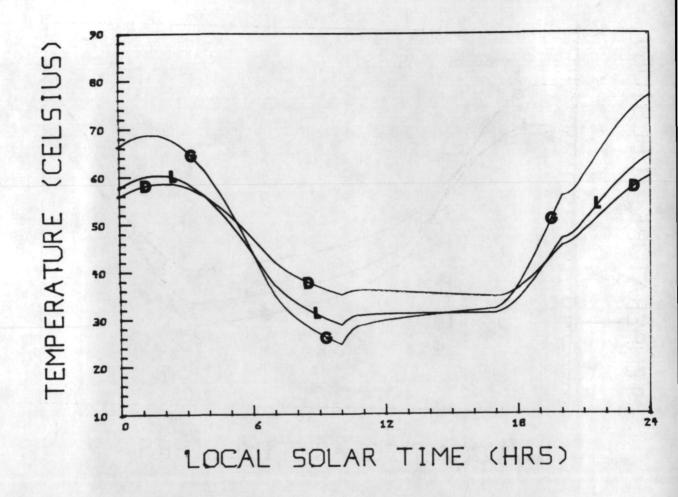
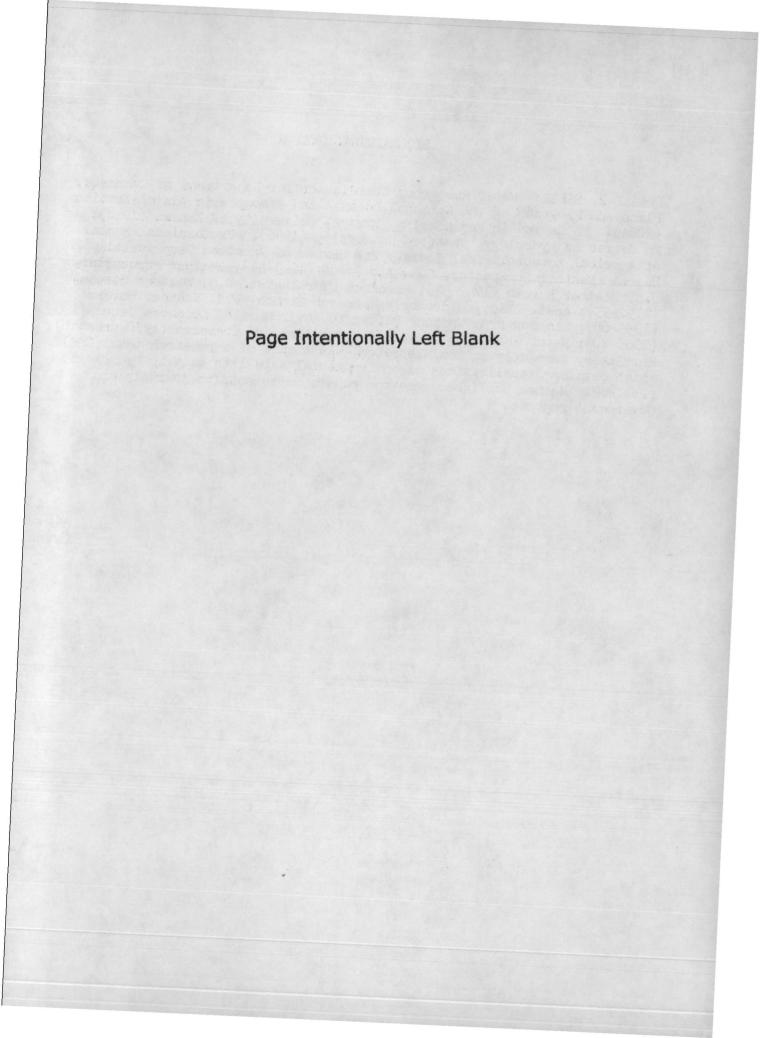


Figure 11. The computed surface temperature variation with time as in figure 10 but modified for impulsive heating at 10 hours local solar time which coincides approximately with the entry of warm air into the test site. Note that near dawn the granite (G), because of its low thermal inertia, is warmer than the dolomite (D) and limestone (L).



#### BIOGRAPHICAL SKETCH

DONALD R. BAKER: Water Resources Coordinator for Department of Commerce, Plans and Programs of the National Oceanic and Atmospheric Administration (NOAA). BS degree in Engineering Physics, University of Kansas (1948); MS degree in Hydrology, Stanford University (1968). Professional Member of Americal Meteorological Society and Member of American Geophysical Union. Weather Forecaster, U.S. Air Force (1943-46); Weather Forecaster, U.S. Weather Bureau (1949-52); Research Hydrologist, U.S. Weather Bureau (1952-55); Asst. Chief, Hydrologic Research Branch, U.S. Weather Bureau (1955-68); Liaison from Weather Bureau to Environmental Sciences Group (ESG) (1968-70); Water Resources Coordinator for Dept. of Commerce (1970-present). Mr. Baker, currently an administrator, was a part of a research team (ESG) which developed applications of environmental satellite data to hydrologic problems. He has published numerous papers in scientific journals and Government reports.

by Donald R. Baker

National Oceanic and Atmospheric Administration, U.S. Department of Commerce

# 1. Introduction

Large scale mapping of certain hydrologic parameters has economic and scientific importance to the social welfare of mankind. For example, a large proportion of the water necessary for man's water supply, power generation, and inland waterways for transportation comes from snow and ice fields. Comprehensive or repetitive survey of this and other hydrologic parameters over large areas and on a timely basis has been impractical and too expensive by conventional ground-based or airborne stations and vehicles. Given the appropriate sensors and data relay equipment, polar-orbiting and geosynchronous satellites can provide a practical means of securing and relaying such useful information to local users or to data processing and product distribution centers.

Before satellite information can be useful to hydrologists, techniques must be developed to put the data in a form suitable for hydrologic applications. Data used in developing these techniques are from NOAA's environmental satellites and National Aeronautics and Space Administration (NASA) technological satellites. In addition to the unmanned satellites' data, photographs from NASA's manned satellites, such as the Apollo 9 S-065 experiment, have been studied for familiarization with data comparable, in resolution and wavelength, to that expected from future Earth Resources Survey (ERS) satellites. The techniques discussed here are those for delineating snow fields. Essentially only two techniques will be described. First, one based on photographic interpretation; and second, an attempt to automate this delineation of snow fields by data digitization and computer processing and redisplay.

## 2. Satellites and Sensors

Orbits and altitudes are important characteristics of satellites, for it is these characteristics along with those of the sensors that largely determine the resolution and areal coverage of the data. For a single satellite, a polar orbit permits global coverage twice a day provided that the sensor's field of view allows overlap on adjacent orbits. With an Earth-synchronous orbit, a satellite can continuously monitor over one quarter of the Earth provided the sensor has both daytime and nighttime sensing capability. A brief resume of orbit characteristics of those satellites pertinent to this paper are listed in Table 1.

TA	B.	Œ	1

Satellite	Orbit	Altitude
ESSA and ITOS	Near-Polar Sun-Synchronous	1,460 km
Nimbus	Near-Polar Sun-Synchronous	1,110 km
ATS	Equatorial Earth-Synchronous	35,800 km

ESSA - Environmental Survey Satellite ITOS - Improved TIROS Operational Satellite

ATS - Applications Technology Satellite

Sensor's field of view or areal coverage, wavelength it senses, its resolution, and the method of readout are important characteristics in determining the type and amount of data that will be obtained for analysis. The first four sensors described in Table II are carried on the near-polar-orbiting satellites and the fifth sensor is a type used on geosynchronous satellites.

# TABLE II

Sensor	Wavelength	Resolution (Nominal)	Areal Coverage	Remarks
AVCS	0.45-0.65 µm	3.7 km	3150 x 2410 km	Central readout, global coverage, daytime only, daily coverage.
APT	0.45-0.65 μm	3.7 km	3260 x 3260 km	Local readout, daytime only, daily coverage.
SR	0.52-0.73 μm 10.5-12.5 μm	3.7 km 7.4 km	Continuous strip about 3200 km wide	Central and local readout, global coverage, daytime and nighttime, daily coverage.
IDCS	0.45-0.65 µm	3.7 km	2600 x 2600 km	Local readout, daytime only, daily coverage.
SSCC	0.38-0.48 μm 0.48-0.58 μm 0.55-0.63 μm	3.7 km	13,000 km diameter	Central readout, daytime only.
	AVCS - Advance APT - Automat SR - Scannin IDCS - Image I SSCC - Spin Sc			

# 3. Data and Data Handling

The details of the digitizing and computer processing of NOAA's television data have been given elsewhere, so only a brief description is given here. A sensor's signal is converted from analog to digital form and then processed in a computer so that each frame is annotated for such things as time, location, satellite, and date. Frames of data are cropped and mosaiced within the computer with each datum point representing an area of approximately 5 km on a side. Each point within the digitized mosaic gives a measure of the brightness of the Earth's background, including clouds, on an integral scale of 0 to 14. The original brightness values are for variations in response of the camera system and inequalities in solar illumination. The mosaics are mapped onto polar-stereographic and Mercator map projections.

# 4. Snow Field Delineation

There are two approaches to snow field delineation used today in the United States. The first of these is the viewing of individual frames or a daily mosaic of digitized data. These data are displayed on a cathode ray tube device and then photographed to maintain the 15 brightness levels to which they are displayed. Reliable identification of snow cover can be made by use of photo-interpretation techniques that include the following: 1) reference to concurrent cloud observations; 2) recognition of terrestrial features; 3) pattern stability (from day to day); and 4) pattern appearance.

An example of this photo-interpretative technique can be given using figures 1 and 2 (ESSA-9 digitized mosaics of 8 and 10 March 1970). In order to demonstrate the method, nine areas will be referred to:

- 1. The ice lead in Hudson Bay.
- 2. White Sands area in New Mexico.
- 3. Dendritic pattern of the snow in the Canadian and United States Rocky Mountains.
- 4. White area located where the Sierra Nevada should be.
- 5. Dark area to the north of the Great Lakes and which extends to the northwest.
- 6. Ice and snow covered Lakes Winnepeg and Nipigon.
- 7. The snow line in Northcentral United States.
- 8. The Great Lakes.
- 9. Clouds over Southern United States.

Indication of little or no clouds interfering with the view can be gained from topographical or pattern recognition of such features as 1 through 8. In photo-interpretation, knowledge of an area is an important asset. For example, the dark appearing area to the north of the Great Lakes and extending to the northwest is not an area of less snow depth, but an area of relatively dense stands of coniferous trees, which results in the darker tone. In figure 2 some of the features listed above are partially or completely blocked from view by clouds. The ice lead in Hudson Bay is not as discernible as before. The streakiness over this area is quite typical of the appearance of clouds over snow fields. In this figure, White Sands, New Mexico, is not apparent because of clouds in the area. Also because of cloud cover the appearance of the snow fields in the Midwest has changed and the Sierra Nevada snow fields are not visible. After determining which areas are clear of clouds, the snow fields can be delineated by hand compositing the snow line from several of these daily photographs into a snow map.

A second approach to snow line delineation is a technique designed to automatically screen out most clouds. Since the satellite data can be presented digitally, the data can be manipulated within a computer. Knowing that the clouds are generally transitory relative to snow cover, it has been shown that a multi-day compositing of minimum brightness (CMB) from digitized ESSA satellite data has a fair-to-good success in filtering cloud or differentiating the snow cover from the more time-dependent cloud cover. These CMB charts are composited over a selected period of days by saving only the minimum brightness observed for a given array point during the compositing period. The resulting

CMB chart is displayed in 15 brightness levels on a cathode ray film device or in the form of a computer printout in rectified form. Latitude and longitude, as well as geographic and political boundaries, are added electronically during the processing (see figure 3).

Clouds, which are often comparable in brightness to snow and ice, are retained in the CMB chart only when they are present in a given area (i.e., over a particular array point) everyday of the compositing period.

The positioning of snow lines derived from CMB charts has been verified by comparing with snow lines derived from ground observations. The verification showed that this method is very effective for the Great Plains and relatively unforested areas in the Midwest, but rather less so in areas of heavy, coniferous forest.

Figure 3 is a five-day composite of minimum brightness. It includes the data that are presented in figures 1 and 2. Note the ice lead in Hudson Bay, the ice-covered lakes of Winnipeg and Nipigon, the appearance of White Sands, and the disappearance of the bright areas (clouds) in Florida (figure 1) and Texas (figure 2). These are all indications of the ability of the CMB technique to filter clouds from the scene. Further confirmation of cloud filtering is the appearance of the Sierra Nevada snow fields in the CMB. The bright areas in Canada and the United States are snow fields, and it is relatively simple to determine their areal coverage as part of the computer processing.

Preliminary studies leading to computer evaluation of the fraction of the basin covered by snow have been made in the Western Mountain States. To evaluate how well one might expect to do, a comparison was made between satellite photography and aerial survey data. The percentage of basin covered was evaluated by planimetering aerial values of snow cover. Also, percentages of snow cover were computed using maximum resolution of ESSA photographs. When the two percentages of basin covered were compared for several basins in the Southern Sierras, they differed by 5 percent or less. The mean difference in snow line elevation computed from the corresponding satellite and aerial survey for one specific (but typical) basin was about 150 meters. Where snow mapping by satellite is more difficult because of more forest area, narrower basins, and more cloud cover (for example in the Upper Columbia River Basin), the results were not as good. Nevertheless, for several test basins the mean difference in snow line evaluation from satellite data and that measured by aerial survey was less than 300 meters. The snow line was consistently estimated from satellite to be higher than aerial survey measurements, probably due to the effects of dense forests.

# 5. Future Satellite Data

Whereas the snow field evaluations discussed above were made using 3 to 5 km resolution data, there are future satellites (by 1972) that will have sensors capable of 1.5 km to 100 meter resolution. In anticipation of this type of data, photographs with comparable resolution and spectral bandwidths to that expected on future satellites were obtained from the S-065 experiment on Apollo 9. Figure 4 is such a photograph; it shows the snow cover on the Mogollon Rim north of Globe, Arizona. The wavelength interval is from 0.59  $\mu$ m to 0.72  $\mu$ m, and the ground resolution is approximately 100 meters. The picture presents an

area of approximately 285 km on a side. A comparison of this photograph with others taken of the same area at the same time, but with different spectral intervals, indicates only a slight preference of one spectral bandwidth over another for snow line delineation.

From the detail of the snow line seen in figure 4, it is apparent that snow line mapping from ERS satellites will be more comparable to that now done from aerial observations. Furthermore, identification of small clouds over snow field may be done more readily by identifying shadow of clouds. See shadow of small clouds toward lower right corner of figure 4.

# 6. Concluding Remarks

Considerable effort has gone into snow line delineation using available satellite data. Furthermore, increasing emphasis is being put on automated extraction of such information and generation of a useable product for hydrologists. Although nothing has been said, the implications are clear that the impact from future satellite and sensor systems will create an increased demand for computer processing before the data can be used by the hydrologist. If the coarse-resolution, broad spectral band data available from current satellites already create a demand by hydrologists for computer processing of the data, it is obvious there will be an even greater demand for computer analysis and evaluation when the future ERS data represented by figure 4 become available.

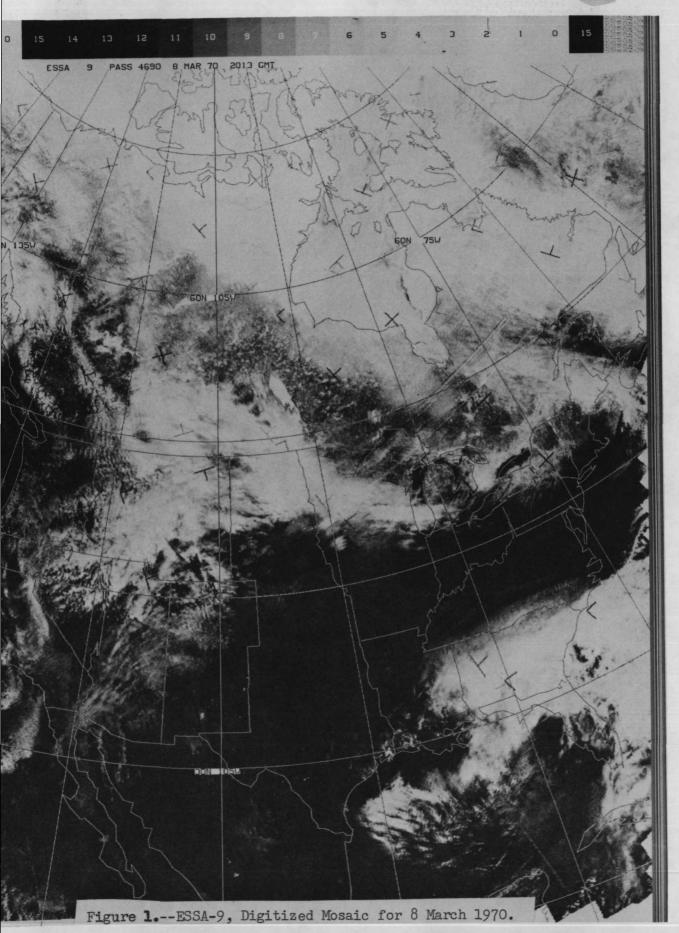
#### BIBLIOGRAPHY

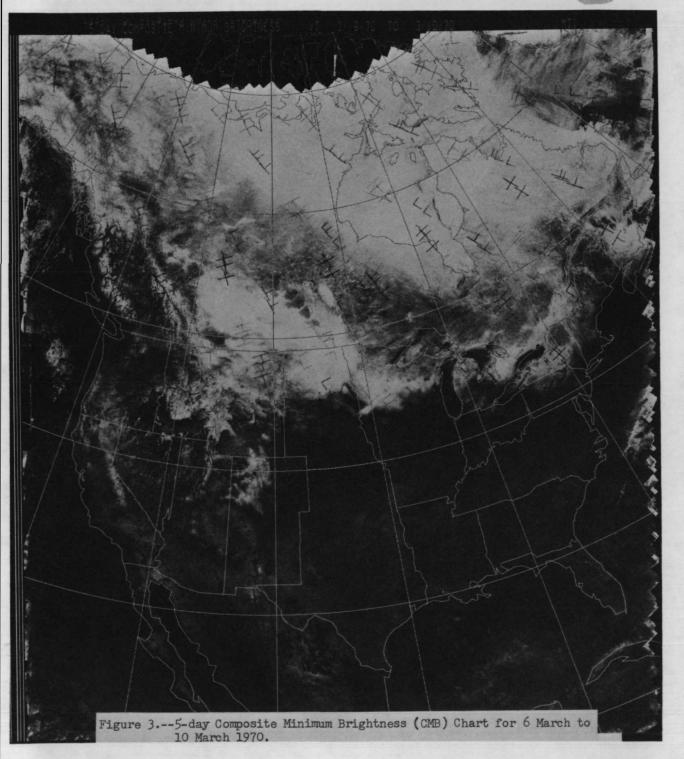
- Barnes, J. C. and Bowley, C. J., "Snow Cover as Mapped from Satellite Photography," Water Resources Research, Vol. 4, No. 2, 1968, pp. 257-272.
- Barnes, J. C. and Bowley, C. J., "The Use of Environmental Satellite Data for Mapping Annual Snow-Extent Decrease in the Western United States," ESSA Contract No. E-252-69(N), Allied Research Associates, Concord, Mass., 1970, 105 pp.
- Bruce, J. P. and Nemec, J., "World Weather Watch and Its Implications in Hydrology and Water Resources Management," WMO/IHD Project Report No. 4, Geneva, Switzerland, 1967, 10 pp.
- McClain, E. P. and Baker, D. R., "Experimental Large Scale Snow and Ice Mapping with Composite Minimum Brightness Charts," <u>National Environmental</u> Satellite Center Technical Memorandum NESCTM-12, Environmental Science Services Administration, Washington, D.C., 1969, 19 pp.
- Popham, R. W., "Satellite Application to Snow Hydrology," WMO/IHD Project Report No. 7, Geneva, Switzerland, 1968, 10 pp.
- World Meteorological Organization, "Scope of the 1972-1975 Plan with Particular Reference to the Meteorological Satellite Sub-System," World Weather Watch Planning Report No. 30, Secretariat of WMO, Geneva, Switzerland, 1970, 124 pp.

#### GLOSSARY

- APT: Short name for Automatic Picture Transmission. Certain satellites of the TIROS and Nimbus series have had special camera and transmitter equipment such that television pictures and radiometer data taken while the satellite is within range of a station on Earth's surface can be received and displayed on relatively simple and inexpensive equipment.
- Compositing: Here it refers to the use of data taken over the same region but at different times.
- Digitization: The process whereby a continuous analog signal received from the satellite is converted to discrete numerical values.
- Earth synchronous: An Earth satellite orbit in which the orbital plane is equatorial and the altitude (35,800 km) such that the velocity of the satellite just matches that of Earth's surface vertically below.
- ESSA photograph: Television image from one of the Environmental Survey Satellites, an operational satellite of the TIROS series.
- Geosynchronous: Same as Earth synchronous.
- Mosaic: Rectified imagery covering a large area that is constructed from single frames taken at intervals throughout a 24-hour period.
- NOAA: National Oceanic and Atmospheric Administration (formerly ESSA), an agency of the U.S. Department of Commerce, which operates the National Environmental Satellite Service.
- Planimetering: A technique for determining the areal extent of a quantity or parameter whose distribution is in mapped form.
- Rectified data: Satellite imagery or scanner measurements that have been mapped onto some standard map projection for Earth's surface, such as Mercator or polar stereographic.
- Resolution: This term usually means "spatial resolution" or "ground resolution."

  It refers in simplest terms to the smallest detail detectible in satellite imagery of clouds or Earth's surface when there is reasonably good contrast between the target(s) and its background.
- Spectral interval (or bandwidth): The width, generally expressed in micrometers (10<sup>-14</sup> cm), of a particular portion of the electromagnetic spectrum a given sensor (e.g. radiometer detector or camera film) is designed to measure or be sensitive to energy received at the satellite from that part of the spectrum.
- Sun synchronous: An Earth satellite orbit in which the orbital plane is near polar and the altitude such that the satellite passes over all places on Earth having the same latitude twice daily at the same sun time.







Page Intentionally Left Blank

### Biographical Sketch

Since 1968 Vincent V. Salomonson has been working for NASA as a research meteorologist in the Laboratory for Meteorology and Earth Sciences, Goddard Space Flight Center, Greenbelt, Maryland. Prior to working for NASA he served as a weather officer in the U.S. Air Force doing weather forecasting for the Strategic Air Command in Newfoundland, Louisiana, and Mississippi. He received a B.S. in agricultural engineering from Colorado State University in 1959, a B.S. in meteorology from the University of Utah in 1960, an M.S. in agricultural engineering from Cornell University in 1964, and a Ph.D. in atmospheric science from Colorado State University in 1968. He has performed research in several areas including the leaching of saline-alkaline soils, erosion magnitudes under furrow irrigation practices, agricultural meteorology and plant climate, radiative transfer and, in particular, anisotropy in reflected solar radiation, satellite meteorology as applied to observations of jet streams, sea surface temperature, cloud statistics, and ozone, and hydrological observations from Nimbus satellites.

Nimbus 3 and 4 Observations of Snow Cover and Other Hydrological Features in the Western Himalayas

by

Vincent V. Salomonson Goddard Space Flight Center

Several of the great rivers of the world begin their flows to the seas in the Himalayan region of southern Asia. Since much of this region is often inaccessible, programs are underway to assess the possibility of monitoring its hydrological features via satellite observations. A series of photographs from the Nimbus 3 and 4 Image Dissector Camera Systems (IDCS), the Nimbus 3 High Resolution Infrared Radiometer (HRIR), and the Nimbus 4 Temperature-Humidity Infrared Radiometer (THIR) has been collected to illustrate and demonstrate the application of these data in observing snow cover and other hydrological features in the Western Himalayas. This collection of imagery shows the relative merits of daily observations of these features in the visible, near infrared (0.7-1.3 µm), and far infrared (10-11 µm) portions of the electromagnetic spectrum with sensors having nominal spatial resolutions between 4 and 8 kilometers. Particular emphasis has been placed on observing features associated with the Indus River because of the economic and social importance of this river in the lives of millions of people.

The resolution and spectral response of the IDCS made it the best system available on Nimbus 3 and 4 for mapping the areal extent of snow cover over the Indus River watershed. This parameter has been measured in terms of the percent of the watershed covered and graphically related to the mean monthly runoff observed at a stream gauging station near the northern border of West Pakistan. The areal extent of the snow cover was assessed on 10 different days during the period from April 1969 to April 1971. As can be seen in Figure 1, during the period of major snowmelt from April to late July 1969 very good agreement between the monthly mean runoff and the snow cover is evidenced. Further efforts to study the stability of this result during the 1970 snowmelt season are in progress.

The contrast between the reflectivity of water and the reflectivity of neighboring vegetation and soil surfaces in the near infrared make the Nimbus 3 HRIR daytime observations very useful in observing the courses of rivers and the locations of lakes in the Tibetan region. As illustrated in Figure 2, nearly the entire course of the Indus River can be observed during cloud free conditions. The paths of many other rivers and many lakes in Tibet can also be easily seen.

The Nimbus  $^4$  THIR monitors the radiation emitted in the 10-11  $\mu m$  region and thereby permits observations of cloud top temperatures and subsequent estimates

of the amount of convective activity occurring over large regions. Figure 3 shows that the extent and character of cloudiness over the Himalayas can be assessed and estimates made of the impact of monsoonal rainfall on Indus River flow.

The overall results of this pilot study clearly indicate that it is feasible to monitor quantitatively the extent of the snow cover over the Indus River watershed during a given year and from one year to another using meteorological satellite imagery that is available on a routine and continuing basis. These observations, in conjunction with other observations taken in the near infrared and far infrared, appear to offer a potentially valuable input for water management systems where conventional observations are either not available or are very costly and difficult to obtain.

ACKNOWLEDGEMENT: The author wishes to acknowledge the support of Mr. James C. Barnes Allied Research Associates, in supplying the photographs.

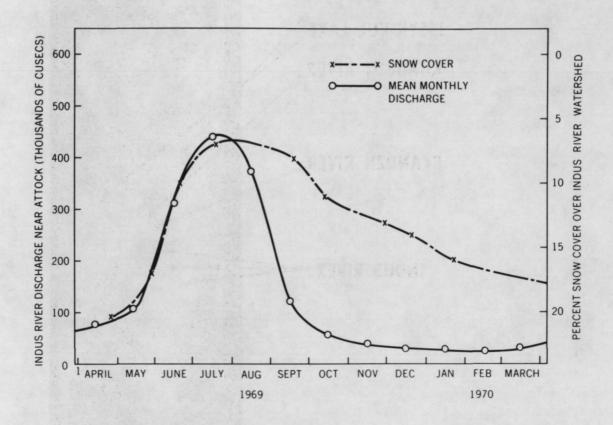


Figure 1. A plot showing the relationship between the percent snow cover over the Indus River watershed and the mean monthly discharge in the Indus River near Attock in West Pakistan. The snow cover area was obtained from the observations of the Nimbus 3 and 4 Image Dissector Camera Systems.

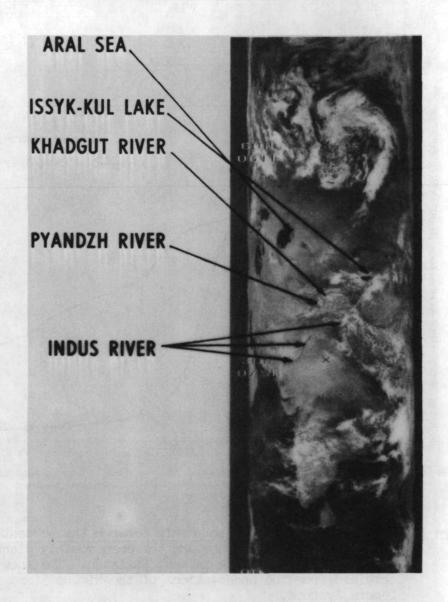


Figure 2. Nimbus 3 High Resolution Infrared Radiometer (HRIR) daytime photofacsimile picture taken over the Himalayas and adjoining regions on orbit 911, 21 June 1969. The spectral response of the HRIR during daytime observations is predominantly in the 0.7-1.3µm region.

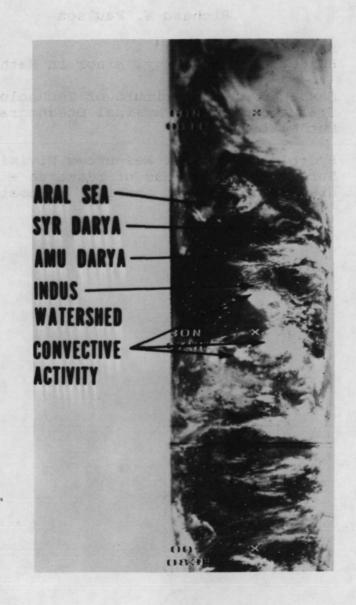


Figure 3. A Nimbus 4 Temperature-Humidity Infrared Radiometer (THIR) 10-11<sub>u</sub>m photofacsimilie picture of the region over and near the Himalayas taken on orbit 1087, 28 June 1970.

# BIOGRAPHICAL SKETCH

# Richard W. Paulson

1958-1962	Hofstra University BS degree in Geology, minor in Mathematics
1962-1966	Massachusetts Institute of Technology Graduate work in Physical Oceanography with minor in Mathematics
1966-1971	Hydrologist, Water Resources Division, U.S. Geological Survey. Major areas of research - estuarine
	dispersion remote sensing automatic data processing

# THE ROLE OF REMOTELY SENSED AND RELAYED DATA IN THE DELAWARE RIVER BASIN

by

Richard W. Paulson U.S. Geological Survey Harrisburg, Pennsylvania

#### INTRODUCTION

For several years the U.S. Geological Survey has operated a system of water-quality monitoring stations in the Delaware River Basin that provides riverine and estuarine water-quality data to water-resources agencies in the basin. This report is a discussion of the planned integration of the existing monitoring and data processing systems with a data-relay experiment proposed for the Earth Resources Technology satellite (ERTS)-A, which will be launched in 1972. The experiment is designed to use ERTS-A as a data relay link for a maximum of 20 hydrologic stations in the basin, including streamgaging, reservoir level, ground water level, and water-quality monitoring stations. This experiment has the potential for reducing the timelag between data collection and dissemination to less than 12 hours. At present there is a significant timelag between the time when the data are recorded at a monitoring site and the water-resources agencies receive the data. The timelag exists because most of these instruments operate in remote locations without telemetry, and the data records are removed manually, generally at a weekly frequency. For most water-quality monitoring, the data do not reach water-resources agencies for a period of 2 weeks to 2 months.

# WATER-RESOURCES MANAGEMENT IN THE DELAWARE RIVER BASIN

Several governmental agencies are concerned with the daily status of the quality and quantity of surface and ground waters in the Delaware River Basin. The lead water resources agency in the basin is the Delaware River Basin Commission (DRBC), which was authorized by the Delaware River Basin Compact, Public Law 87-328. This Compact, whose signatory parties are the United States Government and the states of Delaware, New Jersey, and New York and the Commonwealth of Pennsylvania, became public law in 1961. It requires the DRBC to develop, adopt, and maintain a Comprehensive Plan for the orderly development of the basin's water resources. The Basin Commissioners, who are the governors of the four states and a Presidential appointee (currently the Secretary of the Interior), have a permanent staff that is charged with the management of the water resources of the basin. Projects and areas of

research for the Plan include water supply, flood protection, stream quality, recreation, fish and wildlife, pollution abatement, and regionalization of waste treatment.

The largest single task undertaken by the DRBC has been the abatement of pollution in the Delaware River estuary. This abatement program is designed to improve the estuary's quality to meet the water-quality standards adopted by the Commission in 1968. The pollution-abatement plan includes ".... the adoption of basin-wide regulations for implementing and enforcing the Standards, the assign ment of wasteload allocations to each estuary discharger, and the establishment of a broad surveillance program to keep fulltime check on discharge effluents and stream quality" (DRBC 1968).

Engineering and computer studies of the estuary's capacity to assimilate oxygen-consuming waste provide the DRBC with a basis for assigning wasteload allocations to dischargers once water quality standards were adopted. Soon after the wasteload allocations were issued, estuary dischargers were required to submit, for DRBC approval, schedules of compliance showing how long it would take the particular discharger to complete waste-treatment facilities require to reduce wasteload to meet the allocation. Schedules of compliance by most estuary dischargers should be complete by 1970, and a measurable improvement in the water quality in the estuary is expected to be attained in ".... the-early-to-mid-1970's" (DRBC 1969).

As a Federal-State Compact, the DRBC is a uniquely authorized regulatory agency that has adopted a plan for managing the water resources of the Delaware River basin, including pollution abatement in the Delaware River estuary. The pollution-abatement plan is expected to produce a measurable improvement in water quality in the next several years at a cost of several hundred million dollars. The water-quality monitoring program of the Survey is one of several sources of data for the Commission.

For many years the City of Philadelphia has been interested in the water resources of the Delaware River Basin and the water qualit of the Delaware River estuary. Since 1946, the City's Water Department, which uses the estuary as a major water-supply source, has spent ".... nearly \$300 million to expand and modernize its wastewater system. About \$100 million of this has gone into facilities that directly protect the rivers .... (City of Philadelphia, 1970). In participating in the DRBC's pollution-abatement plan, Philadelphia " .... will expand its water pollution control plants and replace many of the older tributary sewers" at a cost that ".... may exceed \$200 million in the next decade .... " (City of Philadelphia, 1970). The Water Department has supported the operation of the water-quality monitoring system to ".... warn of industrial spills, temperature rises, salt water influx, sewage problems, .... other forms of pollution .... (and to provide) data for long-range prediction of river conditions." (City of Philadelphia, 1970).

A third agency concerned with the daily status of water resources in the basin is the U.S. Geological Survey's Office of the Delaware River Master. The River Master is charged with implementing a Decree of the United States Supreme Court, which resolved a conflict of water-supply need. Water is exported from New York City reservoirs in the upper reaches of the basin to the New York City water supply system. Because the water is exported from the basin it is not available (for other uses) downstream from the reservoirs. During periods of drought the conflicting needs for the exported water by New York City and downstream users have become acutely apparent. When this conflict was brought to the Supreme Court, originally in the early 1930's and again in 1954, the Court decreed limits of withdrawal of water by New York City and a minimum level of streamflow downstream from the reservoirs. on a daily basis, and in accordance with the decree, the River Master prescribes releases of water from New York City reservoirs to maintain the required level of streamflow and monitors withdrawals from the reservoirs for New York City's water supply.

State health and natural resource agencies, municipalities, and Federal agencies, including the Army Corps of Engineers and the Federal Water Quality Administration also have need for water resources information in the basin.

# DELAWARE RIVER BASIN WATER-QUALITY MONITORING AND DATA-PROCESSING SYSTEMS

The Geological Survey's water-quality monitoring system is composed of continuously operating instruments that record dissolved oxygen concentration, temperature, specific conductance at 25° C, and pH at 11 sites in the basin. (See fig. 1) The system, which is cooperatively supported by the Survey, the City of Philadelphia Water Department, the Delaware River Basin Commission, the Delaware Geological Survey, and other local, state and Federal agencies, provides water resources agencies with data on stream quality in the major rivers of the basin in addition to the Delaware River estuary and Delaware Bay.

Many of the monitors operate in remote locations where seasonal ranges in temperature and humidity are large, where sediment, algae, and other debris in the water adversely affect sensors and watersample transfer systems, where ice and wave motion can damage sensors in the stream, and where vandalism contributes to equipment failure. For example, two of the stations frequently operate for long periods of time between servicing visits because they are on islands in the Delaware River estuary and Bay and are very difficult to service, especially during the winter months when high winds and ice make conditions very hazardous. A continuing effort is made to protect the instruments from environmental hazards, and field calibration checks are run on the instruments at every opportunity. Nevertheless, although monitors work well most of the time, they do fail occasionally. As will be discussed subsequently, data must be continuously screened for equipment failures, some of which cannot

be detected in the field.

Data collected by monitors are recorded either on an analog strip chart or a 16-channel paper tape. These data records are retrieved from the monitors weekly by a technician who performs calibration tests on the instruments. The data records are returned to the Survey's Current Records Center (CRC) in Philadelphia where they are computer processed. At the end of each calendar month, data are processed to produce two computer printouts, examples of which are shown in figures 2 and 3. The printout in figure 2 contains a listing of all of the hourly values of one water-quality parameter at one station. Figure 3 is a listing of daily statistics including the daily maximum, mean, minimum, range, and standard deviation, the number of missing hourly values for each day of the month, and a comparison of each day's data with recently adopted DRBC stream quality objectives (standards). Frequently, data for a particular calendar month are not completely processed until 2 weeks to 2 months after that month. The timelag varies within this range as a function of the performance of the monitors.

Although the monitors work very well most of the time, the initial steps in the data-processing system presuppose that malfunction may have taken place during the period between calibration checks. Briefly, the data at the beginning and end points of the data record are compared to independent field analyses of the four monitored parameters, and the data record is computer graphed for human screening. Human intervention in the system serves two purposes. The first purpose is to detect and eliminate spurious data from the data record, and the second is to provide a feedback loop of equipment performance back into the monitoring system. feedback loop is necessary because some monitor malfunctions can only be detected in the data record. For example, an electronic component that behaves erratically at infrequent intervals may not be detected during a routine calibration check but may produce spurious data that can be detected by human or computer screening. Initial screening of data is made a few days after a data record is retrieved, and the feedback loop can then be closed quickly to prevent continued malfunction of the monitor.

Therefore, the data-processing system provides rapid initial screening and release of data, on a monthly basis, to water resources agencies.

The value of the large mass of water quality data presently being collected is diminished because of the timelag between data collection and dissemination. In recognition of this, efforts are made to disseminate some of these data more rapidly. The monitoring station at the Benjamin Franklin Bridge (Pier 11 North) is in one of the most heavily polluted reaches of the estuary and is near the Survey's CRC office. This station is serviced daily, and preliminary water-quality data are released via teletype (figure 4) to several agencies. A summary of water-resources conditions is also placed in a telephone recorder each day and agencies can dial the recorder

directly for information. These releases provide the DRBC with data from a key estuary station. A second key stations is at Reedy Island Jetty, Delaware, where the quality of the water tends to improve after passing through the more upstream Philadelphia-Chester reach of the estuary, where water quality tends to be low. This station also is a key station because it is in the salt water intrusion zone of the estuary and because a large nuclear electric generating station, potentially capable of altering the thermal regime of the estuary, is being constructed near the station. In response to the key role of the station, the DRBC has requested that the Survey install landline telemetry from the Reedy Island monitor to the CRC during fiscal year 1971. Upon installation of telemetry, the daily release in Figure 4 will be expanded to include these data.

In addition to the daily teletype summaries, preliminarly weekly and monthly summaries also are released for data not yet completely through the CRC processing system.

# AN APPROACH TO PROCESSING SATELLITE-RELAYED HYDROLOGIC DATA

It is expected that a maximum of 20 hydrologic sites in the basin will be instrumented with radio telemetry at the time of launch of ERTS-A. The 20 sites will include most, or all, of the water-quality monitors in Figure 1, plus key stream-gaging stations and reservoir and ground-water level stations. Data from these sites will provide water resources management agencies with indices of water-quality, streamflow, reservoir levels, and ground-water levels. In at least one instance the radio telemtry will provide a redundant communications link with a station, because by March 1972 the Reedy Island monitor will have landline telemetry. The landline telemetry will help to provide a sound basis for measuring the utility and accuracy of three modes of operation; (1) no telemetry, (2) conventional landline telemetry, and (3) satellite relayed telemetry.

Radio-telemetry instrumentation, which is still under development, will be designed to broadcast a brief data message from each station once every 90 or 120 seconds. Although the data will be telemetered continually, data will be relayed only when the satellite passes over the station and is simultaneously in view of both the radio transmitter at the station and a receiving station, called an acquisition site. The acquisition site for data relayed from the Delaware River Basin is at the National Aeronautics and Space Administration's (NASA) Goddard Space Flight Center in Greenbelt, Maryland. Figure 5 gives the four or more periods of time, during the daily passes of the satellite over the basin, when a hydrologic station and the acquisition site are both in view of ERTS. A data message is broadcasted every 90 or 120 seconds; so, there will be 5 to 7 data messages sent during a 10-minute period of mutual visibility every 12 hours. Seventeen days are represented in figure 5 because the orbital pattern is repeated at a 17-day frequency.

The NASA Goddard Acquisition Site will have a very high probability of receiving satellite-relayed data from each of the Delaware Basin stations at least once every 12 hours. These data will be processed and relayed by NASA to the CRC on the Bell system teletype network, which is the system the CRC uses for data dissemination. After the CRC receives data from a water resources station the data will be screened before dissemination.

The screening process for data from a particular station, while highly speculative at present, will probably include a comparison of the data with data recently received from the station. This comparison will be done at estuary stations at least because the day to day changes of water-quality conditions usually are small. On the other hand, daily changes in stage can be large at stream-gaging stations, especially during periods of heavy rainfall.

It also will be useful to compare the data with summaries of recent historical data at a station. Summaries for Delaware estuary stations are becoming available as a result of a recent CRC effort to provide water resources agencies with comparisons of recent water-quality conditions to the new DRBC stream-quality objectives. Figures 6, 7, and 8a and b are examples of computer-generated summaries for dissolved oxygen concentrations, temperature, and specific conductance.

The dissolved oxygen concentration summary (Merk, 1970) presented in Figure 6 has time as the ordinate, or vertical coordinate. The water year (October 1 - September 30) is broken down into 122 periods of 3 days each. The abscissa or horizontal coordinate is dissolved oxygen concentration, in milligrams per liter (mg/1), from 0 to 15 mg/1. The period October 1, 1964 - September 30, 1969, or water years 1965-69, is summarized on the graph. The summary indicates the maximum and minimum concentration recorded for each 3-day period during the 5-year period, plus statistical information on the distribution of the 15 daily means. The DRBC stream quality objectives are also plotted to provide a comparison of these data to the objective of the DRBC pollution abatement program. Thus, dissolved oxygen data received from this station can be referenced to this graph to determine whether or not the data are in the range of variation recently experienced. Of course, the graph will have to be updated as water quality conditions improve in the estuary.

The summary for temperature in Figure 7 follows the same general format as the dissolved oxygen graph, except statistical information on the distribution of 15 daily-maximum values (rather than daily means) is plotted with the extremes. As the DRBC stream-quality objective for temperature is stated as the permissible daily maximum rather than the daily average, as is the case for dissolved oxygen, statistical information on the daily mean is given for dissolved oxygen.

Because specific conductance (an indication of total dissolved solids in the water) is not as seasonally dependent as are the two

previous parameters, the computer summaries for this parameter were not ordered by season. The largest contribution of dissolved solids to the estuary comes from ocean salts that disperse upstream. upstream limit of these salts can differ significantly from the vicinity of the station at the Benjamin Franklin Bridge to the station at Reedy Island, a distance of about 50 miles. strength of salinity intrusion into the estuary is strongly correlated to fresh-water inflow to the estuary. Figures 8a and 8b show two computer summaries of specific-conductance data (Paulson, The graph in figure 8a contains cumulative frequency distributions of the daily maximum, mean, and minimum specific conductances that were measured at the Reedy Island station for all days in the period October 1, 1964 to September 30, 1969, when the daily mean flow of the Delaware River at Trenton, N.J. was within 250 cfs (cubic feet per second) of the flow level of 2,000 cfs. Figure 8b is the same graph for that station for the flow level of 11,500 cfs. Notice that the vertical 50 percentile line crosses the daily maximum curve at about 18,800 micromhos (about 33% the salinity of ocean water) in Figure 8a, but the 50 percentile line intersects the daily maximum curve at about 9,300 micromhos (about 15% the salinity of ocean water) in Figure 8b. The Delaware River estuary is a large body of water and does not respond instantly to changes in fresh water inflow. In fact, its response is more adequately described as sluggish. The graphs in Figures 8a and 8b are crude summaries, and the basis for a more refined summary -based on antecedent conditions -- must be determined by further research. Yet, the graphs do provide an expected range for 20 flow intervals that have been summarized for each estuary station.

When the CRC receives satellite-relayed data they will be screened against the hydrologic range and variability of historical station data before being released. Criteria may have to be established to flag data when the hydrologic condition is an extreme condition or outside the range of a permissible level, as established by water resource management officials. Flagging of the data may be provided as a service to management officials.

# CONCLUSION

Frequently, water resources management agencies have difficulty taking action against unfavorable water-resource conditions because of lack of data or knowledge of the condition and of the lack of means to affect a change. The result may be a persistent undesirable condition, such as pollution, or -- as in early 1960's during the Northeast drought -- an imperiled water supply in part of the Delaware River Basin. Difficulty may also be met in coping with short-term natural disasters such as the severe flooding, and concomitant loss of life and property, that occurred in August 1955 when two hurricanes swept across the Delaware River Basin.

In meeting its obligation under the Delaware River Basin Compact, the DRBC has a Comprehensive Plan to develop the water resources of the basin. The Plan will provide the DRBC with the means of safeguarding the basin's water resources. In order to implement the Comprehensive Plan, the DRBC has encouraged and directly supported the system of hydrologic stations maintained by the Survey in the basin and has supported the installation of telemetry at key locations. Thus, progress is being made to overcome some of the conditions that constrain water resources officials from managing the basin's water resources.

The satellite data relay experiment discussed herein will determine whether satellite relay data will be adequate to meet the data needs for responsible river basin management. It should provide the basis for determining whether or not data collected once every 12 hours from a tidal estuary is sufficient to meet these needs when the large ranges of particular parameters are weighed against time of collection within a tidal cycle. For some parameters such a measure may not be adequate, while for others it may.

The experiment will also provide impetus to develop an operational system of real-time data processing and dissemination to handle the large quantity of data that will be obtained from the stations in the basin. A library of the characteristics of hydrologic conditions at each site will be developed as reference material for screening the data as it enters the CRC. Where possible, digital computer techniques for data summarization and screening will be developed. Human intervention in the system will probably be necessary to maintain quality control on the data.

Finally, as water resources agencies develop the means for managing river basins, the results of this experiment will demonstrate the relative merits of satellite relay of data versus conventional means of data telemetry and will provide a basis for the development of operational satellite relay of hydrologic data.

### REFERENCES

- Delaware River Basin Commission, 1968, Annual Report; Trenton, N.J., 21 p.
  - 1969, Annual Report, Trenton, N.J., 21 p.
- City of Philadelphia Water Department, 1970, Clean Streams for Philadelphia, the City's \$500 Million River Cleanup, Philadelphia, Pa., 36 p.
- Merk, Charles F., 1970, A graphical summary of dissolved oxygen data for the Delaware River estuary for water years 1965-69; U.S. Geol. Survey open-file report, 15 p.
- Paulson, Richard W., 1970, A graphical summary of specific conductance data for the Delaware River estuary, as correlated with Delaware River flow at Trenton, N.J.; U.S. Geol. Survey open-file report, 120 p.

### GLOSSARY

- Analog strip chart A continuous recording of the value of a quantity that is made as an inked line on a paper chart.
- Estuary The lower portion of a river affected by oceanic tides.
- Feedback loop The use of the output of a system as a criterion for improving the system's operation.
- Hydrologic station An instrumented field site for recording hydrologic data.
- Observation well A well that is used to monitor the fluctuation of ground-water level.
- Salt water intrusion (influx) The movement of ocean salt into a fresh water river.
- Standard deviation A statistical measure of the spread of data.
- Stream gage A field instrument that indirectly measures the flow of water in a stream or river.
- Thermal regime The normal or regular pattern of temperature.
- Water-quality monitor A field instrument that records one or more physical or chemical measures of water quality.

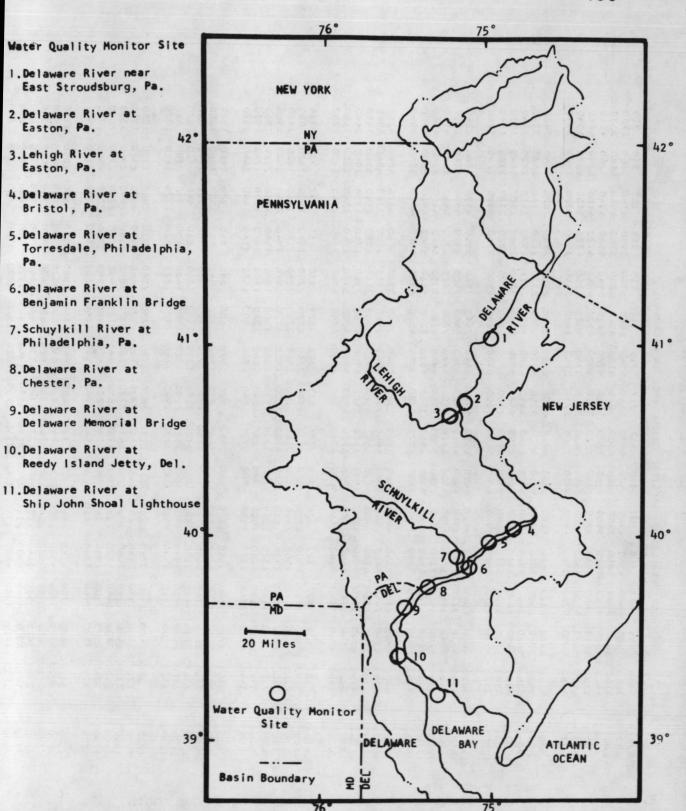


Figure 1.-Map showing location of U.S. Geological Survey water-quality monitors in the Delaware River Basin.

1920 1280

-560

Fi	DISSOLVED DAYGEN DAILY STATISTICS IN MILLIGRAMS PER LITER							
1 fg	DELA	WARE RIVER AT BE	RISTOL	ST	ATION NUMBER	01-4646.00 MII	LE POINT 119.21	JUNE 1963
rom De month								
	DAY NUMBER	MAXIMUM	MEAN	MINIMUM	RANGE	STD. DEV.	NO. OF VALU	JES DEV FRUM DRBL
3A comp Delaware							MISSING FOR THE	
la	162			F 0				
- 8	152 153	6.9	5.6	5.8	1.1	0.3	0	-0.2
ar	154	5.3	5.0	4.8	0.9	0.2	0	-1.5
e m	155	5.0	4.4	4.2	0.8	0.2	0	-2.1
compute are Riv	156	4.5	4.0	3.8	0.7	0.2	0	-2.5
2.5	157	3.9	3.5	3.2	0.7	0.2	0	-3.0
4 6	158	3.4	3.0	2.8	0.6	0.2	Ö	-3.5
	159	3.2	2.8	2.5	0.7	0.2	0	-3.7
er 1	160	3.6	2.9	2.5	1.1	0.3	Ö	-3.6
H F.	161	3.7 -	3.0	2.6	1.1	0.3	0	-3.5
20 00	162	3.7	3.1	2.6	1.1	0.3	0	-3.4
O CT	163	3.4	3.0	2.7	0.7	0.2	0	-3.5
listin Basin	164	3.6	3.1	2.8	0.8	0.2	0	-3.4
10	165	3.8	3.1	2.7	1.1	0.3	0	-3.4
Commis	166	3.5	3.0	2.6	0.9	0.3	0	-3.5
9 6	167	3.8	3.0	2.6	1.2	0.4	0	-2.0
B	168	5.8	4.5	3.1	2.7	0.8	0	-0.5
F. Q.	169	6.4	5.8	4.8	1.6	0.5	0	0.8
8 2	170	6.6	6.3	5.9	0.7	0.2	0	1.3
P. L	171	6.6	6.3	6.0	0.6	0.2	0	1.3
ly	172	6.4	6.2	6.1	0.3	0.1	0	1.2
3	173	6.3	6.1	5.9	0.4	0.1	0	1.1
8 4	174	6.3	6.0	5.6	0.7	0.2	0	1.0
ct a	175	6.7	6.0	5.6	1.1	0.3	0	1.0
4 4	176	6.2	5.9	5.5	0.7	0.2	0	0.9
(0 12-	177	6.0	5.6	5.0	1.0	0.2	0	0.6
13 4	178	5.7	5.4	5.1	0.6	0.1	0	0.4
T H.	179	5.5	5.3	5.1	0.4	0.1	0	0.3
ने दे	180	6.1	5.5	5.0	1.1	0.3	0	0.5
20 01	181	6.2	5.5	5.1	1.1	0.3	. 0	0.5
tatistics d								
H- M								
ty				MON	ATHLY STATIST	ICS		
0, 20		6.9	4.6	2.5	4.4	1.4	0	
and obje					FREQUENCY			
	SUBCLASS	(LOWER BOUND)	2.5 3.0	3.5 4.0	4.5 5.0	5.5 6.0	6.5	
te		RS IN SUBCLASS	120 118	41 28	33 87	122 155	16	
H. 4		NO IN SOURCEAST			,, 0,	,,		
V I								4
SS								0
Ľ.	NO OF OBS	ERVATIONS = 720	TOTAL O	F VALUES =	0.334360E 04	TOTAL OF	SQUARED VALUES = (	0-168473F 05
deviations ectives for		MINUS ISSUED ASS						
JZ DZ								

GEO SURVEY-PH 710-670-3438

WE WISH CONF WITH:

510-650-0815 510-650-0814 510-681-7455 510-681-7478 510-685-9564 END

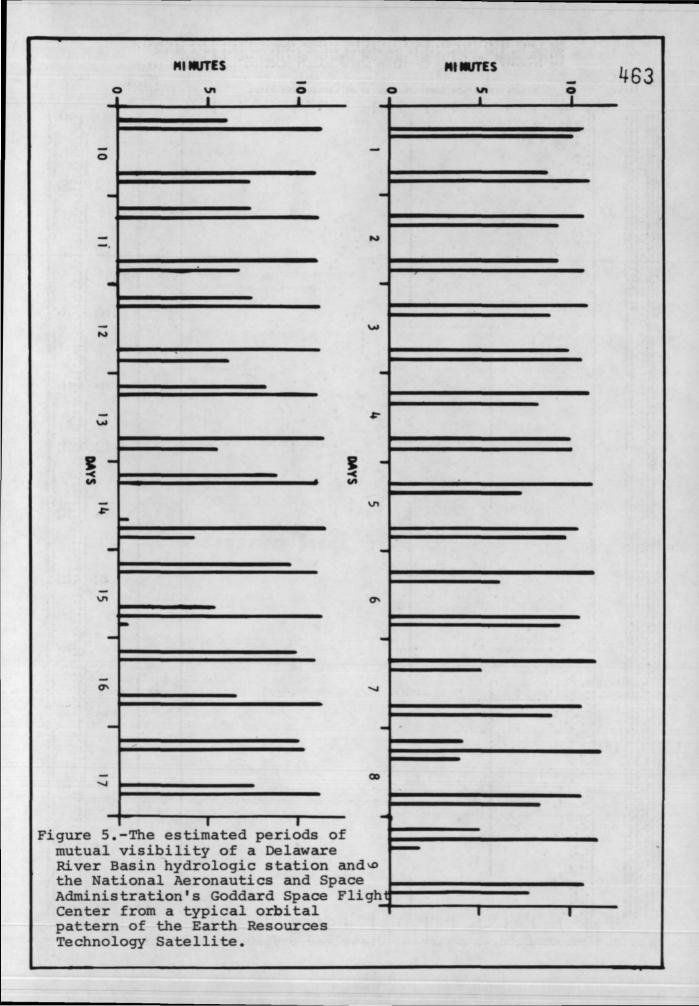
FM: US GEO SURVEY PH

TO: GEO SURVEY TNT, GEO SURVEY HBG, WB-TNT, WB-HBG, DRBC

SUBJ: DAILY WATER QUALITY OF DELAWARE ESTUARY AT BEN FRANKLIN BRIDGE (PIER 11 NORTH) PHILA PA D.O. (MG/L) TEMP . (F) SPEC . COND . (MICROMHOS) DATE PH 6.7 - 6.6 10/1 0.5 - 0.0 76 - 75 399 - 352 398 - 362 75 - 75 10/2\* 0.4 - 0.0 6.7 - 6.7 \* PROVISIONAL MAX AND MIN VALUES (MIDNIGHT - 8AM) END/CRC

GEO SURVEY-PH

Figure 4.-A daily teletype release of Delaware River estuary waterquality data.



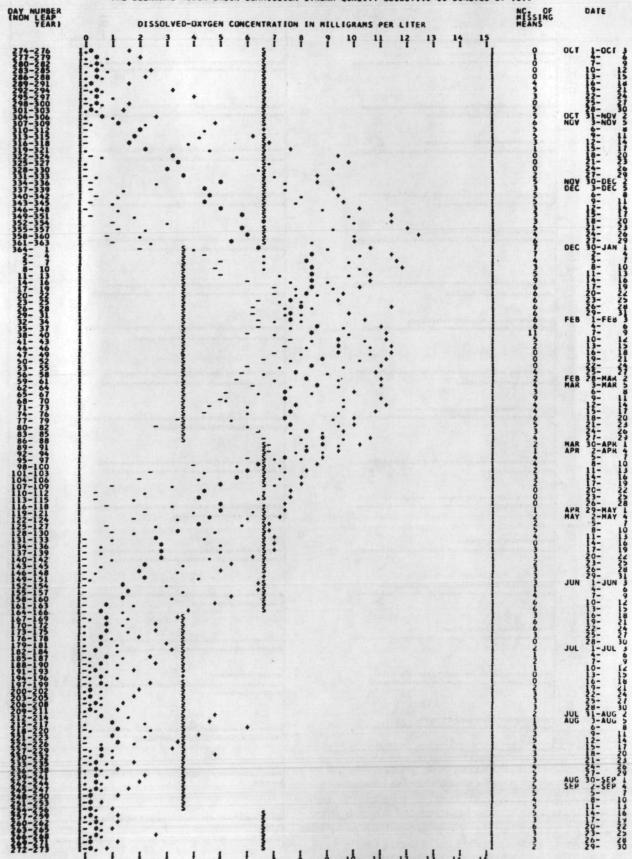


Figure 6.-A computer summary of dissolved oxygen concentration data.

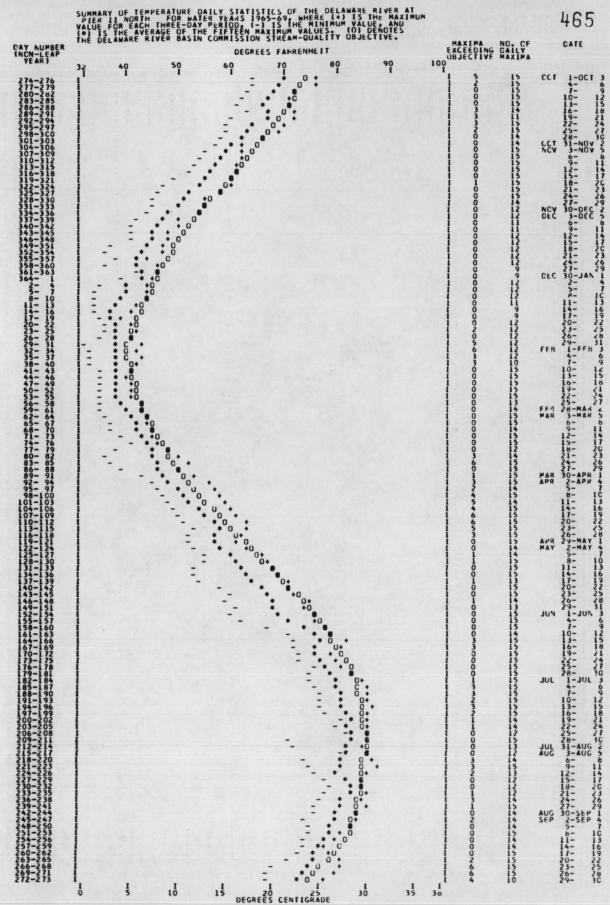


Figure 7.-A computer summary of temperature data.

STATION REEDY ISL

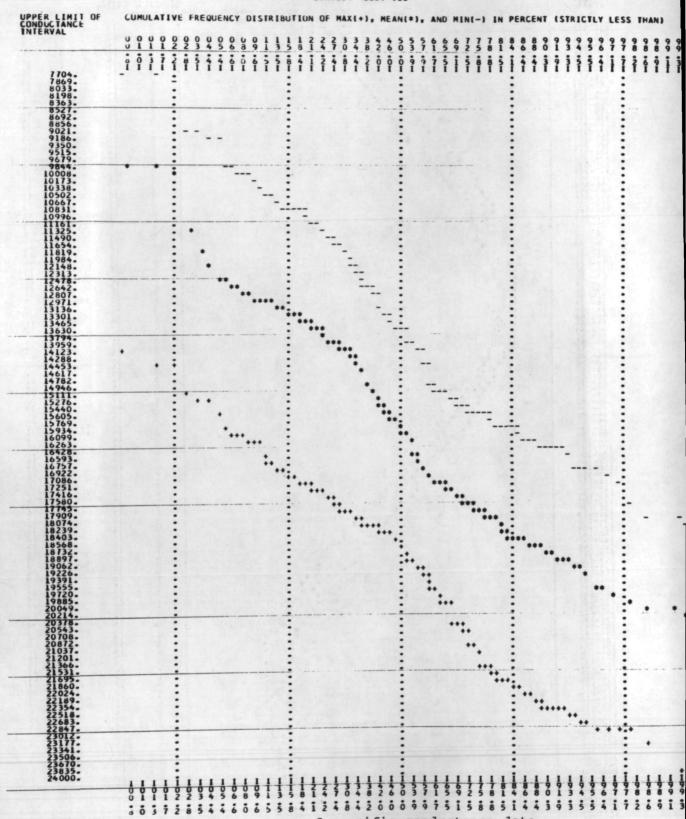


Figure 8a.-A computer summary of specific conductance data.

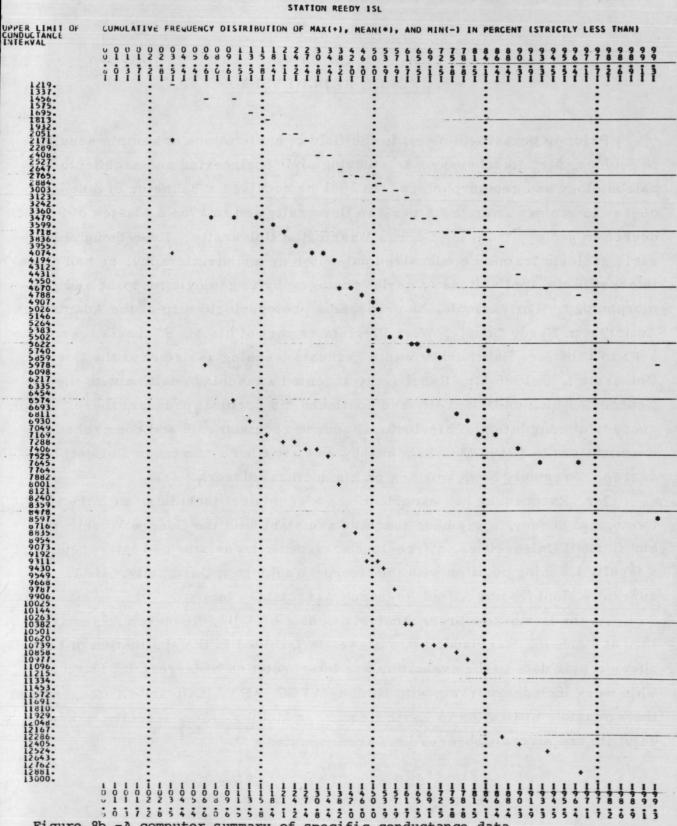


Figure 8b.-A computer summary of specific conductance data.

#### GEORGE RABCHEVSKY

Prior to engaging himself in the field of applications of remote sensing to geology, Mr. Rabchevsky was studying civil engineering and architecture, paleontology and geomorphology. In 1961 he received a Bachelor of Science degree in geology from the American University and in 1963 a Master of Science degree in geology from the George Washington University. Even though his early geologic training emphasized paleontology and stratigraphy, he had an early interest in the applications of aerial photography to geologic mapping and geomorphology. For example, he prepared a photogeologic map of the Adams Run Anticline in Hardy County, West Virginia as part of his M. S. thesis. From 1963 to 1965 Mr. Rabchevsky was a graduate teaching assistant at the Cornell University. In 1965 Mr. Rabchevsky accepted a teaching position with the George Washington University and continued his doctoral program there. After successful completion of his doctoral course requirements and comprehensive examinations in 1969, Mr. Rabchevsky was awarded a Master of Philosophy degree. Presently he is working on his doctoral dissertation.

Mr. Rabchevsky has experience as a geological technician with the U. S. Geological Survey, a graduate teaching assistant with the George Washington and Cornell Universities, a free-lance scientific translator and interpreter and a faculty teaching position with the George Washington University. He is currently employed by Allied Research Associates, Inc.

At the Earth Resources Analysis Center of Allied Research Associates, Inc. at Lanham, Maryland, he is presently involved in the application of satellite photographic data to the evaluation and interpretation of terrestrial features. This work includes working with Nimbus AVCS, APT, IDCS and IR imagery and their possible utilization in Earth Resources studies. Concurrently, other satellite and aircraft observations are evaluated.

## HYDROLOGIC CONDITIONS VIEWED BY THE NIMBUS METEOROLOGICAL SATELLITES\*

George A. Rabchevsky
Allied Research Associates, Inc.
8805 Annapolis Road
Lanham, Maryland

#### Abstract

The unexploited value of the Nimbus meteorological sensor data relates to the satellites' ability for global, temporal, repetitive and uniform tonal and spatial coverage of the earth's surface. Examples are presented illustrating how synoptic views of large areas increase our interpretive capability and enable us to focus on large targets of interest. The effect of resolution of the Nimbus imaging systems on these observations will be discussed, together with the assessment of the areal and temporal magnitude of changes observed by these systems. Two case studies will be presented exemplifying the satellites' ability for repetitive observations enabling us to monitor phenomena under special conditions. One study deals with changes observed in the Antarctic ice conditions utilizing the Nimbus II and III television picture data. The other study deals with terrestrial changes in the Mississippi River Valley (USA) and the Niger River Valley (Africa), observed primarily in the 0.7 to 1.3 micron spectral band. The tonal variations are brought about by the soil moisture and vegetation boundary changes that correlate with the regional climatic and meteorological conditions. As a conclusion, it will be stressed that the utilization of Nimbus satellite photography for geology and other earth sciences will have to begin prior to the launch of the Earth Resources Technology Satellite (ERTS) planned by NASA for early in 1972.

#### 1. INTRODUCTION

Since 1964, four operational Nimbus satellites have been flown successfully. Even though the satellites were designed primarily for meteorological purposes, substantial information on terrestrial features and phenomena are contained in Nimbus data. Studies of the applications for such data to terrestrial problems have been conducted on a limited scale. This paper will examine the feasibility of applying Nimbus data from the Advanced Vidicon

<sup>\*</sup>Adapted from Nimbus Views Hydrologic Conditions, presented at the First Western Space Congress, Santa Maria, California, 26-29 October 1970.

Camera System (AVCS), Image Dissector Camera System (IDCS) and High Resolution Infrared Radiometer (HRIR) experiments to hydrology and related studies. More in-depth research is, of course, necessary to fully substantiate the hydrologic uses of such data.

#### 2. NIMBUS SATELLITE

Nimbus (Figure 1) was designed by NASA to be a meteorological satellite to provide global meteorological data useful for reliable, long-range weather forecasting. To accomplish this, photographic, infrared and ultraviolet measurements of the clouds, the atmosphere and the earth's surface have been collected (Figure 2).

Tables 1 and 2 present the Nimbus Satellites' launch record, experiments, and other characteristics. As it is evident from Table 2, the accidental elliptical orbit of Nimbus I was to the advantage of geoscientists. The perigee was low enough so that good resolution pictures (as high as 365 m.) were taken of various hydrologic and geologic conditions almost on a global scale. However excellent the Nimbus I imagery was, the new sensing capabilities provided by the 0.7 to 1.3 microns HRIR on Nimbus III (and the 10.5 to 12.5 microns thermal IR on the Nimbus IV) are more useful to some of the studies presented in this paper.

For more technical information on Nimbus operations and applications, the reader is referred to the following standard References, 1 through 11. The data is available from the National Climatic Center (NCC) of National Oceanographic and Atmospheric Administration (NOAA) and from National Space Science Data Center (NSSDC) of NASA. Depending on the user, the data is either free of charge or at cost for both the United States and foreign researchers.

#### 3. BACKGROUND STUDIES

The usefulness of Nimbus data to hydrology is suggested in various publications (8, 12, 13, 14, 15, 16, 17). Brief analyses and more in-depth discussions on inland hydrologic conditions (18, 19, 20) and ice studies (21, 22,

<sup>\*</sup>All figures cited may be found at the end of this report.

NIMBUS EXPERIMENTS AND OPERATION SCHEDULE

Satellite	Launch Date	End of Regular Operations	MRIR	HRIR	AVCS	IDCS	SIRS	IRIS	APT	RTTS	THIR	MUSE	SCR	FWS	BUV	IRLS
Nimbus 1	28 Aug 1964	22 Sept 1964		•	•				•							
Nimbus 2	15 May 1966	15 May 1966	•	•	•				•	16.3	1	303			037	
Nimbus 3	14 Apr 1969	4 Feb 1970	•	•		•	•	•		•						•
Nimbus 4	8 Apr 1970	_				•	•	•			•	•	•	•	•	•

	NIMBUS EXPERIMENTS
MRIR	MEDIUM RESOLUTION SCANNING RADIOMETER - 48 KM RESOLUTION
HRIR	HIGH RESOLUTION SCANNING RADIOMETER - 8 KM RESOLUTION
AVCS	THREE CAMERAS IN TRI-METROGON ARRAY PROVIDING 644 X 3059 KM CROSS TRACK SWATH - 0.08 TO 3.2 KM RESOLUTION
IDCS	DAYTIME CLOUD MAPPING; VIEWS 2576 X 2576 KM AREA PER FRAME - 3.2 KM RESOLUTIO
SIRS	VERTICAL TEMPERATURE PROFILE; SURFACE AND CLOUD TOP TEMPERATURES
IRIS	VERTICAL PROFILES OF TEMPERATURE WATER VAPOR AND OZONE; SURFACE (TERRESTRIAL) COMPOSITION (8.0 TO 12.0 $\mu$ m)
APT	DIRECT DATA READOUT SYSTEM - 3.2 KM RESOLUTION
RTTS	REAL TIME TRANSMISSION SYSTEM - 3.2 KM RESOLUTION
THIR	DAY AND NIGHT SURFACE AND CLOUD TOP TEMPERATURES; ATMOSPHERIC WATER VAPOR MAPPING - 8 KM RESOLUTION
MUSE	CHANGES IN SOLAR RADIATION (UV)
SCR	ATMOSPHERIC TEMPERATURE PROFILE
FWS	ATMOSPHERIC WATER VAPOR; SURFACE (TERRESTRIAL) COMPOSITION (3.4 TO 4.0 $\mu$ m)
BUV	ATMOSPHERIC OZONE DISTRIBUTION
IRLS	DATA COLLECTED FROM PLATFORMS
•	NON-METEOROLOGICAL APPLICATIONS POSSIBLE
•	MARGINAL NON-METEOROLOGICAL APPLICATIONS
	MAINLY METEOROLOGICAL APPLICATIONS

TABLE 2 NIMBUS LAUNCH AND ORBITAL CHARACTERISTICS

	NIMBUS 1	NIMBUS 2	NIMBUS 3	NIMBUS 4	
Launch Vehicle	Thor/Agena B	Thrust-Augmented Thor/Agena B	Thorad/Agena D	Thorad/Agena D	
Launch Site	Western Test Range	Western Test Range	Western Test Range	Western Test Ragne	
	Vandenberg AFB	Vandenberg AFB	Vandenberg AFB	Vandenberg AFB	
	California	California	California	California	
Launch Date	28 Aug 1964	15 May 1966	14 Apr 1969	8 Apr 1970	
	00:57 PDT	00:56 PDT	11:54 PDT	00:18 PDT	
Orbit					
Apogee	931 km	1177 km	1132 km	1096 km	
Perigee	422 km	1095 km	1069 km	1087 km	
Period	99 minutes	108 minutes	107.29 minutes	107.12 minutes	
Inclination	81 <sup>0</sup> retrograde	79.9° retrograde	80.10 retrograde	99.89 retrograde	

23, 24, 25, 26) have also been published. Nimbus data has not been extensively used to map snow cover distributions, snow thickness or run-off in the Northern Hemisphere primarily because the Nimbus satellites (with the exception of Nimbus I) have been launched in spring (see Table 1) and sensor operations terminated prior to the winter seasons.

#### 3.1 AVCS and IDCS Data

The Nimbus AVCS and IDCS pictures have been used to map sea ice distribution and movement in the Arctic and Antarctic. A sampling of existing ice reconnaissance accomplishments over these polar "deserts" includes: location and observations of large tabular iceberg formation and motion; establishment of monthly Antarctic pack ice boundaries; detection and monitoring of leads (polynia) forming in the Antarctic.

Snow cover is an earth resource that has been observed from space for the past decade and will be surveyed by future satellites designed exclusively to view the earth's surface. For general information, Figure 3 illustrates a sampling of snow conditions viewed by the Nimbus satellite.

In the north-central United States, maps of snow distribution derived from meteorological satellite photography are already being used as input to operational flood forecasting (28, 29, 30, 31, 32, 33). Snow surveillance from rapid coverage of large areas and of observations regardless of the remoteness of the region, type of terrain or political boundaries may be conducted from satellites. Because snow accumulation in remote mountainous terrain is the prime source of water for much of the western United States, the advantages of remote sensing from space platforms may be of even greater significance for this part of the country.

Other applications of the Nimbus AVCS and IDCS pictures are the observations of terrestrial rivers and drainage systems, lakes and reservoirs, and marshes. The Nimbus ground resolution will not permit detailed hydrologic analyses but small scale observations are definitely feasible. A small sampling

<sup>\*</sup>ESSA meteorological satellites carrying the Nimbus developed AVCS camera systems have provided data for research studies of snow mapping (28, 29, 30, 31, 32, 33) and for operational application.

of such observations is illustrated in Figure 4. Similar pictures could serve as background information for planning more detailed studies.

Nimbus can also provide a basis for maps of drainage systems useful in interpretations of slope directions, regional relief, relative texture and density of the drainage, drainage patterns and geologic structures. Since absolute relief is not evident from Nimbus photographs, the drainage patterns become valuable to separate highlands from the basins. In some cases, the approximate steepness of the slopes may be inferred from the drainage pattern. Drainage patterns may also reveal bedding and tectonic lineations.

#### 3.2 HRIR Data

The Nimbus nighttime HRIR also measures surface temperatures in cloudfree areas. Since different lithologies and surface covers may cool at different rates, the temperature maps may be useful to geohydrological exploration and location of areas for more efficient irrigation projects.

The Nimbus III daytime HRIR (0.7 - 1.3 micron) has opened up a new dimension to applications of Nimbus data to the earth sciences. The 0.7 to 1.3 micron band responds to reflected solar infrared energy and the observed variations in gray tones (on photofacsimiles) are, therefore, a good relative estimation of the near-IR reflectivity of the terrestrial surficial features. Examples illustrating the application of such data to the monitoring of soil-moisture/vegetation conditions will be presented later in the paper. The daytime HRIR data may also aid in the location of alluvium and sand deposits, especially in areas formerly occupied by ancient rivers and lakes.

An inherent disadvantage of the photofacsimiles is the resolution of the HRIR sensor. The average resolution on photofacsimiles is approximately 8 km. at the subsatellite point (Figure 7). On grid-print maps at one-to-one million scale, Mercator projection, the resolution decreases to about 12 km. The average Nimbus AVCS picture resolution, on the other hand, is approximately 3 km. Resolution requirements, however, vary depending on applications and the media sensed.

#### 4. NIMBUS VIEWS TERRESTRIAL HYDROLOGY

#### 4.1 Polar Ice

Nimbus I was the first weather satellite that provided daily photographic coverage of the polar regions. In cloud-free images, contrast is good for both the AVCS and HRIR polar photography. In the HRIR pictures, however, the pack ice edge is not as clearly delineated as in the AVCS (22) being rather a gradual change in brightness corresponding to the change from the warmer water to the colder ice. Nevertheless, abrupt changes are readily noticeable in the HRIR, such as at the edge of the Antarctic continent where a large temperature difference exists.

The main considerations in identifying the ice/water boundary are (a) the persistence of the ice/water boundary in successive images, (b) pattern characteristics of ice and cloud edges and (c) textural differences between the two (34). The most useful factor is the stability of the pack ice front, i.e. the front position changes little in a 24 to 96 hour period, while cloud patterns may shift rapidly in this time frame. Therefore, clouds may often be positively discriminated from ice simply by comparing location coordinates of successive frames.

Patterns and textures are also important in distinguishing between clouds and ice. Cloud fronts can be identified because of their linear orientation which often extends far beyond the normal limits of pack ice coverage. The "lumpy" characteristic of many cloud masses, may also be useful to identify them as clouds. The lumpy appearance is caused by the long shadows from the higher clouds cast on to the tops of the lower ones. Pack ice relief is normally less than 6 meters so that shadows cast should not be resolved by the satellite system

### Monthly Antarctic Pack Ice Boundary

A map of the average monthly pack ice boundaries from Nimbus II AVCS satellite data is illustrated in Figure 5. A similar study was conducted with the Nimbus I AVCS and HRIR data (23). In general, the determination of the average monthly pack ice boundary produced two valuable sets of information on the hydrology of ice in the Antarctic: (a) the existence of monthly changes (or a lack

of them) in the pack ice boundary and (b) the determination of total area under pack ice cover for each month. The areal extent of Antarctic pack ice is presented in Table 3. The values show a uniform monthly increase in pack ice areal extent in the Weddell Sea area from May to August. Note, however, that the circumpolar coverage is almost identical for months of July and August. Though the July-August boundary shifts considerably in places, the total area under ice cover is almost identical for both months.

To update the 1966 ice position from photographs, Figure 6 illustrates the comparative position of ice boundary as viewed by Nimbus II (1966) and III (1969) satellites. Similar ice boundary fluctuations may also be recorded in other polar regions, as for example, in Greenland and Iceland.

TABLE 3

ANTARCTIC PACK ICE AREA AS DETERMINED FROM NIMBUS 2 AVCS

Month	Continent and Pack Ice Area (km <sup>2</sup> )	Continent Area (km²)	Pack Ice Area (km <sup>2</sup> )	Areal Coverage
May	1.3498 x 10 <sup>7</sup>	7.109 x 10 <sup>6</sup>	6.388 x 10 <sup>6</sup>	"Slice"
June	1.5181 x 10 <sup>7</sup>	7.109 x 10 <sup>6</sup>	8.071 × 10 <sup>6</sup>	from 50°W
July	1.5902 x 10 <sup>7</sup>	7.109 x 10 <sup>6</sup>	8.792 x 10 <sup>6</sup>	clockwise
August	1.6795 x 10 <sup>7</sup>	7.109 x 10 <sup>6</sup>	9.685 x 10 <sup>6</sup>	to 110°E
July	2.9355 x 10 <sup>7</sup>	1.6417 x 10 <sup>7</sup>	1.2938 x 10 <sup>7</sup>	Circumpolar
August	2.9372 x 10 <sup>7</sup>	1.6417 x 10 <sup>7</sup>	1.2955 x 10 <sup>7</sup>	Caroninpolar

#### 4.2 Surface Moisture and Vegetation

#### Mississippi River Valley

Examination of the Nimbus III HRIR daytime (0.7 - 1.3 micron) reflectance data in the lower Mississippi River Valley during the period April-September 1969 revealed the presence of significant variations in pattern and tone. Investigation of the possible causes of the changes through literature review and verbal communications (34, 35, 48) suggests that the changes in reflectivity observed on the successive photofacsimiles (Figure 8) and computer produced grid-print maps (Figure 9) correspond primarily to decreases in soil moisture during the dry (1969) summer season. This moisture decrease affects the vegetal cover (wilted vegetation, poor crop yield) and soil texture and the radiometer, in turn, integrates those changes as higher reflectances.

The changes in the reflected solar radiation are easily seen on the photo-facsimiles and may be expressed in relative quantitative terms from the grid-print maps (Figure 9). An increase in reflectance from 22 May to 9 August correlates with a decrease in rainfall in that area. A reversal to a lower relative reflectance during 12 September was a response to the moisture added to the ground in the form of rain. Based on rainfall statistics alone, and without another ground checks, it is possible to conclude that the fluctuating reflectance patterns are mainly due to the soil-moisture, vegetation and soil texture conditions present in the heavily cultivated flood plain soils of the lower Mississippi Valley.

#### The Ouachita River Flooding

Flooding conditions within the Mississippi River Valley during the spring season have also been detected by Nimbus remote sensing data. As ground-truth an Apollo IX near-infrared picture (Figure 10), taken on 9 March 1969, showed an area of flooding along the Ouachita River near the Louisiana-Arkansas border and tonal changes between intensively cultivated land along the Mississippi River and the less intensive cultivation to the west of it.

Analysis of corrected Nimbus III HRIR grid-print reflectance values for 25 and 30 April show a similar flooding pattern along the Ouachita River (Figure 11). Heavy rainfall on 28 April possibly accounts for the lack of a re-

flectance boundary between the two major vegetation types visible in the Apollo imagery (48).

The 6 June values suggest a reduction of the flooded area. However, a weak northeast-southwest tonal gradient corresponding to the two major vegetation types visible in the Apollo picture has now appeared.

By 9 August, there is a marked reflectance increase in the eastern half of the picture. No rain had fallen in this area in over two weeks. This drought seems to have had a pronounced effect on reflectance in the intensively cultivated area along the Mississippi River with a lesser effect on the different vegetation in the western half of the map. All evidence of the spring flood along the Ouachita River has disappeared by this date.

Even though the 12 September map indicates an overall reduction of reflectance values (due to rainfall of about one inch between 2 and 7 September), the NE-SW vegetation boundary is still evident.

There is no doubt that the Ouachita flood did occur. Not only was it picked up by the Nimbus satellite HRIR sensor, but it was also substantiated by ground-truth, in this case Apollo IX spacecraft imagery. Ground-truth, unfortunately, is not always available for the interpretation of many other remotely sensed hydrological events. The detection of the Ouachita flood on Nimbus imagery, however, offers us quasi-ground-truth for the interpretation of similar temporal reflectance patterns in other regions of the world.

### Niger River Valley

Another terrestrial event monitored by the Nimbus III HRIR and briefly described here has occurred in the vicinity of the inland "delta" of the Niger River, western Africa. Examination of a series of photofacsimile prints from June to November of 1969 revealed marked tonal changes. Additionally, evaluation of the digitzed grid-print maps of the area provides quantitative information on the solar reflectance characteristics of this area.

Photofacsimile data - In general, the transitions in shades of gray from dark along the Guinea coast (Nigeria, Dahomey, Togo, etc.) to moderate gray

and finally into pale gray at approximately 15° N latitude roughly correlate with the broad vegetative zones that include tropical forest, Savannah forest and Savannah grasslands that belt the West African continent south of the Sahara Desert. The transition in IR solar reflectance intensity (expressed in gray tones on prints) is best illustrated on the November 18 nearly cloud-free image, the dry season for tropical West Africa (Figure 12). The shifting regional vegetation boundaries (gray tones) in turn correspond to changes in soil moisture, as a response to the meteorological conditions, are partly illustrated in Figure 11.

A more local ground event is illustrated in Figure 13. The dark pendulous shaped area with its associated side lobes is the great interior "delta" (Pleistocene) of the Niger River. Parts of this region, particularly between Lakes Faguibine and Haribongo, are striated by broadly separated linear dunes of stabilized sand that generally trend northeasterly. Drainage in this region follows the interdune areas that are, in places, several miles wide (Figure 14). The areal, tonal and temporal changes illustrated in Figure 10 most likely correspond to the changing hydrologic and vegetative conditions on the ground. Since Nimbus III HRIR daytime channel senses reflected solar radiation in the 0.7 to 1.3 micron band range, surface water and vegetation absorb more solar radiation than most bare surfaces or dry sands. The increases in the darker tones, therefore, may indicate an increase in soil-moisture content, spread of a denser vegetal cover, local flooding or an increase in evapotranspiration.

A cursory literature examination of ground conditions present in the Niger River Valley south of Timbuktu support the explanation presented above. Table shows the increase of monthly rainfall in the area from April to December. On HRIR imagery reflectances began to drop off sharply in June to August and continued to decrease until their lowest values in October and November. The great volume of water (May to October) inundates the Niger River "delta" (interconnects swamps and lakes) and is partly soaked up by the soil and partly evaporates. The increased ground moisture, in turn, gave rise to the luxuriant vegetal growth as inferred from the varying regional reflectance patterns. It is interesting to note that the Kainje reservoir above Bussa (Nigeria), the Akasombo reservoir on the Volta River, Lake Chad, the inland "delta" of the Niger River above Mopti including Lake Faguibine and Lake Haribongo, and some segments of the Niger River can be delineated with a moderate degree of confidence on the October and

# TABLE 4: MONTHLY RAINFALL (mm.) IN THE NIGER RIVER HEADWATERS MALI, WEST AFRICA (47)

STATION	MONTH										
	APRIL	MAY	JUNE	JULY	AUG.	SEPT.	OCT.	NOV.	DEC.		
вамако	3	54	104	236	276	160	129	0	0		
BOUGOUNI	24	42	177	300	189	245	139	13	0		
SEGOU	0	33	90	170	169	152	72	0	0		
MOPTI	0	4	22	141	268	56	25	0	0		
TIMBUKTU	0	1	0	95	9	37	5	0	0		

November imagery despite the fact that this period marks the beginning of the 'harmattan' season when the atmosphere inland is ordinarily very dusty and nazy to altitudes of about 3050 m. (40).

Furthermore, the varying pendulous-shaped area, repetitively observed on Nimbus imagery corresponds primarily to the Quaternary and Tertiary sediments inderlying the flood plain of this "delta" (Figure 15). And since these sediments are made up of hydromorphic (waterlogged) soils and lacustrine and riverine alluvium (41, 45), their water retention capacity is high. The stored ground water, in turn, supports vegetation growth, to a degree directly proportional to the water capacity. The apparent time lag in the vegetal response to the moisture saturation of soil explains why the "delta" area reflects solar radiation more during the maximum rainfall (July-August) and is at its minimum at the beginning of the dry season (November).

The remote monitoring by Nimbus of a "flood" in the Niger River Valley, may also be indirectly substantiated by the fact that the surrounding area is

marshy and subject to periodic flooding (42).

HRIR digitized data - The Nimbus daytime HRIR data may also be displayed on computer produced grid-print maps. Figures 16 and 17 illustrate the distribution of reflectance patterns in the Niger River Valley expressed in quantitative values. The values have been contoured automatically and then enhanced manually. Notice the gross regional shifts of tonal changes (reflectance values) brought about by seasonal conditions. The reflectance values below 10% shift from approximately 12° and 13° latitude on Figure 13A (July), to 15° and 16° latitude on Figure 13B (August), and Figure 17 (November).

In general, the 7-9% reflectance values over continental areas are indicative of "normal" ground conditions, i.e. moisture stored in the "B" and "C" soil horizons supporting vegetal growth in the "A" horizon. This obviously does not apply to regions underlain by dark colored lithologies, as for examples, lava flows, coal, bituminous limestone, etc. Reflectances below 5-6% are, in turn, correlated with water bodies or extremely hydrous soils (Figure 17). Sands and clouds usually respond with reflectances above the 10-12% values.

Due to the Nimbus HRIR sensor resolution, however, these reflectance value boundaries fluctuate depending on the size and position of water bodies, the time of the year, and the viewing angle. Furthermore, the sensitivity of the HRIR sensor seems to degradate with time, so that progressively somewhat lower reflectances recorded on digitized maps are not necessarily correlative with ground conditions.

A more localized and intriguing reflectance pattern appears in the north-west quadrant of Figure 16. This pronounced NW-SE trending subelongate patter does not always occur, however, on all maps, but seems to appear only after periods of regional rainfall. It may be that this is caused by the run-off being stored in the more porous soils or alluvium; the soil-moisture thus giving rise to the anomalous reflectance pattern. This, however, does not explain completely the reoccurrence of this pattern on different maps. It is hypothesized, therefore, that this feature may represent the ancient course of the Niger River (49). The existence of a former route of the Niger River is not new (50). The significance of this interpretation, however, is in the probable ability of the satellite remote sensors to detect such obscure terrestrial features. The applications of such observations are, of course, obvious and hopefully will

materialize with the initiation of the acquisition of higher resolution imagery from the planned Earth Resources Technology Satellites.

#### 5. CONCLUSIONS AND RECOMMENDATIONS

The foregoing discussion presented a brief look into the feasibility of utilizing Nimbus photographs and imagery for hydrology oriented studies and applications. The value of such data is not just the ability of the Nimbus sensors to pick out local hydrologic features, but also their ability to provide geoscientists with repeated global and synoptic observations. The fact that regional soil-moisture and vegetative changes were observed from an altitude of 966 km. in Mississippi and Niger River Valleys indicates the usefulness of Nimbus data for regional hydrological and ecological projects. In the Antarctic and Arctic Seas, the importance of satellite data for ice hydrology and for near real-time evaluation of ship routing (36, 37, 38, 39) has been expressed repeatedly.

The Earth Resources Technology Satellite (ERTS) is planned for launch by NASA for 1972. The expected repeat coverage from ERTS will enable us to map dynamic terrestrial surface conditions (coastal processes, snowfall and run-off, flooding and drought, vegetation bloom) and classify events and landforms (lakes, rivers, deltas, geologic structures and hazards) on a regional scale for the first time. The presently available Nimbus satellite repeat observations data, therefore, may generate background studies for future more detailed and local applications of the ERTS photographs and imagery.

The following is a tentative list of possible hydrologically oriented studies that may be conducted with the Nimbus data:

- 1. Monitor regional soil-moisture and vegetation conditions (floods and droughts).
- Determine the occurrence and areal changes of snow cover in mountainous areas.
- 3. Correlate snow line changes with snow-melt and subsequent run-off in large watersheds.
- 4. Surveillance of freeze-up and break-up of sea-ice for charting of shipping lanes.

- 5. Track movement of large icebergs for warnings to sea traffic and seamining operations.
- 6. Monitor albedo of the Arctic ice during periods of maximum change (June through August).
- 7. Monitor areal extent and fluctuations of the Antarctic and Greenland ice caps.
  - 8. Monitor and classify ice concentrations and large floes in sea ice.
- 9. Develop techniques to enhance snow and ice texture information available on the direct read (APT) photographic and IR data.
- 10. Develop new classification systems (numerical, optical or geometrical) for lakes and drainage basins using large area coverage photos and imagery.

#### DEFINITIONS AND ACRONYMS

- "A" soil horizon the upper part of soil. It consists of mineral layers of maximum organic accumulation.
- Albedo the percentage of the incoming radiation that is reflected by a natural surface such as the ground, ice, snow, or water.
- Alluvium a general term for all detrital deposits resulting from the operations of modern rivers, thus including the sediments laid down in river beds, flood plains, lakes, fans at the foot of mountain slopes, and estuaries.

  Alluvium may become lithified, as has happened frequently in the past, and then may be termed ancient alluvium.
- Apogee the point in an orbit which is furthest from the center of the earth.
- APT Automatic Picture Transmission.
- AVCS Advanced Vidicon Camera System.
- "B" soil horizon lies under (below) the "A" horizon. It consists of weathered material with an accumulation of clay, iron, or aluminum, or with more or less blocky or prismatic structure.
- BUV Backscatter Ultraviolet Spectrometer.
- "C" soil horizon the "C" horizon, under the "B" horizon, is the layer of unconsolidated, weathered parent material.
- Data orbit the orbit during which data were acquired by the satellite.
- Degradation the lessening of image quality because of noise or any optical, electronic, or mechanical distortions in the image-forming system.
- ERTS Earth Resources Technology Satellite.
- ESSA Environmental Science Services Administration.
- Evapotranspiration a term embracing that portion of the precipitation returned to the air through direct evaporation or by transpiration of vegetation, no attempt being made to distinguish between the two.
- Ferruginous (furruginous) of, pertaining to, or containing iron.
- Floe mass of floating ice some 30 meters to 8 km. across not fast to any shore, formed by breaking up of the frozen surface of a large body of water.

Flood plain - that portion of a river valley, adjacent to the river channel, which is built of sediments during the present regimen of the stream and which is covered with water when the river overflows its banks at flood stages.

FWS - Filter Wedge Spectrometer.

Grid-print maps - computer produced maps of temperature or reflectance values.

Harmattan - a dust-laden land wind on the Atlantic coast of Africa in certain seasons.

HRIR - High Resolution Infrared Radiometer.

Hydrous (hydromorphic) - containing water chemically combined, as in hydrates. IDCS - Image Dissector Camera System.

Imagery - the pictorial representation of a subject produced by electromagnetic radiation emitted or reflected from a subject, or transmitted through the subject, and detected by a reversible-state physical or chemical transducer whose output is capable of providing an image.

Infrared - pertaining to or designating the portion of the electromagnetic spectrum with wavelengths just beyond the red end of the visible spectrum, such as radiation emitted by a hot body. Invisible to the eye, infrared rays are detected by their thermal and photographic effects. Their wavelengths are longer than those of visible light and shorter than those of radio waves, light rays whose wavelength is greater than 700 milli-microns

IR - infrared.

IRIS - Infrared Interferometer Spectrometer.

IRLS - Interrogation Recording and Location System.

Lacustrine - of, or pertaining to, or formed or growing in, or inhabiting, lakes.

Large scale - a large scale map shows a small area of the surface of the earth and with great detail.

Mercator map projection - a conformal map projection of the so-called cylindrical type.

Micron - a unit of length equal to the one one-millionth of a meter.

MRIR - Medium Resolution Infrared Radiometer.

MUSE - Monitor of Ultraviolet Solar Energy.

NASA - National Aeronautics and Space Administration.

Nimbus - an experimental meteorological earth orbiting satellite.

Pack ice - any large area of floating ice consisting of pieces of ice driven closely together.

- PDT Pacific Daylight Time.
- Perigee the point in an orbit which is nearest the center of the earth.
- Photofacsimile a pictorial (photographic) representation of temperature or reflectance values.
- Photography the mapping or surveying of terrain by means of photography. The production of a permanent or ephemeral image of a subject on a medium which is directly exposed to electromagnetic radiation emitted or reflected from the subject, or transmitted through the subject, and is affected by the radiation in direct proportion to the emission, reflection, or transmission characteristics of the subject.
- Polynia a space of open water in the midst of ice.
- Porous containing voids, pores, interstices, or other openings which may or may not interconnect.
- Quaternary the younger of the two geologic periods or systems in the Cenozoic era.
- Radiometer a radiation measuring instrument having substantially equal response to a relatively wide band of wavelengths in the infrared region.

  Radiometers measure the difference between the source radiation incident on the radiometer detector and a radiant energy reference level.
- Regional extending over large areas in contradiction to local or restricted areas.
- Remote sensing in simplest terms, remote sensing is the detection and/or evaluation of objects without direct contact. In a restrictive sense, remote sensing activities include only those involving the detection of the electromagnetic radiant energy.
- Resolution the minimum distance between two adjacent features, or the minimum size of a feature, which can be detected by a photographic or an imaging system. For photography, this distance is usually expressed in line pairs per millimeter recorded on a particular film under specified conditions; as displayed by radar, in lines per millimeter. If expressed in size of objects or distances on the ground, the distance is termed ground resolution.
- Retrograde orbit an orbit with an inclination angle between 90° and 180°, i.e. the satellite has a westward component of motion.
- Riverine pertaining to a river.

RTTS - Real Time Transmission System.

SCR - Selective Chopper Radiometer.

SIRS - Satellite Infrared Spectrometer.

Small scale - a small scale map presents only general features. It covers a large area of the earth, but shows little detail.

Spectral band - an interval in the electromagnetic spectrum defined by two wavelengths, frequencies, or wave numbers.

Subsatellite point - intersection of the local vertical through the satellite with the earth's surface, with the image plane, or with the celestial sphere.

Tertiary - the earlier (older) of the two geologic periods comprised in the Cenozoic era, in the classification generally used. Also, the system of strata deposited during that period.

THIR - Temperature Humidity Infrared Radiometer.

Vidicon - television camera tube.

#### REFERENCES

- 1. General Electric, January 1970: <u>Nimbus IV Reference Manual</u>, Space Division, Valley Forge Space Center.
- General Electric, 1969: <u>Nimbus III Reference Manual</u>, Space Division,
   Valley Forge Space Center.
- 3. National Aeronautics and Space Administration, 1965: Nimbus I High

  Resolution Radiation Data Catalog and Users' Manual, Goddard Space
  Flight Center, prepared by Allied Research Associates, Inc.
- 4. National Aeronautics and Space Administration, 1965: Nimbus I Users'

  Catalog: AVCS and APT, Goddard Space Flight Center, prepared

  Allied Research Associates, Inc.
- 5. National Aeronautics and Space Administration, 1966: Nimbus II Users'

  Guide, Goddard Space Flight Center, prepared by Allied Research
  Associates, Inc.
  - ---, 1966: The Nimbus II AVCS World Montage Catalog.
  - ---, 1966: The Nimbus II HRIR Montage Catalog.
  - ---, 1967: The Nimbus II MRIR Catalog, Vol. I and II.
  - ---, 1966: The Nimbus II Data Catalog, Vol. I, II, III, IV and V.
- 6. National Aeronautics and Space Administration, 1969: The Nimbus III

  <u>Users' Guide</u>, Goddard Space Flight Center, prepared by Allied

  Research Associates, Inc.
  - ---, 1969: The Nimbus III Catalog, Vol. I, Part 1 and 2.
  - ---, 1969: The Nimbus III Data Catalog, Vol. II and III.
- 7. National Aeronautics and Space Administration, 1970: The Nimbus IV Users'

  <u>Guide</u>, Goddard Space Flight Center, prepared by Allied Research

  Associates, Inc.
- 8. Sabatini, R. and J. Sissala, 1968: <u>Project NERO--Nimbus Earth Resources</u>

  <u>Observations</u>, Tech. Rept. No. 7, Contract No. NAS 5-10343, Allied

  Research Associates, Inc.
- 9. Greaves, J. R., J. H. Willand and D. T. Chang, 1968: Observation of Sea

  Surface Temperature Patterns and Their Synoptic Changes Through

  Optical Processing of Nimbus II Data, Final Report, Contract No.

  NASW-1651, Allied Research Associates, Inc.

- Kreins, E. R. and L. J. Allison, 1969: <u>Color Enhancement of Nimbus High</u>
   <u>Resolution Infrared Radiometer Data</u>, Goddard Space Flight Center,
   NASA Publication X-622-69-86.
- 11. Demaso, J. M., R. P. Rappaport and A. Ruiz, 1969: A Digital Color Printer, presented by Allied Research Associates, Inc. at the Electro-Optical Systems Design Conference, New York.
- 12. Rabchevsky, G., 1970: Comments on the Geologic Use of Nimbus I

  Television Photography, Proceedings of the First Western Space
  Congress, Vandenberg Scientific and Technical Societies Council,
  Santa Maria, California.
- 13. Conti, M. A., 1967: Evaluation of Nimbus High Resolution Infrared

  Radiometer (HRIR) Imagery, U. S. Geological Survey, Open File
  Report.
- 14. Neal, J. T., Capt., USAF, 1968: <u>Playa Surface Morphology</u>, Misc. Inv., AFCRL, Environmental Research Paper No. 283, Terrestrial Sciences Lab, Project No. 8623.
- 15. Kuers, G., 1968: Interpretation of Daytime Measurements by the Nimbus I and II HRIR, NASA Publication TN D-4552.
- 16. MacLeod, N. H., 1970: Ecological Interpretation of Nimbus III HRIR Data, Goddard Space Flight Center, NASA Publication X-652-70-98.
- 17. Widger, W., J. Barnes, E. Merritt and R. Smith, 1965: Meteorological

  Interpretation of Nimbus High Resolution Infrared (HRIR) Data, Final
  Report, Contract No. NAS 5-9554, republished as NAS CR-352, Allied
  Research Associates, Inc.
- 18. Hahl, D. C. and A. H. Handy, 1966: <u>Hydrologic Interpretation of Nimbus</u>

  <u>Vidicon Image-- Great Salt Lake</u>, Utah, U. S. Geological Survey,

  Open File Report.
- 19. Pouquet, J., 1969: Possibilities for Remote Detection of Water in Arid and Sub-arid Lands Derived from Satellite Measurements in the Atmospheric Window 3.5 4.2 Microns, paper presented at the International Conference on Arid Lands in a Changing World, Tucson, Arizona.

- 20. Nordberg, J. and R. E. Samuelson, 1965: <u>Terrestrial Features Observed</u>

  <u>by the High Resolution Infrared Radiometer</u> in Observations from the

  Nimbus I Meteorological Satellite, NASA Publication SP-89, pp. 37
  59.
- 21. Sissala, J., 1969: "Observations of An Antarctic Ocean Tabular Iceberg from the Nimbus II Satellite", Nature, Vol. 224, pp. 1285-1287.
- 22. Popham, R. and R. E. Samuelson, 1965: Polar Exploration with Nimbus in Observations from the Nimbus I Meteorological Satellite, NASA Publication SP-89, pp. 47-49.
- 23. Predoehl, M., 1966: "Antarctic Pack Ice Boundaries Established from Nimbus I Pictures", Science, Vol. 153, pp. 861-863.
- 24. Barnes, J. C., D. T. Chang and J. H. Willand, 1969: <u>Use of Satellite</u>

  <u>High Resolution Infrared Imagery to Map Arctic Sea Ice</u>, Document

  No. 8G60F (Final Report, Contract No. N62306-68-C-0276, NASA/

  NAVOCEANO Spacecraft Oceanography Project), Allied Research

  Associates, Inc.
- 25. Bowley, C. J., 1969: <u>Use of Nimbus II APT to Determine the Rate of Ice</u>

  <u>Disintegration and Dispersion in Hudson Bay</u>, Tech. Rept. No. 8,

  Contract No. NAS 5-10343, Allied Research Associates, Inc.
- 26. Knapp, W. W., 1969: "A Satellite Study of the Ice in Antarctic Coastal Waters", Antarctic Journal, Sept. Oct. 1969, pp. 222-223.
- 27. Lowman, P. O., Jr., 1967: Geologic Applications of Orbital Photography, NASA, Tech. Note TN D-4155.
- 28. Popham, R. W., A. F. Flanders and H. Neiss, 1966: Second Progress

  Report on Satellite Applications to Snow Hydrology, Proceedings of
  23rd Annual Meeting, Eastern Snow Conference, Hartford, Conn.
- 29. Barnes, J. C. and C. J. Bowley, 1966: Snow Cover Distribution As Mapped from Satellite Photography, Final Report, Contract No. CWB-11269, Allied Research Associates, Inc.
- 30. Barnes, J. C. and C. J. Bowley, 1968: Operational Guide for Mapping

  Snow Cover from Satellite Photography, Final Report, Contract No.

  E-162-67(N), Allied Research Associates, Inc.

- 31. Barnes, J. C. and C. J. Bowley, 1968: "Snow Cover Distribution as Mapped from Satellite Photography", Water Resources Research, 4, (2), pp. 257-272.
- 32. Barnes, J. C., 1969: Satellite Surveillance of Mountain Snow in the

  Western United States, Final Report, Contract No. E-196-68,

  Allied Research Associates, Inc.
- 33. Barnes, J. C. and C. J. Bowley, 1970: The Environmental Satellite Data for Mapping Annual Snow-Extent Decrease in the Western United States, Final Report, Contract No. E-252-69(N), Allied Research Associates, Inc.
- 34. Sissala, J., 1970: Personal Communique.
- 35. Palmer, W. C., 1970: Personal Communique.
- 36. Gibbs, M. E., 1968: The Utilization of Meteorological Satellite Data in Antarctica, U. S. Naval Support Force--Antarctica, Washington, D.C.
- 37. Freeman, R. F., 1968: <u>Use of Satellite Data</u> at Kodiak in Proceedings, Sea Ice Conference, U. S. Fleet Weather Facility, Navy Department, Suitland, Maryland.
- 38. Whittman, W. I., 1968: <u>Satellite Imagery</u> in Proceedings, Sea Ice Conference, U. S. Fleet Weather Facility, Navy Department, Suitland, Maryland.
- 39. Popham, R. W., 1968: <u>Sea Ice Conference</u> Summarizing and Future Outlook in Proceedings, Sea Ice Conference, U. S. Fleet Weather Facility, Navy Department, Suitland, Maryland.
- 40. Phoenix, D., 1970: Personal Communique.
- 41. D'Hoore, J. L., 1964: Soil Map of Africa, Scale 1/5,000,000, Commission for Technical Cooperation in Africa, Joint Project No. 11, Publication No. 93.
- 42. Dalrymple, R. G., 1970: <u>Cartographic Applications of Orbital Photography</u>, NASA Publication X-644-70-110.
- 43. Environmental Science Services Administration, 1969: Climatological

  Data, Environmental Data Service, U. S. Department of Commerce.
- 44. National Aeronautics and Space Administration, 1968: Earth Photographs

  from Gemini VI through XIII, Scientific and Technical Information

  Division, Office of Technology Utilization.

- 45. Association des Services Geologiques Africains (A.S.G.A.), 1963: Geological Map of Africa, co-edition A.S.G.A. and U. N. Educational Scientific and Cultural Organization (UNESCO).
- 46. Thoren, R., 1969: Picture Atlas of the Arctic, Elsevier Publishing Company.
- 47. Environmental Science Services Administration, 1969: World Weather

  Data Center A, Foreign Data Station, Ashville, North Carolina.
- 48. Sissala, J. and G. Rabchevsky, 1970: <u>Terrestrial Changes Monitored by</u>
  <a href="mailto:the Nimbus Meteorological Satellites">the Nimbus Meteorological Satellites</a>, Proceedings of the First
  <a href="Western Space Congress">Western Space Congress</a>, Santa Maria, California, October 1970.
- 49. Pouquet, J. and G. Rabchevsky, 1970: The Niger (Africa) Interior Delta

  (Macina) Remotely Sensed by the Nimbus II and III Satellite HRIR

  Daytime and Nighttime Radiometers, Allied Research Associates,
  Inc., unpublished in-house report.
- 50. McGinnies, W. G., B. J. Goldman and P. Paylore, 1970: Deserts of the World, The University of Arizona Press.

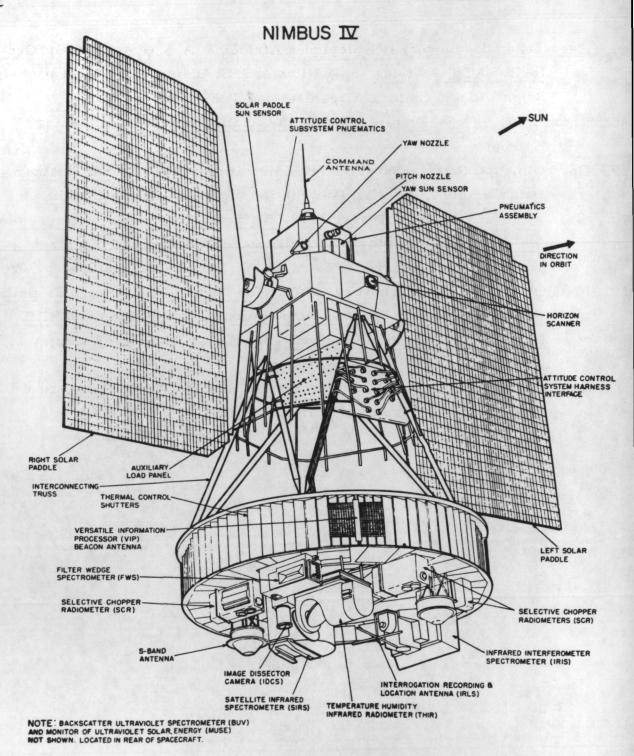


Figure 1: Nimbus IV satellite. The spacecraft is approximately 10 feet tall and I1 feet wide. The base of the satellite houses the sensor instrumentation and other electronic components. The two solar pads continually face the sun and convert solar energy to power the spacecraft. (NASA photo)

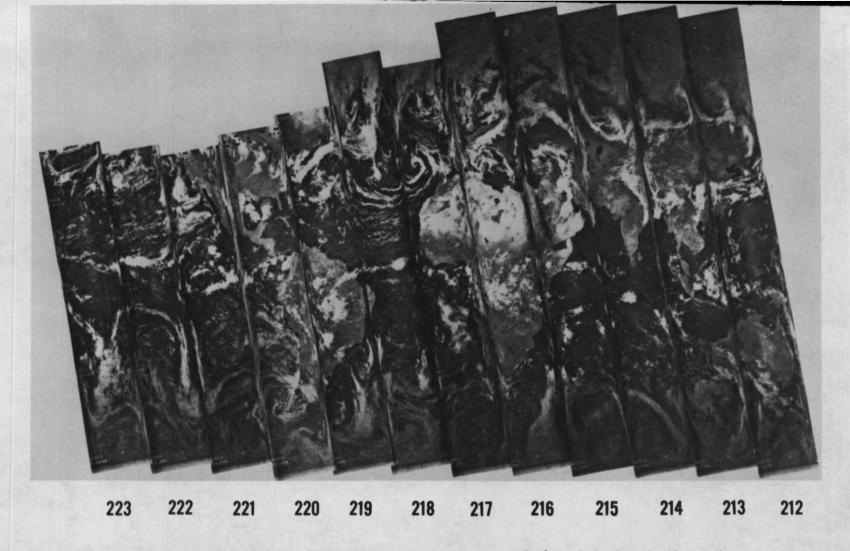


Figure 2: Montage of Nimbus III HRIR Daytime (30 April 1969) photofacsimile strips showing global cloud cover and continent configurations. (All Nimbus pictures were furnished by the NASA Nimbus Project, Goddard Space Flight Center, Greenbelt, Maryland.)

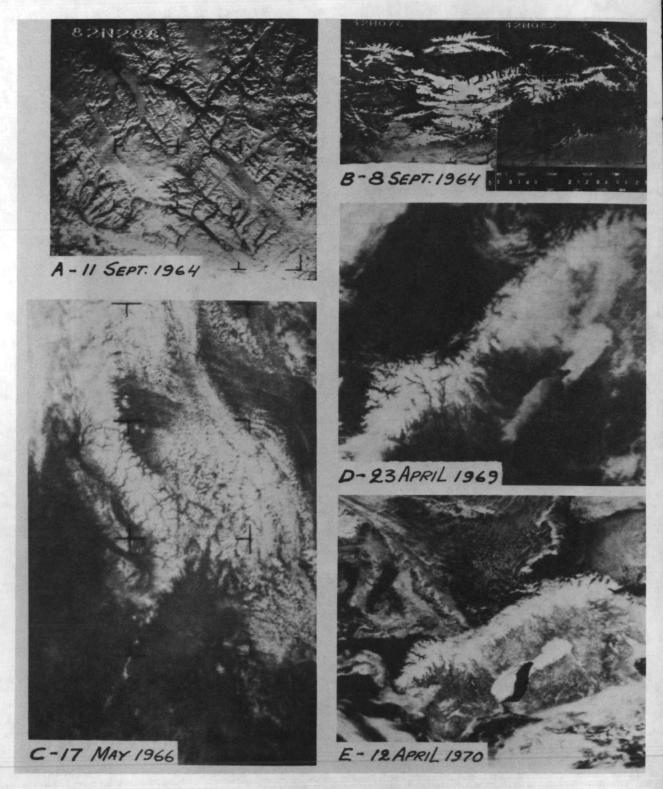


Figure 3: See next page for explanations.

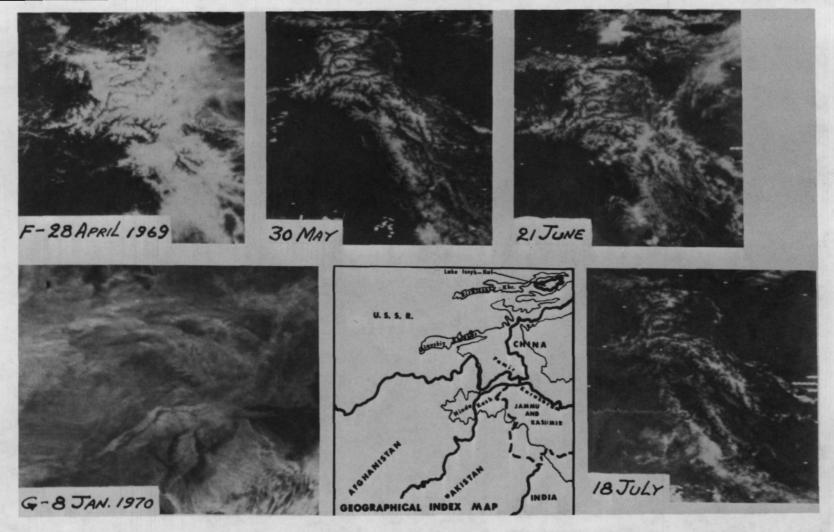
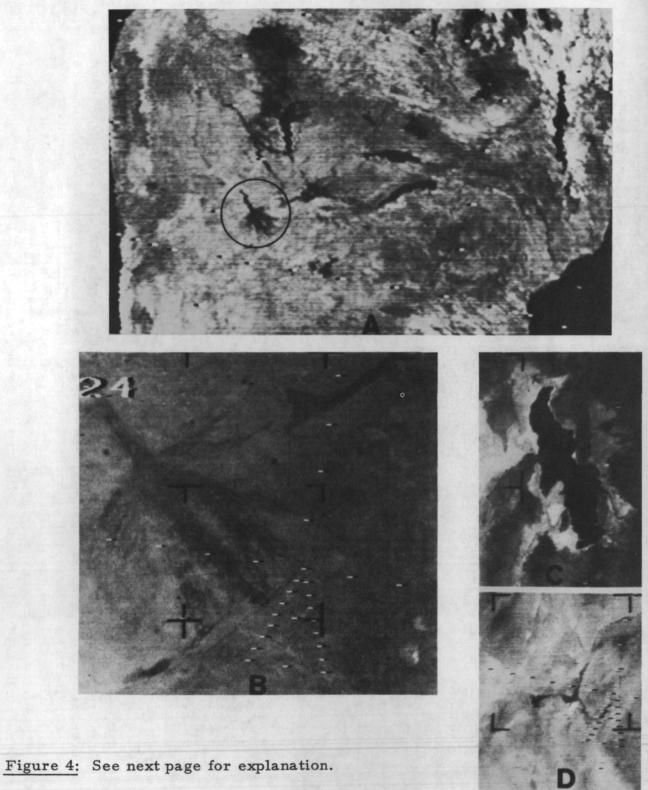


Figure 3: Snow and ice cover distribution viewed by Nimbus satellites: A - Nimbus I AVCS photograph, Ellsemere Island; B - Nimbus I AVCS, Lake Issyk-Kul, Kirgiz U.S.S.R.; C - Nimbus II APT, northwest coast of U.S.A. and southwestern Canada; D and E - Nimbus III and IV IDCS respectively, Scandinavia; F - Nimbus III temporal sequence of IDCS pictures, see map insert for geographical location; G - Nimbus III IDCS, fresh one-half foot snowfall covered a belt from the Blue Ridge Mountains, northeast through eastern Pennsylvania, to northern New Jersey. The remainder of the northeast United States is still covered by the remains of a Christmas snowfall.



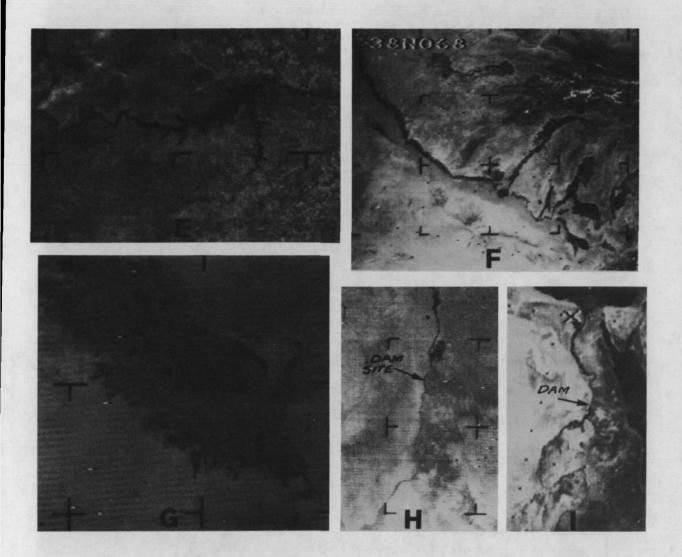


Figure 4: Drainage systems, lakes and reservoirs viewed by Nimbus satellites: A - Nimbus III HRIR (Day), South Africa (Zambezi watershed). The Okavango Basin (circled) is illustrated in B; B - Nimbus I AVCS, Okavango Basin, South Africa; C - Great Salt Lake and Great Salt Lake Desert, Utah (10 September 1964); D - Lake Mead, Nevada (2 September 1964); E - Fort Peck Reservoir, Montana (17 September 1964); F - Nimbus I AVCS, Amu Dary'a River, its tributaries and oases, U.S.S.R. and Afghanistan border area; G - Nimbus I AVCS, Kara Kum Desert, marsh and irrigated cropland along the Amu Dary'a River Delta, U.S.S.R.; H and I - Nimbus I AVCS and Nimbus III HRIR respectively. Arrows point to the site of the Aswan Dam, Egypt. H - Construction of dam four years under way; I - Dam after one year in operation.

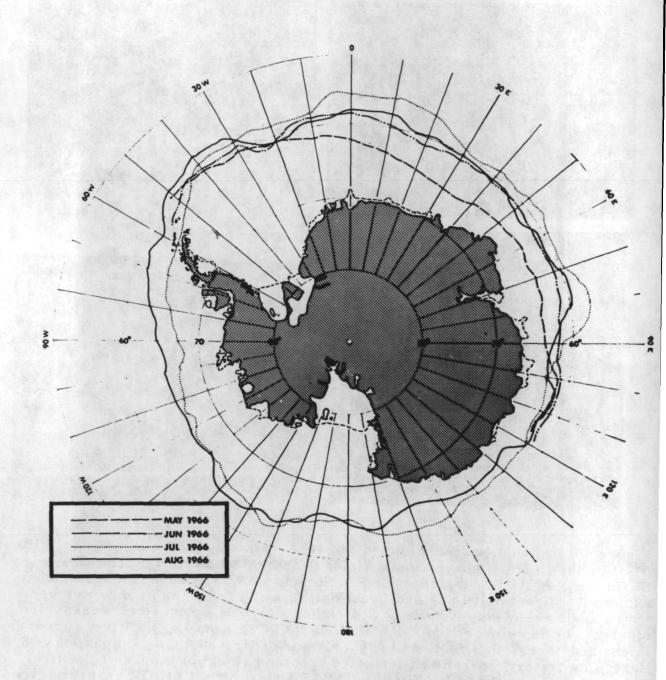


Figure 5: Average monthly Antarctic Pack Ice boundaries derived from Nimbus II AVCS data.

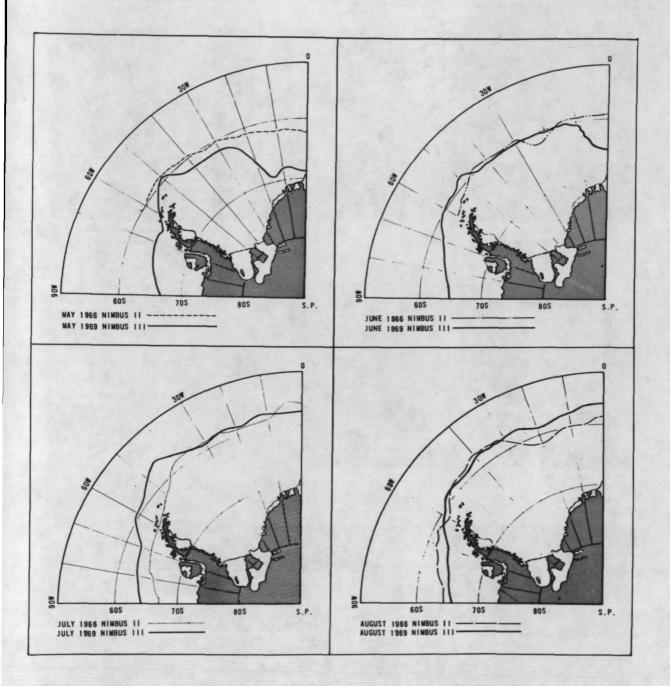
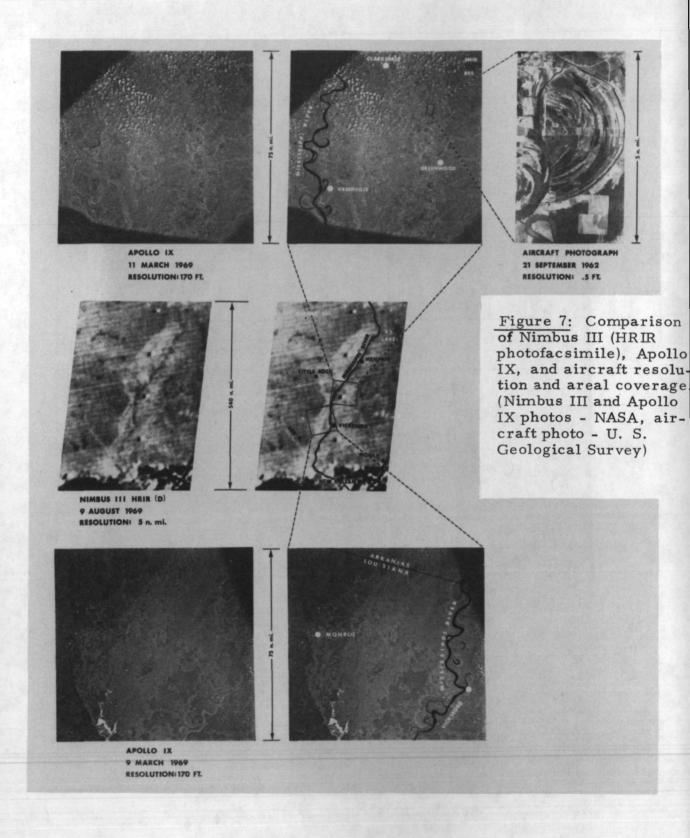
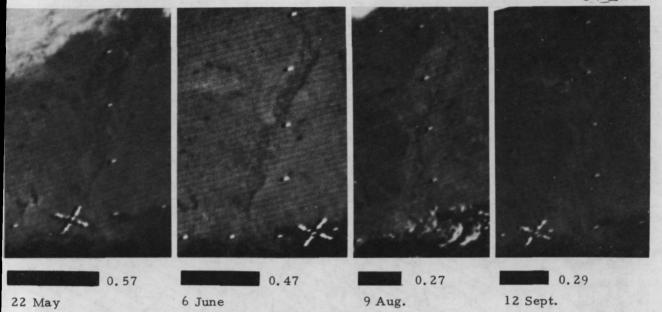


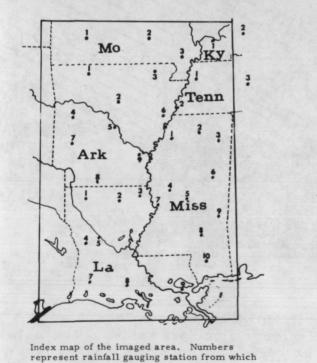
Figure 6: A comparison of monthly fluctuations in the Antarctic Pack Ice boundaries observed by Nimbus II (AVCS) and Nimbus III (IDCS) satellites.





Horizontal bars represent rainfall averages in inches for the week prior to image acquisition. 22 May - rainfall of 0.5 to 2 inches on 18 May; 6 June - rainfall 0.2 to 1.2 inches in Louisiana and Mississippi on 2 June. Light and scattered rainfall elsewhere since 22 May; 9 August - almost no rainfall since 28 July; 12 September - generally heavy rainfall 1 through 12 September. No rainfall from 9 through 12 September (43).

ARKANSAS



information was collected.

#### 1. Clarksdale 1. Harrison 2. Greers Ferry 2. University Walnut Ridge 3. Tupelo 4. Yazoo 3. Blue Mts. Dam Yazoo City 5. Canton Little Rock 5. 6. Forrest City 6. Louisville 7. Narrows Dam 7. Vicksburg 8. 8. Collins El Dorado 9. Meridian 10. Wiggins Dumas KENTUCKY 1. Paducah MISSOURI 2. Madisonville 1. Springfield 2. Ellington LOUISIANA 3. Malden 1. Minden Calhoun Exp. Sta. TENNESSEE Epps 6 W 1. Dyersburg Leesville 2. Memphis Alexandria 3. Centerville

MISSISSIPPI

Gauging stations from which rainfall information was collected.

Baton Rouge Lake Charles Lafayette New Orleans

Figure 8: The varying tonal changes in the Mississippi River Valley illustrated here correspond to solar reflectance recorded by the Nimbus III radiometer (Daytime HRIR) in the 0.7 to 1.3 micron band.

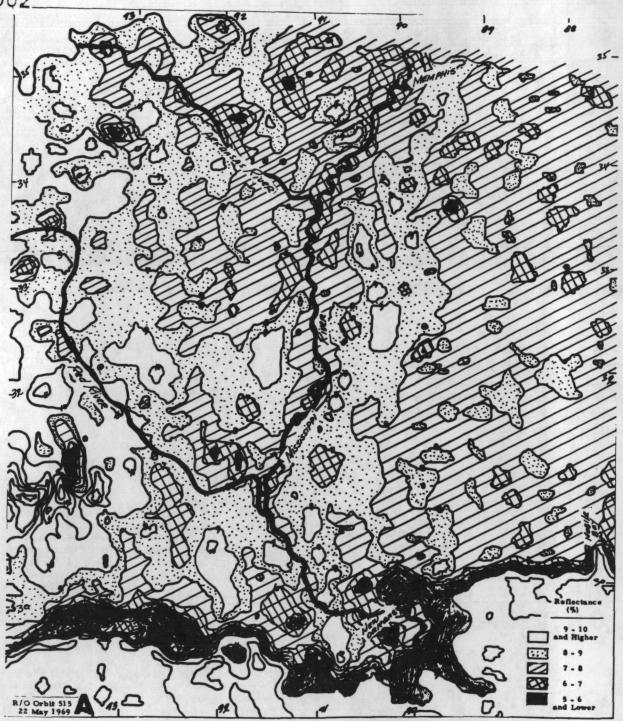


Figure 9: Computer produced (Nimbus III HRIR daytime, 0.7 - 1.3 micron band) maps showing Mississippi River Valley reflectance values. These maps are a digitized product from specially processed analog signals shown pictorially in Figure 8. Such maps are used for more comprehensive analyses of terrestrial features imaged by the Nimbus radiometers. Original scale of grid print map, 1:1 million (Mercator), contoured at 1% interval.

A. Nimbus III HRIR (Day) readout orbit 515, 22 May 1969. Reflectance values along the Mississippi River Valley are lower (6-8%) than on Map B.

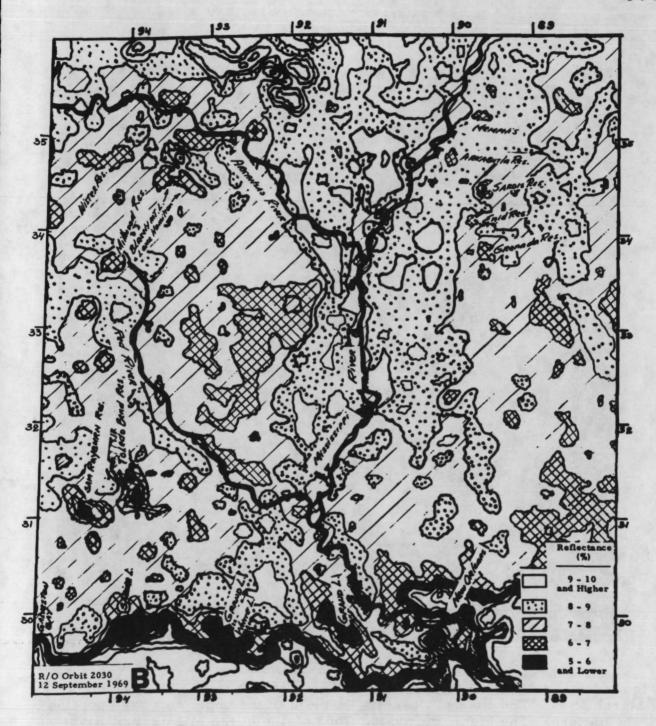


Figure 9 (Continued): Nimbus III HRIR (Day) readout orbit 2030, 12 September 1969. Reflectance values along the Mississippi River Valley are higher (8-10%) than on Map A. See text for explanation of reflectance fluctuations.

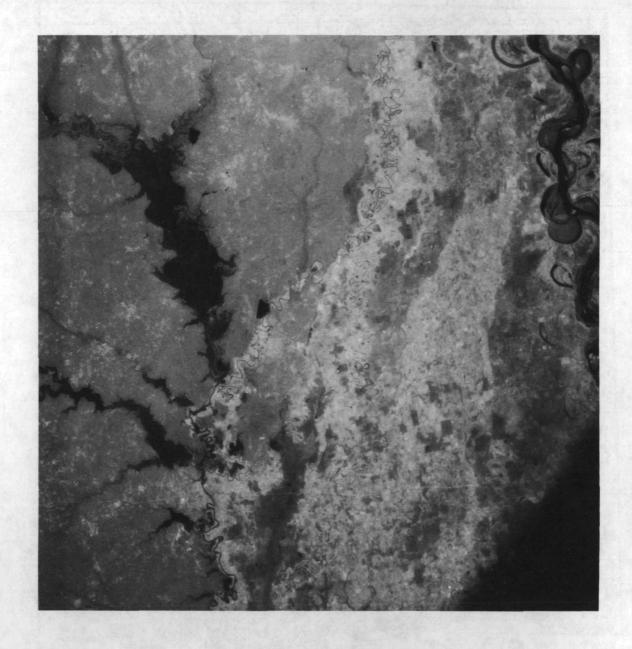
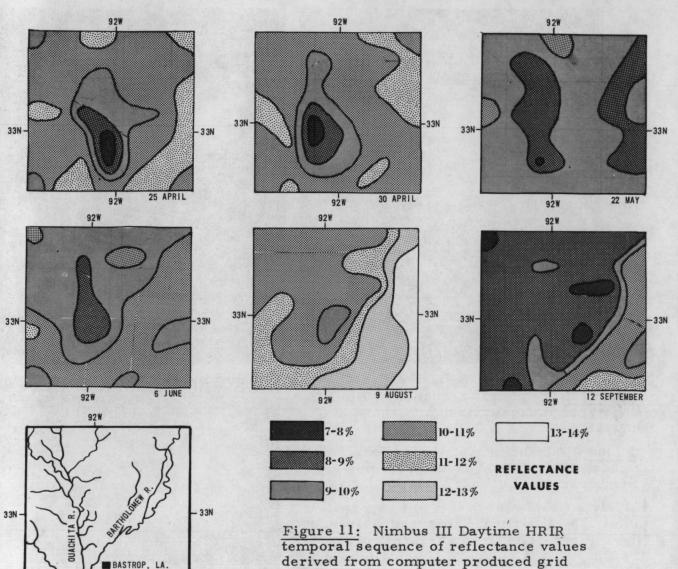


Figure 10: Apollo IX photograph of the lower Mississippi Valley taken on 9 March 1969. The flooded Ouachita River is in the upper left hand portion of the picture. The highly cultivated flood plains of the Mississippi River occupies the right hand portion of the photograph.



92W

temporal sequence of reflectance values derived from computer produced grid print maps. The area is along the Ouachita River at the Louisiana-Arkansas border. Changes in reflectance values and pattern along the Ouachita correlate with lingering effects of an early spring flood. Some of the other patterns correlate with soil and vegetation patterns.





Figure 12: Temporal sequence of Nimbus III (Day) photofacsimile prints showing western Africa.

16 June - Advancing wet season for tropical West Africa; clouds are moving inland from the Gulf of Guinea.

13 July - Clouds move inland to approximately 15° N latitude; storm gyre over Niger River delta; frontal storms over Jos Plateau and northern Nigeria (above Komadiya-Yube and Sokota River Basins).

18 November - Dry season for tropical West Africa. Dust and haze of the harmattan to altitudes of 8-12,000 feet over the Niger River Basin and northern Nigeria.











Figure 13: Temporal sequence of Nimbus III HRIR (Day) photofacsimile prints illustrating the changing tones of the inland "delta" region from August to October corresponds to hydrologic and vegetative conditions on the ground.

Figure 14: Gemini VI photo of the Niger River Valley in central Mali, West Africa. The long dart above and to the right of the striated areas is Lake Faguibine; Lake Haribongo is approximately 100 statute miles below and to the left of it. The city of Timbuktu is between Lake Faguibine and the river. The dark linear pattern south of the river is the result of flooding of stabilized sand dunes. The El Djouf Desert (Sahara) at the upper right is separated from the Aouker Hodh Basin to the west by a cuesta (44). (NASA photo, S65-63247, December 16, 1963)



Figure 15: Geologic and Soil Maps of Niger River Valley South of Timbuktu, Central Mali, West Africa.

- A Geologic Map (45): 1. Quaternary Sediments, 2. Tertiary Sediments, 3. and 4. Pre-Cambrian Lithology, 5. Sands and Dunes, 6. Basic Intrusives, 7. Granites and Pre-Cambrian Lithologies.
- B Soil Map (41): Na Mineral Hydromorphic Soils, Bo Riverine and Lacustrine Alluvium, Ga Sands, Bc Ferruginous Crusts.

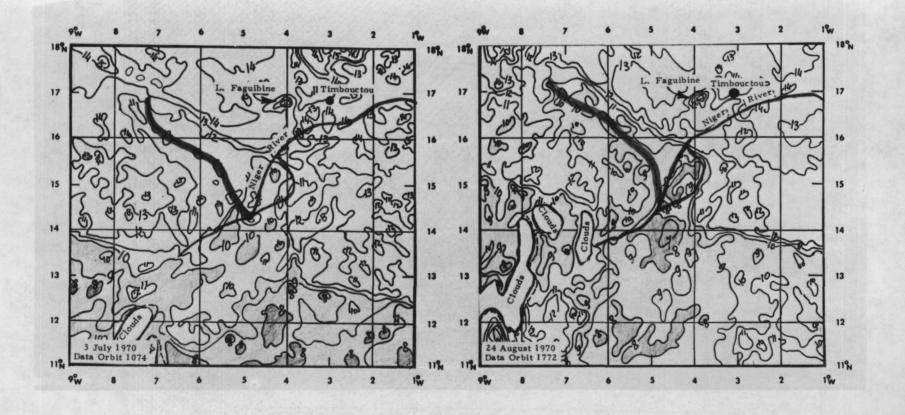


Figure 16: Nimbus III HRIR Daytime Reflectance Values (0.7 - 1.3 spectral band), Central Mali, Africa. Reflectance values lower than 10% are shaded and are indicative of higher soil moisture content and vegetative cover.

Projected former course (Pre-Pleistocene) of the Niger River is accentuated by the heavy shaded line, trending in the NW-SE direction.

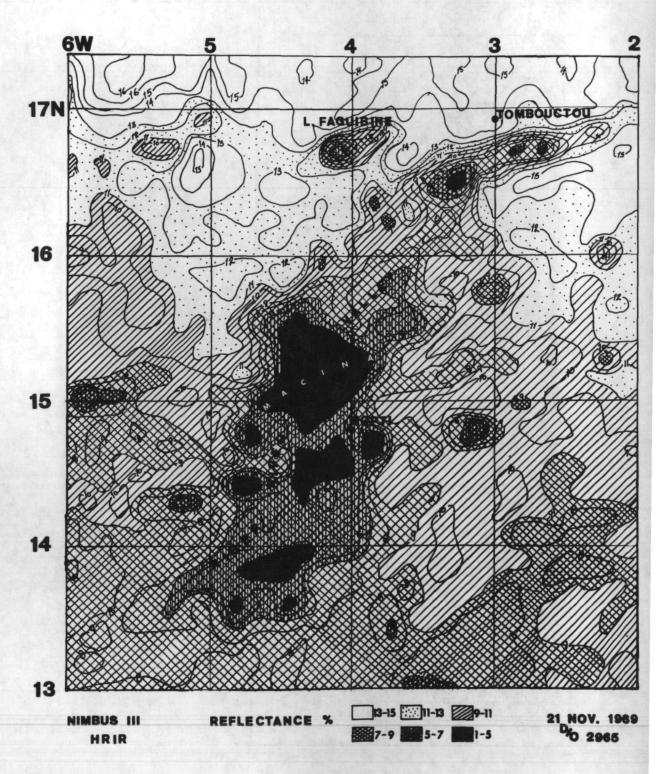


Figure 17: See page 511 for explanation.

Figure 17: Distribution of reflectance values and patterns in the Upper Niger River Valley, Africa, recorded by the Nimbus III HRIR radiometer in the 0.7 - 1.3 spectral band. November in Central Mali is the end of the rainy season ("hivernage") and the beginning of the dry season. The low regional reflectances (compared to July and August maps, Figure 13) are due to the moisture stored in the ground during the wet season, increased evapotranspiration, and the vegetal cover (aquatic and land) that is at its maximum during this season. Reflectance values on this map correspond approximately to the following terrestrial features: 15% and higher: clouds; 12-15%: desert sands (loose material); 11-13%: mostly bare ground (relatively compact); 9-11%: lateritic soil with sparse vegetation; 7-9%: savannah grasslands; 5-7%: vegetation and moisture-saturated flood plain soil; 1-5%: surface water, heavy vegetation, and water-laden ferruginous ground.

RAYMOND M. TURNER is a botanist with the U.S. Geological Survey in Tucson, Arizona. Prior to joining the Survey in 1962, he taught botany at the University of Arizona (1954-1962). Turner attended Utah State University and the University of Utah. After completing his undergraduate studies at those schools he entered Washington State University where he received a Ph.D. in 1954. He has worked on tree growth, palynology, studies of saguaro cactus populations, and the history of changes in Sonoran Desert vegetation. His interest in vegetation led him into the field of remote sensing when he was faced with the need to measure short-term changes in plant volume over areas of several square kilometers.

# MEASUREMENT OF SPATIAL AND TEMPORAL CHANGES IN VEGETATION FROM COLOR-IR FILM

by

Raymond M. Turner

#### INTRODUCTION

When in operation, orbiting satellites, such as those planned for the ERTS Experiments, will have the capacity for following shortterm changes in the appearance of the earth's surface. Weather conditions permitting, a large portion of the earth will be observed at intervals of only a few weeks. Most of the detectable variability on land will indicate either changes in snow cover, in soil moisture, or changes in the amount of green plant material. If measured, changes in vegetation that occur within periods of two or three weeks can be used to pinpoint likely areas for livestock grazing, to help identify crop types and wildland communities, and to estimate primary productivity and evapotranspiration in plant communities. Although measurements of the earth's variable plant cover are of importance to many resource management fields, the ability to estimate the amount of green plant material that covers the soil surface or that is supported by the branches of trees and shrubs remains one of the most elusive measures with which biologists and hydrologists must deal. Recent remote sensing research by the U.S. Geological Survey suggests an approach that may alleviate this data gap. We have been working with techniques which can be used whether the sensing vehicles are conventional aircraft or satellites. Data collection is in a form wholly compatible with current computer technology. Although all of our work has been in an arid area, these techniques should apply to any climatic region.

Most remote sensing studies of vegetation have emphasized measurement of spatial variability: for example, plant community mapping (Higer and others, 1970). A few investigators have used remote sensing techniques to measure plant vigor as it is affected by moisture supply, salinity, or disease (Hoffer and Johannsen, 1969). Measurements of spatial variability do not depend upon repetitive imagery. In contrast, evaluation of temporal variability of vegetation requires multiple observations. Aldrich and Heller (1969) observed vegetation changes over long periods of two and three years in diseased forests by rephotographing the same forested stands. They are probably among the first to apply remote sensing techniques to study changes with time in a vegetation canopy. So far, little attention has been given short-term changes occurring over periods of only a few weeks. The reason for this lies in the special problems that arise when attempting to quantitatively compare multiple photographic observations. Preliminary attempts to standardize repetitive color-infrared photographs will be reviewed in this paper. I wish to emphasize that, as

hydrologists and plant scientists, we have been mainly concerned with ground-truth acquisition. We recognize a potentially important application for the tools of the photogrammetrist and photographic scientist and hope that specialists in these fields may soon apply existing control and calibration techniques to the solution of data needs similar to ours.

Three years ago the U.S. Geological Survey began observing with aerial photographs a 15-mile reach of the Gila River valley in southeastern Arizona (Fig.1). The purpose was to photogrammetrically evaluate short-term changes in the volume of transpiring plant material and to examine relationships between these fluctuations and variations in several hydrologic parameters being intensively studied in the valley. Ground-truth data collected in this intensive investigation of evapotranspiration include ground-water levels, streamflow, rainfall, soil moisture, temperature, humidity, evaporation, radiation, and plant volume (Culler and others, 1970).

The flood plain at the study site is covered by a growth of saltcedar (<u>Tamarix pentandra</u>) of varying density (Fig.2). The adjacent terraces support a short, open forest of mesquite (<u>Prosopis juliflora</u>). Nearby uplands are covered by plant communities comprising such xerophytes as creosotebush (<u>Larrea tridentata</u>), species of <u>Acacia</u>, and various cacti. Stands of each of these plant communities are being studied in our work.

# SELECTION OF THE SENSOR

A readily and continuously available sensing system was needed because our program requires observations of plant changes at two- to three-week intervals. Accordingly, photography was selected as the best technique. Since photographic systems are restricted to wavelengths ranging from just below 0.4  $\mu$  up to 0.9  $\mu$  (Fig.3), this choice narrowed considerably the portion of the electromagnetic spectrum with which we would be dealing. We sought a film or combination of films that could uniquely sense green plant material by taking advantage of the characteristic reflectance of leaves between 0.4 and 0.9  $\mu$ . Within this range, typical leaf reflectance spectra reveal two bands (blue and red) that are greatly affected by chlorophyll absorption, plus a band of relatively high reflectivity in the near infrared region (Fig. 4).

A single black-and-white image could not be used, regardless of the filter employed, because a given grey density value produced by green leaves could be duplicated by many non-plant objects. A combination of two or more images, each recording the energy reflected from plants within different portions of the photographic spectral range was necessary. Black and white multispectral photography was considered but rejected because of the difficulty of exactly aligning the separate black and white images when obtaining densitometer readings from the film.

Another obvious possibility was color diapositive film, either as normal color film or as false-color infrared film. Because of their three-layer construction, these films produce, when exposed, three photo images in one--and the images are perfectly registered.

Without going into detail, note should be made of similarities and a basic difference between regular color film and Ektachrome-infrared (EKIR) film. Both take advantage of the fact that light can be broadly divided into three primary colors-blue, green, and red. (Fig. 4). Furthermore, all colors can be produced by various combinations of these primary colors. Another feature these films have in common is their three-layer construction with the dye content of the superimposed layers selected to produce various combinations of blue, green, and red color in the image when it is viewed with transmitted light. The important difference between these films lies in the sensitivity of the dyes in the three layers: normal color film is sensitive to the same portion of the spectrum as is the human eye; EKIR film sensitivity is shifted toward longer wavelengths so that blues are excluded while invisible infrared is recorded (Fig. 4).

Ektachrome-infrared film was finally selected instead of true color film. Compared to true color film, images of green plants on EKIR film are enhanced and subtle differences between plants are accentuated. This results from the characteristic leaf reflectance properties through the part of the spectral range to which the film is sensitive (Fig.4). As noted by Knipling (1969), the low reflectance of leaves through the visible region is integrated with the high reflectance in the near-IR. Leaf reflectance in these two bands is influenced by two distinct plant systems, one having to do with pigment chemistry, the other with mesophyll anatomy. Both of these systems are closely related to the volume of foliage. Thus, the real advantage of color-IR film over regular color film lies in the ability of the former to sense leaf reflectance in both the visible and near-infrared regions while integrating the effects of two distinct plant traits.

# COLLECTION OF THE DATA

The photographs referred to in this discussion were taken from an elevation 8,500 feet above ground with a K-17 camera equipped with a 6-inch focal length Metragon lens. The film used during the portion of the study covered here was Kodak Ektachrome Aero Film (Type 8443) in 9-inch format. The lens was outfitted with a combination of three filters, Wratten numbers 12, CC20B, and CC30M. This combination was selected following a preliminary study in which 23 different filter combinations were tried according to a system suggested by Fritz (1967). The U.S. Geological Survey took the photographs and processed the film. Photographs were taken between 1000 hours and 1400 hours on 14 different dates between late March and late December 1968.

Optical density values were determined from the three film layers by use of a Macbeth digital read-out transmission densitometer, Model TD-402, outfitted with a 3-millimeter aperture. Readings were made with three filters: Wratten filters, numbers 92, 93, and 94, corresponding to the red, green, and blue spectral bands, respectively. Readings from a fourth filter, number 106 (visual band), were used for some analyses. Absorption characteristics of these filters are shown in figure 5.

As seen in figure 6, dyes in the three EKIR film layers possess overlapping regions of sensitivity and a given layer will be somewhat affected by wavelengths other than those in the range of its dominant sensitivity. By use on the camera lens of the three filters noted earlier (Wratten numbers, 12, CC20B, and CC30M), wavelengths below  $500\,\text{m}_{\mu}$  are excluded and the quantity of light reaching the film is slightly altered in the 500 to 700  $\text{m}_{\mu}$  range to produce a color balance providing maximum detectability of the species with which we are dealing.

In the processed film, the energy received will be expressed as blue green, or red depending on the layer affected. By using a densitometer, a value that is proportional to this energy can be obtained. Because the dyes in the three layers contribute small amounts of color to spectral regions outside the range of their dominant contributions, a density measurement at any point or band along the visible spectrum will be somewhat affected by all three dyes. In photographic parlance, density values of this sort are called integral densities. What is actually needed, though, is a separate density value for each layer with the effect of the other dyes in the tripack removed. This value is called analytical density. The only way to arrive at the analytical density for a tripack film is to derive the values by computation from integral densities. The analytical density values for the three film layers can be determined by matrix analysis if certain characteristics of the dyes are known and provided the green, red, and blue integral density values are read from the same points on the photograph (hence the critical need for exact registry of the images from which the measurements are made).

In practice, density values are obtained by positioning the densitometer aperture over the film by means of a template. The template serves to exactly locate the sample points within the project grid system. With the 8,500 foot photography (scale = 1/17,000) and with a densitometer aperture of 3-millimeter diameter, each sample point corresponds to an area of 0.20 hectares (0.50 acre). Optical density values using the blue, green, and red filters are read from each 0.20 hectare plot.

## ANALYSIS OF DATA

Analysis of repetitive photography presents many problems that arise because of the inescapable changes in photographic conditions from one time to the next. A change in date will usually entail a change in sun angle. If the time of day that the photographs are taken varies, sun angle is again altered. Light intensities vary regularly with the season and randomly with unpredictable variations in atmospheric conditions. Not all the difficulties are related to celestial mechanics or to meteorology, however. Slight changes in film emulsions and in film processing may induce other unwanted effects. Also, variability across individual photographs occurs because of vignetting. As a result of these and still other factors, seasonal differences in color density, attributable solely to changes in plant volume and condition, are confounded with differences due to lack of photographic uniformity. Obviously methods for standardizing and calibrating the photography are essential.

As an illustration of the problems involved, figure 7 shows optical density values obtained from 1300 acres of saltcedar forest as recorded on photographs taken on 14 dates in 1968. Note that the values obtained with each of the filters vary similarly. The red values, which should portray changes in plant volume, are apparently affected by conditions unrelated to this parameter. Obviously an adjustment of the densitometer readings is essential.

To date we have employed few of the controls and calibrations necessary to precisely quantify our measurements and, at best, we are at the semi-quantitative stage. Some of our attempts to obtain standardized measures of plant volume changes will be discussed next.

# CONCLUSIONS

An early attempt by the U.S. Geological Survey to normalize the densitometer readings was accomplished by expressing the color densities obtained with the blue, green, and red filters as percentages of the densities obtained with the visual (number 106) filter (Culler and Turner, 1970). Another standardizing procedure has also been examined. This entails calculating analytical densities from the densitometer readings, converting these adjusted values to transmittances and expressing transmittance for each of the red, green, and blue filters as a percentage of the total red, green, and blue transmittance. In figure 8, red transmittance values adjusted in this manner are shown for 14 dates in 1968. To determine how well this approach can discriminate between areas of different plant density, the densitometer readings for three different saltcedar volume classes are shown. Although detailed ground-truth measurements are lacking for this period, the transmittance values agree with general phenologic observations. The increase in red transmittance from March 22 to April 5 was in response to spring branchlet

growth. The sharp reduction in values between April 19 and May 3 reflects a frost on April 20 which caused partial defoliation. New growth soon restored this loss and the transmittance values increased abruptly in response. The values slowly declined after the maximum of late August as the slow autumnal defoliation typical of the species took place.

As noted in an earlier section, EKIR film is sensitive to two spectral regions that are influenced directly by the amount and condition of green plant tissue. The standardized procedures explained above emphasize energy reflected in the near-IR range and give little stress to reflectance in the red band where plant pigments absorb heavily. Changes in a plant's physiologic condition often result in reduced chlorophyll content. When this occurs, the color balance on EKIR film changes and leaf images change in color from hues of red to yellow hues. There lies in this relationship additional possibilities for normalizing densitometric values obtained from EKIR film. We are currently investigating these possibilities.

Although only preliminary in nature, the results to date encourage us to continue looking for techniques to improve our data gathering capabilities. We feel that a quantitative, seasonal evaluation of the earth's plant covering is feasible and that the potential benefits are great. Solution of this problem is a dual challenge requiring the special skills of the photographic scientist and the resource manager.

# LITERATURE CITED

- Aldrich, R. C., and Heller, R. C. 1969. Large-scale color photography reflects changes in a forest community during a spruce budworm epidemic, in Johnson, P. L. (ed.), Remote sensing in ecology: Georgia Univ. Press, p. 30-45.
- Culler, R. C., and others. 1970. Objectives, methods, and environment--Gila River Phreatophyte Project, Graham County, Arizona: U.S. Geol. Survey Prof. Paper 655-A, 25 p.
- Culler, R. C. and Turner, R. M. 1970. Relation of remote sensing to transpiration of flood plain vegetation: Second Annual Earth Resources Aircraft Program Status Review, National Aeronautics and Space Administration, v. 3, p. 37-1 to 37-8.
- Fritz, N. L. 1967. Optimum methods for using infrared sensitive color films: Photogramm. Eng. v. 33, p. 1128-1138.
- Higer, A. L., Thomson, N. W., Thomson, F. J., and Kolipinski, M. C. 1970. Applications of multispectral remote sensing techniques to hydrobiological investigations in Everglades National Park: Univ. of Michigan, Willow Run Lab. Tech. Report 2528-5-T, 25 p.

- Hoffer, R. M., and Johannsen, C. J. 1969. Ecological potentials in spectral signature analysis, in Johnson, P. L., (ed), Remote sensing in ecology: Georgia Univ. Press, p. 1-16.
- Knipling, E. B. 1969. Leaf reflectance and image formation on color infrared film, in Johnson, P. L. (ed.), Remote sensing in ecology, Georgia Univ. Press, p. 17-29.

### GLOSSARY OF TERMS

- Analytic optical density. The optical density within the spectral range of dominant sensitivity of the individual film layers of a multi-dye layer film.
- Ground-truth data. Information acquired independently of a remote sensing system but describing the object or phenomenon observed by the system.
- Integral optical density. The total optical density of a multidye layer film.
- Opacity. The ratio of the incident to the transmitted (or reflected) light.
- Optical density. The logarithm to the base 10 of the optical opacity.

  Optical density in a multi-dye layer film can be described in two ways, analytic optical density and integral optical density.
- Transmittance. The reciprocal of the opacity.
- <u>Vignetting</u>. The effect of a lens system on a photographic image which produces a fading of the image from the center to the edge of the film.

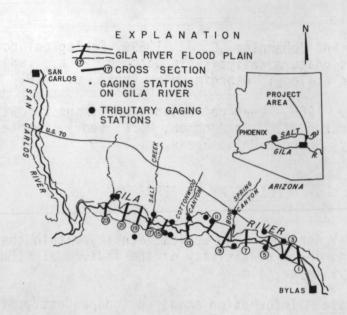


Figure 1.--Map showing location of the U.S. Geological Survey's remote sensing study of vegetation. The numbered cross sections show the location of cleared paths along which instruments for measuring hydrologic parameters are located.



Figure 2.--Unvegetated channel of the Gila River and adjacent flood plain with heavy saltcedar (<u>Tamarix pentandra</u>) growth. Low hills in right midground are sparsely covered with creosote bush (<u>Larrea tridentata</u>) and other desert shrubs.

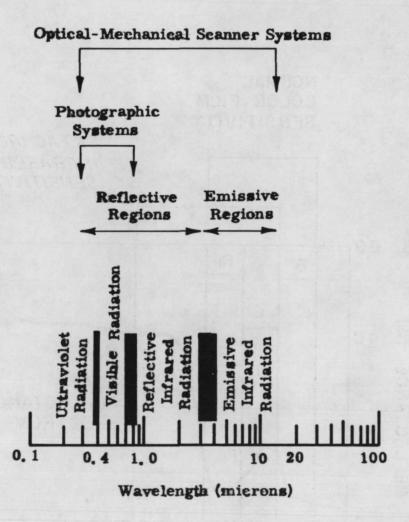


Figure 3.--Portion of electromagnetic spectrum illustrating spectral range of photographic systems.

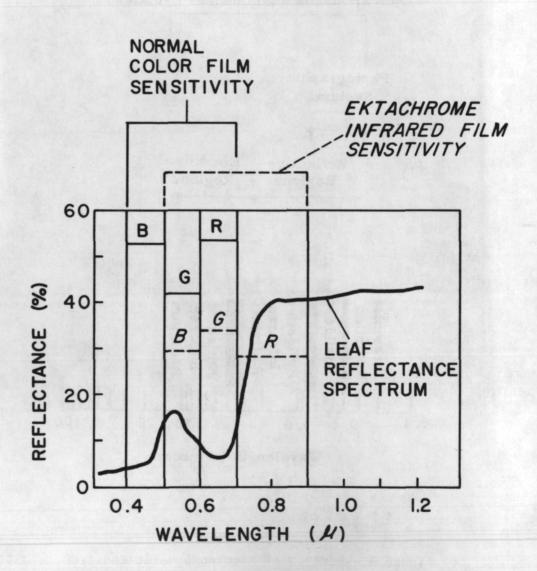


Figure 4.--Typical leaf reflectance curve. The letters indicate the portions of the spectrum which produce the colors blue (B), green (G), and red (R) on normal color film (letters underscored by solid lines) and on Ektachrome infrare film (letters underscored by broken lines).

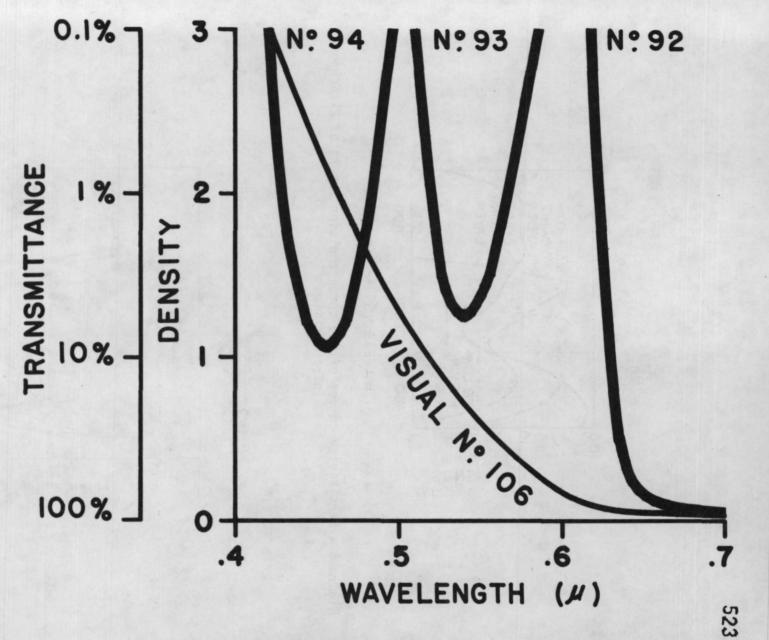


Figure 5.--Absorption characteristics of the densitometer filters used in the film analysis.

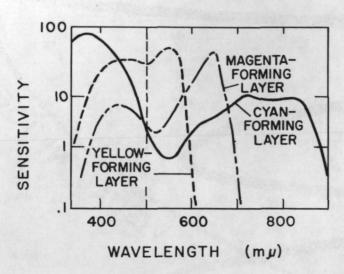


Figure 6.--Sensitivity curves of the three emulsion layers of Ektachrome infrared films.

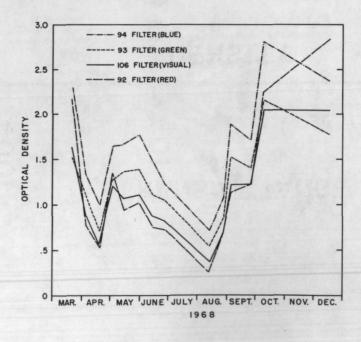


Figure 7.--Average optical densities obtained from Ektachrome infrared photographs of 1300 acres of saltcedar forest. Curves represent densities obtained with the four densitometer filters.

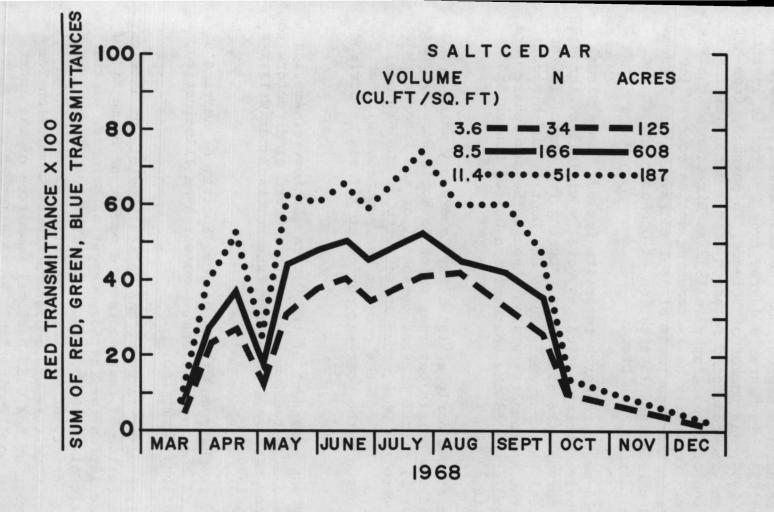


Figure 8.--Seasonal variation of adjusted red transmittances obtained from Ektachrome-IR images of a saltcedar forest, Gila River, Arizona. Data points are mean density values for forest plots representing three different foliage volume classes. N = sample size.

# Seibert Q. Duntley

Professor S. Q. Duntley was born in Bushnell, Illinois in 1911. He received his Bachelor's degree from the Massachusetts Institute of Technology in 1933, his Master's degree from California Institute of Technology in 1935, and Doctor of Science, in physics, from MIT in 1939. He taught and conducted research at MIT until joining Scripps Institution of Oceanography in 1952 as Director of the Visibility Laboratory. Presently he is teaching optics courses for graduate students in the Department of Applied Physics and Information Science and the Scripps Institution of Oceanography at the University of California, San Diego.

Dr. Duntley's major research interests include human visual capability and environmental optics, especially visibility through ocean water and through the atmosphere. During two Gemini flights (V and VII) optical patterns designed by Dr. Duntley and his colleagues to test the astronauts' vision through the atmosphere were laid out over land areas in the southwestern United States and northern Australia.

The program of the Scripps Visibility Laboratory which Dr. Duntley heads had its origin one year prior to World War II. During that war several of the present personnel of the Laboratory were associated with the work, then an activity of the National Research Committee. Much of the program has proceeded without interruption throughout the post-war period at MIT and at Scripps Institution.

Dr. Duntley was president of the Optical Society of America in 1965, and was designated by the Society's board of directors to fill the unexpired term in 1966 of the late Dr. VanZandt Williams, who died in May, 1966.

Dr. Duntley is chairman of the Optical Society of America's representatives to the International Commission on Illumination, also its Publications Committee.

A former director-at-large of the Optical Society of America, Dr. Duntley is a Fellow of that society, a member of Sigma Xi, of the American Association for the Advancement of Science, of the Armed Forces-National Research Council Committee on Vision, and of the Illuminating Society of America. He is the vice-chairman of the U.S. National Committee of the International Commission for Optics and a member of the U.S. National Committee of the International Commission on Illumination. He is a member of the National Academy of Sciences Committee on Observations from Space of Earth

Resources (COSPEAR) and chairman of the COSPEAR Panel on Oceanography and Marine Resources. He is also a member of the newly formed Optical Sciences Center Advisory Group of the University of Arizona.

In 1961, Dr. Duntley was awarded the Frederic E. Ives medal of the Optical Society of America for his distinguished work in optics. At various times he has served as a consultant to the Work Projects Administration, the U.S. Air Force, the U.S. Navy, the General Electric Company, and the Aerospace Corporation.

#### Robert E. Stevenson

Dr. Stevenson is a native Californian, is married, has two sons, and received his academic education at schools and universities in California (A.B. and A.M. from UCLA and Ph.D. from USC).

In 1942, Dr. Stevenson entered the military service and was a navigator for the U. S. Army Air Force. He was recalled to active duty in 1951 as Chief, Photo Interpretation Research, U.S. Air Force. From that duty, he received special commendation for his interpretation techniques with color and infrared films.

From 1953 to 1961, Dr. Stevenson was the Director of Inshore Research, Allan Hancock Foundation, University of Southern Calif. Here he directed all contract research of the ocean environment of southern California for the university. During a sabbatical in 1959, he conducted special research in England for the Office of Naval Research. He has held the position of Research Scientist and Professor of Oceanography and Meteorology, with Texas A & M University and Florida State University. From 1965 through half of 1970, Dr. Stevenson was Assistant Laboratory Director, Bureau of Commercial Fisheries, Galveston, Texas.

Since mid-June, 1970, he has been the Scientific Liaison Officer for the Office of Naval Research, La Jolla, California.

Dr. Stevenson has helped to pioneer the U. S. effort in space oceanography, during the course of which he has been an advisor to the National Council for Marine Resources and Engineering Development, the National Academy of Science, and continues to work with the National Aeronautics and Space Administration to develop space oceanography programs.

#### Almerian R. Boileau

Mr. Boileau was born February 6, 1904. He graduated from the U. S. Naval Academy in Annapolis, Maryland, in 1926 with a degree of B.S. He then served for the next twenty years in the U.S. Navy retiring in 1946 with the rank of Commander. He received his M.A. in physics from San Diego State College in 1951. Since 1953 he has been with the Visibility Laboratory of Scripps Institution of Oceanography engaged in research in the field of atmospheric optics.

Page Intentionally Left Blank

Page Intentionally Left Blank

#### EXPLORATION OF MARINE RESOURCES BY PHOTOGRAPHIC REMOTE SENSING

By

Seibert Q Duntley, Scripps Institution of Oceanography, Robert E. Stevenson, Office of Naval Research, and

Almerian R. Boileau, Scripps Institution of Oceanography

The subject of this paper is the interpretation of photo-graphs in oceanographic remote sensing. The photographs to be presented here were made from spacecraft with two exceptions. Two photographs were made from aircraft.

There were three types of film used to make these photographs: black-and-white, color, and color IR. Black and white photography is well known; it presents pictures in various shades of gray from black to white. Color film presents pictures in color, very nearly as the human eye sees them.

Color IR film presents pictures in color also but not as seen by the human eye. Blue becomes much deeper blue, green is suppressed to some extent, and red is recorded beyond the visual range of the human eye, out in the near infrared. The most noticeable effect of the use of color IR film is that leaf materials which are highly reflective in the infrared part of the spectrum are presented as red.

This slide gives a comparison between color and color IR.

The first remote sensing photograph is in color. It was made in October 1968 by the crew of the Apollo 7 flight. This photograph shows (See Fig. 1) a portion of the Gulf of California, the body of water between Baja, California, and the mainland of Mexico. The spacecraft was north of the photographed area. The photograph was made with the camera looking in a southerly direction.

The bright reflection is from water roughened by wind. The blue color is from smooth, or less rough, water. We believe the streaks in the glitter pattern are oil on the surface of the water. The interesting thing about this photograph is that it confirms the theoretical work relating to the water circulation due to tides and winds.

In this slide (See Fig. 2) we identify the most common components of the ocean color. All of the light is from the sun. Some light appears to come from the sky, but this is, of course, only sunlight scattered by the atmosphere. Consider the direct sunlight falling on smooth water at point A. Of the light which is incident at that point about 2% is reflected at an angle of reflection equal to the angle of incidence and is not seen by the Thus about 98% of the light incident at that point enters the water. Here it encounters scattering particles, water molecules and suspended materials (organic and inorganic), which scatter light. Some of this scattered light returns to the water surface and is seen by the camera. The camera also receives from point A some reflected skylight. Thus the color at point A, as seen by the camera, consists of reflected skylight, light scattered by atmospheric haze, and the color of the ocean water. fortunately, all three of these tend to be blue. Thus from space much of the ocean is seen as a pattern of subtle shades of blue.

At point B, for example, a dark blue portion of the sky is reflected toward the camera. In the water however is a concentration of light scatterers. These might be micro-organisms, schools of fish, or kelp. Often in costal waters the light scatterers are sediments being carried into the sea by rivers. Or they may be sediments being carried away from shore by the tidal action. Deductive reasoning is nearly always used in interpretation of this kind of ocean feature.

The graph on your right shows the absorption coefficient for pure water or the clearest of sea water. As you can see red light (wavelength around 0.6  $\,\mu\,\mathrm{m}$  and longer) is strongly absorbed by the water. Also the violet light at wavelengths from 0.4  $\,\mu\mathrm{m}$  and shorter is also strongly absorbed. The blue and blue-green light is transmitted by clear water to a greater degree than any other part of the spectrum.

Biological activity often gives a green color to the sea. This is because both dead plants and dead animals decompose and the soluble decomposed material is yellow. An accumulation of this yellow stain in the blue water causes the water to have a greenish color. This is common in tidal basins, in bays, and along shores. The dashed curve indicated by Y represents the absorption coefficient for typical bay water.

The dotted line portion of the lower curve, indicated by C, represents the change occurring in ocean water when chlorophyll-bearing green plants (phytoplankton) are present. These plants convert solar energy to food energy and initiate the food chain in the sea. Their concentration is usually too small to give a

definite green color to the sea but a subtle change in the blue color can sometimes be distinguished. Of course the water itself absorbs red light to such a degree that the red absorption of the underwater chlorophyll is lost in remote sensing color photography. The subtle change of blue as shown by the dotted line at C may be discernible in the next photograph.

The area shown in the next color photograph (See Fig. 3) is along the coast of Aden. The Red Sea and the Gulf of Aden are well known for the tremendous plankton blooms that occur in their waters. These growths usually discolor the water, especially near the coasts where the concentrations of the microscopic plants are greatest. There is not always an even distribution of the concentrated blooms, the occurrence being patchy and frequently stretched out in long strings.

In March 1969, the Apollo 9 spacecraft crossed over the Strait of Bab el Mandeb and the astronauts had a perfect view of coastal Aden. In the waters were streamers of discoloration aligned with the light, easterly breezes. Even though no measurements or observations are known from these waters during these orbits, the appearance of the discolored water off Aden is so similar to plankton blooms observed from aircraft that any other interpretation seems unjustified.

Suspended sediments cause the red and infrared reflectance of water to increase so dramatically that the sediment clouds appear in high contrast. It is almost exactly analogous to adding cream to black coffee. Sediment clouds can always be distinguished from bottom features because bottom features do not show when photographed in the region of the spectrum whereas the sediment clouds are extremely prominent. Accordingly, clouds of sediment in clear sea water are easily seen in space photographs and yield valuable information of several kinds of marine resources. This is nicely illustrated in the next color photograph.

The photograph was made by the crew of Gemini 12 as the space-craft passed over the Texas coast November 14, 1966. (See Fig. 4)

The skies were clear and the air was relatively dry. Winds were blowing from the northeast, following a cold front that had moved over the Gulf of Mexico two days before. The direction of the wind was marked clearly by smoke drifting from a marsh fire along the Louisiana coast.

The brisk northerly winds had driven water from the lagoons and estuaries into the Gulf of Mexico. Sediment-laden water (a light bluish color in the photograph) was flowing through all of

the inlets and was caught in the southwesterly coastal current.

Off the coast, large eddies over the shallow Texas shelf (the water depth is 100 meters some 110 kilometers from shore) were outlined by the pattern of suspended sediments and could be seen to carry coastal waters 180 kilometers into the Gulf of Mexico. The seaward flowing currents mark the migration routes of the mature shrimp that live along the Texas coast as they travel to the offshore spawning grounds. By carefully fishing the waters marked by the suspended sediment streams, the shrimp fishermen have developed that fishery into the world's richest.

The next color photograph illustrates the appearance of the ocean bottom in clear ocean water free from sediment plumes.

In December 1965, the Gemini 7 spacecraft passed over the Bahama Islands (See Fig. 5) and a photograph was taken of the Berry Islands that lie to the north of Andros Island. The shallow sand bars and the accompanying surge channels, all composed of brilliant white, calcareous sands, were outlined clearly in this nearly vertical view.

The sands are soft and mobile so that currents, waves, and storm surges readily move and shape the sands. During tropical storms and hurricanes, the surge of water over the Bahama Banks is much greater than normal because of the tremendous masses of water moved in front of the storm by the strong winds. As the waters spill over the banks, large bars and channels are formed that show the direction of the surge. These storm-surge bars are easily noted in this photograph.

Photographs such as this one are of great value in correcting navigational charts. As a result of the study of such photographs a considerable number of chart corrections have been made.

The next color photograph is of the southern portion of Taiwan. (See Fig. 6) The major ocean current systems flow from south to north and around the island of Taiwan. The waters are warm and deeply mixed, having turned northward from the Equatorial Current east of the Philippine Islands. The main axis of the current is east of Taiwan, although its position, as well as its speed, varies seasonally in response to the monsoons of southeast Asia.

On July 19, 1965, the day before this photograph was taken, tropical storm "Nina" was about 180 kilometers east of Taiwan. "Nina" never developed fully and winds of 15 knots were the highest recorded at nearby land stations. By the next day, the storm had dissipated and easterly winds of 4 to 6 knots blew around Taiwan.

When the photograph was taken by the Gemini 4 astronauts, the northern edge of the sun glitter pattern covered the waters adjacent to the southern tip of Taiwan. A range of light-blue colors was produced by the diffuse reflection of the sun from an unevenly roughened sea surface. Winds from the northeast blew across the northerly flowing current to produce the varying roughness of the water. Where the water moved either with the wind, or not at all, the sea surface was smoother and the resulting reflectance color a darker blue than in the flowing current.

As the water flowed north it was parted by the island. As the waters spread away from the island, upwelling took place near shore. The upwelling waters had a smoother surface than those farther seaward. Consequently, they appear to be darker blue than wave-roughened waters. The upwelling water carries nutrients up from the ocean bottom and produces good fishing grounds. We understand that the area of upwelling west of the island has been a good fishing area for years and that the area east of the island is now being exploited.

The science of color measurement can be applied to ocean color. Color measurements can be made, of course, from color photographs by several well established techniques. Such measurements include however, the inaccuracies of color rendering which are inherent in all color photography processes. measurement of ocean color from aerial vehicles or spacecraft is much more accurate. The next two slides show the result of spectroradiometric and colorimetric data obtained by one of the authors using a grating spectroradiometer in an airplane flown some 1300 meters above reefs, sandy shoals, and the Gulf Stream off Dania, Florida. Later the same instrument was mounted in a glass-bottomed boat and returned to the identical ocean locations, where it measured the color of the ocean floor, through the water, directly beneath the boat. (See Fig. 7) The figure on the left shows spectroradiometric curves obtained with the spectroradiometer in the boat, and the figure on the right shows the corresponding measurements when the spectroradiometer was flown at an altitude of 1300 meters. The presence of the reefs and shoals show clearly in the blue and green regions of the spectrum, and the screening effects of the atmosphere are clearly evident in the aerial measurements.

Colorimetric calculations from these data are plotted on a standard chromaticity diagram. (See Fig. 8) The lower, shorter curve represents the loci of the ocean colors as measured from the aircraft. The more saturated ocean colors measured from the glass-bottomed boat are shown by the upper, longer curve.

These are true measurements of ocean color. We are not aware that such measurements have yet been made from space.

Not all ocean color results from the water and its contents, or the ocean bottom, or reflection from the sky. Sometimes reflection of the sun by the surface of the wind roughened sea drastically affects ocean color and in so doing may reveal important clues to marine resources. Consider the geometry in this slide. (See Fig. 9) Parallel sunlight irradiates the surface and at some spot in the ocean a flat water surface would reflect an image of the sun. Although not always within the field of view of the camera, this solar reflection point can always be found, even when the water surface is roughened by wind. When this occurs the image of the sun enlarges into a glitter pattern, the size and shape of which depends upon the surface wind velocity. But even in the presence of wind-driven waves a greater fraction of the area of the sea surface is horizontal than at any other inclination. Thus the center of the glitter pattern stays at the solar reflection point. From the camera position the center of this glitter pattern is dazzling compared with any other point of the field of view and if included in a photograph it is usually overexposed. In our diagram, the water more nearly under the camera may also appear abnormally light because a few unresolved wave facets are tipped at precisely the right angle to reflect sunlight toward the camera. Each wave facet appears like a little piece of sun diminished in brightness by a factor of 2% since that is the reflectance of a clean water surface.

In the lower part of the figure the curve indicates the fractional area of the water-wave surface inclined to reflect sunlight toward the camera. This curve always has its maximum at the center of the sun glitter and the extent of the curve depends upon surface wind velocity. In the example shown, the water appears light wherever a sufficient fraction of the water-wave surface reflects the sun toward the camera. Farther from the glitter center no facets are sufficiently tipped to reflect sunlight to the camera. Here the water appears dark. The glitter pattern in most space photographs appears to have a rather sharp edge. This is partly due to the nonlinear properties of photographic film. Outside the glitter pattern sub-surface phenomena, such as clouds of sediment, can often be seen. Within the glitter pattern however these details are masked by the glitter.

It has already been noted that the extent of the glitter pattern depends upon sea surface roughness. Thus, in nearly calm water the curve is much more steeply peaked than was just shown. While the roughness of the sea depends primarily upon the wind, it is also dependent on the surface tension at the sea surface.

There is an old saying about pouring oil on troubled waters; and mariners have long known that spreading oil upon the surface of the wind-blown sea reduces the surface roughness and facilitates small boat operation for rescue purposes. Natural pils sometimes appear on the surface of the sea as a result of piological activity in the water. This effect is often seen in harbors where such natural vegetable and animal oils are sometimes supplemented by mineral oil from ships. Streaks and patches of oils of any kind can be seen when they occur within the sun glitter because decreased surface tension makes the vater less rough. Lesser roughness means fewer slopes steep enough to cause facets to produce sun glitter. Thus, the oiled areas appear dark in the edge of the sun glitter pattern. In most instances the effect is limited to only a part of the field in view of the camera.

The photograph (See Fig. 10) which illustrates this phenomenon was made from an aircraft flying over San Diego, California.

This black-and-white photograph was made from an aircraft during an aerial survey of the San Diego area several years ago. Fortunately it just happened to show the San Diego harbor at the edge of the glitter pattern. Where the water surface appears light, the water is roughened by the wind. Where the water surface appears dark, a thin film of oil has increased the surface tension causing the water surface to be smoother and therefore less reflective. Incidentally, this black-and-white photograph was made on panchromatic film with a red filter. This, of course, tends to eliminate scattered light from below the water's surface from registering on the photographic film.

The next two photographs are examples of remote sensing from space when color IR film is used. (See Fig. 11.) The first one was made in March 1969 by the Apollo 9 crew. It shows the coast of the United States between Savannah, Georgia, and Jacksonville, Florida. The second was made by a mapping camera being flown at 13 000 meters (42000 feet); it shows several islands in the Florida Keys.

This first color IR photograph of the Georgia coast shows how the blue color of the ocean is accentuated by this type of film. The lighter shades of blue near the coastal islands are believed to be sediment. The vegitation, a dense growth of pine trees, appears red. The mud flats which are shallowly submerged at high tide, are blue gray in color. The channels and waterways through these mud flats are very plainly shown.

This color IR photograph of the Florida Keys shows very claimly the channels and water courses between the two islands

of the Upper and Lower Matecumbe Keys. It is a very good example of how underwater topography can be determined by remote sensing.

There is a great difference in the scale of these last two photographs. The distance along the coastline of Georgia as shown in the preceding slide is about 130 kilometers (80 statute miles) while the section of the road shown in this slide is about 24 kilometers (about 15 miles) long.

## SUMMARY

You have seen several examples of the capabilities of remote sensing.

First, it would appear that the knowledge of where the sediments are, the location of plankton, and determining the area of upwelling water would be of great benefit to the fishing industry.

Second, the use of space photography in remote sensing should be of the greatest value to the cartographers. Corrections to existing charts have already been done due to space photography.

Third, the overall view of the water surface and what can be learned from that view has already been used to confirm theoretical studies of water and wind circulations.

## GLOSSARY

- calcareous Consisting of or containing calcium carbonate.
- artographer Maker of maps and charts.
- not Unit of velocity equal to 1.85 kilometers per hour or 0.515 meters per second.
- nicrometer Unit of length equal to  $1 \times 10^{-6}$  meter (one millionth of a meter).
- hytoplankton Microscopie green plants floating in water.
- lankton bloom Mass or masses of phytoplankton.
- Change in direction of light caused by the light being incident on suspended particles or organisms.
- scatterers Suspended particles or organisms causing scatter.
- spawning grounds Fish breeding areas.

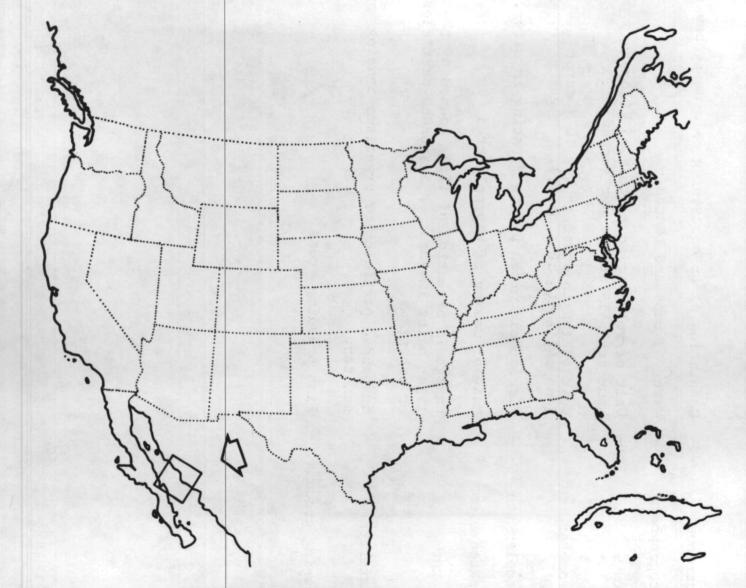


Fig. 1. Area of the Gulf of California shown in first color photograph.

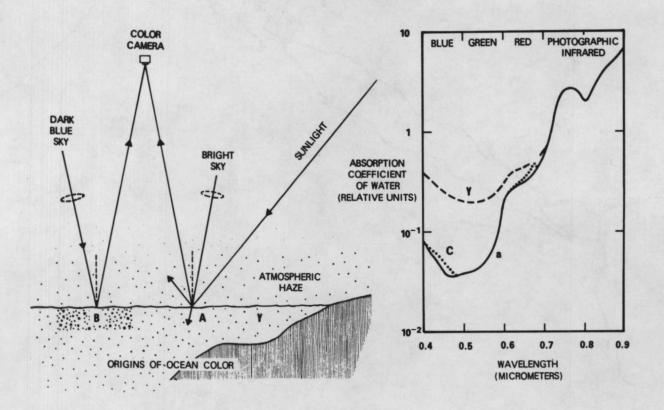


Fig. 2. Origins of Ocean Color.

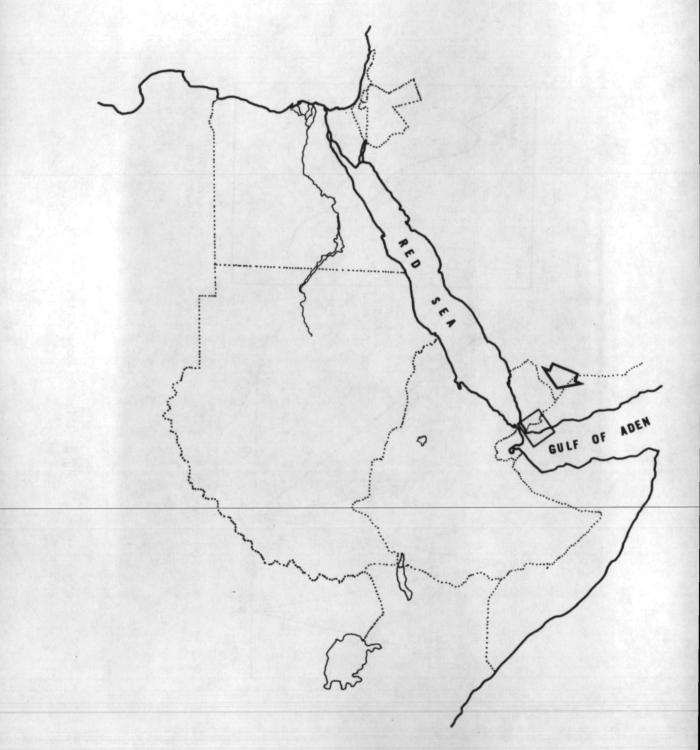


Fig. 3. Aden and the Gulf of Aden shown in second color photograph.

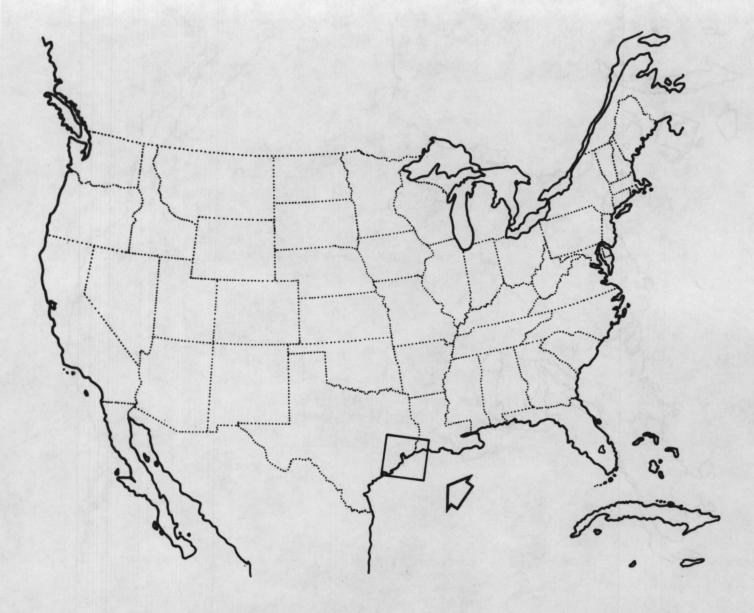


Fig. 4. Texas and Louisiana coastline shown in third color photograph.

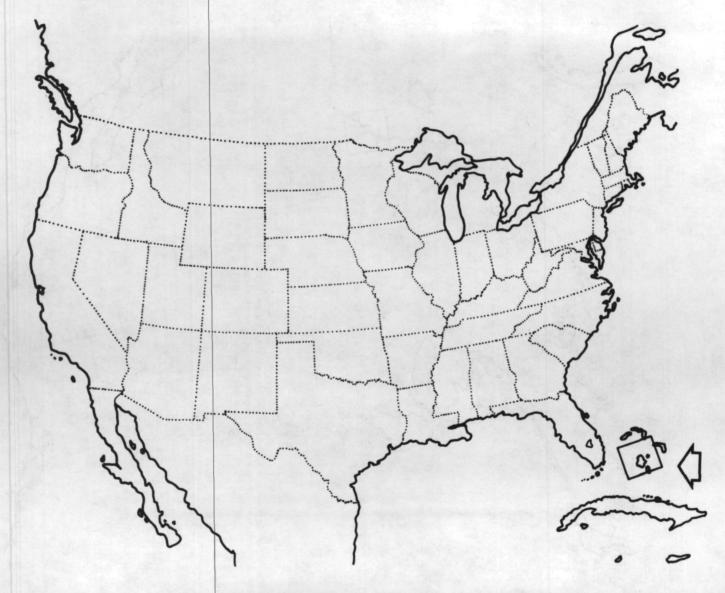


Fig. 5. Area of Berry Islands shown in fourth color photograph.

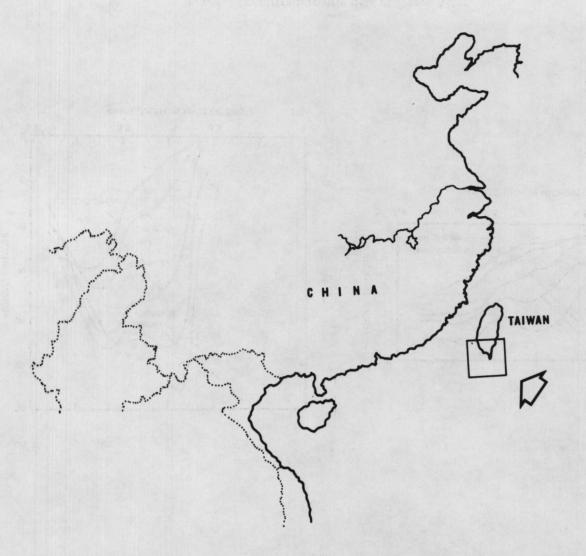
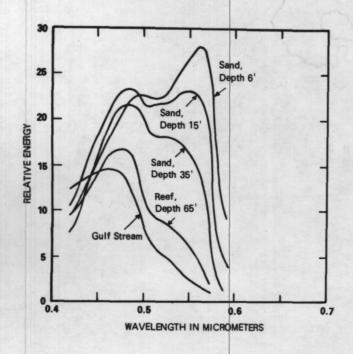


Fig. 6. The part of Taiwan and surrounding ocean shown in fifth color photograph.



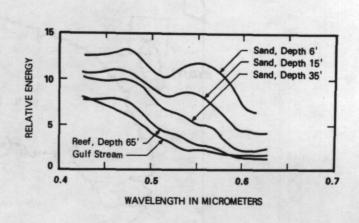


Fig. 7. Spectroradiometric data of Ocean Water.

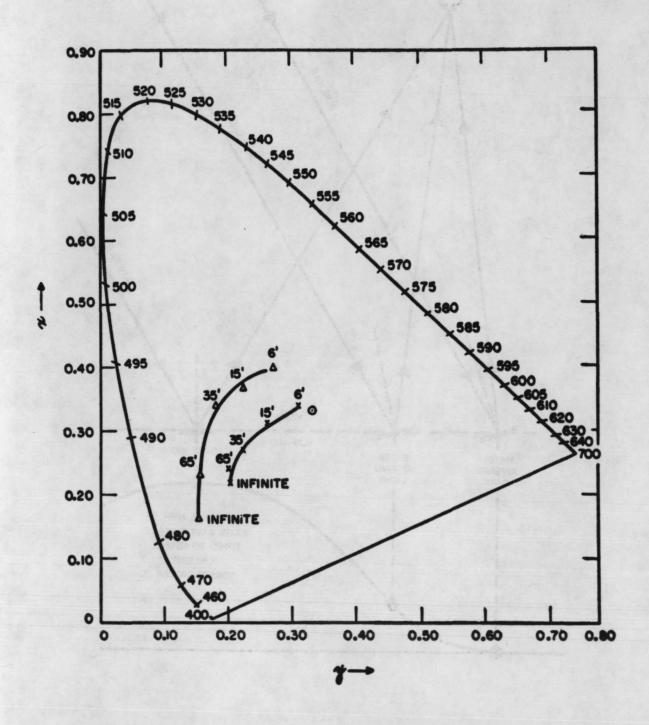


Fig. 8. Chromoticity diagram of data shown in Fig. 7.

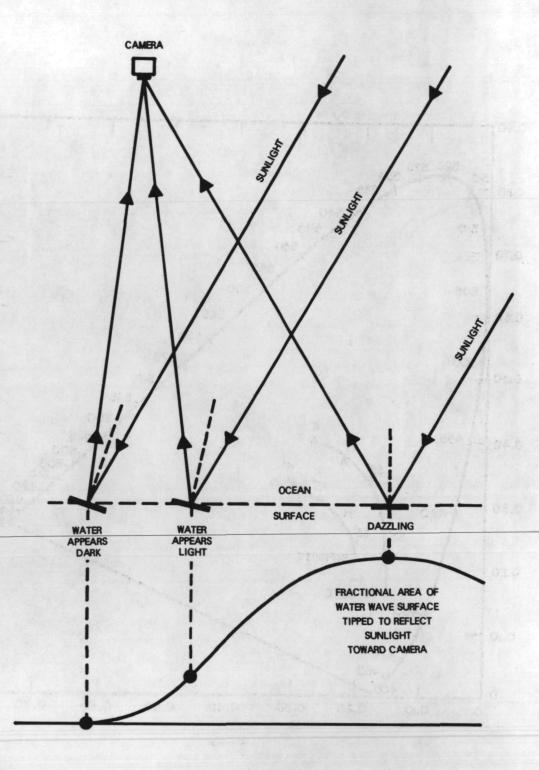


Fig. 9. The geometry of sun glitter patterns.

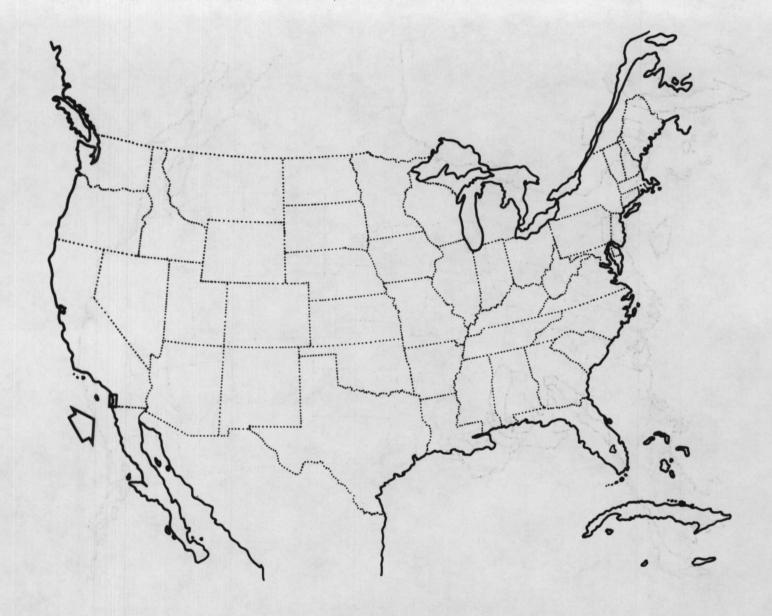


Fig. 10. Location of San Diego harbor shown in black-and-white photograph.

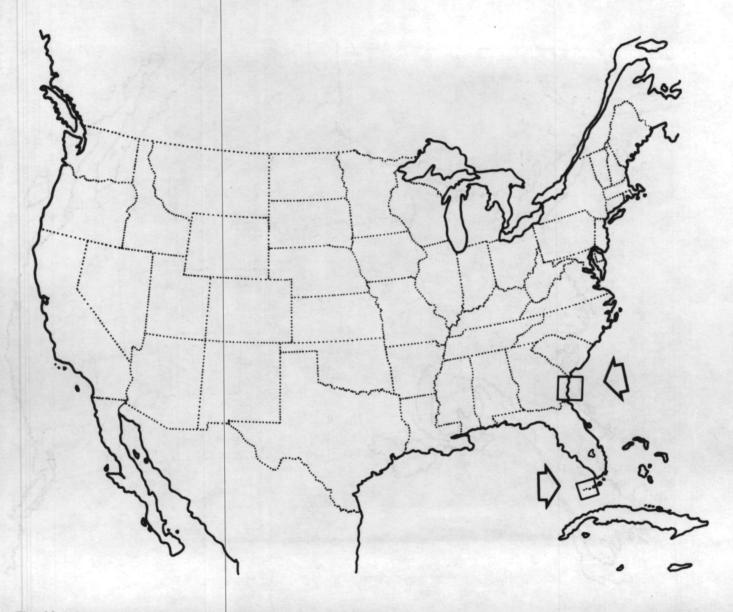


Fig. 11. Areas shown in two Color IR photographs, the coast of Georgia and a part of the Florida Keys.

Page Intentionally Left Blank

#### BIOGRAPHICAL SKETCH

## Robert L. Mairs

Mr. Mairs was born on March 7, 1943, in Alameda, California. He received the B.A. degree in zoology from the University of California, Santa Barbara, in 1966. He has recently completed requirements for the M.S.E. degree in water resource engineering at the Catholic University of America, where his interests were remote sensing of estuarine effluents. From 1965 to 1966, he was involved in the development of infrared sensors for the Santa Barbara Research Center. During 1966, he worked as a biological oceanographer conducting field research on the efficacy of anti-fouling paints. He joined the Naval Oceanographic Office in 1967, and his principal areas of work before joining the Spacecraft Oceanography Project were oriented toward the understanding of coastal oceanographic phenomena. His interests are presently directed toward the application of remote sensors to the study of coastal marine processes.

## OCEANOGRAPHIC INTERPRETATION OF APOLLO PHOTOGRAPHS

Coastal Oceanographic and Sedimentologic Interpretation of Apollo IX Space Photographs; Carolina's Continental Shelf, U. S. A.

Robert L. Mairs

U. S. Naval Oceanographic Office Washington, D. C. 20390

### ABSTRACT

Apollo IX photographs, color band separations, and oceanographic and meteorological data are used in the study of the origin, movement, and dissipation of masses of discolored water on the Carolina's shelf. A model has been developed incorporating jet theory, climatology, currents, surface temperatures, color separations, and other oceanographic data to explain the processes involved in the life cycle of these discolored water masses seen in Apollo photograph AS9-3128.

The "plume-like" patterns of discolored water seen emanating from Ocracoke and Hatteras Inlets are the ebb tide discharges of low density, highly turbid water. Remnant plumes from the previous ebb flow and the boundary between the Gulf Stream and the turbid continental shelf waters are visible further offshore. The photographs show the turbid shelf water being entrained by the Gulf Stream. The intrusion of the Virginia coastal water, which is separated from the Carolina's shelf waters by the Cape Hatteras oceanographic barrier, can be seen to coincide with the 7°C isotherm.

Water mass variability patterns, shown by color space photographs in conjunction with pertinent historical and environmental data plus a concurrent ground truth collection program, can provide valuable synoptic oceanographic data. Space photography is demonstrated to be a powerful tool for the development of a detailed understanding of the basic patterns of circulation, flushing, and mixing on the continental shelves of the world.

### INTRODUCTION

Due to the enormous national investment in space technology over the last few years, the environmental sciences now have a unique global tool: space photography.

Space photographs can produce extremely complete and clear images of the earth's surface, revealing large-scale phenomena and relationships that often cannot be seen from the surface perspective, or at the least are very difficult to grasp from this perspective (Huh, 1969). The intent of this paper is to show that space photographs can be used to detect distinctive water masses, large-scale suspended sediment patterns, and infer coastal and continental shelf processes.

Because ocean water is a complex mixture of solubles, colloids, suspensoids, and biologic matter such as algae, plankton, and seaweed, visible light is absorbed, scattered, and reflected from below the surface in different spectral bands and in varying amounts. These differences create variations in color, brightness, and contrast boundaries on the film. These image variations are the clues by which oceanic masses can be distinguished. If the variable surface water configurations could be detected and plotted regularly, then the resultant charts would provide: (a) a scientific basis for a sampling plan for collection of additional ground truth data, (b) a basis for discriminating between the transient and the more enduring oceanic features, (c) useful data for the surface navigator, and (d) guidance for the fisheries.

The flight of Apollo IX provided several clear, near-vertical color photographs of coastal areas around the world. Of particular interest is the series of photographs taken along the North and South Carolina coasts at various times throughout the mission. Pertinent information concerning some of these photographs can be found in Table 1.

The distribution of turbid waters in one particular photograph, AS9-3128 (Plate 1) illustrates a number of interesting patterns of discolored water that appear to reflect oceanographic conditions on the continental shelf.

Although no ground truth oceanographic data were collected in conjunction with the flight of Apollo IX, meteorological, historical, and oceanographic data are used to interpret the photographs. In addition to these data, photographic color separations of frame 3128 were used in the analysis. Philcò-Ford Corporation (1969) has shown that additional subsurface detail is available from color photography by making color separations in the red, green, and blue regions of the spectrum. A transition in depth penetration is found from red to green to blue. They have found that in the green and blue bands considerable detail is evident in deep waters, whereas the red band yields only near-surface detail.

This paper offers a description and an interpretation of the patterns of discolored water in relation to their origin, movement, and dissipation.

### INTERPRETATIONS

## "Plume-Like" Patterns of Suspended Sediment

In frame 3128, one of the most prominent features is the plume-like pattern of turbid water (Figure 1) which is pouring out through Ocracoke and Hatteras Inlets, N. C. These plumes of discharged water are sharply delineated from the two other distinctive water masses in contact with the plumes (the dark clear coastal waters and the less turbid water outside the plumes). What are the processes that determine the origin, movement, and dissipation of these plumes?

Climatological data supplied by NOAA show near-normal precipitation for March with moderate rainfall on the 9th, 10th, and 11th in various parts of the state. This would indicate significant runoff was being supplied to Pamlico Sound; however, the waters within the Sound appear to be much more turbid than do the waters of the contributing rivers such as the Pamlico and the Neuse, suggesting a relatively small amount of sediment discharge into the Sound. An examination of the contributing rivers and the Pamlico Sound area in the three color separations (Figures 2A, B, and C) should yield information as to the origin of the suspended sediment. The red separation indicates very little suspended sediment is being carried by the rivers, whereas the Pamlico Sound itself appears to be This observation is substantiated by the fact that the amount very turbid. of fine sediment being carried by the contributing rivers was not large enough to account for the amount that appeared to be flowing out. must be some other process operating to cause this turbid water. tological data for Ocracoke and Hatteras Inlets (Table 2) indicate very consistent northwest winds averaging 6 to 17 mph during the period 9-12 These data and the shallowness of Pamlico Sound (less than 15 feet) are strongly suggestive that on 12 March 1969 the turbid waters were being generated in the Sound, dependent on wind-generated shallow water turbulence rather than on heavy rainfall and river discharge.

The tidal origin of the sediment plumes is supported by the fact that the photograph was taken at 1001 EST, which was 4 hours-55 minutes after the predicted ebb current flow began. Slack waters occurred at 0506 and 1154 EST, with the maximum current at 0758 (Table 3). The distribution of the turbid water outside each inlet clearly shows a flow pattern indicative of an ebb-flowing current.

If the plume is of a tidal origin, the horizontal distance it travels as it flows out the inlet could be determined by multiplying the average

velocity during the ebb cycle by the duration.

(average velocity) x (duration) = horizontal distance. (1)

Without direct measurements, the simplest method for determining the average current velocity is to assume that the current-velocity curve approximates a sine or cosine curve. On a cosine curve it is known that the ratio of the mean ordinate to the maximum ordinate is  $2/\pi$ , or 0.637. Therefore, the average current velocity will be the strength of the maximum current multiplied by 0.637.

(0.637) (maximum current) = average current. (2)

Ocracoke Inlet actually has a slightly skewed sine tidal curve (Figure 3); this would not appreciably affect the results, considering the approximations that are made. However, an adjustment must be made to the formula because in this particular instance, the latter low velocity portion of the curve (Figure 3) is not included; from 1001 to 1154 EST. It represents nearly 17 percent of the total area under the curve and covers the currents as they fell from approximately 1.2 knots to 0. Therefore, instead of the area under the curve representing 0.637, a recalculation must be made to take into account the missing portion. Upon measuring the remaining area graphically, one finds that the new ratio of mean ordinate to maximum ordinate is approximately 0.75.

The tidal current table for Ocracoke Inlet (Table 3) shows an average maximum ebb current velocity of 2.1 knots. By applying the approximation Formula 1, the average current velocity should be:

(0.75) (2.1) = 1.6 knots.

Ignoring any interfering effects, a suspended sediment particle that flowed out Ocracoke Inlet at 0506 and was photographed at 1001 should be (from Equation 1):

(2.1 knots) (0.75) (4 hr 55 min) = 7.7 nautical miles outside the inlet.

Measurements from the photograph show the plume extending approximately 6.7 nautical miles out over the shelf.

Here it should be noted that the formula can give only approximate results because the average current is derived through an approximate relationship. More important is the assumption that the suspended particle maintains its velocity throughout its journey, although it undoubtedly does not. Some mixing will obviously take place, and any existing currents will modify its movement. However, a river outflow (in this instance an estuary, but still of hypopycnal nature in the nearshore area) can travel many

miles as a plane jet before density differences between river (estuarine) and oceanic water become so small, due to mixing and sinking, that the uniqueness of the outflow is destroyed (Bates, 1953). Typical density, temperature, and salinity profiles from the shelf waters off Ocracoke Inlet (Figure 4) show the hypopycnal nature of the outflow.

Albertson (1950) has found that the velocity of flow along a jet's axis remains practically equal to the speed of issuance up to a point four channel widths away from the orifice. The Ocracoke Inlet plume extends out over the shelf between four and five inlet widths. Once beyond the limit of four channel widths, lateral turbulence predominates. However, it has been found that, in a two-layer system caused by density differences, not only the above phenomena exists but also the density difference tends to buoy up the outflowing fluids. A two-layer system is difficult to destroy because of the marked stability and the inhibition of vertical or downward mixing caused by the density contrast between layers. Because of density differences, (Figure 4) the ebb flow is basically a surface flow out onto the shelf, whereas the flood flow is basically from the underlying waters. The plume that flows out the inlet during ebb flow does not flow back during flood flow. Some reversal of flow undoubtedly takes place near the inlet mouth, but not enough to destroy the symmetry of the outflow. The sediment plume visible in frame 3569 (Plate 2) off Wynyah Bay, S. C., illustrates the stability of the outflow even during a flood flow.

These data indicate that the plumes are formed by an ebb-flowing current of low density, highly turbid water jetting out onto the shelf through a barrier island inlet. They are cyclic in nature, their origin being linked to each ebb flow. With each change of the tidal flow, they lose the characteristics of a jet and become dependent on the existing winds and currents on the shelf.

For the sediment plume off Ocracoke Inlet to maintain its symmetrical shape on 12 March 1969, the winds and currents in the area would either have had to be rather weak or to move in the same direction as the plume. Data provided by NOAA show a steady resultant northwest wind on 12 March 1969 with an average speed of 16 mph. vector plot of the resultant winds for a period 1-12 March at the Cape Hatteras Station and Figure 6, Haights data (1942), shows the directions and velocities of the average currents accompanying winds blowing from different points of the compass at Capes Hatteras and Lookout. The vector plot (Figure 5) shows that the winds had been blowing from the NW quadrant for four consecutive days and should, according to the Haight chart (Figure 6), generate a wind-driven current moving in a southeasterly direction. However, the fact that the plume is in the lee of the shoreline would decrease the possibility of a strong current in this area because of such a small fetch. This is in agreement with the position and shape of the plume in the photograph as no particular deformation can be detected.

Haights chart (Figure 6) shows that a northeast wind would yield a southwesterly wind-driven current. The effect of prolonged winds from the northeast, is seen in frame AS9-3276 (Plate 3, March 8) of the North Carolina coastal plain. Here the plumes have been driven down the coast in a southwesterly direction as predicted by Haight (1942).

These two photographs, 3128 and 3276, as well as others, all indicate that these plumes are a tidally induced estuarine discharge and that their pattern of travel, once outside the inlet a sufficient distance to overcome the characteristics of a jet, is controlled by the winds and currents prevailing at the time of their discharge.

## Previous Tidal Plumes

In frame AS9-3128, just seaward of the discharge plumes, are sharp sediment boundary lines trailing off from each respective inlet's plume. The lines are aligned to the southeast, and it appears that they are moving in this direction. These sediment lines may represent the remnants of the previous ebb flow discharge plume (Figure 1), because distinct boundaries can still be discerned and the associated waters appear to be more diffuse than the present plume. This should be expected if these features are previous ebb flow plumes as it has been outside the inlet, on the shelf, for a period of from 12 to 17 hours. During this time, differential sinking and turbulent diffusion have undoubtedly taken place causing what seems to be a more dilute turbid water.

An examination of frame 3128 and the three color separations (Figures 2A, B, and C) can make the determination more clear as to whether sinking, mixing, and diffusion have taken place. The red separation (Figure 2A) shows detail only near surface because of the high attenuation coefficient of water in this part of the spectrum. As can be seen in the red separation, the contrast within the present plume is very uniform, suggesting uniformity of composition, and supporting the earlier hypothesis that the plumes flow out of the inlet and maintain their uniqueness for a considerable length of time. The contrast seen along the previous plume line shows a decreasing gradient moving offshore, indicative of sinking. No contrast can be seen further offshore which indicates that the sediments have sunk to a level below that which can be detected in the red band, although they can be seen in the green and blue bands.

Some process or combination of processes must have been operating to cause this sinking. Stefansson and Atkinson (1967) have found that during the winter months, following a period of low air temperature (March 1969 was among the lowest 10 percent of all Marches on record), the temperature-salinity relationships at stations located near the edge of the shelf indicate downwelling of water that has acquired sufficient density by cooling nearshore. The sinking of the turbid water, visible in the three

color separations, to a level of density equilibrium below that of the surface, could be explained by the extremely cold temperatures, the steady NW winds, and the relatively large amount of suspended sediment in the water. Typical winter profiles of the density, temperature, and salinity for this area taken between 23-26 February 1966 (Figure 4) show how this sinking process could take place. There is a progression from the shoreline to the Gulf Stream of cold low salinity estuarine water becoming more saline and warmer (more dense), due to mixing, then flowing under the less dense Gulf Stream associated waters. Equal density levels can be seen trending downward along the outer continental shelf.

The slight south-west bending of the plume can be explained by two separate but interacting phenomena: a generally southwest shelf current and Coriolis Force. Drift bottle experiments made in April and August 1962, described by Gray and Cerame-Vivas (1963) showed conclusively a southwest coastal flow from Cape Hatteras. Stefansson and Atkinson (1967) found that their work on surface density distribution suggested a weak southerly coastal current in Raleigh Bay, N. C. This current was found to follow the depth contours very closely throughout the year. In addition to the southerly shelf currents, Coriolis Force will cause the water currents to bend slightly to the right of the wind direction.

The foregoing interpretation and supporting evidence indicates that these boundary lines and associated turbid waters are a tidal discharge plume from the previous ebb flow. Once they lose the characteristics of their jet flow, they are subject to influences of the existing winds and currents on the shelf. They become subjected to wave-induced mixing, sinking, and dilution and thereby lose their symmetry of shape progressively with increasing time offshore.

A suggested model for the origin and dissipation (life cycle) of the suspended sediment plumes for 12 March 1969 is given in Figure 7.

## Gulf Stream Boundary

In frame 3128, approximately 20 to 30 miles from Ocracoke Inlet, another boundary line is aligned NE-SW as shown in Figure 1. This line represents the contact line between the sediment-laden shelf waters and the Gulf Stream.

The Gulf Stream System is closer inshore off North Carolina than at any point north of Cape Kennedy. The distance from the coast to the inner edge of the Stream generally is about 22 miles from Cape Lookout, 24 miles from Ocracoke Inlet, and 20 miles from Cape Hatteras (Stefansson and Atkinson, 1967). The axis of the Gulf Stream normally lies over the slope between the 100- and 1,000-fathom depth lines. The boundary line in frame 3128 is measured to be 20 miles off Cape Hatteras and as found on

C&GS Chart 1110, 20 miles off Cape Hatteras coast lies halfway between the 100- and 1,000-fathom lines.

Sea surface temperature data for 18 March (NMFS, 1969), six days after the photo, show the Gulf Stream to be very nearly following the 100-fathom line (Figure 8). These data show the North Wall to be fairly straight, and they do not show any meander in the Gulf Stream as might be interpreted from the photograph. However, upon close examination, the sharp boundary line (representing contact) is only present off Cape Hatteras and Hatteras Inlet. The Gulf Stream is visibly in contact with the shelf waters in this area. Off Ocracoke Inlet and to the south, the change in color and apparent density seems to be much more gradual than off Cape Hatteras and represents a gradual sinking and diffusion within the continental shelf waters, rather than the actual margin of the Gulf Stream.

Due to the oblique angle of the photograph, the measurements reported are not exact, but the results from all the lines of evidence do show a close agreement between historical findings (Stefansson and Atkinson, 1967), sea surface temperature charts (NMFS, 1969), and the measurements of the Gulf Stream boundary made directly from the photograph.

The apparent furrows (Figure 1) in the turbid water, that trend in the direction of Gulf Stream flow, indicate that the contact line is being pulled along by the Gulf Stream, much the same as entrained waters would be pulled along by a jet flow. The contact line is very sharp and indicates that sediment is being carried a considerable distance offshore. This movement offshore is very apparent in Plate 3. In contrast, look at the diffuse, sediment line (Plate 1) off the Hatteras Island coast. Here there is no strong current such as the Gulf Stream, so the sediment sinks differentially as mixing takes place.

## Cape Hatteras Oceanographic Barrier

A number of reports mentioned the existence of an oceanographic barrier at Cape Hatteras, separating the northern Virginia coastal waters from the Carolina's shelf waters. The separation of these two water masses is thought to be due to their dissimilarity in temperature and salinity during the winter months. The northern waters are colder, less saline and less dense than the waters on the Carolina shelf. Bumpus (1955) indicated that the shelf waters south of Cape Hatteras did not receive regular intrusions of Virginia coastal waters. Chase (1959) concluded that the extreme changes in temperature and salinity noted at Frying Pan Shoals Lightship was due to the influx of Virginian water which had breached the oceanographic barrier at a time of northeast winds. Bumpus and Pierce (1955) indicated that northeast storms prevalent from November to May often provide sufficient energy to drive northern coastal waters past Cape Hatteras into nearby Raleigh Bay, N. C. Harrison et al (1967) found that

the recovery of seabed drifters and drift bottles south of Cape Hatteras depended on northeast winds. Observations taken at the Diamond Shoals Lightship lend further support to the contention of these workers that northeast winds are necessary to accomplish a break in the oceanographic barrier at Cape Hatteras.

It is postulated that this oceanographic barrier (Figure 1) can be seen in photograph 3128 as a sediment boundary line curving around Cape Hatteras. This frame shows an accumulation of turbid water to the east and southeast of Cape Hatteras overlying the Diamond Shoals area. The turbid water seen to the north of the boundary line is interpreted as an intrusion of Virginian coastal water. This low-salinity, low-temperature water mass from the north flows down Cape Hatteras Island coast onto the Diamond Shoals. Here it seems to be diverted from its southerly flow, forming a large pool of turbid water moving to the east. Without northeast winds, this water mass is unable to break the Hatteras oceanographic barrier, and apparently eddies in this area. Sea surface temperature data (Figure 8) for 18 March 1969 show the colder Virginia coastal waters bending around Cape Hatteras onto the Carolina shelf. If the 7°C isotherm from these data is drawn over the photograph (Figure 9), the area of turbid water and the area of the 7°C water are in very nearly the same position, indicating a slight intrusion of these waters onto the Carolina shelf. But without the strong northeast winds, these colder waters are unable to penetrate further south onto the shelf and instead must flow in an offshore direction.

#### CONCLUSIONS

The main objective of this investigation was to develop and evaluate an interpretive procedure for utilizing space photographs to gain a large-scale understanding of the oceanographic and sedimentologic patterns existent on the continental shelves of the world. The results presented in this paper show that space photography can be used as an efficient means for providing the oceanographer with a permanent record of very detailed near-synoptic data on a very large scale.

Space photography coupled with a properly coordinated program utilizing pertinent historical and routine environmental data with a well planned concurrent ground truth collection program can provide information that will lead to an understanding of the basic patterns of circulation, flushing, and mixing on the continental shelves of the world.

#### REFERENCES

Albertson, M. L., Dai, Y. B., Jensen, R. A., and Rouse, H., 1950, Diffusion of Submerged Jets: Trans. Amer. Soc. Civil Eng., v. 115, p. 639-697.

- 2. Bates, C. C., 1953, "Physical and Geological Processes of Delta Formation," Doctoral Dissertation in Geological Oceanography, Texas A&M.
- 3. Bumpus, D. F., 1955, The Circulation Over the Continental Shelf South of Cape Hatteras: Trans. Am. Geophys. Union, v. 36, p. 601-611.
- 4. Bumpus, D. F., and Pierce, E. L., 1955, The Hydrography and the Distribution of Chaetognaths Over the Continental Shelf, off North Carolina: Deep-Sea Res., supplement to v. 3, p. 92-109.
- 5. Chase, J., 1959, Wind Induced Changes in the Water Column Along the East Coast of the United States: J. Geophys. Res., v. 64, p. 1013-1022.
- 6. Climatological Data, North Carolina, March 1962, v. 74, no. 3, NOAA.
- 7. Gray, I. E., and Cerame-Vivas, M. J., 1963, The Circulation of Surface Waters in Raleigh Bay, N. C.: Limnol. Oceanog., v. 8, p. 330-337.
- 8. Haight, F. J., 1942, Coastal Currents Along the Atlantic Coast of the United States: Coast and Geodetic Survey, Special Pub. No. 230.
- 9. Harrison, W., Norcross, J. J., Pore, N. A., and Stanley, E. M., 1967, The Circulation of Shelf Waters off the Chesapeake Bight: NOAA Professional Paper No. 3.
- 10. Huh, O. K., 1969, "Practical Use of Color Aerial Photography for Coastal Oceanographic Survey," Unpublished Manuscript.
- 11. Local Climatological Data, Cape Hatteras, N. C., March 1969, NOAA.
- 12. Philco-Ford Corporation, 1969, Report on Ben Franklin Spectral Filter Tests, Prepared for U. S. Naval Oceanographic Office.
- 13. Stefansson, U., and Atkinson, L. P., 1967, Physical and Chemical Properties of the Shelf and Slope Waters off North Carolina: Technical Report, Duke Univ. Mar. Lab.
- 14. Tidal Current Tables, 1969, Atlantic Coast of North America, NOAA.

#### GLOSSARY

- 1. Color Band Separations A photographic process by which a Ektachrome color film exposure of wide spectral sensitivity (.4-.7 microns) is split into 3 component spectral bands: blue (.4-.5 microns), green (.5-.6 microns), and red (.6-.7 microns).
- 2. "Plume-Like" Patterns Low density, highly turbid water as it flows from an inlet during an ebb current.
- 3. Remnant Plumes A plume of low density, highly turbid water formed during the previous ebb current.
- 4. Oceanographic Barrier A separation of two water masses due to their dissimilarity in temperature and salinity.



PLATE 1. Apollo IX photograph, AS9-3128, of the North Carolina Coast, taken 12 March 1969, by Astronauts McDivitt, Scott, and Schweickart.

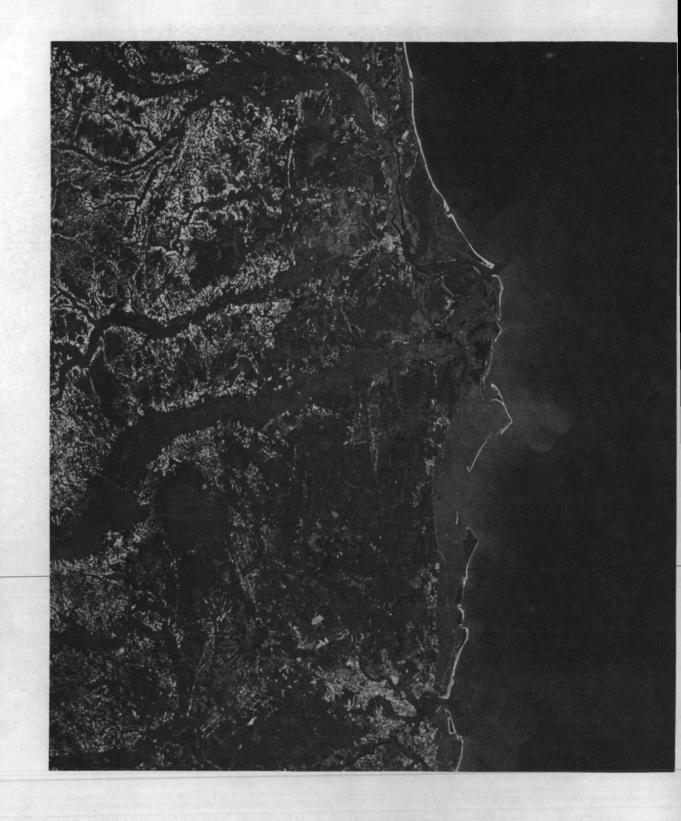


PLATE 2. Enlargement of Apollo IX photograph, AS9-3569, showing Wynyah Bay, S.C., taken 11 March 1969 by Astronauts McDivitt, Scott, and Schweickart.



PLATE 3. Apollo IX photograph, AS9-3276, of the North Carolina Coast taken 8 March 1969 by Astronauts McDivitt, Scott, and Schweickart.

FRAME NO.	DATE		PRINCIPA	AL POIN	T		IMAGE EVALUATION	SUN ELEVATION	TIME	ALTITUDE N. MI.	ONC WAC NO.	PERCENT CLOUD COVER	VIEWING MODE		
			TUDE MIN.		MIN.	PERCENT								DESCRIPTION	
3276	8	35	51N	76	06W	60	Normal	50	1717		G-21	15	Oblique	North Carolina coastal plain, Albermarle Sound, Pamlico Sound	
3568	11	32	48N	80	02W		Normal	49	1622	104	G-21	0	Oblique	East coast of United States, St. Helena Sound, Charleston, Sou Carolina, Santee River	
3569	11	33	06N	79	28W	50	Normal	50	1622	104	G-21	0	Oblique	South Carolina, Charleston, Santee River, Garden City	
3570	11	35	07N	77	04W	0	Normal	50	1623	103	G-21	30	Oblique	North Carolina, Cape Hatteras Wilmington, Atlantic Ocean	
3127	12	34	35N	76	30W	0	Normal	40	1500	116	G-21	15	Vertical	North Carolina, Cape Lookou Pamlico Sound	
3128	12	35	04N	76	01W	0	Normal	40	1501	116	G-21	30	Oblique	North Carolina, Cape Lookout, Cape Hatteras, Pamlico and Albermarle Sounds	

TABLE 1. TIME, POSITION, CAMERA DATA AND SALIENT FEATURES OF SELECTED APOLLO IX PHOTOGRAPHS TAKEN OVER NORTH AND SOUTH CAROLINA COASTS.

## CLIMATOLOGICAL DATA, CAPE HATTERAS, N. C. LATITUDE 35°16'N, LONGITUDE 75°33'W, ELEVATION 7'

		TEN	PERA	TURE (°F	)	PRECIPITATION	PRESSURE	WIND					
	100	y By	1			DESC 2		3361	J.	.H.	FASTES	T MILE	
DATE	MAXIMUM	MINIMUM	AVERAGE	DEPARTURE FROM NORM.	AVERAGE DEW POINT	WATER EQUIVALENT (IN.)		RESULTANT	RESULTANT SPEED (M.P.	AVERAGE SPEED (M.P.	SPEED (M.P.H.)	DIRECTION	
1	53	37	45	-3	41	1.57	29.79	090	7.5	15.4	27	SE	
2	43	37	40	-8	35	.01	29.63	330	20.2	22.7	30	NW	
3	49	36	43	-6	30	0	29.86	330	8.1	12.2	17	NW	
4	44	35	40	-9	30	0	29.82	020	11.9	12.2	22	NNE	
5	44	27	36	-13	25	0	30.06	020	9.6	12.5	23	N	
6	60	27	44	-5	36	.75	29.85	120	6.6	9.2	26	S	
7	57	39	48	-1	40	1.13	29.47	290	12.3	18.3	40	WNW	
8	55	32	44	-6	32	0	29.88	120	1.6	5.8	9	NW	
9	59	37	48	-2	44	.34	29.42	340	6.0	13.8	46	WSW	
10	48	35	42	-8	27	0	29.66	330	11.9	14.8	23	NW.	
11	44	33	39	-11	18	0	29.72	310	17.2	17.7	22	WNW	
12	42	28	35	-15	14	0	29.89	310	14.9	16.0	24	WNW	

# DAILY TEMPERATURE AND PRECIPITATION OCRACOKE INLET, N. C.

		1	2	3	4	5	6	7	8	9	10	11	12
TEMPERATURE	MIN. MAX.	41 51	37 44	34 52	37 49	37 49	33 61	38 57	38 56	46 59	35 55	32 55	41 47
PRECIPITATION		1.00	2.45	0	.40	0	.02	1.71	0	.30	.03	.05	0

TABLE 2. CLIMATOLOGICAL DATA FOR THE PERIOD 1 - 12 MARCH 1969 AT CAPE HATTERAS AND OCRACOKE INLET, N. C. (ESSA 1969).

## OCRACOKE INLET, N. C., CHANNEL ENTRANCE F - FLOOD, DIR. 0° TRUE E - EBB, DIR. 145° TRUE

DAY	SLACK WATER WATER	MAXIMUM TIME	CURRENT VELOCITY (KNOTS)
8	0730	0946	2.0 F
	1306	1604	2.5 E
	1936	2210	2.3 F
9	0142	0440	2.6 E
	0824	1034	1.7 F
	1354	1652	2.3 E
	2030	2258	2.1 F
10	0242	0434	2.4 E
	0924	1134	1.5 F
	1448	1752	2.1 E
	2130	2358	2.0 F
11	0354	0640	2.2 E
	1036	1234	1.3 F
	1600	1858	2.0 E
	2242	0110	1.8 F
12	0506	0758	2.1 E
90.1.44	1154	1346	1.2 F
	1724	2016	2.0 E
	2354		

ABLE 3. TIDAL CURRENT TABLE FOR OCRACOKE INLET, N. C., FOR THE PERIOD 8 - 12 MARCH 1969 (FROM ESSA).

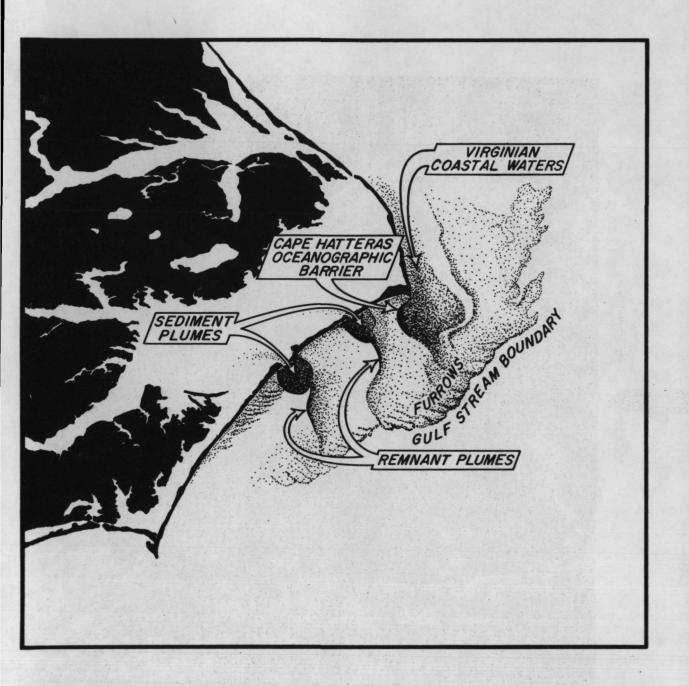


Fig. 1. Oceanographic Analysis of Apollo IX Photograph AS9-3128



Fig. 2A. Red Band Separation



Fig. 2B. Green Band Separation



Fig. 2C. Blue Band Separation

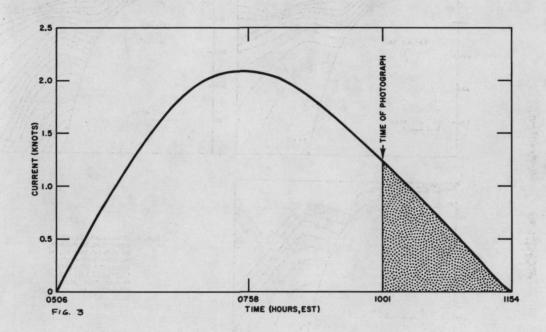


Fig. 3. Theoretical Tidal Current Curve for Ocracoke Inlet, N. C., 12 March 1969

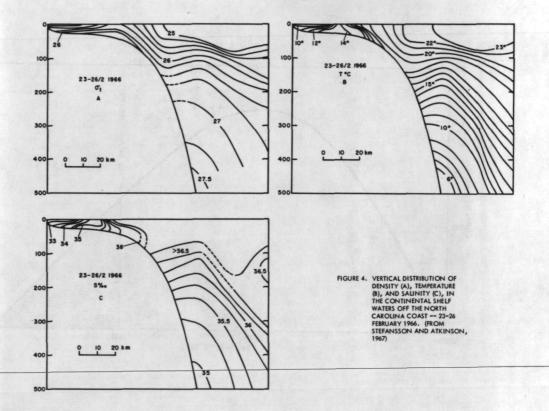


Fig. 4. Vertical Distribution of Density (a), Temperature (b), and Salinity (c) in the Continental Shelf Waters off the North Carolina Coast, 23-26 February 1966 (from Stefansson and Atkinson, 1967)

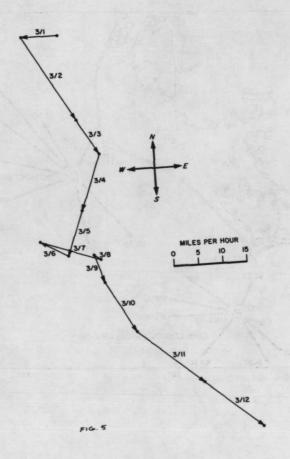


Fig. 5. Vector Plot of Wind Speed and Resultant Direction for Period 1-12 March 1969 at Cape Hatteras, N. C.

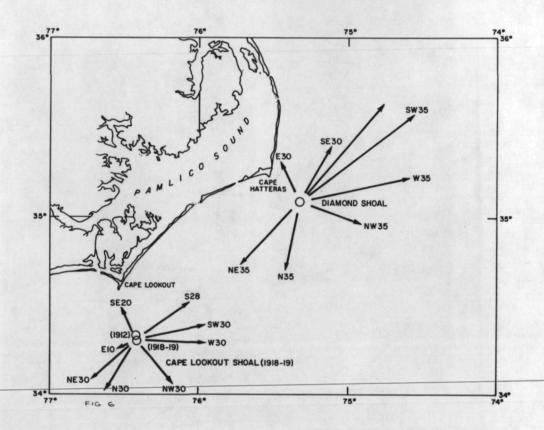


Fig. 6. The Directions and Velocities of the Average Currents Accompanying Winds Blowing from Various Points of the Compass at Capes Hatteras and Lookout (Haight, 1952)

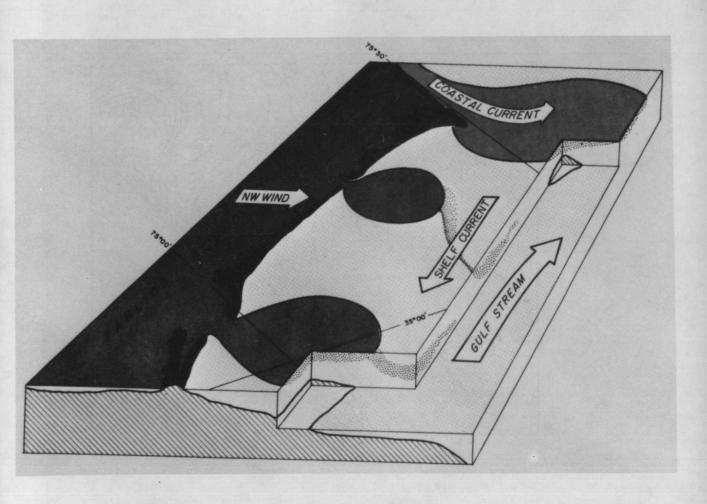


Fig. 7. Theoretical Model for the Formation, Movement, and Dissipation of Discolored Water Masses Seen on the Continental Shelf, 12 March 1969

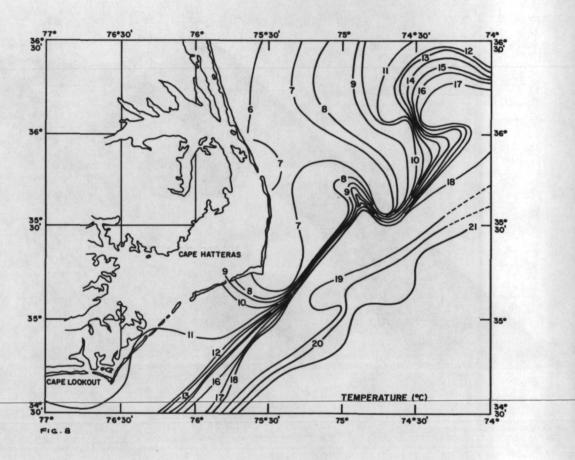


Fig. 8. Sea Surface Temperature Contours off the North and South Carolina Coasts Taken from an Airborne Radiation Thermometer 17,18, 24, 27 March 1969 (National Marine Fisheries Service, 1969)

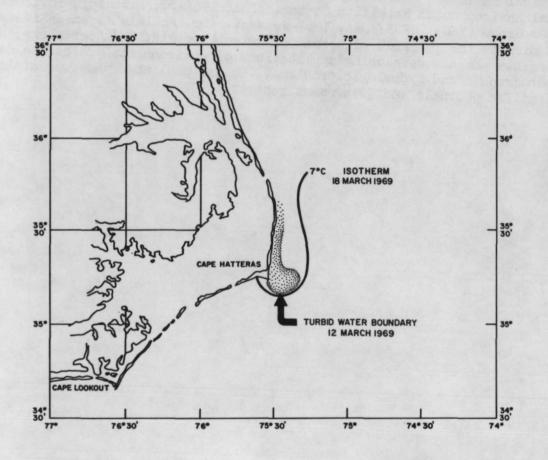


Fig. 9. The 7°C Isotherm from Figure 8 Overlying Apollo Photograph AS9-3128

#### BIOGRAPHICAL SKETCH

E. PAUL MCCLAIN: Research Physical Scientist, National Environmental Satellite Service (NESS) of the National Oceanic and Atmospheric Administration (NOAA). S.M. degree in Meteorology, University of Chicago, 1950; Ph.D. degree in Meteorology, Florida State University, 1958. Professional Member of the American Meteorological Society. Instructor, Dept. of Meteorology, University of Washington, 1950-54; Teaching Assistant and Instructor, Dept. of Meteorology, Florida State University, 1954-57; Instructor and Assistant Professor, Dept. of Geophysical Sciences, University of Chicago, 1957-62; Research Meteorologist, National Environmental Satellite Center, ESSA, 1962-67; Director, Environmental Sciences Group (ESG), NESS/NOAA, 1967-Present. Dr. McClain is an active member of and directs the research of a team of meteorologists, oceanographers, and hydrologists who are developing applications of environmental satellite data to oceanographic and hydrologic problems. He has published numerous articles in scientific journals and Government reports.

#### E. Paul McClain

## 1. Introduction

There are economic and scientific requirements for monitoring polar ice fields, including ice that develops on large subpolar lakes such as our own Great Lakes. Comprehensive and repetitive ice surveys by means of ground parties or by aircraft are hazardous, time-consuming, and prohibitively expensive in the vast, harsh, and poorly accessible regions at high latitudes. A polar-orbiting Earth satellite, however, is a practical means of obtaining much useful sea ice information for operational and research purposes.

Knowledge of sea ice distribution and condition, particularly during periods of formation and breakup, is vital to commercial and military ship movements in the Arctic and Antarctic. More complete and systematic knowledge of the processes of ice buildup, movement, deformation, and decay is needed for the development of analysis and forecasting techniques and effective planning and management of sea transport in polar oceans.

There exists a strong, but not completely known or understood, two-way coupling between the atmosphere and ocean that involves the effects of changing ice fields. This inter-relationship is important in short-period as well as extended atmospheric, hydrologic, and oceanic forecasting. Ice cover, especially the leads and other openings, also plays an important part in the heat balance of polar regions, and this in turn influences atmospheric and oceanic circulation on all scales from local to the general circulation.

The potential of meteorological satellite data for mapping ice fields was quickly recognized after the first pictures from TIROS experimental satellites became available. After the satellite system became fully operational in 1966, and when many countries began receiving their own pictures from the Automatic Picture Transmission (APT) camera system, ice reconnaissance with the aid of satellite pictures became increasingly widespread by the United States, Canada, and other countries with interests at high latitudes. The USSR is also making use of its own and U.S. satellite data for sea ice surveys.

## 2. Use of Meteorological Satellite Data for Sea Ice Mapping

The first of a new generation of Improved TIROS Operational Satellites (ITOS) was placed in orbit 1460 km above Earth last winter. These new NOAA spacecraft combine the global coverage and local readout capabilities, formerly requiring two satellites, in a single satellite. In addition to the television cameras, ITOS-1 carries a two-channel scanning radiometer, one channel detecting visible radiation and the other infrared radiation. Figure 1 is an example of polar ice as it appears in an APT (Automatic Picture Transmission) picture taken by ITOS-1 over the northeast Canada area. APT pictures can be obtained by anyone in the world using relatively inexpensive receiving equipment, and there are now over 500 such local readout stations in over 50 countries.

Although cloud covers much of the Davis Strait in figure 1, first-year pack ice is visible in the lower strait with its southern limits extending southwestward from Disko Island, just off the west coast of Greenland, thence along

the Coast of Labrador to where it blocks the entrace to the Straits of Belle Isle between the Island of Newfoundland and the mainland. Cumberland Sound, Frobisher Bay, and the northeastern side of the Hudson Strait, Ungava Bay, and all of Hudson Bay are completely ice covered with the exception of an elongated area of open water or very thin ice along the eastern side of Hudson Bay.

As is partly evident in figure 1, obscuration of Earth's surface by cloud is a significant problem in the interpretation of ice extent in satellite photographs. Skilled photo-interpretation, making maximum use of landmarks, cloud shadows and comparison of pictures of the same area on two or more successive days, or use of overlapping pictures from successive orbits, is necessary for proper and consistent discrimination between sea ice and clouds.

To automatically and objectively filter clouds from scenes containing ice or snow fields, a method known as minimum brightness compositing was developed. Composite Minimum Brightness (CMB) chart is derived by computer processing of the mapped satellite vidicon data for several successive days, usually five. Only the lowest brightness observed at each grid point during the compositing period is saved for final display. Since cloud-free land or ocean is much less reflective than ice, snow, or clouds, the compositing procedure tends to retain just the slowly changing ice and snow fields, effectively filtering all clouds except those relatively few that persist throughout the period.

The CMB chart is one of the end products of a series of complex data processing steps requiring a high-speed electronic computer. After digitization of the analog television signal from the satellite, the raw data are brightness-normalized for variations in the response of the camera system and for inequalities in solar illumination. The data are then mapped onto a polar stereographic map projection after elimination of overlapping portions of pictures from adjacent orbits. The original brightness (relative) scale of 64 steps is compressed to 15 steps during this process.

Figure 2 is the CMB chart for the 5-day period, May 9-13, 1970, Brightness values have been displayed with a gray scale of 15 steps from white to black. The brightest areas appearing on the CMB chart are ice and snow on Greenland, Iceland, Scandanavia, and elsewhere in areas north of the treeline. Solid pack ice, for example along the east coast of Greenland and in the Baffin Island and Labrador Coast areas, appears almost as bright. Some unfiltered cloudiness will be found on every CMB chart. Fortunately, it is usually distinguishable from snow or ice by being less bright and more ragged or irregular in appearance. Cloud areas also tend to show much more change from one period to the next than do snow or ice areas.

An alternative method of CMB display is by means of computer wherein the brightness values are printed at each point of the array (see fig. 3). When these values are calibrated with respect to external brightness "benchmarks," such as the Greenland ice cap and cloudfree ocean areas, in order to correct for variations within the system, they correlate highly with albedoes (reflectivities) obtained over sea ice by other means. As will be shown in the next section, differences in the CMB values are systematically related to differences in ice concentration and in ice condition (viz. show-covered or puddled).

## 3. Quantitative Delimiting of Sea Ice Conditions

Computer printouts of CMB brightnesses were used to obtain data samples for various areas in the North American Arctic during the period mid-May through mid-September 1969. The southernmost group of areas studied included the following: central Hudson Bay, McClintock Channel, Foxe Basin, and northern Davis Strait. Much change occurred in ice conditions in these areas during the period. Another group consisted of areas near 75°N: northern Beaufort Sea, just west of Banks Isl., McClure Strait, western and eastern Viscount Melville Sound. These areas were characterized mostly by compact or very close pack throughout the period. Another group comprised areas varying in latitude from 68°N to 78°N, but all were characterized by very open pack or ice-free waters throughout the season: western Amundsen Gulf near Cape Bathurst, Chukchi Sea near Cape Lisburne, Barrow Strait just east of Resolute, and Smith Sound between Greenland and Ellesmere Island.

The data for a representative member of each of the above groups (see locations in fig. 4) have been represented in graphical form in figure 5; data for a Greenland ice cap area (Area G) are shown also. Note that the adjusted brightness averages for the ice cap are consistently near a value of 10 on a relative brightness or reflectivity scale of 0-14. The sample taken in western Viscount Melville Sound northeast of Banks Isl. (Area M) is just as bright as Greenland initially, and remains between 9 and 10 through the first third of June. Thereafter it drops rather rapidly in brightness to values between 6 and 7. maintaining this new level through early August. Throughout the remainder of the study period in mid-September it fluctuated between about 3 and 5. According to the Navy's BIRDS EYE Arctic Ocean Ice Reconnaissance Mission (4-69). which passed over this part of Melville Sound on June 3 and again on June 10, this area was characterized by the following ice conditions: 8/8 total concentration of fast ice, 5/8-6/8 multiyear, and 3/8-2/8 thick first-year; no openings, no melting. BIRDS EYE mission 5-69, which reconnoitered this area again on July 28, reported the following: 8/8 total concentration: 6/8 multiyear, 2/8 thick first-year; fractures, many puddles, and a few thaw holes. No BIRDS EYE data were available for August or September in the Melville Sound area, but weekly ice charts issued by the Dept. of Transport, Meteorological Branch of Canada for August show 10/10 concentration in this area, distributed by type as follows: 7/10-6/10 multiyear, and 4/10 or less first-year. Puddles. 3/10 frozen, were reported. During the first half of September the principal change in ice conditions was a decrease to 0/10 of first-year ice and the first appearance of new ice. There was also a trend toward freezing of puddles and the occurrence of snow cover.

In summary, western Melville Sound was characterized by high brightness values (equal to or approaching Greenland values) during the early part of the period when the ice pack was snow covered. Brightnesses decreased by about 30% when the snow melted and puddles developed in late June and through July. The brightness level diminished somewhat more in late August through mid-September as fractures and thaw holes appeared and some of the first-year ice melted. Some of the small peaks interrupting the general downward trend of brightness were associated with stormy periods when persistent cloudiness was not completely filtered by the compositing technique. The upturn in mid-September could also be related to the reported reappearance of some snow cover on the ice.

Central Hudson Bay in figure 5 (Area H) exhibits moderately high brightness averages, near 8, through mid-June, whereupon a remarkably steady decrease sets in, values reaching zero by the first of August. The brightness remains at or very near zero for the remainder of the study period. No BIRDS EYE data were taken over or near this area, so all comparisons are with the Canadian ice charts, the earliest available being for the week ending June 18. Concentrations were reported as 8/10 to ≥9/10, all first year ice, through mid-July, with 1/10-2/10 puddles and 1/10-2/10 thaw holes first being reported the last week of June. The total concentration decreased to 7/10, the fraction given as "medium floe or greater" steadily diminished from 5/10-10/10 to 2/10, and the percentage coverage of puddles increased to 5/10, through the month of July. In the first week of August there was an abrupt decrease in total concentration to 2/10 to 5/10, and by mid-August ice-free conditions were reported in central Hudson Bay.

In summary, the trend of adjusted brightness averages in central Hudson Bay is well correlated with the melting and decreasing concentrations of ice reported in that area.

The final study area given in figure 5 is southwest of Banks Island near Cape Bathurst (Area B) and is representative of those areas that tend to remain ice free throughout the period of study. The highest brightness averages here fell between 2 and 3, but much of the time the values were 1 or under. The high values in May were the result of shorefast ice along the east side of Cape Bathurst extending into the southwest corner of the sampling area. Movement of the sampling area less than 37 km to the NE would have brought the adjusted brightness averages in May to a magnitude of well under 1. The BIRDS EYE flight passed over this area on June 3, June 10, and June 29; in all cases the ice concentrations were reported as zero to ≤1/8. The weekly Canadian ice charts for June 18 through September 13 reported open water in this area southwest of Banks Island, with one exception. The chart for the week ending August 29 showed the sampling area within a narrow finger of 3/10 concentration.

In summary, ice-free conditions in this area were characterized by brightness averages generally ≤1/10 those typical of ice cap or snow covered compact or very close pack ice. Occasional peak CMB values of about 2, such as occurred once in July and several times in August, were associated with periods of persistent cloudiness.

Examination of adjusted CMB averages for a number of Arctic areas during the period mid-May through mid-September of 1969, in conjunction with ice reconnaissance data, ice charts, and meteorological data, indicates that characteristic brightness values are associated with different ice pack concentrations and conditions. These relationships are summarized in Figure 6. Residual cloudiness in the CMB charts presents a minor problem at the lower end of the brightness scale. Thus areas of very open pack or that are ice free may sometimes have brightness values of 2-4, which is the same level associated with open pack concentrations according to figure 6.

Scientists working in this field have stated that surface albedo and its variations are probably the most important regional factor affecting the heat and mass budgets of the Arctic Basin. Since it can be shown that adjusted CMB

values derived from satellite vidicon data are highly correlated with albedoes obtained over sea ice by other means, the technique presented here promises to be a useful tool for sea ice researchers and forecasters.

## 4. Future Prospects for Remote Sensing of Sea Ice from Earth Satellites

Yet other techniques are being developed to extend and improve sea ice surveillance from Earth satellites. It has been shown that infrared radiometer data from NASA's Nimbus satellites can be used to detect major ice features in the darkness of the polar night when television cameras or visible spectrum radiometers are useless. Studies are continuing to determine optimum data processing and display methods to use with NOAA's ITOS scanning radiometer (SR) measurements. The ITOS SR can provide daytime or nighttime thermal infrared data (10.5-12.5 micrometers) at a maximum ground resolution of about 7.5 km and daytime visible data (0.52-0.73 micrometers) at a resolution of about 3.5 km.

The second-generation ITOS, planned to begin in 1972, is scheduled to carry a Very High Resolution Radiometer (VHRR) with both a visible spectrum (about 0.6-0.7 micrometers) and a thermal infrared (10.5-12.5 micrometers) channel. In contrast to the measurements from the SR on the current ITOS, the data from both the channels on the VHRR will have a maximum ground resolution of 925 meters. This significant improvement in resolution, which begins to approach that of the Earth Resources Technology Satellite (ERTS), should improve our capability for detecting and defining sea ice features, concentrations, and conditions.

The multispectral capability of the ERTS A system, also planned to begin in 1972, will be in the visual and near-infrared. It is uncertain at this time how much increase in information content will derive from the multispectral character of the ERTS observation in the case of sea ice applications. The further increase in ground resolution, to 100-200 meters, however, will yield yet better delineation of details in ice features. ERTS B, in 1974, is to be equipped additionally with a thermal infrared channel in the 10 micrometer water vapor "window" region.

Although the 50° inclination of its orbit will preclude viewing of polar areas, the manned NASA SKYLAB spacecraft, planned for late 1972 or early 1973, will carry an Earth Resources Experiment Package with a number of sensors of interest with respect to ice observations. There will be a 6-camera multispectral photographic facility and a 10-band multispectral scanner with more channels in the visible and near infrared, as well as one in the thermal infrared, and ground resolutions will come down in the vicinity of 50+100 meters. More nearly all-weather viewing of sea or lake and river ice should be possible by means of a 13.9 GHz microwave radiometer/scatterometer and a 1.4 GHz microwave radiometer. Even data from the infrared spectrometer could be useful in that it should be possible to determine which specific regions of the IR spectra have the greatest pack ice information content and discriminative capacity with respect to clouds.

#### BIBLIOGRAPHY

- Barnes, J. C., Chang, D. T., and Willand, J. H., "Use of Satellite High Resolution Infrared Imagery to Map Arctic Sea Ice," Final Report, Contract No. N62306-68-C-0276, Allied Research Associates, Concord, Mass., 1969, 109 pp.
- Booth, A. L. and Taylor, V. R., "Meso-scale Archive and Computer Products of Digitized Video Data from ESSA Satellites," <u>Bulletin of American Meteorological Society</u>, Vol. 50, No. 6, 1969, pp. 431-438.
- Bristor, C. L., Callicott, W. M., and Bradford, R. W., "Operational Processing of Satellite Cloud Pictures by Computer," Monthly Weather Review, Vol. 94, No. 8, 1966, pp. 515-527.
- McClain, E. P. and Baker, D. R., "Experimental Large-Scale Snow and Ice Mapping with Satellite Composite Minimum Brightness Charts," ESSA Technical Memorandum NESCTM 12, Dept. of Commerce, Washington, D.C., 1969, 16 pp.
- Potocsky, G. J., "Use of Satellite Photographs to Supplement Aerial Ice Information," <u>Informal Report</u> No. 68-72, U.S. Naval Oceanographic Office, Washington, D.C., 1968, 13 pp.
- Schwalb, A. and Gross, J., "Vidicon Data Limitations," ESSA Technical Memorandum NESCTM 17, Dept. of Commerce, Washington, D.C., 1969, 22 pp.
- Untersteiner, N. and Maykut, G. A., "Numerical Predictions of the Thermodynamic Response of Arctic Sea Ice to Environmental Changes," Memorandum RM-6093-PR, Contract No. F 44620-67-C-0045, Rand Corporation, Santa Monica, Calif., 1969, 173 pp.
- Vasil'ev, K. P., "Use of Meteorological Satellite Data as a Navigation Aid,"
  Trudy No. 36, Problems of Satellite Meteorology (Ed. by I. P. Vetlov &
  G. I. Morskoi), Hydrometeorological Research Center of the USSR, 1968
  (Translation TT 70-50001 for ESSA and NSF, 1970, pp. 46-57).

#### GLOSSARY

- APT: Short name for Automatic Picture Transmission. Certain satellites of the TIROS and Nimbus series have had special camera and transmitter equipment such that television pictures and radiometer data taken while the satellite is within range of a station on Earth's surface can be received and displayed on relatively simple and inexpensive equipment.
- Benchmark: A standard reference location or value used for calibration purposes.
- Compact pack: Defined as 8/8 total ice concentration.
- Compositing: Here it refers to the use of data taken over the same region but at different times.
- Digitization: The process whereby a continuous analog signal received from the satellite is converted to discrete numerical values.
- Fast ice: Sea ice that forms and remains fast, i.e. attached, to the shore.

  Fast ice can extend several hundred kilometers from the coast.
- First-year ice: Also called "winter ice," this is ice that has formed during the current season, and it is generally less than two meters in thickness.
- Medium floe: Ice floes 100-500 meters across.
- Multi-year ice: Also called "polar ice," this is ice that has survived at least two summers, and it is generally two to four meters or more in thickness.
- <u>Multi-spectral</u>: Refers to a sensor system that has two or more radiation detectors or camera films, each measuring in or sensitive to a different interval or band of the electromagnetic spectrum.
- NOAA: National Oceanic and Atmospheric Administration (formerly ESSA), an agency of the U.S. Department of Commerce, which operates the National Environmental Satellite Service.
- Puddled: Refers to a sea ice condition wherein melt water is evident on the surface of the ice.
- Resolution: This term usually means "spatial resolution" or "ground resolution."

  It refers in simplest terms to the smallest detail detectible in satellite imagery of clouds or Earth's surface when there is reasonably good contrast between the target(s) and its background.
- Shorefast ice: Same as "fast ice."
- TIROS: Short name for Television and InfraRed Observation Satellite, a meteorological Earth satellite.
- Water vapor "window": Those portions of the electromagnetic spectrum wherein water vapor in Earth's atmosphere is relatively transparent to, i.e. absorbs weakly, energy emitted from Earth's surface and atmosphere.

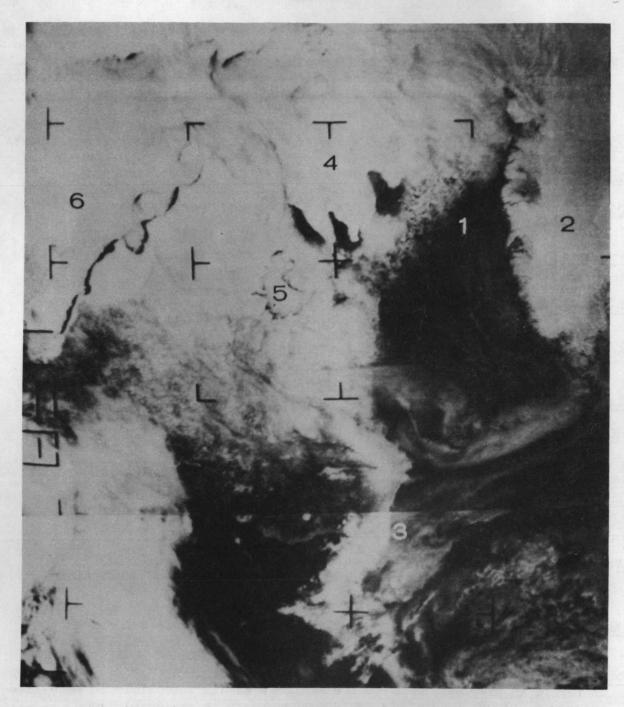
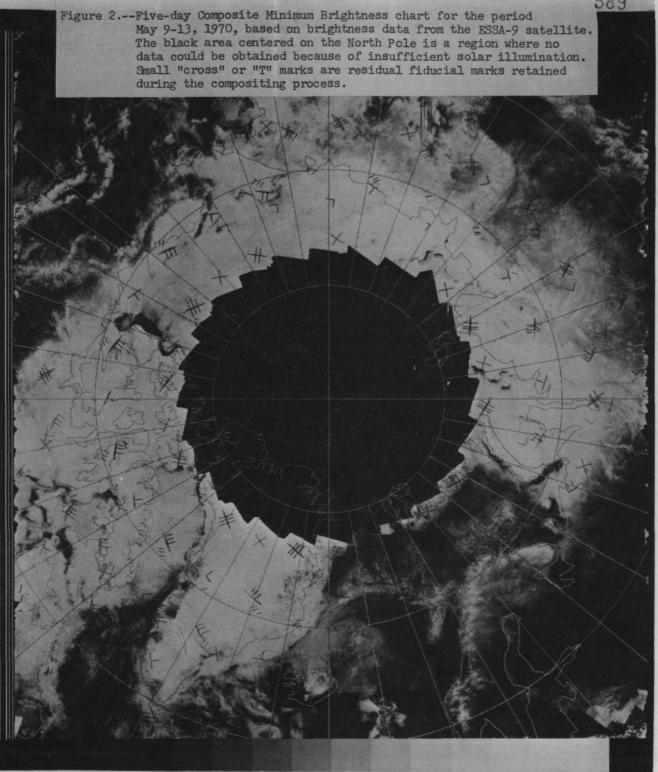


Figure 1.--Composite of two APT pictures from ITOS-1 taken on April 22, 1970.

1) Davis Strait; 2) Greenland; 3) Straits of Belle Isle; 4)

Baffin Island; 5) Ungava Bay; 6) Hudson Bay.



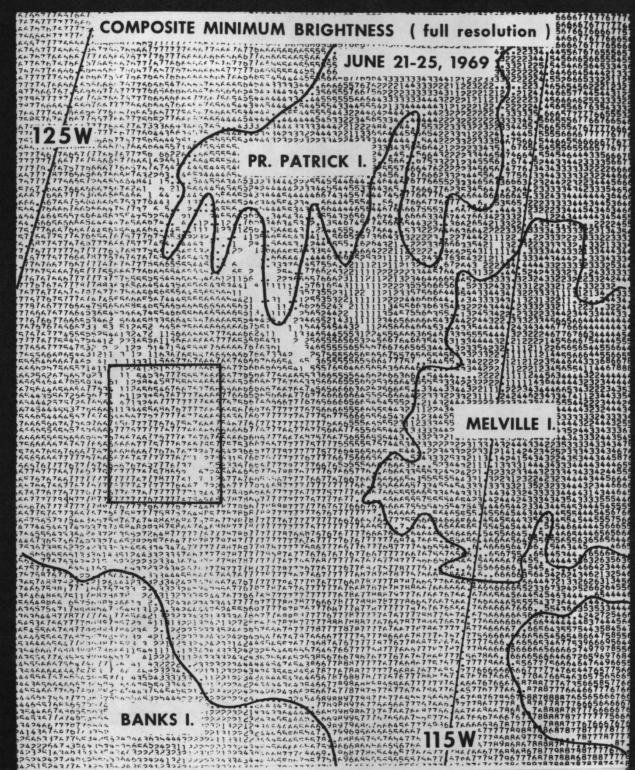


Figure 3.--Portion of a computer printout of the Composite Minimum Brightness (CMB) values for June 21, 1969. Rectangular block is approximately 40 n. mi. (67 km) on a side. The 15-step brightness scale is coded as follows: blank, 1, 2, 3, ... 9, A, B, C, D, E.



# Adjusted Brightness Averages ESSA 9 5 - day CMB Summer 1969

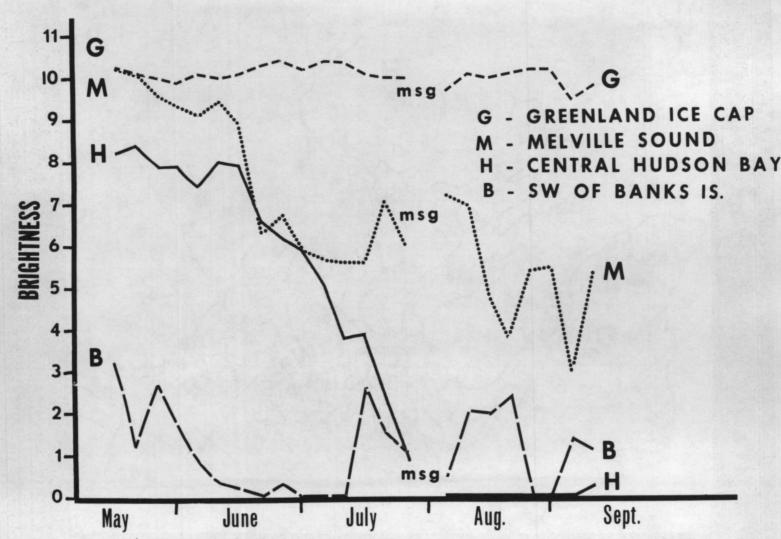


Figure 5.--Adjusted brightness averages for four Arctic areas (see locator map in Fig. 4) as a function of time for the period mid-May to mid-September 1969.

CATE- GORY	ADJUSTED CMB AVERAGE	ICE CONCENTRATION	ICE CONDITION
1	9-10	COMPACT OR VERY CLOSE PACK (10/10-9/10)	SNOW COVERED (>7/10)
2	7-8	COMPACT OR VERY CLOSE PACK (10/10-9/10)	SNOW FREE (< 3/10); LITTLE OR NO PUDDLING (< 1/10)
3	5-6	VERY CLOSE OR CLOSE PACK (9/10-7/10)	SOME PUDDLES AND THAW HOLES (1/10-3/10)
4	2-4	OPEN PACK (6/10-4/10)	MUCH PUDDLING (>3/10) AND ROTTEN ICE
5	0-1	VERY OPEN PACK (3/10-1/10) OR ICE FREE WATERS	

#### BIOGRAPHICAL SKETCH

P. KRISHNA RAO: Research Physical Scientist, National Environmental Satellite Service (NESS) of the National Oceanic and Atmospheric Administration (NOAA). Born in India, M.S. in Geophysics (Andhra University, India), M.S. in Meteorology (Florida State University), and Ph.D. in Meteorology (New York University). Professional member of the American Meteorological Society and Fellow of the Royal Meteorological Society, U.K. 1956-1960: Assistant Research Scientist, Dept. of Meteorology, New York University; 1960-61: Meteorologist with the Canadian Meteorological Service; 1961-Present: Research Physical Scientist, NESS/NOAA. For the last several years Dr. Rao's research efforts have been to develop techniques to understand and use satellite radiation data in meteorological and oceanographic studies. A number of his papers have been published in technical journals, and he has presented papers at national and international meetings.

#### P. Krishna Rao

## 1. Introduction

The distribution of sea surface temperature over large areas of this earth is very useful for many earth resources studies and environmental research. A good estimate of this quantity is essential for certain studies of marine activities, but unfortunately a complete and true picture has not been available due to observational difficulties. Many of the presently available sea surface temperature charts are based on commercial ship reports along the routine shipping lanes, and on data from a few research cruises. These data vary widely in space, time and quality and a global distribution cannot be obtained at short intervals of two or three days.

With the launching of several earth orbiting satellites containing radiometers, it is now possible to measure sea surface temperature under relatively clear sky conditions. Before any attempts could be made to process the data in terms of sea surface temperature on a routine basis, an objective method of determining sea surface temperature from the data was required. One such method has been developed and tested and this technique will be discussed in the next section.

## 2. Surface Temperature Mapping from Satellite Infrared Measurements

The examples presented are based on information obtained from the Improved TIROS Operational Satellite (ITOS). This satellite is equipped with several TV cameras and radiometers. No details of the instrumentation, except a brief description of the radiometer, will be given here. References given at the end will provide additional information on ITOS. ITOS is a three-axis stabilized, earth-oriented spacecraft designed to provide full day and night coverage of the entire surface of the earth on a daily basis. The orbit is circular at 790 nautical miles (1463 kilometers) and near polar in inclination. The scanning radiometer (SR) has two channels; one measures the visible radiation reflected from the earth in the 0.52-0.73 micrometer region during daytime. and the second measures the infrared radiation emitted from the earth in the 10.5-12.5 micrometer region during day and night. If the radiometer looks straight down at Earth's surface, the area instantaneously viewed is about 4 n. mi. (7.4 km) in diameter. The motion of the satellite, together with the action of the scanning mechanism, provides complete coverage without data gaps between successive orbital passes.

The global infrared measurements are stored temporarily on tape on board the satellite for later transmission to the ground and subsequent computer processing. The SR also transmits infrared (SRIR) data in real time directly to Automatic Picture Transmission (APT) stations for local use. These radiation observations are known as the Direct Readout InfraRed (DRIR) data. This information can be displayed on a photo-facsimile recorder and a continuous strip image produced as shown in figure 1. This type of pictorial display is invaluable for qualitative interpretation of the environmental data. The gray scale is arranged such that clouds, snow and ice are shown lighter (less radiant energy reaching the radiometer) and clear and warmer regions are shown darker (more energy reaching the radiometer). A calibrated gray scale wedge can be generated and compared with the picture data to derive quantitative values.

NATIONAL OCEANIC AND ATMOSPHERIC ADMINISTRATION

Figure 1 is an example of nighttime DRIR imagery obtained from the ITOS-1 satellite on 19 October 1970. Some of the prominent features are Cape May, Chesapeake Bay, Delmarva Peninsula, Delaware Bay, warm boundary of the primary Gulf Stream front, a secondary thermal front between the primary one and the coast, and portions of the Great Lakes. Pictures like this obtained at any of the APT stations can be used immediately for many purposes.

For quantitative studies, the digitized IR information is more useful. In quantitative studies the infrared measurements should be corrected for any atmospheric contributions to the observed signal. In the 10.5-12.5 micrometer region, atmospheric water vapor and carbon dioxide are the absorbing consti-The atmospheric contribution varies most with the viewing angle of observation, cloud conditions, and the amount of water vapor within the atmosphere. All the data presented in this paper are corrected for these factors. One of the outputs obtained over a small region of the Gulf of Mexico on the night of 8 September 1970 (approx. 0300 local time) is shown in figure 2. information is derived from a computer program and the temperatures are in degrees Kelvin (K). The area covered is approximately 1.25 degrees latitude -1.25 degrees longitude (or 120.6 x 138.6 km) and each value is a representative temperature for a sub-area of approximately 7.5 x 8.7 km in size, which is essentially the resolution of the present ITOS radiometer. There are about 256 observations over the total area and a detailed analysis can be done. A quick look at the data array shows that in some places the temperature varies as much as 10 K between adjacent sub-areas. Except very near strong current boundaries such large variations in sea surface temperature cannot be accounted These variations can be caused by either clouds or instrumental noise. Subjective methods can be used to eliminate such observations, from sea surface temperature analyses, but this is practicable only for small samples. This approach cannot be used for large scale studies, and objective analysis techniques that can be automated should be used. The method that will be presented here can be used in the other areas of the earth resources studies where the cloudfree observations are required to understand a certain phenomenon.

## 3. Objective Sea Surface Temperature Determination Procedure

The mapping of sea surface temperature from satellite IR observations requires the capability to discriminate the Earth's surface from cloud. With a simple measurement, one might argue that the measurement is either of cloud or of the surface on the basis of only the magnitude of the observed temperature. It is usually impossible to distinguish in this manner the difference between a relatively low opaque or a high thin cloud and the Earth's surface since the associated temperatures may be well within 10 K of one another.

To overcome this problem, a method has been developed to examine a large number of measurements within an area larger than that covered by most cloud masses. From such a sample of measurements, one can determine the surface temperature by making use of the following: (a) the magnitude of the temperature should be highest for the cloudfree observations; and (b) modes dominated by relatively cloudfree observations will be distinct. Since the spatial variability of the sea surface temperature is very small except near the boundaries of major currents and areas of strong upwelling, the statement (b) should hold well over most regions.

The ITOS scans from horizon to horizon in a direction perpendicular to the orbital track and there is data overlap between adjacent orbits. Frequency histograms of these radiation measurements (fig. 3) within a 2.5° latitude/longitude quadrangle (approximately 240 x 280 km) can be generated over large regions. In quadrangles of this size there are 1024 observations. Figure 3 shows one of the computer-produced histograms. The numbers in the left column are coded temperatures (example 120 = 284 K) and run from 89-255. The numbers along the top row, 1-22, identify the various latitude/longitude quadrangles along line 49, section 1 (which gives the location). in each column from 1-22 specify the number of observations in each box that had the indicated temperature (example: For coded temperature 120 under column 15, the value 159 shows the number (or frequency) of observations having that temperature). The numbers in the bottom row indicate the number of observations that were missing from each quadrangle. The histogram presented here is for a three-day composite (September 6, 7, and 8, 1970), and if no data were available in a particular quadrangle, the number in the bottom row should be 3072 (3 x 1024) as in column 4, for example. In column 20, on the other hand, the last number in the column is zero, which means that none of the 3072 observations is missing from that quadrangle.

If there were relatively few clouds in a quadrangle then the histogram should be compact as in column 7. If there are clouds, but it was not completely overcast, then the distribution will be similar to the one in column 15. By examining such frequency distributions one can select the most probable cloudfree temperatures in the area. One such objective method is described below.

In the absence of cloud-contaminated measurements, it can be assumed that the satellite-observed surface temperature distributions in a small area should be Gaussian with a dispersion produced by noise. The standard deviation,  $\sigma$ . of such distributions is equal to the known standard random error of measurement. For a Gaussian distribution, the temperature  $+1\sigma$  from the mean or mode is that temperature on the high temperature wing of the histogram where the change of frequency of observation with temperature is a maximum. When a cloud-contaminated frequency distribution is obtained for an area, it is assumed that this maximum slope, or +  $1\sigma$ , portion associated with the typical cloudfree distribution (clear mode) is identifiable, provided there are sufficient clear spots within the area viewed by the radiometer. Thus, the surface temperature can be defined as the temperature at the point of maximum slope on the high temperature wing of the "clear mode" T (+  $1\sigma$ ), minus the standard error of measurement,  $\sigma$ . This derived value will usually be higher than the observed modal peak temperature because the observed temperature distribution tends to be biased toward lower temperatures when clouds are present.

Figure 4 illustrates the technique by means of two histograms obtained over adjacent quadrangles. Both distributions are skewed toward low temperatures due to cloud contamination. In fact, there were many values below  $280^{\circ}$ K which are not shown. The dispersion on the high temperature side is mainly due to instrumental noise. The high temperature modes shown are produced by a combination of cloud-contaminated and cloudfree observations. Since the standard error of measurements is about  $1.5^{\circ}$ K for the SR on ITOS at these temperatures, the most probable surface temperatures are given by  $T(+1\sigma)$  -  $1.5^{\circ}$ K.

Note that the inferred surface temperature for the more westerly grid square is the same as the modal peak value, indicating that the modal peak is produced predominantly by cloudfree observations. In the other area, however, the modal peak is 3°K lower than the inferred surface temperature, indicating that this peak is produced by cloud-contaminated as well as cloudfree observations (assuming a negligible sea surface temperature gradient over the quadrangle). The observations greater than 301°K are apparently cloudfree, allowing the correct surface temperature to be inferred from the maximum slope of the distribution. The inferred temperatures are in agreement with a nearby ship observation of 301°K.

A complete set of procedures and conditions necessary for reliably specifying sea surface temperatures from histograms of SR temperatures, corrected for atmospheric attenuation, have been devised and put in the form of a computer program. The procedure for specifying the sea surface temperatures is completely objective, and can produce values for a given day over the entire Northern and Southern Hemispheres with a few minutes of computer time. This enables one to bulk process the satellite TR data. The stability of the values increases with the quadrangle size used or through time-compositing because the number of observations that are available for defining the clear modal distribution increases. Also sea surface temperatures for areas where severe cloud contamination exists, or which are not observed due to gaps in satellite coverage, can be inferred through space and time interpolation procedures.

Figure 5 shows the sea surface temperature distribution for the Northern Hemisphere obtained from 3-day composite, 2.5 degree histograms (240 x 280 km) of ITOS nighttime SRIR data. All quadrangles for which temperatures could be specified are indicated by an open circle on the figure. Where these circles are absent, no temperature could be derived because of persistent cloudiness. A few of the cold areas, such as the ones analyzed just west of Baja California and just east of the Philippines, appear to be unrealistic and are evidently due to cloud contamination not adequately handled by the technique. Only with satellites and multiple-day compositing is it possible to cover such large areas and specify temperatures over most of the regions. It is almost impossible to cover such a vast area in a three-day period with conventional observational platforms such as ships or aircraft.

Finally, figure 6 shows a scatter diagram of sea surface temperatures derived from ITOS-SR compared with those reported by the Ocean Station Vessels in the North Atlantic and North Pacific Oceans. Since these vessels take surface temperature measurements at the same depth most of the time, compared to the ships of opportunity, whose reported temperatures correspond to various depths, only the former values were used in the comparison. The root mean square (RMS) difference is about 1.98°K. The difference could be due to a difference between the "skin temperature" and the subsurface temperature measured by ships, or it may be caused by the instrumental calibration of the SB. It has been observed recently that significant noise is introduced by the satellite tape recorder system, which must contribute to the RMS difference noted above. It is also known that ship temperatures vary among themselves with an RMS difference of nearly one degree Kelvin.

## Summary

A technique for deriving sea surface temperatures has been developed and tested with a limited amount of independent data. The technique is completely objective and minimizes the influence of atmospheric absorption, cloud contamination, and instrumental noise on the inferred sea surface temperatures.

Clouds and some amount of instrumental noise will be always present in all observations from earth orbiting satellites. The influence of these elements must be minimized to make a meaningful study of the observed quantities. The technique presented here will be useful in solving this problem.

#### BIBLIOGRAPHY

- Curtis, W. R. and Rao, P. Krishna, "Gulf Stream Thermal Gradients from Satellite Ship and Aircraft Observations," <u>Journal of Geophysical Research</u>, Oceans and Atmospheres, Vol. 74, No. 28, Dec. 20, 1969, pp. 6984-6990.
- Greaves, J. R., Willard, J. H., and Chang, D. T., "Observations of Sea Surface Temperature Patterns and Their Synoptic Changes Through Optimal Processing by Nimbus 2 Data," <u>Final Report</u>, NASA Contract NAS W-1651, Allied Research Associates, Concord, Mass., Sept. 1968, 121 pp.
- Rao, P. K., "Sea Surface Temperature Measurements from Satellite," Mariners Weather Log, Vol. 12, No. 5, Sept. 1968, pp. 152-154.
- Smith, W. L., Rao, P. K., Koffler, R., and Curtis, W. R., "The Determination of Sea-Surface Temperature from Satellite High Resolution Infrared Window Radiation Measurements," Monthly Weather Review, Vol. 98, No. 8, Aug. 1970, pp. 604-611.
- TOS Project/Goddard Space Flight Center, NASA, <u>ITOS</u>, 28 pp., for sale by the Superintendent of Documents, U.S. Government Printing Office, Washington, D.C. 20402. Price: 20 cents.
- Warnecke, G., Allison, L. J., and Foschee, L. I., "Observations of Sea Surface Temperatures and Ocean Currents from Nimbus II," NASA Report No. X-622-67-435, National Aeronautics and Space Administration, Goddard Space Flight Center, Greenbelt, Md., 1967, 9 pp.

#### GLOSSARY

- APT: Short name for Automatic Picture Transmission. Certain satellites of the TIROS and Nimbus series have had special camera and transmitter equipment such that television pictures and radiometer data taken while the satellite is within range of a station on Earth's surface can be received and displayed on relatively simple and inexpensive equipment.
- Compositing: Here it refers to the use of data taken over the same region but at different times.
- Digitization: The process whereby a continuous analog signal received from the satellite is converted to discrete numerical values.
- Gaussian: A statistical term that refers to a "normal" distribution.
- Modes: A statistical term referring to the most frequently occurring value or values in a sample. When the sample is presented in the form of a frequency distribution, the mode(s) appears as a maximum (maxima).
- Photo-facsimile: A method whereby the input voltages from some source are converted to a continuous image by a scanning mechanism that generates gray tones as a function of signal level.
- RMS differences: A statistical term meaning Root Mean Square difference. In the example presented it is obtained by taking the differences between the satellite temperatures and the corresponding ships' temperatures, squaring them, taking the average of the squares, and then obtaining the square root of that value.
- Skewed: If a frequency distribution is not symmetric about its mode it is called "skewed."
- Skin temperature: The temperature of the thin film of the water surface, generally the uppermost fraction of a millimeter.
- Sub-surface temperature: The temperature beneath the water surface, and generally refers to a few meters in depth.
- Thermal front: Transition zone between the two water masses where there is a strong horizontal temperature gradient.
- TIROS: Short name for Television and InfraRed Observation Satellite, a meteorological Earth satellite.
- Upwelling: The process whereby water rises from a lower to a higher depth, usually as a result of divergence and offshore currents.

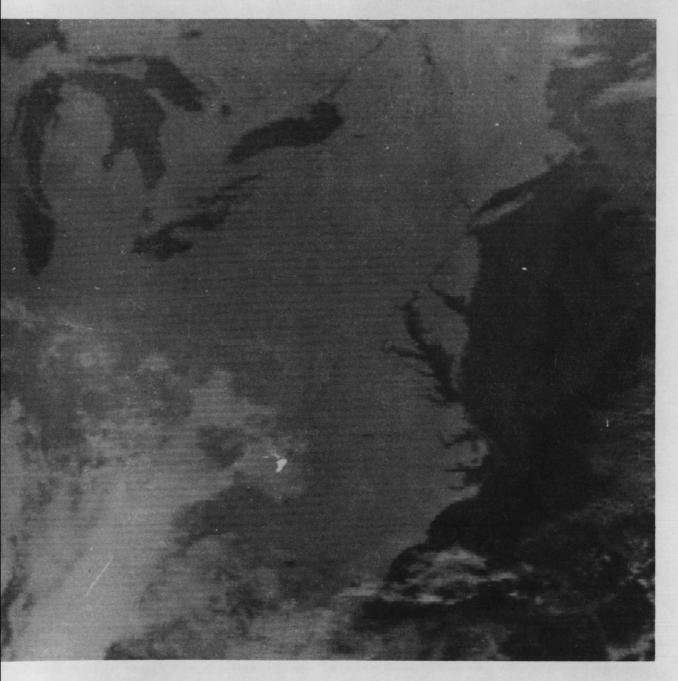
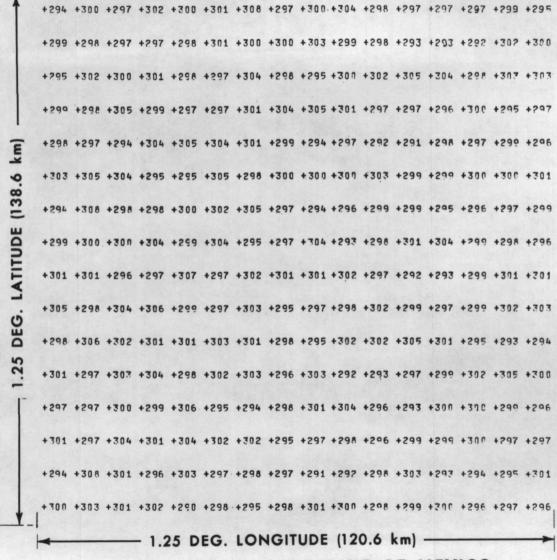


Figure 1.--Direct readout, nighttime infrared imagery obtained from ITOS-1 SEER on 19 October 1970 in the vicinity of the East Coast. The darker is the tone in an area, the warmer is the radiating surface there.



## ITOS 1 SRIR OVER GULF OF MEXICO TEMP. °K SEPT. 8, 1970

Figure 2. -- Example of computer-generated histograms of ITOS-1 STRS data

Figure 3.--Digitized ITOS-1 SRIR data over Gulf of Mexico for 8 September 1970. The temperatures are in degrees Kelvin.

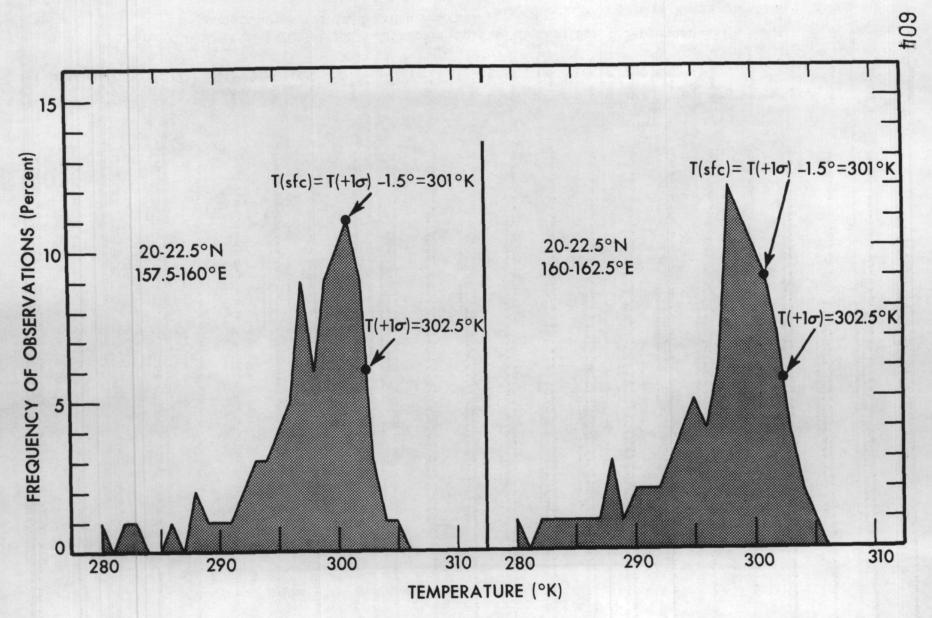


Figure 4.--Sample histograms of corrected ITOS-1 SRIR data showing their relation to sea surface temperature.

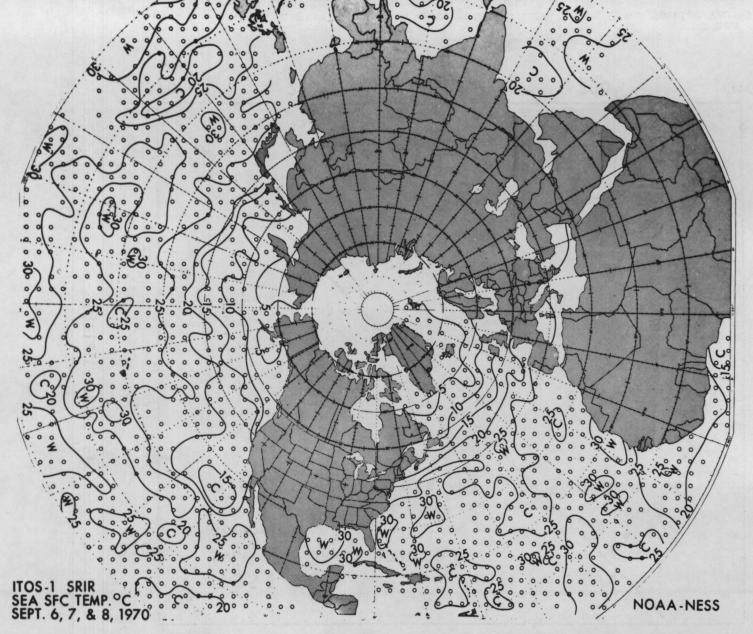


Figure 5.--Three-day (6, 7, and 8 September 1970) composite Northern Hemisphere sea surface temperatures inferred from ITOS-1 SRIR data. The isotherms are labelled in degrees Celsius. Data points are represented by open circles.

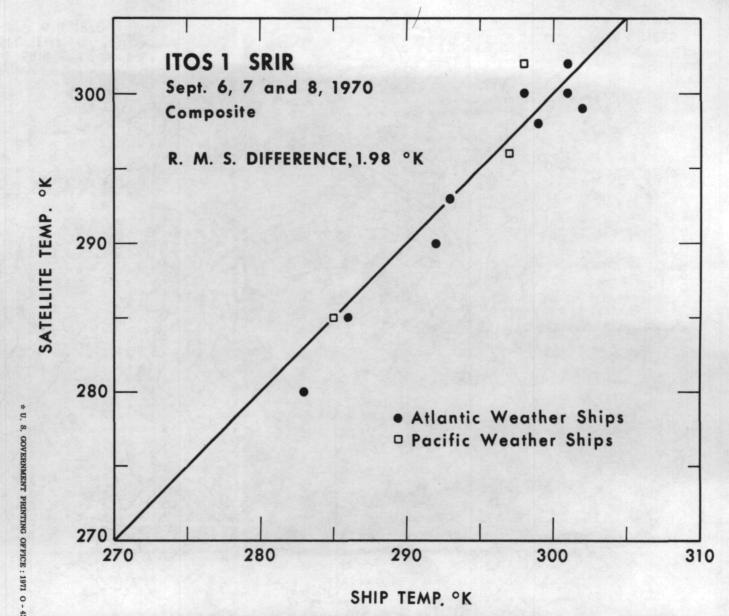


Figure 6.--Scatter diagram of surface temperatures obtained from Ocean Station Vessels versus those inferred from ITOS-1 SRIR data.

PREPARED BY:
NATIONAL AERONAUTICS AND SPACE ADMINISTRATION
OFFICE OF SPACE SCIENCE AND APPLICATIONS
WASHINGTON, D.C. 20546